

Lecture Notes on Multidisciplinary Industrial Engineering
Series Editor: J. Paulo Davim

Ravi Pratap Singh
Mohit Tyagi
Dilbagh Panchal
J. Paulo Davim *Editors*


Proceedings of the International Conference on Industrial and Manufacturing Systems (CIMS-2020)

Optimization in Industrial and
Manufacturing Systems and
Applications

 Springer

Lecture Notes on Multidisciplinary Industrial Engineering

Series Editor

J. Paulo Davim , Department of Mechanical Engineering, University of Aveiro, Aveiro, Portugal

“Lecture Notes on Multidisciplinary Industrial Engineering” publishes special volumes of conferences, workshops and symposia in interdisciplinary topics of interest. Disciplines such as materials science, nanosciences, sustainability science, management sciences, computational sciences, mechanical engineering, industrial engineering, manufacturing, mechatronics, electrical engineering, environmental and civil engineering, chemical engineering, systems engineering and biomedical engineering are covered. Selected and peer-reviewed papers from events in these fields can be considered for publication in this series.

More information about this series at <http://www.springer.com/series/15734>

Ravi Pratap Singh · Mohit Tyagi ·
Dilbagh Panchal · J. Paulo Davim
Editors

Proceedings
of the International
Conference on Industrial
and Manufacturing Systems
(CIMS-2020)

Optimization in Industrial and Manufacturing
Systems and Applications


 Springer

Editors

Ravi Pratap Singh
Department of Industrial and Production
Engineering
Dr. B. R. Ambedkar National Institute
of Technology
Jalandhar, Punjab, India

Mohit Tyagi
Department of Industrial and Production
Engineering
Dr. B. R. Ambedkar National Institute
of Technology
Jalandhar, Punjab, India

Dilbagh Panchal
Dr. B. R. Ambedkar National Institute
of Technology
Jalandhar, Punjab, India

J. Paulo Davim 
Department of Mechanical Engineering
University of Aveiro
Campus Santiago, Aveiro, Portugal

ISSN 2522-5022

ISSN 2522-5030 (electronic)

Lecture Notes on Multidisciplinary Industrial Engineering

ISBN 978-3-030-73494-7

ISBN 978-3-030-73495-4 (eBook)

<https://doi.org/10.1007/978-3-030-73495-4>

© The Editor(s) (if applicable) and The Author(s), under exclusive license to Springer Nature Switzerland AG 2022

This work is subject to copyright. All rights are solely and exclusively licensed by the Publisher, whether the whole or part of the material is concerned, specifically the rights of translation, reprinting, reuse of illustrations, recitation, broadcasting, reproduction on microfilms or in any other physical way, and transmission or information storage and retrieval, electronic adaptation, computer software, or by similar or dissimilar methodology now known or hereafter developed.

The use of general descriptive names, registered names, trademarks, service marks, etc. in this publication does not imply, even in the absence of a specific statement, that such names are exempt from the relevant protective laws and regulations and therefore free for general use.

The publisher, the authors and the editors are safe to assume that the advice and information in this book are believed to be true and accurate at the date of publication. Neither the publisher nor the authors or the editors give a warranty, expressed or implied, with respect to the material contained herein or for any errors or omissions that may have been made. The publisher remains neutral with regard to jurisdictional claims in published maps and institutional affiliations.

This Springer imprint is published by the registered company Springer Nature Switzerland AG
The registered company address is: Gewerbestrasse 11, 6330 Cham, Switzerland

Contents

1	Application of TLBO to Optimize Cutting Variables for Face Milling of Aluminium Alloy Al-8090	1
	Ashutosh Kumar Gupta and Ravi Pratap Singh	
2	Perspective of 4D Printing in Additive Manufacturing	15
	Ajay Sharma and Ajay K. S. Singholi	
3	Sustainable Material Selection for Indian Manufacturing Industries: A Hybrid Multi-criteria Decision-Making Approach	31
	Anbesh Jamwal, Rajeev Agrawal, Monica Sharma, and Anil Kumar	
4	Identification of Barriers in the Implementation of Additive Manufacturing in Indian Scenario	45
	Shivam Verma, Manish Gupta, and Shivam	
5	Application of 3D Scanning for Reverse Manufacturing and Inspection of Mechanical Components	61
	Kailash Chaudhary and Aditya Govil	
6	Optimization Techniques for Response Predication in Metal Cutting Operation: A Review	77
	Rajeev Sharma, Binit Kumar Jha, and Vipin Pahuja	
7	Modelling and Analysis of Barriers in Lean Green Manufacturing Implementation: An ISM Approach	93
	Sarita Prasad, Rao A. Neelakanteswara, and Krishnanand Lanka	
8	Soft Computing Techniques for Predicting Aeration Efficiency of Gabion Stepped Weir	117
	Aayushi Verma, Subodh Ranjan, Umesh Ghanekar, and N. K. Tiwari	

9	Performance Evaluation of Availability of Complex Repairable System and Selection of Optimal Performance Parameters Using Particle Swarm Optimization	123
	Ajay Kumar and Devender Punia	
10	A Study on Characterization of Green Metal Matrix Composites Reinforced with Melon Shell Ash Particulates	141
	Yatan Nagpal, Pardeep Sharma, and Rohit Sharma	
11	Optimizing the Three-Body Abrasion Wear of Quenched and Tempered Steel	153
	Sarika Kumari, Varun Sharma, R. K. Bansal, and Bhuvnesh Bhardwaj	
12	Lean Manufacturing Through PDCA: A Case Study of a Press Manufacturing Industry	167
	Kashmir Singh Ghorha, Rohit Sharma, and Gurraj Singh	
13	Optimization of Changeover Time in a Manufacturing Enterprise Using Single Minute Exchange of Dies (SMED): A Case Study	189
	Aditya Bassi, Harkrit Chhatwal, Nishant Bhasin, Shubham Sharma, and Ruchika Gupta	
14	Study of Development of Various Morphological Phases and Its Effects on the Thermal Coated Specimen—A Review	201
	Sonia Dangi, R. S. Walia, N. M. Suri, and Sumit Chaudhary	
15	Parametric Study on Stainless Steel 316L by Die Sinking EDM for Biomedical Application	215
	Preeti Chauhan, M. A. Saloda, B. P. Nandwana, and S. Jindal	
16	Optimization of Direct Slicing Process Using DICOMS for Additive Manufacturing	231
	Ujjwala Singh Thakur, Vivek Kumar Gupta, Ankit Nayak, and Prashant Kumar Jain	
17	Fatigue Analysis of FRP Laminate Composites	247
	Nitin Johri and Bhaskar Chandra Kandpal	
18	Performance Enhancement of Electro-chemical Discharge Machining by Process Variants: A Review	259
	Pankaj Kumar Gupta, Tapas Bajpai, Nikhil Jain, and Dharmendra Singh	
19	Behaviour of Voided Slab Utilizing Waste Materials	271
	Maninder Singh, Babita Saini, Abhishek Kumar, Ronak Singh Poonia, and Katta Vinay Reddy	

20 Design Considerations for Body-Powered 3D Printed Prostheses with String Mechanism for Upper Limb Disarticulation 283
 Abdul Dhiraj Hussain, Neeraj Radhakrishnan, Mohammed Sarfas, and Vishal Francis

21 Additive Manufacturing of Polymer-Based Bio-implants Using the Fused Filament Fabrication Process 301
 Jasvir Singh and Vishal Francis

22 Design, Applications, and Challenges of 3D-Printed Custom Orthotics Aids: A Review 313
 Ravi Kumar and Saroj Kumar Sarangi

23 Analysis of Carbon Nanotubes Reinforced Functionally Graded Composite Beams by Finite Elements Method 329
 Manish Kumar and Saroj Kumar Sarangi

24 Studies on the Fatigue Performance of Wire and Arc Additive Manufactured SS 904L 343
 Sharath Rajendran, A. Rajesh Kannan, B. Suresha, and N. Siva Shanmugam

25 Heterogeneous Modeling for Fabrication of Anatomical Structure from DICOM Image Using Additive Manufacturing 353
 Vivek Kumar Gupta, Ankit Nayak, Ujjwala Singh Thakur, and Prashant Kumar Jain

26 Improved Local Search Based Grey Wolf Optimization for Feature Selection 371
 Rahul Hans and Harjot Kaur

27 Current Technologies on Electronics Cooling and Scope for Further Improvement: A Typical Review 389
 K. R. Aglawe, R. K. Yadav, and S. B. Thool

28 Numerical Optimization of ZnMgO/CIGS Based Heterojunction Solar Cells via Change of Buffer and BSF Layer 409
 Raushan Kumar, Akhilesh Kumar, and Kumar Saurabh

29 Additive Manufacturing of Large Size Parts Through Retrofitment of Three-Axes CNC Machining Centre 421
 Sagar Kailas Gawali, Narendra Kumar, and Prashant Kumar Jain

30 Investigation of Machining Rate and Tool Wear in Processing of Fe-Based-SMA Through Sinking EDM 439
 Ranjit Singh, Ravi Pratap Singh, and Rajeev Trehan

31	Study of Microstructure, Mechanical and Fracture Properties of Bagasse Ash Powder Strengthened Aluminium Matrix Composites	453
	Vaibhav Singh, Satpal Sharma, and Bhaskar Chandra Kandpal	
32	Analysis of the Surface Roughness Characteristics of EDMed Components Using GRA Method	461
	Vidyapati Kumar and Shankar Chakraborty	
33	Smart Materials for 4-D Printing: A Comprehensive Review	479
	Amit Gupta, P. Sudhakar Rao, and Mohd. Yunus Khan	
34	Composites in Context to Additive Manufacturing	491
	Mohd Shoeb, Lokesh Kumar, Abid Haleem, and Mohd Javaid	
35	A Critical Review on Dissimilar Joining of ASS and FSS	505
	Chetan Tembhurkar, Ravinder Kataria, Sachin P. Ambade, and Jagesvar Verma	
36	Industrial Waste Management in Portugal for Environmental Development	519
	Mayank, Vaibhav Chaturvedi, Tmana Mahajan, Ravi Pratap Singh, Parampreet Kaur, and Amit Arora	
37	Designing a Mechanism to Paint a Conical Shaped Part	535
	Rufus R. Thomas, C. N. Sakhale, M. S. Giripunje, and Sagar D. Shelare	
38	Designing of an Anti Roll Bar to Adjust the Balance and Stability of a Formula Student Car	547
	Ankit Kumar Singh, Ekansh Prasad, and Pradeep Kumar Jain	
39	Study and Comparison of Initial Populations on the Performance of Modified Differential Evolution Algorithm	563
	I. R. Gawai and D. I. Lalwani	
40	Evaluation of Smart Bio-materials in Orthopedics and Tissue Engineering	587
	Pravin S. Nerkar, Sanket J. Tawale, Shailesh M. Saoji, and Akshay D. Doye	
41	Design and Development of Novel Multipoint Epicyclic Superfinishing Tool	601
	Muhammad Osama, Faiz Iqbal, Dilshad Ahmad Khan, and Zafar Alam	
42	Investigation on Mechanical Properties of Himalyan Extract Reinforced Epoxy Composite	621
	Ajay Chauhan, Vikram Singh, and Shiv Kumar	

43 Minimizing Solid Not Fat Loss in Whey During Paneer Manufacturing Using Taguchi Orthogonal Array 633
Sudip Banerjee, N. M. Suri, Sumankant, Subrata Kumar Bag,
and Sandeep Kumar Khatkar

44 Features and Functions of Filament Operated 3D Printer Nozzles: A Review 645
Krishnanand, Vatsal Mittal, Varanjot Singh,
Amar Kumar Branwal, and Mohammad Taufik

45 Extruder Design in Pellets Operated 3D Printers: A Review 661
Krishnanand, Varanjot Singh, Vatsal Mittal,
Amar Kumar Branwal, and Mohammad Taufik

46 Smart Magnetorheological (MR) Finishing Technology and Its Applications 677
Rahul Vaishya, Vivek Sharma, Vikas Kumar, and Rajeev Verma

47 Development of Sheet Metal Die by Using CAD and Simulation Technology to Improvement of Quality 687
Amrapali L. Ramteke, Shubash N. Waghmare, Sagar D. Shelare,
and Piyush M. Sirsat

Chapter 1

Application of TLBO to Optimize Cutting Variables for Face Milling of Aluminium Alloy Al-8090



Ashutosh Kumar Gupta and Ravi Pratap Singh

Abstract This paper presents an implementation of the Taguchi design and sanitized teaching–learning based optimization application to optimize MRR and MT in a CNC face milling operation. The Taguchi orthogonal array (DOE), is a time-efficient and cost-effective experimental technique. In this study spindle speed, feed rate and depth of cut are the input variables, and MRR and MT are the responses. An orthogonal array of L_9 is used for experimentation and a regression equation is developed using obtained value of responses later this equation is used as an objective function in TLBO algorithm to get an optimal machining combination.

Keywords Face milling · MRR · Machining time (T_c) · Taguchi design · S-TLBO

1.1 Introduction

The main goal(s) of machining in the real life are to obtain maximum productivity, minimum operational cost, lower production time and better machining quality. Improvement in the productivity and production time could be obtain by referring Material Removal Rate (MRR) and Machining Time (MT). The usual optimization technique can optimize machining objective(s) by using methods like Taguchi-Grey method, Full-Factorial method and RSM. Modern optimization techniques like PSO, TLBO, GA, NSGA-II, ANFIS and ABC and its variants are called soft computing optimization methods. Now, soft computing is tending over conventional technique because these soft computing techniques are fast and more accurate. Teacher Learning Based Optimization (TLBO) is used for optimization in this paper which is a modern (non-traditional) optimization technique suggested by Rao and Savsani [1].

A. K. Gupta · R. P. Singh (✉)

Department of Industrial and Production Engineering, Dr B R Ambedkar National Institute of Technology, Jalandhar, Punjab 144011, India

e-mail: singhrp@nitj.ac.in

1.2 Literature Review

Shandilya et al. [2] performed multi-objective parameter optimization using TLBO, GA and RSM and compared their optimization results. The experiments were performed on Electric discharge machining by taking S_{OFF} , S_{ON} , I_p and A_c as input parameter and cutting rate, surface roughness as output parameter. The material Inconel-825 and Molybdenum wire were selected as workpiece and tool wire respectively. The absolute error between experimental result and optimized result using optimization techniques for Cutting Rate was 2.89%, 1.50% and 4.04% and for Surface Roughness 0.30%, 0.45% and 0.37% respectively. The optimized result of TLBO for CR and SR was good in comparison to GRA and GA.

Advanced materials have also been reported to be machined using non-traditional cutting approaches too [3–5]. Muaz and Choudhary [6] performed nano-finishing of AISI-4340 steel using nano powder of TiCN/Al₂O₃/TiN that had been used during experimental investigation in flat end milling machine. A set of experiments were undertaken using different parameters each time and optimized. The hybrid analysis results validated by multi-objective genetic algorithm, confirmed that the method's produced values within appropriate tolerance levels. It was found that low viscosity fluids deliver improved results during MQL. This was done with the aim of reducing the effects at making the process environment-friendly and reducing waste [6].

Siddique and Thakur [7] used CNC end milling for optimization of various input parameters of Aluminium 7075 using non-conventional approach. For design the trail experiments Taguchi L₉ orthogonal array and for optimization teaching–learning based optimization method was used. Cs, doc and feed were selected as process variables and SR was taken as output (response) parameter.

The optimization of alloys has been emphasized in previous investigations [8–11]. Pillai et al. [12] investigated process variables for the end milling of Al 6005A. The process parameter spindle speed, tool path strategies and feed rate were taken into consideration to study their effect on machine time and SR. It was found that tool path strategies had maximum aspect on performance parameter whereas feed rate had minimum aspect. Taguchi-Grey relation analysis was used estimate optimal process parameter and verified with ANOVA. It was found that raster tool path strategies resulted lower SR in compare of irregular and offset tool strategy.

Mahesh and Rajesh [13] used fuzzy logic with Taguchi orthogonal array L₂₇ simultaneously to maximize the MRR and minimize SR. The experimentation was performed for Al 7075 with input parameter speed, nose radius and depth of cut on CNC end milling. The dimension of work-piece was 590 mm × 55 mm × 20 mm. Two orthogonal array L₉ was prepared for experiment first with coolant ON condition and second with coolant OFF condition which was used to calculate the tool-wear. The confirmatory experiment showed that surface roughness decreased to 0.14 μm and MRR increased to 2304 mm³/min. The most affecting parameter was found that surface roughness and material removal rate. Modeling and multi-response optimization have also been reported to be quite necessary and crucial aspect while dealing with machining of advanced alloys [14–18].

Lu et al. [19] investigated optimization techniques in the high-speed end milling of SDK tool steel. The responses taken for evaluation were surface roughness, tool life and MRR corresponding to type of milling, axial and radial doc, feed per tooth and ss. PCA was applied to find weightage of responses for relative improvement of responses. The result was found that when GRA is added with PCA gives better results nearest to experimental value [19].

Lungu et al. [20] explored the effect of feed and cutting speed by using FEM simulation on the responses like temperatures, cutting force and chip formation. The simulation was carried out for AISI 1045 and AISiMgMn Al Alloy later the simulation result was verified by experimental runs. Parameters like cutting speed, feed rate and depth of cut were main parameters so kept variable to show the effect on responses while other parameters were kept constant during simulation and experimentation. For the simulation, orthogonal cutting was performed on deform 2D software. The result was found that cutting forces and temperature increases with increase in the feed rate but cutting speed has lesser influence on cutting force. Due to properties of AISI 14045 the temperature was relatively high during turning. Value obtained by simulation was significantly close experimental test [20].

1.3 Experimental Work

1.3.1 *Experimental Setup and Material*

In this experiment, cutting of Al-8090 is performed on MAXMILL 3-axis milling machine at NIT Jalandhar. Al 8xxx series are alloy of mainly aluminium and lithium which have good mechanical, thermal property. So, it is used to make a component of high strength with low mass density. Aluminium-8090 is considered as workpiece of dimensions (145 mm × 70 mm × 45 mm), the tool of diameter 25 mm and Tungsten Carbide (TiC) inserts is used in performing experiments. Raster face milling cutting of faces is performed. The chemical properties and mechanical properties of aluminium-8090 are shown in Table 1.1.

1.3.2 *Design of Taguchi Method*

The set of experiments have been designed using Taguchi method which is based on orthogonal array. By using these Taguchi's orthogonal arrays, number of experiments can be minimized which outcomes reduced effort, time and experimental cost. Taguchi's L_9 is used for the experimental design in requisition to obtain optimum cutting conditions for minimum tool machining time and maximum Material Removal Rate. Spindle speed, feed per tooth and depth of cut are taken as process variables and machining time and material removal rate are taken as responses.

Table 1.1 Chemical and mechanical property of Al 8090

Chemical properties		Mechanical property	
Element	Content (%)	Property	Matric
Aluminum, (Al)	93–96.2	Tensile strength (S_{ut})	470 MPa
Lithium, (Li)	2.2–2.7	Yield strength (S_{yt})	375 MPa
Copper, (Cu)	1–1.6	Elongation at break	7% (approx.)
Magnesium, (Mg)	0.60–1.3	Elastic modulus (E)	80 GPa
Iron, (Fe)	≤ 0.30	Shear strength (S_{ys})	275 MPa
Zinc, (Zn)	≤ 0.25	Hardness, Brinell (@load 500 kg; thickness 10.0 mm)	121
Silicon, (Si)	≤ 0.20	Density (g/cm^3)	2.54 g/cm^3
Titanium, (Ti)	≤ 0.10	Melting point	600–655 °C
Chromium, (Cr)	≤ 0.10		
Manganese, (Mn)	≤ 0.10		
Zirconium, (Zr)	0.040–0.16		
Other (each)	≤ 0.050		
Other (total)	≤ 0.15		

Process variables and their levels are given in Table 1.2. Tool parameters and other machining conditions are kept constant during experiments. Width and length of cut is also fixed constant during experiment (Table 1.3).

Table 1.2 Control variables and their levels

S. No.	Input (control) variables	Unit	Level 1	Level 2	Level 3
1	SS (n)	rpm	1600	2400	3200
2	FR (f)	mm/tooth	0.15	0.20	0.25
3	DOC (d)	mm	0.60	0.90	1.20

Table 1.3 Design of experiments: Taguchi L_9 (3^3) orthogonal array

Trial No.	Spindle speed (n)	Feed rate (f)	Depth of cut (d)
1	1600	0.15	0.6
2	1600	0.20	0.9
3	1600	0.25	1.2
4	2400	0.15	0.9
5	2400	0.20	1.2
6	2400	0.25	0.6
7	3200	0.15	1.2
8	3200	0.20	0.6
9	3200	0.25	0.9

1.3.3 TLBO Optimization Technique

Optimization is a procedure to find best optimum value of input parameters which gives appropriate value of pre-defined function. Optimization may be divided into two categories Single Response optimization and Multi Response optimization. Optimization Process of the predefined function may be of maximization or may be minimization type. TLBO is much easier to understand and implement as well as it does not have complexity with respect to tuning of the algorithmic parameters unlike other algorithms because there are only two tuning parameters over here. This TLBO algorithm explains two phase of the learning first is Teacher phase and second is Learner phase.

Teacher Phase: This is first phase of Algorithm in which learners learn from the teacher depending on his or her capability. A teacher attempts to increase the improve result of the class in the subject trained by him or her.

T_i and M_i is the teacher and mean at any iteration i respectively. T_i will try to improve M_i near its own aim (let M_{new}). Teaching factor which will decide mean value need to be changed.

$$\text{Difference Mean}_i = r(M_{new} - TF \times M_i) \quad (1.1)$$

where TF can be either 1 or 2 and r is random no. between $[0,1]$

$$\text{Teaching_Factor} = \text{round}[1 + \text{rand}(0, 1)(2 - 1)] \quad (1.2)$$

$Y_{new,i}$ is the update value of $Y_{old,i}$. $Y_{new,i}$ will be accepted if it gives better value.

$$Y_{new,i} = Y_{old,i} + \text{Difference Mean}_i \quad (1.3)$$

- (a) **Learner Phase:** It is the 2nd phase of the algorithm in which learners increase their learning knowledge by relating between themselves. A learner interrelates randomly with a other learners for improve his or her knowledge with another learner (Fig. 1.1).

For $i = 1 : P_n$

Select 2 learners randomly let Y_i and Y_j where $i \neq j$

if $F(Y_i) < F(Y_j)$

$$Y_{new,i} = Y_{old,i} + r_i(Y_i - Y_j) \quad (1.4)$$

else,

$$Y_{new,i} = Y_{old,i} + r_i(Y_j - Y_i) \quad (1.5)$$

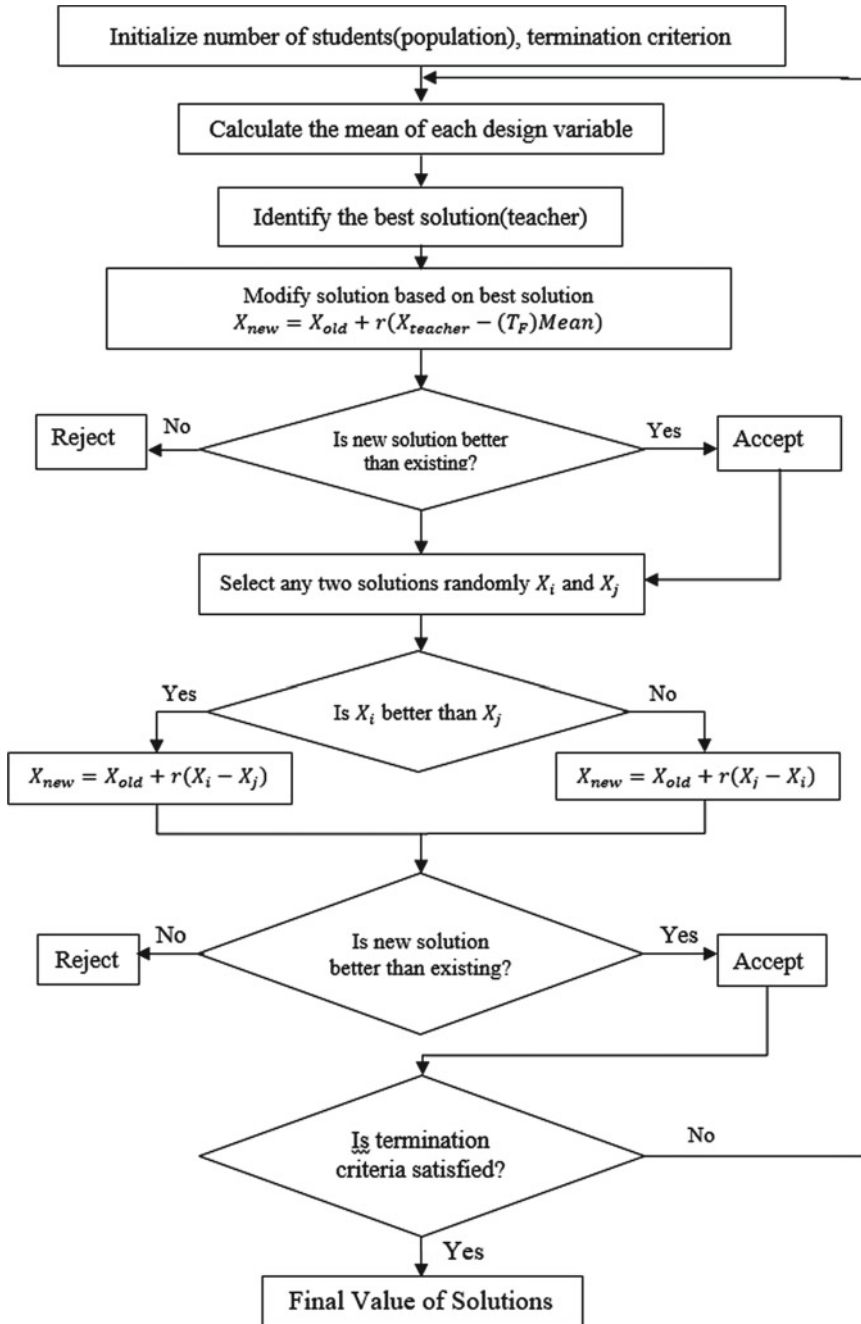


Fig. 1.1 Flow chart of TLBO

```

end (if)
end (for)
Accept  $Y_{new,i}$  if it is better solution
    
```

1.4 Result and Discussion

The result of the Machining time and Material removal rate of each trial are shown in Table 1.4. The variation of output parameter (i.e. Machining time and MRR) at each trial are shown in Figs. 1.2 and 1.3 respectively. The interaction plot for Machining time and MRR is shown in Figs. 1.4 and 1.5 respectively. The figures (interaction plots) clearly shows that the variation of depth of cut has low effect

Table 1.4 Response table

Trial No.	SS (<i>n</i>)	FR (<i>f</i>)	DoC (<i>d</i>)	MRR	MT
1	1600	0.15	0.6	7200	21.2500
2	1600	0.20	0.9	14,400	15.9375
3	1600	0.25	1.2	24,000	12.7500
4	2400	0.15	0.9	16,200	14.1667
5	2400	0.20	1.2	28,800	10.6250
6	2400	0.25	0.6	18,000	8.5000
7	3200	0.15	1.2	28,800	10.6250
8	3200	0.20	0.6	19,200	7.9688
9	3200	0.25	0.9	36,000	6.3750

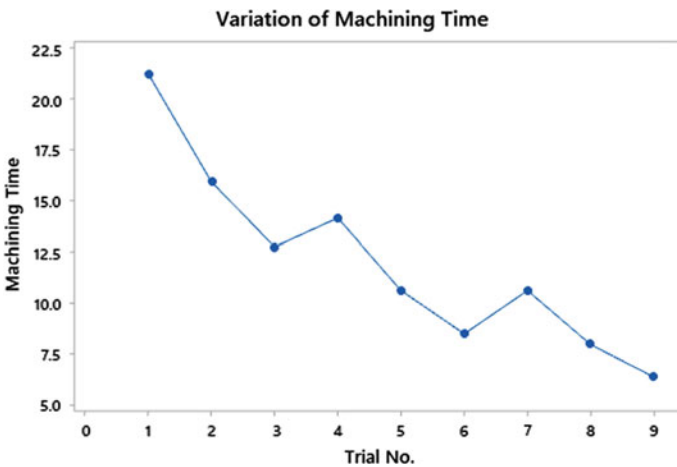


Fig. 1.2 Variation of MT versus trial no.

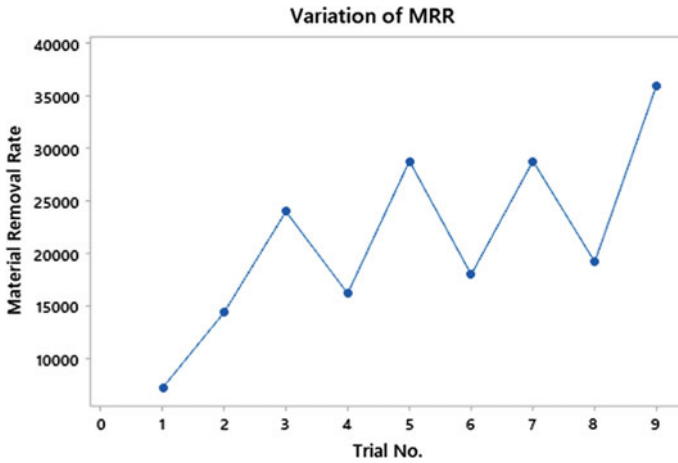


Fig. 1.3 Variation of MRR versus trial no.

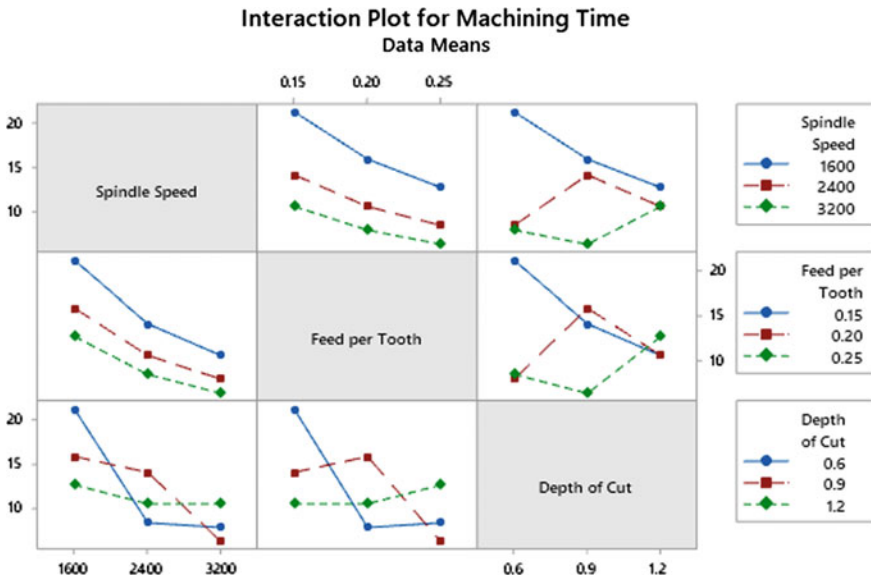


Fig. 1.4 Interaction plot for machining time

for Machining time and spindle speed has low effect for MRR. The optimization is performed on Teaching Learning Based Optimization Technique. The regression equation generated by Minitab 19.2 for MT and MRR are shown by Eqs. (1.6) and (1.7).

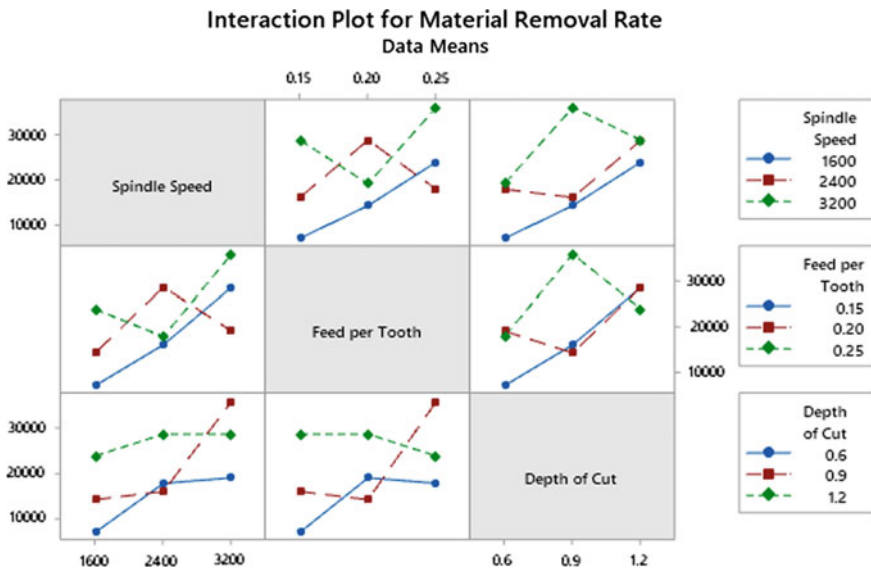


Fig. 1.5 Interaction plot for MRR

1.4.1 Regression Equation

$$\text{Machining Time} = 38.64 - 0.005202 \times n - 61.4 \times f - 2.07 \times d \quad (1.6)$$

$$\text{Material Removal Rate} = -33600 + 8.00 \times n + 86000 \times f + 20667 \times d \quad (1.7)$$

The MRR of Al-8090 during milling increases with doc and feed rate (Fig. 1.4). The increment in MRR with increasing doc and feed rate are observed in the literature. The increment in feed rate increased the metal removal rate by increasing the feed of workpiece (Fig. 1.4) but the effect of SS (n) is not significantly more on MRR. It is observed that at higher feed rate and doc, MRR is high.

The MT of Al-8090 during milling increases with ss and feed rate (Fig. 1.5). The increment in MT with increasing ss and feed rate are observed in the literature. The increment in feed rate increased the machining time by increasing the feed of workpiece (Fig. 1.5) but the effect of doc(d) is not significantly more on MT. It is observed that at higher feed rate and ss, MRR is high.

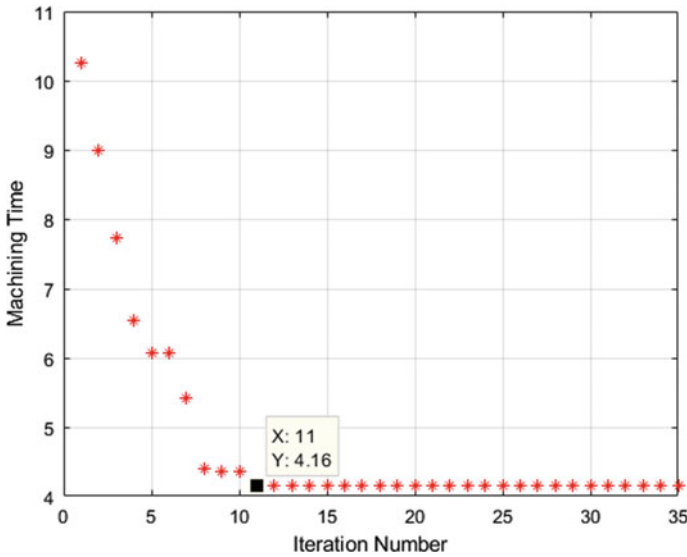


Fig. 1.6 Convergence plot for machining time

1.4.2 Optimization Using sTLBO

1.4.2.1 Single Objective Optimization

The single response optimization for machining time and material Removal Rate is performed in terms of machining process variables using sTLBO algorithm in this part. For getting optimum value Machining Time, Eq. (1.6) is formulated by Regression analysis and used as the fitness function for optimization. The plot between Machining Time and Iteration number is shown in Fig. 1.6. After applying TLBO algorithm, optimum combination of input parameters for minimum MT (**4.1596 s**) is SS (3200 rpm) feed per tooth (0.25 mm/tooth) and DoC (1.2 mm). Similarly, for MRR Eq. (1.7) is used as an objective function for optimization. The plot between material Removal Rate and Iteration number is shown in Fig. 1.7. Maximum MRR (**383,000 mm³/min**) is obtained at SS (3200 rpm) Feed per Tooth (0.25 mm/tooth) and DoC (1.2 mm).

1.4.2.2 Multi-objective Optimization

In this presented work priori approach is used for optimization of MT and MRR. The main aim is to minimize MT and maximize MRR. The normalized function (F) by using priori method is taken from Eq. (1.8). An algorithm is written on matlab 2018a and performed for multi-objective optimization.

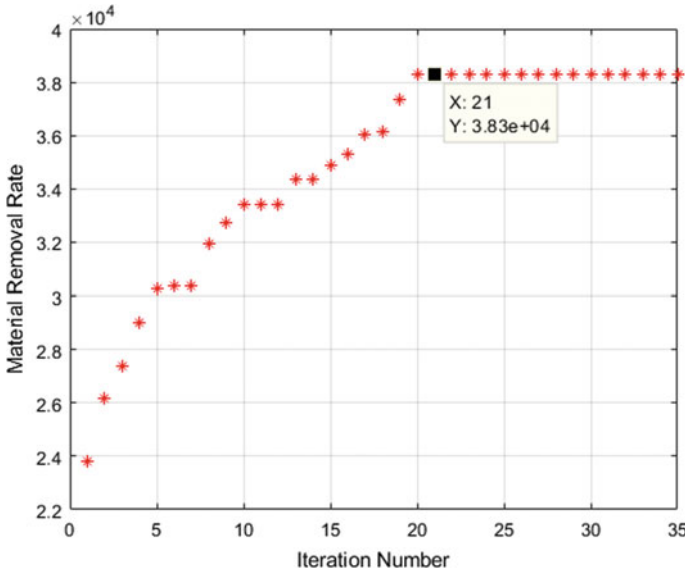


Fig. 1.7 Convergence plot for MRR

$$F = w_1 \left(\frac{MT}{MT_{MIN}} \right) - w_2 \left(\frac{MRR}{MRR_{MAX}} \right) \tag{1.8}$$

where w is weight factor ($w_1 = w_2 = 0.5$) and MT_{MIN} is the minimum value of Machining Time and MRR_{MAX} is maximum material removal rate.

The plot between Multi-Objective function and Iteration number is shown in Fig. 1.8. The Result for minimum MT (4.16 s.) and maximum MRR (383,000 mm³/min.) is obtained by Multi-Objective TLBO algorithm at Spindle Speed (3200 rpm) Feed per Tooth (0.25 mm/tooth) and Depth of Cut (1.2 mm).

1.5 Conclusion

1. TLBO is a powerful algorithm, easy to use in complex problems where the input parameters are not connected directly. It gives accurate Value of Machining Time and Material removal rate in face milling operation.
2. For optimization using TLBO the best suited face milling parameter for Al 8090 are minimum MT (4.16 s.) and maximum MRR (383,000 mm³/min.) at Spindle Speed (3200 rpm) Feed per Tooth (0.25 mm/tooth) and Depth of Cut (1.2 mm).

This work can be moved forward in two directions, Firstly, by adding more output parameter like Tool wear, Surface Roughness etc. Secondly by investigating more cutting tool and work-piece material.

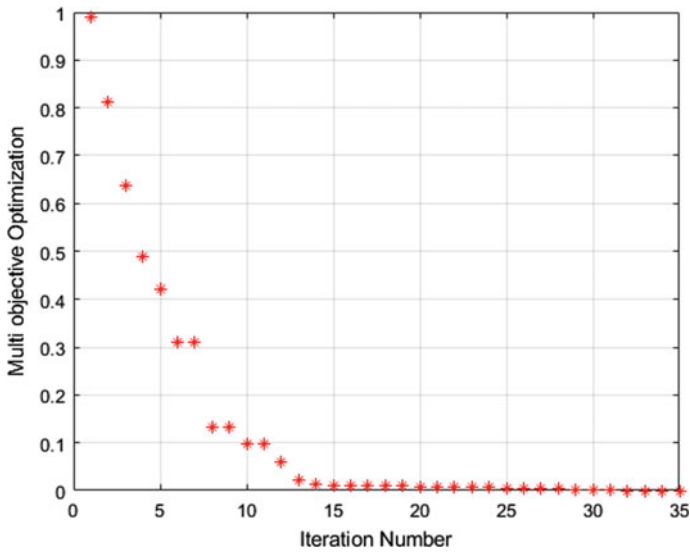


Fig. 1.8 Plot for multi-objective optimization

References

1. Rao, R.V., Savsani, V.J., Vakharia, D.P.: Teaching-learning-based optimization: A novel method for constrained mechanical design optimization problems. *CAD Comput. Aided Des.* **43**(3), 303–315 (2011)
2. Shandilya, P., Rouniyar, A.K.: Multi-objective parametric optimization on machining of Inconel-825 using wire electrical discharge machining, pp. 1–13 (2020)
3. Singh, R.P., Singhal, S.: Rotary ultrasonic machining: a review. *Mater. Manuf. Process.* **31**, 1795–1824 (2016)
4. Singh, R.P., Singhal, S.: Investigation of machining characteristics in rotary ultrasonic machining of alumina ceramic. *Mater. Manuf. Process.* **32**, 309–326 (2017)
5. Singh, R.P., Tyagi, M., Kataria, R.: Selection of the optimum hole quality conditions in manufacturing environment using MCDM approach: a case study. In: *Operations management and systems engineering*, Springer, Singapore, pp. 133–152 (2019)
6. Muaz, M., Choudhury, S.K.: Experimental investigations and multi-objective optimization of MQL-assisted milling process for finishing of AISI 4340 steel. *Meas. J. Int. Meas. Confed.* **138**, 557–569 (2019)
7. Siddiqui, F., Thakur, P., Mumbai, N.: Optimal selection of parameters in CNC end milling of Al 7075 T6 alloy by (2019)
8. Singh, R.P., Singhal, S.: Rotary ultrasonic machining of macor ceramic: an experimental investigation and microstructure analysis. *Mater. Manuf. Process.* **32**, 927–939 (2017)
9. Singh, R.P., Singhal, S.: Experimental investigation of machining characteristics in rotary ultrasonic machining of quartz ceramic. *J. Mater. Des. Appl.* **232**, 870–889 (2018)
10. Singh, R.P., Kataria, R., Kumar, J., Verma, J.: Multi-response optimization of machining characteristics in ultrasonic machining of WC-Co composite through Taguchi method and grey-fuzzy logic. *AIMS Mater. Sci.* **5**, 75–92 (2018)
11. Singh, R.P., Kumar, J., Kataria, R., Singhal, S.: Investigation of the machinability of commercially pure titanium in ultrasonic machining using graph theory and matrix method. *J. Eng. Res.* **3**, 75–94 (2015)

12. Unnikrishna Pillai, J., Sanghrajka, I., Shunmugavel, M., Muthuramalingam, T., Goldberg, M., Littlefair, G.: Optimisation of multiple response characteristics on end milling of aluminium alloy using Taguchi-Grey relational approach. *Meas. J. Int. Meas. Confed.* **124**, 291–298 (2018)
13. Mahesh, T.P., Rajesh, R.: Optimal selection of process parameters in CNC end milling of Al 7075–T6 Aluminium alloy using a Taguchi-fuzzy approach. *Procedia Mater. Sci.* **5**, 2493–2502 (2014)
14. Singh, R., Singh, R.P., Tyagi, M., Kataria, R.: Investigation of dimensional deviation in wire EDM of M42 HSS using cryogenically treated brass wire. *Mater. Today: Proc.* (2019). <https://doi.org/10.1016/j.matpr.2019.08.028>
15. Singh, R.P., Singhal, S.: An experimental study on rotary ultrasonic machining of macor ceramic. *J. Engg. Manuf.* **232**, 1221–1234 (2018)
16. Singh, R.P., Singhal, S.: Rotary ultrasonic machining of alumina ceramic: Experimental study and optimization of machining responses. *J. Eng. Res.* **6**, 01–24 (2018)
17. Tyagi, M., Panchal, D., Singh, R. P., Sachdeva, A.: Modeling and analysis of critical success factors for implementing the IT-based supply-chain performance system. In: *Operations management and systems engineering*. Springer, Singapore, pp. 51–67 (2019)
18. Singh, R.P., Kataria, R., Singhal, S.: Decision-making in real-life industrial environment through graph theory approach. In: *Computer Architecture in Industrial, Biomechanical and Biomedical Engineering*. IntechOpen (2019). <https://doi.org/10.5772/intechopen.82011>
19. Lu, H.S., Chang, C.K., Hwang, N.C., Chung, C.T.: Grey relational analysis coupled with principal component analysis for optimization design of the cutting parameters in high-speed end milling. *J. Mater. Process. Technol.* **209**(8), 3808–3817 (2009)
20. Lungu, N., Croitoru, S.M., Bişu, C.F., Dumitraşcu, C., Borzan, M.: The influence of the cutting speed and feed rate on the machinability ratings in machining of AISI 1045 carbon steel and AISi1MgMn aluminium alloy. *Appl. Mech. Mater.* **436**, 194–204 (2013)

Chapter 2

Perspective of 4D Printing in Additive Manufacturing



Ajay Sharma and Ajay K. S. Singholi

Abstract The present paper discusses an overview about 4D printing and its applications in different areas. The overview consists of basic discussion on 3D printing or also termed as Additive manufacturing (AM), its operating technique and materials used to make products. 4D printing is based on 3D printing technique and the only difference is that, it uses smart material to print the required product. Information regarding smart materials, their types and method of operation or working is discussed in the paper. Shape shifters, shape memory alloys, shape memory polymers, gels and other active smart materials are some of the significant and most commonly used smart materials which are mentioned in the paper. The paper also includes the various affecting factors and modes by which the response stimulus is generated among the smart materials and accordingly performs the stimulus action. Discussion on stimulus response by effect of heat, water, electric as well as magnetic field, light rays etc. are briefly mentioned in the paper. Lastly, application of 4D printing technology in various fields such as mechanical, medical, commercial, general purpose have been discussed along with scope and suggestions to implement its use further is added in the conclusion.

Keywords Additive manufacturing (AM) · 4D printing · Shape memory polymer (SMP) · Shape memory alloy (SMA) · Shape memory hybrids (SMH) · Shape memory material (SMM) · Response · Stimulus

2.1 Introduction

The term additive manufacturing (AM) is the most efficient technology in order to fabricate three-dimensional (3D) shape structures which are complicated and likely to be hard in fabrication by using conventional manufacturing process [1]. At present, most of the methods used in AM are layer based. Although, these kinds of techniques

A. Sharma (✉)

USICT, Guru Gobind Singh Indraprastha University, New Delhi, India

A. K. S. Singholi

GB Pant Engineering College, New Delhi, India

have its own flaws, for example the slow speed and the components manufactured bear anisotropic stiffness (in single direction they are weak in comparison to other directions). Newly, derived by Kirigami and Origami, an exclusive AM based techniques on self-folding models have been developed so as to solve the issues of the traditional approach of layer based manufacturing. The self-folding models; their approach in additive manufacturing is known as 4D printing [2].

The concept of 3D printing permits any consumer to design and generate their own products as per their need, the products created also has almost least possible wastage. Now, with the technique of 4D printing, AM will be significantly impacted by the means of economy and community in the coming decade [3–5].

However, developments are still carried out and researches are progressively being made in additive manufacturing in reference to technologies related to 3D printing and applications, one of the foremost innovative breakthroughs is combining the concept of 3D printing with smart materials to generate such products which can alter their shape with respect to time. Additionally, the products printed via 4D printing technique can self-transform responding to some stimuli with respect to time [6].

2.1.1 Augmented Printing Using 3D Technology

Rapid Prototyping is commonly referred as manufacturing in layers, as it generates a 3D physical model in solid form in consecutive layer by layer manner, by diffusion of printing material which controlled by a computer [7]. There are several types of additive manufacturing of 3D printing process which depends on the handling of the material. In few cases, material in form of liquid is controlled, it might be also in molten form, or in the form of laminates which can be cut out and then joined together to reform the required shape [8, 9].

Augmented Reality (AR) can be defined as collaboration of techniques which permits mixing in real time comprising the input content produced by computer along with live visual display in video form. The concept when is used in combination with 3D printing it is known as Augmented Printing. AR is basically based on virtual reality technique and communicates with the real world as well as virtual world. The simultaneous existence of real environment as well as virtual models enables anyone to observe and visualize complicated concepts, and advance in newer activities which cannot be fulfilled by any other technique [10].

2.1.2 Shape Memory Effect

Shape memory effects form the basic factor in the alteration of 4D of the initial stage modelling specification considering the impression of stimuli and additionally retrieve the path details for the accessibility in the future to the constituted shapes.

Relating to the uniformity of temporary or instant shapes, the shape memory effect might be single way (1-W), double way (2-W), triple way (3-W) or it can be multiple-way [11]. The SMEs comprises of two phases, the initial phase provides the ability to program which forecasts the temporary specifications of the samples that printed on the other hand the next phase is the stage of actuation that signifies the recovery of the shape, printed permanently back through stimulus.

2.1.3 Impact on Different Sectors and Applications

AM technology has been applied in various and varied sectors. The technology is used in China for construction purpose. They were able to build a 10 story building within a day. Additive manufacturing are widely used in medical field in making different products [12]. One of the applications is in creating artificial organs which are similar to real organs. Also AM technique is used in making prosthetic parts for the body [9]. They are cheap and durable and hence save cost. In engineering field especially in mechanical sector, small components of complex machines are built by 3D printing using several materials such as, PLA, Fiber composites etc. [7]. Further electronic devices such as cell phones, speakers, multimedia devices etc. are making their most of the components via 3D printing technique [13].

2.2 3D Printing Technology

Several authors have researched on 3D printing technology and have defined it as per their own prospective. Here are few definitions: 3D printing structures the object or the product in several layers; 3D printing technique creates the output product in several layers accumulated together; the accuracy and the effectiveness of molding regarding the product are comparatively low. Depending on the assimilated innovation comprising the virtual model of the product which is targeted or its 3D modelling, the 3D mould for printing, intelligent mold injection, the “3D printing” technique is presented exclusively and it is assumed to emerge as newer trend in the industries of manufacturing, and additionally they have wider prospects in application [14].

The process of 3D printing involves developing products directly by the means of aligning layer deposition of the material on one another until the final object is created. The alignment of layer is done by any of the several methods based on the type of technology utilized. This technique permits to design and model parts which are complicated and hence overcoming the cost for assembly additionally. The process of 3D printing is deprived of tools which ultimately reduces the overall time consumptions [15].

The technology of 3D printing is the techniques that enables in giving the most effective technique in designing of any product, its manufacturing as well as prototyping. This technique provides fabrication of several products that are cost effective,

have high utility, can be altered on maximum scale, and are highly efficient in energy consumption against the wide range of applications [16].

2.2.1 *Benefits of Additive Technology Over Conventional Manufacturing*

The knowhow might significantly declines the requirement for stocks since the design can be converted in digital form, resulting in delegation in the process of manufacturing. When the manufacturing of products is accomplishing closer to the end target, there will be decline in the cost for logistics and also reduces the influence over environment. Ultimately the time needed for the sales production will also be reduced [17].

Minimizing the cost for tools, as in additive manufacturing, tools are not required. Hence, this provides a supreme deal comprising tractability as in reference to adapting as per the market and declining or even minimizing, the included cost (fabricating tool, its inspection as well as maintenance) when contradicted with conventional manufacturing technique (Fig. 2.1). Depending upon the CAD model generated in 3D, even the complicated design models such as hollow interiors, varying thickness geometry, interior channels as well as non-uniform shape geometries etc. can be easily produced. This is otherwise a time taking and costly process in conventional manufacturing [18].

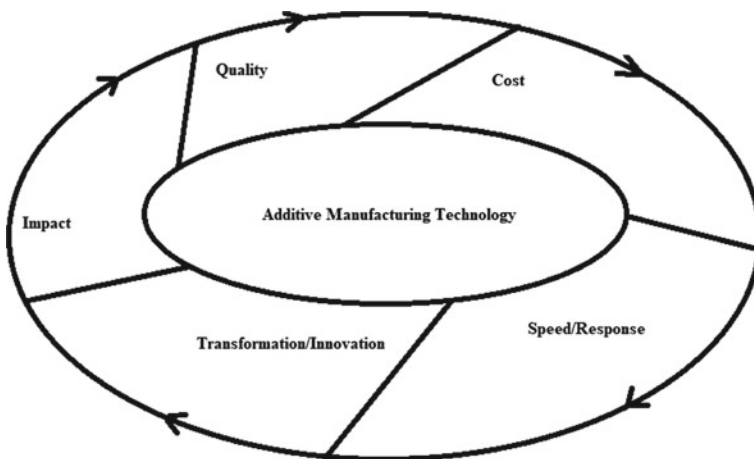


Fig. 2.1 Key advantages of AM over traditional manufacturing [17]

2.3 Shape Memory Materials Used in Printing

Recently the shape memory materials (SMMs), specifically which are polymeric in nature, have begun to grab much attention, as they are subjected to a belief that they add on a new dimensional constraint to the material properties, and exhibits the capability to re-shape the design and model of the object. The most important feature of SMMs is that they can return back to their original shape to the initial condition once any stimulus is applied [19].

Investigations have resulted in emergence of several materials having the capability to “memorize” a non-permanent shape provided, and further “recover” back to the actual shape which is permanent when exposed to external stimuli. This is the “shape memory effect” (SME) which remains the feature of entire SMMs. SME is significantly a wide process, and a broad range of materials such as alloys of metal, polymers, ceramic materials, system of super-molecules in addition with crystalline structure are found to be under SME [20].

2.3.1 *Shape Memory Hybrids (SMH) and Shape Memory Composites*

In the current scenario, shape memory hybrids (SMH) is growing as an exclusive member among the Shape memory materials. The ideology of SMH is characterized by its easy availability which enables any normal person to design and produce their customized SMM so as to encounter their requirements as per their area of application [21]. Shape memory hybrids use which is made from more than one type of molecules together as one hybrid material. They have the same properties of smart material which is that it can alter its shape with respect to time when an external stimulus is given [22].

Shape memory composites are basically smart materials with polymeric properties or a combination of polymers which can change its shape when exposed under moisture, light or radiation, magnetic field, electric field, temperature variation etc. and further regain its actual shape if the stimulus is stopped with respect to time [23].

2.3.2 *Smart Materials*

Smart materials also referred as functional materials have the capability to change themselves as per the conditions of the environment which is; they have the ability to alter themselves by mean of external stimuli physically and are hence have the fitment in the surrounding. Usually these conversions include transformation of energy (Fig. 2.2). Therefore, smart materials for instance can transform mechanical

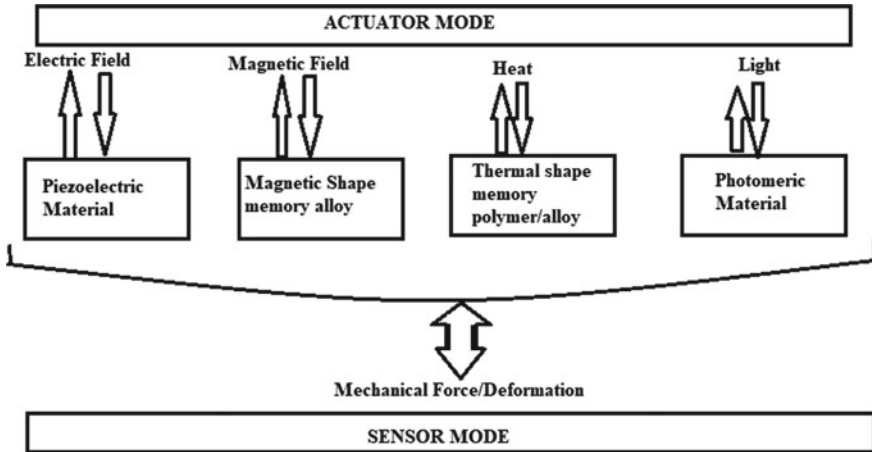


Fig. 2.2 Smart material action overview [7]

energy in form of electrical energy and vice versa. These resemble the smart materials in form of sensors and actuators [24]. Smart materials include all the categories of SMPs, SMAs, SMHs, shape memory active composites and others like gels that exhibit memory effect. One such example of smart material is hydrogel. Hydrogel has the property to undergo deformation and change its shape when water is added to it. The change in the shape is as per the desire of the experiment performed. The change of shape can be one way or two ways [25].

2.3.2.1 Classification of Smart Materials

The 4D printing can be described as additive manufacturing along with dimension of time; this allows any function or shape to change with variation of time when subjected to some external stimulus for instance self-folding movement of a flat 4D printed sheet in such a way that converted in to a closed box when subjected to some stimuli. The other form of folding may be curling, spiral shape or bending at an angle.

Domain of components and various categories tangled in 4D printing [26] are shown and described as follows and shown in Fig. 2.3:

1. Technology of 3D printing: Fused filament fabrication (FFF), Direct ink write (DIW), Digital light processing (DLP), inkjet printing, SLS and SLA.
2. Stimuli for 4D printing: thermal stimuli, photo stimulus, water stimulus, chemical (Chemo) stimulus, and stimulation by magnetic field exposure.
3. 4D printing material system: single active SMP, liquid crystal elastomer, single or composite hydrogel, SMP composites, and other multifunctional materials.
4. 4D printing applications: Active origami, Active actuators, smart packaging, Meta materials, tissue engineering and biomedicine.

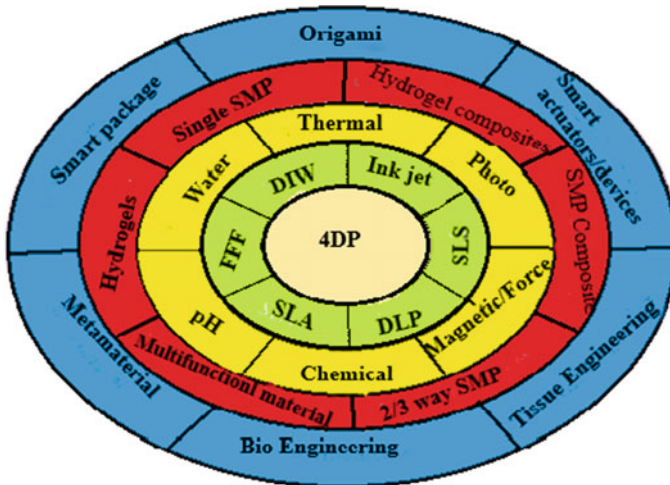


Fig. 2.3 Classification structure of smart materials [27]

Piezoelectric materials are such materials which generate a voltage whenever any stress is incorporated on them. This is a reversible process, hence when a voltage is passed across any sample; it will generate stress inside the sample itself. Appropriately structures made from these materials hence can be used for bending, expansion or contraction when any such voltage is incorporated [28].

Thermo-responsive materials are such materials that can withstand several shapes at different temperatures. They can change their shape form and gain back the original shape on application of heat. In this process, they generate a force actuating in nature. Shape memory alloys, for instance nitinol, which is a mixture of titanium and nickel that bears resistance against corrosion similar to that of stainless steel, makes it a perfect material for biochemical products [29].

Magneto-restrictive materials closely related to piezoelectric, have their response restricted to only magnetic field instead of electric field. These materials are basically utilized in low frequency, sonar transducers that have high power, actuators comprising hydraulics and motor, in addition with SMA Nitinol. Limiting magneto materials are promising materials in order to get active damping vibrations [30].

PH-sensitive materials are such materials which alter their color due to change in the acidity. This type of materials can be utilized in paints which can alter the color to depict corrosion in any metal component beneath [31].

Electro-chromic materials are able to change their color when any voltage is applied. A basic example of such material is the Liquid crystal display, materials which are photochromic, that alter their color in response to source of light. There are several paints which are thermochromics and photochromic, and they change their color when heat is applied or light is exposed on them [28].

Polymer gels, a typical example is hydrogel, which have cross linked structure of polymers bloated with solvent medium for instance water. The gel is capable of expansion as well as shrinking (~1000 times) by little variation in temperature or pH [32].

2.4 4D Printing

The concept of 4D printing is to print real life products as similar to additive manufacturing but using smart materials such as SMPs or SMAs as printing materials [33]. As discussed earlier, smart materials can respond to specific stimuli when provided such as light source, thermal variation, moisture etc. The concept is simple and aims to print such prototypes that can alter their shapes and size with respect to time as desired by the user. Shape shifting materials are such examples of 4D printing [34].

2.4.1 *Classification of 4D Printing Based on Printing Methods*

2.4.1.1 SLA (Stereolithography)

The Stereolithography (SLA) principle is based on process of photo-polymerization that allows the transformation of monomers of liquid/ oligomer to a solid polymer, basically by utilizing ultra violet rays, the radiation triggers the photo-initiator in the mixture that activates the reaction of polymerization in those respective areas directly [35]. This high-end technology uses laser techniques in the treatment of layer-above-layer comprising resins of photopolymer. Ultimately, the process of direct digital manufacturing (DDM) is incorporated which generates components directly from the CAD file [17]. Zolfagharian et al. [36] worked on patterns of self-assembling actuators printed by 4D printing method using the method of SLA. The shape memory polymer used in the work can bend itself from a remote distance when exposed to ultra violet lights. The heats from the UV rays were responsible for bending the product as hydrogel inks were used for absorbing the heat.

Chong et al. [37] used cross linked poly lactic acid ink and utilized 4D printing technique in producing flexible electronic circuits by the method of SLA. He used iron oxide as Nano particles in the ink for better stimulus results under UV lights. He created several small 3D components that can be used in soft robotics, electronics etc.

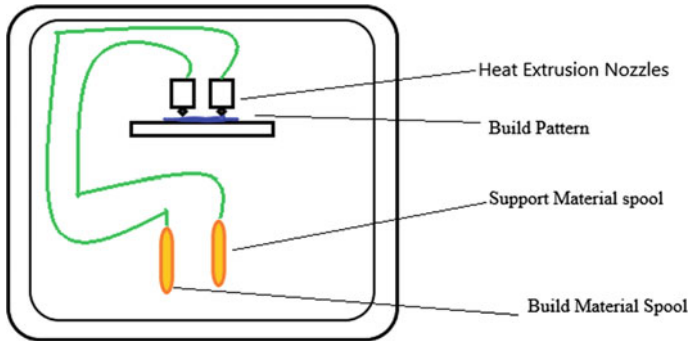


Fig. 2.4 Process of FDM method [43]

2.4.1.2 FDM Printing

In the present days, the maximum printing done in 4D is carried out by Polyjet 3D systems which enables photopolymers through UV rays, hence can transmit a uniform and glossy surface and material properties of several types [38]. Although, the system needs costly investment at beginning and maintenance periodically, in comparison with FDM systems. Particularly the, trays in built and the nozzle of extrusion ought to be replaced for the system of FDM nevertheless the overall expense is less compared to the polyjet system print heads [39].

In the process of FDM printing (Fig. 2.4), the component is generated in layers by melting a thermoplastic material which is diffused on the printer bed through a nozzle with lesser diameter. The component can be made from any CAD model in STL file format. The filament is generally in between 1.75 and 3.0 mm [40].

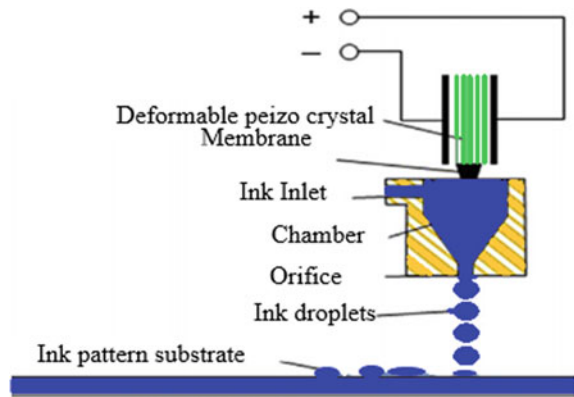
Kollamaram et al. [41] worked on FDM printing technique on low temperature deposition in 3D printing of thermolabile drugs. Attempts were made to print a low melting and thermolabile drugs by degrading the temperature of FDM process. Two materials such as Kollidon VA64 and Kollidon 12PF were studied in the research. He found that due to heating the drug degrades gradually.

Kür and Eren [42] worked on FDM type 3D printing in creating 3D parts from ABS material to be used for electrical devices and few mechanical devices. The author used multi walled carbon nanotubes for fused deposition so that the final product obtained becomes electronically active.

2.4.1.3 Inkjet Printing

Free Nano-printing (FNP) was the first technique to incorporate inkjet printing for 4D printing method. The process of FNP gives big opportunity to obtain high specific energy since the loading of material is increased with respect to particular surface area and more specific power since the porous structure is hierarchical simultaneously. In this method (as shown in Fig. 2.5) the droplets of GO comprised of several

Fig. 2.5 Process of Inkjet printing [46]



concentrations were frosted to solid form rapidly by putting them on a cold substrate that had the temperature of $-25\text{ }^{\circ}\text{C}$ [44]. The ink in pure aqueous form used for printing eliminates the requirement for unwanted fillers since only moisture was utilized as the GO dispersant. The resourceful dispersion of inkjet freeze printing along with technique of freeze casting allows a uniform comfortable recognition of complicated 3D shapes and structured aerogels [45].

2.4.1.4 Selective Laser Melting (SLM)

The SLM is a method of additive manufacturing also termed as 3D printing that includes complicated and working components generated by consecutive layers of melting power material with help of a beam of laser [47]. This method is broadly utilized in NiTi (nickel titanium which is a shape memory alloy as material. since the NiTi material has very broad application, they are progressively developed either in form of bulk or porous form material by the means of modern process of manufacturing such as SLM.

The process of SLM includes the technique of 3D printing that is comprised of complicated 3D geometries produced by melting and then solidifying the material in several adjoined layers over one another. The complicated structures and free hand fabrication is provided by SLM which is a great chance to develop and grow further to next level in implementing the NiTi alloys to very complex components (for instance medical sector, devices used in surgery or bone implants, actuators etc.) [48, 49].

Dabiri et al. [50] aimed to research in the fatigue characteristics of several types and grades of steel manufactured through selective laser melting technique. The study included parameters such as surface quality, building orientation, heat treatment, energy density and service condition of the end product. Zheng et al. [51] studied and found that due to heating in the selective laser melting process products made from material alumina ceramics develop cracks. Hence, attempts were made to develop

specimen materials from (Al_2O_3) by SLM technique so as to overcome the cracking of ceramics.

2.4.2 Classification Based on Types of Stimulus Material Used in 4D Printing

2.4.2.1 Variation of Temperature as Stimuli

Thermoplastics can be induced by the application of heat as stimuli. In fact, heat is utilized or variation in temperature to incorporate shape memory self-healing and self-assembly in response stimuli in thermoplastics [52]. Solicitation of a stimulus like heat then enables reoccurrence to the enduring shape, which is “stored” by the means of covalent bonds. Self-healing materials are capable of restoring degraded functionality, often in the form of structural damage to the bulk material [32].

2.4.2.2 Impact of Water Used for Stimuli

The recovery of shape from deformation comprising shape memory polymers can be agitated by presence of water since the effect of plasticizing in the molecules of water, which elevates the workability of chains of macromolecules. If any smart material is hydrophilic or soluble in water, the recovery of shape might be triggered [53]. The water effect on such smart materials is in the manner to implement expansion or shrinking of the product on addition of water. This feature is characterized by water molecules which actuate the smart material to deform or reform its shape [54]. Hydrogel is one of the moisture or water responsive smart materials.

2.4.2.3 Impact of Magnetic Field in Reshaping and Shaping of SMPs

The working principle of Magnetic Shape Memory Alloy (MSMA) is somewhat similar to the functioning of shape memory alloys as it responds when subjected to magnetic field. The mode of working allows increasing significantly the dynamical bandwidth of the device since instead of a thermo-mechanical it uses a magneto-mechanical energy conversion process [55]. The MSMA material have the characteristics to reshape themselves when they are exposed to any magnetic field. The source can be from electromagnets as well. Ni–Mn–Ga is one such material which belongs to MSMA [56].

2.4.3 Advantages and Applications of 4D Printing

Several sectors and areas such as engineering, medical, aerospace, electronic devices, artificial tissues or organs etc. (more mentioned in Fig. 2.6) can be benefitted with the 4D printing technology. Here are few of them listed below:

1. **In medical field:** the implants produced by the 4D printing method are directly implemented in the body of the patient. This enables in easy operation and makes is more trustworthy and reliable [57].
2. **In aircrafts:** one such instance is the utilization of fiber epoxy resin of carbon which gives reduction in weight by 40% when compared to that of aluminum. The creators of Airbus A380 utilize approximately 25% of their parts of the aircraft completely made out of 4D printing technique, where as Boeing 787 uses almost 50% of the parts from 4D printing [58].
3. **In mechanical field:** A new example using for design and manufacture of turbines blades of wind turbine has been demonstrated using 4D printing process. The blades of wind turbine are made from 4D printing as they are more flexible and can withstand maximum wind load without failure. 4D printed paradigms avoid the bend test coupling BTC of the blades, hence preventing it from getting damaged [59].
4. **In automobile sectors:** In the recent years the technique of 4D printing is utilized in automotive sectors such as making spring suspensions of vehicles specially leaf springs. The smart material enables to get the required curvature among the leaves using 4D printing [60].
5. **In electrical field:** automated assembly or substances which are programmed structurally are flourishing and their usage in the field of electrical field is growing such as in robotics, PV, antenna and measuring instruments etc. The geometries having the ability to alter them reverse have large usability in sector of soft robotics. In the electronics field, the solvent ink is utilized for printing in 3D and a transformed product is assumed to be obtained. Here, the 4D printing

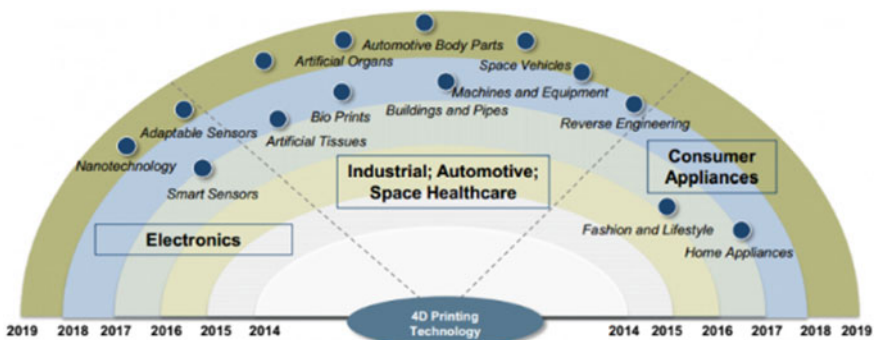


Fig. 2.6 Application of 4D printing technology: a forecast (www.machinedesign.com)

has excellent application since it has negligence of droplet spreading and can print non uniform as well as varying thickness products [61].

2.4.4 Scope of 4D Printing and Application and Advantage in General

1. Environment responsive home appliances and product with improved comfort and features [54].
2. Shoes which can transform themselves according to the use required [9].
3. Buildings that could assemble and disassemble themselves [9].
4. Printing bio components that can be implanted to human body [62].
5. In aeroplane wings that responsive to the flow of air for better lift [58].
6. Alternative to Smart valves and sensors used in pipe showing response to pressure flow [28].

2.5 Conclusion and Future Scope

As 3D printing continues to grow in its applications and evolve high quality materials at large scales, it is sure that this new concept of 4D printing would provide many ingenious ways in creating highly functional and complex surfaces. In intelligent material structure 4D printing has vast scope of involvement as environment sensitive house and structures are in their development phase. However, research and development of 4D printing with different aspects will definitely have impact on traditional additive manufacturing applications. Several types of 4D printing techniques including use of various smart materials and type of response stimulus has been discussed in the paper. We can say that still 4D printing is in its nascent phase and need to be work more to explore its full strength. In the near future, with 4D printing technology we will be able to provide substitute to intelligent material structures integrated with drivers and sensors assembled using traditional methods. The majority of use of this technology is in medical field such as making artificial tissues, organs, implants etc. However, in technical sector, especially in mechanical field, the concept of 4D printing is utilized mostly in the automotive industries. In machine industries it still remains a big challenge to implement products made based on 4D concept of printing and using them in workshops or industries.

References

1. Qiu, C.: Helical Kirigami-enabled centimeter-scale worm robot with shape-memory-alloy linear actuators. *J. Mech. Robot.* **7**, 1–10 (2015)
2. Kwok, T., Wang, C.C.L., Deng, D., Zhang, Y., Chen, Y.: 4D printing for freeform surfaces: design optimization of origami and Kirigami structures, no. 213 (2017)
3. Jiang, R., Kleer, R., Jiang, R., Kleer, R., Piller, F.T.: Predicting the future of additive manufacturing: a delphi study on economic and societal implications of 3D printing for 2030 *Technological Forecasting & Social Change Predicting the future of additive manufacturing: a Delphi*

- study on economic and societal implications of 3D printing for 2030. *Technol. Forecast. Soc. Chang.* (2017)
4. Jackiewicz, J.: Manufacturing of instructional aids for students at low cost by means of 3D printing. *Mater. Manuf. Processes* **32**(10), 1116–1130 (2017). <https://doi.org/10.1080/10426914.2016.1257135>
 5. Sun, M.G., Rojdamrongratana, D., Rosenblatt, M.I., Aakalu, V.K., Yu, C.Q.: 3D printing for low cost, rapid prototyping of eyelid crutches. *Orbit* (2018). <https://doi.org/10.1080/01676830.2018.1445760>
 6. Chung, S., Song, S.E., Cho, Y.T.: Effective software solutions for 4D printing: a review and proposal. *Int. J. Precis. Eng. Manuf. Green Tech.* **4**(3), 359–371 (2017)
 7. Ahn, S., Montero, M., Wright, P.K.: Anisotropic material properties of fused deposition modeling ABS. *Rapid Prototyp. J.* (2012)
 8. Le Duigou, A., Castro, M., Bevan, R., Martin, N.: 3D printing of wood fibre biocomposites: from mechanical to actuation functionality. *JMADE* **96**, 106–114 (2016)
 9. Mpofu, T.P., Mawere, C., Mukosera, M.: The impact and application of 3D printing technology, June 2014 (2016)
 10. Lara-prieto, V., Bravo-quirino, E., Rivera-campa, M.Á., Enrique, J.: An innovative self-learning approach to 3D printing using multimedia and augmented reality on mobile devices. *Procedia Procedia Comput. Sci.* **75**(81), 59–65 (2015)
 11. Pei, E., Hsiang, G.: Technological considerations for 4D printing: an overview. *Prog. Addit. Manuf.* (2018)
 12. Birbara, N.S., Otton, J.M., Pather, N.: 3D modelling and printing technology to produce patient-specific 3D models. *Hear. Lung Circ.* **28**(2), 302–313 (2019)
 13. Tahalyani, J., Khanale, M., Kandasubramanian, B.: Dielectric polymeric compositions for improved electrical properties of flexible electronics. Elsevier Inc. (2018)
 14. Yang, W., Jian, R.: Research on intelligent manufacturing of 3d printing/copying of polymer. *Adv. Ind. Eng. Polym. Res.* (2019)
 15. Jasveer, S., Jianbin, X.: Comparison of different types of 3D printing technologies. *Int. J. Sci. Res. Publ. (IJSRP)* **8**(4), 1–9 (2018)
 16. Bailey, C., Stoyanov, S., Tilford, T., Turloukis, G.: 3D-Printing And Electronic Packaging (2014)
 17. Attaran, M.: The rise of 3-D printing: the advantages of additive manufacturing over traditional manufacturing. *Bus. Horiz.* (2017)
 18. Jiménez, M., Romero, L., Dom, I.A., Dom, M.: Additive manufacturing technologies: an overview about 3D printing methods and future prospects, vol. 2019 (2019)
 19. Lv, P., Wang, C.C.: CR (2017)
 20. Uto, K., Deforest, C.A., Kim, D.: 5.2—Soft Shape-Memory Materials. Elsevier Inc. (2016)
 21. Wang, C.C., Huang, W.M., Ding, Z., Zhao, Y., Purnawali, H.: Cooling- /water-responsive shape memory hybrids. *Compos. Sci. Technol.* **72**(10), 1178–1182 (2012)
 22. Yao, Y., et al.: Fabrication and characterization of auxetic shape memory composite foams. *Compos. Part B* **152**(May), 1–7 (2018)
 23. Zhao, J., Li, J., Li, Y., You, J.: Thermoplastic shape memory composites with enhanced recovery stress and recovery ratio based on double roles of PVAc-g-GO. *Compos. Commun.* **13**, 52–56 (2019)
 24. Drossel, W., Meinel, F., Bucht, A., Kunze, H., Giebichenstein, B.: The field of smart materials Smart materials for smart production—a cross-disciplinary Costing models for capacity optimization in Industry 4. 0: trade-off between used capacity and operational efficiency. *Procedia Manuf.* **21**, 197–204 (2018)
 25. Wu, D., Xie, X., Kadi, A.A., Zhang, Y.: SC. *Chinese Chem. Lett.* (2018)
 26. Khare, V., Sonkaria, S., Lee, G., Ahn, S., Chu, W.: From 3D to 4D printing—design, material and fabrication for multi-functional multi-materials (2017)
 27. Kuang, X., et al.: Advances in 4D printing: materials and applications (2018)
 28. Kamila, S.: Introduction, classification and applications of smart materials : an overview, Feb 2015

29. Briseño, S., et al.: Materialia NiTi shape memory alloy helices through the hydriding—dehydrating method. *Materialia* **5**, 13–15 (2019)
30. Rastogi, P., Kandasubramanian, B.: Breakthrough in the printing tactics for stimuli-responsive materials: 4D printing. *Chem. Eng. J.* (2019)
31. Nadgorny, M., Xiao, Z., Chen, C., Connal, L.A.: Three-dimensional printing of pH-responsive and functional polymers on an affordable desktop printer (2016)
32. Bekas, D.G., Tsirka, K., Baltzis, D., Paipetis, A.S.: Self-healing materials: a review of advances in materials, evaluation, characterization and monitoring techniques. *Compos. Part B* **87**, 92–119 (2016)
33. Mao, Y., et al.: 3D printed reversible shape changing components with stimuli responsive materials. *Nat. Publ. Gr.* 1–13 (2016)
34. Gladman, A.S., Matsumoto, E.A., Nuzzo, R.G., Mahadevan, L., Lewis, J.A.: Biomimetic 4D printing, vol. 15, Apr 2016
35. Mauricio, A., Rodriguez-herandez, J.: Polymers for additive manufacturing and 4D-printing: materials, methodologies, and biomedical applications. *Prog. Polym. Sci.* (2019)
36. Zolfagharian, A., Kaynak, A., Khoo, S.Y., Kouzani, A.: Pattern-driven 4D printing sensors and actuators A: physical pattern-driven 4D printing. *Sens. Actuat. A. Phys.* **274**, 231–243 (2018)
37. Chong, S., Pan, G., Chin, J., Show, P.L.: Integration of 3D printing and Industry 4.0 into engineering teaching
38. Kollamaram, G., Croker, D.M., Walker, G.M., Goyanes, A., Basit, A.W., Gaisford, S.: Low temperature fused deposition modeling (FDM) 3D printing of thermolabile drugs. *ScienceDirect* **7(5)**, 41–43 (2016)
39. Ly, S.T., Kim, J.Y.: 4D printing—fused deposition modeling printing with thermal-responsive shape memory polymers. *Int. J. Precis. Eng. Manuf. Green Tech.* **4(3)**, 267–272 (2017)
40. Singh, R., Kumar, R., Farina, I., Colangelo, F., Feo, L., Fraternali, F.: Multi-material additive manufacturing of sustainable innovative materials and structures, pp. 1–14 (2019)
41. Kollamaram, G., Croker, D.M., Walker, G.M., Goyanes, A., Basit, A.W., Gaisford, S.: Low temperature fused deposition modeling (FDM) 3D printing of thermolabile drugs. *Int. J. Pharm.* (2016)
42. Kür, H., Eren, O.: FDM 3D printing of MWCNT reinforced ABS nano-composite parts with enhanced mechanical and electrical properties, 37, July 2018, pp. 339–347 (2019)
43. Stratasys.com: FDM and PolyJet 3D printing a global leader in applied additive technology solutions FDM and PolyJet 3D printing (2017)
44. Khoo, Z.X., et al.: 3D printing of smart materials: a review on recent progresses in 4D printing, July 2015
45. Zhang, F., Wei, M., Viswanathan, V.V., Swart, B., Shao, Y.: Nano Energy 3D printing technologies for electrochemical energy storage. *Nano Energy* **40**(May), 418–431 (2017)
46. Killard, A.J.: 4—Screen printing and other scalable point of care (POC) biosensor processing technologies. Elsevier Ltd. (2017)
47. Van Humbeeck, J.: additive manufacturing of shape memory alloys. *Shape Mem. Superelasticity* **4(2)**, 309–312 (2018)
48. Dadbakhsh, S., Vrancken, B., Kruth, J., Luyten, J., Van Humbeeck, J.: Materials science & engineering a texture and anisotropy in selective laser melting of NiTi alloy. *Mater. Sci. Eng. A* **650**, 225–232 (2016)
49. Petrovskaya, T.S., Toropkov, N.E., Mironov, E.G., Azarmi, F.: 3D printed biocompatible polylactide-hydroxyapatite based material for bone implants. *Mater. Manuf. Processes* **33(16)**, 1899–1904 (2018). <https://doi.org/10.1080/10426914.2018.1476764>
50. Afkhami, S., Dabiri, M., Alavi, S.H., Björk, T., Salminen, A.: Fatigue characteristics of steels manufactured by selective laser melting. *Int. J. Fatigue* **122**, Dec 2018, 72–83 (2019)
51. Zheng, Y., Zhang, K., Liu, T.T., Liao, W.H., Zhang, C.D., Shao, H.: Cracks of alumina ceramics by selective laser melting. *Ceram. Int.* **45(1)**, 175–184 (2019)
52. Lee, C., Boydston, A.J., Nelson, A.: *SC. Prog. Polym. Sci.* (2019)
53. Hu, J., Meng, H., Li, G., Ibeke, S.I.: A review of stimuli-responsive polymers for smart textile applications, May 2012

54. Huang, W.M., Yang, B., Zhao, Y., Ding, Z.: Thermo-moisture responsive polyurethane shape-memory polymer and composites: a review, pp. 3367–3381 (2010)
55. Hubert, A., Calchand, N., Le Gorrec, Y., Gauthier, J.: Magnetic shape memory alloys as smart materials for micro-positioning devices. HAL Id: hal-00720674, Aug 2012
56. A.I. Pristupag, Magnetic-field-sensitive polymer composite materials, vol. 409 (2014)
57. Javaid, M., Haleem, A.: *SC. Clin. Epidemiol. Glob. Heal.* (2018)
58. Ntouanoglou, K., Stavropoulos, P., Mourtzis, D.: 4D printing prospects for the aerospace industry: a critical review Mourtzis review 4D Printing Prospects for the Aerospace a critical Costing models for capacity optimization in Industry 4. 0: Trade-off between used capacity and operational efficiency. *Procedia Manuf.* **18**, 120–129 (2018)
59. Momeni, F., Sabzpoushan, S., Valizadeh, R.: Plant leaf-mimetic smart wind turbine blades by 4D printing. *Renew. Energy* **130**, 329–351 (2019)
60. S. Van Hoa; Development of composite springs using 4D printing method. *Compos. Struct.* (2018)
61. Mohanta, K.: 4D printing—will it be a game-changer?, pp. 3–5 (2018)
62. Zarek, M., Mansour, N., Shapira, S., Cohn, D.: 4D printing of shape memory-based personalized endoluminal medical devices, vol. 201600628, pp. 1–6 (2016)

Chapter 3

Sustainable Material Selection for Indian Manufacturing Industries: A Hybrid Multi-criteria Decision-Making Approach



Anbesh Jamwal, Rajeev Agrawal, Monica Sharma, and Anil Kumar

Abstract At the present time, Sustainable materials play an important role to make the balance between environment and manufacturing. Many strategies and models have been developed in this field to improve the cost effectiveness in industries. In the last few years Govt. policies among the global and customer pressure has forced many industries to adopt sustainable materials for the manufacturing processes in industries to promote sustainability and maintain the eco balance. The increase in global carbon emission through the manufacturing processes has also forced Indian industries to adopt sustainable practices in their business. Among these, all strategies selection of sustainable materials plays an important role in the adoption of sustainable manufacturing practices in industries. The aim of this research work is to propose a Hybrid Multi-criteria-based model to evaluate the best sustainable materials for Indian manufacturing industries as India is a fast growing nation at the global level. The indicators are collected from an existing literature review and through the questionnaire survey circulated to Indian manufacturing industries. The proposed model of sustainable materials adoption is validated with a case study in the Indian additive manufacturing industry. In the end, this study concludes with the limitation, managerial implications, and future scopes. It is expected that this study will be helpful for Indian manufacturing industries which are adopting sustainable materials in their manufacturing processes.

Keywords Sustainable manufacturing · Sustainable materials · Additive manufacturing · Materials selection · Fuzzy-TOPSIS

A. Jamwal (✉) · R. Agrawal
Department of Mechanical Engineering, Malaviya National Institute of Technology, J.L.N. Marg,
Jaipur, Rajasthan 302017, India

M. Sharma
Department of Management Studies, Malaviya National Institute of Technology, J.L.N. Marg,
Jaipur, Rajasthan 302017, India

A. Kumar
Guildhall School of Business and Law, London Metropolitan University, London, UK

3.1 Introduction

The manufacturing industries in India have a great effect on our environment, economy, and health [1]. The rapid urbanization among the globe has led to many environmental problems such as resource depletion which affect our environmental sustainability [2]. Developing nations like India are working on new innovations and technologies to compete with developed nations [3]. Besides this, Indian industries are now working on maintaining the environmental sustainability to reduce carbon emissions during the manufacturing processes [4]. Sustainability manufacturing focuses on the manufacturing practices which don't or having less effect on the environment during practices [5]. Generally, manufacturing practices in industries produce many types of emission in which carbon emission is the cause of worry at the present time because it is responsible for global warming and environment pollution [6]. Sustainable manufacturing focuses on reducing these emissions during the manufacturing practices in industries. Global policies and customer pressure among the industries have forced all types of industries to adopt sustainable manufacturing practices [7]. Sustainable manufacturing also focuses on the use of those manufacturing processes which don't lead to any health issues for customers and employees as well as other communities [8]. The main drivers of sustainable manufacturing are conservation of natural resources, recycling the products, waste management, and environmental protection using environmentally friendly processes, pollution control using fewer carbon emissions [9]. There are many enablers of which decide the sustainability of the organization in which: Sustainable design, sustainable materials selection, sustainable machining, sustainable packaging, sustainable supply chains, sustainable material disposal, and sustainable recycling are important. Sustainable material selection is an emerging research area in India because inappropriate material selection for manufacturing processes causes higher carbon emissions hence results in environmental pollution [10]. Another reason for sustainable material selection is that now Indian customers are more conscious about the environmental and economic issues so industries are now under pressure to adopt sustainable materials [11, 12]. Apart from these issues, manufacturing industries in India are now considering the material selection process as an important part of the manufacturing and considering as sustainability pillar [13, 14]. The present manufacturing trend across the globe is not only about the financial benefits to the industry but industries are also focusing on the long-term impact of manufacturing on present and future generations by sustainable manufacturing. The term sustainable manufacturing is focused on the consideration of all three pillars of sustainability i.e. economic, social and environmental during the manufacturing and reduction of carbon emissions by promoting eco-friendly manufacturing processes.

1. The objective of present research work is to identify the criteria list for sustainable materials selections for Indian additive manufacturing industries from the survey and literature review which is based on Indian manufacturing industries.
2. Ranking of criteria based on the data collected from the additive manufacturing industries.

3. Prioritize the materials used in additive manufacturing industries with the consideration of sustainability pillars with the help of Fuzzy-TOPSIS methodology.

To meet the present objectives of the study Fuzzy-TOPSIS methodology is used. In Sect. 2 sustainable manufacturing studies have been mentioned in additive manufacturing industries. Section 3 consists of the problem description. Section 4 consists of the solution methodology used in the present study. Section 5 describes the research design and Sect. 6 describes the application of Fuzzy-TOPSIS in the material selection in Indian additive manufacturing industries which is further followed by results and conclusions.

3.2 Research Gap

The use of sustainable powders and materials in the additive manufacturing industries has a very large market at the global level. However, it is limited in developing countries like India due to a lack of a proper framework for material selection [15]. There has been a lot of research work carried out in sustainable materials in the past few years [16–19]. These studies were focused on the selection of sustainable materials which leads to the production of sustainable products through additive manufacturing [20, 21]. Few studies show the issues in sustainable manufacturing in additive manufacturing industries but there is no study that is carried out for sustainable material selection for additive manufacturing industries in a developing nation like India [22]. This study is first attempt to develop a hybrid framework for sustainable material selection for additive manufacturing industries in India which is based on all three pillars of sustainability. In this study, various materials and powders were used in additive manufacturing industries that have been taken and then through the TBL criteria of sustainability best among the alternatives is selected. The criteria and materials were chosen with the consultation with experts from additive manufacturing industries and researchers currently working on additive manufacturing.

3.3 Additive Manufacturing Industry Case Illustration

In the present study case study has been in the additive manufacturing industry. Data of various metals used in the additive manufacturing industry is collected from the industry and then specific values of their mechanical and physical properties are collected from databases. Further, the three all the factors have been categorized into the three categories which are based on the sustainability measurements. In Indian additive manufacturing industries, sustainable manufacturing studies are reported and there is no study that reports about the sustainable material selection for the Indian additive manufacturing industries. From the literature survey, it is found that

Table 3.1 Criteria for the additive manufacturing industries

Criteria	Symbol
Environmental	ENV
Social	SCO
Economical	ECO

developed countries are now focusing on the adoption of sustainable materials over the traditional materials to reduce the negative impact of manufacturing processes on the environment. Sustainable practice around the globe has forced developing nations like India to adopt sustainable material selection but in Indian industries, there are no proper criteria for the sustainable material selection for additive manufacturing industries. In the present study, there are 19 alternatives were chosen with 3 criteria with the discussion with additive manufacturing experts and academia. Further, the questionnaire survey is circulated to the industry and academia to collect the data. Inputs given by experts were processed and ranking of criteria and alternatives is done with the fuzzy-TOPSIS. Tables 3.1 and 3.2 show the alternatives and criteria chosen for the study.

In the present study case study has been in the additive manufacturing industry. Data of various metals used in the additive manufacturing industry is collected from

Table 3.2 Alternatives for sustainable material selection for industries

Alternative	Symbol	Criteria
Global warming contribution	ENV1	ENV
Healthy industry environment	ENV2	ENV
Environment form	ENV3	ENV
Waste management	ENV4	ENV
Transportation and production activities	ENV5	ENV
Recycle and reuse	ENV6	ENV
Natural resources consumption	ENV7	ENV
Land occupied	ENV8	ENV
Health and safety	SCO1	SCO
Ecological and social acceptability	SCO2	SCO
Availability and adaptation	SCO3	SCO
Political issues	SCO4	SCO
Resistance against natural contamination	SCO5	SCO
Maintenance and operation cost	ECO1	ECO
Investment cost	ECO2	ECO
Energy efficiency	ECO3	ECO
Financial risks	ECO4	ECO
Tax contributions	ECO5	ECO
Meeting volatile customer demands	ECO6	ECO

the industry and then specific values of their mechanical and physical properties are collected from databases. Further, the three all the factors have been categorized into the three categories which are based on the sustainability measurements. In Indian additive manufacturing industries, sustainable manufacturing studies are reported and there is no study that reports about the sustainable material selection for the Indian additive manufacturing industries. From the literature survey, it is found that developed countries are now focusing on the adoption of sustainable materials over the traditional materials to reduce the negative impact of manufacturing processes on the environment. Sustainable practice around the globe has forced developing nations like India to adopt sustainable material selection but in Indian industries, there are no proper criteria for the sustainable material selection for additive manufacturing industries. In the present study, there are 19 alternatives were chosen with 3 criteria with the discussion with additive manufacturing experts and academia. Further, the questionnaire survey is circulated to the industry and academia to collect the data. Inputs given by experts were processed and ranking of criteria and alternatives is done with the fuzzy-TOPSIS. Tables 3.1 and 3.2 show the alternatives and criteria chosen for the study.

3.4 Solution Methodology

Generally, the conventional TOPSIS method discussed the identification of the best alternative among the number of alternatives and criteria using the shortest distance from the negative ideal solution of the problem and the positive ideal solution of the problem. In general, a positive ideal solution gives the maximum benefit to the industry at the minimum cost and in a negative ideal solution, it is reversed [23, 24]. The distinguishing feature of the Fuzzy-TOPSIS method as compared to the TOPSIS method is that in place of crisp weights for the alternatives and criteria. Triangular fuzzy numbers used in the problem to represent the linguistic judgement of experts from industry and academia. In the present section, the Fuzzy TOPSIS methodology is proposed [25]. The only limitation of the traditional TOPSIS technique is that the crisp inputs are used for the selection of the alternative. There may be imprecise human judgement due to the crisp inputs raking of the alternatives. Steps of fuzzy-TOPSIS techniques are discussed below:

- Develop a comparison matrix (m_{ij}) of the alternatives with the different criteria by the use of linguistic variables presented in Table 3.5.
- Obtain the normalized decision matrix by using the equation presented below:

$$r_{m_{ij}} = \left\{ \begin{array}{l} \left(\frac{a_{m_{ij}}}{x_{ij}^+} + \frac{b_{m_{ij}}}{x_{ij}^+} + \frac{c_{m_{ij}}}{x_{ij}^+} \right), \quad \forall_{ij}, x_{ij}, \text{ is a positive criterion} \\ \left(\frac{x_{ij}}{a_{m_{ij}}} + \frac{x_{ij}}{b_{m_{ij}}} + \frac{x_{ij}}{c_{m_{ij}}} \right), \quad \forall_{ij}, x_{ij}, \text{ is a negative criterion} \end{array} \right\} \quad (3.1)$$

- Obtain a weighted normalized decision matrix using the equations given below:

$$\tilde{V} = [\tilde{v}_{ij}]_{m \times n} \quad (3.2)$$

$$\tilde{v}_{ij} = r_{mij} \otimes w_j \quad (3.3)$$

- d. Determine the FNIS (Fuzzy negative ideal solution) and FPIS (Fuzzy positive ideal solution) as follows:

$$\begin{aligned} A^- &= \{v_1^-, v_2^-, \dots, v_n^-\}, \text{ where} \\ v_j^- &= \{\max(v_{ij}) \text{ if } j \in J'; \min(v_{ij}) \text{ if } j \in J''\}, \quad j = 1, 2, \dots, n. \end{aligned} \quad (3.4)$$

Here, J' is the negative criteria.

$$\begin{aligned} A^+ &= \{v_1^+, v_2^+, \dots, v_n^+\}, \text{ where} \\ v_j^+ &= \{\max(v_{ij}) \text{ if } j \in J''; \min(v_{ij}) \text{ if } j \in J'\}, \quad j = 1, 2, \dots, n. \end{aligned} \quad (3.5)$$

Here, J'' is the positive criteria.

- e. Calculation of distance from each alternative FNIS and FPIS as follows:

$$d_i^- = \left\{ \sum_{j=1}^n (v_{ij} - v_{ij}^-)^2 \right\}^{1/2}, \text{ where } i = 1, 2, \dots, m. \quad (3.6)$$

$$d_i^+ = \left\{ \sum_{j=1}^n (v_{ij} - v_{ij}^+)^2 \right\}^{1/2}, \text{ where } i = 1, 2, \dots, m. \quad (3.7)$$

- f. Calculation for (CC_i) closeness coefficient for each alternative as follows:

$$CC_i = \frac{d_i^-}{d_i^- + d_i^+}, \quad i = 1, 2, \dots, m \quad (3.8)$$

- g. Ranking of alternatives for the material selection by CC_i values in the descending order.

3.5 Application of Methodology

This section illustrates the application of Fuzzy-TOPSIS in the selection of sustainable materials for Indian additive manufacturing industries. In the first phase, the data is collected from the industries using the questionnaire survey and a sustainable model is developed to select the best sustainable material for industries which is based on the TBL. The criteria and alternatives for the present study are finalized through the discussion with the expert reviews. 3 criteria with the 19 alternatives

Table 3.3 Linguistic expressions

Linguistic variables	Corresponding Fuzzy number
Very low	(0, 0, 2)
Low	(0, 2, 4)
Medium	(2, 4, 6)
High	(4, 6, 8)
Very high	(6, 8, 10)
Excellent	(8, 1, 10)

Table 3.4 Pairwise comparison for different criteria

Criteria	Environmental	Economical	Social
Best criteria: environmental	1	5	7
Environmental			7
Economical			5
Social			1
Worst criteria: social			

were selected for the study. The linguistic expression used in the present research work is shown in Table 3.3.

Table 3.8 shows the main criteria’s computational results; CR value of main criteria is less than zero which is due to the high consistency among the pairwise comparison (Tables 3.4, 3.5, 3.6 and 3.7).

Table 3.5 Pairwise comparison for environmental criteria

BO	ENV1	ENV2	ENV3	ENV4	ENV5	ENV6	ENV7	ENV8
Best criteria: ENV1	1	4	8	3	4	4	5	8
ENV1								8
ENV2								6
ENV3								1
ENV4								4
ENV5								5
ENV6								4
ENV7								4
ENV8								5
OW	Worst criteria: ENV3							

Table 3.6 Pairwise comparison for social criteria

BO	SCO1	SCO2	SCO3	SCO4	SCO5
Best criteria: SCO4	2	3	3	1	4
SCO1					6
SCO2					6
SCO3					5
SCO4					7
SCO5					4
OW	Worst criteria: SCO5				

Table 3.7 Pair-wise comparison for the Economic criteria

BO	ECO1	ECO2	ECO3	ECO4	ECO5	ECO6
Best criteria: ECO5	5	3	2	4	1	2
ECO1						5
ECO2						5
ECO3						6
ECO4						4
ECO5						7
ECO6						4
OW	Worst criteria: ECO6					

Table 3.8 Criteria weights with CR

Criteria	ξ^*	Weights	CR
Environmental		0.69221	
Social	2.00222	0.07680	0.53661
Economical		0.23085	

3.6 Results and Discussion

The results obtained from the present research work and application of Fuzzy-TOPSIS methodology is presented in Figs. 3.1, 3.2 and Table 3.9. Table 3.9 represents the results obtained from the application of the proposed methodology. In the present study three main pillars of sustainability: Economic, social and environmental is considered which the TBL are also. In this study weights for criteria and alternatives are determined using the best worst method and the global weights of alternatives have been calculated. Among all the three criteria it is found that the environmental aspect has a great influence on additive manufacturing industries rather than the other two aspects. It is found that in developing nations like India environmental factors are important factors that influence the sustainability issues in industries. The depletion of natural resources affects the environmental balance. It is a major issue for the

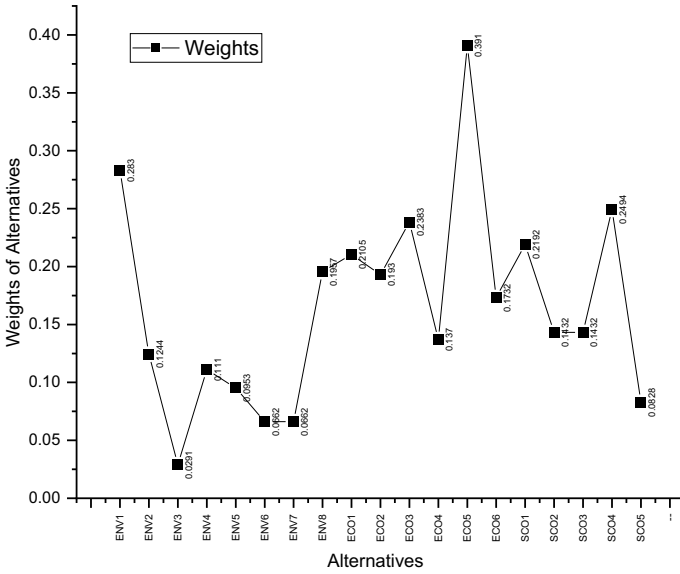


Fig. 3.1 Alternatives weights for sustainable material selection

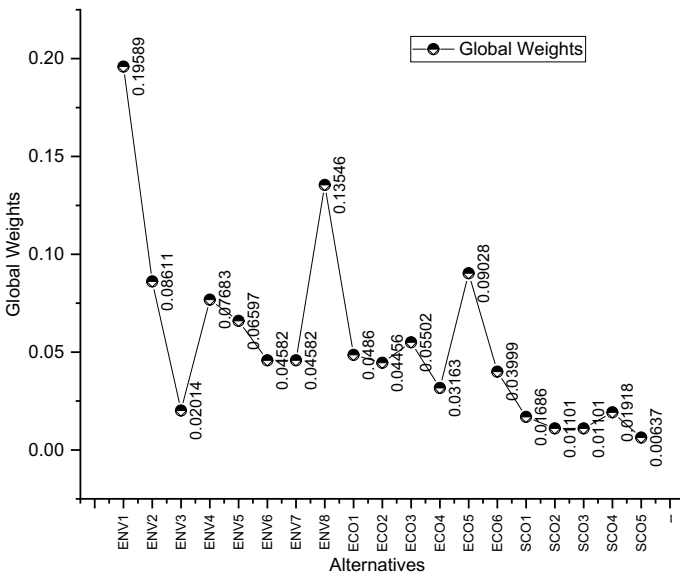


Fig. 3.2 Global weights of alternatives

Table 3.9 Ranking of alternatives with their respective criteria

Alternative	Symbol	Criteria	Rank
Global warming contribution	ENV1	ENV	1
Healthy industry environment	ENV2	ENV	4
Environment form	ENV3	ENV	14
Waste management	ENV4	ENV	5
Transportation and production activities	ENV5	ENV	6
Recycle and reuse	ENV6	ENV	9
Natural resources consumption	ENV7	ENV	10
Land occupied	ENV8	ENV	2
Health and safety	SCO1	SCO	16
Ecological and social acceptability	SCO2	SCO	17
Availability and adaptation	SCO3	SCO	18
Political issues	SCO4	SCO	15
Resistance against natural contamination	SCO5	SCO	19
Maintenance and operation cost	ECO1	ECO	8
investment cost	ECO2	ECO	11
Energy efficiency	ECO3	ECO	7
Financial risks	ECO4	ECO	13
Tax contributions	ECO5	ECO	3
Meeting volatile customer demands	ECO6	ECO	12

industries to meet the demands of customers while considering the environmental factors and following the standards. Sustainability plays an important role to fulfill the customer requirements while reducing the negative impacts of processes on the environment. The ranking of criteria is ENV > ECO > SOC in our sustainable model for material selection for Indian additive manufacturing industries. In this study, it is found that environmental factor consideration should be given more importance for Indian manufacturing industries for sustainable manufacturing practices in the additive manufacturing industries. In the last few years, there have been many advancements in processing techniques for the materials for additive manufacturing purposes, especially for metal additive manufacturing. The environmental criteria having eight alternatives which can be ranked as ENV1 > ENV8 > ENV2 > ENV4 > ENV5 > ENV6 > ENV7 > ENV3. The effect of global warming due to additive manufacturing ranked one among all the alternatives. It is found that conventional materials contribute to large CO₂ emissions and other environmental problems that can be solved by the use of sustainable eco-friendly materials. In a healthy industry, the environment is which also affects the sustainability practices in Indian additive manufacturing industries. Choosing the right criteria for Indian manufacturing is a challenging task as it requires a validated model with less cost. The economic criteria alternatives are ranked as ECO5 > ECO3 > ECO1 > ECO2 > ECO6 > ECO4.

Based on the data collected from the industries and academia experts tax contribution plays an important role in sustainability practices. It is further followed by energy efficiency. Indian industries are now focusing on the adoption of sustainable manufacturing practices [26, 27]. Sustainable materials plays an important role in Sustainable manufacturing practices [28, 29]. This is the reason now industries are more focused towards the adoption of sustainable materials and machining methods.

Renewable sustainable energy sources have very little impact on the environment. Ranking for the social criteria is $SOC4 > SOC1 > SOC2 > SOC3 > SOC5$. It is found that political issues are a very important factor for Indian additive manufacturing industries which is further followed by health and safety.

The main aim of the present research work is to develop a sustainable model for the material selection for Indian additive manufacturing industries with the consideration of TBL. The criteria and alternatives in present research work are ranked by the Fuzzy-TOPSIS method.

3.7 Conclusion and Future Scope

The present concept of sustainable development is becoming more popular in developing nations like India due to Govt. polices and pressure from consumers to considering environmental factors. With an increase in the population of India pollution is also increasing day by day which also results in depletion of natural resources at a very fast rate. Indian industries are the large contributors in the world industrialization in which some are following sustainable manufacturing practices. But these studies are very limited especially when it comes to additive manufacturing industries. It is still a major problem for the Indian industries to select sustainable materials with the concept of sustainable development. In the present paper, a framework is developed and proposed for the Indian additive manufacturing industries with the consideration of TBL. There were 3 criteria with 19 alternatives finalized after the survey and then the BWM method is considered for the weight calculations. The last phase of the study is about the ranking the alternatives by Fuzzy-TOPSIS method. It is expected that this study can provide a sustainable model for the material selection for the Indian additive manufacturing industries.

Acknowledgements Author(s) received financial support from the TEQIP-3 sponsored project “Exploration of sustainable manufacturing in Indian manufacturing industries” for this research work.

References

1. Jamwal, A., Aggarwal, A., Gupta, S., Sharma, P.: A study on the barriers to lean manufacturing implementation for small-scale industries in Himachal Region (India). *Int. J. Intell. Enterpr.*

- 6(2–4), 393–407 (2019)
2. Singh, P.L., Sindhvani, R., Dua, N.K., Jamwal, A., Aggarwal, A., Iqbal, A., Gautam, N.: Evaluation of common barriers to the combined lean-green-agile manufacturing system by two-way assessment method. In: *Advances in Industrial and Production Engineering*, pp. 653–672. Springer, Singapore (2019)
 3. Gautam, N., Ojha, M.K., Swain, P., Aggarwal, A., Jamwal, A.: Informal investigation of fourth-party and third-party logistics service providers in terms of Indian context: an AHP Approach. In: *Advances in industrial and production engineering*, pp. 405–413. Springer, Singapore (2019)
 4. Mayyas, A., Omar, M.A., Hayajneh, M.T.: Eco-material selection using fuzzy TOPSIS method. *Int. J. Sustain. Eng.* **9**(5), 292–304 (2016)
 5. Anupam, K., Lal, P.S., Bist, V., Sharma, A.K., Swaroop, V.: Raw material selection for pulping and papermaking using TOPSIS multiple criteria decision making design. *Environ. Progress Sustain. Energy* **33**(3), 1034–1041 (2014)
 6. Govindan, K., Shankar, K.M., Kannan, D.: Sustainable material selection for construction industry—a hybrid multi criteria decision making approach. *Renew. Sustain. Energy Rev.* **55**, 1274–1288 (2016)
 7. Girubha, R.J., Vinodh, S.: Application of fuzzy VIKOR and environmental impact analysis for material selection of an automotive component. *Mater. Des.* **37**, 478–486 (2012)
 8. Azimifard, A., Moosavirad, S.H., Ariafar, S.: Selecting sustainable supplier countries for Iran's steel industry at three levels by using AHP and TOPSIS methods. *Resour. Policy* **57**, 30–44 (2018)
 9. Wittstruck, D., Teuteberg, F.: Integrating the concept of sustainability into the partner selection process: a fuzzy-AHP-TOPSIS approach. *Int. J. Logist. Syst. Manag.* **12**(2), 195–226 (2012)
 10. Query ID="Q4" Text="Unable to parse this reference. Kindly do manual structure" Chaharsooghi, S.K., Ashrafi, M.: Sustainable supplier performance evaluation and selection with neofuzzy TOPSIS method. In: *International Scholarly Research Notices*, 2014 (2014)
 11. Yong, D.: Plant location selection based on fuzzy TOPSIS. *Int. J. Adv. Manuf. Technol.* **28**(7–8), 839–844 (2006)
 12. Melugiri-Shankaramurthy, B., Sargam, Y., Zhang, X., Sun, W., Wang, K., Qin, H.: Evaluation of cement paste containing recycled stainless steel powder for sustainable additive manufacturing. *Constr. Build. Mater.* **227**, 116696 (2019)
 13. Majeed, A., Zhang, Y., Ren, S., Lv, J., Peng, T., Waqar, S., Yin, E.: A big data-driven framework for sustainable and smart additive manufacturing. *Robot. Comput. Integr. Manuf.* **67**, 102026 (2020)
 14. Sanchez-Rexach, E., Johnston, T.G., Jehanno, C., Sardon, H., Nelson, A.: Sustainable materials and chemical processes for additive manufacturing. *Chem. Mater.* **32**(17), 7105–7119 (2020)
 15. Agrawal, R., Vinodh, S.: State of art review on sustainable additive manufacturing. *Rapid Prototyping J.* (2019)
 16. Al-Ghamdi, K.A.: Sustainable FDM additive manufacturing of ABS components with emphasis on energy minimized and time efficient lightweight construction. *Int. J. Lightweight Mater. Manuf.* **2**(4), 338–345 (2019)
 17. Vijay, Y., Sanandiya, N.D., Dritsas, S., Fernandez, J.G.: Control of process settings for large-scale additive manufacturing with sustainable natural composites. *J. Mech. Design* **141**(8) (2019)
 18. Rocha, V.G., Saiz, E., Tirichenko, I.S., García-Tuñón, E.: Direct ink writing advances in multi-material structures for a sustainable future. *J. Mater. Chem. A* **8**(31), 15646–15657 (2020)
 19. Lee, H.T., Song, J.H., Min, S.H., Lee, H.S., Song, K.Y., Chu, C.N., Ahn, S.H.: Research trends in sustainable manufacturing: A review and future perspective based on research databases. *Int. J. Precis. Eng. Manuf.-Green Technol.* 1–11 (2019)
 20. Leng, J., Ruan, G., Jiang, P., Xu, K., Liu, Q., Zhou, X., & Liu, C.: Blockchain-empowered sustainable manufacturing and product lifecycle management in industry 4.0: a survey. *Renew. Sustain. Energy Rev.* **132**, 110112 (2020)
 21. Machado, C.G., Winroth, M.P., Ribeiro da Silva, E.H.D.: Sustainable manufacturing in Industry 4.0: an emerging research agenda. *Int. J. Prod. Res.* **58**(5), 1462–1484 (2020)

22. Hernandez Korner, M.E., Lambán, M.P., Albajez, J.A., Santolaria, J., Ng Corrales, L.D.C., Royo, J.: Systematic literature review: Integration of additive manufacturing and industry 4.0. *Metals* **10**(8), 1061 (2020)
23. Wang, J.W., Cheng, C.H., Huang, K.C.: Fuzzy hierarchical TOPSIS for supplier selection. *Appl. Soft Comput.* **9**(1), 377–386 (2009)
24. Singh, P.K., Sarkar, P.: A framework based on fuzzy AHP-TOPSIS for prioritizing solutions to overcome the barriers in the implementation of ecodesign practices in SMEs. *Int. J. Sustain. Dev. World Ecol.* **26**(6), 506–521 (2019)
25. Ashtiani, B., Haghighirad, F., Makui, A., Ali Montazer, G.: Extension of fuzzy TOPSIS method based on interval-valued fuzzy sets. *Appl. Soft Comput.* **9**(2), 457–461 (2009)
26. Jamwal, A., Agrawal, R., Sharma, M., Kumar, V.: Review on multi-criteria decision analysis in sustainable manufacturing decision making. *Int. J. Sustainable Eng.* 1–24 (2021)
27. Jamwal, A., Agrawal, R., Sharma, M., Kumar, V., Kumar, S.: Developing a sustainability framework for Industry 4.0. *Procedia CIRP*, **98**, 430–435 (2021)
28. Jamwal, A., Agrawal, R., Sharma, M.: Life cycle engineering: past, present, and future. In *Sustainable Manufacturing* (pp. 313–338) (2021) Elsevier
29. Jamwal, A., Agarwal, R., Sharma, M., Kumar, A., Kumar, V., Garza-Reyes, J.A.: Machine learning applications for sustainable manufacturing. A Bibliometric-based Review for Future Research. *J. Enterprise Inf. Manage.* (2021). <https://doi.org/10.1108/JEIM-09-2020-0361>

Chapter 4

Identification of Barriers in the Implementation of Additive Manufacturing in Indian Scenario



Shivam Verma, Manish Gupta, and Shivam

Abstract Additive manufacturing, also known as 3D printing is a material joining technology based on layer-by-layer deposition. AM technologies have capabilities to reduce lead time, to increase material efficiency, to deal with complexity in production, to reduce time and labor in construction, making cell-based organs in healthcare technologies and is an important part of Industry 4.0. Countries like the USA, China, South Korea, Japan are taking a leap in the adaptation and making patents in AM technology, India is being slow in the adaptation and implementation of this technology. This gap is governed by several barriers which are needed to be addressed. This study identifies the barriers prevailing in Indian scenario towards the adaptation of AM technologies using Fuzzy ISM methodology and classify them on the basis of dependence power and driving power and also level their hierarchy in Fuzzy ISM model. Some critical barriers like Compatibility, Initial Cost, Lack of talent etc. are identified and considered for analysis.

Keywords Additive manufacturing · Fuzzy ISM · Barriers · India · Implementation

4.1 Introduction

Additive Manufacturing (AM), also known as 3D Printing is a modern material joining manufacturing technology which is generally based on layer-by-layer deposition and creating a 3D object by using digital file. This technology has been used to produce prototype for years but recent technological advancements like increase in number of materials, speed, accuracy, bionics lead AM to produce whole part with the help of little or more post processing. Today, this technology is being used for functional parts, fit and finish components, mold and tooling and visual proof of concept [1] in various fields like automotive sector, health sector, Research and Development

S. Verma · M. Gupta · Shivam (✉)
Department of Mechanical Engineering, Motilal Nehru National Institute of Technology
Allahabad, Prayagraj, India

etc. Cost reduction, increased efficiency, innovation, prototyping, product development etc. are the main reasons which are motivating the industries to adopt this technology [1].

In 2018, AM market reached \$9.1 billion with a growth rate of 18% [2] and it is expected to reach \$23.79 billion by 2025 [3] with \$7.65 billion in North America, \$7.18 billion in European and Middle Eastern Countries, \$5.56 billion in Asia Pacific Countries with 70% business share of China only and \$1.11 billion by rest of the world [4]. Although Asia Pacific contributes 23.79% of Global additive manufacturing market but the contribution of India is less than 2.2% as compared to other major economies like China (13%), Japan (9.2%) [4]. India has become the 6th largest economy in the world with a phenomenal growth rate of 7.3% but somehow India is being slow in the race of adaptation of AM technologies and considered as a follower country in the categories of Leader, Challengers and Followers in a report published by AT Kearney group [5]. Interestingly growth of global AM market has not been able to make the grade as it was forecasted few years ago for e.g. Global AM market was expected to reach \$13 billion in 2018 [1] but it reached \$9.1 billion in 2018 [2]. Differences show that there are some challenges and barriers which are creating gap between implementing AM technologies in India and other developing and developed nations and those barriers are needed to be addressed. This paper is organized as literature review, methodology, results, discussion, conclusion, limitation and future scope.

4.2 Literature Review

Additive Manufacturing, as the name suggests it adds material to make the object. It is commonly known as 3D Printing. It uses CAD software or 3D scanner to create the 3D geometry file and then this geometry is transferred to printer to deposit or fuse the material layer by layer.

Diffusion of AM technologies in India is relatively slow as compared to other countries, it consists about 2.2% with total of 23.79% market of Asia Pacific compared to China (13%) and Japan (9%) [4]. Major contributors are electronic industry (24.1%), automotive sector (21.2%), industrial sector (13.8%), aerospace sector (10.8%), architectural sector (5.1%) and educational sector (3%), medical sector (15%) in India. Indian AM market is expected to reach at \$79 million by 2022. With the arrival of new startups in AM like 3D Dexter, Aha3D, Imaginarium India, AM in India is gaining some momentum but due to lack of centralized approach this technology is still in its nascent stage in India. India is being slow in the adoption of Additive Manufacturing technologies so there is a need to address the barriers which are leading to the slow adoption rate.

To identify the barriers in implementation of AM in India, literature search, published interviews of industry experts, industry reports have been used. These barriers are then discussed with experts for their relevance and they are chosen in the manner that relationship between them can be established. Barriers have been

Table 4.1 Frequency of citation

Sr. No.	Barriers	References
1	Resistance to change (a) Resistance of acquiring new skill (b) Fear of losing jobs	[6, 7]
2	Initial cost (a) High printer cost (b) Training and skill development cost (c) AM technology implementation cost (d) IT security cost	[6, 8–10]
3	Lack of talent/experience (a) Designer unavailability	[6, 11, 8, 9, 12]
4	Compatibility: dependence on other industries	[10]
5	Technical limitations (a) Speed of large-scale production (b) Surface finish (c) Hazardous chemicals used in post processing (d) Material development	[6, 8–10]
6	Intellectual property threat and security (a) AM sabotage (b) Design data theft (c) Intellectual property rights	[13, 9, 14]
7	Management support	[15, 8]
8	Status of India in R&D towards AM	[9]
9	Lack of awareness	[6, 16]
10	Lack of government support	[17, 9]
11	Technology versus expectation mismatch	[16]

identified as follows, frequency of citation of different barriers is shown by Table 4.1.

- (a) **Resistance to change:** Workers show resistance in acquiring new skill after doing conventional work for years. AM technologies are followed by automation so fear of losing job increases resistance among worker to adopt technology [7]. These barriers among workers lead to resistance of management support to adopt AM.
- (b) **Initial Cost:** Industrial grade 3D printers requires high cost and is too much for medium and small scale industries of India, extra 30–40% custom duty makes it more costlier [9]. Skilled labor, IT security cell also increases the initial cost of AM implementation [9].
- (c) **Lack of Experience/Talent:** Only 3% students of India get enrolled in vocational training courses after higher secondary school. According to a report by Manpower group, employers find 58% difficulty in job filling due to lack of talent [18]. AM technologies demands high skilled worker availability in CAD based systems.

- (d) **Compatibility: Dependence on other industries:** Successful implementation of AM technologies depends on the mutual intersection of two supply chains i.e. if there is an industry which is producing parts through AM technologies then there must be a consumer industry willing to buy it [10].
- (e) **Technical limitations:** Chemicals used for post processing and UFP (Ultrafine particles) from printing have been observed causing some health threats [19], speed of large scale production and breakeven point have been observed at 42 for Selective Laser Sintering on comparison to high pressure die casting [20]. Strength of layer needs additional methods to restructure the required properties [8]. Intrinsic properties such as holes, degenerating facets have been observed during conversion from CAD to STL file [21].
- (f) **Intellectual Property threats and Security:** A research published by Gartner states that there would be loss of \$100 billion per year by the end of 2018 [9] because of IPR threats. Even complex parts can be scanned and printed easily without the consent of copyright holder [13]. Less efficient security system can lead to technical theft and AM sabotage [14].
- (g) **Management Support:** Successful implementation of technology in any industries is supported by its management, it is done by adapting technology, making workers comfortable about technology and provide training to workers.
- (h) **Status of India in R&D towards AM:** India's investment on R&D is stagnant at 0.6–0.7% of GDP for 20 years as compared to other developing and developed economies which is around 2.5–3.0% of GDP. Construction 3DP can play a vital role in Housing for All mission by Government of India, a decent amount of research publications and case studies can help industries to implement this technology [6]. Only few number of Institutions are offering master's program in additive manufacturing specialization [9].
- (i) **Lack of Awareness:** A survey done on 186 stakeholders of construction industries states that only 72% have heard this technology from newspaper and videos and only 7% of them have researched on this topic to know more about it [6]. According to AM startups like Think3D and 3Ding, lack of awareness is main reason for slow adoption of AM technologies in India [16].
- (j) **Lack of Government Support:** The leading countries in AM technologies like USA, China, South Korea, Russia have developed nation action plan on Additive Manufacturing, such action plans are missing in Indian context and high custom duty of around 35–40% on industrial level printer are also increasing the initial cost of implementation [9]. AM output product are kept in 28% GST slab, making these less attractive to adopt.
- (k) **Technology versus Expectation Mismatch:** According to the lead member of 3D printing venture Think3D Prudhvi, there is a mismatch between technology and expectation of people regarding cost, quality and speed. People want their product to be really quick and do not distinguish between 2D printing and 3D printing. Gartner hype cycle put only few AM application in plateau of productivity and maximum AM application in slope of enlightenment, which signifies only few AM application have been stabilized at ground level and remaining are yet to be commercialized.

4.3 Methodology

Taking barriers from academic literature, published interviews and industrial reports, now to find relationship among these barriers Interpretive Structural Modeling (ISM) methodology will be used. ISM methodology transform poorly articulated data into visible and well defined data [22]. Some important studies have been performed using ISM methodology which includes, finding enablers for flexible manufacturing system in India [23], for the analysis of barriers in implementing solar power installations in India [24], in analyzing the interaction of criteria, sub criteria for supplier selection in supply chain environment [25], etc.

Fuzzy ISM Methodology: To make ISM model more sensitive Fuzzy based ISM methodology is used. Some important studies have been performed using Fuzzy ISM which includes, to identify and analyze the barriers in solar energy implantation in Indian rural sector [26], to analyze the barriers in green supply chain management implementation [27], to find the enablers for Indian Manufacturing Sector competitiveness [28], etc. Citation of various barriers in the literature is shown in Table 4.1. Flow chart of ISM fuzzy model is shown in Fig. 4.1 [15].

Since ISM methodology uses binary values for assigning the weights to the factor i.e. 0 or 1, it does not provide the strength of relationship to the factors. In fuzzy based ISM methodology strength to relationship is provided on the scale of 0–1. Table 4.2 will be used for providing relationship to the factors [28].

4.3.1 Fuzzy Direct Relationship Matrix

Fuzzification increases the sensitivity of conventional MICMAC. It is done by introducing fuzzy input as shown in the table. Using values in the table, fuzzy direct relationship matrix of barriers of implementation AM in Indian Scenario is shown by Table 4.3.

4.3.2 Fuzzy Indirect Relationship

The indirect relationship signifies the hidden impact of the factor which are overlooked in direct relationship. Composition operator of fuzzy relation is used to find indirect relationship between barriers. Some common compositions are max–min, max product, max average. Let us assume the fuzzy relation matrix R showing relationship between x_1, y_1, y_2 and fuzzy relation matrix S showing relationship between y_1, y_2, z_1 . To find interrelationship between x_1, z_1 through variable y_1, y_2 we can use above mentioned composition.

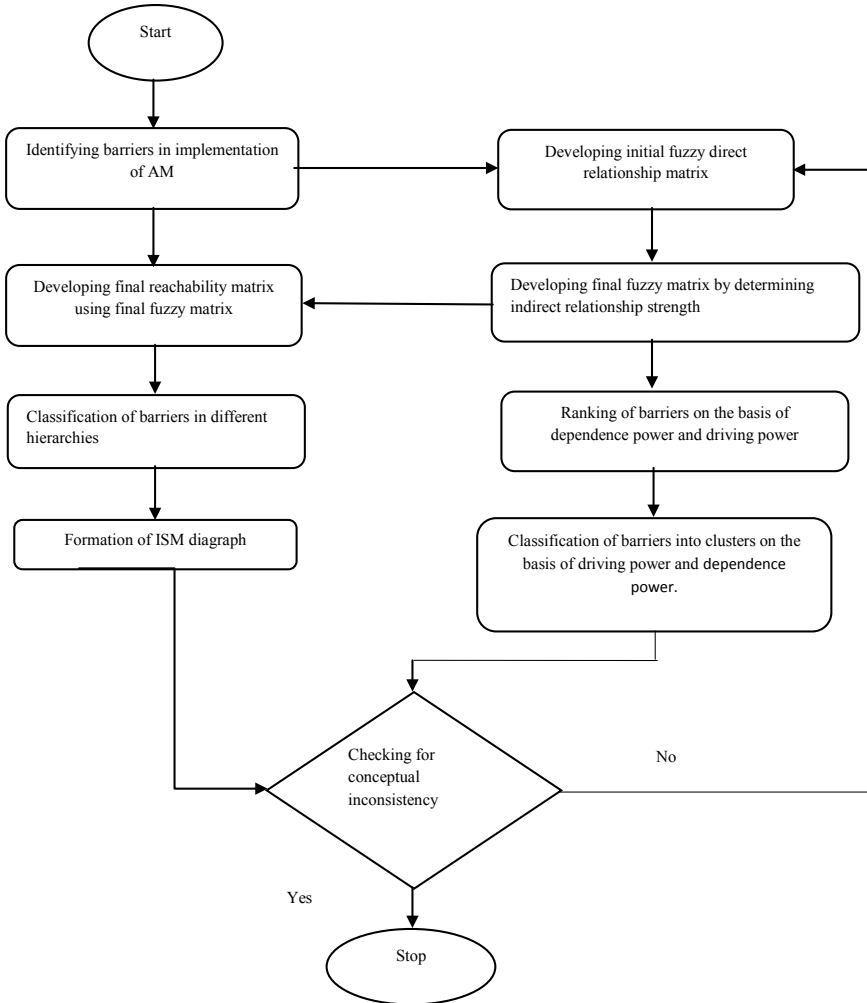


Fig. 4.1 Fuzzy ISM methodology

Table 4.2 Relationship strength values

Relative strength	No	Very low	Low	Medium	High	Very high	Full
Value	0	0.1	0.3	0.5	0.7	0.9	1

$$R = \begin{matrix} & \begin{matrix} y_1 & y_2 \end{matrix} \\ \begin{matrix} x_1 \\ .5 \end{matrix} & \begin{pmatrix} .7 & .5 \end{pmatrix} \end{matrix}$$

$$S = \begin{matrix} y_1 \\ y_2 \end{matrix} \begin{pmatrix} z_1 \\ .9 \\ .3 \end{pmatrix}$$

Table 4.3 Fuzzy direct relationship matrix

S. No.	Barriers	1	2	3	4	5	6	7	8	9	10	11
1	Resistance to change	1	0	0.3	0	0	0	0.3	0.1	0.3	0	0.3
2	Initial cost	0.1	1	0.1	0.7	0	0.3	0.9	0	0.1	0.3	0.1
3	Lack of experience/talent	0.3	0.3	1	0.1	0	0	0.3	0.1	0.5	0.3	0.5
4	Compatibility: dependence on other industries	0	0.5	0.1	1	0	0.5	0.7	0	0.3	0	0.1
5	Technical limitations	0.1	0.9	0	0.7	1	0	0.9	0.1	0.1	0.3	0.7
6	Intellectual property issue and threats	0	0.7	0	0.5	0.1	1	0.7	0.1	0	0.7	0.1
7	Management support	0.5	0	0.5	0.1	0	0.3	1	0.3	0.1	0.3	0
8	Status of India in R&D towards AM	0	0.3	0.5	0.1	0.3	0.5	0	1	0.1	0.9	0.1
9	Lack of awareness	0.5	0	0.5	0.1	0	0.1	0.1	0.3	1	0.1	0.7
10	Lack of government support	0.1	0.5	0.5	0	0.7	0.7	0.9	0.7	0.5	1	0.3
11	Technology versus expectation mismatch	0.3	0	0	0.1	0	0	0	0	0	0	1

Matrix R is showing direct relationship between x_1, y_1, y_2 variables and matrix S is showing direct relationship between y_1, y_2, z_1 . To calculate the indirect relationship between x_1, z_1 , following compositions are used. Relationship strength of x_1 to y_1 is represented by $x_1_y_1$ and same representation have been followed for other variables.

Max min composition: R.S

$$x_1_z_1 = \max (\min (x_1_y_1, y_1_z_1), \min (x_1_y_2, y_2_z_1))$$

$$x_1_z_1 = \max (\min (0.7, 0.9), \min (0.5, 0.3))$$

$$x_1_z_1 = \max (0.7,0.3).$$

$$x_1_z_1 = 0.7$$

Max product Composition: R.S

$$x_1_z_1 = \max((x_1_y_1 * y_1_z_1), (x_1_y_2 * y_2_z_1))$$

$$x_1_z_1 = \max ((0.7*0.9), (0.5*0.3))$$

$$x_1_z_1 = \max (0.63,0.15)$$

$$x_1_z_1 = 0.63$$

Max-average composition: R.S

$$x_1_z_1 = \max ((x_1_y_1 + y_1_z_1)/2, (x_1_y_2 + y_2_z_1)/2)$$

$$x_1_z_1 = \max ((0.7 + 0.9)/2, (0.5 + 0.3)/2)$$

$$x_1_z_1 = \max (0.8,0.4)$$

$$x_1_z_1 = 0.8$$

Values obtained from max–min, max-product, max-average composition for relation of x_1 to z_1 are 0.7, 0.63, 0.8 respectively. Since relation of x_1 to y_1 is high (0.7), and relation of y_1 to z_1 is very high (0.9) so indirect relationship between x_1 and z_1 should be less than high (0.7). Since max–min composition yields a relationship of 0.7, max-average composition yields a relationship of 0.8 and max-product yields a relationship of 0.63, so among mentioned, max-product composition is more prominent to calculate indirect relationship between barriers. Max product composition has also shown some promising results in the past [26, 28]. For the fuzzy direct relationship table, max product algorithm will be applied since it contains large number of iterations, a MATLAB program have been created to calculate indirect relationship. Iterations will be repeated till we get fuzzy stabilized matrix i.e., values do not change on performing repetitive max-product algorithm.

4.3.3 *Fuzzy Stabilized Matrix*

After repetitive iterations of max-product composition, a final stabilized fuzzy matrix is obtained which contains transitivity. Stabilized matrix will be used to make binary matrix by assigning 1 for values greater than 0.5 and 0 for the values less than 0.5. Fuzzy stabilized matrix is shown by Table 4.4.

4.3.4 *Final Binary Reachability Matrix*

Now with the help of fuzzy stabilized matrix, final reachability matrix is constructed with all interrelationship between barriers. Fuzzy values greater or equal to 0.5 will be considered as 1 and values less than 0.5 will be considered as 0. Final Reachability Matrix from stabilized fuzzy matrix is given by Table 4.5.

4.3.5 *Level Partitioning*

The final reachability matrix will be used to group factors into different levels. The antecedent set (A) and reachability set (R) are obtained for each factor from final reachability matrix. Reachability set consist of factor itself and other factors which this factor may help to achieve and Antecedent set consist of factor itself and another factor, which may help to achieve this factor. In final reachability matrix the row will represent reachability set while column will represent antecedent set. To level the factors intersection set (I) is found between Reachability set and Antecedent set and if for a certain factor $\{R\} = \{I\}$ then that factor is considered in top level. Summary of Barriers after performing all the iteration is given in Table 4.6.

Table 4.4 Final fuzzy stabilized matrix

S. No.	Barriers	1	2	3	4	5	6	7	8	9	10	11	D.P
1	Resistance to change	1.000	0.090	0.300	0.063	0.063	0.090	0.300	0.100	0.300	0.090	0.300	2.696
2	Initial cost	0.450	1.000	0.450	0.700	0.210	0.350	0.900	0.270	0.225	0.300	0.225	5.080
3	Lack of experience/talent	0.300	0.300	1.000	0.210	0.210	0.210	0.300	0.210	0.500	0.300	0.500	4.040
4	Compatibility: dependence on other industries	0.350	0.500	0.350	1.000	0.245	0.500	0.700	0.245	0.300	0.350	0.210	4.750
5	Technical limitations	0.450	0.900	0.450	0.700	1.000	0.350	0.900	0.270	0.225	0.300	0.700	6.245
6	Intellectual property issue and threats	0.350	0.700	0.350	0.500	0.490	1.000	0.700	0.490	0.350	0.700	0.343	5.973
7	Management support	0.500	0.210	0.500	0.150	0.210	0.300	1.000	0.300	0.250	0.300	0.250	3.970
8	status of India in R&D towards AM	0.405	0.567	0.500	0.441	0.630	0.630	0.810	1.000	0.450	0.900	0.441	6.774
9	Lack of awareness	0.500	0.170	0.500	0.132	0.189	0.189	0.243	0.300	1.000	0.270	0.700	4.193
10	Lack of government support	0.450	0.630	0.500	0.490	0.700	0.700	0.900	0.700	0.500	1.000	0.490	7.060
11	Technology versus expectation mismatch	0.300	0.050	0.090	0.100	0.031	0.050	0.090	0.031	0.090	0.045	1.000	1.878
Dependence power		5.055	5.117	4.990	4.486	3.978	4.369	6.843	3.916	4.190	4.555	5.159	52.659

Table 4.5 Final binary matrix using fuzzy stabilized matrix

Sr. No.	Barriers	1	2	3	4	5	6	7	8	9	10	11	D.P
1	Resistance to change	1	0	0	0	0	0	0	0	0	0	0	1
2	Initial cost	0	1	0	1	0	0	1	0	0	0	0	3
3	Lack of experience/talent	0	0	1	0	0	0	0	0	1	0	1	3
4	Compatibility: dependence on other industries	0	1	0	1	0	1	1	0	0	0	0	4
5	Technical limitations	0	1	0	1	1	0	1	0	0	0	1	5
6	Intellectual Property issue and threats	0	1	0	1	0	1	1	0	0	1	0	5
7	Management support	1	0	1	0	0	0	1	0	0	0	0	3
8	Status of India in R&D towards AM	0	1	1	0	1	1	1	1	0	1	0	7
9	Lack of awareness	1	0	1	0	0	0	0	0	1	0	1	4
10	Lack of government support	0	1	1	0	1	1	1	1	1	1	0	8
11	Technology versus expectation mismatch	0	0	0	0	0	0	0	0	0	0	1	1
Dependence power		3	5	5	4	3	4	7	3	3	3	4	44/44

Table 4.6 Level classification

Barriers	Reachability set	Antecedent set	Intersection set	Level
Resistance to change	1	1, 7, 9	1	I
Technology versus expectation mismatch	11	3, 5, 9, 11	11	I
Lack of experience/talent	3, 9	3, 7, 8, 9, 10	3, 9	II
Lack of awareness	3, 9	3, 9, 10	3, 9	II
Management support	7	2, 4, 5, 6, 7, 8, 10	7	III
Initial cost	2, 4	2, 4, 5, 6, 8, 10	2, 4	IV
Compatibility	2, 4, 6	2, 4, 5, 6	2, 4, 6	IV
IPR threats and security	4, 6	4, 6, 8, 10	4, 6	IV
Technical limitations	5	5, 8, 10	5	V
Status of R&D in AM	8, 10	8, 10	8, 10	VI
Government support	8, 10	8, 10	8, 10	VI

4.4 Results

Nine clusters have been defined on the basis of Driving Power and Dependence Power as LL, ML, HL, LM, MM, HM, LH, MH, HH, L signifies Lower, M signifies Medium, H signifies High. It is very less likely that a barrier having low dependence and low driving power as well as high dependence and high driving power hence cluster LL and HH are empty. It can be seen in Fig. 4.2: Barrier Classification that barriers are divided in four cluster as LM, MM, HM, MH where LM stands for lower driving power and Medium dependence power. As conceived in the literature Lack of Government Support, India’s status in R&D are in HM cluster and last at level 6 in hierarchy level driving other barriers. Technical limitation, Initial Cost, IPR threats, Compatibility, Lack of awareness, Lack of experience are in MM cluster and ranked as level V, IV, IV, II, II level of hierarchy. Management Support is in MH cluster and at level III in hierarchy. Resistance to change and Technology versus Expectation Mismatch is in LM cluster with very little driving power and considerable dependence power and are at level I in hierarchy. Barriers summary is given by Table 4.7. Fuzzy ISM model is shown by Fig. 4.3.

4.5 Discussion

Final ISM model which is constructed with the help of Fuzzy stabilized matrix clearly shows that Lack of Government support, Status of India in R&D towards AM, Technical limitations are crucial factors in the implementation of additive manufacturing in Indian scenario and these factors are then followed by initial cost, Dependence on other industries, IPR threat, Management Support, Lack of awareness, Lack of

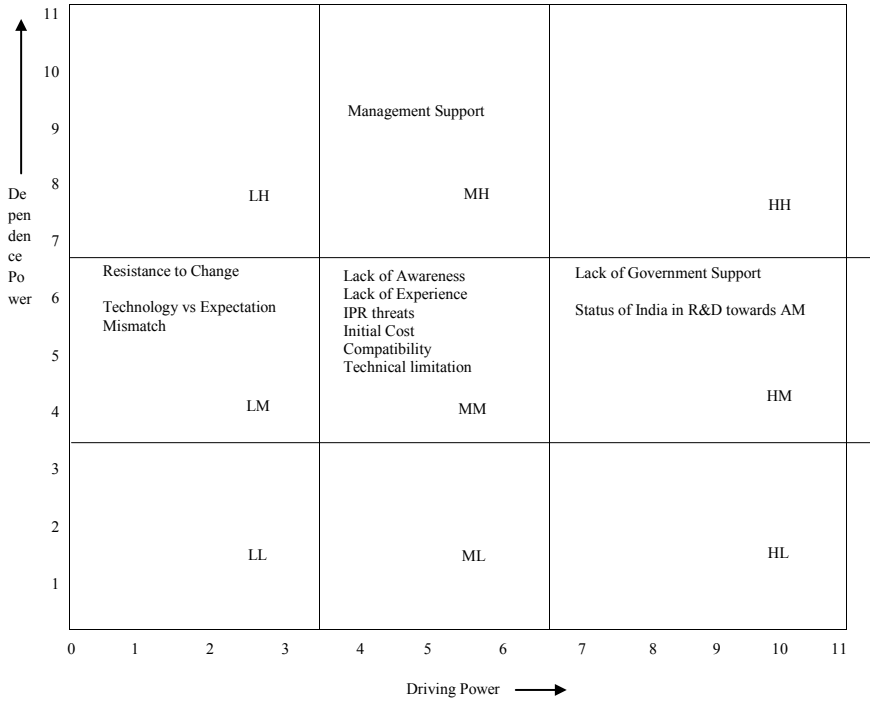


Fig. 4.2 Barrires classification (MICMAC analysis)

talent in AM technology, all these factors combined leads to resistance to change and technology versus expectation mismatch.

Government of India launched FAME (Faster Adoption and Manufacture of Hybrid Vehicle in India) scheme in two phases in order to adopt Electric and Hybrid Vehicle [29], absence of such framework in implementing Additive Manufacturing technology and subsidies provided by government on Industrial level 3D printers and its associated products are increasing its initial cost of investments. Initial cost is also affected by unavailability of experienced worker; management have to invest a large amount on training. Status of India in Research and Development towards AM technologies is also present due to gap between Industries and Institutions. There are also very lesser institutions in India which are providing specialization in AM technologies which leads to the technical limitations of AM technologies and can be minimized if there is active participation between industry and institutions. IPR threats are also needed to be tackled with high IT security system which increases the initial cost of AM implementation. Industries tends to be sceptic about new technologies in their supply chain so an industry which is seeking to adapt AM technology can not apply in its supply chain until other supply chain don't want to. These factors combined leads to less management support. In India only 3% of students who are entering in upper secondary level join vocational or technical

Table 4.7 Barriers summary

Barriers	Driving power	Dependence power	Driving power—dependence power	Rank	Level	Cluster
Resistance to change	2.696	5.055	-2.359	9	I	LM
Initial cost	5.080	5.171	-0.091	7	IV	MM
Lack of experience/talent	4.040	4.990	-0.950	8	II	MM
Compatibility	4.750	4.483	0.266	5	IV	MM
Technical limitations	6.245	3.978	2.266	3	V	MM
IPR threats	5.973	4.369	1.604	4	IV	MM
Management support	3.970	6.843	-2.873	10	III	MH
Status of R&D in AM	6.774	3.916	2.857	1	VI	HM
Lack of awareness	4.193	4.190	0.003	6	II	MM
Government support	7.060	4.555	2.505	2	VI	HM
Technology versus expectation mismatch	1.878	5.159	-3.281	11	I	LM

courses and very less vocational training courses are offered below secondary level and hence due to lack of skill availability, 58% of employers find difficulty in filling the job vacancies. A survey done in Indian Built Sector with 186 stakeholders towards AM concludes that 86.04% people thought that AM is more about prototyping and concept proofing and were not aware about the actual construction process it can carry out [6]. With advanced and cheap technological development in AM it can be vastly used in construction process like making toilets and home at very faster rate.

Departmental and Worker's resistance to change is merely a driving barrier, leads to less management support but a dependent barrier on the above-mentioned barriers. Lack of awareness and lack of experience in AM technologies leads to mismatch between actual technology and expectation.

Various national action plan by different countries like China's Additive Manufacturing Industry Promotion Plan 2015–16 and 2017–20, South Korea's 3D Printing Development Council, United States of America's National Additive Manufacturing Innovation Institute are some classic examples in which government played a key role in the development of AM related technologies, such programs are need of the hour for India. These initiatives can improve the conditions of Research and Development in AM technologies and will lead to reduce technical limitations and initial cost of implementation. Vocational courses at the pre secondary school level can

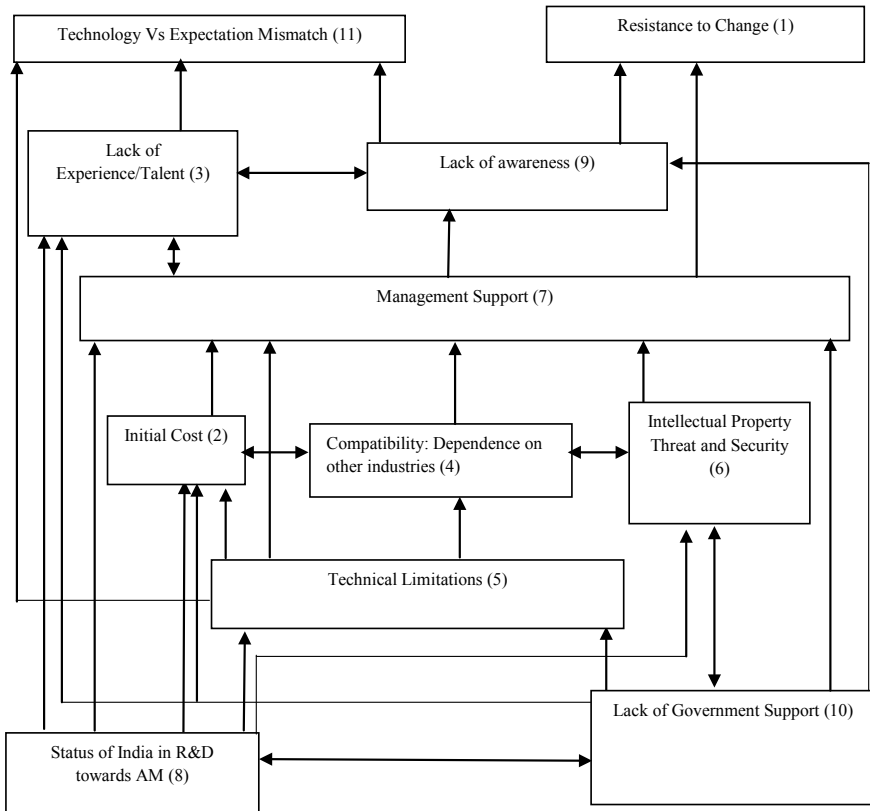


Fig. 4.3 Fuzzy ISM model

also inculcate curiosity and innovation towards technology among students. Technical workshop and short-term courses can be very helpful in industries to make people aware about the technology and filling gap between technology and expectations mismatch. More the worker and organization is aware about the technology and its implication less the resistance they will offer. Additive Manufacturing is also a major part of Industry 4.0 and can help India achieve a leap towards it, all it needs a good framework to implement.

4.6 Conclusion

This study identifies the barriers prevailing in implementation of Additive Manufacturing in India, finds their driving power and dependence power and level them using Fuzzy ISM methodology. Number of researcher and AM industry experts also agree on the point that with the arrivals of AM based startups, AM technologies adoption

is gaining momentum in India but due to absence of national plan of AM implementation like USA, China, South Korea, Japan, this adaptation has not accelerated yet. Government support also leads to decrease in initial cost of implementation. Industries and Universities are needed to collaborate to reduce technical limitation, Industries can help University choose project as per their requirement. To inculcate awareness about technology some workshops can be organized with in the industries about technological changes and its effects frequently so that there will be familiarization with the technology and worker offer less resistance to adopt. Additive manufacturing is being considered as pillar for future manufacturing, we need to eradicate these barriers as fast as we can otherwise there will be loss for Indian Manufacturing sector in long run.

4.7 Limitation and Future Scope

Barriers are selected on the basis of literature, published interviews and articles from different industrial organisations, however some more barriers may exist on the ground level. In this study Fuzzy ISM methodology have been used. Results are based on expert opinions which depends on one's knowledge and expertise in AM technology, which are judgemental in nature. Barriers can also be quantified and more accurate results can be obtained. Different approaches like AHP can also be used to rank the barriers.

This study sheds little light on why these barriers are existing, a separate detailed study can be done on the root cause of these barriers prevailing. A separate study of the solutions of identified barriers can also be performed.

References

1. Johnson, D.: 3D printing the next revolution in industrial manufacturing, pp. 1–10 (2016). <https://doi.org/10.1016/j.micromeso.2014.04.051>
2. Sher, D.: AM global market.pdf (2018)
3. Research, G.V.: AM future forecast.pdf (2018)
4. Frost & Sullivan's Global 360° Research Team: Global Additive Manufacturing Market 2023—Forecast', Frost & Sullivan, May 2016, pp. 20–25 (2016)
5. Sean, M., et al.: 3D printing: disrupting the \$12 trillion manufacturing sector, pp. 1–8. [https://doi.org/10.1364/AO.23.000134\(2017\)](https://doi.org/10.1364/AO.23.000134(2017))
6. Anjum, T., et al.: Purview of 3DP in the Indian Built Environment Sector. *Procedia Eng.* **196**(June), 228–235 (2017). <https://doi.org/10.1016/j.proeng.2017.07.194>
7. Mellor, S., Hao, L., Zhang, D.: Additive manufacturing: a framework for implementation. *Int. J. Prod. Econ.* **149**, 194–201 (2014). <https://doi.org/10.1016/j.ijpe.2013.07.008>
8. Manda, V.R., Kampurath, V., Msrk, C.: 3D printing and its effect on outsourcing: a study of the Indian aircraft industry. *J. Aerosp. Technol. Manag.* **10**, 1–22 (2018). <https://doi.org/10.5028/jatm.v10.862>
9. Panneerselvam, P.: Additive manufacturing in aerospace and defence sector: strategy of India. *J. Defence Stud.* **12**(1), 39–60 (2018)

10. Rogers, H., Baricz, N., Pawar, K.S.: 3D printing services: classification, supply chain implications and research agenda. *Int. J. Phys. Distr. Logist. Manag.* **46**(10), 886–907 (2016). <https://doi.org/10.1108/IJPDLM-07-2016-0210>
11. Berman, B.: 3-D printing: the new industrial revolution. *Bus. Horiz.* **55**(2), 155–162 (2012). <https://doi.org/10.1016/j.bushor.2011.11.003>
12. Sudheer, N., et al.: Implementation of additive manufacturing in educational institutions by enrichment of technology, pp. 7–10 (2017)
13. Kietzmann, J., Pitt, L., Berthon, P.: Disruptions, decisions, and destinations: enter the age of 3-D printing and additive manufacturing. *Bus. Horiz.* **58**(2), 209–215 (2015). <https://doi.org/10.1016/j.bushor.2014.11.005>
14. Yampolskiy, M.: Security of additive manufacturing: attack taxonomy and survey. *Additive Manuf.* **21**, 431–457 (2017). <https://doi.org/10.1016/j.addma.2018.03.015>
15. Dwivedi, G., Srivastava, S.K., Srivastava, R.K.: Analysis of barriers to implement additive manufacturing technology in the Indian automotive sector. *Int. J. Phys. Distr. Logist. Manag.* **47**(10), 972–991 (2017). <https://doi.org/10.1108/IJPDLM-07-2017-0222>
16. Ranipeta, S.S.: 3D printing lacks awareness in India, but can the few startups in this space change that? Accessed From: The News Minute (2017)
17. India: Tracking additive manufacturing industry (2019). Available at: <https://www.maschinenmarkt.international/english/global/articles/839606/>
18. Development, S.: SUMMARY Skill Development for Industry 4.0 (2016)
19. Wohlers, T.: ‘Wohlers Report 2015: Additive Manufacturing and 3D Printing State of the Industry Annual Worldwide Progress Report. Wohlers Associates, pp. 1–34 (2014)
20. The Economist Intelligence Unit: Adding it up: the economic impact of additive manufacturing, p. 24 (2018)
21. Matta, A. K., Ranga Raju, D. and Suman, K. N. S. (2015) ‘The Integration of CAD/CAM and Rapid Prototyping in Product Development: A Review’, *Materials Today: Proceedings*, 2(4–5), pp. 3438–3445. doi: <https://doi.org/10.1016/j.matpr.2015.07.319>
22. Attri, R., Dev, N., Sharma, V.: Interpretive Structural Modelling (ISM) approach: an overview. *Res. J. Manag. Sci.* **2**(2), 3–8 (2013). <https://doi.org/10.1108/01443579410062086>
23. Raj, T., Shankar, R., Suhaib, M.: An ISM approach for modelling the enablers of flexible manufacturing system: the case for India. *Int. J. Prod. Res.* (2008). <https://doi.org/10.1080/00207540701429926>
24. Ansari, M.F., et al.: Analysis of barriers to implement solar power installations in India using interpretive structural modeling technique. *Renew. Sustain. Energy Rev.* **27**, 163–174 (2013). <https://doi.org/10.1016/j.rser.2013.07.002>
25. Kannan, G., Haq, A.N.: Analysis of interactions of criteria and sub-criteria for the selection of supplier in the built-in-order supply chain environment. *Int. J. Prod. Res.* **45**(17), 3831–3852 (2007). <https://doi.org/10.1080/00207540600676676>
26. Sindhu, S., Nehra, V., Luthra, S.: Identification and analysis of barriers in implementation of solar energy in Indian rural sector using integrated ISM and fuzzy MICMAC approach. *Renew. Sustain. Energy Rev.* **62**, 70–88 (2016). <https://doi.org/10.1016/j.rser.2016.04.033>
27. Govindan, K., et al.: Barriers analysis for green supply chain management implementation in Indian industries using analytic hierarchy process. *Int. J. Prod. Econ.*, 1–14 (2013). <https://doi.org/10.1016/j.ijpe.2013.08.018>
28. Kumar, D., Agrawal, R., Sharma, V.: Enablers for competitiveness of Indian manufacturing sector: an ISM-fuzzy MICMAC analysis. *Procedia Soc. Behav. Sci.* **189**, 416–432 (2015). <https://doi.org/10.1016/j.sbspro.2015.03.200>
29. What is FAME India Scheme?—Indian Economy (2019). Available at: <https://pib.gov.in/newsite/PrintRelease.aspx?relid=191377>. Accessed 23 Nov 2019

Chapter 5

Application of 3D Scanning for Reverse Manufacturing and Inspection of Mechanical Components



Kailash Chaudhary and Aditya Govil

Abstract Reverse manufacturing creates another object similar to the existing object. The point cloud data developed with the help of 3D scanning is used for manufacturing of the complex objects. The cost and time of the reverse manufacturing is less than that of the conventional methods. 3D scanner is an important part of 3D printing ecosystem which is playing most important role in latest research in mechanical engineering. The advantage of 3D scanner consists of ease of use, which derives from the shorter scanning duration and the less demanding skill requirement of the operator. Another advantage of the 3D scanning consists in the higher number of acquired surface points which statistically leads to more accurate description of complex parts. For example, mechanical parts like naval vessels, submarines, weapon systems, engines and hulls do not have 3D CAD files and they can be repaired with the help of 3D scanner in a very efficient and easy manner. 3D scanned data is directly used to make changes in programming of artificial intelligent based welding and machining processes. A lot of time and in turn money can be saved using this advanced technique because traditional measurement methods like callipers, rulers etc. consume time and skill. In this research work, reverse manufacturing is applied to propellers of a local aero model manufacturer. It was found that use of 3D scanners in combination with Coordinate Measuring Machine (CMM) helps in measurement of the features with good quality and accuracy in a very short span of time. Results based on comparison of reverse manufacturing with traditional method related to dimensional accuracy and mechanical properties will be presented in full paper.

Keywords Reverse manufacturing · 3D scanning · 3D printing · CMM · Dimensional accuracy · Mechanical properties

K. Chaudhary (✉) · A. Govil
Department of Mechanical Engineering, M.B.M. Engineering College, Jai Narain Vyas University, Jodhpur, India

5.1 Introduction

Reverse engineering creates another object similar to the existing object. Objects having free formed surfaces can only be reverse engineered with the help of 3D scanning. The point cloud data developed with the help of 3D scanning CAD model is used for manufacturing these types of objects. The cost of the reverse engineering is less than the cost of conventional methods. Even the time required to manufacture an object by reverse engineering incorporating a 3D scanner is just a quarter of the time required by conventional methods. 3D scanner is a most important part of 3D printing ecosystem which is playing most important role in latest reverse engineering scenario.

The advantage of 3D scanner consists of ease of use, which derives from the shorter scanning duration and the less demanding skill requirement of the operator. Another advantage of the 3D Scanning consists in the higher number of acquired surface points which statistically leads to more accurate description of complex parts like aerofoil along with the blade root. Similarly, it can be used effectively to acquire the entire trailing edge of the gas turbine geometry. Using 3D scanners in combination with coordinate measuring machine (CMM), the mechanical part model can be measured with most features with good quality and accuracy in a very short span of time. Parts that are fragile are easily inspected with the help of 3D scanning technology because it is non contact type inspection. Some parts which have burrs, flatness and roundness error are also problematic with CMM and other conventional methods but for 3D scanners these are just a matter of seconds to give accurate results.

It is the process of creating a computer model of an object that exactly replicates the form of the object. Laser scanners are used to capture the 3D data of the object, and this data is transferred to the computer where it is aligned, edited and finalized as a complete 3D model.

Advantages of digital modelling are:

- Digital Modelling generally offers a faster and more cost effective solution.
- It presents a great solution for creating solid models when an object has organic contours.
- Offers excellent dimensional accuracy and can be utilized for comparative analysis.
- Rapid NURBS Dumb Solid models can be utilized as a base for design work.
- Digital models can be visualized in rendering software as a solid object, which is great for seeing the overall shape and contour of the model.
- It saves digital monuments without any depreciation for infinite time.
- These digital models are great source of information which can be used for training and research purpose.

Table 5.1 List of main criteria and sub criteria for application of 3D scanning in field of inspection and reverse engineering

Code	Criteria	Sub criteria	References
QC	Quality control	Quick response industries	[1]
RE	Reverse engineering	3D modelling; CAD reconstruction	[2]
AM	Additive manufacturing	Time and cost of final products	[3]
AA	Automotive application	Rapid prototyping	[4]
IN	Inspection	Dimensional measurements	[5]
ST	Scanning technology	3D scanning; automotive application	[6]

5.2 Research Background

Applications of 3D scanning technologies show potential for the diverse application in the materials and manufacturing field. Recently 3D scanning technology is developing to ensure that they can be used by both new and experienced users alike for multiple applications providing most seamless workflow yet. 3D scanning is one of the fastest, safest, and most cost effective ways of achieving high quality 3D models of all kinds of objects [7]. These devices are highly user friendly and portable so that user can have full opportunity to take advantage of the working environment and high end technology available. The application of 3D scanning in field of inspection and reverse engineering has been shown by various authors under different criteria in different industries has been presented in Table 5.1.

5.3 Research Methods

5.3.1 Theory of Proposed Work

Reverse engineering is a kind of engineering which takes full advantage of an Existing object. The main objective is to produce another object similar to already create part. For this we need to have complete information about the existing object. This information can be collected efficiently with the help 3D scanner. In this dissertation our aim is to describe the use of 3D scanner in Reverse engineering. Data collected from the scanner is utilized in different software. These softwares help us to create mesh, repair it, and orientate it and to define the position of mesh. So designs of the components can also be modified while reverse engineering. In this way we can not only save our time but also our valuable resources which are spent in developing designs and modifications. After 3D scanning and manipulating the data obtained with it the object is then 3D printed with the help of 3D printer. Technology used in 3D printer nowadays is called fused filament modelling. Material used in this technology is not only cheap but can also be recycled which can further lead to cost effectiveness.

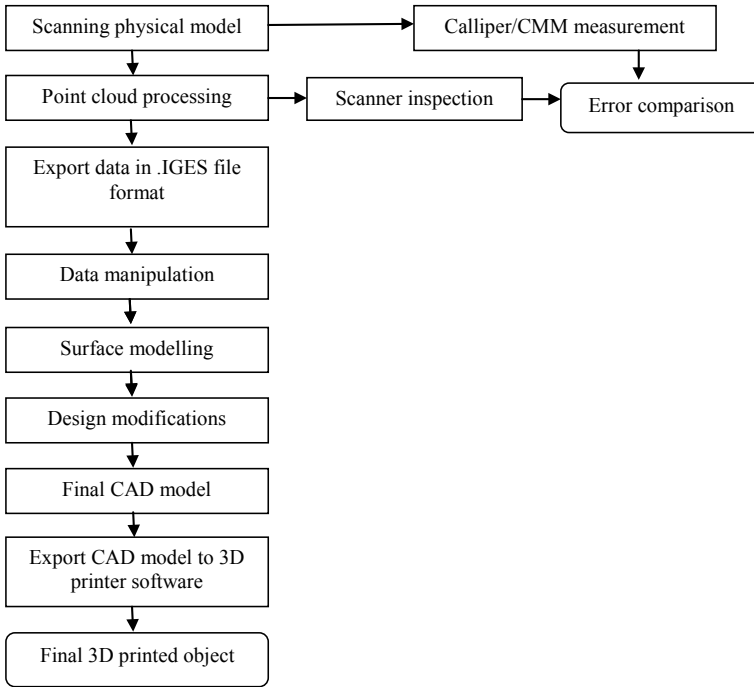


Fig. 5.1 3D scanning process and its application in inspection and reverse engineering

Some materials which are used in 3D printing are acrylonitrile butadiene styrene (ABS), polyamide (nylon), polylactic acid (PLA), wood, stereolithographic materials (epoxy resins), wax, silver steel, photopolymers and photo carbonates. But in this study only nylon and PLA were used to print the final mechanical components. PLA is the cheapest material among all the material available in the market whereas nylon is a much costlier along with better materialistic properties (Fig. 5.1).

5.3.2 Flow Chart of Proposed Work

5.4 Case Study

To exemplify the application of proposed framework, propeller of a RC plane is considered which is presently being manufactured by injection moulding by Sharma aero models Pvt. Ltd. Jodhpur, India. Since these propellers rotate at extraordinary rates so they are subjected to high risk of failure and due to which these propellers remain in good demands from the customers throughout the year. Firstly, company did not have the CAD model of the propeller so they wanted to have the digital model of

the propeller for design purpose. Secondly, company was facing several customized demands of the propeller and company was unable to fulfil these demands as it was not economically viable to make multiple moulds to serve variety of demands in countable numbers hence company decided to adopt method of reverse engineering to cater demands. Major modification which has been done in this work is that two rotor propeller was scanned and modified into three rotor propeller in addition of reverse engineering of two rotor propeller. Moreover to assess the application of 3D scanner in field of inspection same propeller was also inspected with callipers/CMM. The measurements obtained were also verified by the dimensional results obtained with the help of 3D scanner.

5.4.1 Scanning of Propeller

The Einscan-SE shining 3D scanner was used in this study utilizing structured light technology to provide a fast and extensive capture of complex surfaces. Millions of points are captured from the surface of the object in a single view. Each scan consumed 8 s t capture a single view and so propeller was scanned in total eight scans to capture full geometry of the propeller under auto scan mode. Before scanning scanner was calibrated to detect the position of camera and projector in relation to the object so as to obtain actual camera parameters and get more accurate results. It is all done with the help of a calibration board fixed on a holder over the turntable and if its successful only than scanning is started. A total of 3.5 min took to scan whole propeller out of which 2 min was consumed in calibration and 1.5 min or completing scanning of the propeller (Figs. 5.2 and 5.3).

As the propeller is made up of Nylon glass filled material surface of propeller reflects light and so to get the right point cloud information it was painted with a developer spray. The final scanned propeller is shown in below image. Propeller is one of those devices having the most complex geometry because there is change in



Fig. 5.2 Original propeller to be scanned



Fig. 5.3 scanner and calibration board

the slope of the rotor as we move away from the hub of the propeller. Even the hub has a varying internal section like a nozzle. Initially we tried to scan the propeller with the help of a low cost 3D scanner but this attempt did not work because to scan such complex designs it is needed to rotate the scanner 360 °C around the object without disturbing the position of scanner and the object. So a low cost scanner can always be used for objects having simple prismatic design features. Finally Ein scan-SE shining 3D scanner was used to complete the scan of the propeller. This is a structured light 3D scanner having a automatic turntable to rotate the object round the clock to have a fast and extensive capture of complex surfaces. In each scan the scanner capture millions of points from the surface of the object. Before scanning the object it is needed to input the number of scans the user wants to do in one complete round of the turntable. So the scanning of the propeller was done in total 8 steps so as to capture each and every point present on the surface of the propeller (Fig. 5.4).

5.4.2 Generation of CAD Model from the Scanning Data

The scan data obtained finally is not the exact copy of the surface of the physical model due to presence of holes and damages on the surfaces. The scan data was saved in IGES file format so that it can be edited to construct the CAD model. In this study ProE was the software used to transform the point cloud data into a conceptual surface model.

Following points were followed to obtain an accurate 3D model:

- Converting triangular meshes into polygonal meshes.
- Cleaning abnormal polygon meshes.
- Creation of a global wireframe that encompasses all individual patch boundaries that have no practical use in final model.
- Redefining the surfaces by smoothing.



Fig. 5.4 Scanned propeller

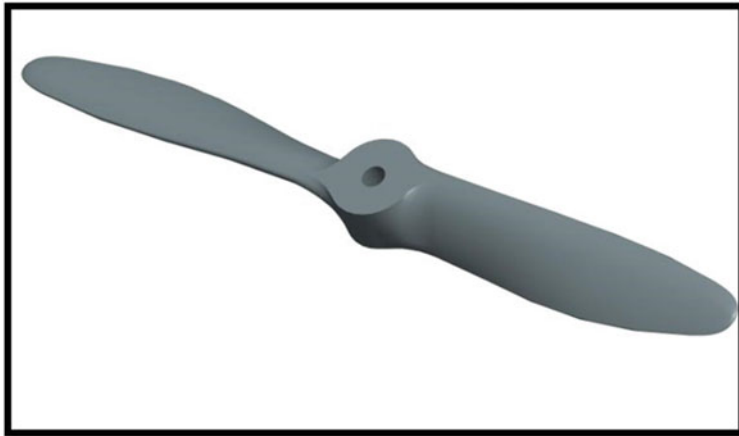


Fig. 5.5 Final CAD model

- Removal of holes that are formed because of regions not captured by 3D scanner.
- Achieving a structure as close as possible to the set of geometrical features of original object (Fig. 5.5).

5.4.3 Modification in Design of CAD Model

Since CAD model now has been successfully obtained without any need of any skilled designer we can also make some modifications in design as per our requirements. The main aim is to add one more rotor blade to the propeller according to



Fig. 5.6 New modified propeller having three rotors

the need of the company. This whole process was completed by the software ProE in couple of hours with the help of powerful editing tools in the software. Complete editing was done in 1.5 h. This was the final model generation step and so it is needed to keenly confirm with 3D data. It was easily completed with low user skill and low computational burden which shows the usefulness of reverse engineering. This is one of the greatest advantage of this technology that there is always a possibility of modification in design after generating the use of die get eliminated which helps to save a big amount of initial investment done by the company and on other side customized requirements of customers are also get fulfilled without spending any huge amount. These applications enable product optimization to improve the final product quality and to increase the competitiveness of the products. Following Fig. 5.6 shows the three rotor propeller made by modification in scanned data during designing.

5.4.4 3D Printing of Propeller

After the 3D surface representation of an object is generated, the next step is to create a model using rapid prototyping. This process comprised two steps: (1) convert the model into STL (standard triangle language) format which is the standard model format for rapid prototyping machines and printers and (2) slice the model for rapid prototyping operations. The software has a module which converts STL file into a part program. The STL files consist of normal and vertices coordinates of every triangle on the surface in form of a set program. In this work a 3D printer is employed to

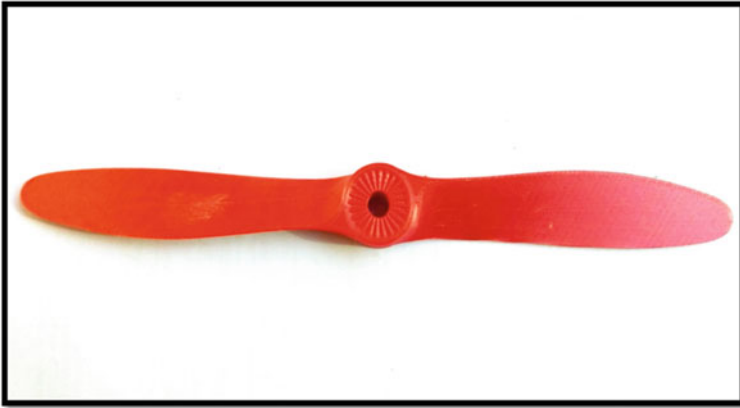


Fig. 5.7 Final 3D printed propeller

manufacture the propeller that run on fused deposition modelling technology. Before manufacturing the STL file is imported into slicing software which generates the tool paths of 3D printer by generating G codes which contains required instruction given by the user for the extruder. In this work software named CURA is utilized in combination with 3D printer of ENDER company to 3D print the propeller. In this work a red coloured filament of PLA (polylactide) was used to 3D print the propeller. Final 3D printed propeller is shown in Fig. 5.7.

5.4.5 Inspection

Inspection adds to the cost of manufactured component so it shows how worthy it is to search other ways of inspection different from traditional methods. Low cost high volume objects require little inspection but on the other hand high cost low volume objects like airplanes, turbines, dies etc. require an efficient way of inspection. Inspection can also be fully automated with the help of 3D scanners. The number of workers employed in a firm can be reduced significantly. Coordinate measuring machine (CMM) is a mechanical method to measure components which have its own limitations also. 3D scanners eliminates almost all of these limitations. In this paper there has been showed that how future of inspection control technology can be overridden by 3D scanners. Following Fig. 5.8 shows the inspection results obtained by a 3D scanner.

A CMM measuring machine can have errors along 6 different axes. This means that accurate calibration is needed to be done every time before taking the measurements so that errors can either be fixed or integrated into the data. Measurement from CMM is done after successful calibration. The part to be measured is firmly clamped on the worktable so that when probe of CMM touches the part there should not be any

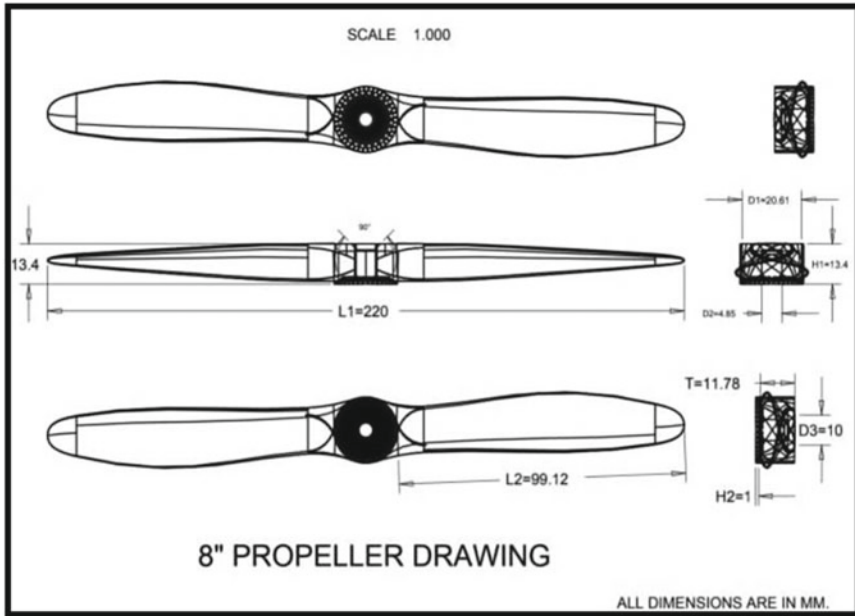


Fig. 5.8 Inspection results obtained by 3D scanner

vibration and movement in part which can disrupt the results. Parts to be measured are clamped in such a orientation such that probe can reach to maximum dimensions because change in part orientations causes errors. Minimum will be the orientation maximum will be the accuracies in the measurement results. Dimensions like length, cylindricity, angularity etc are measured with the help of respected modules in the software of CMM. Results obtained are instantly displayed and saved in the computer automatically. Figure 5.9 clearly shows the measurement of the propeller in the CMM.

5.5 Results

5.5.1 Results for Reverse Engineering

The procedures how these results are obtained are described in detail above. These results clearly describe the advantages and shortcomings of employing reverse engineering in a industrial firm. Sharma aero models Ratanada, Jodhpur was also involved in this work to provide some traditional manufacturing details about injection moulding process.



Fig. 5.9 CMM (Mitutoyo Crysta M574 plus)

Two Rotor Propeller

See Table 5.2.

Three Rotor Propeller

To manufacture three rotor Propeller company has to prepare a new mould which cost it to 60,000 Rs. and further some variable charges also are added to the final cost. Moreover according to the company Sharma aero models Ratanada, Jodhpur demands of three rotor propellers is limited to less than 40 units per year. This one of the main reason that company has to refuse customers of three rotor propellers because company cannot afford production of three rotor propeller with a costly mould for such a low demand of products. But if these types of propeller are

Table 5.2 Results for two rotor propeller

S. no.	Parameters	Injection moulding	Reverse engineering
1	Time elapsed to manufacture one propeller	1 h	4 h
2	Material employed	Nylon	PLA
3	Cost of material per unit gram	18 Rs.	9 Rs.
4	Cost of manufacturing one unit of propeller when production is less than 2.5 thousand units	180 Rs.	100 Rs.
5	Cost of manufacturing one unit of propeller when production is more than 2.5 thousand units	80 Rs.	100 Rs.

Table 5.3 Results obtained for three rotor propeller

S. no.	Parameters	Time (h)	Material used	Total cost incurred per part
1	Time elapsed in preparation of part to be scanned	0.025	PLA	200 Rs.
2	Time elapsed in calibration of the scanner for scanning	0.041		
3	Time elapsed in scanning of the propeller	0.16		
4	Time elapsed in generation of CAD model	1		
5	Time elapsed in 3D printing of the propeller	5.25		
6	Time elapsed in finishing the solid 3D model with a sand paper	0.5		
7	Total time elapsed to prepare the propeller	7.05		

produced with the help of reverse engineering employing a 3D scanner than following interesting results were obtained (Table 5.3).

5.5.2 Inspection with 3D Scanner

The second part of this work is based on comparing the dimensions of the propeller by inspecting with a CMM, vernier calliper and 3D scanner. Same scanner used in reversed engineering is employed here to obtain the results related to inspection. Inspection with 3D scanners can be automated easily with assembly line which is not possible with large coordinate measuring machines which are very costly also. So inspection with scanning helps to reduce work force employed in inspection and also helps to decreases cost of the product. Results successfully prove that 3D scanners measures dimensions in very less time with accurate results. Comparison of the inspected dimensions of a propeller with callipers and 3D scanner is shown in Table 5.4.

Comparison of dimensions of propeller with CMM and 3D scanner is shown in Table 5.5 which clearly indicates that 3D scanners have accuracy almost equal to coordinate measuring machines. Apart from accuracy 3D scanners offer various other capabilities such as portability, flexibility, low cost, faster results, less demanding skills, better connectivity with softwares and compatibility with modern world industry 4.0.

Table 5.4 Inspection results with 3D scanner

S. no.	Notation	Dimension name	Dimensions with 3D scanner (mm)	Dimensions with calliper (mm)	Actual dimensions (mm)
1	L1	Length of propeller	202.5	203	203
2	L2	Length of each blade	89.12	89.35	90
3	D1	External diameter of hub	20.61	20	20
4	D2	Internal diameter of hub on back side	4.85	5	5
5	D3	Internal diameter of hub	10	10	10
6	H1	Total height of propeller hub	13.4	14.2	14
7	H2	Height of teethes on hub	1	1	1
8	T	Height of hub without teethes	11.78	12	12

Table 5.5 Inspection results from CMM and 3D scanner

S. no.	Notation	Dimension name	Dimensions with 3D scanner (mm)	Dimensions with CMM (mm)	Actual dimensions (mm)
1	L1	Length of propeller	202.5	203.2425	203
2	L2	Length of each blade	89.12	90.2325	90
3	D1	External diameter of hub	20.61	20.0054	20
4	D2	Internal diameter of hub on back side	4.85	5.0045	5
5	D3	Internal diameter of hub	10	9.89009	10
6	H1	Total height of propeller hub	13.4	14.0801	14
7	H2	Height of teethes on hub	1	1.0002	1
8	T	Height of hub without teethes	11.78	11.8900	12

5.6 Conclusion

3D optical scanning technology can deliver accuracy for complex machine parts used in various industrial sectors and how reverse engineering can be useful for manufacturing from existing products. These studies about reverse engineering and inspection with help of 3D scanner clearly demonstrate their potential application in field of production and Industrial technology. Reverse engineering is one of the best forms to manufacture prototypes or short productions.

The first part of this wok demonstrates how successfully the propeller is made with the help of reverse engineering. Not only a two rotor propeller but also a three rotor propeller three rotor propeller is made without any help of design engineer. If the company makes this propeller with help of 3D printing than it would be more economical if total production is less than 2500 units of propeller which is clearly observed in above graph (Fig. 5.10). In injection moulding process initial cost per unit is high before a certain threshold because of the mould cost. Therefore if number of units produced is not above that threshold company has to bear loss only. Moreover a lot of designing time is also saved while employing a reverse engineering which helps to increase the speed of product delivery in the market as well.

The second part of this work is based upon inspection of propeller dimensions with the help of a 3D scanner. Scanners have immense potential to replace traditional measuring devices like coordinate measuring machine, callipers etc. because of their flexibility to integrate with the assembly lines in production firms. 3D scanners are best to fulfil the demands of modern manufacturing environment to achieve quality and quantity both. Above Fig. 5.11 graphically shows the comparison of results obtained by 3D scanner and CMM with respect to the actual dimensions of the propeller. Results obtained indicate that 3D scanners and CMM have not

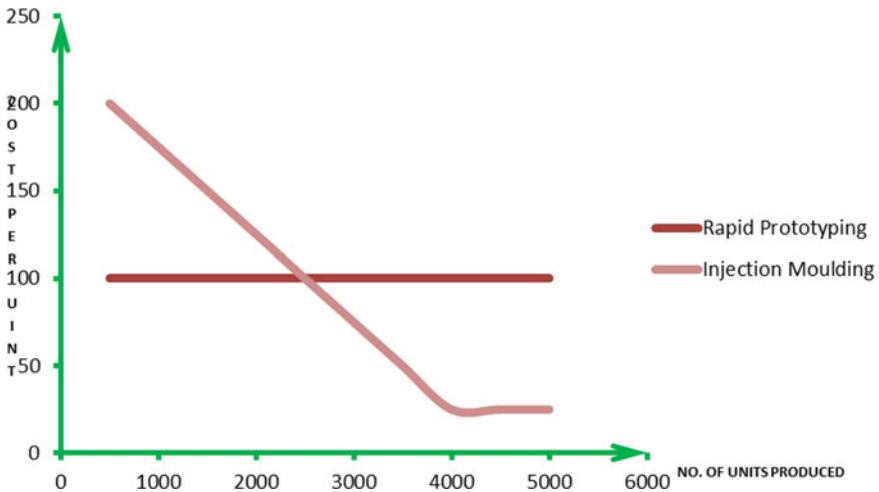


Fig. 5.10 Graphical description of conclusion

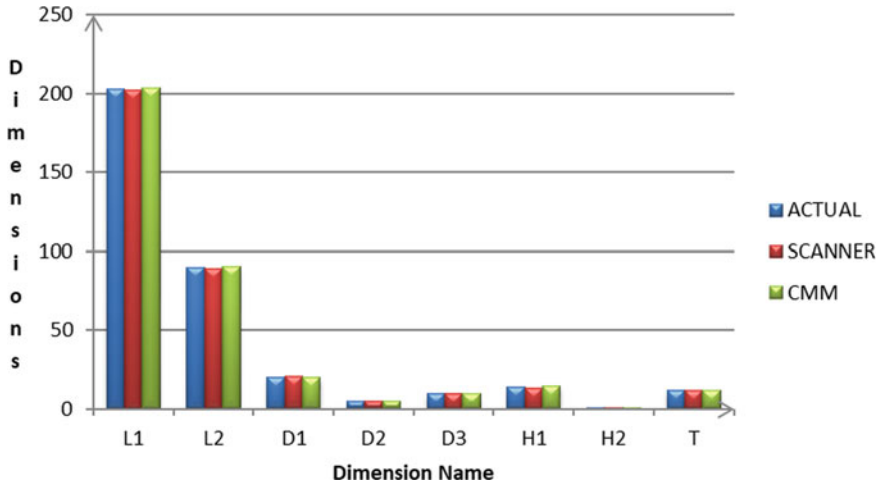


Fig. 5.11 Graphical description for inspection results

much difference in the measurement values. In addition of such good measurement capabilities like CMM scanners also have flexibility, portability, accuracy and speed which make them useful in industry 4.0 in future.

L1	Length of propeller	D1	External diameter of hub	D3	Internal diameter of hub	H2	Height of propeller hub
L2	Length of each blade	D2	Internal diameter of hub on back side	H1	Total diameter of propeller hub	T	Height of hub without teeth

Advantages of the above approach can be summarized as follows:

- The ease and speed of acquiring information from the product.
- The ability of to reconstruct the data using multiple surface patches.
- The advanced processing features of the software which enables modifications in design of the product with minimum skill requirement in addition to reverse engineering.
- The compatibility with different software packages available.
- Minimum wastage and maximum usage because here manufacturing technique involved is a additive process.

References

1. Yao, A.W.L.: Applications of 3D scanning and reverse engineering techniques for quality control of quick response products. *Int. J. Adv. Manuf. Technol.* **26**, 1248–1288 (2005)

2. Buonamici, F., Carfagni, M., Furferi, R., Governi, L., Lapini, A., Volpe, Y.: Reverse engineering modeling methods and tools: a survey. *J. Comput. Aided Des. Appl.* 1–29 (2017)
3. Paulic, M., Irgolic, T., Balic, J., Cus, F., Cupor, A., Brajhih, T.: Reverse engineering of parts with optical scanning and additive manufacturing. In: *Conference on Intelligent Manufacturing and Automation*, vol. 69(2014), pp. 790–803
4. Sansoi, G., Docchio, F.: Three dimensional optical measurements and reverse engineering for automotive applications. *J. Robot. Comput. Integr. Manuf.* **20**, 359–367 (2004)
5. Matache, G., Dragon, V., Puscasu, C., Vilag, V., Paraschiv, A.: A comparison between 3D scanning and CMM dimensional inspection of small size gas turbine. *Bull. Transilvania Univ. Brassov* **4**(53), 1–7 (2011)
6. Kus, A.: Implementation of 3D optical scanning technology for automation application. *J. Sens.* **9**, 1967–1979. ISSN 1424-28220 (2009)
7. Varady, T., Martin, R.R., Cont, J.: Reverse engineering of geometric models- an introduction. *J. Comput. Aided Des.* **29**(4), 255–268 (1997)

Chapter 6

Optimization Techniques for Response Predication in Metal Cutting Operation: A Review



Rajeev Sharma, Binit Kumar Jha, and Vipin Pahuja

Abstract At the Present time speedily changing in manufacturing industries, so optimization techniques is use for response predication in metal cutting operation. Now a day's increasing demand of quality of product. These all types of optimization techniques play important role in quality and productivity. In this paper show a review about both types of optimization techniques such as conventional and non-conventional optimization techniques. Many types of conventional optimization techniques are used for optimization of machine parameters included dynamic programming, goal programming, linear programming, sequential unconstrained minimization technique, simplex method etc. And the latest optimization techniques included Taguchi design, Response surface method (RSM), Fuzzy logic system (FLS), Genetic algorithm, Scatter search techniques, Partial Swarm optimization (PSO), Multi optimization genetic algorithm etc.

Keywords Parameters optimization · Linear programming · Genetic algorithm · Taguchi design · Response surface method

6.1 Introduction

Today, Metal cutting is assume significant part in designing ventures. In this exploration of metal cutting centers, input measure boundaries and highlights of apparatuses setting influence proficiency of cycle and reaction. The cycle of parametric improvement is utilized for upgrade in cycle effectiveness through break down and figure out which information factor influence reaction **Montgomery** [1].

The robotization of metal cutting cycle has grown really after some time because of increase from many part of designing with accomplishing higher machining execution [2]. In this paper numerous kinds of demonstrating strategies and execution of these procedures dependent on relapse investigation [3], fluffy rationale technique [4] and ANN (fake neural organization) (fu 2003). In this articles examined

R. Sharma (✉) · B. K. Jha · V. Pahuja
Department of School of Manufacturing Skill, Bhartiya Skill Development University, Jaipur,
India
e-mail: Rajeev.sharma@ruj-bsdu.in

Taguchi streamlining strategy [5], Mathematical programming [6], RSM (Response surface technique) (Motogomery, 2001), Simulated toughening [7] and GA (Genetic Algorithm) (Goldberg 2002). Execution of advancement strategies in genuine—life cutting cycle, these procedures have numerous restrictions and suspicions are concentrated in writing [8].

In this exploration shows that a model for multi-pass turning activity and for profundity of cut unique writing computer programs is utilized [9]. In this articles populace—based method PSO is created [10]. Issues are acknowledged in finding the experimental exhibition conditions for cutting edge Tool plans in light of the fact that these are covered up under automated information bases in restrictive programming [11], as verified in late examinations [12]. In this articles, critically review of optimization techniques for metal cutting process. A universal plan/structure for optimization of process parameters study in metal cutting mechanism.

6.2 Literature Review

6.2.1 *Conventional Optimization Techniques*

Prasad et al. [13] in this paper research completed for deciding the cycle boundaries in turning activity and build up a streamlining module. The target of this examination is minimization of creation. The straight and mathematical programming strategies are utilized for settling detailed models. Gopalakrishan and khayyal [14] have talked about a logical device that's utilized for determination of machine boundaries in turning activity. In this examination, mathematical writing computer programs is utilized for minimization the complete expense of machining and ISPO-10 evaluation utilized as device.

Hinduja et al. [15] in this examination, dissected such sort of condition whose have max. Creation and minimization of unit cost in turning activity. In this exploration ideal outcome was limited to a feed rate to profundity of cut by chip slowing down limitations. Some of different factors included force, mathematical exactness and surface unpleasantness (SR). Sundaram [16] fine turning activity AISI 4140 steel and solidified carbide utilized as a device. What's more, in this exploration objective writing computer programs is utilized for choice of cycle boundaries. Ermer and kromidiharajo [17] this exploration, for taking care of issues identified with multi pass machining and for this issue a numerical model was created. They utilized steel as HSS and carbon steel as work piece. Petropoulos [18] mathematical improvement programming strategies is utilized for ideal cutting boundaries, for example, speed and feed rate.

Brewer [19] in this examination finds that cutting force is more compelling boundary with unit cost by utilizing Lagrangian multipliers streamlining method. Bhattacharya et al. [20] has investigated unit cost for turning activity and cycle boundaries, for example, cutting force and surface unpleasantness improvement by utilizing

Lagrangian strategy. Walvekar and Lambert [21] upgraded feed rate and reducing speed for least creation expense by utilizing mathematical programming. Gilbert [22] in this paper contemplated, improvement of cycle boundary with min. creation rate and greatest creation rate. Armarego and Brown [23] have advancement machine boundary by utilizing differential count. Taylor [24] diverse logical and exploratory methodology for advancement of machine boundary has been researched.

6.2.2 Latest Optimization Techniques

6.2.2.1 Taguchi Method

See Table 6.1.

Process of Taguchi Optimization Techniques

See Fig. 6.1.

6.2.2.2 RSM (Response Surface Method)

Gianni Campatelli et al. [32] in this paper focused on minimization of power consumption in a milling process on a modern CNC (computer Numerical Control) machine. The experiments were investigation to evaluate and optimization of process parameter such as depth of cut, cutting speed and the axial by using response surface method. All the experiment was complete by dry lubrication. Tung-Hsu et al. [33] in this paper research on nano particles. A Nano particle is produce through wet milling machine. In this research, process parameter is optimization by Taguchi, RSM and GA integrated and fined optimal process parameter.

Nanda et al. [34] in this paper, experimental work conducted by abrasive jet machine. The parametric optimization of process parameter to box-behnken design of RSM with output parameter such as SR, MRR and flaring dia. The result was validate by SEM. Raman Kumar et al. [35] this research work carried out on sustainable manufacturing process with minimization of energy consumption, optimal surface roughness and better MRR. The designs of experimental were conducted on EN 353 alloy steel with tungsten carbide insert used as a tool. The optimization of process parameter such as feed rate, cutting speed, depth of cut and noise radius with repose parameter such as MRR, SR.

Amran et al. [36] this research have investigated of process parameter in drilling process and optimization of process parameter by RSM. Experimental work was carried with 20 set of experiment. These process parameter such as (feed rate, drill diameter, spindle speed). After this optimization, find that spindle speed is more effective parameter compare to other.

Table 6.1 Literature review on Taguchi method

S. No.	Author	Research
1	Tlhabadira et al. [25]	In this research, experimental investigation on milling machine by using Taguchi optimization technique and Autodesk fusion. In this research optimization of process parameters such as feed rate, cutting speed, depth of cut with surface roughness. Experimental were conducted on M00TS as w/p material and DMC635V DMG ECOLIVE, Siemens 810D, CNC vertical milling machine and carbide insert
2	Vikas Sharma et al. [26]	Purpose of this research is that find optimal process parameter for single and multi-optimization resulting in an optimal value of MRR (metal removal rate) and tool wear. The experiments were completed on inconel 718 and copper cadmium as a tool
3	Nimo Singh et al. [27]	In this paper, described about optimization of process parameters such as current, electrolyte concentration, feed rate and flow rate of electrolyte concentration with response parameter such as Surface roughness (SR) and MRR (metal removal rate) by using taguchi method. And find out that electrolyte concentration is more effective parameter
4	Krishna Kumar et al. [28]	In this research paper, optimization of process parameter of micro Electro discharge machining by Taguchi orthogonal array. The micro machining is complete on SIC material. XRD, SEM and EDX technique were analyzed for study of micro EDM characteristics
5	Sanchit Kumar et al. [29]	In this paper focused on better surface quality of w/p in micro machining operation. For this surface finish, optimization of process parameter through Taguchi orthogonal array technique. And it was see that diameter of tool & pulse rate these parameter is more effective parameter
6	Hanen et al. [30]	In this paper, optimization of process parameter such as ball of mass, velocity of disc, powder of mass and the time of timing on mechanosynthesis of hydroxyfluorapatite by using Taguchi optimization method
7	Rasik Upadhye and Ishwar Pkeswami [31]	In this paper research carried Out that optimize process parameter of casting manufacturing. The optimization of process parameters is complete by maximization S/N ratio and min. noise factor through Taguchi method

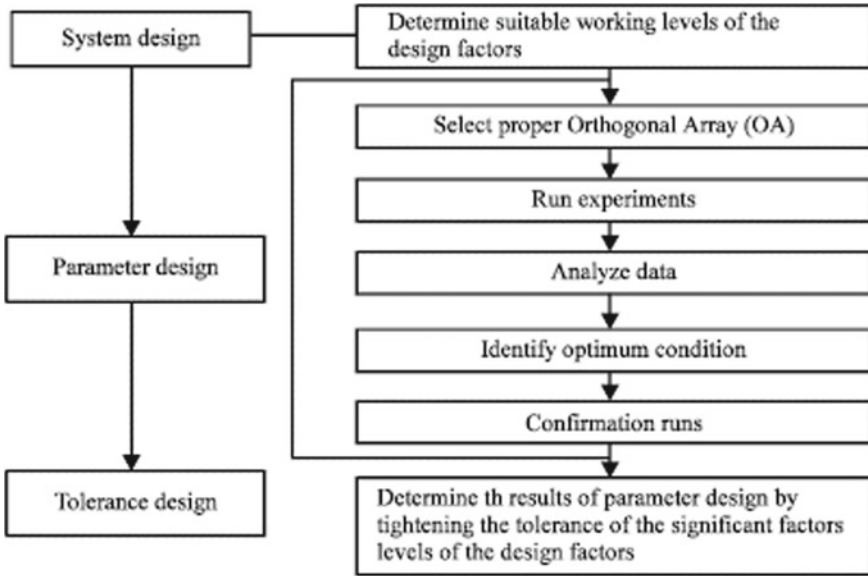


Fig. 6.1 Shown flow chart of Taguchi Method

Carmita Camposeco-Negrete [37] this research paper present experiment works on turning of AISI 6061 T6 aluminum. The main purpose of this research that minimization of energy consumption and maximization of MRR. The optimization of process parameter by CCD (Central composite design) and find that feed rate is more significant process parameter. Daramola et al. [38] the purpose of this research, optimal cutting condition (Maximization of MRR and Lower surface roughness). L50 experiments set were designed in Minitab and optimization by RSM and Taguchi method.

Huawei Song et al. [39] in this article, parametric examination of feed rate, shaft speed, laser pulse and profundity of cut with output parameter, for example, is cutting force. After the trial work, results advancement through Taguchi and Response surface technique (RSM) and found that RSM improvement strategy instigated relative less cutting force. Table 6.2 indicating list of parameters and level.

Table 6.2 List of parameters and level [39]

Parameters	Notation	Level-1	Level-2	Level-3	Level-4
Feed rate (f)	A	0.24	0.28	0.32	0.36
Spindle speed (v)	B	420	480	540	600
Depth of cut (a _p)	C	16	20	24	28
Pulse (p)	D	40	44	48	52

Table 6.3 Level of machining parameters [40]

Input parameters	Level-1	Level-2	Level-3
SOD	1	1.5	2
Flow rate	60	120	180
Speed	100	150	200
Pressure	200	300	400

Selvam et al. [40] in this paper parametric optimization through Response surface method (RSM) under following parameters which showing in Table 6.3.

With output parameter which is related to quality characteristics. After the optimization, it was observed that optimal process parameters within the selected range: traverse abrasive flow rate of 115 g/min, SOD of 1 mm, speed of 145 mm/min and water pressure of 200 MPa.

Asit Kumar Parida and Kalipada Maity [41] in this examination, the hot turning of Monel-400 has been performed to explore the impact of four machining factors (cutting velocity, feed rate, profundity of cut and work piece temperature) on flank wear and surface harshness. The work piece has been warmed with a combination of oxygen and fluid oil gas. The examinations have been done dependent on face centered composite design (CCD). Response surface system (RSM) has been utilized to play out the numerical displaying of flank wear and surface unpleasantness. The impact of individual boundary on reactions has been assessed utilizing ANOVA examination. The anticipated model for flank wear and surface harshness acquired from the relapse condition shows great concurrence with the examination results. A greatest mistake of 13% and 7% of flank wear and surface harshness has been seen between the reproduced and trial results separately.

Amit Kumar et al. [42] in this examination, machinability of Inconel 825 by Graphenenano powder blended EDM has been explored. Three response parameters in particular material expulsion rate (MRR), Tool wear rate and Ra have been recognized to assess measure execution. Response surface Method (RSM) has been utilized to direct the investigation. It has been seen that MRR, SR and TWR are generally impacted by top current (IP), GV and pulse on schedule. Further, surface morphology of the produced surface has been examined by taking FESEM pictures, which shows a similarly better surface.

Amran et al. [43] this paper examines the impacts of penetrating parameters, for example, feed rate, drill diameter and spindle speed across on a superficial level harshness and surface of bored opening by applying RSM. There are three components under scrutiny, in this manner, by applying RSM there will be 20 test perceptions. The base surface harshness estimated for the opening was 1.06 μm at mix of 2000 rpm shaft speed, 78 mm/min feed rate and 2.5 mm drill distance across. While the greatest surface harshness of 2.59 mm was estimated at the blend of 250 rpm axle speed, 153 mm/min feed rate and 3.5 mm drill measurement. One factor plot investigation found that the main boundary was shaft speed followed by drill measurement and feed rate. Hence, surface harshness diminished while speeding up, feed rate and drill distance across. There were associations between all the boundary of shaft

Table 6.4 Input process parameters [43]

Parameters	Level-1	Level-2	Level-3
Depth of cut	0.3	0.45	0.6
Spindle speed	800	1000	1200
Feed rate	40	50	60
Tool nose radius	0.4	0.6	0.8

speed, feed rate and drill distance across in boring cycle under scrutiny. Table 6.4 indicating factor name and levels.

Sanjeevi et al. [44] this paper plans to foresee the ideal arrangement of surface harshness utilizing Response Surface Methodology in surface pounding machining measure. Reaction surface Methodology extricated for input boundaries planning to surface granulating measure. EN 24 steel machining with different speed, profundity of cut and feed rate timing. The surface harshness of the machined work piece estimated by the customary pointer test. At that point information and yield boundaries feed into the RSM and created ANOVA and relapse condition to deliver the ideal arrangement. Table 6.5 indicated level of information factor and name.

Karthik Pandiyan and Prabaharan [45] in this work, AA6351 amalgam steel work piece machined by CNC machine focus is assessed by Response Surface Methodology with a target capacity of acquiring great surface get done with utilizing single device tasks and improvement strategies for finding the estimations of the cycle factors that produce alluring estimations of the reaction. Table 6.6 speak to enter measure boundaries and levels.

Alagarsamy et al. [46] in present examination, aluminum grid composite strengthened with 15 wt% zirconium dioxide (ZrO₂) particulates was manufactured through mix projecting course. Electric release machining (EDM) was done to machine the delivered composite utilizing copper anode. Heartbeat current, beat on-schedule and heartbeat off-time were picked as information boundaries and surface harshness (SR)

Table 6.5 Parameter level [44]

Level of input parameter	Name	Range of parameters
1	Depth of cut	0.1–0.9
2	Feed rate	1.5–6
3	Speed	1100–1500

Table 6.6 Process parameters and levels

Factor name	Level-1	Level-2	Level-3
Feed rate	40	50	60
Spindle speed	800	1000	1200
Tool nose radius	0.4	0.6	0.8
Depth of cut	0.3	0.45	0.6

was considered as yield machining execution trademark. The exploratory arrangement has been embraced by Box Behnken design (BBD) of response surface method (RSM). This procedure was utilized to built up a numerical model for investigate the machining execution trademark. Besides, investigation of change (ANOVA) was applied to discover the impact of each machining boundary and their communications on SR. It has been seen that beat current was the most transcendent boundary on SR followed by beat on-schedule.

Process of RSM Method

See Fig. 6.2.

6.2.2.3 PSO (Particles Swarm Optimization)

Costra et al. [47] in this research, all experiment conducts by using multi-pass turning process. In this research optimization of these process parameters such as (cutting velocity, depth of cut, feed rate) by Particle swarm optimization). The purpose of this research, minimize of unit cost. Lee and Ponnam Balam [48] have focused on multi-pass turning process. The purpose of this research, minimize unit production cost. Chen et al. [49] in this paper, research was carried out on turning thin walled circular cylindrical sheet. The purpose of this research maximize Metal removal rate (MRR). The optimizations of process parameters such as cutting speed, feed rate, cutting depth for maximize MRR.

Zainal et al. [50] this research was completed by end milling operation for purpose minimize surface roughness (Ra). For this, optimization of process parameter by using PSO. The result compared with Taguchi optimization method. PSO result was more optimal compared Taguchi. Yildiz [51] Multi cutting tool, process parameter (cutting speed, feed rate), and purpose- maximize total profit rate, better than hybrid PSO (PSRE) HDRE. Sun and Zhang [52] cutting of boring bar manufacturing process, the purpose of research—desired frequency, process parameter (pressure, cutting speed, feed rate, depth of cut) and these process parameter is optimize by PSO technique.

Mellal and Williams [53] in this paper research work complete by grinding operation process for purpose of maximize MRR. For this research, optimization of process parameter by PSO and PSO result is compared with TLBO for validation. Bobby Oedy Pramoedyo et al. [54] in this research focused on integrated optimization technique for optimum response such as thrust force. Torque, hole exit delimitation and hole entry delimitation by drilling operation. The research work carried on carbon fiber reinforced polymer.

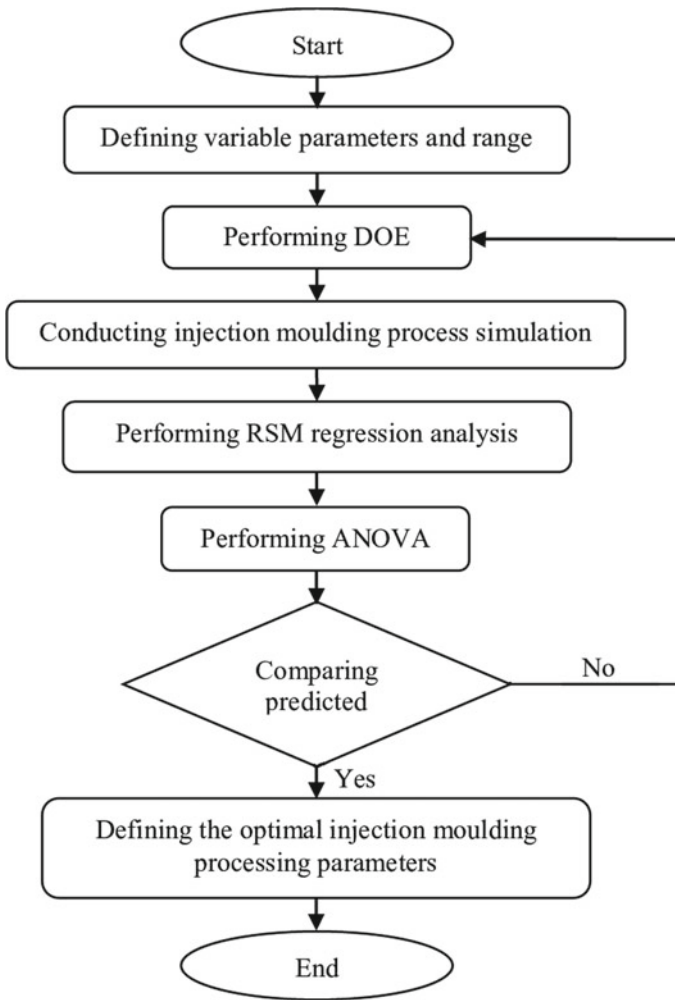


Fig. 6.2 General Process of RSM Optimization Techniques

6.2.2.4 Genetic Algorithm (GA) and Fuzzy Logic System (FLS)

Umashankar Gupta et al. [55] the accuracy is significant for axisymmetric parts. In this paper hereditary calculation is applied to discover limit cylindricity. For exactness part cylindricity resilience is one significant boundary. In this examination, acquired ideal estimation of cylindricity; mistake 5.40035 μm , speed-250 m/min, feed rate-0.23, profundity of cut-0261, instrument nose span 1.2 mm.

Sathiya Narayanan et al. [56] in this paper zeroed in on turning procedure on AISI H13 steel as a work piece and carbide instrument in CNC turning. L27 set of test lead by CNC turning machine. What's more, after get relapse examination,

for connection between input measure boundaries and yield measure boundaries. The profundity of cut is more huge cycle boundary on MRR and feed rate is more compelling boundary on SR (Ra). The reason for this exploration, limit SR and expand MRR by advancement by GA.

Durairaj and Gowri [57] in this paper, studied on CNC turning operation on inconel 600 alloy used as a work piece and titanium carbide as a tool. In this paper non-linear regression analysis is used for find relation ship between output and input process parameters. Genetic algorithm is applied for optimize of process parameters such a speed, depth of cut and feed rate with SR and tool wear as a response. The optimum performance of cutting are feed rate micron m/rev., depth of cut 30 μm m and cutting speed 25 m/min. Vedat Saras and Cetin Ozay [58] in this paper focused on RSM (response surface method), Artificial neural network(ANN) and NSGA-II were applied for used for modeling and multi objective optimization of Al 6351/Egg Shell Reinforced Composite.

Ramon Quiza et al. [59] in this paper focused on multi objective optimization technique based on genetic algorithm in turning operation. And parametric optimization of process parameter by genetic algorithm. The purpose of this research, tool life and operation time. Haber et al. [60] this research work carried out by drilling process. The purpose of research was that analysis of cutting force by fuzzy model with triangular membership function. In this paper analysis of input parameter such as feed rate and depth of cut with cutting force by use 49 no. of rules and find that when increasing cutting force then depth of cut is also increasing. Dong and Wang [61] in this paper, research was complete on milling machine. The purpose of research was that prediction of surface roughness. In this paper, process parameter such as spindle speed, feed rate, depth of cut was analysis with SR. and find that ANFIS with LOO-CV approach effective way for prediction of SR.

Lian et al. [62] the reason for this examination was investigation of cutting power on turning activity by fluffy rationale model with three-sided enrollment work. In this AND sensible activity is utilized. After this work acquired that the GPFC can lessen the troubles in deciding a fitting enrollment work and fluffy standards. Skrabalak et al. [63] the motivation behind this exploration was that lessening the no of miniature break and surface harshness boundary by fluffy rationale model with Electro Chemical release machining.

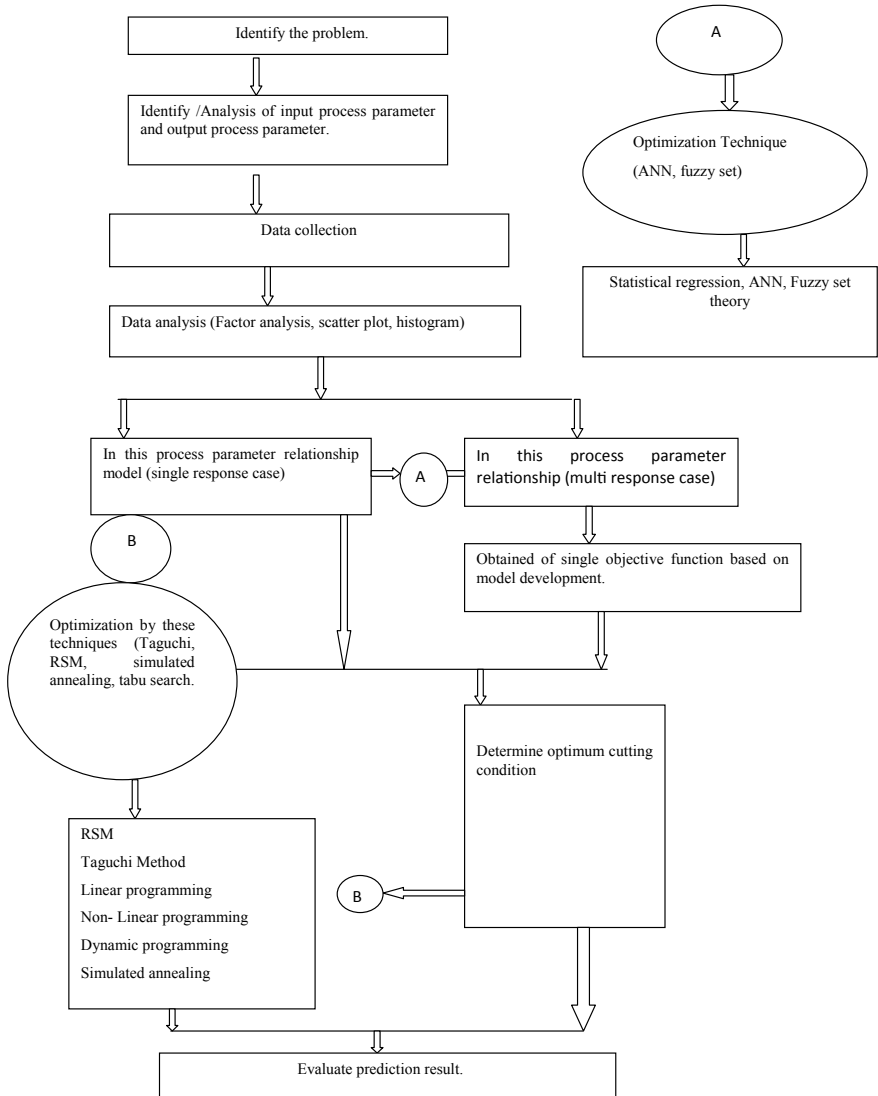
6.3 Characteristics of Optimization Techniques

See Table 6.7.

Table 6.7 Characteristics of optimization technique

S. No.	Optimize technique	Characteristics of optimization technique
1	Response surface method	In response surface strategy (RSM) streamlining successive of examination is conceivable in metal cutting activity. Reaction surface strategy is a measurable enhancement procedure which utilizes quantitative information which is connected from analysis to decide relapse model and to advance select put measure boundary
2	Taguchi method	Taguchi strategy is most helpful enhancement technique in which a progression of experimentation might be directed. Taguchi strategy applied both discrete reaction and proceeds with reaction
3	Genetic algorithm	A genetic calculation is an improvement procedure that utilization for taking care of the two kinds of issue, for example, unconstrained and obliged. In GA, produce a populace of point at every emphasis and best point in the populace approach on an ideal outcome
4	Simulated annealing	Simulated strengthening is measure advancement technique that is use for tackling bound-obliged and unconstrained kinds of issue. The mimicked toughening is technique, in which actual cycle of warming a material and afterward gradually bringing down the temp. to diminish imperfection so limiting the framework energy
5	Tabu search	Tabu search method enhancement technique created by F. W. Glover in 1986 which method is formalized in 1989. Forbidden pursuit technique is a metaheuristic search strategy utilizing neighborhood search strategies utilized for numerical improvement. Unthinkable pursuit might be applied any sorts of issue for advancement. Forbidden pursuit is a subsidiary free methodology that might be applied to multi-minima (or maxima), straight (or non-direct), and discrete (or nonstop) reaction work

6.4 A Generic Structure for Process Parameter Optimization



6.5 Conclusion

In this paper, a literature review of optimization techniques that use for response prediction in metal cutting operation.

- Lagrange's strategy, mathematical programming, objective programming, and dynamic programming these wide ranges of streamlining methods applied in the past for enhancement of different machining measure.
- But Today's in serious market most recent improvement strategies are effectively applied for increment profitability and nature of item. A survey of writing on enhancement strategies has uncovered that there are, specifically, effective mechanical uses of plan of test based methodologies for ideal cycle boundary.
- Taguchi strategy and Response surface technique is generally applied. These are precise methodology of demonstrating and assurance of ideal or close ideal cutting conditions has indicated a fascinating potential with regards to both item and cycle quality improvement of metal cutting.

References

1. Montgomery, D.C.: Introduction to Statistical Quality Control, 2nd edn. Wiley, New York (1990)
2. Tan, F.P., Creese, R.C.: A generalized multi-pass machining model for machining parameter selection in turning. *Int. J. Prod. Res.* **33**(5), 1467 (1995)
3. Montgomery, D.C., Peck, E.A.: Introduction to Linear Regression Analysis, 2nd edn. New York (1992)
4. Zadeh, L.A.: In: Yager, R.R., Ovchinnikov, S., Tong, M., Nguyen, H.T. (eds.) *Fuzzy Sets and Application: Selected Papers* (1973)
5. Ross, P.J.: *Taguchi Techniques for Quality Engineering*. McGraw-Hill, New York (1989)
6. Hillier, F.S., Lieberman, G.J.: *Operations Research*, 2nd edn. CBS, Delhi (1999)
7. Kirkpatrick, K., Gelett, C.D., Vecchi, M.P.: *Optimization by Simulated Annealing* (1983)
8. Osborne, D.M., Armacost, R.L.: Review of techniques for optimizing multiple quality characteristics in product development (1996)
9. Youssef, A.Y., Beauchamp, Y., Thomas, M.: Comparison of a full factorial experiment to fractional and Taguchi's method in a lathe dry turning operation. *Comput. Ind. Eng.* **27** (1994)
10. Kennedy, J., et al.: *Particles Swram Optimization* (1997)
11. Sandvik, A.B.: *Coroplan Process Planning Software and Coroplan User Manual*. Sandvik Automation, GmbH (1981)
12. Ostafiev, D.: Multiple constraint optimization analysis and software for selecting machining condition on rough turning operation. Ph.D. thesis. University of Melbourne, Melbourne (1999)
13. Prasad, A.V.S.R.K., Rao, P.N., Rao, U.R.K.: Optimal selection of process parameters for turning operations in a CAPP system. *Int. J. Prod. Res.* **35**, 1495–1522 (1997)
14. Gopalakrishnan, B., Khayyal, F.A.: Machine parameter selection for turning with constraints: an analytical approach based on geometric programming. *Int. J. Prod. Res.* **29**: 1897–1908 (1991)
15. Hinduja, S., Petty, D.J., Tester, M., Barrow, G.: Calculation of optimum cutting conditions for turning operations. *Proc. Inst. Mech. Eng.* **199**(B2), 81–92 (1985)
16. Sundaram, R.M. An application of goal programming technique in metal cutting. *Int. J. Prod.* (1978)

17. Ermer, D.S., Kromordihardjo, S.: Optimization of multi-pass turning with constraints. *J. Eng. Ind.* **103**, 462–468 (1981)
18. Petropoulos, P.G.: Optimal selection of machining rate variable by geometric programming. *Int. J. Prod. Res.* **11**, 305–314 (1973)
19. Brewer, R.C., Rueda, R.: A simplified approach to the optimum selection of machining parameters. *Eng. Dig.* **24**(9), 133–150 (1963)
20. Bhattacharya, A., Faria-Gonzalez, R., Inyong, H.: Regression analysis for predicting surface finish and its application in the determination of optimum machining conditions. *Trans. Am. Soc. Mech. Eng.* **92**, 711 (1970)
21. Walvekar, A.G., Lambert, B.K.: An application of geometric programming to machining variable selection. *Int. J. Prod. Res.* **8**, 3 (1970)
22. Gilbert, W.W.: 1950 Economics of machining. In: *Machining—Theory and Practice*. American Society of Metals (1950)
23. Armarego, E.J.A., Brown, R.H.: *The Machining of Metals*. Prentice Hall, Englewood Cliffs (1969)
24. Taylor, F.W.: On the art of cutting metals. *Trans. ASME* **28**, 31–35 (1907)
25. Thahadira, I., Daniyan, I., Masu, L., Vanstanden, L.R.: Process design and optimization of surface roughness during M200 TS milling process using the Taguchi method. In: *29th CIRP Design* (2019)
26. Sharma, V., Misra, J.P., Singhal, P.: Optimization of process parameters on combustor material using Taguchi & MCDM method in electro-discharge machining (EDM). *Mater. Today Proc.* **18**, 2672–2678 (2019)
27. Singh, N., Singh, G., Devi, M.B.: Optimizing the process parameters of ECM using Taguchi method (2020)
28. Kumar, K., Srivastav, A.S., et al.: Experimental investigation into the micro-EDM characteristics of conductive. *Sic. Ceram. Int.* **42**, 1597–1610 (2016)
29. Kumar, S., Singh, G., Agarwal, S.: Optimization the machining parameters of surface roughness during. *Mater. Today. Proc.* (2019)
30. Hanan, S.N., Millot, N., Salman, E.B.: Study of the effect of milling parameters on mechanosynthesis of hydroxyfluorapatite using the Taguchi method. *PT* (2019)
31. Upadhye, R., Pkeswami, I.: Optimization of sand casting process parameter using Taguchi method in foundry. *IJERT* **1**(7) (2012)
32. Campatelli, G., Lorenzini, L., Scipaa, A.: Optimization of process parameters using a RSM for minimizing power consumption in the milling of carbon steel. *J. Clean. Prod.* **66**(2014), 309e316 (2019)
33. Hou, T.-H., Su, C.-H., Lia, W.-L.: Parameters optimization of a nano-particle wet milling process using the Taguchi method, RSM and GA. *Powder Technol.* **173**, 153–162 (2007)
34. Nanda, B.K., Mishra, A., et al.: Experimentation and optimization of process parameters of abrasive jet drilling by surface response method with desirability based PSO. In: *ICAAMM-2016* (2016)
35. Kumar, R., Singh, P., Singh, S.: Multi objective optimization using different methods of assigning weights to energy consumption responses, surface roughness and MRR during rough turning operation. **S0959-6526**(17), 31247–7 (2017)
36. Amran, M.A., Salmah, S., Hussein, N.I.S., et al.: Effects of machine parameters on surface roughness using RSM in drilling process. In: *The Malaysian International Tribology Conference* (2013)
37. Camposeco-Negrete, C.: Optimization of cutting parameters using RSM for minimizing energy consumption and maximizing cutting quality in turning of AISI 6061 T6 aluminum. *J. Clean. Prod.* (2014)
38. Daramola, O.O., Thahadira, I., Olajide, J.L., et al.: Process design for optimal minimization of resultant cutting force during the machining of Ti-6Al-4V: RSM and desirability function analysis. *Procedia CIRP* **84**(2019), 854–860 (2019)
39. Song, H., Dan, J., Li, J., Jing, Du., Xiao, J., Jianfeng, Xu.: Experimental study on the cutting force during laser-assisted machining of fused silica based on the Taguchi method and response surface methodology. *J. Manuf. Processes* **38**, 9–20 (2019)

40. Selvam, R., Arunkumar, N., Karunamoorthy, L.: An investigation on machining characteristics in abrasive water jet machining of hybrid laminated composites with SiC nano particles. *Mater. Today Proc.* (2020). <https://doi.org/10.1016/j.matpr.2020.06.193>
41. Kumar Parida, A., Maity, K., Modeling of machining parameters affecting flank wear and surface roughness in hot turning of Monel-400 using response surface methodology (RSM). *Measurement* (2019). <https://doi.org/10.1016/j.measurement.2019.01.070>
42. Kumar, A., Kumar, S., Mandal, A., Dixit, A.R.: Investigation of powder mixed EDM process parameters for machining Inconel alloy using response surface methodology. *Mater. Today Proc.* **5**, 6183–6188 (2018)
43. Amrana, M.A., Salmaha, S., Husseina, N.I.S., Izamshabb, R., Hadzleyb, M., Sivaraosb, Kasimb, M.S., Sulaimanb, M.A.: Effects of machine parameters on surface roughness using response surface method in drilling process. *Procedia Eng.* **68**, 24–29 (2013)
44. Sanjeevi, R., Kumar, G.A., Krishnan, B.R.: Optimization of machining parameters in plane surface grinding process by response surface methodology. *Mater. Today Proc.* (2021). <https://doi.org/10.1016/j.matpr.2020.04.075>
45. Karthik Pandiyan, G., Prabaharan, T.: Optimization of machining parameters on AA6351 alloy steel using response surface methodology (RSM). *Mater. Today Proc.* <https://doi.org/10.1016/j.matpr.2020.01.369>
46. Alagarsamy, S.V., Ravichandran, M., Sakthivelu, S., et al.: Optimization of electric discharge machining parameters on surface roughness for Al/ZrO₂ composite through response surface methodology. *Mater. Today Proc.* (2020). <https://doi.org/10.1016/j.matpr.2020.01.344>
47. Costa, A., Celano, G., Fichera, S.: Optimization of multi-pass turning economies through a hybrid particle swarm optimization technique. *Int. J. Adv. Manuf. Technol.* **53**, 421–433 (2011)
48. Lee, Y.Z., Ponnambalam, S.G.: Optimisation of multipass turning operations using PSO and GA-AIS algorithms. *Int. J. Prod. Res.* **50**(22), 6499–6518 (2012)
49. Chen, D., Lin, B., Han, Z., Zhang, Y.: Study on the optimization of cutting parameters in turning thin-walled circular cylindrical shell based upon cutting stability. *Int. J. Adv. Manuf. Technol.* **69**, 891–899 (2013)
50. Zainal, N., Zain, A.M., Radzi, N.H.M., Othman, M.R.: Glowworm swarm optimization (GSO) for optimization of machining parameters. *J. Intell. Manuf.* **27**(4), 797–804 (2016)
51. Yildiz, A.: A new hybrid differential evolution algorithm for the selection of optimal machining parameters in milling operations. *Appl. Soft Comput.* **13**, 1561–1566 (2013)
52. Sun, Y.S., Zhang, Q.: Optimization design and reality of the virtual cutting process for the boring bar based on PSO-BP neural networks. *Neural Comput. Appl.* **29**(5), 1357–1367 (2018)
53. Mellal, M.A., Williams, E.J.: Parameter optimization of advanced machining processes using cuckoo optimization algorithm and hoopoe heuristic. *J. Intell. Manuf.* **27**, 927–942 (2016)
54. Pramoedyo, B.O., Norcahyo, R., et al.: *Eng. Sci. Technol. Int. J.* (2019)
55. Gupta, U., Viayak, U., Appala, G., et al.: Mathematical modelling and optimisation of cylindrical form parameter in CNC turning using RSM and GA. *Mater. Today Proc.* **5**:19985–19996 (2018)
56. Sathiya Narayanan, N., Baskar, N., Ganesan, M.: Multi objective optimization of machining parameters for hard turning OHNS/AISI H13 material using GA. *IMME17* (2018)
57. Durairaj, M., Gowri, S.: Parametric optimization for improved tool life and surface finish in micro turning using GA. *IConDM* (2013)
58. Chukwuemeka, C., Uzoma, C.: RSM and ANN modeling for production of Al 6351/egg shell reinforced composite: multi objective optimization using GA. *MTCOMM* (2019)
59. Quiza, R., Rivas, M., Brindis, E.A.: Genetic algorithm-based multi-objective optimization of cutting parameters in turning processes (2006)
60. Haber, R.E., Toro, R.M.D., Gajate, A.: Optimal fuzzy control system using the cross-entropy method: a case study of a drilling process. *Inf. Sci.* **180**(14), 2777–2792 (2010)
61. Dong, M., Wang, N.: Adaptive network-based fuzzy inference system with leave-one-out cross-validation approach for prediction of SR. *Appl. Math. Model.* **35**(3), 1024–1035 (2011)

62. Lian, R.J., Lin, B.F., Huang, J.H.: A grey prediction fuzzy controller for constant cutting force in turning. *Int. J. Mach. Tools Manuf.* **45**(9), 1047–1105 (2005)
63. Skrabalak, G., Zybura-Skrabalak, M., Ruszaj, A.: Building of rules base for fuzzy-logic control of the ECDM process. *J. Mater. Process Technol.* **149** (2004)

Chapter 7

Modelling and Analysis of Barriers in Lean Green Manufacturing Implementation: An ISM Approach



Sarita Prasad, Rao A. Neelakanteswara, and Krishnanand Lanka

Abstract Lean and green manufacturing is used in firms to achieve better financial, operational and environmental performance. Many researchers concentrated on the integration of these two paradigms in firms. Still, limited researchers have tried to investigate the barriers for firms which creates hindrance in the way of implementation of lean-green. This research is an attempt to identify and analyse the barriers for lean and green manufacturing, also to analyse the relationship among barriers and their effects on the implementation process. A hierarchical structure model has developed with the help of ISM (Interpretive Structural Modelling) and the strength of relationship among barriers have analysed with the help of MICMAC analysis. A nine-level ISM model for barriers has developed which shows ‘Market competition and uncertainty’ at the top position and other barriers such as ‘Lack of government support to integrate green practices’, ‘Lack of environmental awareness’ and ‘Governmental environmental laws and regulations and deficient enforcement’ are at the bottom position of the model.

Keywords Barriers · Lean and green paradigm · Lean manufacturing · Green manufacturing · Interpretive structural modelling · MICMAC analysis

7.1 Introduction

7.1.1 Background of Lean and Green Manufacturing

Fast changes in market demand, globalisation and awareness about the environment have forced the companies to modify and maintain their processes to adopt a proactive role towards cleaner process [4]. Nowadays, companies are more focusing on environmental management techniques for sustainable development. Several researchers have conducted a study and demonstrated that lean is very helpful to achieve sustainability in manufacturing system. Dhingra et al. [8] studied the synergies between lean and green manufacturing. This approach will help the firm to fulfil customer

S. Prasad (✉) · R. A. Neelakanteswara · K. Lanka
Department of Mechanical Engineering, National Institute of Technology, Warangal, India

volatile demands and sustain market competition [27]. Research shows that these two paradigms have widely explored separately, but the combined effect of lean and green study is limited. This kind of research will encourage the organisation to integrate lean and green strategies to obtain maximum synergies, high profits, clean-corporate image by reducing environmental waste, improved worker health and safety and reduced consumer risks. Lean and green manufacturing is the perfect blend of two approaches which focuses to reduce the non-value added activities in manufacturing system with the adoption of advanced environmental friendly technology.

Huo et al. [12] have analysed the effect of lean- green manufacturing in the supply chain. The study found that on the customer side, lean will help the supply chain to achieve social, environmental and economic sustainability and green will enable the system to achieve improvement in environmental performance. Whereas in the supplier side, green will allow the system to achieve higher sustainability as it will direct improve the social and economic performance and lean will only enhance the financial performance [3]. Green manufacturing approach focuses on the environmental related issues and also focus on the end of the life cycle of products. These issues have fetched the attention from various industries practitioners, government bodies, customers and consumers across the world [15]. Manufacturing firms are more concerned about the material selection, green design approach, production with less environmental pollutions, gas emissions, recycling of materials etc. [24]. Lean manufacturing approach helps the firms to achieve profits with a significant reduction in waste production activities and cycle time with improved quality [23].

Sindhvani et al. [27] investigated the combined approach of lean-green and agile manufacturing to address its barriers and limitation. Researchers have developed various tools to measure the leanness and greenness of the organisations. The challenge to implement lean and green is not only limited to the approach of implementation but also includes managerial, workers behaviour, technical and government rules. These barriers are related to each other in a sophisticated manner and need to be appropriately analysed. These barriers are having a different impact when implementing lean-green in manufacturing industries. Hence it is important to investigate the main barriers of lean and green manufacturing, their relationship and dependency among each other.

7.1.2 Need for the Study

The literature survey conducted over lean and green manufacturing resulted in various articles which discussed the barriers of lean and green manufacturing in various industries. These studies show the barriers/obstacles experienced by industry practitioners during the implementation of lean and green. It is necessary to understand that each barrier has its effects which creates hurdles in the path of lean green implementation. It is important to analyse the effect of each barrier on lean and green implementation which will help the practitioners to adopt certain corrective measures. This modelling process of barriers will help the industry practitioners to focus on most

critical barriers and analyse the relationship among these barriers. In the literature, there are various studies which focus on the drivers of lean and green manufacturing implementation in various industries. But, the studies related to the identification of barriers for lean and green manufacturing are limited. Hence it creates a strong need for a study which identify the significant barriers of lean and green and develops a model to analyse the relationship among barriers. This approach will provide a smooth roadmap for lean and green implementation in manufacturing industries.

7.1.3 Research Objective

The main aims of this study are

- (1) To identify the barriers of the lean-green manufacturing process.
- (2) To develop a hierarchical model to show the relationship among barriers through ISM model.
- (3) To categorise the barriers into four division through MICMAC approach.

The modelling approach will help the researchers and practitioners to analyse the contextual relationship among these barriers and make their strategies accordingly. The literature review conducted in the study will show the contributions of many researchers in the identification of barriers for lean and green manufacturing. Later, MICMAC analysis is used to categories the barriers in four parts. The MICMAC analysis helps the firms to analyse the dependency among barriers.

7.1.4 Organization of Paper

The paper is structured into eight sections. Section 7.2 comprises of literature review about lean green barriers and various approaches used for modelling. Section 7.3 comprises identification of barriers from literature. Section 7.4 consist of the discussions of study. Section 7.5 comprises the description of the methodology. Section 7.6 consist the actions towards the elimination of barriers. Section 7.7 consist of managerial implications. At last Sects. 7.8 and 7.9 comprise the conclusions, future study and limitations of the study.

7.2 Literature Review

The literature review comprises of studies related to the ISM approach applied to identify and analyse the relationship among barriers of lean-green implementation in organisations. This study aim was to prioritise the barriers of lean-green manufacturing and also helps to build a better understanding of the lean and green concept and

their challenges. Vinodh and Asokan [30] conducted a study to analyse the obstacles for adaption of lean six sigma with environmental consideration. This study developed an ISM model in which barriers like lack of commitment from the management, lacking in training programmes and poor education and funding constraint for green process appeared at the bottom position. Other barriers such as challenges during the adoption of environmental strategies, strict government rules and policy, poor attitude to achieve sustainability, communication gap and inadequate monitoring for defects are found at the upper position in the model.

Cherrafi et al. [6] used a combined approach of systematic literature review and ISM to analyse the relationship among barriers of green lean implementation. The study found that less awareness about environmental impact and lack of support from the government are the significant barriers for green-lean initiatives as it placed at the bottom of the model. Kumar et al. [15] implemented the ISM approach to see the connection among barriers to adapt green lean six sigma during the product development process. Competition and uncertainty found to be the topmost barrier in the model and lack of support from total top management placed at the lower position. Thanki et al. [28] analysed the success factor for lean-green implementation and suggested that support from government is the most significant factor in the model. Besides, that green disposal initiative and organisational capabilities are also significant factors for lean green implementation. Prasad et al. [23] analysed the relationship among enablers for lean manufacturing implementation through the combined approach of ISM and IRP (Interpretive Ranking Process) for Bulgarian SMEs. Caldera et al. [3] study propose four critical enablers and six critical barriers to achieve sustainability in SMEs. The most critical barrier found in the study is the lack of financial resources.

Ojo et al. [22] discussed the impact of green supply chain management (GSCM) and its barriers in construction firms. They found that barriers such as unawareness of public, insufficient knowledge about environmental sustainability, less support from management, lacking support in legal terms and lacking support from government are the crucial barriers for GSCM. Yadav et al. [32] conducted a study to identify the barriers for lean six sigma (LSS) and found that 'lack of top management attitude', 'lack of LSS project training and education' and 'lack of strategic planning' are the most important barriers. Siegel et al. [26] presented a systematic model to show the relationship among the critical factors for green-lean practices for small and medium enterprises (SMEs). The study shows that the lack of metrics and measurement is the most important challenge for green lean implementation in SMEs. Tiwari et al. [29] found lack of customer focus, absence of lean management, inadequate capital investment, leadership and resistance to change are the critical lean barriers in the Indian automobile industry.

7.3 Barriers Identification

Barriers can be explained as an obstacle or hurdle which slow down the progress of work. The organisation faces many barriers during the implementation of lean-green manufacturing. These barriers have selected from the previous study through a systematic literature review (SLR). Five steps of review are followed as (1) problem description/ objectives, (2) locating studies, (3) articles selections, (4) in-depth analysis of articles and (5) results of the study. Barriers identified in the study are explained below:

- 1. The necessity of high investments/fund constraint**
Lean and green implementation requires advanced technology and proper design structure in the manufacturing system. Adoption and implementation of these techniques require a high amount of investment in the manufacturing process.
- 2. Lack of top management involvement in adopting green lean initiative**
The role of top management in the successful adaption of any new techniques is much necessary and important. Top management of firms can provide support to the lower level structure of the firm to implement green lean techniques. Top management plays an important role in design ideas and strategic decisions in the firm while implementing lean and green.
- 3. Lack of communication and cooperation between departments/Information gap**
The communication among employees of various departments in the manufacturing firm and exchanging information with each other are very important in any firm. The communication and cooperation between departments can help to build an efficient base for lean and green manufacturing.
- 4. Resistance to change due to past failures**
It is necessary for any organization to be well prepared for the required changes in the manufacturing process while implementing lean and green techniques. Employees of any manufacturing firms having tendency to resist the changes in the daily routine work pattern while implementing new techniques. Manufacturing companies should consider on these internal challenges which comprise the structural (machines, technology etc.) and infrastructural (business pattern/practices) changes.
- 5. Lack of training**
The implementation process of lean and green require proper training and consultancy to the employees of the firm to know the basic knowledge and ethics of green and lean manufacturing. The implementation of green and lean manufacturing requires the equal involvement of managers as well as workers in the firm.
- 6. Lack of Human resource**
Human resource is an important resource for any industry. Availability of workers, raw materials and technology are important parameters for the implementation of lean-green techniques. Unavailability of any of the resources can

results in a big hurdle in implementation. Support from well-trained workers can enable the manufacturing system to execute the planned tasks on time with better decision making.

7. **Lack of government support to integrate green practices**
The government can help the firm to implement new advanced green techniques in the firm. Government policies, rules and regulations can mandate the firms to implement such strategies in the production process and reduce the emissions. The greening of the manufacturing process can be influenced by several factors such as rules and regulations, trade regulations and policies.
8. **Lack of awareness in customers/customer non-involvement in greening**
Customer choice is the prime important factor in any business. Companies always design and manufacture the products in such a way that it fulfils the customer needs. Environmental awareness among customers can significantly force the manufacturing firm to adopt new green techniques. In this way, pressure from the customer can make the firm to adopt lean and green techniques and produce economic products with environmental consideration.
9. **Market competition and uncertainty**
In today's world of uncertain customer demands and market competition, it is very difficult for a company to implement lean and green techniques. Uncertainty in the market always acts as a major obstacle for any new techniques. The market uncertainty can create several competitive priorities such as quality of products, flexibility, responsiveness, quick delivery and new product development with environmentally friendly use.
10. **Poor supplier commitment**
The supplier can help the firms to make the supply chain sustainable with lean initiatives. Collective efforts by the supply chain members can help the implementation of lean and green in a manufacturing firm.
11. **Lack of technical expertise/technical barriers (poor R&D)**
Poor technical expertise can create a barrier in terms of adoption of new green and lean techniques.
12. **Lack of information technology implementation**
Technology up-gradation can help the firms to change the organizational features and to become more competitive in the market. The lack of information technology implementation in the organization creates a big hurdle in the adoption of lean and green techniques.
13. **Lack of environmental awareness**
Awareness about the environmental impact can motivate the manufacturing firm to implement new green and lean techniques. This will also help the firm to achieve economic, environmental and social sustainability.
14. **Lack of management skill and knowledge/poor team management**
The implementation of lean-green approach requires skilled management with proper team coordination. Resistance from top management and poor team management can create a hurdle in the implementation of the lean green practice.

15. **Lack of ethical standards and corporate social responsibility**
Corporate social responsibility can make a firm to be more responsible towards the environment and also it encourages the firm to be socially accountable.
16. **Lack of recycling and reuse efforts of the organisation**
Adoption of recycling and reuse practices are important for firms to become economic and environmentally sustainable.
17. **Lack of organization encouragement**
Lack of encouragement from the organization can hinder the information flow in the supply chain.
18. Poorly organised culture in adopting the green and lean system.
19. Governmental environmental laws and regulations and deficient enforcement
20. Restrictive company policies towards product/process maintenance/Poor infrastructure.

7.3.1 Locating and Selection of Studies

The articles were searched using string related to the main theme of research. Search string includes Lean paradigm, Green paradigm, Lean and Green manufacturing, Barriers, Obstacles, Challenges and Failures. This search string used in electronic engine databases such as Elsevier (sciencedirect.com), Emerald (emeraldgroupublishing.com), IEEE (ieeexplore.ieee.org), Taylor and Francis (taylorandfrancis.com), Inderscience (inderscience.com), Web of Science (apps.webofknowledge.com) and Google Scholar (scholar.google.com). A total sample of 120 articles was selected those belongs to lean and/or green manufacturing. However, only 70 papers of this sample discussed the barriers and drivers for lean and green implementation. In this way, a total of 20 papers have further considered for the study. The main purpose of this research is to identify and analyse the generic barriers of lean and green manufacturing which can be applicable to various industries such as manufacturing industry, service industry etc. The structure of the research is shown in Fig. 7.1.

7.3.2 Analysis and Synthesis

In this study, the thematic approach has been used to synthesis the qualitative research. With this approach, 20 barriers have selected for study; summarised in Table 7.1. In the study, many barriers are identified from lean and green separately since no prior work has published in this direction. These barriers are further discussed with experts from industry and scholars to modify it and make it more relevant and suitable to consider for lean and green barriers. Many researchers explained in their studies that the combination of these two concepts would inherit the same barriers and challenges as they faced individually, as these concepts share various similarities (Ng et al. [21]). Campos and Vazquez-Brust [4] have described the integrated tool

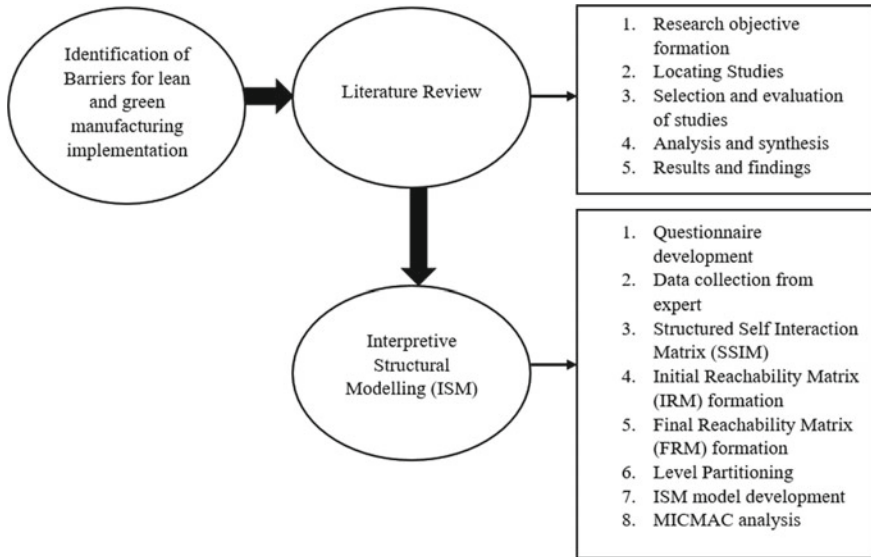


Fig. 7.1 Structure of research approach

approach of lean-green techniques which can implement together to achieve environmental performance and operational efficiency. Therefore this study also supports the implementation of an integrated approach of lean-green in organisations to achieve sustainability performance. It will be very tough for the companies to remove all the barrier for the first time during the lean and green implementation. As these barriers can affect each other during the implementation process. This direct the research to know and analyse the dependency relationship among different barriers in the organisation.

7.4 Methodology

7.4.1 Interpretive Structural Modelling

ISM method is used to develop a model which form a hierarchical level structure to depict the relationship and interaction between variables of the study [15]. It provides the most straightforward way to develop a complicated structure model on the basis of complex variables. The steps in the ISM model approach is as follows [6, 15, 18, 23]:

- Identification and selection of variables (barriers) for the study.
- Defining the contextual relation among barriers with the help of the experts' team.

Table 7.1 Barriers in lean and green implementation

S. No.	Barriers	References
1	The necessity of high investments/fund constraint	Mudgal et al. [20], Luthra et al. [16], Giunipero et al. [11], Mathiyazhagan et al. [18], Jayant and Azhar [13], Drohomeretski et al. [10], Salonitis and Tsinopoulos [25], Dhull and Narwal [9], Kumar et al. [15], AlManei et al. [2], Cherrafi et al. [6]
2	Lack of top management involvement in adopting Green lean initiative	Massoud et al. [17], Mudgal et al. [20], Luthra et al. [16], Giunipero et al. [11], Mathiyazhagan et al. [18], Jayant and Azhar [13], Ojo et al. [22], Salonitis and Tsinopoulos [25], Dhull and Narwal [9], Mittal et al. [19], AlManei et al. [2]
3	Lack of communication and cooperation between departments/information gap	Massoud et al. [17], Mathiyazhagan et al. [18], Abdullah et al. [1], Kumar et al. [15], Cherrafi et al. [6]
4	Resistance to change due to past failures	Mudgal et al. [20], Abdullah et al. [1], Salonitis and Tsinopoulos [25], Mittal et al. [19], AlManei et al. [2], Cherrafi et al. [6]
5	Lack of training courses/consultancy/institutions to train, monitor and mentor the progress specific to each industry	Mathiyazhagan et al. [18], Jayant and Azhar [13], Dhull and Narwal [9], Kumar et al. [15], Cherrafi et al. [6]
6	Lack of human resource/poor quality of human resources	Luthra et al. [16], Mathiyazhagan et al. [18], Dhull and Narwal [9], Kumar et al. [15], Cherrafi et al. [6]
7	Lack of government support to integrate green practices	Luthra et al. [16], Mathiyazhagan et al. [18], Jayant and Azhar [13], Ojo et al. [22], Cherrafi et al. [6]
8	Lack of awareness in customers/customer non-involvement in greening	Luthra et al. [16], Mathiyazhagan et al. [18], Jayant and Azhar [13], Mittal et al. [19], Kumar et al. [15]
9	Market competition and uncertainty	Luthra et al. [16], Giunipero et al. [11], Jayant and Azhar [13], Dhull and Narwal [9], Kumar et al. [15]
10	Poor supplier commitment/reluctant to change towards green and lean in the supply chain (unwilling to exchange information)	Luthra et al. [16], Kasim and Ismail [14], Mathiyazhagan et al. [18], Drohomeretski et al. [10], Dhull and Narwal [9]
11	Lack of technical expertise/technical barriers (poor R&D)	Luthra et al. [16], Mathiyazhagan et al. [18], Jayant and Azhar [13], Abdullah et al. [1], Dhull and Narwal [9]

(continued)

Table 7.1 (continued)

S. No.	Barriers	References
12	Lack of environmental awareness/lack of knowledge about environmental impacts	Massoud et al. [17], Mathiyazhagan et al. [18], Jayant and Azhar [13], Ojo et al. [22], Cherrafi et al. [6]
13	Lack of management skill and knowledge/poor team management	Carleysmith et al. [5], Kumar et al. [15], Cherrafi et al. [6]
14	Lack of ethical standards and corporate social responsibility	Mathiyazhagan et al. [18], Jayant and Azhar [13], Dhull and Narwal [9]
15	Lack of recycling and reuse efforts of the organisation	Mathiyazhagan et al. [18], Jayant and Azhar [13], Cherrafi et al. [6]
16	Lack of information technology implementation	Luthra et al. [16], Jayant and Azhar [13], Dhull and Narwal [9]
17	Lack of organization encouragement	Luthra et al. [16], Dhull and Narwal [9], Mittal et al. [22]
18	Poor corporate culture separating environmental and continuous improvement decisions/poorly organised culture in adopting green and lean system	Luthra et al. [16], Mathiyazhagan et al. [18], Cherrafi et al. [6]
19	Governmental environmental laws and regulations and deficient enforcement	Massoud et al. [17], Kasim and Ismail [14], Dhull and Narwal [9]
20	Restrictive company policies towards product/process maintenance/poor infrastructure	Mudgal et al. [20], Giunipero et al. [11], Mathiyazhagan et al. [18]

- Structured Self Interaction Matrix (SSIM) is developed to show the pairwise comparison between barriers.
- SSIM is converted into an initial reachability matrix and further analysed for transitivity rule. The rules of transitivity can be explained as if variable X is having a relationship with variable Y and variable Y is having a relationship with variable Z; then, variable X will also have a relation with variable Z.
- After checking the transitivity rule, final reachability matrix (FRM) is developed.
- Level partition of variables.
- A digraph is drawn with the help of FRM.
- After removal of transitivity links, resulting digraph is represented as final ISM model by mentioning the statements in place of variables nodes.

7.4.2 Questionnaire Development and Data Collection

ISM method depends on the data collected based on the experts' opinions and suggestions. In this study, twelve experts were approached belonging to various manufacturing companies. In the initial stage, all experts were explained about the lean and green approach, benefits, importance and objective of this study. After the frequent

7.4.5 Final Reachability Matrix (FRM)

FRM matrix is obtained after checking the rule of transitivity in initial reachability matrix [6]. The developed final reachability matrix is shown in Table 7.4. This matrix is further analysed to develop reachability and antecedent set for every variable. Reachability set of a variable comprises the variable itself and all the variables which it helps in achieving it. The antecedent set also includes the variable itself and all the variables which are helping to achieve it. If a barrier got same set value for reachability and intersection set, then it is considered as a top-level barrier in ISM model. The same procedure is followed until all barriers will get ranks. The level partitioning can be seen in Table 7.5.

7.4.6 Level Partitioning

In the FRM, the reachability set and antecedent set were found for each barrier [31]. On one hand, the reachability set includes the barrier itself with all the other barriers which it helps to achieve. On the other hand, the antecedent set includes barriers itself with all the other barriers which are helping to achieve to it. The barriers with the same reachability and intersection set considered as the first-level barrier in ISM modelling. This process is continued until all the barriers obtained a rank. The level partitioning for the study can be seen in Table 7.5. This levelling process helps to develop the digraph which can finally be converted into ISM model after removing the transitivity links.

7.4.7 Formation of ISM Model

Based on FRM, a digraph was drawn. In the next step, all the transitivity links have removed and node numbers have replaced with corresponding barriers. The final ISM model is shown in Fig. 7.2. The study suggests that ‘lack of government support to integrate lean green practices’, ‘lack of environmental awareness’ and ‘government environmental laws and regulations and deficient enforcement’ are the most critical barriers for lean and green manufacturing implementation as it comes at the bottom position of ISM model. ‘Market competition and uncertainty’ has identified as the top position barrier in ISM model.

Table 7.4 Final reachability matrix

S. No.	1	2	3	4	5	6	7	8	9	10	11	12	13	14	15	16	17	18	19	20	Driving power
1	1	1	1	1	0	0	0	1	1	1	1	0	1*	1	1	1	1	1	0	1	15
2	1	1	1	1*	0	0	0	1	1	1	1	0	1	1	1	1	1	1	0	1	15
3	0	0	1	0	0	0	0	1	1	1	0	0	0	1	0	0	0	1	0	1	7
4	0	0	1*	1	0	0	0	1	1	1	1	0	0	1	1	1	1	1	0	1	12
5	1	1	1	1	1	1	0	1	1	1	1	0	1	1	1	1	1	1	0	1	17
6	1	1	1	1	1	1	0	1	1	1	1	0	1	1	1	1	1	1	0	1	17
7	1	1	1	1	1	1	1	1	1	1	1	1	1	1	1	1	1	1	1	1	20
8	0	0	0	0	0	0	0	1	1	1	0	0	0	0	0	0	0	0	0	0	3
9	0	0	0	0	0	0	0	0	1	0	0	0	0	0	0	0	0	0	0	0	1
10	0	0	0	0	0	0	0	1	1	1	0	0	0	0	0	0	0	0	0	0	3
11	0	0	1	0	0	0	0	1	1	1	1	0	0	1	1	1	0	1	0	1	10
12	1	1	1	1	1	1	1	1	1	1	1	1	1	1	1	1	1	1	1	1	20
13	1	1	1	1	0	0	0	1	1	1	1	0	1	1	1	1	1	1	0	1	15
14	0	0	0	0	0	0	0	1	1	1	0	0	0	1	0	0	0	0	0	0	4
15	0	0	1	0	0	0	0	1	1	1	1	0	0	1	1	1	0	1	0	1	10
16	0	0	1	0	0	0	0	1	1	1	1	0	0	1	1	1	0	1	0	1	10
17	0	0	1	1	0	0	0	1	1	1	1	0	0	1	1	1	1	1	0	1	12
18	0	0	1	0	0	0	0	1	1	1	0	0	0	1	0	0	0	1	0	1	7
19	1	1	1	1	1	1	1	1	1	1	1	1	1	1	1	1	1	1	1	1	20
20	0	0	1	0	0	0	0	1	1	1	0	0	0	1	0	0	0	1	0	1	7
Dependance power	8	8	16	10	5	5	3	19	20	19	13	3	8	17	13	13	10	16	3	16	225

Table 7.5 Level partitioning

S. No.	Reachability set	Antecedent set	Intersection set	Level
1	1, 2, 3, 4, 8, 9, 10, 11, 13, 14, 15, 16, 17, 18, 20	1, 2, 5, 6, 7, 12, 13, 19	1, 2, 13	VII
2	1, 2, 3, 4, 8, 9, 10, 11, 13, 14, 15, 16, 17, 18, 20	1, 2, 5, 6, 7, 12, 13, 19	1, 2, 13	VII
3	3, 8, 9, 10, 14, 18, 20	1, 2, 3, 4, 5, 6, 7, 11, 12, 13, 15, 16, 17, 18, 19, 20	3, 18, 20	IV
4	3, 4, 8, 9, 10, 11, 14, 15, 16, 17, 18, 20	1, 2, 4, 5, 6, 7, 12, 13, 17, 19	4, 17	VI
5	1, 2, 3, 4, 5, 6, 8, 9, 10, 11, 13, 14, 15, 16, 17, 18, 20	5, 6, 7, 12, 19	5, 6	VIII
6	1, 2, 3, 4, 5, 6, 8, 9, 10, 11, 13, 14, 15, 16, 17, 18, 20	5, 6, 7, 12, 19	5, 6	VIII
7	1, 2, 3, 4, 5, 6, 7, 8, 9, 10, 11, 12, 13, 14, 15, 16, 17, 18, 19, 20	7, 12, 19	7, 12, 19	IX
8	8, 9, 10	1, 2, 3, 4, 5, 6, 7, 8, 10, 11, 12, 13, 14, 15, 16, 17, 18, 19, 20	8, 10	II
9	9	1, 2, 3, 4, 5, 6, 7, 8, 9, 10, 11, 12, 13, 14, 15, 16, 17, 18, 19, 20	9	I
10	8, 9, 10	1, 2, 3, 4, 5, 6, 7, 8, 10, 11, 12, 13, 14, 15, 16, 17, 18, 19, 20	8, 10	II
11	3, 8, 9, 10, 11, 14, 15, 16, 18, 20	1, 2, 4, 5, 6, 7, 11, 12, 13, 15, 16, 17, 19	11, 15, 16	V
12	1, 2, 3, 4, 5, 6, 7, 8, 9, 10, 11, 12, 13, 14, 15, 16, 17, 18, 19, 20	7, 12, 19	7, 12, 19	IX
13	1, 2, 3, 4, 8, 9, 10, 11, 13, 14, 15, 16, 17, 18, 20	1, 2, 5, 6, 7, 12, 13, 19	1, 2, 13	VII
14	8, 9, 10, 14	1, 2, 3, 4, 5, 6, 7, 11, 12, 13, 14, 15, 16, 17, 18, 19, 20	14	III
15	3, 8, 9, 10, 11, 14, 15, 16, 18, 20	1, 2, 4, 5, 6, 7, 11, 12, 13, 15, 16, 17, 19	11, 15, 16	V
16	3, 8, 9, 10, 11, 14, 15, 16, 18, 20	1, 2, 4, 5, 6, 7, 11, 12, 13, 15, 16, 17, 19	11, 15, 16	V
17	3, 4, 8, 9, 10, 11, 14, 15, 16, 17, 18, 20	1, 2, 4, 5, 6, 7, 12, 13, 17, 19	4, 17	VI
18	3, 8, 9, 10, 14, 18, 20	1, 2, 3, 4, 5, 6, 7, 11, 12, 13, 15, 16, 17, 18, 19, 20	3, 18, 20	IV
19	1, 2, 3, 4, 5, 6, 7, 8, 9, 10, 11, 12, 13, 14, 15, 16, 17, 18, 19, 20	7, 12, 19	7, 12, 19	IX

(continued)

Table 7.5 (continued)

S. No.	Reachability set	Antecedent set	Intersection set	Level
20	3, 8, 9, 10, 14, 18, 20	1, 2, 3, 4, 5, 6, 7, 11, 12, 13, 15, 16, 17, 18, 19, 20	3, 18, 20	IV

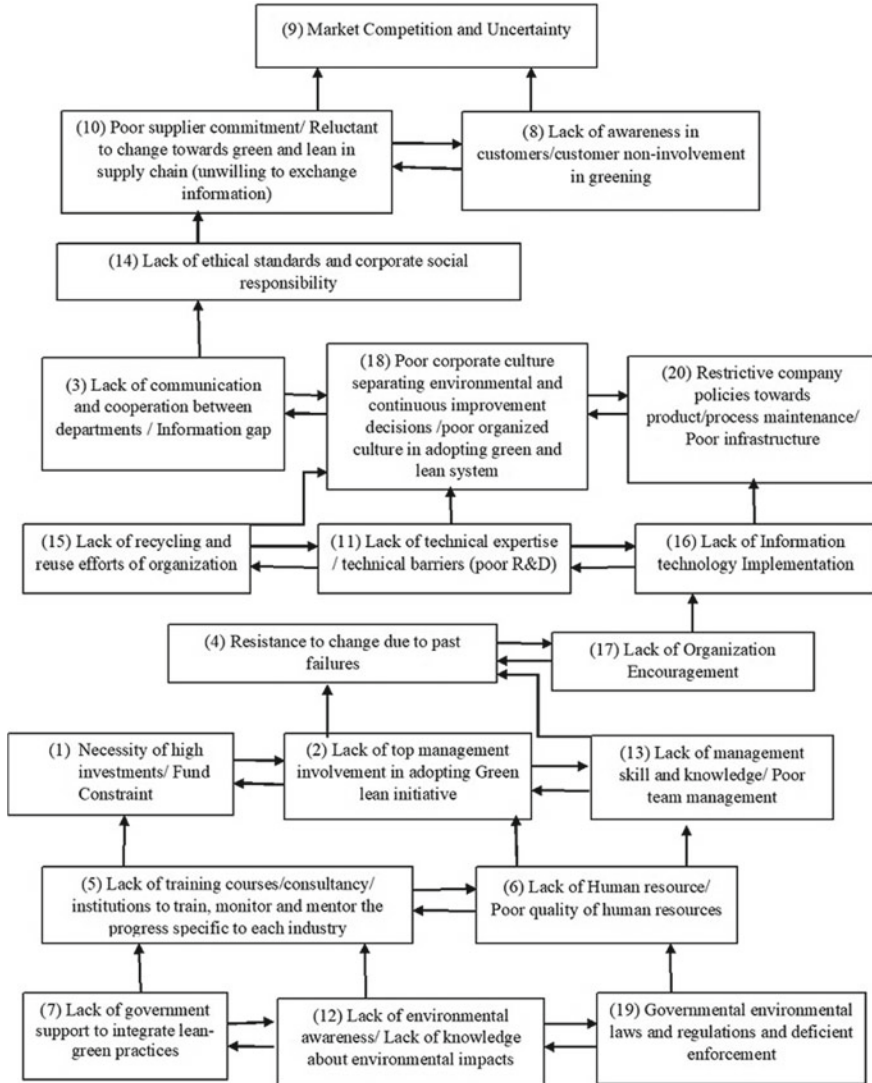


Fig. 7.2 ISM model for barriers in lean green implementation

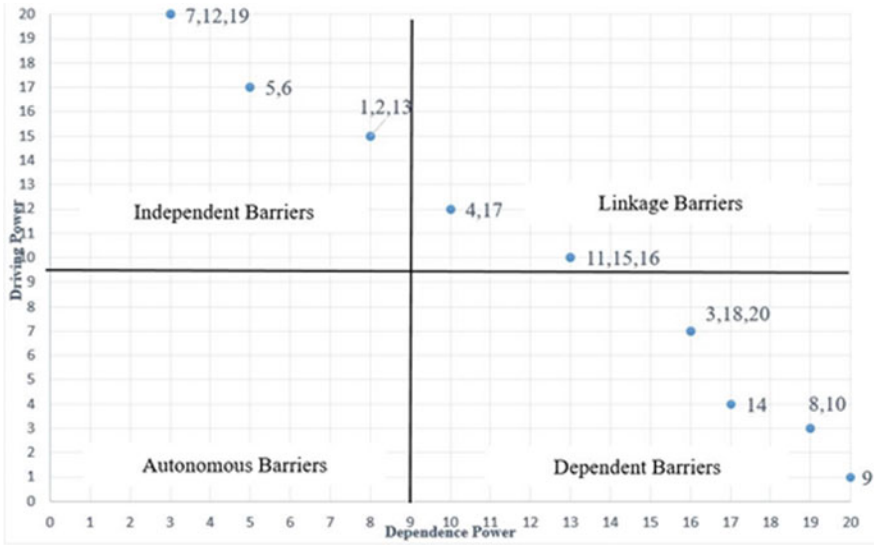


Fig. 7.3 MICMAC analysis

7.4.8 MICMAC Analysis

The MICMAC analysis is developed to investigate and analyse the dependency and driving powers of barriers [15]. The value of powers of each barrier was calculated in final reachability matrix. The MICMAC analysis is shown in Fig. 7.3. In this figure, barriers were categorised in four cluster or quadrants. These four quadrants are autonomous, dependent, independent and linkage.

1. **Autonomous barriers:** Barriers with low driving and dependence power fall in the autonomous category. No barriers were found in this category.
2. **Dependent barriers:** Barriers with high dependence power and less driving power come under the dependent category. It includes Information gap, poorly organised culture in adopting the green and lean system, process maintenance/Poor infrastructure, lacking in terms of ethical standards, lack of awareness in customers/customer non-involvement in greening, market competition and uncertainty and poor supplier commitment/Reluctant to change towards green and lean in the supply chain (unwilling to exchange information).
3. **Linkage barriers:** Barriers with high dependence power and high driver power come under linkage. It includes resistance to change due to past failures, lack of Organization Encouragement, lack of technical expertise/technical barriers (poor R&D), lack of recycling and reuses and lack of information technology implementation.

4. **Independent barriers:** Barriers with more driving power and weak dependence power will come under independent. It includes lack of support from the government, lack of environmental awareness, governmental environmental laws and regulations and deficient enforcement, lack of training courses, the necessity of high investments/fund Constraint, lack of commitment from the management side and poor management skill and knowledge/Poor team management.

The categorisation of barriers based on MICMAC analysis is essential for the organisation, as it will help to define the role of each barrier. This analysis will help to describe the impact of one category barriers on the other category barriers. As per MICMAC analysis, the barriers belongs to the independent will support the barriers belongs to linkage. Similarly, barriers of independent and linkage categories will support the barriers of the dependent category.

7.5 Discussion of Findings

Nowadays, sustainability has gained a lot of attention by academician and industrial experts [6]. The integrated lean-green paradigm will encourage the organisation to achieve sustainability [7]. Although this integrated strategy is beneficial for the organisation, it faces varies challenges during the implementation of lean-green (Cherraffi et al. [6]). Without better understanding and knowledge of these barriers, the organisation cannot effectively implement lean and green in their projects. This research finds the significant barriers facing by the organisations during the implementation of lean green. Barriers were further analysed through the ISM approach with the help of the expert team, which consist of academic and industrial professionals. The research finding of the study is given below.

- Lack of support from the government in the integration of lean-green practices, lack of knowledge about environmental impact, government environmental laws/regulations and deficient enforcement found as the primary barriers for lean green implementation. Cherraffi et al. [6] conducted a study to find barriers in the green lean implementation process and found that environmental practices are influenced by stakeholders group, management and government involvement. Government rules and regulations, schemes to support lean and green practices and promotional advertisement will help the organisations to be aware of its importance and benefits. It has also observed that despite the willingness of adoption the green techniques in organisations, the adoption and implementation level is low due to lack of knowledge about the benefits that can be the low cost-efficient product from environmental practices.
- MICMAC analysis shows that no barriers are autonomous barriers; it means this study confirms that all barriers included in the research play an important role. So the barriers selected in this study can act as an essential challenge towards the implementation of the lean-green project.

- In the study, some of the barriers identified belong to human resource management. These barriers include lacking in training courses for employees, lack of monitoring to see the progress of industry, lack of top management involvement, and lack of management skill and knowledge/Poor team management. It is clear from the study that a skilled worker will help to implement the green lean techniques in organisations. Studies show that lack involvement of human resources will lose the opportunity to achieve sustainable benefits from lean and green manufacturing [6].
- The study also includes financial barriers such as the necessity of high investments and fund Constraint. To implement a new approach/technique some initial funds are required. These funds constraint barrier is considered as an essential barrier in academic literature [2, 9, 10, 25]. So the findings of the research are common from the reported literature. Fund constraint includes mainly the difficulty to get bank loans by the organisations to adopt new green techniques due to lack of support from the government.
- Barriers related to managerial aspects, employee behaviour and technological advancement are also challenging for the organization, which need to be overcome by the firm. Barriers such as Resistance to change due to past failures, Lack of technical expertise/technical barriers (poor R&D) and Lack of communication/cooperation between departments are the barriers which need to explore more by the firm's management.

7.6 Elimination of Barriers

This section comprises of remedial actions suggested by the experts and researchers to eliminate or decrease the effect of barriers in the organisation. The development of the circular economy can overcome the lack of support provided by the government, lack of environmental awareness, governmental environmental laws and regulations and deficient enforcement. Circular economy deals with the conceptualisation of integrated thinking of economic profit and impact on environmental performance [3]. The lean and green initiative requires proper training for employees [6]. It is necessary to educate and train management people as well as workers to ensure the commitment and teamwork management in the organisation.

The organisation can implement various strategies to become internally capable of implementing lean and green manufacturing. One strategy can be the collaboration work with a research organisation, academic institution and getting guidance support from the government to conduct training courses, to get assistance towards the process and to find opportunities for funds. This can help the organisation to minimise their cost in terms of consultation charge, which incurred while getting technical assistance. Also, it will help to improve the skill and knowledge of workers. The necessity of high investments/Fund Constraint barriers can be overcome by the development of financial institution which can provide funding to organisations to start implementing lean and green manufacturing.

Support from the government to use an integrated approach of lean-green and making rules, regulation and policies will also help the organisations to get insurance from the bank to compensate with the risk involved during the adaption process. Application of new techniques can help the organisation to implement 3R (reduce/reuse/remanufacture) policies which encouraged the organisation to be environmentally sustainable. Use of information technology will also help the system to be aware of the waste in the system and to know the customer preferences towards sustainability. The communication between the departments, better policies, infrastructure and supplier support will help the companies to identify the problem in the system, also to monitor and develop action plans to see the progress until achieving goals.

7.7 Managerial Implications

Based on MICMAC analysis in the study, it is found that driving and linkage barriers for lean green manufacturing have to be properly determined by the management and should be removed at the earliest. The developed ISM model will help the management to prioritize these barriers through a hierarchical structure of the model. Barriers that belong to dependence category also influence the other barriers and can affect the implementation process of lean and green in the company. Based on ISM method and MICMAC analysis, the firm's management can avoid these barriers with the help of below implications:

- **Beginning Phase**—Management should have to train the firm's workers and create awareness about the benefits of these techniques which includes environmental friendly practices. The lean and green approach will help the firm to face the competition in the global market.
- **Continuous improvement in manufacturing system**—Management should have to focus on the non-value-added activities which contain various emissions also. These activities and generated waste have to be continuously monitored and reduced with the help of advance technology.
- **Customer orientation**—Management should have to appreciate customer choices and awareness about environmental impacts. Firms need to share information about the firm's efforts towards adaption of lean and green strategies in the supply chain.

The implementation of lean and green techniques should be observed in three main phases of product development. These phases are the design and planning phase, development phase and production phase. The removal of driving barriers can help the firms to integrate the lean and green techniques in the planning phase. After that managing the linkage barriers can help the firms to implement the integrated approach in the development phase. At last, the removal of dependant barriers will help the firm to implement lean and green manufacturing in the production phase.

7.8 Conclusions

In the literature review, many researchers have reported about the integrated approach of lean and green manufacturing and barriers for its implementation [3, 6, 15, 19, 26, 27]. Very limited studies have focused on the solutions for these barriers which can help the organizations to implement lean and green manufacturing in the firm. The study analyses the barriers of lean green implementation and their relationship among each other through ISM modelling approach. This study proposes possible solutions to eliminate these barriers from manufacturing organizations. A systematic literature review has conducted as the first step towards this study to identify the potentials barriers of lean and green manufacturing. The barriers are the hurdles in the way of implementing the lean-green approach. In this study, twenty barriers were identified and further analysed with ISM approach to see their relationship with each other [7, 15, 18].

ISM approach used to analyse the contextual relationship among variables (barriers) to see their importance towards lean green implementation process. These barriers which create hurdles in the implementation process of lean and green manufacturing can be considered as a major challenge for managers and technical experts in the manufacturing industry. Based on the input received from the expert's team, an SSIM matrix was developed which is the first step of the ISM approach. The ISM approach modelled the barriers into nine levels. ISM approach develops a model which shows that Market Competition and Uncertainty, Poor supplier commitment and Lack of awareness in customers barriers acquire the topmost levels in ISM model. It shows that these barriers have less impacts on the implementation process of lean and green manufacturing. These barriers are having less impact than the other barriers of the study. Kumar et al. [15] found in the study that market competition and uncertainty gives very less impact to other barriers. Kumar et al. [15] also suggested that lack of awareness in customer about the environmental impact and poor supplier commitment barriers are comparatively easy to eliminate from the manufacturing system.

In the third and fourth level, a total of four barriers are placed namely: Lack of ethical standards and corporate social responsibility, Lack of communication and cooperation between departments, Poor corporate culture separating environmental and continuous improvement decisions and Restrictive company policies towards product. Barriers at the same level show an equal impact on the lean and green manufacturing implementation process. The barriers found at the bottom position in the ISM model are crucial for the lean and green. The barriers found at the bottom positions are Lack of support from the government in the integration of lean-green practices, lack of knowledge about environmental impact, government environmental laws/regulations and deficient enforcement. These barriers are driving the other barriers during lean and green implementation. Cherrafi et al. [6] concluded that lack of government support to integrate lean and green practice and lack of knowledge about environmental impact are the primary barriers for lean and green

manufacturing implementation. Support from the government can help the organizations to be more aware of the importance and potential benefits of lean and green practices.

These barriers are further analysed by MICMAC approach to recognise the driving and dependence power of these barriers. In this process, these barriers were further categorised into four types as independent, dependent, linkage and autonomous. The categorization of barriers is based on the driving and dependence power of barriers. Study shows that eight barriers are classified as independent barriers, seven barriers are classified as dependent and five barriers are classified as linkage barriers. The result from MICMAC analysis shows that all the barriers included in the study are important and hence can be considered as a significant challenge for the organisation while implementing lean and green manufacturing.

The results and finding of this study will help various organisations to develop theoretical knowledge about lean and green and its implementation to achieve economic and environmental sustainability. The developed model through the ISM approach can be helpful for management and industrial professionals to measure the impact of barriers and take preventive action to avoid them. This study will also be helpful for policymakers to formulate and develop such policies which help and support the organisation to become sustainable. Due to the generic approach of study, these barriers identification will help many organisations in various sectors such as manufacturing, service, healthcare and transport. These all sectors are getting pressure from customers and market competition to operate more sustainably and produce the product in a greenway.

7.9 Future Study and Limitations

In the future perspective, several other barriers can be find based on the geographical location of the industry, specific to the industry and the firm's size. The limitation of the research is that the model developed in the study is solely based on expert judgement and opinions of experts. The opinions of the expert can be biased. The result of this study is not specific to one particular industry, so the barriers for other industry may be different. The study can be validated to a particular industry, company size or country. This study includes twenty barriers for lean green implementation, but in the future study, these can be extended with further analysis. This study can also be validated through structural equation modelling (SEM) with empirical analysis.

References

1. Abdullah, M., Zailani, S., Iranmanesh, M., Jayaraman, K.: Barriers to green innovation initiatives among manufacturers: the Malaysian case. *RMS* **10**(4), 683–709 (2016)

2. AlManei, M., Salonitis, K., Xu, Y.: Lean implementation frameworks: the challenges for SMEs. *Proc. CIRP* **63**, 750–755 (2017)
3. Caldera, H.T.S., Desha, C., Dawes, L.: Evaluating the enablers and barriers for successful implementation of sustainable business practice in ‘lean’ SMEs. *J. Clean. Prod.* **218**, 575–590 (2019)
4. Campos, L.M.S., Vazquez-Brust, D.A.: Lean and green synergies in supply chain management. *Supply Chain Manag. Int. J.* **21**(5), 627–641 (2016)
5. Carleysmith, S.W., Dufton, A.M., Altria, K.D.: Implementing lean sigma in pharmaceutical research and development: a review by practitioners. *R&D Manag.* **39**(1), 95–106 (2009)
6. Cherrafi, A., Elfezazi, S., Garza-Reyes, J.A., Benhida, K., Mokhlis, A.: Barriers in green lean implementation: a combined systematic literature review and interpretive structural modelling approach. *Prod. Plann. Control* **28**(10), 829–842 (2017)
7. De, D., Chowdhury, S., Dey, P.K., Ghosh, S.K.: Impact of lean and sustainability oriented innovation on sustainability performance of small and medium sized enterprises: a data envelopment analysis-based framework. *Int. J. Prod. Econ.* 107087 (2018)
8. Dhingra, R., Kress, R., Upreti, G.: Does lean mean green? *J. Clean. Prod.* **85**, 1–7 (2014)
9. Dhull, S., Narwal, M.: Drivers and barriers in green supply chain management adaptation: a state-of-art review. *Uncertain Supply Chain Manage.* **4**(1), 61–76 (2016)
10. Drohomerski, E., da Costa, S.G., de Lima, E.P.: Green supply chain management. *J. Manuf. Technol. Manage.* (2014)
11. Giunipero, L.C., Hooker, R.E., Denslow, D.: Purchasing and supply management sustainability: drivers and barriers. *J. Purchasing Supply Manag.* **18**(4), 258–269 (2012)
12. Huo, B., Gu, M., Wang, Z.: Green or lean? A supply chain approach to sustainable performance. *J. Clean. Prod.* **216**, 152–166 (2019)
13. Jayant, A., Azhar, M.: Analysis of the barriers for implementing green supply chain management (GSCM) practices: an interpretive structural modeling (ISM) approach. *Procedia Eng.* **97**, 2157–2166 (2014)
14. Kasim, A., Ismail, A.: Environmentally friendly practices among restaurants: drivers and barriers to change. *J. Sustain. Tourism* **20**(4), 551–570 (2012)
15. Kumar, S., Luthra, S., Govindan, K., Kumar, N., Haleem, A.: Barriers in green lean six sigma product development process: an ISM approach. *Prod. Plann. Control* **27**(7–8), 604–620 (2016)
16. Luthra, S., Kumar, V., Kumar, S., Haleem, A.: Barriers to implement green supply chain management in automobile industry using interpretive structural modeling technique: an Indian perspective. *J. Ind. Eng. Manag.* **4**(2) (2011)
17. Massoud, M.A., Fayad, R., El-Fadel, M., Kamleh, R.: Drivers, barriers and incentives to implementing environmental management systems in the food industry: a case of Lebanon. *J. Cleaner Prod.* **18**(3), 200–209 (2010)
18. Mathiyazhagan, K., Govindan, K., NoorulHaq, A., Geng, Y.: An ISM approach for the barrier analysis in implementing green supply chain management. *J. Clean. Prod.* **47**, 283–297 (2013)
19. Mittal, V.K., Sindhvani, R., Kapur, P.K.: Two-way assessment of barriers to lean–green manufacturing system: insights from India. *Int. J. Syst. Assur. Eng. Manage.* **7**(4), 400–407 (2016)
20. Mudgal, R.K., Shankar, R., Talib, P., Raj, T.: Modelling the barriers of green supply chain practices: an Indian perspective. *Int. J. Logistics Syst. Manag.* **7**(1), 81 (2010)
21. Ng, R., Low, J.S.C., Song, B.: Integrating and implementing Lean and Green practices based on proposition of Carbon-Value Efficiency metric. *J. Cleaner Prod.* **95**, 242–255 (2015)
22. Ojo, E., Mbowe, C., Akinlabi, E.T.: Barriers in implementing green supply chain management in construction industry. In: *International Conference on Industrial Engineering and Operations Management* (2014)
23. Prasad, S., Baltov, M., Rao, N., Lanka, K.: Interdependency analysis of lean manufacturing practices in case of Bulgarian SMEs: interpretive structural modelling and interpretive ranking modelling approach. *Int. J. Lean Six Sigma* (2020)
24. Russell-Smith, S.V., Lepech, M.D., Fruchter, R., Meyer, Y.B.: Sustainable target value design: integrating life cycle assessment and target value design to improve building energy and environmental performance. *J. Clean. Prod.* **88**, 43–51 (2015)

25. Salonitis, K., Tsinopoulos, C.: Drivers and barriers of lean implementation in the Greek manufacturing sector. *Proc. CIRP* **57**, 189–194 (2016)
26. Siegel, R., Antony, J., Garza-Reyes, J.A., Cherrafi, A., Lameijer, B.: Integrated green lean approach and sustainability for SMEs: from literature review to a conceptual framework. *J. Clean. Prod.* 118205 (2019)
27. Sindhwani, R., Mittal, V.K., Singh, P.L., Aggarwal, A., Gautam, N.: Modelling and analysis of barriers affecting the implementation of lean green agile manufacturing system (LGAMS). *Benchmark. Int. J.* (2019)
28. Thanki, S.J., Thakkar, J.: Interdependence analysis of lean-green implementation challenges: a case of Indian SMEs. *J. Manuf. Technol. Manage.* (2018)
29. Tiwari, R.K., Tiwari, J.K.: Prioritization of barriers to lean implementation in Indian automotive small and medium sized enterprises. *Manage. Prod. Eng. Rev.* **9** (2018)
30. Vinodh, S., Asokan, P.: ISM and Fuzzy MICMAC application for analysis of lean six sigma barriers with environmental considerations. *Int. J. Lean Six Sigma* (2018)
31. Warfield, J.W.: Developing interconnected matrices in structural modeling. *IEEE Trans. Syst. Men Cybern.* **4**(1), 51–81 (1974)
32. Yadav, G., Desai, T.N.: A fuzzy AHP approach to prioritize the barriers of integrated lean six sigma. *Int. J. Quality Reliab. Manage.* (2017)

Chapter 8

Soft Computing Techniques for Predicting Aeration Efficiency of Gabion Stepped Weir



Aayushi Verma, Subodh Ranjan, Umesh Ghanekar, and N. K. Tiwari

Abstract The paper investigates the modeling performance of aeration efficiency (E20) of gabion stepped weir with varying steps (no step, one step and two steps) by using soft computing techniques. The output values of aeration efficiency are computed using Random Forest (RF) and Artificial Neural Network (ANN). The actual aeration efficiency is taken by conducting experiments in laboratory flume and taking mean size, porosity, discharge, drop height and Reynolds number as input parameters. For comparing the results by these soft computing techniques standard statistical parameters such as coefficient of correlation (CC) and root mean square error (RMSE) are utilized. RF obtained the coefficient of correlation and root mean square error value of 0.8738 and 0.0649 compared to the values of 0.9357 and 0.0550 respectively attained by ANN. The findings of this paper will help in selecting better modeling technique for predicting the aeration efficiency of gabion stepped weir.

Keywords Aeration efficiency · Artificial neural network · Gabion stepped weir · Random forest

8.1 Introduction

Aeration is a mass transfer of oxygen from atmosphere to a liquid or substance. For improving the aeration efficiency (E20), the hydraulic structures can be used as the essential elements as they create strong turbulent mixing along with bubble entrainment at the structure but they block the longitudinal movement of marine life flow and disrupt the movement of chemical and physical material, impacting the water environment. Aeration efficiency and aeration performance of gabion stepped weir is studied by many investigators [1, 5, 8; and many others].

A. Verma (✉) · S. Ranjan · N. K. Tiwari
Department of Civil Engineering, National Institute of Technology, Kurukshetra, Haryana
136119, India

U. Ghanekar
Department of Electronics and Communication Engineering, National Institute of Technology,
Kurukshetra, Haryana 136119, India

Soft computing models, such as Artificial Neural Network (ANN), Genetic Algorithms (GA), Gaussian Processes (GP), Random Forest (RF), Multi-linear regression (MLR), Support Vector Machines (SVM), and etc. have been extensively used in past few years by investigators in several parts of civil engineering. These models are applied to predict efficiency of aeration under various flow conditions and dimensions. Soft computing technique has been implemented as a substitute to traditional regression equations provided in the literature for modeling complex problems. Recently, many investigators such as [2, 3, 6, 7], have applied soft computing method for their studies.

Two soft computing models are used to predict aeration efficiency of gabion stepped weir models and are compared with each other. The present study examines the predicting potential of Random Forest and Artificial Neural Network for gabion weir.

8.2 Random Forest

Random Forest adds to bagging another layer of randomness. Successive trees in bagging don't rely on previous trees; each constructed individually using a data set bootstrap sample. In the end, prediction is made by a simple majority vote. Besides creating each tree using specific data bootstrap sample, RF alters how the regression trees are developed. Compared to many other classifiers, this rather counterintuitive strategy is reliable against over fitting, including neural network, support vector machine and discriminant analysis, and results in very good efficiency. The number of trees to grow, and the number of features to create a tree at each node are two user-defined parameters essential to produce a RF regression. RF algorithm can also be used during the modeling stage to define the value of each variable. To evaluate the relevance of an input variable, a random noise is substituted for each variable in turn. The resulting degradation in the consistency of the model is a variable-importance indicator. The degradation in model quality is evaluated for out-of-bag validation data by the variation in root mean square error. In this study, we applied RF regression to predict the aeration efficiency of gabion stepped weir.

8.3 Artificial Neural Network

Artificial Neural Network (ANN) is a computational method based on the biological nervous system but much of the biological complexity is overlooked. It is accomplished by the ANN with a large amount of highly integrated processing elements (neurons), operating in tandem to solve particular problems, such as forecasting and pattern recognition. Feed forward ANN model is used in this paper in which the data is processed in forward direction only. ANN includes a difficult task of selecting parameters including the number of hidden nodes, number of iterations and learning

Table 8.1 Values of user-defined parameters of ANN

Hidden layer node	Momentum	Learning rate	Training time
6	0.1	0.2	6000

rate. Determining suitable network architecture for a specific problem is necessary, because the topology of the network impacts the computational complexity and generalization capabilities. The three layers (input, hidden and output layer) in ANN are connected with no feedback connections. After trying various network structures, the number of nodes in the hidden layer is decided, as no theory is available up till now to know the hidden layers essential for any given task. During the training process, the user defined parameters are adjusted to get the optimal results. The values for user-defined parameters are mentioned in Table 8.1.

8.4 Experimental Setup

The data for this study are taken by the experiments performed in the hydraulics laboratory of Department of Civil Engineering, NIT, Kurukshetra by [4] using a rectangular steel flume of 25 cm width (26.4 cm at the outlet end), 30 cm height and 4 m length. It has a storage tank at the downstream end of length 125 cm, width 60 cm and depth 60 cm. For recirculation of water, a 2HP pump is used which provides a range of 0.5–6 l/s. On the upstream side, a tank is attached with a metal screen which acts as a barrier to control the turbulence. Discharge is calculated by cipoletti weir on the downstream side.

The gabion stepped models consist of following dimensions: Model 1 has no step gabion weir with dimension 52 cm × 24 cm × 25 cm; Model 2 has one step gabion weir with dimension 26 cm × 24 cm × 12.5 cm of each step; and Model 3 has two step gabion weir with dimension 17.33 cm × 24 cm × 8.33 cm of each step.

8.5 Data Set

The data used in this paper consists of 63 observations, out of which 65% of total data set was taken for training data set and remaining 35% data are taken for testing data set. Discharge, Porosity, Mean size of material, Drop height and Reynolds number has been used for input, and aeration efficiency is used as output. The characteristics for data set are specified in Table 8.2.

Table 8.2 Characteristics of training and testing dataset

Input parameters	Units	Training data			
		Minimum	Maximum	Mean	Standard deviation
Discharge (q)	m ³ /s/m	0.0066	0.0236	0.01736	0.0069
Drop height	cm	0.9	17.82	10.12	3.854
D50	mm	15.6	40.8	27.22	10.376
Porosity	%	21	41.2	29.2325	6.2888
Re	–	6625	23,625	17,400	6953.93
Efficiency (E20)	%	0.04	0.76	0.219	0.1688
		Testing data			
		Minimum	Maximum	Mean	Standard deviation
Discharge (q)	m ³ /s/m	0.0124	0.0234	0.0191	0.0042
Drop height	cm	2.5	14.7	9.075	3.845
D50	mm	15.6	40.8	27.3478	10.8257
Porosity	%	21	41.2	28.687	6.76
Re	–	12,416.67	23,416.67	19,108.7	4213.707
Efficiency (E20)	%	0.07	0.62	0.1804	0.119

8.6 Result and Discussion

In this study, values of RF and ANN models are used for calculation of correlation coefficient and root mean square error by using training and testing dataset. Performance of the models in training and testing set are stated in Tables 8.3 and 8.4. The result suggests better performance of ANN in terms of correlation coefficient (CC) and root mean square error (RMSE) in both training and testing data set compared to RF with this dataset. A significant improvement in accuracy by ANN regression shows that it can be used in prediction of aeration efficiency of gabion stepped weir.

Figures 8.1 and 8.2 shows the relation between actual data set and predicted data set of aeration efficiency of Gabion stepped weir for training and testing set,

Table 8.3 Performance of soft computing techniques using training data

Techniques	CC	RMSE
RF	0.9920	0.0299
ANN	0.9924	0.0268

Table 8.4 Performance of soft computing techniques using testing data

Techniques	CC	RMSE
RF	0.8738	0.0649
ANN	0.9357	0.0550

Fig. 8.1 Actual versus predicted values for training data set

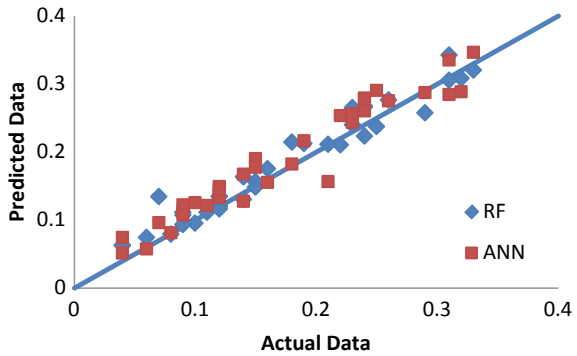
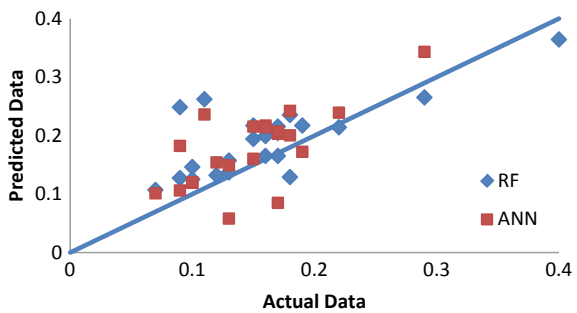


Fig. 8.2 Actual versus predicted values for testing data set



respectively. From Fig. 8.2 it can be seen that few of the values are far off from the line in the case of ANN.

Figure 8.3 shows the variation of predictive values and actual values of aeration efficiency (E20) with number of dataset. From this plot it is clear that Predictive values by ANN approach is in good agreement with actual experimental performance; while RF is deviating at few of the dataset of the two soft computing methods.

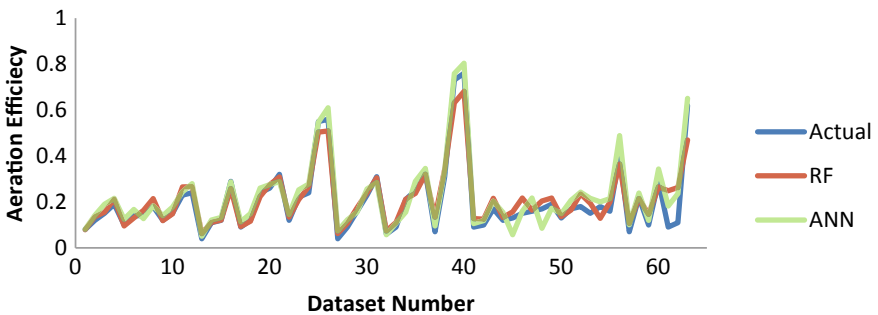


Fig. 8.3 Variation in predictive values by RF and ANN in comparison of actual value

8.7 Conclusion

The present experimental work has been conducted to predict the aeration efficiency of gabion stepped weir with different number of steps and with three different size of the gravel material. The predicted values of aeration efficiency through gabion weir were computed using RF and ANN by taking mean size, porosity, discharge, drop height, Reynolds number as input parameters. ANN gives the better result among the two modeling techniques used with CC 0.9357 and RMSE 0.0550 compared to RF with CC 0.8738 and RMSE 0.0649. Hence ANN can be successfully used in estimation of aeration efficiency of gabion stepped weir.

References

1. Al-Fawzy, A.M., Al-Mohammed, F.M.: Dissipation of energy of flow by conventional type of gabion weir. In: IOP Conference Series: Materials Science and Engineering, vol. 584, No. 1, p. 012038. IOP Publishing (2019, Aug)
2. Deswal, S.: Modeling oxygen-transfer by multiple plunging jets using support vector machines and Gaussian process regression techniques. *Int. J. Civ. Environ. Eng.* **5**(1), 1–6 (2011)
3. Hamed, M.M., Khalafallah, M.G., Hassanien, E.A.: Prediction of wastewater treatment plant performance using artificial neural networks. *Environ. Modelling Softw.* **19**(10), 919–928 (2004)
4. Luxmi, K.M.: Aeration at the Gabion Weir. M.Tech Diss., National Institute of Technology, Kurukshetra (2019)
5. Mohamed, H.I.: Flow over gabion weirs. *J. Irrig. Drainage Eng.* **136**(8), 573–577 (2010)
6. Roushangar, K., Alami, M.T., Shiri, J., Asl, M.M.: Determining discharge coefficient of labyrinth and arced labyrinth weirs using support vector machine. *Hydrol. Res.* **49**(3), 924–938 (2018)
7. Sattar, A.A., Elhakeem, M., Rezaie-Balf, M., Gharabaghi, B., Bonakdari, H.: Artificial intelligence models for prediction of the aeration efficiency of the stepped weir. *Flow Meas. Instrum.* **65**, 78–89 (2019)
8. Wüthrich, D., Chanson, H.: Hydraulics, air entrainment, and energy dissipation on a Gabion stepped weir. *J. Hydraulic Eng.* **140**(9), 04014046 (2014)

Chapter 9

Performance Evaluation of Availability of Complex Repairable System and Selection of Optimal Performance Parameters Using Particle Swarm Optimization



Ajay Kumar and Devender Punia

Abstract In this research study, the steady and transient state availability is modeled using Markov Methods and Particle Swarm Optimization (PSO) has been implemented for selections of optimal parameters for a complex repairable screw manufacturing system. The considered system is modeled structurally representing its various constituent elements/components and their interconnections. The various failure and repair rates of the various elements of the considered system are calculated practically studying the maintenance records of the past history. Performance analysis of availability is done to observe the dependency/criticality of the various failures and repair rate. The transient state analysis is carried out to calculate the mean time to failure of system. The PSO gives the optimal availability at various combinations of performance parameters at various particle size and iterations. The results of this paper will be valuable for the maintenance engineer and plant staff to achieve best possible feasible/optimum system performance by selection of appropriate performance parameter for maximizing the availability of system and to plan appropriate maintenance strategies.

Keywords Maintenance strategies · Modeling · Complex systems · Repair and failure rates · Performance analysis · Particle swarm optimization · Availability

9.1 Introduction

Increasing the demands of industrial revolution with the advancement depends upon the functioning of complex machinery and equipment. The necessary concepts and tools of industry provide discipline by reliability engineering and repair it's performed by raising the utilization of its resources. In the process industry required that different components or equipment used whenever needed. If the equipment fail sometimes it is impossible to recover it, which leads to overall system failure. A high

A. Kumar (✉) · D. Punia

Department of Mechanical Engineering, Deen Bandhu Chhotu Ram University of Science and Technology, Murthal, Sonapat, India

level of complexity characterized by today's technological system like nuclear power plant, aircraft, and production industries like chemical, screw, thermal etc. Industrialization got to expand newly products and make better modern products to raise meet consumer demands so on survive and increase during a vicious competitive environment. Product quality and reliability are critical carrying capacity factors and hence the most concerns of process industries. Kumar [17] studied the availability optimization of rice processing plant and device a maintenance plan for maximum profit. Weichert et al. [37] analyzed a progress within the process industry and also the developed available data due to the markov process, improve production processes by large attention in optimization methods and integrating machine learning. Singhal and Sharma [33] discussed an article produce a new technique for behavior analysis of systems through fuzzy Kolmogorov's differential equations and Particle Swarm Optimization. Markov modeling has been formulated of differential equations and uncertainty in data of system in fuzzy environment. KDEs (Kolmogorov's Differential Equations) are derived and then their solutions are obtained by Runge-Kutta 4th Order Method. The PSO (Particle Swarm Optimization) improved the solutions obtained above. Li et al. [18] discussed probabilistic and a systematic availability for periodical investigation system which may obtain instantaneous availability and average availability of periodical investigation system under repair-time distributions. Agrwal et al. [1] analyzed an EPBTBM is utilize for making an irrigation tunnel by RAM (reliability, availability and maintainability). Dahiya et al. [4] discussed a system of sugar industry in which a mathematical model is formulated and reliability approach is used. The formulated mathematical model considers failure and repair rates as exponential distribution. The differential equations are expanded by using Markov method and reliability. Sharifi et al. [29] analyzed that work on a system including k-out-of-n subsystem along with common cause failures and short circuit for the components in various subs in adding to components failures. System availability has affected by these two failures show by Markov model. Wu et al. [38] proposed a semi-Markov multi-state repairable system is take part uncertainty model with a reduction on transition time. To search out the optimal number of transition times of integer nonlinear programming is solved by algorithm. Kumar [10] developed a computational software for evaluation of availability of pre heat exchanger using the PSO and make comparison of the results with other optimization technique. Kumar [11] studied the multi-condition degraded manufacturing production system and optimized the performance parameters using PSO. Bolvashenkov et al. [2] presented the Markov technique to the comparison between analyses of various sorts of adhesion electric motors for evaluation the reliability correlated expense of the propulsion systems. Determine of reliability correlated and average availability developed by the Markov technique for considering aging process of electrical motors and vehicle operational conditions. Liu et al. [19] proposed a Markov approach is expanded to deal with variety generation during a two-stage system. Supported the presented mathematical model, determine transient quality performance by analytical formulas also including the setting time, quality loss and real-time product quality. López-Campos et al. [20] studied a strategy to initiate e-maintenance plans that incorporate the database of tools for RCM, CMMS and results from the CBM. Tsarouhas [35]

analyzed a tool to look at the present operations management of the industry system. When reducing production costs then, engineers and managers are going to be ready to make the proper resolve about the system, productivity and optimizing capacity. Velásquez and Lara [36] studied the primary of reliability investigation, it has been involved to the preparation and design of short circuit. Kumar et al. [16] analyzed the various reliability compute like reliability, profit function, availability and M.T.T.F. Laplace transformation, supplementary unsteady technique. Qiu et al. [23] studied optimal maintenance policies and availability of a system is going through periodical inspections and find out analytical result of system are derived. Kumar et al. [14] used probabilistic approach for a Markov-Birth-Death process with the help of mathematical formulation is find out analysis of availability, performance modeling and developed a model of fabric finishing system. Kumar and Tiwari [15] proposed a PSO approach is apply to find out optimization and performance analysis for CSDGB filling system. Markov Approach is to performed mathematical modeling and exponential distribution for failures and repairs rates. Goyal and Ram [6] determined the measures reliability of a series and parallel system with mathematical model has been designed and the system is analyzed under the observation of preventive maintenance and equipment failures. Kumar and Garg [12, 13] examine the performance analysis of brewery plant and optimize the availability function using particle swarm optimization technique. Ram and Manglik [26] presented a multi-state is repairing manufacturing system of a mathematical model with several of failures like partial, human, catastrophic and common cause is associating waiting time to repair. Laplace transformation and supplementary variable technique is used for determine reliability measures like availability, reliability, MTTR, MTTF, sensitivity analysis. Malik and Goel [21] studied cost and availability analysis is containing of two module system and these modules can work in reduced and complete capacity. Sabouhi et al. [28] discussed the result of component stability and repair on the reliability and availability is too significant of three common types of plants that is STPP, GPPP and CCPP. Repair rate, steady-state analysis and failure rate analysis of plants are derived from the mathematical expression. Rao and Naikan [27] an availability modeling is proposed a MSD technique and is to analyze the dynamic conduct of repairable system. Ram and Kumar [25] studied the Laplace transformation, variable technique, Markov process theory and reliability models are determined for paper mill plant system. He et al. [7] analyzed periodic preventive maintenance and periodic inspection of a system is to find and correct hidden failures that give to raise cost per unit time. Singh and Rawal [32] Laplace transforms and supplementary is used to study the system. Maintenance cost has been discussed by different operation of reliability namely MTTF, state transition probabilities, availability and profit function. Manglik and Ram [22] determined the reliability is used by Laplace transformation. Khanduja et al. [9] presented the maintenance planning and steady state action is for the bleaching system. A probabilistic approach is used for Markov birth-death process to find out mathematical modeling. Soro et al. [34] determined the availability is developed by a model and function of multi-state degraded system is for reliability function and production rate subjected to imperfect preventive maintenance and minimum repair. Sharma and Kumar [31] composite industrial system is achieved

high performance by the modification of RAM (reliability, availability and maintainability) analysis. Genetic algorithm and Lambda-Tau methods are applied for system to expression for RAM analysis. Sharma and Kumar [30] carried out design change for RAM analysis is to acquire increase mean time to failures or minimum failures and system behavior is find out by Markov model. Dhillon and Shah [5] studied the production of a system with three-state devices is affected by common cause failure, human error, maintenance policies and redundancy. He and Wang [8] studied the optimization problems are by a CPSO (co-evolutionary particle swarm optimization approach). Chen and Trivedi [3] presented a joint optimization of maintenance policy and inspection rate is by SMDP, and condition based maintenance of optimal maintenance policy is searching by Markov decision program (MDP) algorithm. Levantesiet. al. [24] carried out a systematic method is for calculating the performance of non-parallel production lines along with deterministic processing times.

9.2 System Description

Metal Gathering Machine is produced the perfect “gain flow” of metal employing heat and up-setting effect applied both parallel on work-piece. It provides with homogeneous and accurate gathering results. These machines are engaged for the assembly of wide selection of head forming like beads, collar and flange, required with in the manufacturing of parts like valves heads, Flange Bolts, and bobbins etc. The Metal Gathering Machine system is consisting of the following five elements:

Subsystem (A): This subsystem includes of one unit (heating unit). Failure of unit considered as the total failure of the system.

Subsystem (B): It includes of one unit (upper clamping unit). Failure of unit considered as the total failure of the system.

Subsystem (C): It includes of one unit (lower clamping unit). Failure of unit considered as the total failure of the system.

Subsystem (D): It includes of one unit (temperature controller). Failure of unit considered as the total failure of the system.

Subsystem (E): It includes of one unit (work piece holder). Failure of unit considered as the total failure of the system.

These elements D1–D5 are arranged in series configuration and the block diagram is presented by Fig. 9.1.

9.2.1 Notation Used

Table 9.1 shows the notations used symbolically for the performance analysis and

Fig. 9.1 Block diagram of metal gathering machine system

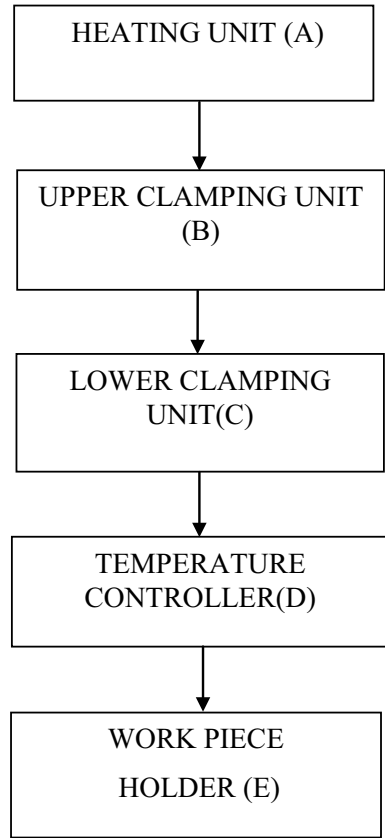


Table 9.1 Notations assumed in performance modelling of metal gathering machine system

Notations used in metal gathering machine					
State	Block diagram	Transition diagram	Full capacity (without standby)	Full capacity (with standby)	Reduced capacity
Notations	Figure 9.1	Figure 9.2	ABCDE	–	–
State	Failed state	Failure rates	Repair	–	–
Notations	abcde	$\alpha_1-\alpha_5$	$\beta_1-\beta_5$	–	–

modelling of the Metal Gathering Machine system which are used for generation of transition/Probability state diagram.

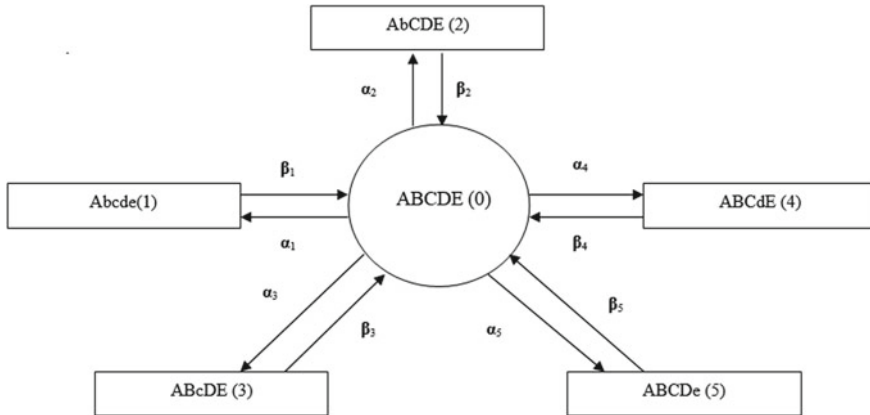


Fig. 9.2 Transition diagram of metal gathering machine system

9.2.2 Assumptions

In order to carry out performance modelling of Metal Gathering Machine System of a Screw manufacturing system, it is assumed that:

1. Failure and repair rates follow the decaying exponential curve and are independent of each other.
2. Only single element or their component fails at any particular instant of time keeping other element in good working state.
3. In case of presence of standby unit the failure of every element is through a reduced capacity working phase
4. If a system recovered it will be considered perfectly working state.
5. Switch-over devices for standby unit are considered almost perfect.

9.2.3 Data Collection

Failure rate is a function of time and presented as the proportion of total quantity of failures (N) and time (t) duration. In accordance with the behavior of bathtub curve, during early phase of its working, the failure rates are more. During the normal life of system operation, it reduces to a steady value which can be assumed steady state and due to wear and tear; it rise again at the end. The proper values of such failure and repair rates are collected practically for the particular element from the process history record, daily operation reports, maintenance report sheet etc., available in the considered Screw manufacturing plant for a period of six month after observations and discussions with maintenance engineers which are given in Table 9.2. The availability matrix explores the possibilities of an assortment of proper

Table 9.2 Failure and repair rates of metal gathering machine system of a screw manufacturing plant

Subsystems	Ranges of failure rates	Ranges of repair rates
Heating Unit	0.00322–0.00722	0.033–0.073
Upper clamping unit	0.00164–0.00564	0.017–0.057
Lower clamping unit	0.00163–0.00563	0.019–0.059
Temperature controller	0.00321–0.00721	0.032–0.072
Work piece holder	0.00421–0.0082	0.041–0.081

selection of failure/repair rates and corresponding availability levels of the elements of a Screw manufacturing plant.

9.3 Performance Modelling

A system or component can be one of three states failed, working or reduced state. The probabilities are related with these states on the basis of a continuous or discrete. The steady state analysis is used for evaluation of probability of being in same state or the other at any time. In availability and reliability analysis, the major performance measures variables are failure probability, the probability of being returned to an available state, repair rate and failure rate. The Markov analysis, one of the most widely used reliability analysis methods is developed by Andrei Andreyevich Markov, who was a Russian mathematician, is applied under the constraint that process is homogenous.

9.3.1 Structural Modelling

For operational illustration of the Metal Gathering Machine System, a transition diagram using the notations as represented in Table 9.1 is drawn, which represents the probabilities of all feasible states (full working condition, reduced working condition and failed condition).

Markov graph has been used to draw the transition diagram of considered system which pictorially exhibits the Markov process and different possible probability of the state is represented by nodes of branches in transition diagram of the Metal Gathering Machine System. Markov model is denoted by a probability matrix whose

typical element P_{ij} represents the transition probability from the state 'i' to a mutually exclusive state 'j'. Figure 9.2 shows the transition diagram of Metal Gathering Machine System.

9.3.2 Mathematical Modelling

The Chapman-Kolmogorov difference-differential equations corresponding to the transition diagram as given in Fig. 9.2 are formulated using mnemonic rule. These equations are:

$$(d/dt + \alpha_1 + \alpha_2 + \alpha_3 + \alpha_4 + \alpha_5)P_0(t) = \beta_1P_1(t) + \beta_2P_2(t) + \beta_3P_3(t) + \beta_4P_4(t) + \beta_5P_5(t) \quad (9.1)$$

$$(d/dt + \beta_1)P_1(t) = \alpha_1P_0(t) \quad (9.2)$$

$$(d/dt + \beta_2)P_2(t) = \alpha_2P_0(t) \quad (9.3)$$

$$(d/dt + \beta_3)P_3(t) = \alpha_3P_0(t) \quad (9.4)$$

$$(d/dt + \beta_4)P_4(t) = \alpha_4P_0(t) \quad (9.5)$$

$$(d/dt + \beta_5)P_5(t) = \alpha_5P_0(t) \quad (9.6)$$

With initial condition at time $t = 0$.

$$P_i(t) = 1 \quad \text{for } i = 0 \\ = 0 \quad \text{for } i \neq 0$$

Steady state availability of Metal Gathering Machine.

By putting $d/dt = 0$ at $t \rightarrow \infty$ in Eqs. (9.1–9.6) the steady state probabilities are given as:

$$P_1 = \alpha_1/\beta_1P_0 \quad (9.7)$$

$$P_2 = \alpha_2/\beta_2P_0 \quad (9.8)$$

$$P_3 = \alpha_3/\beta_3P_0 \quad (9.9)$$

$$P_4 = \alpha_4/\beta_4P_0 \quad (9.10)$$

$$P_5 = \alpha_5/\beta_5 P_0 \quad (9.11)$$

$$P_0 = (\beta_1 P_1 + \beta_2 P_2 + \beta_3 P_3 + \beta_4 P_4 + \beta_5 P_5) / (\alpha_1 + \alpha_2 + \alpha_3 + \alpha_4 + \alpha_5) \quad (9.12)$$

$$\sum P = 1$$

$$P_0 + P_1 + P_2 + P_3 + P_4 + P_5 = 1 \quad (9.13)$$

On putting the values of P_1, P_2, P_3, P_4, P_5 , in term of P_0 in Eq. (9.13) and we get

$$P_0\{1 + (\alpha_1/\beta_1 + \alpha_2/\beta_2 + \alpha_3/\beta_3 + \alpha_4/\beta_4 + \alpha_5/\beta_5)\} = 1$$

$$P_0(1 + Z) = 1$$

The formulation of steady state availability for Metal Gathering Machine System (A_v) may be estimated by adding the probabilities of working states only.

$$\text{Availability } (A_v) = P_0 = 1/(1 + Z) \quad (9.14)$$

9.4 Performance Analysis

Equation 9.14 provides the overall availability (A_v) of the system availability as function of its failure rates (α_i) and repair rates (β_i) which includes all possible working states. The maximum availability of the system is considered for all feasible values of (α_i, β_i). Table 9.3 provides the decision matrices corresponding to each element of a Metal Gathering Machine System of a Screw manufacturing industry.

9.5 Result Discussion

The steady state analysis is shown in Table 9.3 and Fig. 9.3, it is noted that effect of failure and repair rates of Heating unit for the longer span of time availability of the system. With the increase of failure rate from 0.00322 to 0.00722, the system availability decrease by 7.56% and for the increase of repair rate from 0.033 to 0.073, availability of the system gain by 3.74%. For the system Upper Clamping unit, with the increase of the failure rate from 0.00164 to 0.00564, the system availability decrease by 13.70% and with the increase of repair rate from 0.017 to 0.057, the availability of the system increase by 4.77%. With the increase of the failure rate from

0.00163 to 0.00563 for the Lower Clamping unit, the system availability decrease by 12.44 and increase of repair rate from 0.019 to 0.059, the availability of the system increased by 4.07%. In case of Temperature Controller sub system, the increase of the failure rate from 0.00321 to 0.00721, the system availability decrease by 7.75% and the increase of repair rate from 0.0032 to 0.0072, the availability of the system increased by 3.9%. From the table it can be concluded that for the subsystem Work piece Holder, the increase of failure rate from 0.00421 to 0.00821, the system

Table 9.3 Decision Matrices Of The Elements Of A Metal Gathering Machine system

<i>Heating unit</i>						
	β_1					
α_1	0.033	0.043	0.053	0.063	0.073	Constant values
0.00322	0.6744	0.6849	0.6916	0.6962	0.6996	$\alpha_2 = 0.00164$
0.00422	0.6609	0.6741	0.6827	0.6886	0.6930	$\beta_2 = 0.017$
0.00522	0.6479	0.6637	0.6740	0.6811	0.6865	$\alpha_3 = 0.00163$
0.00622	0.6354	0.6536	0.6655	0.6739	0.6801	$\beta_3 = 0.029$
0.00722	0.6234	0.6438	0.6573	0.6667	0.6738	$\alpha_4 = 0.00321$
						$\beta_4 = 0.032$
						$\alpha_5 = 0.00421$
						$\beta_5 = 0.041$
<i>Upper clamping unit</i>						
	β_2					
α_2	0.017	0.027	0.037	0.047	0.057	Constant values
0.00164	0.6744	0.6910	0.6990	0.7036	0.7066	$\alpha_1 = 0.00322$
0.00264	0.6487	0.6738	0.6860	0.6932	0.6980	$\beta_1 = 0.033$
0.00364	0.6248	0.6574	0.6735	0.6831	0.6896	$\alpha_3 = 0.00163$
0.00464	0.6027	0.6418	0.6615	0.6734	0.6813	$\beta_3 = 0.019$
0.00564	0.5820	0.6269	0.6499	0.6639	0.6733	$\alpha_4 = 0.00321$
						$\beta_4 = 0.032$
						$\alpha_5 = 0.00421$
						$\beta_5 = 0.041$
<i>Lower clamping unit</i>						
	β_3					
α_3	0.019	0.029	0.039	0.049	0.059	Constant values
0.00163	0.6744	0.6881	0.6950	0.6992	0.7019	$\alpha_1 = 0.00322$
0.00263	0.6513	0.6722	0.6828	0.6893	0.6937	$\beta_1 = 0.033$
0.00363	0.6297	0.6569	0.6711	0.6798	0.6856	$\alpha_2 = 0.00164$
0.00463	0.6095	0.6424	0.6597	0.6705	0.6777	$\beta_2 = 0.017$
0.00563	0.5905	0.6285	0.6488	0.6614	0.6700	$\alpha_4 = 0.00321$
						$\beta_4 = 0.032$
						$\alpha_5 = 0.00421$
						$\beta_5 = 0.041$

(continued)

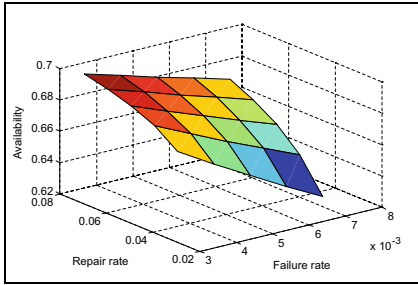
Table 9.3 (continued)

<i>Temperature controller</i>							
	β_4						Constant values
α_4	0.032	0.042	0.052	0.062	0.072		
0.00321	0.6744	0.6854	0.6924	0.6972	0.7007		$\alpha_1 = 0.00322$
0.00421	0.6605	0.6744	0.6833	0.6895	0.6940		$\beta_1 = 0.033$
0.00521	0.6471	0.6638	0.6744	0.6819	0.6873		$\alpha_2 = 0.00164$
0.00621	0.6343	0.6534	0.6658	0.6745	0.6808		$\beta_2 = 0.017$
0.00721	0.6220	0.6434	0.6574	0.6672	0.6745		$\alpha_3 = 0.00163$
							$\beta_3 = 0.019$
							$\alpha_5 = 0.00421$
							$\beta_5 = 0.041$
<i>Work piece holder</i>							
	β_5						Constant values
α_5	0.041	0.051	0.061	0.071	0.081		
0.00421	0.6744	0.6837	0.6901	0.6947	0.6983		$\alpha_1 = 0.00322$
0.00521	0.6635	0.6746	0.6823	0.6880	0.6923		$\beta_1 = 0.033$
0.00621	0.6529	0.6658	0.6748	0.6814	0.6864		$\alpha_2 = 0.00164$
0.00721	0.6427	0.6572	0.6674	0.6749	0.6807		$\beta_2 = 0.017$
0.00821	0.6328	0.6489	0.6602	0.6685	0.6750		$\alpha_3 = 0.00163$
							$\beta_3 = 0.019$
							$\alpha_4 = 0.00321$
							$\beta_4 = 0.032$

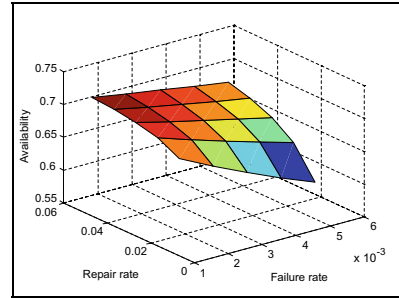
availability decreased by 6.16%. Similarly with the increase of repair rate from 0.041 to 0.081, the availability of the system increased by 3.54%.

The Transient state analysis is done using Ranga Kutta approach considering the tome duration for a year. The Mean time between failures is calculated to be 255 days. The variation of availability of Metal Gathering Machine system with time is shown in Table 9.4 and Fig. 9.4.

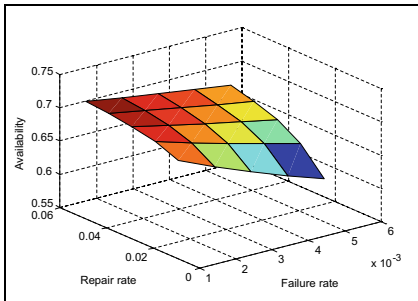
The Particle Swarm Optimization technique is used for finding out the best combination of failure rate and repair rate considering the availability function (Eq. 9.14) as objective function. The numbers of iterations are considered from 50 to 2000 in interval of 50 and numbers of particles are considered from 16–20. The results are shown in Table 9.5. The optimum availability achieved is 77.9% which is at 16 numbers of particles and 100 numbers of iterations as shown in Table 9.5. The corresponding failure and repair rates are given in Table 9.5.



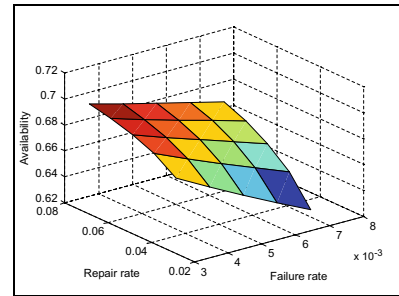
Heating Unit



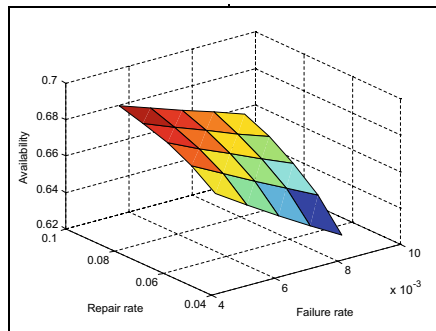
Upper Clamping Unit



Lower Clamping Unit



Temperature Controller



Work piece Holder

Fig. 9.3 Effects of elements failure and repair rates on availability of Metal Gathering Machine system

9.6 Conclusion

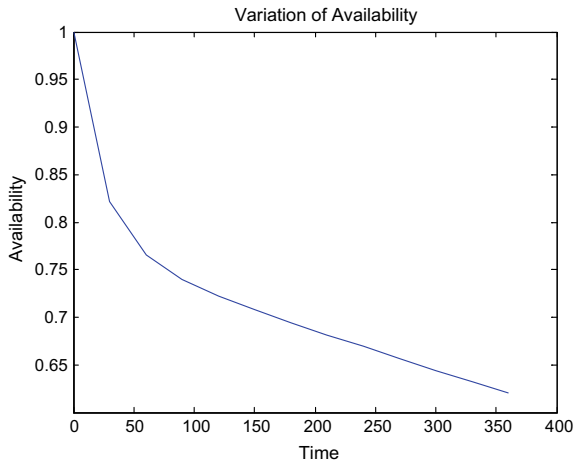
With an increase in the complexities of real industrial systems, maintenance decision making has become a challenge for maintenance managers. In the present study, the Screw manufacturing industry is considered to study the performance analysis of

Table 9.4 transient state variation of availability

Time (days)	Availability
0	1.0000
30	0.8211
60	0.7650
90	0.7396
120	0.7225
150	0.7080
180	0.6947
210	0.6818
240	0.6692
270	0.6567
300	0.6444
330	0.6322
360	0.6201

MTBF = 255

Fig. 9.4 Variation of availability with time for material gathering machine



availability. The different approaches Markov method and particle swarm optimization is utilised in present study. In this study the availability function of considered system is optimised using different combination of failure and repair rates. In the transient state analysis it is clear that after some time the behaviour of the system become steady state. From the PSO table result the plant engineer can select ant combination of failure or repair rate considering the economic criteria for optimum availability of the system. The result of this study will be beneficial for planning the maintenance schedule of considered industry.

Table 9.5 Failure and repair rates corresponding to availability using PSO

S. No.	n	N	α_1	α_2	α_3	α_4	α_5	β_1	β_2	β_3	β_4	β_5	A_4
1	16	50	0.003573	0.00385502	0.00202852	0.00350762	0.0069508	0.04872331	0.05674093	0.05153663	0.038061	0.073814413	0.77870123
2	16	100	0.003798	0.00308367	0.00309974	0.0032203	0.00764613	0.03539792	0.05583234	0.05785333	0.071292	0.070918781	0.779415461
3	16	200	0.004044	0.00225026	0.00225065	0.00333407	0.00662185	0.06605431	0.04718804	0.0483522	0.040817	0.064283219	0.741068426
4	16	500	0.003655	0.0028055	0.00458312	0.00409128	0.00739544	0.05651692	0.05558523	0.05412228	0.047766	0.047677944	0.755364786
5	16	1000	0.003838	0.00463577	0.00334149	0.00335981	0.00746536	0.0714609	0.0482594	0.03837037	0.03771	0.051699221	0.748846793
6	16	1500	0.004148	0.00254674	0.00292467	0.00626184	0.00792618	0.06546405	0.03387321	0.0555719	0.065999	0.068087609	0.724490035
7	16	2000	0.00458	0.00233179	0.00229525	0.00664882	0.00751865	0.04585732	0.03827491	0.04462069	0.063335	0.058018649	0.693445625
8	17	50	0.00375153	0.0040169	0.002447	0.00354368	0.006893	0.037697	0.03074992	0.04360098	0.05789887	0.0654505	0.733723078
9	17	100	0.00356057	0.0051656	0.00266195	0.00319306	0.007749	0.0496552	0.0408511	0.03307669	0.06244371	0.07384699	0.759791069
10	17	200	0.00472005	0.0040624	0.00354905	0.00380412	0.007453	0.0503472	0.04936502	0.04372565	0.05387502	0.06443607	0.708999995
11	17	500	0.00476758	0.0027173	0.00558457	0.00393046	0.007734	0.0574508	0.04312328	0.04629052	0.05383676	0.04611851	0.679234546
12	17	1000	0.00345237	0.0032467	0.00326127	0.00600825	0.008153	0.0365370	0.02895962	0.04276631	0.03832164	0.04210880	0.721336971
13	17	1500	0.00416308	0.0042643	0.00452867	0.00470187	0.0074115	0.0519119	0.042377	0.04937711	0.03395573	0.06030902	0.709041046
14	17	2000	0.00464714	0.003701	0.00303427	0.00548693	0.007111	0.044144	0.04607837	0.05441929	0.04757818	0.06884222	0.698613173
15	18	50	0.0036665	0.0026336	0.0046569	0.00627937	0.006421	0.03363107	0.03672099	0.04658508	0.04545317	0.076039257	0.678036108
16	18	100	0.0040549	0.0041043	0.0030521	0.00543238	0.007659	0.06078895	0.0345406	0.03963249	0.0487151	0.063596026	0.707773045
17	18	200	0.0045822	0.0045705	0.0021656	0.00384825	0.007257	0.06808927	0.0397595	0.03674633	0.07071467	0.0444408659	0.710345485
18	18	500	0.0037650	0.0018344	0.0016937	0.00420004	0.007727	0.06805154	0.02272403	0.04636565	0.0673139	0.076650766	0.754459444
19	18	1000	0.0035802	0.0033076	0.0024394	0.00377989	0.006801	0.06065304	0.03123096	0.04744763	0.0490252	0.058411447	0.745085443
20	18	1500	0.0045514	0.0055324	0.0020146	0.00380429	0.007795	0.04752181	0.0490382	0.02777038	0.0605737	0.072342295	0.711524948
21	18	2000	0.0044085	0.0046333	0.0033948	0.00614486	0.007826	0.05699708	0.04259951	0.04942933	0.0532533	0.045785366	0.707674233
22	19	50	0.0032845	0.0020916	0.00362263	0.0041106	0.00632369	0.0371995	0.03769526	0.055728	0.05458025	0.04385771	0.740498327
23	19	100	0.0036468	0.00257502	0.00480893	0.00325453	0.00629727	0.0447511	0.05430842	0.04923656	0.0442739	0.04426571	0.729849747

(continued)

Table 9.5 (continued)

S. No.	n	N	α_1	α_2	α_3	α_4	α_5	β_1	β_2	β_3	β_4	β_5	A_4
24	19	200	0.0042282	0.00286331	0.00332035	0.00545855	0.0076088	0.0505606	0.04272795	0.03870751	0.05557574	0.06910718	0.704075858
25	19	500	0.0038809	0.00234753	0.00217927	0.00349997	0.00637178	0.0713202	0.03978231	0.0562659	0.05828964	0.08001353	0.741514205
26	19	1000	0.0042732	0.0043466	0.00247862	0.00329638	0.0068193	0.0368409	0.03679702	0.02905704	0.06288649	0.0554561	0.697003957
27	19	1500	0.0047026	0.00525216	0.0038006	0.00625136	0.00807509	0.0638968	0.05544197	0.04921023	0.06967372	0.05178872	0.706142727
28	19	2000	0.0032924	0.00548953	0.0038721	0.0051167	0.00702097	0.0395118	0.04198712	0.05088125	0.04065213	0.04373586	0.735615482
29	20	50	0.0039263	0.0040344	0.0022580	0.0044596	0.007901	0.06394362	0.02633852	0.03556022	0.04617923	0.059495284	0.709652546
30	20	100	0.0035416	0.0057020	0.0026715	0.0065207	0.00922	0.04606206	0.02747227	0.04874059	0.04641394	0.056394618	0.706733514
31	20	200	0.0040149	0.0037940	0.0039633	0.0066445	0.008011	0.04594876	0.03833434	0.04971809	0.06853332	0.071712251	0.709190612
32	20	500	0.0034398	0.0045858	0.0020981	0.0063999	0.006334	0.05948802	0.04075957	0.04405871	0.06343763	0.054167961	0.729717616
33	20	1000	0.0035968	0.0041162	0.0030889	0.0064038	0.008052	0.04362816	0.05400223	0.04300045	0.07140971	0.0800046093	0.739217163
34	20	1500	0.0039657	0.0049184	0.0045388	0.0065836	0.007864	0.06887459	0.05366046	0.05608143	0.066611641	0.062608086	0.726815959
35	20	2000	0.0046881	0.0033722	0.0021592	0.0032908	0.007665	0.05942815	0.02585716	0.05716891	0.04436967	0.068525598	0.726746462

References

1. Agrawal, A.K., Murthy, V.M.S.R., Chattopadhyaya, S.: Investigations into reliability, maintainability and availability of tunnel boring machine operating in mixed ground condition using Markov chains. *Eng. Fail. Anal.* **105**, 477–489 (2019)
2. Bolvashenkov, I., Herzog, H.G., Frenkel, I., Khvatskin, L.: Using Markov reward model for decision making in the choice of optimal type of traction electric motor for icebreaking ship. In: *Ecological Vehicles and Renewable Energies (EVER)*, 2018 Thirteenth International Conference on, pp. 1–6. IEEE (2018, Apr)
3. Chen, D., Trivedi, K.S.: Optimization for condition-based maintenance with semi-Markov decision process. *Reliab. Eng. Syst. Safety* **90**(1), 25–29 (2005)
4. Dahiya, O., Kumar, A., Saini, M.: Mathematical modeling and performance evaluation of A-pan crystallization system in a sugar industry. *SN Appl. Sci.* **1**(4), 339 (2019)
5. Dhillon, B.S., Shah, A.S.: Availability analysis of a generalized maintainable three-state device parallel system with human error and common-cause failures. *J. Quality Maintenance Eng.* **13**(4), 411–432 (2007)
6. Goyal, N., Ram, M.: Series-parallel system study under warranty and preventive maintenance. In: *Math. Appl. Eng.* 97–113 (2017)
7. He, K., Maillart, L.M., Prokopyev, O.A.: Scheduling preventive maintenance as a function of an imperfect inspection interval. *IEEE Trans. Reliab.* **64**(3), 983–997 (2015)
8. He, Q., Wang, L.: An effective co-evolutionary particle swarm optimization for constrained engineering design problems. *Eng. Appl. Artif. Intell.* **20**(1), 89–99 (2007)
9. Khanduja, R., Tewari, P.C., Kumar, D.: Steady state behavior and maintenance planning of bleaching system in a paper plant (2011)
10. Kumar, A.: Availability optimisation of pre-heat exchanger system with random repair and failure rates using PSO. *Int. J. Reliab. Saf.* **12**(4), 327–347 (2018)
11. Kumar, A.: Performance evaluation of multi-state degraded industrial production system and selection of performance measure using PSO: a case study. *Int. J. Prod. Quality Manage.* **25**(1), 1–17 (2018)
12. Kumar, A., Garg R.K.: Decision support system for maximum availability of series-parallel system using particle swarm optimization. *Int. J. Intell. Enterprise* **3**(2), 148–169 (2016a)
13. Kumar, A., Garg, R.K.: Availability analysis and evaluation of series parallel system using soft computing technique. *Int. J. Reliab. Saf.* **10**(4), 346–367 (2016b)
14. Kumar, A., Pant, S., Singh, S.B.: Availability and cost analysis of an engineering system involving subsystems in series configuration. *Int. J. Quality Reliab. Manage.* **34**(6), 879–894 (2017)
15. Kumar, P., Tewari, P.: Performance analysis and optimization for CSDGB filling system of a beverage plant using particle swarm optimization. *Int. J. Ind. Eng. Comput.* **8**(3), 303–314 (2017)
16. Kumar, R., Tewari, P., Khanduja, D.: Parameters optimization of fabric finishing system of a textile industry using teaching–learning-based optimization algorithm. *Int. J. Ind. Eng. Comput.* **9**(2), 221–234 (2017)
17. Kumar, A.: Performance modelling and optimisation of the rice processing industrial system using PSO. *Int. J. Ind. Syst. Eng.* **34**(2), 224–240 (2020)
18. Li, J., Chen, Y., Hung, H.: Availability modeling for periodically inspection system with different lifetime and repair-time distribution. *Chin. J. Aeronaut.* (2019)
19. Liu, S., Du, S., Xi, L.: Transient analysis of quality performance in two-stage manufacturing systems with remote quality information feedback. *Comput. Ind. Eng.* **117**, 262–281 (2018)
20. López-Campos, M.A., Márquez, A.C., Fernández, J.F.G.: The integration of open reliability, maintenance, and condition monitoring management systems. In: *Advanced Maintenance Modelling for Asset Management*, pp. 43–78. Springer, Cham (2018)
21. Malik, N., Goel, P.: Cost benefit and availability analysis of two modules with perfective maintenance. *Int. J. Appl. Eng. Res.* **11**(3), 1774–1780 (2016). ISSN 0973-4562

22. Manglik, M., Ram, M.: Reliability analysis of a two unit cold standby system using Markov process. *J. Reliab. Stat. Stud.* **6**(2), 65–80 (2013)
23. Qiu, Q., Cui, L., Gao, H.: Availability and maintenance modelling for systems subject to multiple failure modes. *Comput. Ind. Eng.* **108**, 192–198 (2017)
24. Levantesi, R., Matta, A., Tolio, T.: Performance evaluation of continuous production lines with machines having different processing times and multiple failure modes. *Perform. Eval.* **51**(2–4), 247–268 (2003)
25. Ram, M., Kumar, A.: Paper mill plant performance evaluation with power supply in standby mode. *Int. J. Quality Reliab. Manage.* **32**(4), 400–414 (2015)
26. Ram, M., Manglik, M.: An analysis to multi-state manufacturing system with common cause failure and waiting repair strategy. *Cogent Eng.* **3**(1), 1266185 (2016)
27. Rao, M.S., Naikan, V.N.A.: Availability modeling of repairable systems using Markov system dynamics simulation. *Int. J. Quality Reliab. Manage.* **32**(5), 517–531 (2015)
28. Sabouhi, H., Abbaspour, A., Fotuhi-Firuzabad, M., Dehghanian, P.: Reliability modeling and availability analysis of combined cycle power plants. *Int. J. Electr. Power Energy Syst.* **79**, 108–119 (2016)
29. Sharifi, M., Khoshniat, S.: Optimization the availability of a system with short circuit and common cause failures. *Int. J. Ind. Math.* **11**(4), 239–248 (2019)
30. Sharma, R.K., Kumar, S.: Performance modeling in critical engineering systems using RAM analysis. *Reliab. Eng. Syst. Saf.* **93**(6), 913–919 (2008)
31. Sharma, S.P., Kumar, D.: RAM analysis of the press unit in a paper plant using genetic algorithm and Lambda-Tau methodology. In: *Applications of Soft Computing*, pp. 127–137. Springer, Berlin, Heidelberg (2009)
32. Singh, V.V., Rawal, D.K.: Availability, MTTF and cost analysis of complex system under preemptive resume repair policy using copula distribution. *Pakistan J. Stat. Oper. Res.* **10**(3), 299–312 (2014)
33. Singhal, N.E.H.A., Sharma, S.P.: An efficient approach for availability analysis through fuzzy differential equations and particle swarm optimization. *Iranian J. Fuzzy Syst.* **16**(3), 161–173 (2019)
34. Soro, I.W., Nourelfath, M., Ait-Kadi, D.: Performance evaluation of multi-state degraded systems with minimal repairs and imperfect preventive maintenance. *Reliab. Eng. Syst. Saf.* **95**(2), 65–69 (2010)
35. Tsarouhas, P.: Statistical techniques of reliability, availability, and maintainability (RAM) analysis in industrial engineering. In: *Diagnostic Techniques in Industrial Engineering*, pp. 207–231. Springer, Cham (2018)
36. Velásquez, R.M.A., Lara, J.V.M.: Reliability, availability and maintainability study for failure analysis in series capacitor bank. *Eng. Fail. Anal.* **86**, 158–167 (2018)
37. Weichert, D., Link, P., Stoll, A., Rüping, S., Ihlenfeldt, S., Wrobel, S.: A review of machine learning for the optimization of production processes. *Int. J. Adv. Manuf. Technol.* 1–14 (2019)
38. Wu, B., Cui, L., Fang, C.: Reliability analysis of semi-Markov systems with restriction on transition times. *Reliab. Eng. Syst. Saf.* 106516 (2019)

Chapter 10

A Study on Characterization of Green Metal Matrix Composites Reinforced with Melon Shell Ash Particulates



Yatan Nagpal, Pardeep Sharma, and Rohit Sharma

Abstract Composite materials can be used to reinforce agricultural waste in different engineering fields. Use of these wastes as reinforcement results in environmentally friendly, cost-effective product growth. In present work, melon shell ash (MSA) was used as a reinforcement; while Al7% of SiMg alloy was a metal matrix for the production of composite material. Different weight percentages of 0, 3, 6, 9 and 12 of MSA particles of size 30 μm was used to develop composite materials for investigation. X-Ray fluorescent (XRF) resolute the characterization of prepared MSA powder which revealed the presence of SiO_2 , K_2O and Al_2O_3 . Scanning electron micrographs (SEMs) have been investigated for the homogeneous dispersion of MSA particles in the developed materials. The hardness and tensile strength of material was improved from 47.9 VHN to 74 VHN and from 160 to 201 MPa respectively; with increase in the MSA contents from 0wt% to 12 wt%. Also, a decrease in impact energy from 18 to 12 J, ductility from 8.3 to 5.5 was observed with the increase in MSA contents. Wear resistance improved by increasing the content of MSA particles. Developed material can be used in the automotive industry where the material's properties can be changed to meet certain requirements.

Keywords Aluminium alloy · Composites · Melon shell ash · Microstructure · Ultimate tensile strength (UTS)

10.1 Introduction

In the field of materials production, agricultural waste resulted in low-cost metal matrix composites, resulting in positive effects on both the environment and human

Y. Nagpal (✉)

Research Scholar, Amity University, Uttar Pradesh Noida, India

P. Sharma

Department of Mechanical Engineering, Panipat Institute of Engineering and Technology, Panipat, India

R. Sharma

Department of Mechanical Engineering, Amity University, Uttar Pradesh Noida, India

beings [1, 2]. Aluminum metal matrix composites (AMMCs) have shown widespread attention over the last few decades. In today's scenario, with the rapid development of composite materials, there has been an enormous growth in the manufacturing, aviation and automotive industries. The main objective to manufacture metal matrix composite was to combine the desired properties of high strength metals with ceramics, high elastic modulus, ductile properties etc., in order to produce the new material with the intermediate mechanical characteristics between matrix alloy and ceramic reinforcement [3, 4]. Composite materials have presented a good mixture of mechanical, chemical and tribological characteristics that cannot be accomplished by traditional aluminum metal matrix [5]. Aluminium composites possessed certain physical properties such as low density, increased fatigue strength, light weight, high rigidity, low cost and relevant characteristics [6]. AMMCs find use in rail brake disk, diesel piston, hydraulic brake system components, connecting rod, etc. [7].

Several reinforcements such as AlN, Si₃N₄, graphite, SiC, B₄C, TiC, zirconium, Al₂O₃, TiB₂ etc. have been used to manufacture AMMCs. Aluminium strengthened with SiC, Al₂O₃ or B₄C is commonly used MMCs with improved properties at reduced production costs that have motivated various engineers to use AMMCs for different purposes such as pistons, brake rotor, drive shafts etc. [8]. These AMMCs showed improved mechanical, tribological properties and improved corrosion resistance [9, 10]. Al–Si alloy has become popular in recent years due to its extensive use in ship and aeronautical radar systems due to improving mechanical characteristics, lower density, strong heat dissipation characteristics etc. than pure Al [11]. The availability of reinforcement such as SiC, Si₃N₄, Al₂O₃ (synthetic reinforcement) in various application is well known; but they are not produced on a large scale in some of the developing countries like India. The import of these synthetic reinforcements from developed nations includes high foreign currency exchange due to which they are available at a relatively high cost in local market [12].

In order to overcome the high cost of chemical replacements, there is an alternative way to explore various types of agricultural waste, such as coconut shell, baggase, rice husk, bamboo leaf, ground nutshell etc. for the manufacture of AMMCs [13–15]. Agricultural waste is also available at a very low cost, with the advantage of being environmentally friendly. Such agricultural wastes have a high content of refractory materials; hematite (Fe₂O₃), silica (SiO₂), alumina (Al₂O₃) [16]. Various researchers developed AMMCs by taking these agricultural wastes as reinforcement material [17–22]. Melon shell is another abundantly available agricultural waste across various region of India. Melon shell is an agricultural waste; the dumping of which resulted into damage of land and environmental threat to human beings too where it is dumped [23]. However, melon shells can be utilized effectively by converting the melon shell into ash powder under controlled burning conditions.

10.2 Literature Review

Hassan and Aigbodion [24] prepared an egg-shell particle reinforced Al-Cu-Mg matrix composite by stir casting process. The mechanical properties were checked experimentally and the findings showed an improvement in the tensile strength and hardness of the composite with the addition of egg shell particles at different weight percentage (2–12) while the impact strength was found to be reduced.

Shanmugavel et al. [25] prepared Al alloy-red mud reinforced metal matrix composite by powder metallurgy process and further studied the optimization and wear behavior of composite. The experimental test was performed and an investigation was carried out indicating an improvement in the wear resistance of composite to the addition of red mud as reinforcement.

Dwivedi et al. [26] developed A356 aluminium alloy SiC and FA reinforced hybrid matrix composite by electromagnetic stir casting process. The experimental analysis consisted of the preparation of five composite samples at various wt% of the SiC and FA particles respectively and microstructure and mechanical properties of the composites have been investigated. The findings showed an improvement in the tensile strength and hardness of the composite with the addition of SiC and FA as reinforcement, while overall impact strength, fatigue strength and density were found to be reduced with a substantial increase in SiC and FA as reinforcement. The microstructural behavior showed a uniform distribution of the two reinforcements in a small clusture matrix.

Kumar et al. [27] prepared Al-4.5wt%Cu with Bamboo Leaf Ash (BLA) reinforced matrix composite by stir casting technique. The mechanical and tribological properties were investigated and results were analyzed that showed an increase in hardness of a composite with decrease in density with addition of BLA as reinforcement. The results also showed the enhancement of wear resistance of a composite.

Abdulwahab et al. [19] developed A356 aluminium alloy composite reinforced with MSA by stir casting method. The tribological behavior of a composite was determined and the findings showed an increase in wear resistance of a composite on addition of wt% of MSA as reinforcement.

Suleiman et al. [28] fabricated Al-12wt%Si MSA reinforced matrix composite by stir casting technique. The experimental analysis was done and mechanical properties were investigated and analyzed. The results showed that hardness and tensile strength were found to be increased while % elongation and impact strength were substantially reduced with increase in wt% of MSA as reinforcement and wear resistance was also enhanced with addition of MSA as reinforcement.

The present work was therefore based on the use of MSA by strengthening it with Al6101 alloy to produce AMMCs by casting process. In the case of AMMCs, different percentage reinforcements (0–12% in step 3%) of MSA particles (30 μm) were varied. Tensile strength, percentage elongation, hardness, energy impact and rate of wear were evaluated for various AMMCs developed. The microstructures of the AMMCs formed have been investigated by SEM.

Table 10.1 XRF analysis of melon shell ash

Oxides	SiO ₂	K ₂ O	Al ₂ O ₃	LOI	CaO	Fe ₂ O ₃	SO ₃	Na ₂ O	ZnO	MnO	MgO
wt%	84.00	5.00	3.30	2.30	2.35	1.32	0.65	0.53	0.47	0.38	0.35

10.3 Experimental Procedure

10.3.1 Preparation of MSA

MSA powder was formed after a proper heat treatment (30 h in furnace) from melon. Melon shell had been processed in a perforated metallic drum for the development of MSA, which is further processed at 620–680 °C for 3 h. Heat treatment was done for reducing the carbonaceous and volatile constituents present in MSA powder [18, 23]. The obtained MSA powder was ball milled to reduce the particle size to 30 μm.

10.3.2 Elemental Analysis of MSA

Various elements present in carbonized MSA were determined by XRF. Proper amount of MSA powder was measured by weighing balance and after grinding this was compacted in a hydraulic depression to develop pellet. Developed pellets were tested by Energy Dispersive X-Ray (Spectroscopy) (EDX) at 1.2 mA current and 25 kV voltages. It will take approximately 20 min for stimulation in the presence of X-rays. Various elements present in carbonized MSA are shown in Table 10.1.

10.3.3 Development and Testing of Composites

Aluminium alloy Al6101 of commercial grade was taken as metal matrix. Table 10.2 depicts various elements present in metal matrix used in present work.

The manufacturing of AMMCs takes place by orthodox casting route. An accurate amount of metal matrix was heated in an electric furnace equipped with graphite stirrer. Preheating of MSA powder takes place in a separate electric furnace and is blended with the molten base alloy. The mixture was then stirred for 15 min at 550 RPM with the help of stirrer operated by an electric motor. A semi-automatic

Table 10.2 Chemical composition of base metal Al6101

Aluminum Al 6101	97.6%	0.06%	0.03%	0.10%	0.50%	0.35%	0.03%	0.30–0.70%	0.10%
Element	Al	B	Cr	Cu	Fe	Mg	Mn	Si	Zn

muffle furnace was constantly operated at 780 °C during the whole blending. From the graphite crucible, the molten mixture was placed in a preheated (460° C) steel mould. An appropriate time was provided to the molten mixture to get it solidifies in steel mould. Different characterizations were performed on the heat treated (T-6) composite. All AMMCs at different percentage reinforcement were developed adopting the same procedure. The Scanning Electron Microscope was applied for the metallographic investigation of the developed composites. X-ray diffractometer (XRD) was used to obtain peaks and patterns according to the composition. Mitutoyo make (MVK-H1, England) Vickers hardness tester was used at a load of 500 g for a dwell time of 20 s at ten different locations for evaluating hardness of all samples. ASTM E08 standard [29] was implemented for the preparation of tensile specimen. The assessment of UTS was made by computerized universal testing machine. The impact toughness was evaluated on Izod Impact Machine. Samples for wear testing were developed as per ASTM G99-95 principle. The evaluation of wear on developed composites was accomplished by Pin-on-disc tribometer at 55–65% humidity and 35 °C temperature. The pins used on tribometer (in present work) had 6 mm diameter and 50 mm height. After the 30 min run, the pin (individually for each composite) was removed from the tribometer and the surface was prepared for metallographic analysis. The end surface of worn pins was first cleaned and then polished with 400, 600, 800, 1000, and 1200 grit size abrasive papers respectively. The wear rate was computed by loss of weight per unit time. An electronic weighing balance (± 0.1 mg resolution) was used for the investigation of loss in weight in a developed composite.

10.4 Results and Conversation

10.4.1 MSA Evaluation

Various elements present in carbonized MSA were evaluated by XRF and is given in Table 10.1. Silica (84.00 wt%) has maximum percentage followed by K_2O (5.00 wt%), Al_2O_3 (3.30 wt%), CaO (2.35 wt%), Fe_2O_3 (1.32 wt%) and Na_2O , SO_3 , ZnO , MgO , MnO were present as traces in very small quantity respectively (Table 10.1).

10.4.2 Microstructure of Composites

As-cast Al6101 alloy micrograph is displayed in Fig. 10.1a. It is revealed from the Fig. 10.1a, that silicon; the main constituent of the alloy was spread uniformly and found soluble in aluminium metal matrix. Figure 10.1b–e shows the micrographs of various reinforced composites with 3–12 wt% of MSA particles.

It is revealed from Fig. 10.1b that the light black portion of silica was MSA powder; it was the major constituent of MSA powder as verified in the XRF. Figure 10.1c–e

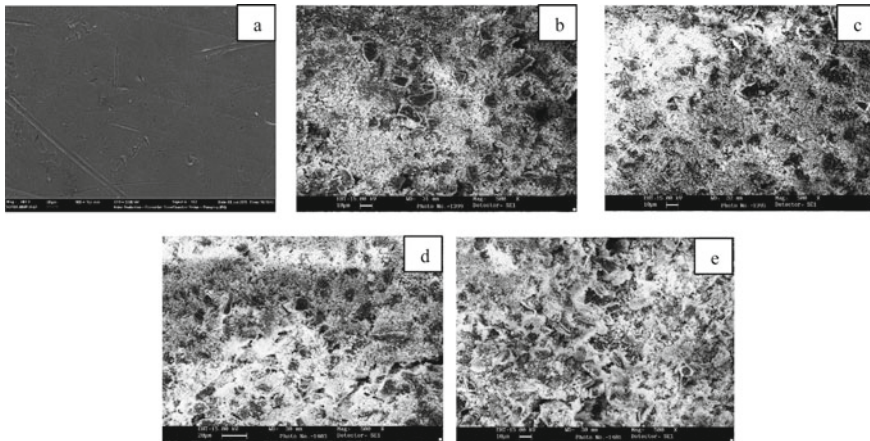


Fig. 10.1 a SEM micrograph of 0 wt% reinforced MSA particles, b 3 wt%, c 6 wt%, d 9 wt%, e 12 wt% reinforced MSA particles

shows the microstructures of composites developed by 6, 9, and 12 wt% of MSA particles respectively. These micrographs showed the same behavior with increased light black portion of SiO_2 as the wt% of MSA powder increased. A good bonding has been observed between MSA particles and base alloy along with the non-considerable gap in between the base alloy and MSA particles [30, 31]. All the manufactured composites showed few discontinuities with uniform dispersal of MSA particles in the base alloy. MSA particles showed both good preservation and interfacial bonding with aluminum metal matrix at various wt% of MSA particles (Fig. 10.1b–e). The wettability of MSA particles was improved by the addition of magnesium in small quantity during stirring. MSA particles showed increased dispersion with increasing wt% of reinforcement (Fig. 10.1b–e). These observations are in agreement as obtained in previous research [32].

The results of XRD analysis for 12 wt% MSA reinforced composite in the form of diffractogram is shown in Fig. 10.2. Peaks were matched using Match (phase identification from powder diffraction version 2) software and the possible phases were identified. As observed that aluminium has larger peaks than SiO_2 , K_2O , Al_2O_3 , CaO etc. which are main constituents of MSA powder. XRD pattern confirms that the SiO_2 , K_2O , Al_2O_3 particles present in MSA ash neither react with aluminium matrix nor produce any other compound except SiO_2 , K_2O and Al_2O_3 .

10.4.3 Hardness Analysis

An increase in wt% of MSA particles in the composite has a positive sign for hardness. Figure 10.3 exhibit the variations in hardness values at different MSA particles percentage composition. The hardness of the Al6101 alloy was 47.9 VHN and

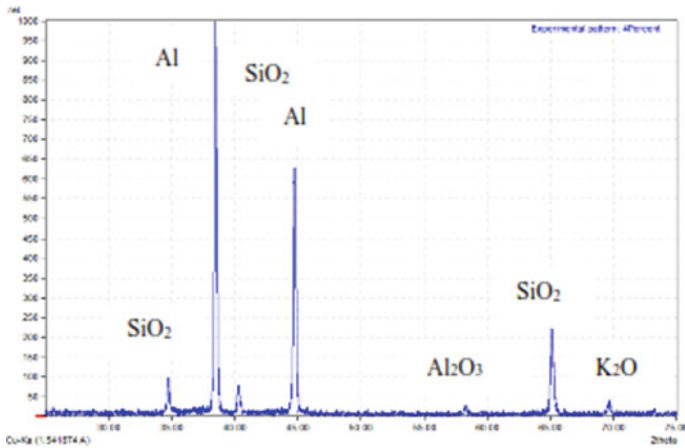
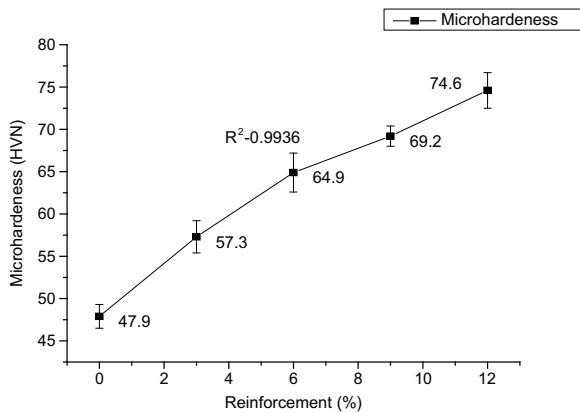


Fig. 10.2 XRD pattern of Al6101 alloy reinforced with 12 wt% MSA particles

Fig. 10.3 Variation of micro-hardness with weight percentage of MSA particle addition



increased to 74 VHN at 12 wt% of MSA particles. This enhancement in hardness could be attributed because of presence of hard and brittle element such as SiO₂, Al₂O₃, Fe₂O₃, K₂O etc. in the MSA powder as revealed in the XRF analysis.

The dislocation density at the interface has been increased due to the difference in the thermal expansion coefficient of base alloy and MSA material, which in turn increases the strength of the composites [33, 34].

10.4.4 Tensile Strength and Percentage Elongation

UTS variation for various composites (MSA particle wt%) is shown in Fig. 10.4. Such MSA particles support the tensile behavior of the reinforced composites. When the

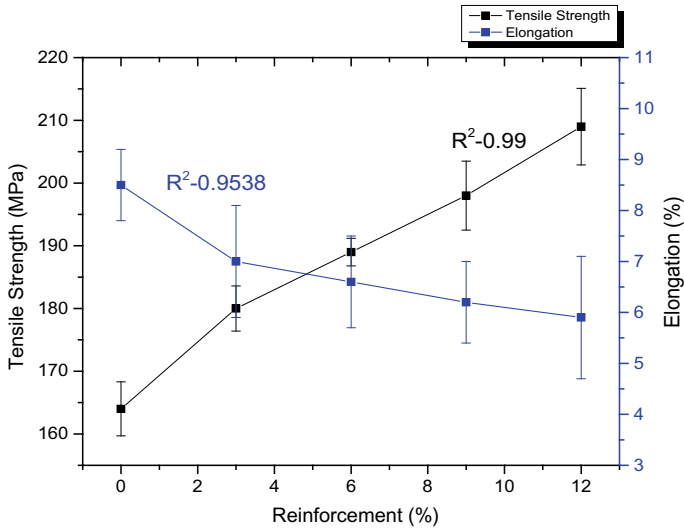


Fig. 10.4 Variation of tensile strength and percentage elongation with weight percentage of MSA particle addition

load is applied to these composites, the reinforced particles serve as a barrier to disruption. Same results had been observed in case of rice husk ash [35–38]. Tensile strength of the composites increased as MSA particles acts as filler and showed higher resistance to the applied load. Figure 10.4 presents that the volume fraction of MSA particulates has a negative impact on the ductility of the composites.

This decrease may be due to the emergence of brittle form, hard particulate matter or clustering of MSA particles in the composites. Previous authors have obtained the same results [39, 40].

10.4.5 Impact Toughness

Impact strength of base alloy and composites has been depicted in Fig. 10.5. MSA particle additions have a negative impact on the impact strength of the composites. The interfacial cracking and particle cracking of the MSA reinforced particles were the prime mechanism of impact fracture [41]. The natures of particles were brittle and hard along with the poor tendency against the resistance to severe-crack propagation [16]. It is clear that addition of 3–12 wt% of MSA particles negatively affect fracture toughness of reinforced composites. Similar results were revealed by other researchers too [30, 31].

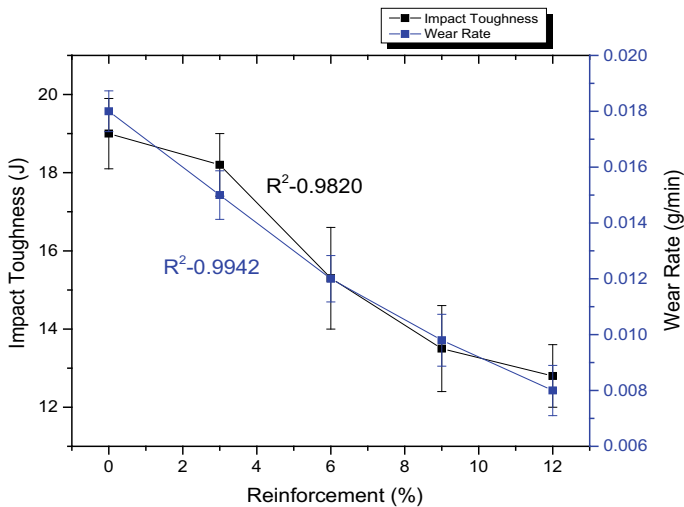


Fig. 10.5 Variation of impact toughness and wear rate with weight percentage of MSA particle addition

10.4.6 Wear Properties of Composites

Figure 10.5 revealed that the MSA particle has a positive impact on the wear resistance. The wear resistance of developed materials is significantly larger than the base alloy (Al6101) due to the reinforcement; which was having higher SiO₂ content that was treated as a load department constituent. High content of MSA particulates; limits the distortion of the base alloy against the load. Furthermore, the wear rate of composites at higher MSA particles wt% is lower and similar results for wear rate were revealed in previous research [38]. The morphologies of Al6101 alloy and the 12 wt% MSA particles reinforced composite was depicted in Fig. 10.6. It is revealed from the Fig. 10.6 that the chipping and micro cutting were the prime reasons for material removal in the composite (Fig. 10.6b) at a load of 60 N. Composite with 12 wt% MSA particle also revealed the abrasion marks and a shallow cutting process found as compared with the Al6101 alloy without any load (Fig. 10.6a). These results are also in accordance with the previous research [39–41].

10.5 Concluding Remarks

1. SEM micrographs exposed the fairly uniform dispersion of MSA particles in metal matrix.
2. Hardness improved from 47.9 to 74.6 VHN with the addition of MSA reinforcement particles (0–12%).

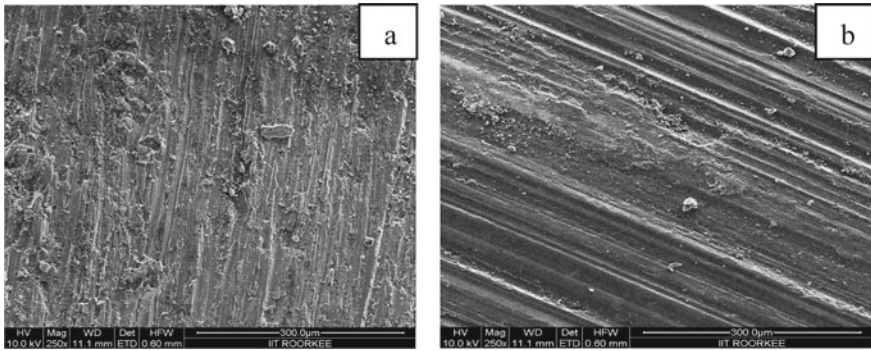


Fig. 10.6 SEM morphology of Al6101 alloy **a** without load, **b** reinforced with 12 wt% of MSA particles at applied load (60 N)

3. The tensile strength of the composites increased from 160 to 201 MPa, percentage elongation reduced from 8.3 to 5.5% and impact toughness decreased from 18 to 12 J with the addition of MSA reinforcement particles (0–12%).
4. Wear resistances improved by using MSA as reinforcement particulates. The wear rates in the composites decreased from 0.017 to 0.0076 g/min with the addition of MSA reinforcement particles (0–12%).
5. Micro-cutting was the main reason for deterioration in both Al6101 alloy and 12 wt% reinforced composites.
6. Being an agricultural waste MSA can be used as a good alternate to imported reinforcement such as Al_2O_3 , SiC, TiC, Si_3N_4 , AlN, B_4C , TiB_2 etc. available, as it is cheap and environmental friendly too.

References

1. Suleiman, I.Y., Abdulwahab, M., Awe, F.E.: Influence of particulate loading on the mechanical properties of al-4.5 Cu/GSA composite. *Nig. J. Eng.* **23**, 86–97 (2016)
2. Alaneme, K.K., Adewale, T.M., Olubambi, P.A.: Corrosion and wear behaviour of Al–Mg–Si alloy matrix hybrid composites reinforced with rice husk ash and silicon carbide. *J. Mater. Res. Technol.* **3**(1), 9–16 (2014)
3. Hashim, J., Looney, L., Hashmi, M.S.J.: Metal matrix composites: production by the stir casting method. *J. Mater. Process. Technol.* **92**, 1–7 (1999). [https://doi.org/10.1016/S0924-0136\(99\)00118-1](https://doi.org/10.1016/S0924-0136(99)00118-1)
4. Kala, H., Mer, K.K.S., Kumar, S.: A review on mechanical and tribological behaviors of stir cast aluminum matrix composites. *Proc. Mater. Sci.* **6**, 1951–1960 (2014). <https://doi.org/10.1016/j.mspro.2014.07.229>
5. Senthilvelan, T., Gopalakannan, S., Vishnuvarthan, S., Keerthivaran, K.: Fabrication and characterization of SiC, Al_2O_3 and B_4C reinforced Al–Zn–Mg–Cu alloy (AA 7075) metal matrix composites: a study. *Adv. Mater. Res.* **622**, 1295–1299 (2013)

6. Senthilkumar, P., Manimaran, R., Krishna Reddy, Y.: Evaluation of mechanical properties of hybrid Al7009 nanocomposite. In: *Energy Sources, Part A: Recovery, Utilization, and Environmental Effects*, pp. 1–9 (2019). <https://doi.org/10.1080/15567036.2019.1624876>
7. Saravanan, S.D., Kumar, M.S.: Effect of mechanical properties on rice husk ash reinforced aluminum alloy (AlSi10Mg) matrix composites. *Proc. Eng.* **64**, 1505–1513 (2013). <https://doi.org/10.1016/j.proeng.2013.09.232>
8. Ramanathan, A., Krishnan, P.K., Muraliraja, R.: A review on the production of metal matrix composites through stir casting—Furnace design, properties, challenges, and research opportunities. *J. Manuf. Processes.* **42**, 213–245 (2019). <https://doi.org/10.1016/j.jmapro.2019.04.017>
9. Anilkumar, H.C., Hebbar, H.S., Ravishankar, K.S.: Mechanical properties of fly ash reinforced aluminium alloy (Al6061) composites. *Int. J. Mech. Mater. Eng.* **6**(1), 41–45 (2011)
10. Kok, M.: Production and mechanical properties of Al₂O₃ particle-reinforced 2024 aluminium alloy composites. *J. Mater. Process. Technol.* **161**(3), 381–387 (2005). <https://doi.org/10.1016/j.jmatprotec.2004.078>
11. Bandil, K., Vashisth, H., Kumar, S., Verma, L., Jamwal, A., Kumar, D., Singh, N., Sadasivuni, K.K., Gupta, P.: Microstructural, mechanical and corrosion behaviour of Al–Si alloy reinforced with SiC metal matrix composite. *J. Compos. Mater.* **53**, 4215–4223 (2019). <https://doi.org/10.1177/2F0021998319856679>
12. Aigbodion, V.S.: Potential of using bagasse ash particle in metal matrix composite. Ph.D. Work, Department of Metallurgical and Materials Engineering, Ahmadu Bello University, Samaru, Zaria, Nigeria (2010)
13. Karthikeyan, A., Nallusamy, S.: Investigation on mechanical properties and wear behavior of Al–Si–SiC-graphite composite using SEM and EDAX. In: *IOP Conference Series: Materials Science and Engineering*, vol. 225, No. 1, p. 012281 (2017). IOP Publishing. <https://doi.org/10.1088/1757-899X/225/1/012281>
14. Alaneme, K.K., Olubambi, P.A.: Corrosion and wear behaviour of rice husk ash—Alumina reinforced Al–Mg–Si alloy matrix hybrid composites. *J. Mater. Res. Technol.* **2**(2), 188–194 (2013)
15. Madakson, P.B., Yawas, D.S., Apasi, A.: Characterization of coconut shell ash for potential utilization in metal matrix composites for automotive applications. *Int. J. Eng. Sci. Technol.* **4**(3), 1190–1198 (2012)
16. Kumar, G.V., Rao, C.S.P., Selvaraj, N.: Mechanical and tribological behavior of particulate reinforced aluminum metal matrix composites—a review. *J. Min. Mater. Characterization Eng.* **10**(01), 59 (2011)
17. Wu, S.Q., Wang, H.Z., Tjong, S.C.: Mechanical and wear behavior of an Al/Si alloy metal-matrix composite reinforced with aluminosilicate fiber. *Compos. Sci. Technol.* **56**(11), 1261–1270 (1996). [https://doi.org/10.1016/S0266-3538\(96\)00085-1](https://doi.org/10.1016/S0266-3538(96)00085-1)
18. Obasi, N.A., Ukadilonu, J., Eze, E., Akubugwo, E.I., Okorie, U.C.: Proximate composition, extraction, characterization and comparative assessment of coconut (*Cocos nucifera*) and melon (*Colocynthis citrullus*) seeds and seed oils. *Pak. J. Biol. Sci.* **15**(1), 1 (2012). <https://doi.org/10.3923/pjbs.2012.1.9>
19. Abdulwahab, M., Dodo, R.M., Suleiman, I.Y., Gebi, A.I., Umar, I.: Wear behavior of Al-7% Si-0.3% Mg/melon shell ash particulate composites. *Heliyon* **3**(8), e00375 (2017). <https://doi.org/10.1016/j.heliyon.2017.e00375>
20. Surappa, M.K.: Aluminium matrix composites: challenges and opportunities. *Sadhana* **28**(1–2), 319–334 (2003). <https://doi.org/10.1007/BF02717141>
21. Prasad, N.: Development and Characterization of Metal Matrix Composite Using Red Mud an Industrial Waste for Wear Resistant Applications (Doctoral dissertation) (2006)
22. Hebbar, H.S., Ravindra, K.G.: Study of the mechanical and tribological properties of aluminium alloy—SiCp composites processed by stir casting method. *Int. Conf. Adv. Mech. Eng.* (2008)
23. Olorunmota, R.T., Ofuya, T.I., Idoko, J.E., Ogundeji, B.A.: Effect of rice husk and melon shell wastes as possible grain protectants in cowpea storage. *J. Adv. Biol. Biotechnol.* 1–9 (2017). <https://doi.org/10.9734/JABB/2017/37114>

24. Hassan, S.B., Aigbodion, V.S.: Effects of eggshell on the microstructures and properties of Al–Cu–Mg/eggshell particulate composites. *J. King Saud Univ. Eng. Sci.* **27**, 49–56 (2015). <https://doi.org/10.1016/j.jksues.2013.03.001>
25. Shanmugavel, R., Sundaresan, T.K., Marimuthu, U., Manickaraj, P.: Process optimization and wear behavior of red mud reinforced aluminum composites. *Adv. Tribol* (2016). <https://doi.org/10.1155/2016/9082593>
26. Dwivedi, S.P., Sharma, S., Mishra, R.K.: Microstructure and mechanical behavior of A356/SiC/Fly-ash hybrid composites produced by electromagnetic stir casting. *J. Braz. Soc. Mech. Sci. Eng.* **37**, 57–67 (2015). <https://doi.org/10.1007/s40430-014-0138-y>
27. Kumar, B.P., Birru, A.K.: Tribological behavior of aluminium metal matrix composite with addition of bamboo leaf ash by GRA-Taguchi method. *Tribol. Industry* **40** (2018)
28. Suleiman, I.Y., Salihu, S.A., Mohammed, T.A.: Investigation of mechanical, microstructure, and wear behaviors of Al-12% Si/reinforced with melon shell ash particulates. *Int. J. Adv. Manuf. Technol.* **97**, 4137–4144 (2018). <https://doi.org/10.1007/s00170-018-2157-9>
29. Standard ASTM: E8: Standard Test Method for Tension Testing of Metallic Materials. ASTM International, West Conshohocken (USA) (2004)
30. Prasad, D.S., Krishna, A.R.: Tribological properties of A356. 2/RHA composites. *J. Mater. Sci. Technol.* **28**(4), 367–372 (2012)
31. Zuhailawati, H., Samayamuththirian, P., CH, M.H.: Fabrication of low cost of aluminium, matrix composite reinforced with silica sand. *J. Phys. Sci.* **18**(1), 47–55 (2007)
32. Pathak, J.P., Singh, J.K., Mohan, S.: Synthesis and Characterisation of Aluminium-Silicon-Silicon Carbide Composite (2006)
33. Sahin, Y.: Wear behaviour of aluminium alloy and its composites reinforced by SiC particles using statistical analysis. *Mater. Des.* **24**(2), 95–103 (2003). [https://doi.org/10.1016/S0261-3069\(02\)001437](https://doi.org/10.1016/S0261-3069(02)001437)
34. AlanemeaΨ, K.K., Alukob, A.O.: Production and age-hardening behaviour of borax premixed SiC reinforced Al–Mg–Si alloy composites developed by double stir-casting technique. *West Indian J. Eng.* **34**(1), 2 (2012)
35. Suresh, K.R., Niranjan, H.B., Jebaraj, P.M., Chowdiah, M.P.: Tensile and wear properties of aluminum composites. *Wear* **255**(1–6), 638–642 (2003). [https://doi.org/10.1016/S0043-1648\(03\)00292-8](https://doi.org/10.1016/S0043-1648(03)00292-8)
36. Surappa, M.K.: Synthesis of fly ash particle reinforced A356 Al composites and their characterization. *Mater. Sci. Eng. A* **480**(1–2), 117–124 (2008)
37. Torralba, J.D., Da Costa, C.E., Velasco, F.: P/M aluminum matrix composites: an overview. *J. Mater. Process. Technol.* **133**(1–2), 203–206 (2003). [https://doi.org/10.1016/S0924-0136\(02\)00234-0](https://doi.org/10.1016/S0924-0136(02)00234-0)
38. Prasad, D.S., Krishna, A.R.: Production and mechanical properties of A356. 2/RHA composites. *Int. J. Adv. Sci. Technol.* **33**, 51–58 (2011)
39. Das, S., Dan, T.K., Prasad, S.V., Rohatgi, P.K.: Aluminium alloy—rice husk ash particle composites. *J. Mater. Sci. Lett.* **5**(5), 562–564 (1986)
40. Gupta, V.K., Gupta, M., Sharma, S.: Process development for the removal of lead and chromium from aqueous solutions using red mud—an aluminium industry waste. *Water Res.* **35**(5), 1125–1134 (2001)
41. Della, V.P., Kühn, I., Hotza, D.: Rice husk ash as an alternate source for active silica production. *Mater. Lett.* **57**(4), 818–821 (2002)

Chapter 11

Optimizing the Three-Body Abrasion Wear of Quenched and Tempered Steel



Sarika Kumari, Varun Sharma, R. K. Bansal, and Bhuvnesh Bhardwaj

Abstract The present study investigates the wear behaviour of Quenched and Tempered Steel (Hardox 400) under three-body abrasion wear testing conditions using dry sand rubber wheel testing rig under dry wear conditions at room temperature. Design of experiments approach using face centred design was used to investigate the correlations between resultant wear loss and input parameters (viz. Applied load, speed and flow rate of abrasives) using silicon carbide sand with 100–150 grit size. The results revealed that, among all the parameters studied, the load was found to be the most significant parameter affecting the wear rate followed by abrasive flow rate and the rotational speed of the rotating rubber wheel.

Keywords Quenched and tempered steel · Design of experiments · Face centred design · Dry sand rubber wheel testing

11.1 Introduction

Abrasion wear is one of the unceasing problems which are highly prevalent in earth-moving and mining industries. As per different studies, it has been estimated that around 50% of all wear problems in these industries are because of abrasion [1, 2]. To cater this issue of three-body abrasion problem, several studies have been reported related to the identification and implementation of possible solutions [3]. One of the widely used solutions to address this issue was the usage of abrasion resistant wear plates which possesses high hardness and extremely high strength, and the most commonly used wear plates are JFEEH 400, Hardox 400, 21988/JN/HBW555XCr21 etc. [4, 5]. Different components such as dump truck bodies, stripping shovels, buckets for earthmoving machineries etc. are manufactured from such plates which

S. Kumari (✉) · V. Sharma · R. K. Bansal
Department of Industrial and Production Engineering, Dr B R Ambedkar National Institute of Technology, Jalandhar, India

B. Bhardwaj
Department of Mechanical Engineering, Jaipur Engineering College and Research Centre, Jaipur, Rajasthan, India

are subjected to low and high stress three-body abrasion wear conditions [6, 7]. In order to evaluate the wear performance of these plates under three-body abrasive wear conditions, dry sand rubber wheel (DSRW) laboratory test has been developed as per ASTM G65 standard [8]. However, the experimentation carried out using this test involves the usage of different process variables (such as load, speed, abrasives type, abrasives size etc.) which have significant influence on the wear performance of the tested specimens. Hence, owing to the complexity of the problem, various design of experimentation (DOE) techniques have been proposed and implemented in literature to identify the relationship of such variables and the material wear performance [9, 10]. Taguchi method was used by Sahin et al. to develop a mathematical model for predicting the abrasion wear response of different plain carbon steels in terms of sliding distance, load and abrasive grain size [11]. Gray-based Taguchi method was successfully implemented to obtain a relationship between specific wear rate and different independent variables such as sliding speed, load and percentage variation of metallic compound in metal matrix composites [12]. Response surface methodology (RSM) was effectively implemented by researchers to establish a relationship between testing variables such as sliding velocity, sliding distance, applied load etc., and response variable such as wear volume, mass loss etc. [13]. Several investigators have used the factorial design based on design of experiments approach to establish a close correlation between the independent and dependent variables of the abrasion wear [14]. Although differing in practise, the methods are conceptually the same but differ substantially in terms of their predicting ability.

Keeping in view the literature reviewed, many of methods currently in use may have limited reliability and validity. Also, there are only few reports available in open literature wherein the detailed abrasion wear studies related to wear plates have been carried out. Thus, this piece of study was carried out to investigate the three-body abrasion wear performance of Hardox 400 steel using design of experiments approach with face centred design of response surface methodology. The scanning electron microscopy was done to understand the underlying wear mechanism involved during three-body abrasion wear of these steels. The results depicted the valid contrast between the predicted and actual values of the abrasion wear.

11.2 Material and Method

The material used in this study was in the form of wear plates of Hardox 400 steel possessing the thickness of 20 mm and chemical composition consisting of carbon (0.32%), Mn (1.46%), Ni (1.50%), Cr (2.50%), Si (0.70%), P (0.025%) and Fe (balance). The wear plates were received in the quenched and tempered condition having hardness of 400 HBW and tensile strength of 1250 MPa [15].

Three-body abrasion wear performance of the selected material in the form of wear rate was evaluated using dry sand rubber wheel test (DSRW), which involve number of input variables such as load, speed, abrasive flow rate etc. To establish the relationship between such input variables and wear rate as output variable, face

Table 11.1 Independent variables and levels of experimentation

Factors	Notation	Units	Levels		
			- 1	0	1
Load	A	N	40	60	80
Speed	B	RPM	100	175	250
Flow rate	C	gm/min	150	200	250

centred design (FCD) based on response surface methodology was used. The wear parameters and their levels used in the study are listed in Table 11.1, and the design matrix consisting of different experimental sets/runs obtained using FCD is shown in Table 11.2. Dry sand rubber wheel experiments were conducted on Hardox 400 steel specimens of size (76.2 × 25.4 × 12.7) mm as per design matrix shown in Table 11.2. During each test, the specimens were abraded against silicon carbide (SiC) abrasives as shown in Fig. 11.1, of the size range 100–150 grit under different loading conditions, and the results thus obtained in the form of mass loss (gm) are also shown in Table 11.2.

Table 11.2 Design matrix based on FCD and experimental results

Std.	Run	A: load (N)	B: speed (RPM)	C: flow rate (gm/min)	Wear (gm)
1	7	40	100	150	0.950
2	6	80	100	150	2.100
3	2	40	250	150	0.597
4	14	80	250	150	1.390
5	16	40	100	250	1.819
6	5	80	100	250	3.060
7	3	40	250	250	1.145
8	19	80	250	250	2.281
9	18	40	175	200	1.233
10	1	80	175	200	2.240
11	12	60	100	200	1.993
12	4	60	250	200	1.292
13	10	60	175	150	1.025
14	9	60	175	250	1.815
15	13	60	175	200	1.526
16	15	60	175	200	1.454
17	17	60	175	200	1.510
18	8	60	175	200	1.500
19	11	60	175	200	1.563
20	20	60	175	200	1.536

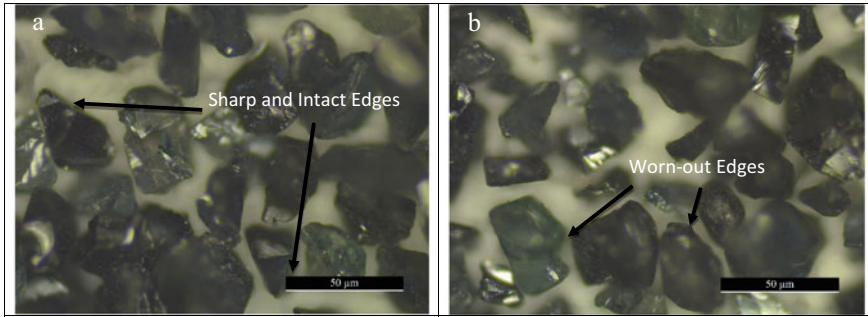


Fig. 11.1 The optical micro images for **a** unused, and **b** used dry sand abrasive particles

11.3 Results and Discussion

For the purpose of this study, the effect of different process variables (load, speed and abrasive flow rate) on the wear rate of substrate material was evaluated using FCD based on RSM through Design Expert software. The systematic analysis through this technique involves the development of design matrix, development and analysis of mathematical model through regression and analysis of variance (ANOVA) and finally the optimization of parameters.

11.3.1 Development of Empirical Relation Between Wear Variables and Wear Rate

11.3.1.1 Validating the Assumptions of ANOVA

The assumption of normal distribution is the first assumption of ANOVA and is validated through the normal probability of residuals as shown in Fig. 11.2. Since the residuals for wear rate are mostly lying on the straight line and hence are normally distributed, this validates the first assumption. The second assumption of constant variance is depicted through residuals versus the predicted plot shown in Fig. 11.3. Since there is no predefined pattern in the plot, so the second assumption is validated [10].

Figure 11.4 shows the Predicted versus Actual plot for the generated model in the design expert software. Similarly, Fig. 11.5 represents the Residual versus Run plot for the model generated.

Fig. 11.2 Normal probability plot of residuals for validating first assumption of ANOVA

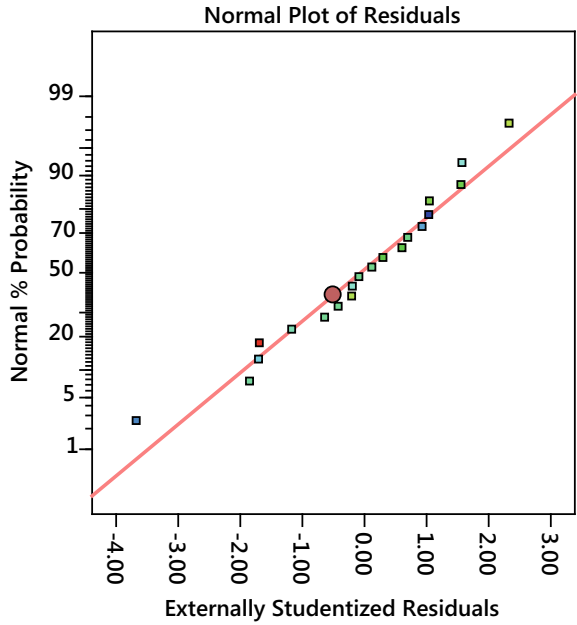


Fig. 11.3 Residual versus predicted plot for validating second assumption of ANOVA

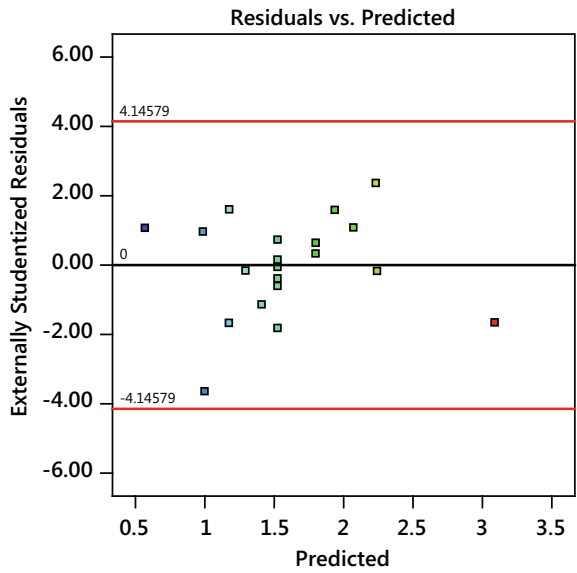


Fig. 11.4 Predicted versus actual plot for validating of ANOVA

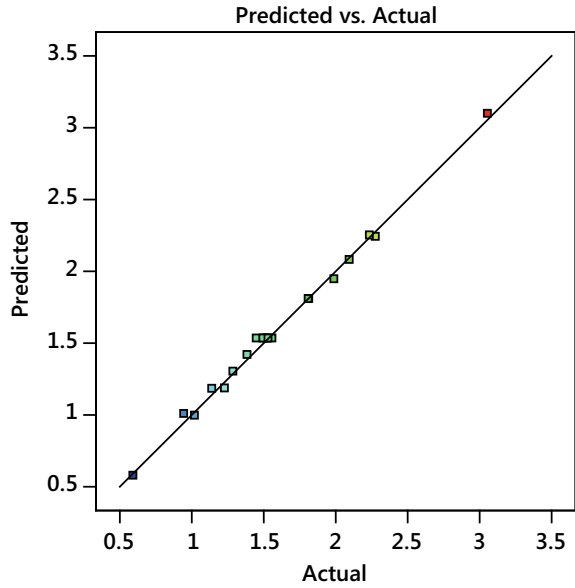
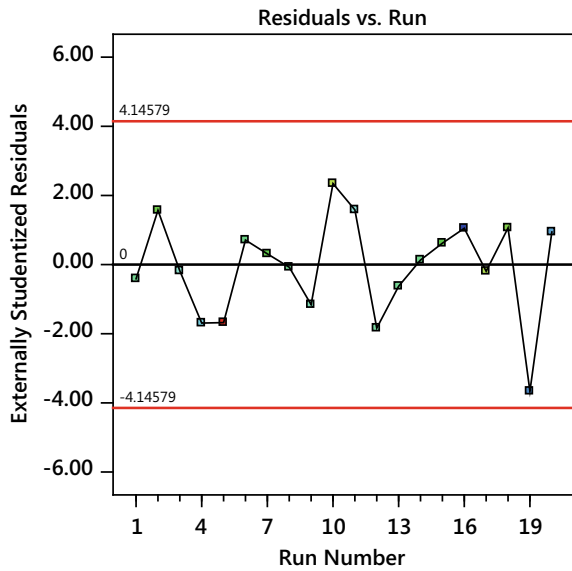


Fig. 11.5 Residual versus run plot for validating of ANOVA



11.3.1.2 Analysis of Variance (ANOVA) for Wear Rate

The analysis of variance for wear rate was carried out at the confidence level of 95% and is shown in Table 11.3. The table shows that the “Prob. > F” value for the wear rate mathematical model, is less than 0.0001 and is lesser than 0.05, which

Table 11.3 ANOVA table for wear rate

Source	Sum of squares	DF	Mean square	F value	p-value Prob. > F
Model	5.770	9	0.641	269.658	< 0.0001
A-Load	2.838	1	2.838	1193.576	< 0.0001
B-Speed	1.035	1	1.035	435.298	< 0.0001
C-Flow Rate	1.647	1	1.647	692.641	< 0.0001
AB	0.027	1	0.027	11.222	0.0074
AC	0.024	1	0.024	9.903	0.0104
BC	0.019	1	0.019	7.997	0.0179
A ²	0.094	1	0.094	39.471	< 0.0001
B ²	0.023	1	0.023	9.521	0.0115
C ²	0.048	1	0.048	20.085	0.0012
Residual	0.024	10	0.002		
Lack of fit	0.017	5	0.003	2.477	0.1710
Pure error	0.007	5	0.001		
Cor total	5.794	19			
Std. Dev.	0.049		R-squared		0.996
Mean	1.601		Adj R-squared		0.992
C.V. %	3.045		Pred R-squared		0.957
Press	0.248		Adeq precision		73.102

implies that the model is significant and depicts the accurate prediction of wear rate. Also, the value of “Prob. > F” for different model terms and their interactions is less than 0.05, which states that the terms significantly affect the prediction ability of the model. Further, the “Prob. > F” value for lack of fit is 0.1710 (greater than 0.05) and is insignificant. Further analysis of the ANOVA table shows that the R² value and adjusted R² value are close to each other and are within the limit of 20% [16].

The analysis of variance as discussed above clearly depicts the high accuracy of prediction through the mathematical model developed in Eq. 11.1.

$$\begin{aligned}
 \text{Wear} = & -1.101 - 0.033 * \text{Load} - 0.005 * \text{Speed} \\
 & + 0.028 * \text{Flow Rate} - 3.85000\text{E} - 005 \\
 & * \text{Load} * \text{Speed} + 5.42500\text{E} - 005 \\
 & * \text{Load} * \text{FlowRate} - 1.30000\text{E} - 005 \\
 & * \text{Speed} * \text{Flow Rate} + 4.61817\text{E} - 004 \\
 & * \text{Load}^2 + 1.61292\text{E} - 005 * \text{Speed}^2 \\
 & - 5.27088\text{E} - 005 * \text{FlowRate}^2
 \end{aligned}
 \tag{11.1}$$

11.3.2 Effect of Testing Conditions on Wear Rate

The effect of the process variables (load, speed and flow rate) on the wear rate of the substrate materials was as shown in the singles factor plots in Fig. 11.6.

The interactions between the process variables and the combined behavior of the variables were depicted as shown in Fig. 11.7.

The effect of process variables (Load, speed and abrasive flow rate) on the wear loss of substrate material is shown in the form of 3D plots.

Figure 11.8 shows the response surface for abrasion wear loss in terms of applied load and rotational speed at the constant abrasives flow rate of 200 gm/min. It is evident from the figure that the wear loss increases with the increase in load from 40 to 80 N. This behaviour could be attributed to the fact that at lower value of load the mode of abrasion was rolling which changed to sliding/grooving mode with the increase in load [17]. It is further observed from the figure that the wear loss reduced with the increase in speed of rotation of rubber wheel however the rate of reduction is much lower with the increase in load.

Figure 11.9 shows the interaction effect of load and abrasive flow rate on the wear loss of testing specimens when subjected to the rotational speed of 175 rpm. The plot depicts that the abrasive flow rate has positive influence on the wear loss, which

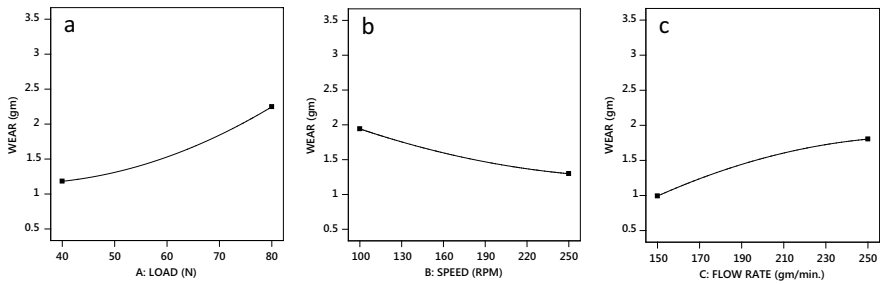


Fig. 11.6 One factor plots **a** load versus wear, **b** speed versus wear and **c** flow rate versus wear

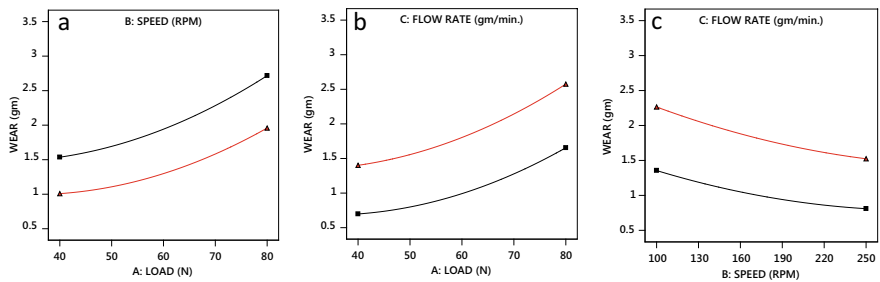


Fig. 11.7 Interaction plots for the process variables **a** load and speed w.r.t wear: **b** load and flow rate w.r.t wear: and **c** speed and flow rate w.r.t wear

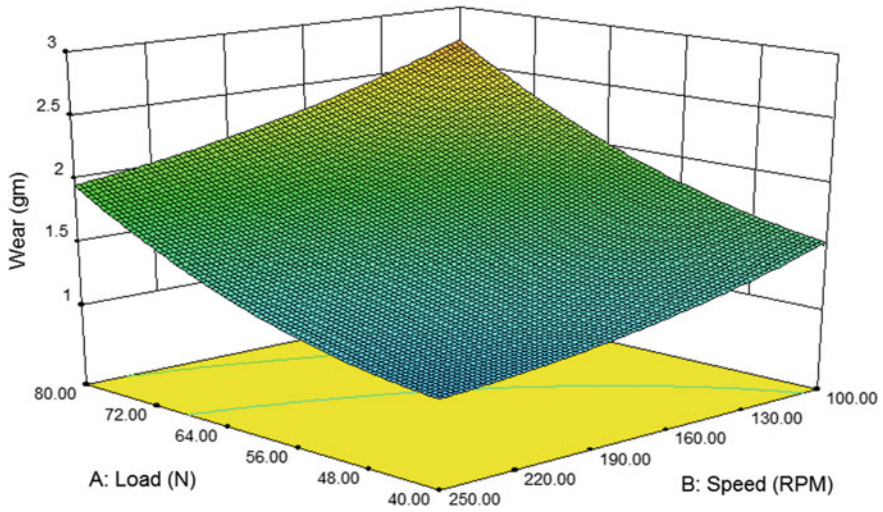


Fig. 11.8: 3D plot for wear loss in terms of load and speed at the flow rate of 200 gm/min

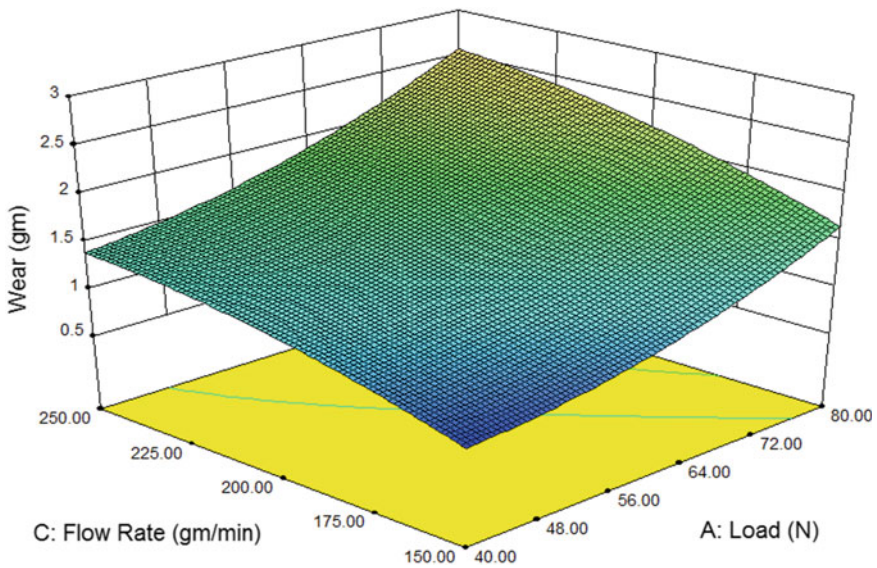


Fig. 11.9 3D plot for wear loss in terms of load and flow rate (speed = 175 rpm)

could be due to the participation of larger number of abrasive particles in abrasion of substrate with the increase in flow rate. The interaction of flow rate with the load shows that the mass loss is on the higher side for higher flow rate for all the load values changing between 40 and 80 N. Further, the mass loss variation between the

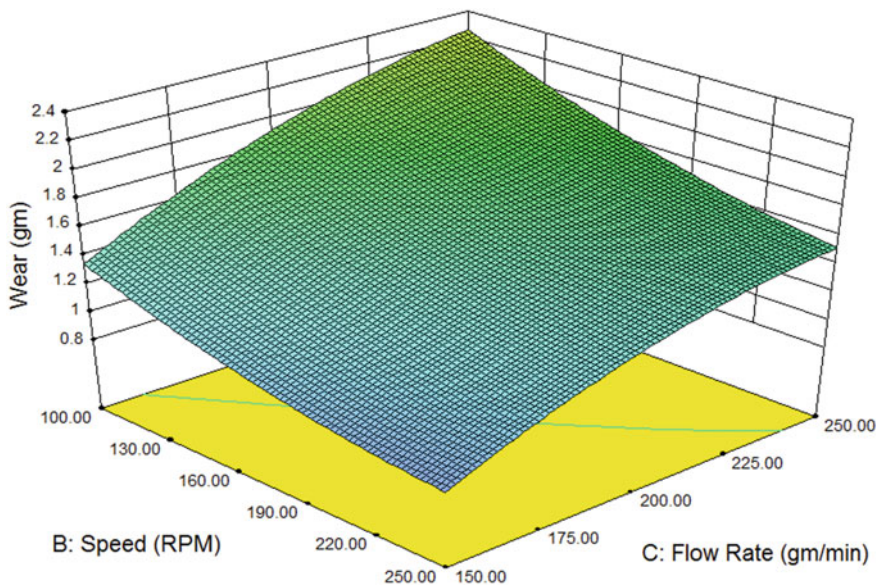


Fig. 11.10 3D plot for wear loss in terms of speed and flow rate (load = 60 N)

wear curves is somewhat higher for a load of 80 N as compared to 40 N load. This could be accredited to the dominating effect of applied load at higher values.

Figure 11.10 shows the 3D plot illustrating the interaction effect of speed and abrasive flow rate on the abrasion wear of substrate material at the constant load of 60 N. The plot show that with an increase in speed the wear loss reduces, however, the flow rate has positive effect on the wear loss. It is further observed that the maximum amount of wear loss occurred at the minimum speed of 100 rpm and maximum abrasive flow rate of 250 gm/min.

Figure 11.11 Represents the influence of process variable i.e. speed, load and flow rate with respect to the wear of the substrate material. Where the corner of the cube represents the interactions between any two variables w.r.t the wear.

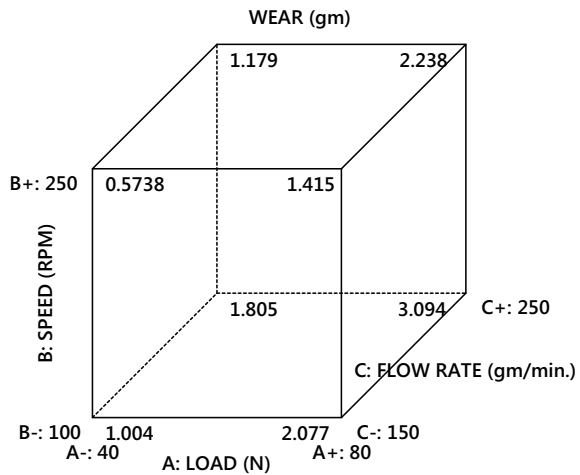
11.3.3 Optimization and Confirmation Experiments

In order to estimate the maximum and minimum wear loss of Hardox 400 steel within a range of input variables, the optimal solutions are reported in Table 11.4. Further the confirmation runs were carried out at the optimum testing conditions to validate the prediction ability of the empirical model. The results obtained are shown in Table 11.4, which clearly depicts that the percentage error between predicted and experimental values lies within the range of 5%. This demonstrates that the

Table 11.4 Optimization results for three-body abrasion test (DSRW)

Test condition	Load (N)	Speed (RPM)	Abrasive flow rate (gm/min)	Wear loss (mg)		% error
				Experimental	Predicted	
Minimum	40	250	150	0.597	0.576	3.5
Maximum	80	100	250	3.060	2.937	4.0

Fig. 11.11 The cube representation for the process variables w.r.t wear



developed mathematical model predicts the wear loss of substrate material with high effectiveness and accuracy.

Figure 11.12, represents the optimized ramp results for the wear at maximum and minimum wear by the model. The desirability for the both the optimized ramp plots was 1.

11.3.4 S.E.M Images

The S.E.M images were obtained for both minimum and maximum wear rate. It can be observed that for the load condition at 40 N with speed at 250 RPM with abrasive flow rate of 150 gm/min, the wear rate tracks were shallow and less craters channels were formed under the abrasion test as shown in Fig. 11.13a. Similarly, for the maximum conditions it can be observed that for the load condition at 80 N with speed at 100 RPM with abrasive flow rate of 250 gm/min, the wear rate tracks were much higher in number and craters channels were with higher depth formed as shown in Fig. 11.13b.

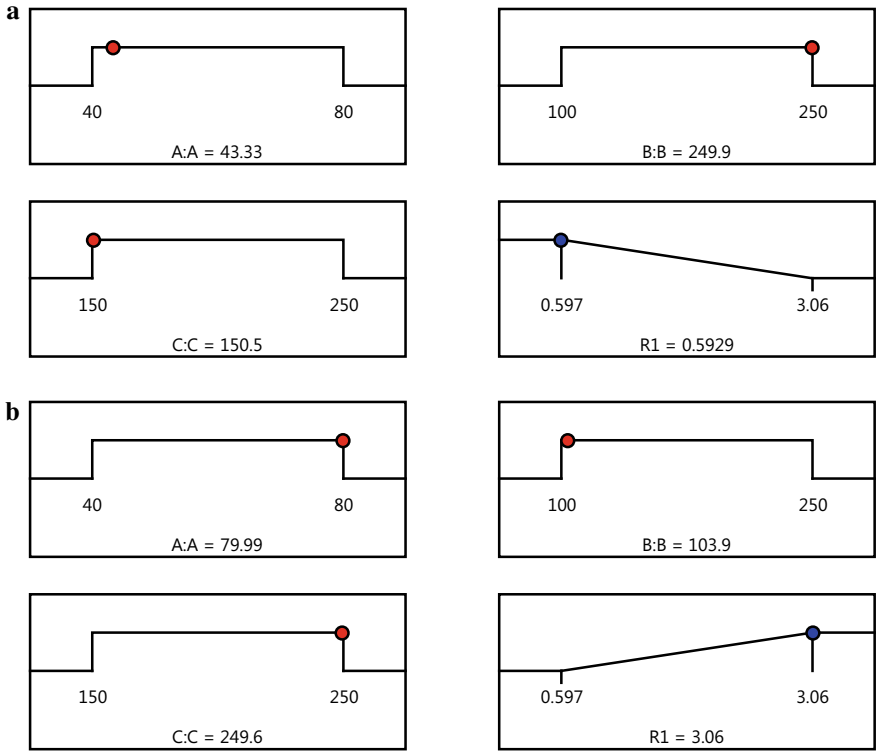


Fig. 11.12 The optimized results obtained from the model for **a** minimum wear, and **b** maximum wear

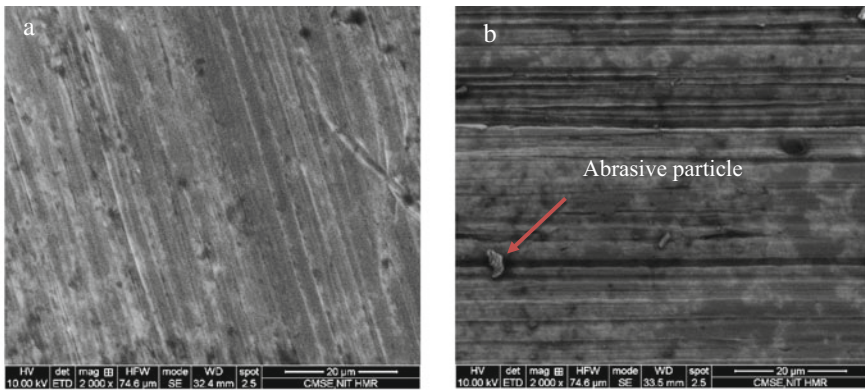


Fig. 11.13 The S.E.M. images obtained for **a** minimum wear rate, and **b** maximum wear rate

11.4 Conclusions

The main conclusions of this work are drawn together and are presented as follows:

1. The load, speed and abrasive flow rate shows the significant effect on wear loss of Hardox 400 steel. Also, the interaction of load and speed, load and flow rate, and speed and flow rate were also found to be the significant model terms affecting wear loss.
2. Among all the independent variables, load and abrasive flow rate increased the wear loss with the contribution of 49.18% and 28.54% respectively. However, the speed of rotation reduced the wear loss by contributing 17.93% in the model.
3. The maximum wear loss of Hardox 400 occurred when the load was 80 N, speed was 100 rpm and abrasive flow rate was 250 gm/min. On the contrary, the minimum wear loss occurred at the load of 40 N, speed of 250 rpm and flow rate of 150 gm/min.
4. The confirmation experiments conducted at the maximum and minimum wear testing conditions shows the excellent prediction capability of the developed mathematical model.

References

1. Stachowiak, G.W., Batchelor, A.W.: Engineering Tribology, 4th edn. Butterworth-Heinemann, Boston (2014)
2. Petrica, M., Badisch, E., Peinsitt, T.: Abrasive wear mechanisms and their relation to rock properties. *Wear* **308**(1–2), 86–94 (2013)
3. Misra, A., Finnie, I.: A review of the abrasive wear of metals. *J. Eng. Mater. Technol.-Trans. ASME* **104**(2), 94–101 (1982)
4. Adamiak, M., Gorka, J., Kik, T.: Structure analysis of welded joints of wear resistant plate and constructional steel. *Archives Mater. Sci. Eng.* **46**(2), 108–114 (2010)
5. Khrushchov, M.M.: Principles of abrasive wear. *Wear* **28**(1), 69–88 (1974)
6. ANSI/AWS: Specification for Welding Earthmoving, Construction, and Agricultural Equipment. AWS D14. 3/D14. 3M, pp. 1–82 (2010)
7. Sharma, V., Shahi, A.S., Kumar, S.: Influence of different filler weld wire chemistries on metallurgical and mechanical behavior of ultrahigh strength steel welded joints. *Proc. Inst. Mech. Eng. Part L J. Mater. Des. Appl.* **233**(11), 2280–2300 (2019)
8. ASTM: Standard Test Method for Measuring Abrasion Using the Dry Sand/Rubber Wheel Apparatus. ASTM G65-04, ASTM International, pp. 1–12 (2010)
9. Hutchings, I.M.: *Tribology: Friction and Wear of Engineering Materials* CRC Press (1992)
10. Montgomery, D.C.: *Design and analysis of experiments*, 6th Edition Set. John Wiley & Sons, Limited (2007)
11. Sahin, Y.: Optimal testing parameters on the wear behaviour of various steels. *Mater. Des.* **27**(6), 455–460 (2006)
12. Dharmalingam, S., Subramanian, R., Somasundara Vinoth, K., Anandavel, B.: Optimization of tribological properties in aluminum hybrid metal matrix composites using Gray-Taguchi method. *J. Mater. Eng. Perform.* **20**(8), 1457–1466 (2010)
13. El-Tayeb, N.S.M., Yap, T.C., Brevem, P.V.: Wear characteristics of titanium alloy for cryogenic sliding applications. *Tribol. Int.* **43**(12), 2345–2354 (2010)

14. Ravindran, P., Manisekar, K., Narayanasamy, P., Selvakumar, N., Narayanasamy, R.: Application of factorial techniques to study the wear of Al hybrid composites with graphite addition. *Mater. Des.* **39**, 42–54 (2012)
15. Buglacki, H., Smajdor, M.: Mechanical properties of abrasion-resistant Hardox 400 steel and their welded joints. *Adv. Mater. Sci.* **4**(2(4)), 5–8 (2003)
16. Myers, R.H., Montgomery, D.C., Anderson-Cook, C.M.: *Response Surface Methodology: Process and Product Optimization Using Designed Experiments*. Wiley (2009)
17. Stevenson, A.N.J., Hutchings, I.M.: Development of the dry sand/rubber wheel abrasion test. *Wear* **195**(1–2), 232–240 (1996)

Chapter 12

Lean Manufacturing Through PDCA: A Case Study of a Press Manufacturing Industry



Kashmir Singh Ghorha, Rohit Sharma, and Gurraj Singh

Abstract Globalization has resulted in increased market competition. A large number of choices in the market have affected the behaviour of the customer. They expect high-quality goods at low prices and with short delivery times. It is, therefore, necessary for any industry to improve its existing production standards on a continuous basis in order to satisfy the needs of its customers and thus, save their market share. The continuous improvement projects help in optimizing the use of available resources through waste reduction which helps in improving manufacturing cost and product quality. The paper discusses a case study in which the productivity of a press manufacturing company is improved through a continuous improvement strategy. The paper is focused on the use of the Plan-Do-Check-Act (PDCA) cycle to improve the marking standards of a heavy component known as Dish End used in the link frame mechanical press. A marking jig is designed and manufactured to improve the marking cycle time of Dish End manufacturing and it has resulted in a reduction of 255 min of the marking process.

Keywords Continuous improvement · PDCA · Lean manufacturing · Marking jig · Productivity improvement

12.1 Introduction

The rapid changes in technology and increased product variety have led the industries to implement continuous improvement strategies to remain competitive. Any industry needs to focus on continuous improvements in their speed, efficiency, and customer value in order to satisfy the changing customer demands. The ability to improve the processes on a continuous basis decides the long term health of any industry [21].

K. S. Ghorha (✉) · R. Sharma

Department of Mechanical Engineering, Lovely Professional University, Phagwara, India

G. Singh

Department of Industrial and Production Engineering, Dr. B R Ambedkar National Institute of Technology, Jalandhar, India

The continuous improvement efforts can expect incremental improvement over time or breakthrough improvement all at once [20].

PDCA cycle is an iterative, four-step technique to improve processes, products, services and to solve troubles on a continuous basis. It is developed by Dr. William Edwards Deming. It is sometimes called PDSA, the Deming Wheel, or Deming Cycle. He created a tool that helps in finding out the causes for which product fails to meet customer expectations, what changes are required to be done, and then testing the solutions in a continuous feedback loop. The four phases of PDCA are:

- (a) Plan: This phase involves the identification and analysis of the problem, development of the hypotheses about what the issue may be, and decision about which one to test.
- (b) Do: This phase involves testing of the potential solution specifically on a limited area first and measurement of the effects.
- (c) Check: This phase involves the study of the results obtained in the previous step, their effectiveness, and decision regarding whether the hypotheses are supported or not.
- (d) Act: Depending on the analysis done in the previous step, further actions are decided in this phase. For example, if the solution is successful then the next step is to implement it on a larger scale. But if the solution is not successful then it is time to think about other potential solutions.

The PDCA cycle is an effective approach for problem-solving. It not only manages change but also ensures that potential solutions are appropriately tested before committing their implementation on a larger scale. Moreover, it is useful in all kinds of environments or any kind of industry [5].

Along with a sound methodology, continuous improvement projects also need a sound analysis tool. The critical examination technique is a very effective way of analyzing the problem at hand. This technique is used to examine the recorded facts. In this technique, each element of the process or work currently being done and documented in the form of a chart passes through a systematic and progressive series of questions. The aim is to determine the facts for which it is carried out. Based on the facts found the changes are made in order to develop a new and better method of doing work. The questioning technique used in this method helps in lowering the chance of missing any information which may contribute to developing better ways of doing work. The widely used procedure for conducting critical examination contains two sets of questions named primary questions and secondary questions. The primary questions help in finding out the importance of the activity currently being done while secondary questions help in finding out the alternative ways of doing work. The critical examination technique is summarised in Table 12.1.

The primary questions cover five main work elements named as the purpose of work, means used to perform that work, place of work, the sequence of work, and person involved in the work. The prime focus of the primary questions is to reveal every aspect of the work so that work should be understood in detail and more clearly. This understanding of the work in depth further reveals parts of the work which are unnecessary or lacks efficiency. The prime focus of the secondary questions is to

Table 12.1 Critical examination chart

Work elements	Primary questions	Secondary questions
Purpose of work	What is achieved? Is it compulsory? If Yes, then why?	What else could be done?
Means used	How is it done? Why that way?	How else could it be done?
Place of work	Where is it done? Why there?	Where else could it be done?
Sequence of work	When is it done? Why then?	When else could it be done?
The person involved in work	Who does it? Why that person?	Who else could do it?

find alternatives to the unnecessary work or the inefficient parts of the work found through primary questions so that a better method can be developed. The analysis through critical examination technique helps in removing the inefficiencies from the system and thus, makes the processes standardized.

The standardized work results in a smooth workflow, high quality, rejection-free production, and optimum efficiency. It eliminates the variability from the processes resulted from several causes such as unnecessary movements, search for tools, operator skill variation, and adjustments and thus makes the work predictable. After the implementation of the standardized work, it is necessary to constantly work for further improvement of the developed standards. The work should be reviewed daily to find out the abnormalities and issues which can be eliminated in time to achieve more precise work procedures.

This case study adopts the PDCA approach to frame the problem at hand, uses critical examination technique to identify the parts of the work which are unnecessary and lacks efficiency, and standardized the work processes through the development of better ways of doing work.

12.1.1 Background of the Case Study

The case study is done at Link Frame Mechanical Press (LFMP) manufacturing company. The company is engaged in the manufacturing of mechanical and hydraulic presses. The major target sector of the company is the automobile sector. The position of the company before the start of the productivity improvement project was as follows.

The company had experienced an increase in the demand for the Air Tanks and had forecasted a 20–30% increase in the demand for the next 2 years. On the other side, the company was facing a problem of high marking time and rework of the component known as Dish End used in the Air Tanks of the LFMP. The rework was due to the connection flanges welded on the Dish End which produced a miss-match

issue with the pipelines at the assembly stage processes. This scenario had forced the company to improve the existing production capacity and to lower the manufacturing cost by improving the existing production standards.

This situation gave the authors an opportunity and a case study is done on the Dish End manufacturing process of the same company to improve the marking time and rework activities. The PDCA cycle combined with the critical examination technique is used as a continuous improvement tool in the study to find out the main causes of the high marking time and rework activities, development of the solution, and its implementation to remove the existing problem.

12.1.2 Introduction to the Product

The product under study is a Dish End which is a part of the Air Tank used in LFMP. The various applications of the LFMP are in the automobile sector, defence, white goods production, shipyard, aeronautical, railways, and nuclear sector. It is widely used in the automobile sector for forming various sheet metal components used in different automobiles. This press transforms the rotational force of a motor and flywheel into a translational force of slide which performs the pressing action. The major components of this press are: bottom head, moving bolster, slide, uprights, crown, die cushion, and an air tank as shown in Fig. 12.1. The tie rods are used to assemble the subassemblies of these major parts during the assembly of the press. The purpose of the Air Tank in LFMP is to store air for the counterbalance cylinders of the press. In the Air Tank, two Dish Ends are used. The Air Tank consists of a long cylindrical shell closed at both ends with the help of Dish Ends welded to it as shown in Fig. 12.2.

In LFMP, two Air Tanks are used. So, per press four Dish Ends are manufactured. These Air Tanks are connected to the counterbalance cylinders of the press through pipelines that connect the flange of Dish End to the flange of the counterbalance cylinder.

12.2 Literature Review

Seidel and Arndt [19] applied a productivity assurance program for strategic productivity improvement in complex job shop environments where a multitude of technological and non-technological factors are involved. The study suggested that this method as compared to other existing productivity improvement methods is easy to apply and does not require complex evaluation procedures for the determination of meaningful parameters on which improvement decisions can be made. This methodology consisted of the following main steps: (1) Identifying the general requirements of high productivity set by a company's specific type of production process, (2)

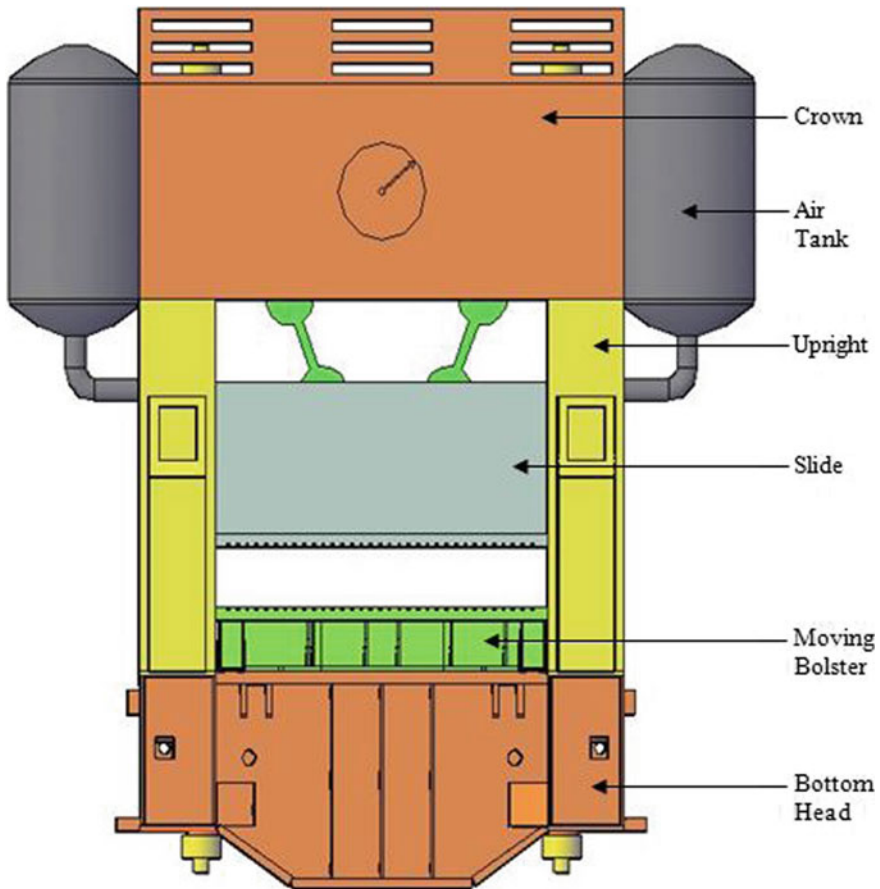


Fig. 12.1 LFMP with air tanks

Analyze the company's position and productivity levels concerning these requirements, (3) Identify opportunities for productivity improvement, (4) Develop improvements, (5) Implement improvements, (6) Monitor the result and go back to step no. 2. Chandra [22] achieved a saving of 3.35 h in processing time in a manufacturing unit through the application of work-study. The main focus was on the application of time study and method study techniques. The study discussed how these techniques help in eliminating unnecessary waste and in the design of improved ways of performing the job in minimum time. Al-Saleh [1] worked in the inspection station of a motor vehicle for the improvement of productivity. The research work used the time study and motion study techniques to identify and eliminate the bottlenecks in the inspection process of the vehicle. The ARENA software was used to estimate the results that can be achieved through the suggested changes. The methodology adopted in the study had the following steps: (1) Process mapping, (2) Bottleneck identification

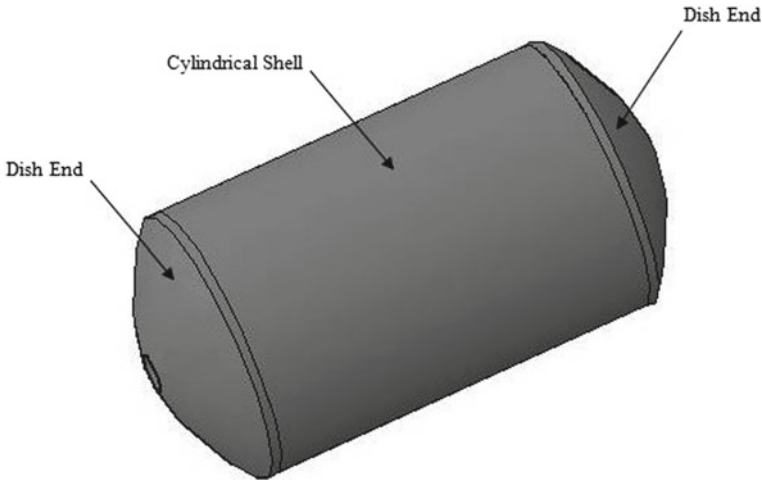


Fig. 12.2 Air tank

through analysis, (3) Eliminating the bottlenecks through motion study, (4) Standard time calculations for the new methods developed. The tools used for data collection are operation charts, flow charts, and man-machine charts. Through motion study, new hand motions were introduced and the non-value added motions were eliminated in inspection stage 1 of the periodic inspection process. The study achieved a productivity improvement of 174.8% in the inspection of the vehicle. Hassanali [6] improved the productivity of a construction equipment manufacturing industry through the application of work-study techniques. The main focus of the study was on the improvement of material utilization and worker productivity. The study found underutilization of the available resources in the yard area. The method study was used to understand the current operations conducted. The analysis of the existing operation resulted in the development of the proposed productivity model. The techniques used to collect the data were operation charts, string diagrams, and flow charts. The development of improved methods through the new productivity model resulted in the improvement of worker's attendance and inventory within one month of the installation of the new model. Hemanand et al. [7] worked in the automotive industry to improve productivity through the application of lean manufacturing techniques. The target of the study was to reduce the unnecessary motion wastes hidden at various points of the production process. The methodology adopted includes the detailed study of the plant layout and process mapping of the plant followed by the identification and elimination of bottlenecks or wastes. The process flow charts and time study technique was used for the data collection. The study found a high idle time of workers and a lot of material handling through manual means. The study worked on the improvement of the plant layout to reduce the unnecessary motion waste resulting in the operator idle time and high material handling time. The study used the gravity feeder to connect all the machines to reduce material handling time.

The positions of different machines changed to balance the line and eliminate the operator idle time. A delivery window was opened between two stations to reduce the material handling motions. The study achieved an 11.95% increase in the productivity of the plant. Marri and Shaikh [12] improved the productivity of the textile industry through the use of work-study techniques. The aim was to eliminate the wastes from the current processes. The study used the method study technique to understand in detail the current operations of the industry to identify bottlenecks and waste. The time study was also used in the research work to set the time standards for certain operations. The method study mainly contains the following steps: (1) Select the area, (2) Record the necessary information, (3) Examine the recorded facts carefully, (4) Develop the improved methods, (5) Define the developed solutions, (6) Install the proposed methods, (7) Maintain the result obtained. The data collection tools used in this method were operation charts, flow charts, string diagrams, man-machine charts. The critical examination tool was used along with the 5W2H tool for the identification of facts and developing new solutions. The study improved the material handling equipment, developed the proper instruction charts for workers, manuals for machine inspections, installed racks for the different tools, improved the utilization of space through a new layout, and developed incentive rewards for labour. Barbole et al. [4] reduced the cost of manufacturing through cost control techniques. The study was conducted at Piaggio vehicles to reduce the material cost of the production process. The cost reduction techniques used in the study were value engineering, kaizen costing, and inventory management. The study concluded that the cost reduction techniques like quality control, budgetary control, and value engineering play a vital role in low-cost manufacturing for the industries where the material cost is 70% of the total cost. Khatun [9] used industrial engineering techniques like work-study and capacity study for productivity improvement in the garment industry. The study started with the use of the method study technique in order to record the detail of current operations along with the time taken by these operations. The time taken was obtained by the use of the time study technique. The breakdown method was used in the study to note the various elements (in sequence) involved in each operation. The study developed a plant layout that helped in efficient bundle tracking, eliminating lot mix-up, use of self-inspection, and increased worker efficiency. The study also discussed the role of industrial engineering techniques in productivity improvement by comparing the two different set of industries. Kumar and Mahto [10] optimized the assembly line of the packaging industry through the process analysis technique. In the process analysis technique, the focus is on finding the wastages and non-value addition activities in the existing processes of the production for the sake of improving the current productivity. The ABC classification was employed in the study for selecting the items which are important for customers in the analysis process. The study identified bottlenecks in the production line in terms of workstations. These bottleneck workstations were rearranged in order to eliminate the waiting time. Kayar and Akalin [8] improved the efficiency of the assembly line and production through the use of method study. The study was conducted in a textile company. The method study helped in increasing the production of blouses by 30 numbers per day. The study reported an increase in the efficiency of the assembly

line by 7.83%. Through method study, new and improved methods were developed for the production of blouses which lowered the manpower and number of machines required than the previous methods. The study also improved the utilization of the work floor area. The research showed that method study is a very important tool for increasing productivity without an increase in the production cost. Kumar and Kumar [11] used the concept of standardization in order to implement lean manufacturing in the automotive parts manufacturing industry. The study was focused on the importance of standardized work for eliminating and reducing waste in the manufacturing processes and thus improving productivity. The methodology adopted in the study has the following steps: the study of current processes and flow of material, documenting the work in proper order through various data collection tools, critical examination of the recorded facts, use of work standardization techniques to develop new standards, implementing the proposed standards, and monitoring the results obtained. The study reported a decrease in the manpower from 4 to 3, a reduction in work-in-process inventory by 26%, and setups reduced by 66.68%. Pampanelli et al. [15] applied the lean and green model to improve the utilization of resources and lower the total cost in terms of energy and mass flow in the manufacturing industry. The concept of a cross-functional kaizen team at the cell level is used in the study. The study started from a production cell level and after getting satisfactory results the study was implemented in other parts of the manufacturing. The prime focus was to improve the material flow, reduce energy consumption and waste generation. The methodology used in the study is: (a) Stabilization of the value, (b) Identification of environmental aspects and environmental impacts, (c) Measurement of the environmental value stream, (d) Improvement of the environmental value stream, (e) Continuous improvement. The study confirms a 30–50% reduction in resource use and a total cost reduction of 5–10% for energy and mass flow in the manufacturing unit. Rahman et al. [16] focused on the use of the kanban system for lean manufacturing in small and medium enterprises. The study also identified the factors which create problems for implementing the kanban system in Malaysian SMEs. The study was conducted in the industry manufacturing automotive parts. The observation method and structured interviews are used for the data collection in the study. The study identified the following problems in implementing the kanban system: improper inventory management, lack of participation from top management, employees and supplier, and lack of quality control and quality improvements. Sayem et al. [18] developed a quality control model in the apparel industry for productivity improvement by minimizing the rework in the production process. The study was focused on the identification, quantification, and elimination of the variations and their sources in order to ensure the production right for the first time. The model developed also achieved a reduction in cost and throughput time. The methodology used in the study includes the following steps: current quality system mapping, identification of defects at different stages, ranking the defects through Pareto analysis, categorization of the defects through cause and effect, and developing a quality inspection model. The study achieved a 40%, 50%, and 55% reduction in the rework for the sewing section, stitching section, and thread section respectively. Athalye et al. [3] worked in the automobile industry to reduce the cost with the help of industrial engineering

tools. At first, the importance and use of various industrial engineering tools were studied through the help of a questionnaire and personal interview techniques. The study concluded that the use of cost reduction tools has increased a lot than other methods in the last 10 years. The study was conducted in the stamping unit of the industry with the aim of reducing the operation cost. The double die hold technique was used to increase the productivity of the 600 T press. The work reported Rs. 1,877,088 saving annually. Mori et al. [13] discussed the different types of tools used to improve the productivity of the manufacturing units. The study discussed the following tools along with their importance and use: Time and motion study technique, optimum utilization of available resources, parallel work centers, use of automation, process analysis technique, non-value addition activities and their elimination, Line balancing, 6 s method, 5 s method, direct observation technique, and cellular manufacturing. Antonioli et al. [2] worked in the automotive industry which manufactures the air conditioning systems for the vehicles with the aim of improving the productivity of the line. The study focused on the standardization technique, reduction or elimination of non-value addition activities, and continuous improvements in order to eliminate the waste in the manufacturing process. The results show an increase in the productivity and efficiency of both machines and operators. The overall equipment effectiveness was increased by 16%. The methodology adopted consists of the following main steps: (1) Mapping of the existing processes (2) Identification of wastes, critical points and difficulties in implementing the lean tools (3) implementing Kaizen and standard work technique for improvements. (4) The result analysis through OEE. Rosa et al. [17] improved the quality and productivity of steel wire-rope manufacturing through Lean and PDCA tools. The methodology used consists of the following steps (a) Mapping of the existing operations by value stream mapping, (b) Identification of wastes and bottlenecks, (c) Development of solutions (d) Implementation of upgraded procedures for equipment (e) Eliminate waste (f) Improve through PDCA. The results obtained show that productivity is increased by 41%. Neves et al. [14] implemented the lean tools in trimming products for the sake of continuous improvement and fast adaptation to the changes in the market. The study focused on the identification of problems and developing answers through the PDCA cycle, 5 s, 5W2H tools. The target was process standardization, increasing profit by value addition. The results shows 10% increase in the useful available time of operators. The methodology used contains 5 stages: (1) Dissection of manufacturing processes, (2) Identification of waste and quality problems, (3) Use of root-cause analysis, (4) Application of suitable lean tools, (5) Analysis of the results obtained.

The review of different case studies on productivity improvement has suggested that the use of continuous improvement techniques produce different results in different manufacturing environments. Moreover, no single technique can be considered as best and it is suggested that the use of a combination of different continuous improvement techniques produce better results.

12.3 Methodology Used

The PDCA cycle is used as a methodology for improving the rework in the assembly stage processes of the Dish End and to lower its high marking time at the fabrication stage processes. The various steps used in the methodology are shown in Fig. 12.3.

12.3.1 Plan

In this step, the complete data related to the manufacturing process of Dish End and its use in the Air Tank at the assembly stage processes is collected through direct observation, feedback from concerned personnel, and time study techniques. The outline process chart (from fabrication stage processes to assembly stage processes) of the Dish End is made as shown in Table 12.2. This chart shows the various manufacturing operations in sequence along with their time taken.

After making the process chart, the critical examination of each operation involved in the process is done through the critical examination technique in which series of

Fig. 12.3 Methodology used

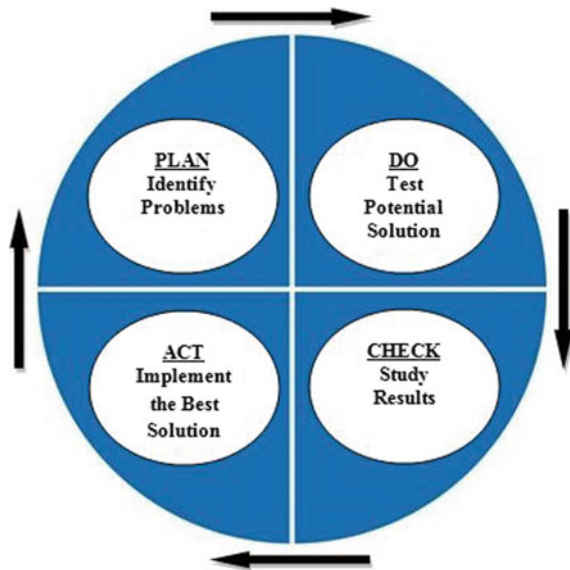


Table 12.2 Outline process chart of the dish end per press

Operation	Number	1	2	3	4	5	6	7	8	9	10	11	12	13	14
	Time taken (min)	15	60	360	104	614	708	106	914	105	224	119	112	204	94

primary and secondary questions are asked about the process at hand to identify the problems and better ways of doing work. One such example is shown in Table 12.3. This table shows the critical examination chart made for operation no. 3 of the Dish End manufacturing. In this chart, operation no. 3 is examined on five main elements of the work that is the purpose of operation, means used to do the operation, place where the operation is performed, the sequence of the operation in the process, and person involved in the operation. Firstly, the primary questions are asked on these five elements of the work, and these questions helped in understanding the work performed in the operation, unnecessary part of the operation, and lack of efficiency in the operation. So, the following primary questions are asked:

- (a) What is achieved in the operation? Is it necessary? If yes, then why is it necessary?
- (b) What means are used to perform the operation? Why the operation is performed that way?
- (c) At what place the operation is performed? Why is it performed at that place?
- (d) What is the sequence of the operation in the process? Why is it performed in that sequence?
- (e) Who performs the operation? Why that person?

Secondly, the secondary questions are asked on the five main elements of the work and these questions helped in finding the alternatives to the unnecessary part of the work and lack of inefficiencies found through the primary questions. So, the following secondary questions are asked:

- (a) What else could be done to achieve the required value addition more effectively and efficiently?
- (b) What other means can be utilized to achieve the required value addition more effectively and efficiently?
- (c) Where else the work could be done to achieve the required value addition more effectively and efficiently?
- (d) What another sequence could be followed to achieve the required value addition more effectively and efficiently?
- (e) Who else could do the work to achieve the required value addition more effectively and efficiently?

In a similar manner, the critical examination of all the operations of the manufacturing operations of Dish End is done and individual critical examination charts are made. Through the critical examination of the operations of the process the following main points are observed:

- (a) On top of the Dish End, a marking operation is done manually through geometrical instruments by the marker at the fabrication stage (see Fig. 12.4). This marking operation is done in order to locate the exact position on the Dish End as per drawing for the welding of connection flange on the Dish End.
- (b) The marking operation is done on the marking table and the whole procedure includes the following steps in sequence: preparation of the marking table, the

Table 12.3 Critical examination chart of operation no. 3 of the dish end

Critical examination chart for operation no. 3		
	Questions	Answers
1	Purpose	
		Marking on the top of Dish Ends in order to locate the correct area where connection flanges are to be welded
	Is it necessary?	Yes
	If Yes. Why it is necessary?	It is the requirement of the design. There is a need to locate the exact position for the welding of connection flanges on the Dish End which ensures proper matching of the connection flanges of the Dish End with the pipelines of the press at the assembly stage processes
	What else could be done?	The marking is necessary but it is an old traditional method which is very slow and not foolproof. Because of the manual element in the procedure chances of errors are high. So, a fast, accurate and foolproof method of marking needs to be developed
2	Means	
	How is it done?	It is done manually with the help of geometrical instruments after placing the job on the levelling blocks set on the marking table
	Why that way?	Marking with geometrical instruments is the basic method which works on every tailor made product
	How else could it be done?	A marking jig can be designed and manufactured which can make this manual marking faster and error free
3	Place	
	Where is it done?	It is done on the marking tables

(continued)

Table 12.3 (continued)

Critical examination chart for operation no. 3		
	Why there?	Marking tables are necessary in order to mark correctly through geometrical instruments
	Where else could it be done?	Marking jig can be designed which can eliminate the use of the marking tables and setting of the component. The use of jig can allow marking on any levelled surface
4	Sequence	
	When is it done?	It is done after the arrival of the Dish Ends to the fabrication shop from cutting yard. This is the first operation performed on the Dish Ends in the fabrication shop
	Why then?	It is a planned sequence according to the manufacturing requirement of the component
	When else could it be done?	No issues with the sequence of the operation
5	Person	
	Who does it?	Qualified marker
	Why that person?	Technical person is required for that task
	Who else could do it?	He is the best person for the current situation

setting of levelling blocks on the marking table, setting of the Dish End on the levelling blocks, locating and marking the center of the Dish End manually through geometrical instruments, and marking of the area where connection flange is to be welded on the Dish End.

- (c) After marking, in the next operation, the marked area on the Dish End is removed with the help of a gas cutting operation. This is done to create an opening on the Dish End for the welding of the connection flange as per drawing.
- (l) In the next operation, the connection flange is welded on the Dish End (see Fig. 12.5) inside the opening made in the previous operation.
- (e) After welding of connection flange on the Dish End, these Dish Ends are welded to the sides of the Air Tanks in the next series of operations.
- (f) In the next step, the Air Tanks (with welded Dish Ends) are assembled on the press at the assembly shop. The pneumatic pipeline of the press is connected to the Dish Ends of the Air Tanks through the welded connection flanges.



Fig. 12.4 Marking on the dish end

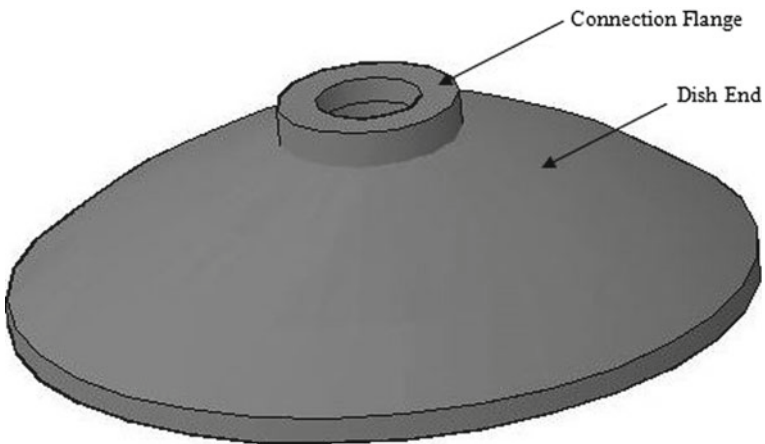


Fig. 12.5 Connection flange welded on the Dish End

In the above manufacturing process of the Dish End, the following two problems are observed:

- (a) The marking operation is very slow and the marker takes around 1.5 h to mark one Dish End. This means 360 min per press which is a very high cycle time.
- (b) At the time of the assembly of the pneumatic pipeline with the connection flange of the Dish End, sometimes deviation is observed in the alignment of

the connection flange and the pipeline. This results in the rework activities of the Dish End in order to eliminate the deviation.

Further analysis of these two problems through direct observation and feedback from the concerned personnel revealed that the deviation between the connection flange and pipeline results from the errors in the center location step of the marking operation. Due to manual marking, sometimes the marker locates the wrong center of the Dish End which results in deviations at assembly stage processes. The use of an old traditional method of manual marking with geometrical instruments consume lots of time. The variation in the skill level of the markers also contributes to high marking time and rework activities. So, it is decided that the manual marking operation must be replaced with some jig that can locate the center of the Dish End without any error and makes the marking operation quick and error-free.

12.3.2 Do

Based on the previous findings, a marking jig is designed and manufactured as shown in Fig. 12.6 to overcome the problems identified. There were two main requirements in the design part of the jig:

- (a) The jig should locate the center of the Dish End quickly and accurately.
- (b) It should be light in weight so that it can be used by a single person easily.

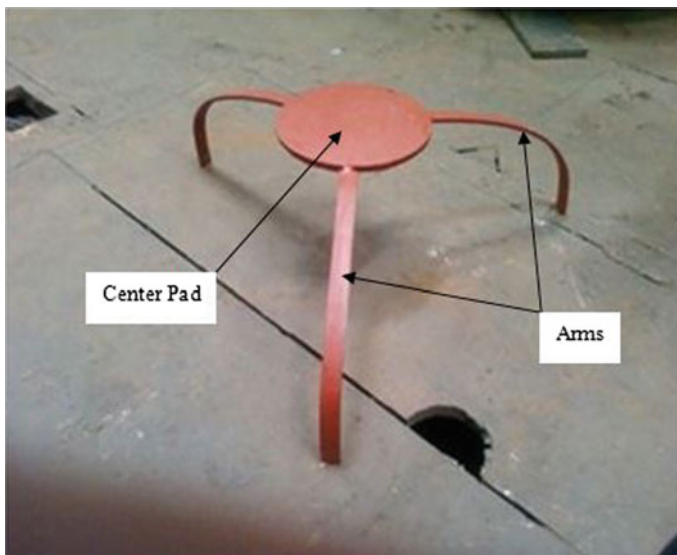


Fig. 12.6 Marking jig

In order to achieve these two requirements, only two main elements are used in the jig. These are named as center pad and arms of the jig. The jig has one center pad and three arms are welded to it. The angle between the arms is 120° . The purpose of the center pad of the jig is to serve as a template that can be used by the marker to mark the area on the Dish End for the connection flange. The center pad allows the marker to mark the area without the use of centering and divider which is a time-consuming method. Now marker can directly take the impression of the center pad with a scribe which is an easy and fast method. The purpose of the arms of the jig is to locate the center pad accurately and fast to the desired area on the Dish End. The condition for the arms was that their profile should be made in such a way that they should lock the position of the center pad of the jig exactly at the desired location on the Dish End. This condition demands exact matching of the profile of the arms and center pad with the profile of the Dish End. In order to achieve this, the profile of the center pad and the arms is made through the same die-set in which the Dish Ends are manufactured. This ensured the complete matching of the jig arms with the Dish End at the time of marking and avoids any variation in the location of the center of the Dish End during the marking operation. In order to ensure the lightweight of the jig, only three arms arranged at 120° with respect to each other are used and these are effective in locating the center pad of the jig to the required place on the Dish End fast and accurately.

12.3.3 Check

The marking jig is tested firstly on two sets of Dish Ends as shown in Fig. 12.7. In order to test the working and accuracy of the jig the following checking procedure is adopted:

- (a) Two dummy sets of the Dish End are manufactured and marking is done on these two sets through the jig with the new method. The marking time through the new method and jig is recorded by the time study technique.
- (b) Two dummy sets of cylindrical shells are also manufactured for these two dummy sets of Dish Ends in order to make two dummy Air Tanks by following the complete procedure which is followed for the real product.
- (c) Then these two dummy Air Tanks are used at the assembly shop during the assembly of the actual LFMP.
- (d) In order to check the accuracy of the new method, a complete dummy pipeline is made between the flange of the counterbalance cylinder of the press to the connection flanges of the Dish Ends attached to both the dummy Air Tanks.
- (e) After the completion of this dummy assembly, the complete procedure is inspected by the quality control inspector and a final report is generated by the quality control department of the company.

The final inspection report revealed that the assembly is free from any deviation and instructed the planning department of the company to make a job order for the

Fig. 12.7 Marking jig on the dish end



implementation of the new method for the actual product. The result of the time study done for the new method showed that the new method of marking takes only 30 min in comparison to 90 min taken by the old method. So, the use of jig and a new method of marking resulted in a time saving of 60 min per Dish End. The following procedure is used in the marking of Dish End in the new method:

- (a) In the new method, the use of the marking tables and levelling blocks in order to set the job is optional. The job can be placed on any surface for the marking operation. So, this new way of marking provides an opportunity to eliminate the step of marking table preparation.
- (b) Unlike the old method, there is no need to locate the center of the Dish End through geometrical instruments. Because this is achieved through the marking jig that locates the center itself. So, in the new method, after placing the job on any levelled surface, the marker has to just put the jig on the job for locating the center. Thus, the step of the center location is completely eliminated.
- (c) After placing the jig on the job, the marker takes the impression of the center pad of the jig onto the Dish End through a scribe and thus, the time-consuming method of marking through centering and divider is completely eliminated.
- (d) After taking the impression of the center pad, the jig is removed and the remaining marking procedure remains the same as that of the old method. A quick comparison between the old and the new method is summarised in Table 12.4.

Table 12.4 Comparison of old and new method

Operation	Old method	New method
1.1	Preparation of marking table	Marking table is optional
1.2	Levelling of the job on blocks	Levelling is optional
2.1	Location of the center through geometrical instruments	It is not required as the jig itself locates the center
2.2	Marking with geometrical instruments	Marking with the jig and geometrical instruments

12.3.4 Act

After the successful trial of the marking jig on the two dummy sets of the Dish End, the new procedure of marking is documented in the form of process charts and these charts are displayed at all the work stations of the Dish End. A training session is arranged with all the concerned markers, supervisors, and shop head in which complete guidance is provided to them regarding the new method. This is done in order to eliminate any kind of confusion at different work stations. Finally, the new process is implemented in all the presses. And the whole process is closely monitored for the next 50 Dish Ends in order to collect more information about the problems or any challenges observed in the new process. The direct observation and the feedback collected from the concerned personnel revealed that the solution implemented for the marking operation of Dish End is successful and it has eliminated the deviation problem and the marking time is reduced significantly.

12.4 Result and Discussion

The aim of the study was to reduce the high marking time and rework activities related to Dish End manufacturing in the case company. In order to achieve that aim, the PDCA approach was used as a methodology for the case study. In the first stage, the data was collected through direct observation, feedback, and time study techniques and a process chart is made which is critically analysed through critical examination technique. The first stage of the study helped in identifying two main causes which were responsible for the high marking time and rework activities. The causes were the manual marking procedure and variations in the skill of the markers. In the second stage, a marking jig was designed and manufactured in order to eliminate the manual element from the marking procedure which was time-consuming and responsible for the marking errors. In the next stage, the proposed solution was tested and implemented successfully.

The main aim of the proposed solution was to make a foolproof center location procedure in the marking process because it was identified as a source of error and time consumption. In order to achieve that the marking jig was designed in such a

manner that it should locate the center correctly and quickly. This is done through the three arms attached to the center pad of the jig. These arms locate the center pad of the jig exactly to the required position on the Dish End. To achieve this foolproof location of the center, the profile of the center pad and the arms of the jig is matched perfectly with the profile of Dish End. This is achieved by manufacturing the jig profile in the same die-set in which the profile of Dish Ends is manufactured.

The marking jig has improved the marking time significantly. In the previous method, the marking was done manually through geometrical instruments, and on average 90 min per Dish End and 360 min per press were consumed in the marking process as 4 Dish Ends are used in a press. Now with the help of a marking jig, the marking time per Dish End is reduced to 30 and 120 min per press. From the rework reports collected from the quality department, it is found that per press on an average 15 min were consumed in the Dish End rework activities as shown in Fig. 12.8.

Due to the implementation of the new marking jig, the 15 min of rework per press is also eliminated. The total savings achieved are given in Table 12.5.

The consistency of the proposed solution was also checked through the time study of the marking operation of 50 Dish Ends done through marking jig. These 50 Dish Ends were marked by 5 different markers and each marker had marked 10 Dish Ends. This was done to see whether the skill of the marker has any effect on the new method. And it is found that all the markers took similar time (close to 30 min) for the marking operation. The results of the time study of the new method for 50 Dish Ends are shown in Table 12.6.

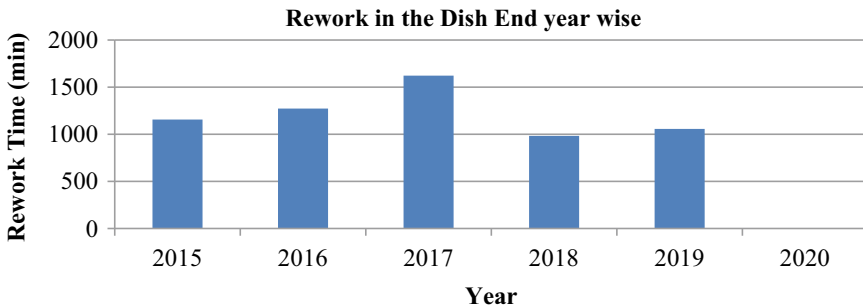


Fig. 12.8 Rework in the dish end year wise

Table 12.5 Savings per press

S. No.	Activity	Without Jig	With Jig	Time saved (min)
		Time (min)	Time (min)	
1	Setup	60	60	0
2	Marking	360	120	240
3	Rework	15	0	15
Total savings				255

Table 12.6 Time taken by markers with the new method

Time taken per dish end (min)										
S. No.	1	2	3	4	5	6	7	8	9	10
Marker 1	29	28	27	29	27	29	30	27	28	27
Marker 2	27	31	29	28	32	28	27	29	27	28
Marker 3	28	30	28	27	27	28	28	29	30	29
Marker 4	29	27	29	29	28	30	29	28	28	28
Marker 5	27	31	30	28	31	28	27	29	27	30

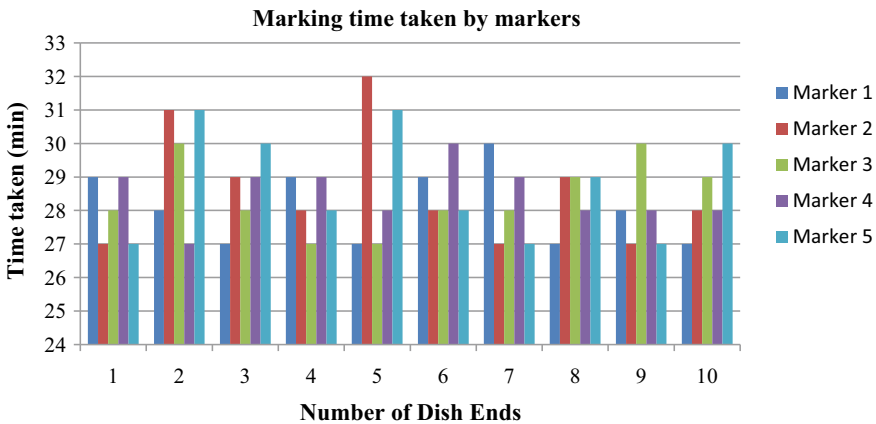


Fig. 12.9 Comparison of time taken (marker wise) for 10 sets of dish end

The comparison of the time taken by 5 different markers for the marking of 10 different sets of the Dish Ends is shown in Fig. 12.9.

12.5 Conclusion

Continuous improvement activities to improve the existing production standards are of high priority for any industry in order to sustain itself in a competitive market. The PDCA is a very effective tool in resolving new and reoccurring problems in any industry. The iterative approach of PDCA helps in the testing of proposed solutions and assessing results in a waste-reducing cycle. The study concludes that the marking jigs can give better results than manual marking processes. The marking jig developed for Dish End manufacturing has reduced the cycle time by 255 min per press. The case study will be useful for other similar processes of different industries and will help the process engineers in decision making.

References

1. Al-Saleh, K.S.: Productivity improvement of a motor vehicle inspection station using motion and time study techniques. *J. King Saud. Univ. Eng. Sci.* **23**(1), 33–41 (2011)
2. Antonioli, I., Guariente, P., Pereira, T., Ferreira, L.P., Silva, F.J.G.: Standardization and optimization of an automotive components production line. *Proc. Manuf.* **13**, 1120–1127 (2017)
3. Athalye, A., Gera, P., Madan, A.R.: Study and analysis of cost reduction techniques in press part production: a case study of stamping unit. *Int. J. Sci. Res. (IJSR)* **4**(1), 3247–3252 (2015)
4. Barbole, A.N., Nalwade, Y.D., Parakh, S.D.: Impact of cost control and cost reduction techniques on manufacturing sector. *Indian Streams Res. J.* **3**(5), 1–8 (2013)
5. Deshpande, V.A.: Application of plan-do-check-act cycle for quality and productivity improvement—a review. *Int. J. Res. Appl. Sci. Eng. Technol.* **5**(1), 1997–2001 (2017)
6. Hassanali, K.N.: A productivity model utilising a work study approach for performance measurement. *J. Assoc. Prof. Eng. Trinidad Tobago* **40**(1), 13–25 (2011)
7. Hemanand, K., Amutbuselvan, D., Raja, S.C., Sundararaja, G.: Improving productivity of manufacturing division using lean concepts and development of material gravity feeder—a case study. *Int. J. Lean Thinking* **3**(2), 102–116 (2012)
8. Kayar, M., Akalin, M.: A research on the effect of method study on production volume and assembly line efficiency. *Tekstil ve Konfeksiyon* **24**(2), 228–239 (2014)
9. Khatun, M.M.: Application of industrial engineering technique for better productivity in garments production. *Int. J. Sci. Environ. Technol.* **2**(6), 1361–1369 (2013)
10. Kumar, N., Mahto, D.: Productivity improvement through process analysis for optimizing assembly line in packaging industries. *Glob. J. Res. Eng.* **13**(3), 1–4 (2013)
11. Kumar, R., Kumar, V.: Literature review and implications of standard work implementation in indian industry—a case study. *Int. J. Latest Trends Eng. Technol. (IJLTET)* **4**(3), 50–63 (2014)
12. Marri, H.B., Shaikh, G.Y.: The role of productivity improvement tools and techniques in the textile sector during manufacturing. In: *Proceedings of the 2012 International Conference on Industrial Engineering and Operations Management Istanbul, Turkey, July 3–6* (2012)
13. Mori, V.K.V., Kanchava, Y.B., Karetha, P.A., Charola, M.B.: Productivity improvement by use of time study, motion study, lean tool 's and different strategy for assembly of automobile vehicles. *Int. J. Sci. Res. Dev.* **3**(02), 2060–2065 (2015)
14. Neves, P., Silva, F.J.G., Ferreira, L.P., Pereira, T., Gouveia, A., Pimentel, C.: Implementing lean tools in the manufacturing process of trimmings products. *Proc. Manuf.* **17**, 696–704 (2018)
15. Pampanelli, A.B., Pauline, F., Andrea, M.B.: A lean and green model for a production cell. *J. Cleaner Prod.* **85**, 19–30 (2014)
16. Rahman, N.A.A., Sariwati, M.S., Mashitah, M.E.: Lean manufacturing case study with Kanban system implementation. *Proc. Econ. Fin.* **7**, 174–180 (2014)
17. Rosa, C., Silva, F.J.G., Ferreira, L.P.: Improving the quality and productivity of steel wire-rope assembly lines for the automotive industry. *Proc. Manuf.* **11**, 1035–1042 (2017)
18. Sayem, A., Islam, M.A., Khan, M.M.A.: Minimization of reworks in quality and productivity improvement in the apparel industry. *Int. J. Eng. Appl. Sci.* **1**(4), 147–164 (2014)
19. Seidel, R.H.A., Arndt, G.: Productivity improvement in job shop production. *CIRP Ann. Manuf. Technol.* **37**(1), 421–424 (1988)
20. Singh, J., Singh, H.: Performance enhancement of a manufacturing industry by using continuous improvement strategies—a case study. *Int. J. Prod. Quality Manage.* **14**(1), 1–30 (2014)
21. Sraun, J.S., Singh, H.: Continuous improvement strategies across manufacturing SMEs of Northern India—an empirical investigation. *Int. J. Lean Six Sigma* **8**(2), 1–5 (2017)
22. Chandra, P.V.: An effort to apply work and time study techniques in a manufacturing unit for enhancing productivity. *Int. J. Innov. Res. Sci. Eng. Technol.* **2**(8), 4050–4058 (2007)

Chapter 13

Optimization of Changeover Time in a Manufacturing Enterprise Using Single Minute Exchange of Dies (SMED): A Case Study



**Aditya Bassi, Harkrit Chhatwal, Nishant Bhasin, Shubham Sharma,
and Ruchika Gupta**

Abstract This paper presents a case study where the implementation of lean techniques in the changeover time of stereo in a Flexo printing machine were investigated to study its impact. During this study, the problem with high changeover time during printing were investigated through SMED (Single minute exchange of dyes). The research includes the analysis of current system depicting the existing problems within the company. The methodology aims to analyse the root cause of existing problems and thus provide implementation of improvement plan. At the end of the investigation, a few solutions were successfully implemented. The results demonstrates the steps taken to optimize the changeover time which was reduced to around 29 min. Thereby, an improvement of 10% was achieved. Hence, decreasing the changeover time resulted in increased productivity and processing time in the manufacturing unit.

Keywords SMED · Quick change over time · Internal and external activities · 5S

13.1 Introduction

Lean management was originated from Toyota production house and as stated by many authors it works on exaggerating the products value by streamlining the operations in a production setup. Lean methodologies can be enforced in the manufacturing sector in various ways such as reduction in defects, shortening of the lead time and reducing the changeover time. There are variety of lean methodology tools like identifying and sorting of Value Added and Non-Value-Added activities, 5S, SMED (Single Minute Exchange of Dies), Kaizen, Standardized Work and JIT (Just in time).

In these modern times, application of lean six sigma has spread all around the globe. These techniques are often implemented in the manufacturing industry in order to reduce the cost of production, maintain the product quality and sustaining a

A. Bassi (✉) · H. Chhatwal · N. Bhasin · S. Sharma · R. Gupta
Amity University Noida, Greater Noida, Uttar Pradesh, India

good customer relation. One of the tools which we used in our research project was SMED. It is an approach to reducing output and quality losses due to changeovers. C/O (Changeover) time is the amount of time consumed between the last piece of present product and the first piece of the next product. Reducing the changeover time helps the big, medium-sized and small-scale industries to meet the customers demand and thus leads to increase in their profits. In this method the process is studied by doing videography and examined on multiple occasions. After this process, all the activities are listed down and are segregated into internal (when the machine is running) and external activities (when the machine is stopped). The aim is to convert as many internal activities to external ones in order to reduce the overall time of production and hence meet the customers demand. 5S (Sort, set in order, Shine, Standardize and sustain) is a method that consists of five Japanese words which focuses on setting everything in order and sustaining the workplace clean. This eventually allows the workforce perform their job in a systematic manner without risking their life.

This paper aims to present the implementation sequence and level of importance regarding Lean-SMED techniques at a non-woven bag manufacturing firm.

13.2 Research Background

These days, organizations need to make the products as indicated by the necessities and prerequisites of their customers. Apart from that, customers also desire their product to be delivered on time and for that the lead time for the production is the key. For that, lean production system must be in place as it gives an edge to the companies who implement them in this highly competitive market. For a lean system, the removal of non-value adding activities and wastes is very imperative. Ohno [1] describes waste as any activity that does not value to the product from the customer's point of view. To reduce such non-value activities or wastes, there are a variety of tools that can be used like 5S, Value Stream Mapping and SMED.

Single Minute Exchange of Dies, or simply SMED assures a less changeover time and efficient transition of the machine setup usually less than ten minutes as explained by Shingo [2]. The Changeover time is the total amount of time elapsed between the last product produced in the previous run of the machine to the first different product produced in the next run. This amount of time is spent on cleaning and altering preparing the machine setup for next product. A setup can be defined as the transitioning of a machine to produce a product to a different product. Sousa et al. [3] describes that implementation of SMED involves a deep analysis of each and every setup operation. Setup operations can be characterized as Internal and External Setup. A literature review by Yash and Nagendra [4] covers the implementation of SMED by saying that it may represent the key factor for providing more flexibility and enhanced product flow in the manufacturing unit. Moreover, the main steps for implementing SMED includes judging the current state process, separating the internal and external activities and streamlining the process of changeover.

Goubergen and Landeghem [5] categorized three reasons for reducing setup times which includes Flexibility, Bottlenecks and Costs minimization. Flexibility is due to the large variety of products and any manufacturing company should react quickly according to the customer needs in order to maintain its reputation in the market. Bottlenecks should be minimized to maximize the availability for producing more. Costs minimization is very important as in any manufacturing unit, the production costs are directly proportional to the machine performance.

A critical evaluation of Shingo's methodology on SMED by McIntosh et al. [6] argues that the application of improvement techniques in some of the stages of SMED does not always prove to be effective. Whereas, a study by Abraham et al. [7] demonstrated the effectiveness of SMED by reducing the setup time of a press machine by 75%. This was achieved by identifying the bottlenecks and eliminating the non-value-added activities from the existing process leading to significant improvement in productivity.

SMED is one of the ideal methods to strengthen the output and minimize the quality loss in any manufacturing process as said by Prof. Nagaraj A. Raikar [8]. Apart from the value-added benefits, decreasing the changeover time results in additional advantages such as cost reduction, standardization, and better workload as showed by Ribeiro et al. [9]. The Overall Equipment Efficiency (OEE) increases by decreasing the equipment downtime with Changeover as explained by Rahul and Naik [10] in a case study.

There are many more examples of the application of SMED that can be found to prove that this tool can be applied in a plethora of industries. One such example can be of a pharmaceutical company by Gilmore and Smith [11] where the setup time was reduced from 28.8 to 8.25 h with the help of SMED.

13.3 Methodology

The Lean six sigma project being reported here was carried out Planet Green Innovations which is part of Sterimed Group of companies. The company was recently facing major problems in the management of their inventory specifically the maintenance of their inventory levels. During the operations of the ongoing project, Changeover times were considered as the scope for improvement where some Lean Six-Sigma tools were applied and appropriate suggestions were given for improvement. The technique which was used is called SMED. The steps taken in the project are explain below.

13.3.1 Data Collection

Data collection is the initial phase of any Lean Six Sigma project. It is that phase where we are able to identify the customer and the requirements for the product and

Table 13.1 Translation matrix

V.O.C	CTQ	CTQ measure	CTQ specification
Huge pending orders	Change over time	Overall production rate	Reduction in change over time by 22%

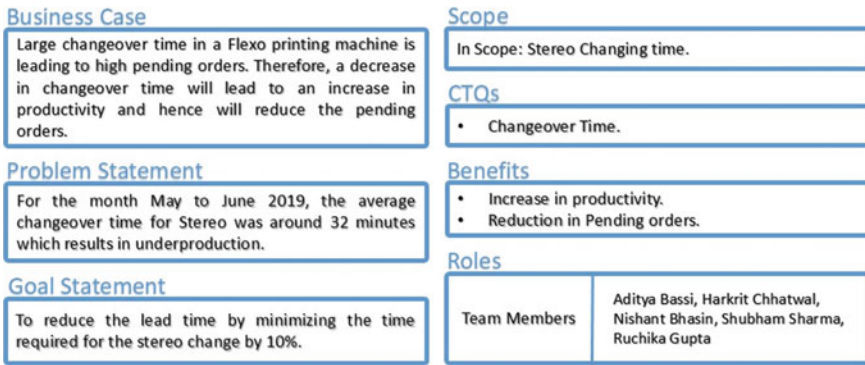


Fig. 13.1 Project charter

services. This phase plays a vital role as it helps in identifying the goals and aligns the project by laying the groundwork that will allow the team to remain focused.

One of the first phases of data collection is to identify the VOC (Voice of Customer) and the various steps required to convert it into CTQ (Critical to Quality). The conversion of VOC to CTQ is depicted below in Table 13.1. The table showcases the company’s demand to increase the Overall Production rate to complete the huge existing and Pending orders and aims at achieving it by reducing the changeover time by approximately 22%.

Once the translation matrix is generated, next step is to construct a project charter which will exhibit the Problem Statement, Goal Statement and the benefits of carrying the project. The project charter shown in Fig. 13.1 displays the problem statement which mentions a large changeover time in the manufacturing, consequences of which are reduction in productivity and decrease in company’s revenue. Furthermore, the goal statement defines minimization of stereo changeover by 10% in order to increase the operation productivity.

13.3.2 Data Analysis

Often many tend to avoid the analyse phase as we are able to identify the problems earlier only in our project. But this phase is important because it clearly defines how well the process is currently performing and identifies how much the process can be

improved. We are able to develop hypotheses which helps us to validate and identify vital root causes of the problem in hand (Fig. 13.2).

One of the prime Lean six sigma tools used to find the root cause of the problem is the Ishikawa or the Fishbone diagram. It is a drill down process which enables us to point out the factors, causes and sub causes of the desired problem. In other words, we can say it helps in identifying the root cause of the given problem we look to find solutions for.

The cause and effect diagram depicted factors which effected the most on the inaccurate inventory levels. The major factors are:

- **Material not available**—one of the problems the operators tends to face is the unavailability of the material (cloth roll) at the appropriate time. This leads to increase in the non-value-added time and decreases the productivity.
- **Operator Training**—Lack of training plays a vital role as an unskilled worker will obviously take more time for setting up the new stereo and the roller on the machine.
- **Unavailability of tools**—During the setting up of the new stereo and the roller there are certain tools which are required. Often, they are not found because of misplacement. This causes delay and increase in change over time (Fig. 13.3).

Furthermore, in the analysis phase of the project we noted down the changeover time for stereo change for the month of June. The above table represents the data that was collected for the month of June. Every day the number of changeovers used

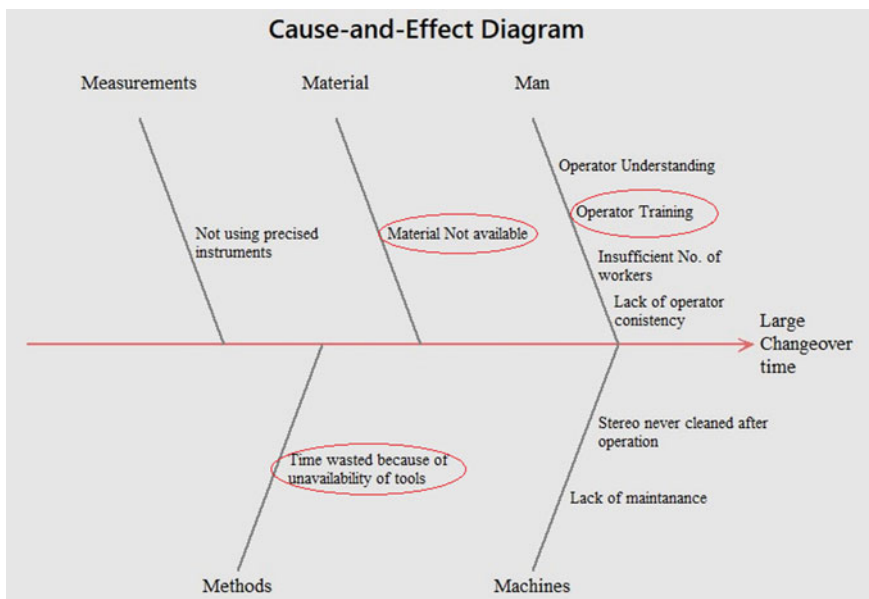


Fig. 13.2 Cause and effect diagram

Stereo Changeover time (June)	Average Changover time per day	Date	Changeover time
32	33.3	02 June 2020	33.3
37		03 June 2020	27
31		04 June 2020	34
25	27.0	05 June 2020	28.3
29		06 June 2020	25.5
27		07 June 2020	34
30	34.0	08 June 2020	29.8
34		09 June 2020	35
38		10 June 2020	36
29	28.3	11 June 2020	37
28		12 June 2020	35.5
28		13 June 2020	34.3
26	25.5	14 June 2020	28.5
25		15 June 2020	25.5
35	34.0	16 June 2020	34
33		17 June 2020	26
31	29.8	18 June 2020	32.5
28.5		19 June 2020	33.5
36	35.0	20 June 2020	34.5
37		mean	31.8
32			
35	36.0		
37			
36			
40	37.0		
35			
38	35.5		
33			
30.5	34.3		
38			
29	28.5		
28			
25	25.5		
26			
33	34.0		
35			
23	26.0		
29			
27	32.5		
38			
35	33.5		
32			
33	34.5		
36			

Fig. 13.3 Changeover times

to vary depending upon the number of daily orders. We first noted the timings for every changeover and later took the each day in order to understand and represent it in a more productive manner. We plotted a graph represents the recorded time for changeover over the given month of June. The vertical axis represents the average changeover time on a specific day while the horizontal axis showcases different days of the month. On calculations the linear changeover time for the month of June came out to be 31.8–32 min. On further analysis and study of the manufacturing process

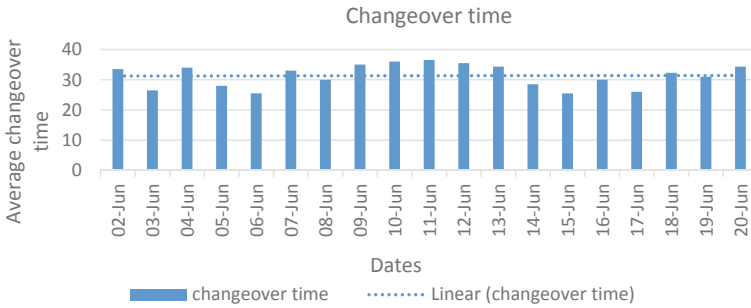


Fig. 13.4 Changeover time graph

we aimed at reducing this changeover time by 10% which will be able to make significant change in the productivity of the unit (Fig. 13.4).

13.3.3 Improvement Scope

One of the first steps in the improvement phase is the listing down of all the activities which takes place in the production of the certain product. Table 13.2 showcases all the steps which are performed in the production operation.

Once all the activities were stated, we then identified and segregated the External Activities. Moreover, we were poised to find out all the waste activities (Tables 13.3 and 13.4).

13.3.4 Implementation and Control Phase

After the identification of the all the steps and the internal, external and waste activities certain solutions were proposed according to the problems faced by the enterprise. Table 13.5 will showcase all the improvement solutions suggested and how these measures will bring change (Fig. 13.5).

The following images shows the implementation of the tag system in the industry. It can be clearly depicted that tags are now used on the cloth rolls specifying appropriate information required by the operator which will help him in identifying the rolls from the inventory.

Once the recommended solutions were proposed and started to get implemented in the unit, our next step in the project was to again calculate the changeover times after a period of 2–3 months to observe how much reduction we were able to achieve with our suggestions.

Figure 13.6 displays the changeover time readings in a graphical format. The vertical axis represents the average changeover time on specific days while the

Table 13.2 Production operation

S. No.	Steps
1.	Stock roll material was brought from the store
2.	Two people pick up the ink tray from the machine and then place it down on the floor
3.	They filled the ink back to the barrel which will not be used for the next job
4.	The operators then started cleaning the floor where the tray was kept
5.	The machine operator collected the stereo and altered it to the required dimensions
6.	On the back of the stereo double-sided tape was applied and extra tape was removed
7.	The operator observed the stereo for air bubbles and removes the bubbles with the help of a sharp pin
8.	The required stereo cylinder was searched and picked as per job specifications
9.	There was a search for Allen keys on the shop floor
10.	One of the operators unscrew the stud bolt and the already placed cylinder was removed
11.	The new required cylinder was then cleaned as it was already containing an old stereo
12.	Then the operator pasted the new stereo on the cylinder
13.	The empty cloth roll was removed from the machine
14.	After this there was a weight for the new stock material to arrive
15.	The shaft and the hub were attached to the new cloth Rolland it was put back on the machine
16.	After the preparation of the stereo on the cylinder, it was linked back to its position on the flexo machine
17.	Then one operator tightens the stud bolt using Allen key while the other prepares the required ink colour
18.	The required ink tray was then cleaned with the help of thinner
19.	This tray was put back to its location on the machine and was then filled with required ink
20.	The gap between the stereo and the cloth was adjusted on the machine
21.	The machine was then started and the operator continuously checked the printed face by measuring with scale
22.	While doing this he observes any problem with the printed material and stops the machine if required
23.	The machine was again started with the appropriate adjustment

horizontal axis depicts the various days. On analysis and calculations, the average changeover time came out to be 28.91–29 min (Fig. 13.7).

The following graph depicts a comparison between the mean changeover time at the initial phase and the mean changeover time after the implementation of the desired suggestions. The difference came out to be in the region of 10% from the earlier figure of 31.90–32 min to 28.91–29 min.

Table 13.3 Internal activities

S. No.	Internal activities
1.	Two people pick up the ink tray from the machine and then place it down on the floor
2.	They filled the ink back to the barrel which will not be used for the next job
3.	The operators then started cleaning the floor where the tray was kept
4.	The machine operator collected the stereo and altered it to the required dimensions
5.	On the back of the stereo double-sided tape was applied and extra tape was removed
6.	The operator observed the stereo for air bubbles and removes the bubbles with the help of a sharp pin
7.	The required stereo cylinder was searched and picked as per job specifications
8.	There was a search for Allen keys on the shop floor
9.	One of the operators unscrew the stud bolt and the already placed cylinder was removed
10.	The new required cylinder was then cleaned as it was already containing an old stereo
11.	Then the operator pasted the new stereo on the cylinder
12.	The empty cloth roll was removed from the machine
13.	After this there was a weight for the new stock material to arrive
14.	The shaft and the hub were attached to the new cloth Rolland it was put back on the machine
15.	After the preparation of the stereo on the cylinder, it was linked back to its position on the flexo machine
16.	Then one operator tightens the stud bolt using Allen key while the other prepares the required ink colour
17.	The required ink tray was then cleaned with the help of thinner
18.	This tray was put back to its location on the machine and was then filled with required ink
19.	The gap between the stereo and the cloth was adjusted on the machine

Table 13.4 External and waste activities

S. No.	External activities	Waste activities
1.	Sometimes cleaning of extra ink tray	Cleaning up of the floor where the ink tray is kept
2.	Stock roll material was brought from the store	Excess amount of tape is first applied and then it is removed which is considered as a waste activity
3.	The machine was then started and the operator continuously checked the printed face by measuring with scale	There is always a search for stereo cylinder to start a new job
4.		There is a search for Allen keys as the shop floor is always messed up
5.		A waiting for the stock material is observed

Table 13.5 Recommended solutions

Recommended solution	Implementation
1. Preparation of Stereo while the machine is running	The machine operators can prepare the stereo for the next order while the flexo printing machine is running. This will eventually save a lot of time in changeovers
2. Implementation of 5S	Implementation of 5S can help in solving a variety of problems in the industry <ul style="list-style-type: none"> • One of S in 5S is set in order. Set in order can be achieved by allotting proper slots for the tools to be kept • Furthermore, we proposed the idea of installing of a proper rack for the rollers to be kept in a systematic manner so that it becomes easy to identify it • Another solution we recommended was introducing of tags which will be applied on each cloth roll stating specific information about the cloth roll
3. Systematic dispatch of material from store	After careful analysis we suggested the firm to start a timely routine about at what time and what quantity of material can be dispatched from the store. This was suggested after we found that there was inadequate space available on the shop floor and thus it will lead to less claustrophobic WIP inventory
4. Proper training	Proper training should be given to the workforce to follow the system introduced
5. Weekly Maintenance of machine	A proper schedule is suggested for weekly maintenance of the machines in order to reduce the stoppage of production due to machine breakdown



Fig. 13.5 Tag system

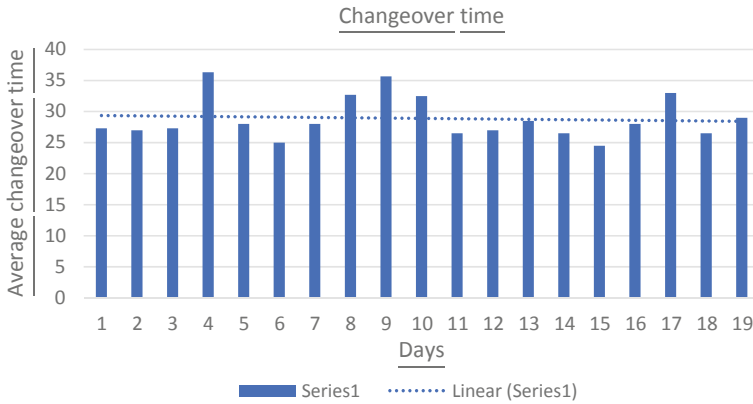
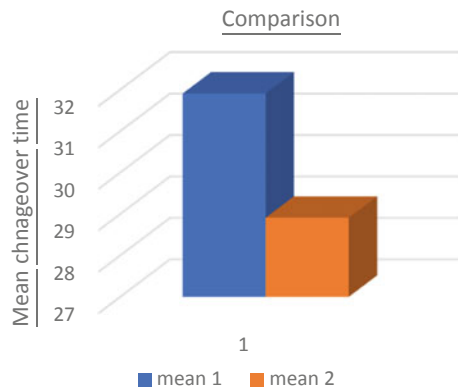


Fig. 13.6 New changeover times

Fig. 13.7 Comparison graph



13.4 Conclusion

The SMED technique of Lean Six Sigma tools was very helpful in conducting this project. Cause and effect diagram was an vital tool to identify the root causes of the problem and played significant part in completion of the project. On successful closure of the project we were able to reduce the mean changeover time by 10 %.

Acknowledgements We would like to thank Dr Gurtej Singh Narang, Head of Research and Development, Planet Green innovations—A Sterimed Group Company for allowing us to perform a Lean Six Sigma project related to the inventory issues in their organization and optimization of the issues using Lean Six Sigma.

References

1. Ohno, T.: *Toyota Production System: Beyond Large-Scale Production*. Productivity Press, Cambridge (1988)
2. Shingo, S.: *A Revolution in Manufacturing: The SMED System*. Productivity Press, Cambridge (1985)
3. Sousa, R.M., Lima, R.M., Carvalho, J.D., Alves, A.C.: An industrial application of resource constrained scheduling for quick changeover. In: *IEEE International Conference on Industrial Engineering and Engineering Management, IEEM 2009*, pp. 189–193 (2009)
4. Yash, D., Nagendra, S.: Single minute exchange of dies: literature review. *Int. J. Lean Thinking* **3**(2), 27–37 (2012)
5. Goubergen, D., Landeghem, H.: Rules for integrating fast changeover capabilities into new equipment design. *Robot. Comput. Integr. Manuf.* **18**, 205–214 (2002)
6. McIntosh, R.I., Culley, S.J., Mileham, A.R., Owen, G.W.: A critical evaluation of Shingo's 'SMED' (single minute exchange of die) methodology. *Int. J. Prod. Res.* **38**(11), 2377–2395 (2014)
7. Abraham, A., Ganapathi, K.N., Motwani, K.: Setup time reduction through SMED technique in a stamping production line. *SASTECH J.* **11**(2), 47–52 (2012)
8. Raikar, N.A.: Reduction in setup time by SMED methodology: a case study. *Int. J. Latest Trends Eng. Technol. (IJLTET)* **5**(4) (2015)
9. Ribeiro, D., Bragaa, F., Sousab, R., Carmo-Silvab, S.: An application of the SMED methodology in an electric power controls company. *Rom. Rev. Precis. Mech. Optic Mechatron.* **40**, 115–122 (2011)
10. Rahul, R.J., Naik, G.R.: Application of SMED methodology—a case study in small scale industry. *Int. J. Sci. Res. Publ.* **6**(8), 1–4 (2012)
11. Gilmore, M., Smith, D.J.: Set-up reduction in pharmaceutical manufacturing: an action research study. *Int. J. Oper. Prod. Manage.* **16**, 4 (1996)

Chapter 14

Study of Development of Various Morphological Phases and Its Effects on the Thermal Coated Specimen—A Review



Sonia Dangi, R. S. Walia, N. M. Suri, and Sumit Chaudhary

Abstract Thermal spray coating techniques have been widely used for improving the surface properties of the specimen like corrosion resistance, hardness, friction resistance, wear resistance, erosion resistance etc. All these properties not only depend on the type of coating material but also on the surface morphology. The work material during thermal spray came across critical operating conditions like high temperature, pressure. Moreover, the coating morphology also depends on the size, type and shape of the coating material. This showed a noticeable effect on the performance of the coated surface. The different characterization techniques are available to study the morphological properties of the coated samples. In this review, the effect of various parameters on the surface morphology of thermal spray coating has been studied.

Keywords Morphology · Thermal spray coating · Tribology · SEM · Porosity · Cracks

14.1 Introduction

Coating techniques for protecting the substrate material from atmosphere have been used from ancient times. The advanced coating methods not only protect the substrate but enhancing the performance of the substrate. The advanced coating techniques enable multiple effects like protection from corrosion and erosion, reduction in wear, achieve desired friction by inducing desired hardness, atmospheric inertness, depositing desired material over the substrate and reinforcing the substrate material etc. [1–5]. There are various coating methods like PVD, CVD, Sol–gel, Electroplating and Thermal Spray each having its advantages and drawback in the field of application [6]. Some of the coatings are easy to achieve and cost-effective but the purpose is to provide a layer of desired material for atmospheric protection or

S. Dangi (✉) · R. S. Walia · N. M. Suri
Production and Industrial Engineering Department, PEC, Chandigarh, India

S. Chaudhary
Mechanical Engineering Department, Thapar Institute of Engineering & Technology, Patiala, India

aesthetics. The material subjected to dynamic load, erosion, wear and friction has to be coated such that the coating should service the adverse working conditions [7–10].

Thermal spray coating emerged as one such coating techniques in which the coating material has been sprayed over the substrate material at high temperature (upto 15,000 °C), the flow of particles is assisted by high velocity gas/air. Classification of various thermal spray coating techniques is depending on heat source i.e. plasma spray coating, high velocity oxyfuel coating (HVOF), arc spray coating [11–15].

The most common thermal spray coating method is Plasma spray coating, in this method the temperature of the heat source is more than 15,000 °C. The molten accelerated particles of coating material move towards the substrate and strike the substrate with a governed speed. The continuous bombardment of the particles on the substrate resulted in the formation of a dense layer of coating [16–18]. The coating density in the case of HVOF and arc spray coating is less as compared to plasma spray coating. High heat in the case of plasma spray coating resulted in stress induced to the specimen. The thermal spray coating can be applied to a wide variety of substrate and coating material such as metals, ceramics, polymers, composites etc. The multilayer coating of the same or different compositions can also be achieved via thermal spray coating [19, 20].

The mechanical, thermal, tribological, electrical and chemical performance and properties of the coated specimen depend on the coating parameters, coating material and another important parameter is the coating morphology [21–23]. Most of the major properties and performance of the coating depends on the morphology. In this review article the impact of coating morphology on the various properties of the coated specimen has been discussed. The review focuses on the different thermal spray coating methods applied for coating the variety of substrate materials.

14.2 Mechanism of Coating Build-Up

The principle of material deposition is quite similar for all the coating methods. The heat source in the form of arc or flame has been used for depositing the desired coating material over the substrate surface. The temperature of the flame may go upto 15,000 °C and the high velocity of carrier gas assists the impact of coating material over the substrate [24, 25]. The flame generated moved towards the substrate material through the nozzle. The coating material is supplied to the heated flame and forced towards the substrate. The coating material having thermal energy due to heat transfer from the flame and kinetic energy due to the momentum transfer by the carrier gas strikes the substrate in solid, semi-solid or molten state and gets deposited over the surface of the substrate [26–29].

In the case of cold spray coating, the coating material doesn't melt so the coating is achieved by plastic deformation due to the impact velocity of heated material.

Whereas, in the case of thermal spray coating, the coating material gets melted and the molten material gets deposited due over the substrate surface [6, 30].

The substrate surface should be clean from physical and chemical impurities as the coating material and the substrate may have mechanical interlocking and metallurgical bonding. The first layer of material deposited on the substrate governs the thermo-physical properties of the coating. The multiple passes of the flame result in multilayer coating over the surface [31–33].

14.3 Morphological Development for Thermal Spray Coatings

The coating material has a very vital role and it affects the quality of the coated specimen largely. The mechanical and chemical properties of the coating material affect the coating but it has been observed morphology of coating material before coating plays a very important role the determining the properties of coated specimens. The morphological development of coating depends mainly on substrate material, coating material, gas dynamics and coating process. Figure 14.1 shows all the major parameters affecting the coating process. Moreover, the morphology of the

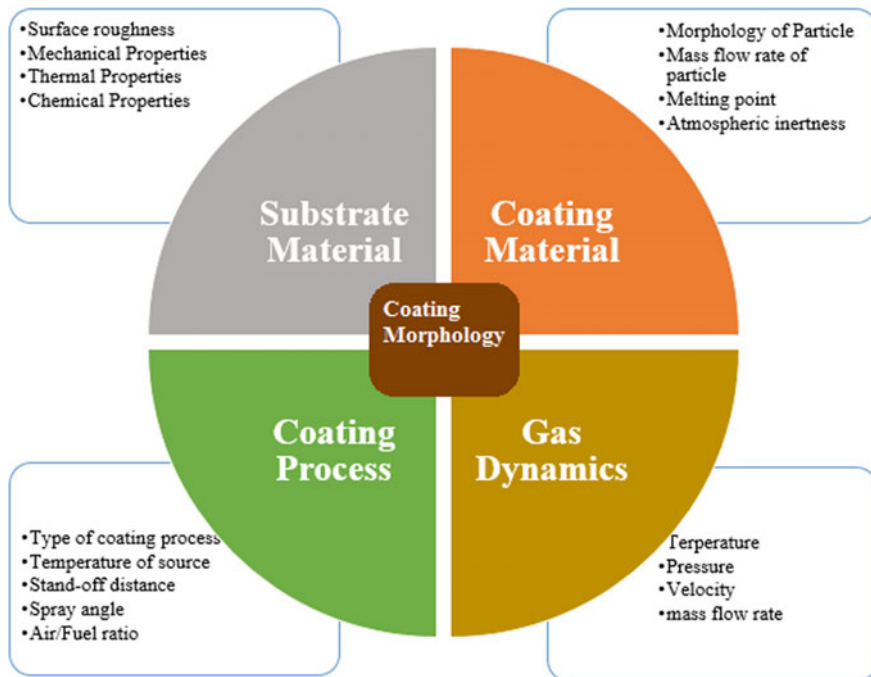


Fig. 14.1 Parameters affecting coating morphology

coating deposited on the specimen also affects the mechanical, chemical, thermal and tribological performance of the coated specimen.

14.3.1 Morphology of Coating Material

The morphology of coating material is one of the very crucial parameters which affects the performance of the coating. The coating material having the same particle size and chemical composition reported different mechanical, chemical, thermal, tribological, electrical behavior as there was some morphological difference observed among the coating materials used. The particles which are deposited by complete melting are least affected by their initial morphology [28]. Still, the effect of initial morphology for those particles has also been reported by the researches. There might be a possibility that the particles don't get melted completely and deposited by the mechanical action, in that case, the initial morphology of particles governs the morphology of coating and the performance of the coating. The particle morphology may provide the solidification front for the coating. The solid particles assist the grain growth and directional solidification of the molten material [34, 35].

The particle morphology may affect the direction of motion, the velocity of particles through the feed mechanism or spray gun. The particles having non-aerodynamic morphology may create an obstacle in the movement, the actual mass flow rate in this case decrease and cause clogging of the spray gun. The particles having spherical morphology move smoothly without many obstacles whereas the annular particles experience large drag created by the carrier gas. The hard coating material having annular morphology causes the wearing of spray gun as the sharp edges present on the annular morphology to strike the spray gun and plough the material of gun due to the high drag force created by the carrier gas. This affects the accuracy of the process which is minimum in the case of spherical morphology [36–38].

The annular morphology coating material has a larger surface area as compared to spherical morphology. These materials show a higher heat transfer rate i.e. it gets heated in cold quickly. The peak temperature obtained in case of annular morphology may be higher than the spherical morphology but these particles lose heat very swiftly, as a result, the solidification rate is very high which results in smaller grains [28]. The bigger size coating materials can't melt completely, the grain growth in such cases has been governed by the initial morphology of the particles. The annular morphology assists the heat transfer rate as the morphology of coating material becomes spherical the heat transfer rate decreased. The slower heat transfer rate may be responsible for the bigger grain size but the presence of voids on the coated samples resulted in decreased elastic modulus and toughness [39–41].

The density of coating also depends on the plastic deformation of the under-melted coating material. The coating material having higher plastic deformation, the coating produced might be more closely packed and the voids eliminated. This results in a very dense coating. The substrate initial temperature also governs the morphology of the coating. If the substrate initial temperature is less than 200 °C,

the bonding of coating on the substrate would not be strong due to the poor wetting of the substrate surface and the morphology produced would be irregular [42, 43]. The partial melting of coating material may result in decreased efficiency as there is a possibility of rebounding of particles from the substrate surface (Fig. 14.2).

14.3.2 Morphology of Coated Material

The thermal spray coating over the substrate surface is generally obtained by either spherical, elliptical, or any other annular splats combing together to create a lamellar microstructure. The molten or semi-molten droplets of coating material strike the substrate with high velocity. The molten droplets may be micro or nano in size which strikes the substrate and the cohesion between the substrate and coating material assists the formation of a stable layer of coating over the surface. The morphology of coated material primarily has deposited material, voids, porosity, semi-melted material. Each having a different effect on the performance and properties of the coating. The lamellar microstructure is governed by the process parameters such as morphology and size of coating material, the velocity of particles, flame temperature, angle on impingement etc. The molten coating material has a huge affinity for agglomeration, such agglomeration result in the enhanced size of the coating material over the surface. The morphological characteristics observed in the thermal spray coated specimen shown in Figs. 14.3 and 14.4 are voids, porosity, delamination, spalling, interface contamination, cracks, unmelted particles, pull-outs, oxidation, metal inclusion [26, 44–48].

14.3.2.1 Porosity

The porosity in thermal spray coating may go upto 8–10% depending upon the type of process, solidification rate, initial morphology of particles. Porosity in the case of plasma spray coated was observed more than HVOF thermal spray coating. In the case of plasma spray coating, there might be a lesser impact of coating material on the substrate or splashing of the molten material from the surface due to a high melting point, which resulted in higher porosity [49].

As the deposition in case of thermal spray coating is lamellar i.e. the deposition is such that one layer gets deposited over the other. Due to the impact of accelerated coating material, the previous layer of deposition gets flattened over the surface and the porosity present in the previously coated layer disappears, hence the density of coating increases. The deposition of more and more layers over the surface enhances the density of the coating [50–54]. There have been some crakes and porosity observed on the interface of the respective layers that is generally termed as voids. These voids affect the mechanical, chemical, thermal, and electrical properties of the coated material. The globular voids present at the parting line may be carried to the upper surface of the coating and form open pores. These voids act as

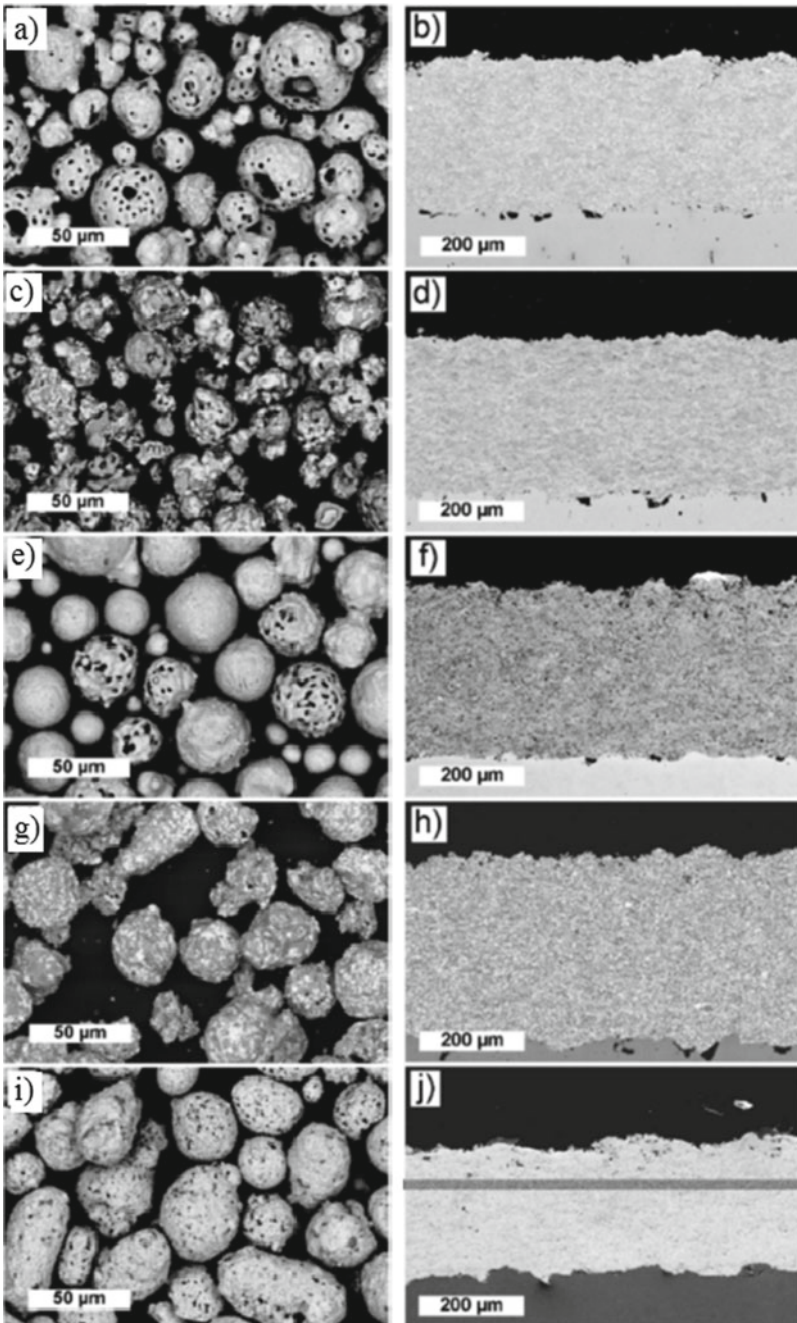


Fig. 14.2 SEM micrographs of the various coating material (left) and obtained thermal sprayed coatings (right): Cr_3C_2 -50NiCrMoNb (a, b), Cr_3C_2 -25NiCr (c, d), Cr_3C_2 -25NiCr (e, f), Cr_3C_2 -37WC-18NiCoCr (g, h) and WC-10Co4Cr (i, j) [66]

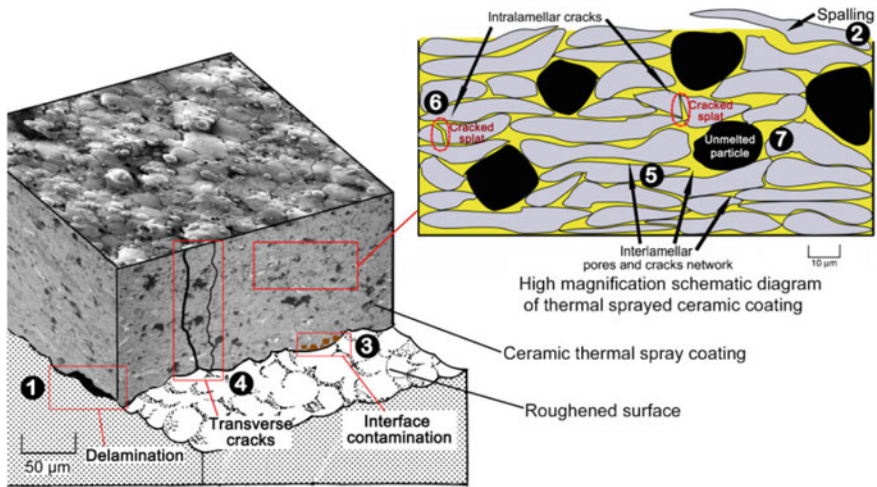


Fig. 14.3 Typical ceramic coating microstructure (1) delamination (2) spalling (3) interface contamination (4) transverse crack (5) inter-lamellar pores (6) inter-lamellar cracks (7) unmelted particles [44]

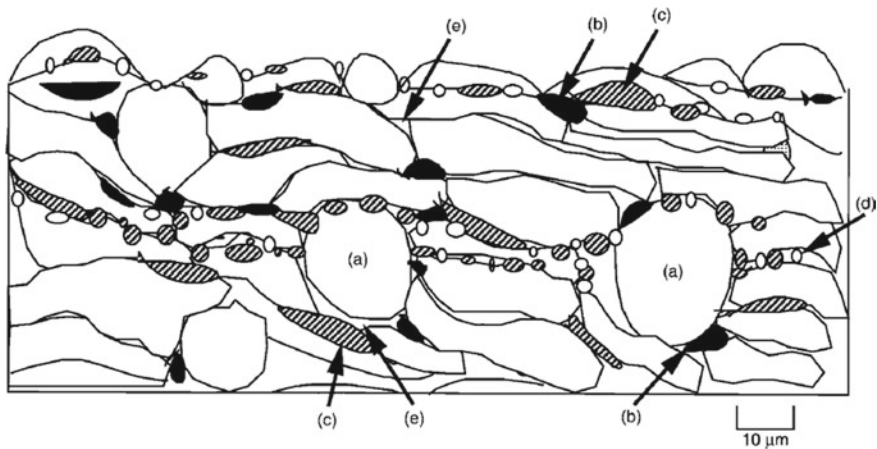


Fig. 14.4 Schematic illustration of metallic coating microstructure (a) unmelted particles (b) oxides (c) debris (d) fine particles (e) porosity [26]

launchpad oxidation of the material. The vapours from the chemical reaction formed and produce porosity in the coating. the dirt and inclusion of foreign material is also responsible for voids generation. The inter-lamellar pores due to rapid solidification resulting in micro-cavities. These pores may act as a crack propagation site and the rate of reaction at these sites increases drastically when working under elevated

temperature and pressure. The pores provide a site for air hence decrease the thermal and electrical conductivity of the coating [55–57].

14.3.2.2 Cracks

The cracks can be commonly observed in the thermal spray coating. The cracks may be present on the interface of substrate and coating are known as delamination. Such types of cracks are produced due to less impact of coating material striking on the substrate so the cohesive forces become weak and result in delamination. The transverse cracks may also be observed in the coating which is perpendicular to the substrate surface. The coating obtained is in the form of lamellar i.e. deposition of one layer of coating over the other. There might be a possibility of cracking at the inter-lamellar site. Such cracks are very critical as they reduce the fatigue life of the coating [58, 59]. These cracks get widen heat treated as observed by Lui et al. shown in Fig. 14.5 [60].

The cracks reduce the fatigue life of the coating and the coated specimen. These cracks widen and propagate to the surface resulting in sudden failure of the coating. These cracks may also act as the site for the accumulation of internal stresses in

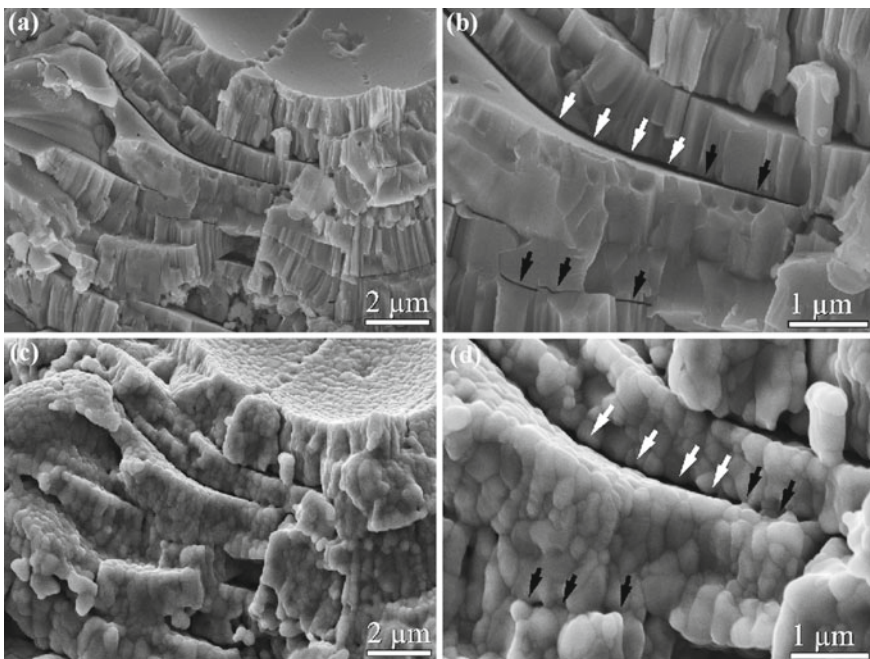


Fig. 14.5 Morphological investigation of LZO thermal spray coating **a, b** as sprayed **c, d** thermal exposer at 1300 °C for 2 h [43]

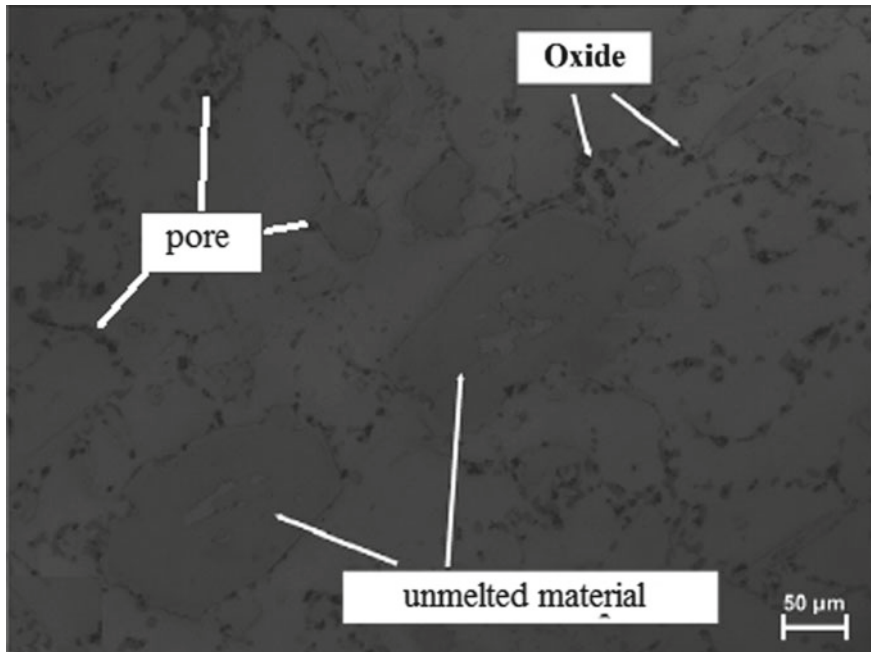


Fig. 14.6 Microstructure of coated Babbitt alloy [65]

the coating. The voids formed due to cracking may be responsible for accelerated oxidation of the specimen [61].

14.3.2.3 Unmelted Coating Material

The high melting point material or large size coating material doesn't melt completely and gets deposited on the substrate surface. Another reason may be the refractoriness of the material which reduces the heat transfer from the source to the material or the low-temperature heat source [62–64]. These unmelted particles cause stress concentration in the coating. The localized oxidation had also been observed at the site of unmelted particles shown in Fig. 14.6. The unmelted particles strike the lamellar with a high impact compared to the fully molten material. This results in increased microhardness and density of the coating [65].

14.3.2.4 Oxidation

The atmospheric contamination observed mainly in a metallic coating known as oxidation. The oxidation of substrate or coating may occur at different stages of thermal spray coating. The uncleaned substrate may prove to a carrier for the initial

oxidation at the interface of the substrate and coating. The coating material came across an elevated temperature which increases the rate of oxidation. The coating material sprayed over the substrate may react with the carrier gas and cause oxidation. The lamellar sites proved to be one of the very common locations for oxidation [67–69]. The oxidation of particles continues thereafter at the sites such as pores or cracks, where the atmospheric gasses could react with the substrate material. The mechanical, chemical, electrical, thermal properties etc. had been hugely affected by oxidation [70, 71].

14.4 Conclusions

The thermal spray coating has very wide applications right from mechanical components to aerospace applications, automobile, medical equipments, electronics and electrical etc. The effectiveness of coating not only depend on the substrate or coating material alone, but also on the microfeatures like morphological characteristics of coating material and coating obtained.

The morphology of coating material affects its followability through the nozzle, heat transfer rate, melting of the particle, impact velocity, mass flow rate etc. All these have some impact on some splat formation and other properties of the coating. The splat formation and shape have a major impact on the solidification and lamellar formation.

The coating gets deposited over the surface in the form of multi-layer lamellar and the density of coating enhances when the depositing layer strikes the previously deposited lamellar. There are some characteristics like voids, porosity, delamination, spalling, interface contamination, cracks, unmelted particles, pull-outs, oxidation, metal inclusion observed in the thermal spray coating, each having an impact on the various properties of the thermal spray coating.

References

1. Martins, R., Amaro, R., Seabra, J.: Influence of low friction coatings on the scuffing load capacity and efficiency of gears. *Tribol. Int.* **41**, 234–243 (2008)
2. Kamps, T.J., Walker, J.C., Wood, R.J., Lee, P.M., Plint, A.G.: Reproducing automotive engine scuffing using a lubricated reciprocating contact. *Wear* **332–333**, 1193–1199 (2015)
3. Goyal, T., Walia, R.S., Sidhu, T.S.: Surface roughness optimization of cold sprayed coatings using Taguchi method. *Int. J. Adv. Manuf. Technol.* **60**, 611–623 (2012)
4. Priest, M., Dowson, D., Taylor, C.: Predictive wear modelling of lubricated piston rings in a diesel engine. *Wear* **231**, 89–101 (1999)
5. Mierbach, A., Hildyard, M., Parker, D., Xu, H.: Piston ring performance modelling. In: T&N Technical Symposium Paper (1995)
6. Tyagi, A., Walia, R.S., Murtaza, Q., Pandey, S.M., Tyagi, P.K., Bajaj, B.: A critical review of diamond like carbon coating for wear resistance application. *Int. J. Refract. Metals Hard Mater.* **78**, 107–122 (2018)

7. Miguel, J.M., Vizcaino, S., Lorenzana, C., Cinca, N., Guilemany, J.M.: Tribological behavior of bronze composite coatings obtained by plasma thermal spraying. *Tribol. Lett.* **42**, 263–273 (2011)
8. Torres, B., Garrido, M.A., Rico, A., Rodrigo, P., Campo, M., Rams, J.: Wear behaviour of thermal spray Al/SiCp coatings. *Wear* **268**, 828–836 (2010)
9. Spencer, K., Fabijanic, D.M., Zhang, M.X.: The use of Al-Al₂O₃ cold spray coatings to improve the surface properties of magnesium alloys. *Surf. Coat. Technol.* **204**, 336–344 (2009)
10. Wilden, J., Schnick, T., Wank, A., Materials, C.: Performance of HVOF nanostructured diboride composite coatings. In: *Proc. Int. Therm. Spray Conf. Essen, Ger.*, pp. 1033–1037 (2002)
11. Tyagi, A., Walia, R.S., Murtaza, Q.: Tribological behavior of temperature dependent environmental friendly thermal CVD diamond coating. *Diamond Related Mater.* **96**, 148–159 (2019)
12. Vignesh, S., Shanmugam, K., Balasubramanian, V., Sridhar, K.: Identifying the optimal HVOF spray parameters to attain minimum porosity and maximum hardness in iron based amorphous metallic coatings. *Def. Technol.* **13**, 101–110 (2017)
13. Pandey, S.M., Walia, R.S., Murtaza, Q.: Effect of NiCr on dry sliding wear of high carbon iron-molybdenum composite plasma spray coating. *Int. J. Precis. Technol.* **8** (2018)
14. Pandey, S.M., Murtaza, Q., Walia, R.S.: Study of dry wear behavior and morphological characteristic of 60%Mo-20%NiCr-10%Mo+Fe based alloy coating by atmospheric plasma spray technique. *Adv. Mater. Process. Technol.* **3**, 393–406 (2017)
15. Tyagi, A., Pandey, S.M., Walia, R.S., Murtaza, Q.: Characterization and parametric optimization of tribological properties of Mo blend composite coating. *Mater. Res. Express* **6** (2019)
16. Jiang, C., Xing, Y., Zhang, F., Hao, J.: Microstructure and corrosion resistance of Fe/Mo composite amorphous coatings prepared by air plasma spraying. *Int. J. Min. Met. Mater.* **19**, 657–662 (2012)
17. Kobayashi, K., Yano, S., Inoue, A.: Fe-based metallic glass coating produced by smart plasma spraying process. *Mater. Sci. Eng. B* **148**, 110–113 (2008)
18. Kishitake, K., Era, H., Otsubo, F.: Characterization of plasma sprayed Fe-17Cr-38Mo-4C amorphous coatings crystallizing at extremely high temperature. *J. Therm. Spray Technol.* **5**, 283–288 (1996)
19. Tyagi, A., Walia, R.S., Murtaza, Q.: Tribological behavior of HVOF carbon coating for wear resistance application. *Mater. Res. Express* **6**, 67–77 (2019)
20. Muthu, S.M., Arivarasu, M.: Investigations of hot corrosion resistance of HVOF coated Fe based superalloy A-286 in simulated gas turbine environment. *Eng. Fail. Anal.* **107**, 104224 (2020)
21. Wu, J., Zhang, S., Sun, W., Gao, Y., Wang, J.: Enhanced corrosion resistance in Fe based amorphous coatings through eliminating Cr-depleted zones. *Corros. Sci.* **136**, 161–173 (2018)
22. Zhang, C., Chan, K., Wu, Y., Liu, L.: Pitting initiation in Fe-based amorphous coatings. *Acta Mater.* **60**, 4152–4159 (2012)
23. Berman, D., Narayanan, B., Cherukara, M.J., Sankaranarayanan, S.K.R.S., Erdemir, A., Zinovev, A., Sumant, A.V.: Operando tribochemical formation of onion-like-carbon leads to macroscale superlubricity. *Nat. Commun.* **9**, 1164 (2018)
24. Cheng, D., Xu, Q., Lavernia, E.J., et al.: The effect of particle size and morphology on the in-flight behavior of particles during high-velocity oxyfuel thermal spraying. *Metall. Mater. Trans. B* **32**, 525–535 (2001)
25. de Villiers Lovelock, H.L.: Powder/processing/structure relationships in WC-Co thermal spray coatings: a review of the published literature. *J. Therm. Spray Technol.* **7**, 357–373 (1998)
26. Tucker, R.C.: *ASME Handbook: Thermal Spray Technology*, vol. 5A (2013)
27. Technology, T.S., Tucker, R.C.: *Introduction to Coating Design and Processing*, vol. 5 (2013)
28. Nouri, A., Sola, A.: Powder morphology in thermal spraying. *J. Adv. Manuf. Process.* **e10020**, 1–19 (2019)
29. Nayak, H., Krishnamurthy, N., Shailesh, R.A.: Studies on plasma sprayed thermal barrier coating with increase in coating thickness. *Tribol. Ind.* **40**(3), 420–432 (2018)

30. Siao, A., Ang, M., Berndt, C.C., Siao, A., Ang, M., Berndt, C.C.: A review of testing methods for thermal spray coatings: a review of testing methods for thermal spray coatings **6608** (2014)
31. Pawlowski, L.: *The Science and Engineering of Thermal Spray Coating*. Wiley, Hoboken (2008)
32. Fauchais, P.L., Heberlein, J.V.R., Boulous, M.I.: *Thermal Spray Fundamentals from Powder to Part*. Springer, Berlin (2014)
33. Davis, J.R.: *ASME Handbook of Thermal Spray Technology* (2004)
34. Ben Ettouil, F., Mazhorova, O., Pateyron, B., Ageorges, H., El Ganaoui, M., Fauchais, P.: Predicting dynamic and thermal histories of agglomerated particles injected within a d.c. plasma jet. *Surf. Coat. Technol.* **202**, 4491–4495 (2008)
35. Bouneder, M., Ageorges, H., El Ganaoui, M., Pateyron, B., Fauchais, P.: Direct current plasma spraying of mechanofused alumina-steel particles, October 2009
36. Ghadami, F., Aghdam, A.S.R.: Improvement of high velocity oxy-fuel spray coatings by thermal post-treatments: a critical review. *Thin Solid Films* **678**(February), 42–52 (2019)
37. Schneider, K.E., Belashchenko, V., Dratwinski, M., Siegmann, S.: *Thermal Spraying for Power Generation Components*. Wiley, Hoboken (2007)
38. Rokni, M.R., Nutt, S.R., Widner, C.A., Campagne, V.K., Harbe, R.H.: Review of relationship between particle deformation, coating review of relationship between particle deformation, coating microstructure, and properties in high-pressure cold spray. *J. Therm. Spray Technol.* (2017)
39. Rad, D.T.M.R., Hussain, A.M.T.: *Beyond Traditional Coatings: A Review on Thermal-Sprayed Functional and Smart Coatings*, vol. 28, no. 4. Springer, US (2019)
40. Mikli, V., Kafrdi, H., Kulu, P., Besterct, M.: Characterization of powder particle. *Proc. Estonian Acad. Sci Eng.* **7**, 22–34 (2001)
41. Gu, S., Kammis, S.: Bonding mechanism from the impact of thermally sprayed solid particles. *Metall. Mater. Trans.* **40**, 2664–2674 (2009)
42. Picas, J.A., Punset, M., Baile, M.T., Martin, E., Fom, A.: Effect of oxygen/fuel ratio on the in-flight particle parameters and properties of HVOF WC-CoCr coating. *Surf. Coat. Technol.* **205**, S364–S368 (2011)
43. Chi, W., Sampath, S., Wang, H.: Ambient and high-temperature thermal conductivity of thermal spray coatings. *JTTEE* **5**, 773–778 (2006)
44. Siao, A., Ang, M., Berndt, C.C., Siao, A., Ang, M., Berndt, C.C.: A review of testing methods for thermal spray coatings. *Int. Mater. Rev.* **59**, 179–223 (2014)
45. Sun, S.D., et al.: Microstructure, abrasive wear and corrosion characterisation of laser metal deposited Fe-30Cr-6Mo-10Ni-2C alloy. *Wear* **438–439**, 203070 (2019)
46. Zhang, J., Guo, X., Jung, Y., Li, L., Knapp, J.: Microstructural non-uniformity and mechanical property of air plasma-sprayed dense lanthanum zirconate thermal barrier coating **1**, 11–16 (2014)
47. Si, C, Duan, B., Zhang, Q., Cai, J., Wu, W.: Wear-resistance properties of subsonic flame sprayed amorphous Fe–Mo–Cr–Co coating with extremely high amorphous rate. *Integr. Med. Res.* 1–12 (2020)
48. Xiao, J., Liu, Q., Li, J., Guo, H., Xu, H.: Microstructure and high-temperature oxidation behavior of plasma-sprayed Si/Yb₂ SiO₅ environmental barrier coatings. *Chin. J. Aeronaut.* **32**(8), 1994–1999 (2019)
49. Coatings, P.: Porosity and its significance in plasma-sprayed coatings. *Coatings* **9**, 1–19 (2019)
50. Thirumalaikumarasamy, D., Shanmugam, K., Balasubramanian, V.: Establishing empirical relationships to predict porosity level and corrosion rate of atmospheric plasma-sprayed alumina coatings on AZ31B magnesium alloy. *J. Magnes. Alloys* **2**, 140–153 (2014)
51. Mancini, C.E., Berndt, C.C., Sun, L., Kucuk, A.: Porosity determinations in thermally sprayed hydroxyapatite coatings. *J. Mater. Sci.* **36**, 3891–3896 (2001)
52. Konyashin, I.Y., Chukalovskaya, T.V.: A technique for measurement of porosity in protective coatings. *Surf. Coat. Technol.* **88**, 5–11 (1997)
53. Curran, J.A., Clyne, T.W.: Porosity in plasma electrolytic oxide coatings. *Acta Mater.* **54**, 1985–1993 (2006)

54. Mutter, M., Mauer, G., Mücke, R., Guillon, O., Vaßen, R.: Correlation of splat morphologies with porosity and residual stress in plasma-sprayed YSZ coatings. *Surf. Coat. Technol.* **318**, 157–169 (2016)
55. Ekberg, J., Ganvir, A., Klement, U., Creci, S., Nordstierna, L.: The influence of heat treatments on the porosity of suspension plasma-sprayed yttria-stabilized zirconia coatings. *J. Therm. Spray Technol.* **27**, 391–401 (2018)
56. Son, S.-H., Lee, H.-J., Park, Y.-J., Kim, J.-H.: Preparation of conducting polymer composites: effects of porosity on electrical conductivity. *Polym. Int.* **46**, 308–312 (1998)
57. Khal, H.E., Cordier, A., Batis, N., Siebert, E., Georges, S., Steil, M.C.: Effect of porosity on the electrical conductivity of LAMOX materials. *Solid State Ionics* **304**, 75–84 (2017)
58. Al-Fadhli, H.Y., Stokes, J., Hashmi, M.S.J., Yilbas, B.S.: HVOF coating of welded surfaces: fatigue and corrosion behaviour of stainless steel coated with inconel-625 alloy. *Surf. Coat. Technol.* **200**, 4904–4908 (2006)
59. Padilla, A., Velasquez, J.A., Berrios, E.S., Cabrera, P.: Fatigue behavior of a 4140 steel coated with a NiMoAl deposit applied by HVOF thermal spray. *Surf. Coat. Technol.* **150**, 151–162 (2002)
60. Liu, T., Luo, X., Chen, X., Yang, G., Li, C., Li, C.: Morphology and size evolution of interlamellar two-dimensional pores in plasma-sprayed $\text{La}_2\text{Zr}_2\text{O}_7$ coatings during thermal exposure at 1300 °C. *J. Therm. Spray Technol. Ref 12* (2015)
61. Voorwald, H.J.C., Souza, R.C., Pigatin, W.L., Cioffi, M.O.H.: Evaluation of WC-17Co and WC-10Co-4Cr thermal spray coatings by HVOF on the fatigue and corrosion strength of AISI 4340 steel. *Surf. Coat. Technol.* **190**, 155–164 (2005)
62. Zhang, C., Guo, R.Q., Yang, Y., Wu, Y., Liu, L.: Influence of the size of spraying powders on the microstructure and corrosion resistance of Fe-based amorphous coating. *Electrochim. Acta* **56**, 6380–6388 (2011)
63. He, J., Ice, M., Dallek, S., Lavernia, E.J.: Synthesis of nanostructured WC-12 pct Co coating using mechanical milling and high velocity oxygen fuel thermal spraying. *Metall. Mater. Trans. A* **31A**, 541–553 (2000)
64. Wu, Y., Lin, P., Chu, C., Wang, Z., Cao, M., Hu, J.: Cavitation erosion characteristics of a Fe–Cr–Si–B–Mn coating fabricated by high velocity oxy-fuel (HVOF) thermal spray. *J. Mater. Lett.* **61**, 1867–1872 (2007)
65. Roberto, P., Alcover, C., Geraldo, A., Pukasiewicz, M.: Tribology international evaluation of microstructure, mechanical and tribological properties of a Babbitt alloy deposited by arc and flame spray processes. *Tribiol. Int.* **131**, 148–157 (2019)
66. Matikainen, V., Koivuluoto, H., Vuoristo, P.: A study of Cr_3C_2 -based HVOF- and HVAF-sprayed coatings: abrasion, dry particle erosion and cavitation erosion resistance. *Wear* **446–447**(January), 203188 (2020)
67. Kiilakoski, J., Langlade, C., Koivuluoto, H., Vuoristo, P.: Surface & coatings technology characterizing the micro-impact fatigue behavior of APS and HVOF-sprayed ceramic coatings. *Surf. Coat. Technol.* **371**(October 2018), 245–254 (2019)
68. Thirumalaikumarasamy, D., Shanmugam, K., Balasubramanian, V.: Corrosion performance of atmospheric plasma sprayed alumina coatings on AZ31B magnesium alloy under immersion environment. *J. Asian Ceram. Soc.* **2**, 403–415 (2014)
69. Khan, Z.S., et al.: Thermal cycling behavior and hot corrosion performance of the plasma sprayed $\text{Er}_2\text{Si}_2\text{O}_7$ coatings deposited on Cf/SiC composites. *J. Asian Ceram. Soc.* **3**(1), 123–129 (2015)
70. Wang, Y., Zhou, C.: Hot corrosion behavior of nanostructured Gd_2O_3 doped YSZ thermal barrier coating in presence of $\text{Na}_2\text{SO}_4 + \text{V}_2\text{O}_5$ molten salts. *Prog. Nat. Sci. Mater. Int.* **27**(4), 507–513 (2017)
71. Zro, M.C.Y.O., Singh, J., Kumar, S., Mohapatra, S.K.: An erosion and corrosion study on thermally sprayed WC-Co-Cr powder. *Wear* **438–439**(January), 102751 (2019)

Chapter 15

Parametric Study on Stainless Steel 316L by Die Sinking EDM for Biomedical Application



Preeti Chauhan, M. A. Saloda, B. P. Nandwana, and S. Jindal

Abstract The electric discharge machine has been acknowledged as a better technique for modification of the surface for biomedical implants. It has many advantages over previously used techniques. Machining by EDM holds many advantages like an increase in wear resistance due to microstructural changes, deposition of oxide and carbide layer over workpiece which enhances the corrosion resistance of material and porosity of material also increases which encourages ingrowth of tissue and transportation of body fluid into it. Increases in surface roughness of elements increase the surface area available for interaction with the bone so higher surface roughness (SR) of biomaterial shows better bone fixation with it than smoother surfaces. In growth of tissues is revealed with higher SR. The parametric study was performed, aiming at increasing the SR of SS 316L for biomedical use and graphite as an electrode was used. Effect of variation in Current (I_d), pulse on time (T_p) and servo voltage (V_d) on SR were studied. Taguchi method was used to evaluate maximum SR. ANOVA was used to identify the most significant factor.

Keywords EDM · Biomedical · Graphite · SS 316L · SR · Taguchi

15.1 Introduction

EDM is used in manufacturing, automotive and aerospace industries for production of complex geometries and finishing of parts [1]. Even nowadays some nonconductive material can also be machined for example zirconia and alumina but it requires coating of conductive material over it to initiate sparking. Once the spark is initiated hydrocarbon oil degenerates into hydrogen and carbon which helps in further sparking and material gets removed. Material from workpiece is removed using thermal energy by erosive effect. It is different from other traditional machining techniques as it does not have physical contact between tool and workpiece which eradicates many problem like chatter, vibration, mechanical stresses which reduces

P. Chauhan (✉) · M. A. Saloda · B. P. Nandwana · S. Jindal
Department of Mechanical Engineering, College of Technology and Engineering, Udaipur,
Rajasthan, India

chances of tool failure [2] and even delicate parts can be easily machined like washing machine agitators. It has wide application in production of mould, dies [3, 4], medical equipment, optical instruments, thin-walled separators in nuclear industry [5] and sports equipment etc. EDM is replacing other traditional machining methods like drilling, grinding, polishing and milling etc. [6]. Figure 15.1 shows important output and input parameters of EDM. Figure 15.2 explains classification of spark erosion machining.

In EDM as shown in Fig. 15.3 replica of tool is formed on workpiece. Material from workpiece is removed using thermal energy produced by sparking between workpiece and tool filled with dielectric fluid between them. EDM is mostly used method for the production of close tolerance shapes, 3D complex shapes. Thermal energy causes the vaporization of material from workpiece and material is removed.

Advantages of EDM machining are:

- Complicated shapes can easily be made by EDM machining.
- Elements with close tolerances can be manufacture by EDM
- Material with any hardness and toughness can be easily machined by EDM.
- As there is no contact between workpiece and tool so material can be machined without any distortion.
- EDM machining is more suitable for delicate material which cannot take stress of traditional machining methods.
- Mirror surface finish can also be obtained by EDM machining by introducing powder additives in dielectric fluid.

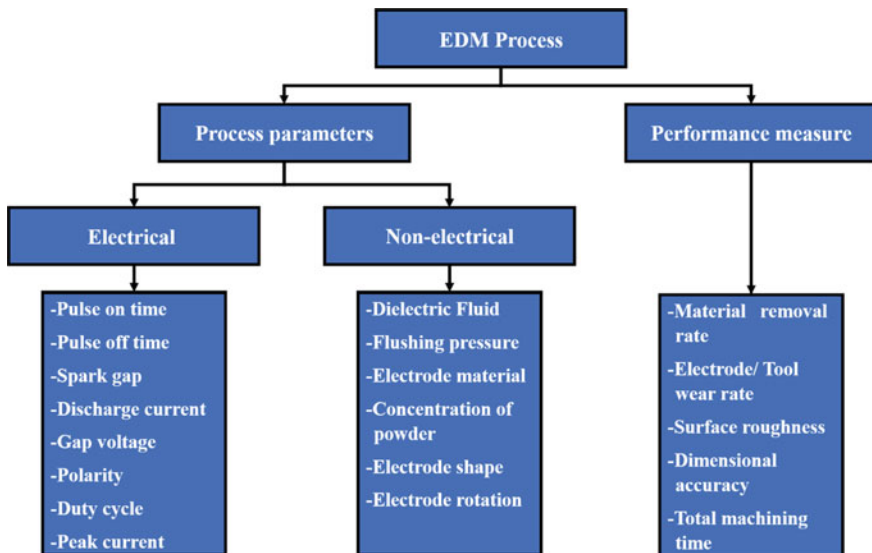


Fig. 15.1 Important output and input parameters for the EDM process [7]

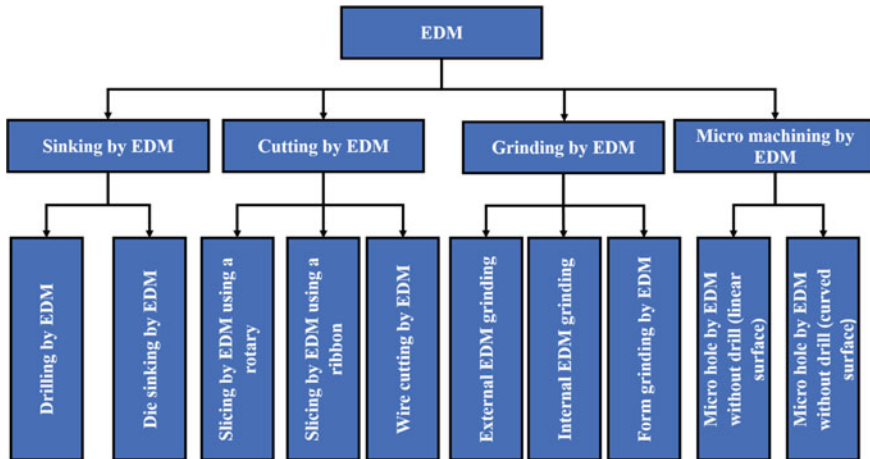


Fig. 15.2 Classification of spark erosion machining [8]

- Due to chip formation in traditional machining methods burs are left on workpiece where as in EDM machining no burs are left on workpiece.

Generally, tool and workpiece are connected with positive and negative polarity respectively where the tool behaves as cathode and workpiece as an anode. Dielectric fluid is an electrically neutral liquid that has some dielectric constant. As the dielectric fluid has some breakdown voltage therefore potential applied between tool and workpiece should be greater than its breakdown voltage otherwise the current will not flow between tool and workpiece. There is RC relaxation circuit in which capacitance gets charged due to the supply of DC power voltage and after that, it gets discharged. When the capacitor discharges its charge between tool and workpiece with minimum resistance. The spark occurs between tool and workpiece which has minimum resistance. There is a minimum resistance between the inter-electrode as there is less gap between these electrodes.

A very large amount of potential is supplied between tool and workpiece when the capacitor gets discharged after charging. An electric field is generated due to electrostatic force which directs electrons from tool towards the workpiece. The electron will move towards workpiece in dielectric fluid when the bond energy of electron is less. Then electron travels with very high velocity and this velocity depends on the potential which is supplied through the capacitor. The electron will move towards the workpiece and collide with the molecules. This collision between electron and molecules generates more positive ions and electrons due to which high concentration of these ions between tool and workpiece within the minimum electrode gap takes place. The positive ion moves in direction of the tool while electrons move towards the workpiece which results in the sparking known as “Plasma Channel”.



Fig. 15.3 ZNC 250 electric discharge machine

The electron collides with the workpiece at a very high velocity. The kinetic energy of these electrons converts into thermal energy which removes the material from the workpiece. This material is removed due to vaporization and melting. The collision of positively charged ions is also responsible for material removal but as their concentration is very less so they result in very less material removal. The plasma channel collapses when the supply of potential between tool and workpiece is stopped. The pressure is generated which removes molten material from the workpiece.

From last few years, to increase MRR, tool is given ultrasonic assisted vibration and tool vibrates, it increases flushing away of debris from workpiece which increases MRR and SR remains unaffected. Rotation of tool also increases the MRR. Some appropriate powder additives in dielectric fluid are being used to improve SR and decreases tool wear. Water as dielectric fluid is being used over other hydrocarbon dielectric fluid for safe environment as decomposition of hydrocarbon oil releases carbon monoxide and methane which is harmful for environment.

15.2 Research Background

Modification of surface for biomaterials is very important for improved surface morphology. There are various techniques available for surface modification like CVD, anodising, PVD and nitriding etc. but due to weak adhesion, bond cannot sustain under repeated loading conditions in corrosive environment and these techniques have become inefficient. Before these techniques coating is required i.e., grit blasting and shot peening which results in increase of production cost [9]. EDM has been recognized for Surface modification of biomaterials in recent years [10]. Elements machined by EDM shows good biocompatibility. Human osteoblast cell reveals better cell proliferation when machined by EDM. EDM machined surface requires no surface preparation as required by other techniques. Corrosion resistance and hardness is improved when machined by EDM which is desirable for biomedical implants. EDM machined samples are preferable substances for MG-63 cells of human osteoblast as per adhesion and growth is concerned [9, 11, 12].

Texture and nature of implant surface defines the behaviour of cells and tissue [13]. More is the surface roughness of elements more is the surface area available for interaction with the bone. Higher surface roughness of biomaterial shows better bone fixation with it and in growth of tissues is revealed with higher surface roughness [13–16]. Main aim of increasing surface roughness is to improve cellular activity. Higher surface roughness obtained by EDM results in deposition of oxide and carbide layers on material which enhances adhesion and ingrowth of bone derived cells [17]. EDM machined surfaces shows improved wear resistance [18, 19]. Porosity of EDM machined surface is increased [20] which enhances the growth of mineralized tissue into pore space which allows body fluid to be transported through interconnected pores [21]. Deposition of oxide and carbide layer after EDM machining results in increase of corrosion resistance and biocompatibility [9]. Table 15.1 explains different types of biomaterials.

SS 316L is mostly used biomaterial as shown in Fig. 15.4 due to low cost, excellent fabrication properties, high fatigue resistance, easy availability, good corrosion resistance, high fracture toughness and good biocompatibility [22–24]. In stainless steel 316L, L stands for low carbon percentage i.e., 0.03%. Table 15.2 shows SS 316L's chemical composition. Graphite was used as tool for machining as shown in Fig. 15.5. Graphite produces more carbide phases on EDM machined surfaces which

Table 15.1 Characteristics of metallic biomaterials (grades ranged from 5 excellent score, to 1, poor score) [27]

Characteristics	Stainless steel	Co-based alloys	Ti-based alloys
Machinability			
Conventional	5	1	1
Advanced	5	3	3
Corrosion resistance	2	3	4
Biocompatibility	1	2	3
Wear resistance	2	2	1
Bioactivity	1	1	1



Fig. 15.4 Machined workpiece

Table 15.2 Chemical composition of stainless steel 316L [28]

Elements		C	Mg	Si	P	S	Cr	Mo	Ni	N
Composition %	Min	–	–	–	–	–	16.0	2.0	10.0	–
	Max	0.03	2.0	0.75	0.045	0.03	18.0	3.0	14.0	0.10



Fig. 15.5 Graphite electrode

increases the corrosion resistance of workpiece. Graphite as electrode gives higher surface roughness [25, 26].

Graphite is non-metal which is commonly used in industries as electrode for EDM machining. Graphite has high melting point which makes it more stable than other electrode material. It is comparatively cheaper than other electrodes. It has low density and can be easily machined into desired shape of electrodes. Graphite produces more carbide phases on EDM machined surfaces which increases corrosion resistance of workpiece.

15.3 Research Methods

Whole work was carried out on ZNC-250 Electric Discharge Machine. Schematic diagram of experimental setup is shown in Fig. 15.6. ZNC 250 die sinking EDM was used which has 3 axis x, y and z. Range of x, y and z axis is 250 mm, 250 mm and 200 mm respectively. It has maximum capacity of operating platform of 200 mm. It has maximum processing speed of $200\text{mm}^3/\text{min}$. It consumes maximum power of 6 kW. The machine can hold workpiece of maximum of 200 kg and tool of 25 kg.

SR is a measure of texture of workpiece measured after machining was done. SR is measured by Mitutoyo SURFTTEST SJ-210 as shown in Fig. 15.7. SS 316L was used with dimension $32 \times 32 \times 150$ mm as work piece material. Graphite electrode with dimension $20 \times 20 \times 100$ mm was used as tool.

Surface roughness is measured by contact between Mitutoyo SURFTTEST SJ-210 and workpiece. Technique used here for measuring surface roughness is post process technique and measured by stylus profilometer which has diamond stylus tip. It is moved over machined workpiece and surface roughness is measured. This instrument

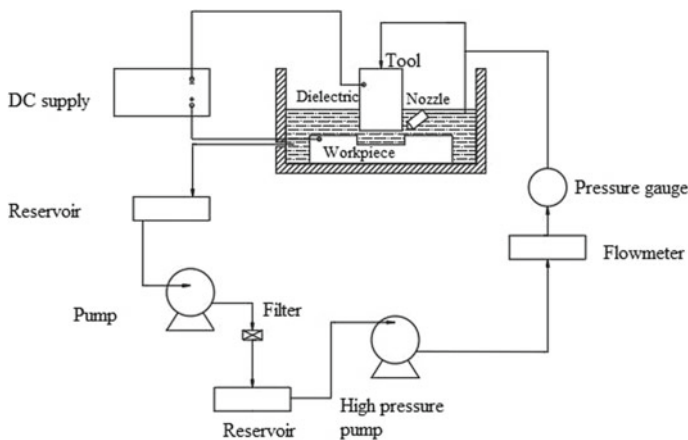


Fig. 15.6 Experimental setup



Fig. 15.7 Mitutoyo SURFTEST SJ-210

uses differential inductance method for detection method. It has measuring range of $360\ \mu\text{m}$ ($-200\ \mu\text{m}$ to $+160\ \mu\text{m}$). Radius of tip is $5\ \mu\text{m}$. Stylus is made of diamond. Radius of skid curvature is $40\ \text{mm}$. Drive range of detector is $21\ \text{mm}$. Its least count is $0.001\ \mu\text{m}$. Bottom configuration has V-shaped trough. The surface roughness is measured by Mitutoyo SURFTEST SJ-210 and data stored in it can be recovered by SPC, Printer or by inserting memory card in it. Here memory card has been used for retrieval of data. Following steps has been performed for insertion of memory card into it and for storing data in it as shown in Fig. 15.8.

In EDM Dielectric fluid use here is Divyol spark erosion oil—25. Machining has to be carried out in absence of oxygen in order to avoid oxidation, when oxidation occurs it leads to poor surface conductivity of workpiece and hinders the further machining of workpiece. That's why dielectric fluid is used as medium to have oxygen free environment for machining. It should have enough sturdy dielectric resistance so that it does not break down easily and while sparking it should be thermally resistant. Most commonly used dielectric fluid are kerosine and deionised water. Tap water can not be used as dielectric fluid as it ionises easily due to presence of salts in it. Dielectric fluid flows over workpiece and tool and removes eroded material from workpiece and helps in further efficient machining of workpiece.

SR has been calculated and examined using Taguchi by Minitab 18. Various steps in Taguchi has been shown in Fig. 15.9. Orthogonal array minimizes number of trials, so it is most effective as it handles number of variables and vast data. Three different parameters i.e., T_p , I_d and V_d are varied and their effect on SR has been studied and design matrix for various parameters are shown in Table 15.3. L9 orthogonal array

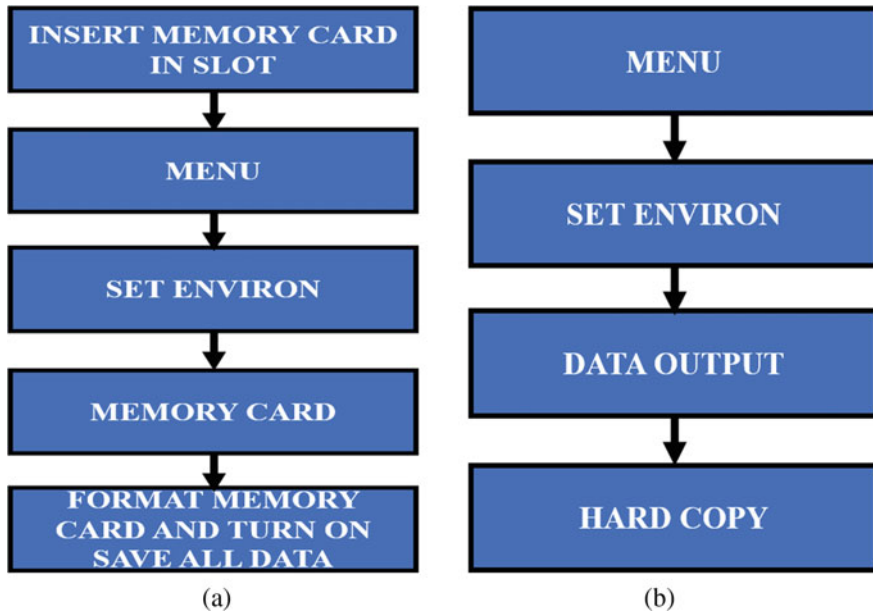


Fig. 15.8 **a** To insert memory card and **b** to store data perform following functions in instrument

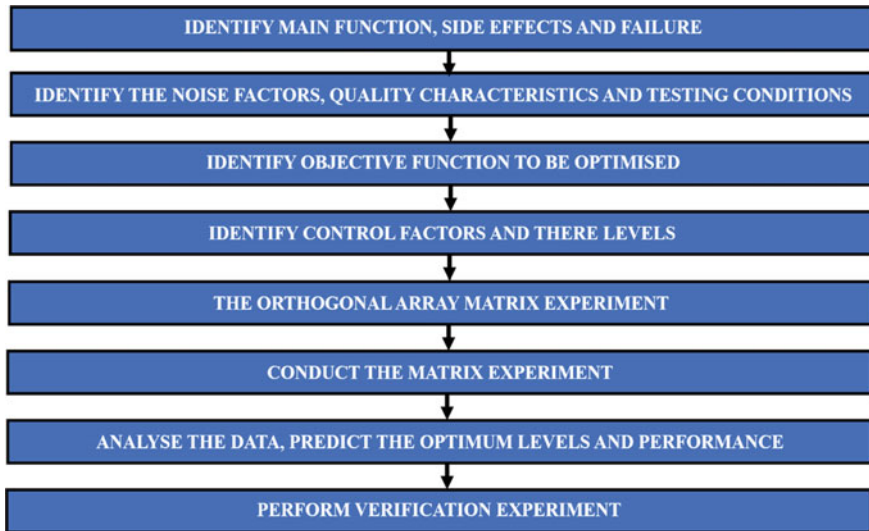


Fig. 15.9 Flow chart for steps in Taguchi design

Table 15.3 Design matrix

S. No.	I_d	T_p	V_d
1	10	50	3
2	10	350	5
3	10	650	7
4	14	50	5
5	14	350	7
6	14	650	3
7	18	50	7
8	18	350	3
9	18	650	5

was selected for evaluating maximum SR. Larger the better option was selected. ANOVA was used to identify most significant factor.

15.4 Result Discussion

Three parameters T_p , I_d and V_d are varied and their effect has been studied. In this study high range of parameters has been opted as the aim is to increase SR of biomaterial stainless steel 316L for biomedical application. Here T_{off} has been kept constant as with various study it was concluded that T_{off} has very less effect or variation on SR. Here T_{off} taken was 40 μ s. As high range of T_p and I_d has been opted which causes more material removal and more debris, so to provide sufficient time for flushing away of eroded material T_{off} was selected so.

Table 15.4 shows experimental results of machined surface of SS 316L. Larger

Table 15.4 Design matrix

S. No.	Independent parameters			Response	
	I_d (A)	T_p (μ s)	V_d (V)	SR (μ m)	S/N ratio
1	10	50	3	5.752	15.1964
2	10	350	5	10.061	20.0528
3	10	650	7	11.351	21.1007
4	14	50	5	8.055	18.1213
5	14	350	7	11.530	21.2366
6	14	650	3	13.960	22.8977
7	18	50	7	10.501	20.4246
8	18	350	3	14.277	23.0927
9	18	650	5	18.244	25.2224

the better option was considered in Taguchi as the aim was to increase SR of material for biomedical use.

Main effect of plot for means graph has been obtained by Taguchi method by software Minitab 18. Main effect plot for means reveals optimization of process parameters at which one can get optimised result for response. Here SR is response and current, pulse on time and servo voltage are factors and for optimization of results higher the better has been chosen. Results of Fig. 15.10 reveals that maximum SR is obtained at combination of parameter I_d 18 A, T_p 650 μ s and V_d 5 V.

Figure 15.11 shows how surface roughness is varied when there is increase in parameters I_d and T_p . Here as we can see in the graph when T_p increases from 50 to 650 μ s for I_d 10 A there is increases in SR. similarly for I_d 14 A and 18 A for increase in T_p SR is increasing. This graph clearly shows that SR increases with increase in I_d and T_p .

In Fig. 15.12 interaction plot is shown between V_d and T_p . Here we can see how graph for SR varies with these two parameters. When V_d increases from 3 to 7 V for T_p 50 μ s there is linear increase in SR. For T_p 350 μ s SR initially decreases then increases for increase in V_d from 3 to 7 V. For T_p 650 μ s SR first increases from 3 to 5 V then it decreases from 5 to 7 V. It is concluded that increase in T_p SR. Whereas for V_d SR increases from 3 to 5 V and then SR decreases from 5 to 7 V.

Figure 15.13 shows interaction plot between I_d and V_d for SR. here for I_d 14 A SR increases for increase in V_d from 3 to 7 V. For I_d 14 A SR initially decreases then increases for V_d from 3 to 7 V. For I_d 18 A, SR increases with increases in value of V_d from 3 to 5 V and there is further decrease in SR with increase in value of V_d from 5 to 7 V. From interaction plots shown above clearly states that SR increases as I_d and T_p increases, whereas with V_d initially SR increases then decreases.

SR plot for 3D surface shown in Figs. 15.14, 15.15 and 15.16 can be seen above. It can be clearly seen that with increase of T_p and I_d , SR. Surface roughness is highly influenced by T_p and then I_d . V_d has very less effect on SR. Only slight change on

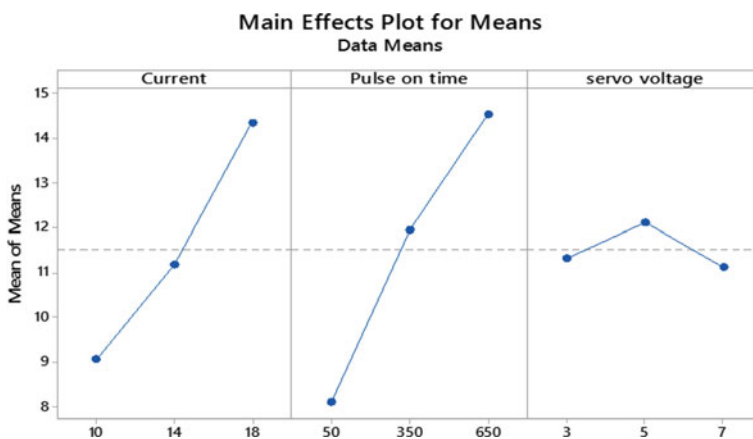


Fig. 15.10 Main effect plot for means of SR

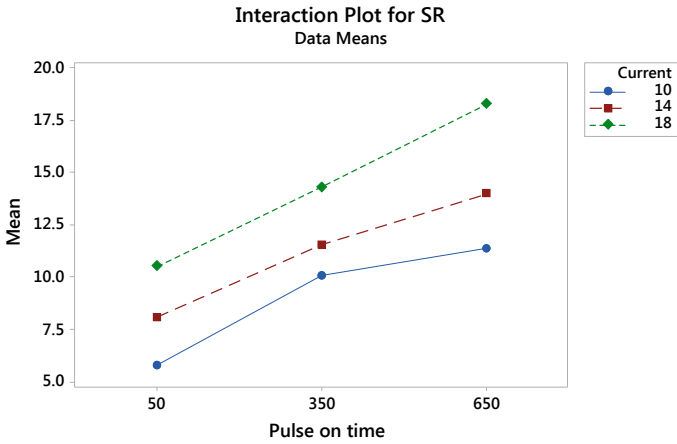


Fig. 15.11 Interaction plot for SR between I_d and T_p

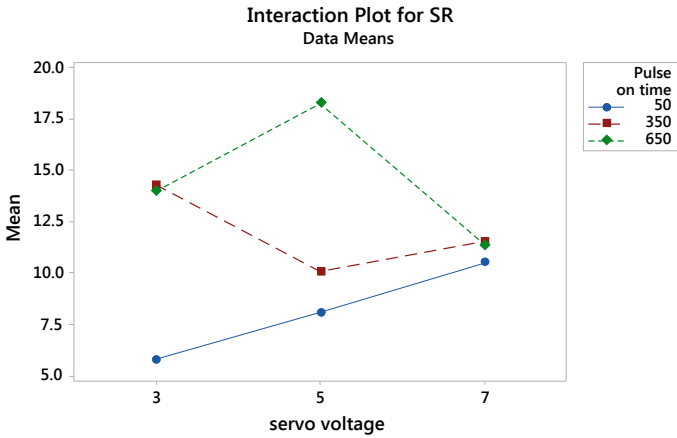


Fig. 15.12 Interaction plot for SR between T_p and V_d

SR can be seen due to change in V_d . From literature survey it was observed that T_p and I_d highly affects SR and increases in value of these parameters increases SR. That's why high value of these parameters was chosen as the main aim of this study was to increase SR which is beneficial for biomedical implants. Maximum surface roughness has been obtained at peak value of T_p 650 μ s, peak value of I_d 18 A and 5 V V_d .

From Table 15.5 it was observed that as T_p and I_d increases SR increases. Increase in V_d results in increase of SR but further increase in V_d leads to decrease of SR.

From Table 15.6, it was observed that T_p and I_d has p value less than 0.05 which shows that these two factors are significant and affects the response i.e. SR. Whereas

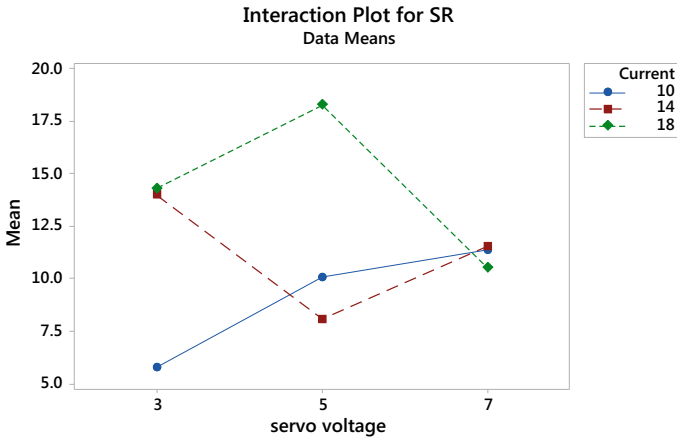
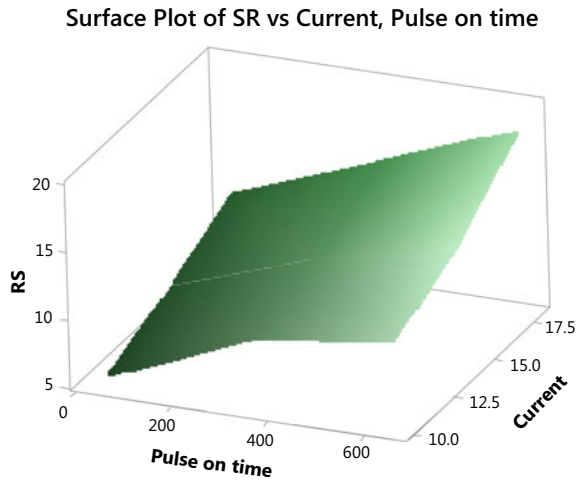


Fig. 15.13 Interaction plot for SR between I_d and V_d

Fig. 15.14 3D surface graph for SR between I_d and T_p



V_d has p value which is greater than 0.05 which shows that V_d is not significant factor and it does effect response much i.e. SR. T_p is most significant factor followed by I_d . V_d has least effect on SR. As I_d increases, supplied energy between tool and workpiece also increases which results in larger crater size of machined workpiece higher is the value of I_d more is the SR. When T_p is increased, supply of energy duration is increased. Hence energy is supplied for longer duration more material is melted and crater size produced is large in size and results in increase of SR. Increase of SR is higher with T_p than I_d . Effect of V_d on SR is not significant as change of V_d has lesser effect on SR.

Fig. 15.15 3D surface graph for SR between I_d and V_d

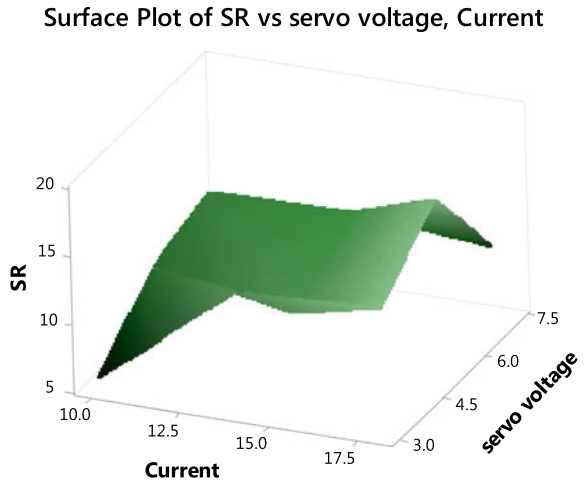


Fig. 15.16 3D surface graph for SR between T_p and V_d

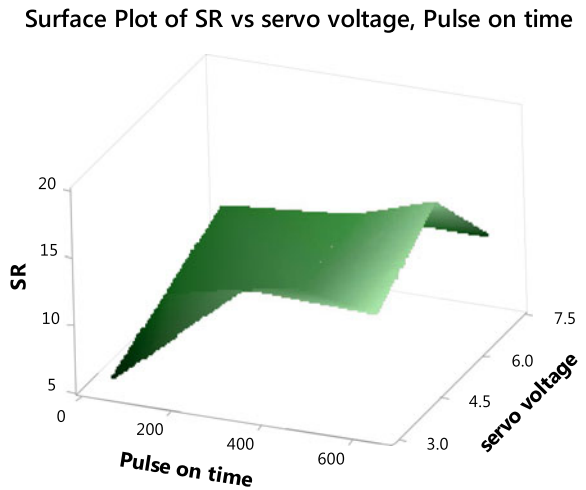


Table 15.5 Rank table for S/N ratio and control machining parameters for SR

Level	I_d	T_p	V_d
1	18.78	17.91	20.40
2	20.75	21.46	21.13
3	22.91	23.07	20.92
Delta	4.13	5.16	0.74
Rank	2	1	3

Table 15.6 Rank table for S/N ratio and control machining parameters for SR

Source	DF	Adj SS	Adj MS	F-Value	P-Value
I_d	2	42.445	21.2226	74.78	0.013
T_p	2	62.575	31.2873	110.24	0.009
V_d	2	1.651	0.8255	2.91	0.256
Error	2	0.568	0.2838		
Total	8	107.238			

15.5 Conclusion

Following conclusions were drawn from experimental results.

- For SR T_p and I_d are most significant factors. Out of which T_p has more effect on SR than I_d .
- With increases in T_p from 50 to 650 μs SR also increases because as T_p increases energy supplied duration increases which results in crater of larger size on workpiece and hence SR is increased.
- Similarly as I_d increases from 10 to 18 A SR increases. As I_d is increased energy supplied is increased which causes higher temperature and larger crater size and hence SR is increased.
- V_d does not have significant influence over SR, change in V_d has very less effect on SR. As V_d is increased from 3 to 5 V, there is slight increase in SR. As it further increase to 7 V, there is slight decrease in SR.
- Maximum SR 18.244 μm is observed at set of parameters T_p 650 μs , I_d 18 A and V_d 5 V.

References

1. Ho, S.H., Newman, S.T.: State of the art electrical discharge machining (EDM). *Int. J. Mach. Tools Manuf.* **43**, 1287–1300 (2003)
2. Abbas, N.M., Solomon, D.G., Bahari, M.F.: A review on current research trends in electrical discharge machining (EDM). *Int. J. Mach. Tools Manuf.* **47**, 1214–1228 (2007)
3. Barman, S., Vijay, Nagahanumaiah, Puri, A.B.: Surface texture and elemental characterization of high aspect ratio blind micro holes on different materials in micro EDM. *Procedia Mater. Sci.* **6**, 304–309 (2014)
4. Nanimina, A.M., Rani, A.M.A., Ginta, T.L.: Assessment of powder mixed EDM: a review. In: *Proceedings of the 4th International Conference on Production, Energy and Reliability, ICPER (2014)*
5. Volosova, M.A., Okunkova, A.A., Povolotskiy, D.E., Podrabinnik, P.A.: Study of electrical discharge machining for the parts of nuclear industry usage. *Mech. Ind.* **16**, 706 (2015)
6. Pandey, A., Singh, S.: Current research trends in variants of electrical discharge machining: a review. *Int. J. Eng. Sci. Technol.* **2**, 2172–2191 (2010)

7. Ubaid, A.M., Dweiri, F.T., Aghdeab, S.H., Al-Juboori, L.A.: Optimization of electro discharge machining process parameters with fuzzy logic for stainless steel 304 (ASTM A340). *J. Manuf. Sci. Eng.* **140**, 1–13 (2018)
8. Rajesh, R., Anand, M.D.: The optimization of electro discharge machining process using response surface morphology and genetic algorithms. *Procedia Eng.* **38**, 3941–3950 (2012)
9. Prakash, C., Kansa, H.K., Pabla, B.S., Sanjeev, P., Aggarwal, A.: Electric discharge machining—a potential choice for surface modification of metallic implants for orthopedic applications: a review. *J. Eng. Manuf.* **230**, 1–30 (2015)
10. Kumar, V., Beri, N., Kumar, A.: Electric discharge machining of titanium and alloys for biomedical implant applications: a review. *Int. J. Res. Anal. Rev.* **3**, 120–128 (2018)
11. Chauhan, P., Saloda, M.A., Nandwana, B.P., Jindal, S.: Review on research trends in electric discharge machining for biomedical application. *TEST Eng. Manage.* **83**, 2689–2696 (2020)
12. Harchuba, P., Cákóváb, L.B., Stráskýa, J., cákóváb, M.B., Novotná, K., Ceka, M.J.: Surface treatment by electric discharge machining of Ti–6Al–4V alloy for potential application in orthopaedics. *J. Mech. Behav. Biomed. Mater.* **7**, 96–105 (2011)
13. Alla, R.M., Ginjupalli, K., Upadhya, N., Shammas, M., Ravi, R.K., Sekhar, R.: Surface roughness of implants: a review. *Trends Biomater. Artif. Organs* **25**, 112–118 (2011)
14. Saini, M., Singh, Y., Arora, P., Arora, V., Jain, K.: Implant biomaterials: a comprehensive review. *World J. Clin. Cases* **3**, 52–57 (2015)
15. Buser, D., Schenk, R.K., Steinemann, S., Fiorellini, P.P., Fox, C.H., Stich, H.: Influence of surface characteristics on bone integration of titanium implants: a histomorphometric study in miniature pigs. *J. Biomed. Mater. Res.* **25**, 889–902 (1991)
16. Shalabi, M.M., Gortemaker, A., Hof, M.A.V., Jansen, J.A., Creugers, N.H.J.: Implant surface roughness and bone healing: a systematic review. *J. Dent. Res.* **85**, 496–500 (2006)
17. Strasky, J., Janecek, M., and Harchuba, P., 2011. Electric Discharge Machining of Ti-6Al-4V Alloy for Biomedical Use. *WDS'11 Proceedings of Contributed Papers*, 11. 127–131.
18. Shunmugam, M.S., Philip, P.K.: Improvement of wear resistance by EDM with tungsten carbide P/M electrode. *Wear* **171**, 1–5 (1994)
19. Güngör, E., Ekmekçi, B.: Wear resistance of electrical discharge machined surfaces. In: Conference: 3rd International Symposium on Innovative Technologies and Science, At Universidad Politecnica de Valencia, Valencia, Spain, vol. 1, pp. 1080–1089 (2015)
20. Mahamat, A.T.Z., Rani, A.M., Husain, P.: Machining of cemented tungsten carbide using EDM. *J. Appl. Sci.* **11**, 1–7 (2011)
21. Dewidar, M.M., Khalil, K.A., Lim, J.K.: Processing and mechanical properties of porous 316L stainless steel for biomedical applications. *Trans. Nonferrous Met. Soc. China* **17**, 468–473 (2017)
22. Singh, R., Dalhotre, N.B.: Corrosion degradation and prevention by surface modification of biometallic materials. *J. Mater. Sci.* **18**, 725–751 (2007)
23. Simionescu, N., Benea, L.: Corrosion behavior of 316L stainless steel as biomaterial in physiological environment. In: 13th Annual Conference on Materials Science Metal and Manufacturing, Paris, France, November 2017
24. Mariotto, S.F.F., Guido, V., Cho, L.Y., Soares, C.P., Cardoso, K.K.: Porous stainless steel for biomedical applications. *Mater. Res.* **14**, 146–154 (2011)
25. Muttamara, A., Borwornkiatkaew, W., Pronpijit, A., Nuanchom, S.: Effect of graphite electrode to surface's characteristic of EDM. In: MATEC Web of Conferences, vol. 177, pp. 1–4 (2016)
26. Suhardjono: Characteristics of electrode materials on machining performance of tool steel SKD11 with EDM sinking. *ARPN J. Eng. Appl. Sci.* **11**, 986–991 (2016)
27. Aliyu, A.A.A., Abdul-Rani, A.M., Ginta, T.L., Prakash, C., Axinte, E., Razak, M.A., Ali, S.: A review of additive mixed-electric discharge machining current status and future perspectives for surface modification of biomedical implants. *Hindawi Adv. Mater. Sci. Eng.* **2017**, 1–23 (2017)
28. Azom: Stainless Steel Grade 316L Properties, Fabrication and Applications (UNS S31603) (2004). <https://www.azom.com/article.aspx>. Viewed on Nov 2018

Chapter 16

Optimization of Direct Slicing Process Using DICOMS for Additive Manufacturing



**Ujjwala Singh Thakur, Vivek Kumar Gupta, Ankit Nayak,
and Prashant Kumar Jain**

Abstract In this article, processing of Computed Tomography (CT) scan data using the principle of direct slicing is discussed. Various segmentation algorithms are compared for fetching the region of interest. Otsu thresholding automates the selection of global threshold value than any intermediate thresholding algorithm and hence it is used for segmentation in presented research work. Further respected contour has been created by selecting the most optimum edge detection technique out of Sobel, Robert, Prewitt and Canny. Canny edge detection produces more sharper edges. Thus, an improvised algorithm of Canny is used which is also relevant for preservation of weak edges. The contour is compared to its Standard Tessellation Language (STL) file, generated in MIMICS software. The coordinates of the two models are superimposed at a given slice height and compared for the deviation of sliced area and perimeter of the two models. Results show that an improvised method of direct slicing with accurate segmentation and edge detection techniques can obtain the precise sections, improve the part's shape and maintain the outward direction of normal and can therefore overcome the inadequacies of the STL.

Keywords CT scan · STL · Segmentation · Edge detection

16.1 Introduction

Additive Manufacturing (AM) is a process of layer by layer deposition of material to fabricate a 3D object. Unlike to subtractive manufacturing, AM process fabricates the object from Computer Aided Design (CAD) model of defined geometry without use of specific tooling. The capability to fabricate parts with offers the cost saving unlike time-consuming conventional manufacturing processes like machining, casting etc.

U. S. Thakur · V. K. Gupta · A. Nayak (✉) · P. K. Jain
Mechanical Engineering Discipline, PDPM Indian Institute of Information Technology, Design
and Manufacturing, Jabalpur, Madhya Pradesh 482005, India
e-mail: ankitnayak@iiitdmj.ac.in

A. Nayak
Banasthali Vidyapith, Vanasthali, Rajasthan 304022, India

The AM system manufactures parts of good quality in minimal overall time. The manufacturing world has witnessed its evolution since last three decades. Earlier, AM process was only used for prototyping purpose, popularly known as Rapid Prototyping (RP). Nowadays, AM has been adopted by many industries to make functional products to reduce the product development cycle time.

Design of CAD model is one of the main prerequisites step of AM process. CAD model of required geometry which is to be fabricated are modelled using CAD software packages such as Solid Works, Pro/Engineer, and Catia. This step is indistinguishable for all the AM process.

In this step, design of model is done in CAD software and is converted into Standard Tessellation Language (STL) file format. The STL file format converts CAD model into triangulated surface data. In AM process, STL file format become de-facto standard file format which was accepted commonly.

The generated STL file is exported to software which it is sliced into layers to get contour information. In accordance of basic principle of AM process any model fabricated layer by layer manner, hence it is necessary to slice the model into layer. Various open source software available online such as Flash Print, Slicer, Replicator-G, and RepRap, etc. that slices the given model. Software not only provides contour information but also set values of different process parameters to get good surface finish as well as strength.

Standard Tessellation Language (STL) is considered as a de-facto standard for the Additive Manufacturing (AM) industry. However, aiming at the errors [1] with STL, alternatives are proposed for input to AM systems. Direct slicing aims at slicing the Computer Aided Design (CAD) model directly and transferring the resultant contours to the RP process. This method overcomes all the drawbacks while using an intermediate tessellation in addition to reduced processing time. CT Scans are emerging as popular sliced contours due to its well-known connectivity and used extensively in medical imaging and 3D modeling and virtual prototyping as well.

Direct Slicing can generate precise sliced contours [2] from original CAD models and obviates the error-detection and repairing process of STL files. Segmentation and Edge Detection is applied on the CT-Scans [3] to generate the region of interest after which the boundaries of ROI is detected. This iteration continues for the subsequent layers once the contour of one layer is defined. The 3D model is printed by assigning the contours as a tool path.

Medical image segmentation [4] is a procedure for extracting the “Region of Interest” through an automatic or semi-automatic process. Most techniques are based on region and boundary properties. Thresholding [5] is one such technique in which image is formed from regions with respective pixel value. It comprises a value in histogram that divides intensities in two parts. The first part is the “foreground” having pixels with intensities greater than or equal to the threshold and the latter is the “background” having pixels with intensities less than the threshold. However, it does not take into account the spatial information of the image which leads to noise and intensities in inhomogeneities. Otsu method is another technique which is proposed to automate the selection of threshold value. The goal is to find an optimum value of global thresholding. It chooses the threshold to minimize the intra

class variance of black and white cluster pixels. The threshold value that maximizes the between class variance is chosen to be the optimal threshold.

Once the region of interest is selected, edge detection [6] is done to form the boundaries of the objects where the edge separates between the objects and the background, overlapping objects. Many edge detection methods [6] like the Sobel, Prewitt and Canny are proposed in the literature. Canny operator generates equally good edges with smooth continuous pixels and thin edge compared with other operators which cannot produce smooth and thin edges.

The need for reconstructing the 3D geometry by stacking up the DICOMS has always been essential for the biomedical applications. Surgeries are done to remove the cancerous area of bone in bone cancer. If the cancer is near a joint, then the whole joint has to be removed and replaced with an artificial one. An implant generally called as prosthesis is assembled generally in the knee joint assembly or the hip point assembly. The correct implant is designed by the accurately choosing the region and describing its boundary in the corresponding slices. However, since the whole joint is removed, the CT-scan of that area will be missing. One method to resolve the issue is to patch the surfaces homogenously but accuracy is severely affected. Therefore, a much better alternative is to interpolate the contours in the missing region. Accurate interpolation leads to the exact reconstruction of the implant.

16.2 Direct Slicing

The CAD model is sliced directly, and the resultant contours are transferred to the Additive manufacturing process. This process can be used as an alternative to intermediary tessellation files. Rapid prototyping models are widely used for a variety of applications. It is essential to maintain the integrity of the product throughout its manufacturing. The requirement of the RP models for engineering applications along with the need for model integrity demands a satisfactory method of defining RP data. This method should be capable in overcoming the disadvantages of tessellation. The significance of direct slicing can be seen in producing cylindrical shapes. It takes less processing time than the tessellation and has smaller file size. It performs better in obtaining smooth surface geometry and takes less time than the manual finishing.

16.3 Adaptive Slicing

The Direct slicing method overcomes the disadvantages of ST. However, it is inefficient in slicing the model with varying curvatures in horizontal and vertical directions. One solution to this problem is the adaptive slicing or slicing method for varying thickness. Various studies have been done with faceted surfaces for parametrizing the cusp height to slice STL files. Some methods are developed to determine the variable thickness using optimization. An algorithm is developed to design an adaptive slicing

procedure for a parametric surface. In this process the thickness is calculated on the basis of maximum vertical curvatures at different points. The Marching algorithm is also developed for the adaptive slicing of STL files.

16.4 Implementation of Direct Slicing

Several procedures are used for slicing a solid model. The specifications about the part's highest and lowest point have to provide in the beginning of slicing algorithm. The lowest Z coordinate of the part is the bottom and the highest Z coordinate is the top, when the slicing is done is Z direction. The tags of the slices are put together, and the function is called consecutively for slicing of the part. The program also includes an adaptive slicing procedure.

It depends on the alteration of parts. If the section of a part does not undergo any change in an interval, the layer thickness is modified to maximum layer thickness which is input parameter. This parameter is not taken into account in case adaptive slicing is not desired. The section is disregarded if it has the same geometry as the section corresponding to the standard layer thickness. The section is added to the assembly of sheet if it is equal to the section corresponding to maximum layer thickness. The sectioning takes place halfway between the standard and the maximum layer thickness and a middle section is created if it is not equal.

16.5 Proposed Algorithm

Direct Slicing produces accurate slice contours from original CAD models. Segmentation and Edge Detection is applied on the CT-Scans to generate the region of interest after which the boundaries of ROI are detected. This iteration continues for the subsequent layers once the contour of one layer is created. The 3d model is printed by assigning the contours as a tool path.

Image segmentation is extracting the "Region of Interest" through an automatic or semi-automatic process. Most techniques are based on the properties of region and boundary. Thresholding is a technique in which image is formed from regions with different values of gray level. It consists of a particular value from the intensity sample data that divides intensities in two parts. The former division is usually the "main or the front portion" having pixels whose intensities are equal to or greater than the threshold and the latter portion is the "background" which consists of the remaining pixels. However, it does not take into account the spatial information of the image which can lead to noise and in homogeneities. Otsu method is another technique which automates the selection of threshold value. The goal is to find an optimum value of global thresholding. It is assumed that an image has two-pixel classes. It chooses the threshold to minimize the intra class variance of black and white cluster pixels. Optimal threshold value maximizes the between class variance.

Once the region of interest is selected, edge detection is done to form the boundaries of the objects where the edge separates the objects from its background. Many algorithms like the Sobel, Prewitt and Canny are proposed in the literature. Canny operator generates smooth and thin edges with continuous pixels compared with other operators which cannot produce smooth and thin edges.

In this paper, region comprising the spongiol bone in the CT scan are fetched using two different algorithms. The image obtained after the processes are compared to the actual image which is derived from MIMICS. The two images are overlapped over each other in MATLAB and the overlapping area and perimeter in percentage is calculated and compared for accuracy.

There are two algorithms, developed for the synthesis of images which are as follows:

16.6 Manual Thresholding

In this algorithm, the range of the region of interest has to be provided in Hounsfield units by the user through an open interface. Once the range is obtained, the algorithm performs the thresholding operation by screening the pixels which falls into the range and discards the remaining area. The screened pixels are stored in a matrix. Once the thresholding is done, edge detection is performed for getting the boundary. The perimeter of the binary image is fetched using the BWPERI command in MATLAB. Thus, the object with its boundary is obtained and converted as a spatial figure in MATLAB and its coordinates are saved as shown in Fig. 16.1.

Fig. 16.1 Flowchart for the manual thresholding operation

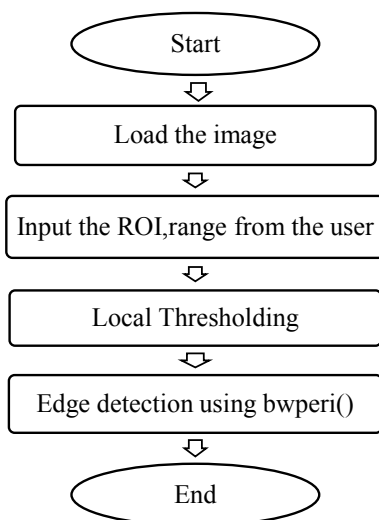
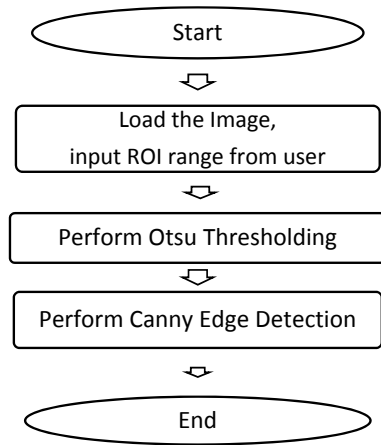


Fig. 16.2 Flowchart for Otsu thresholding algorithm



16.7 Otsu Thresholding

In this algorithm, Otsu thresholding with n levels are used initially for segmentation. Canny operator is then used for the edge detection as shown in Fig. 16.2. The coordinates of the obtained image are saved in another matrix for further use.

16.8 Improved Otsu Thresholding with Improvised Canny Algorithm

In this algorithm, an improved Otsu threshold segmentation method [7] is proposed to get better region of interest. Firstly, `multithresh` command is used to automate the value of thresholds. It segments the image into N levels by Otsu thresholding method. Each level contains the pixels which lie between threshold limits. Once the level that contains the region of interest is selected by the user, contour density is calculated for that corresponding image. If number of contours in the image exceeds a limit, it may be difficult to get the accurate region of interest since the unwanted regions are included. Hence, further segmentation is done using `multithresh` and the iteration is continued for two levels. This process provides the image with accurate region of interest.

An improvised version of canny edge detection [8] is used to get the contour. The image initially is noised with a salt and pepper [9] and decomposed to 2D wavelet transformation, whereby soft thresholding is done to filter and smoothen of the noise. The inverse of wavelet decomposition is then done to restore the original image with region of interest. Canny operation is performed in the obtained image. Thus, the boundary differentiating the object is finally achieved as shown in Fig. 16.3. The

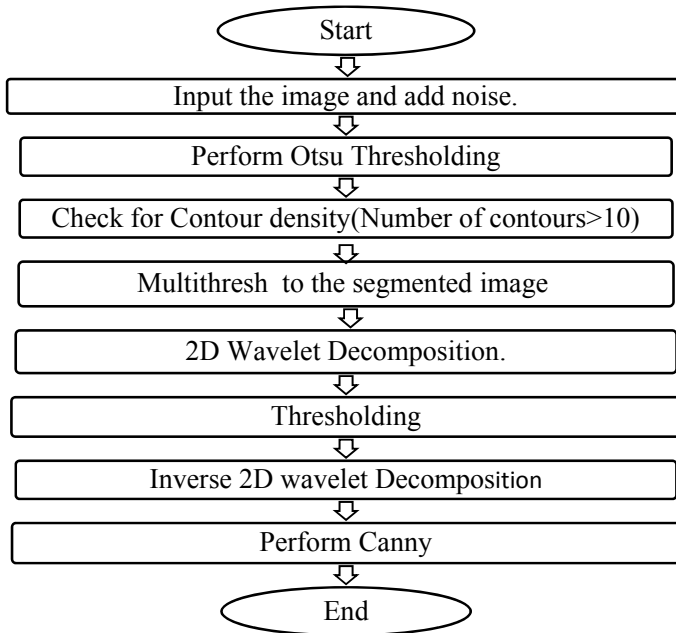


Fig. 16.3 Flowchart for Improved Otsu and improved Canny algorithm

figure is converted as a spatial figure in MATLAB software and its coordinates are stored.

16.9 Flowchart of Operations

The flowchart and processes for completing each module is specified in Figs. 16.1, 16.2 and 16.3.

16.10 Experimentation

The images generated by the three processes are generated in MATLAB and stored with their coordinates in matrix respectively. The original region of spongier and compact bone of the CT scan is generated by creating a mask in mimics [10] software. The masked image is imported in MATLAB and is stored as a spatial figure and its coordinates are saved. Each of the figures generated by the above process is overlapped with the masked image and coordinates are grouped as coinciding or

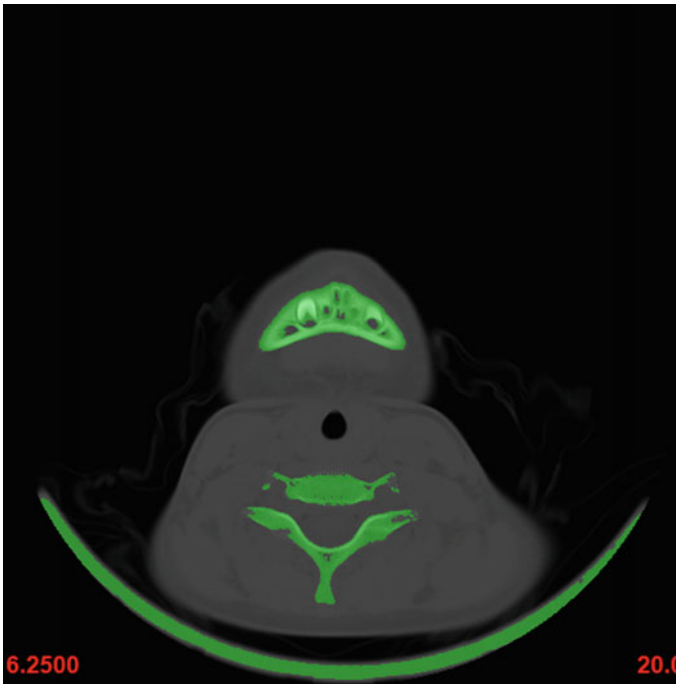


Fig. 16.4 Region of compact and spongy bone in DICOM image in MIMICS

distinguishing. Thus, percentage of overlapping area and perimeter are calculated (Figs. 16.4, 16.5, 16.6 and 16.7).

16.11 Development of Intermediate Planar Contour and Applications

To view a 3D object from several cross sections, various approaches were made using different interpolation techniques. There were some surface based theories proposed for the interpolation. The surface-based approach is detecting two dimensional contours that describe the edges of the interested object on a slice by slice basis. One surface-based method is to interpolate the cardinal splines when the B Spline represents the cross section. In this way, a surface is reconstructed by lofting method. In the cuberille based approach the representation of an object is by creating a subset of the set of all voxels and representation of the surface is by the set of directed faces which separate voxels in the object from voxels in the back- ground. The surface representations are obtained by joining the boundaries by planar surface elements. As shown in Fig. 16.8. The triangulation process creates a collection of

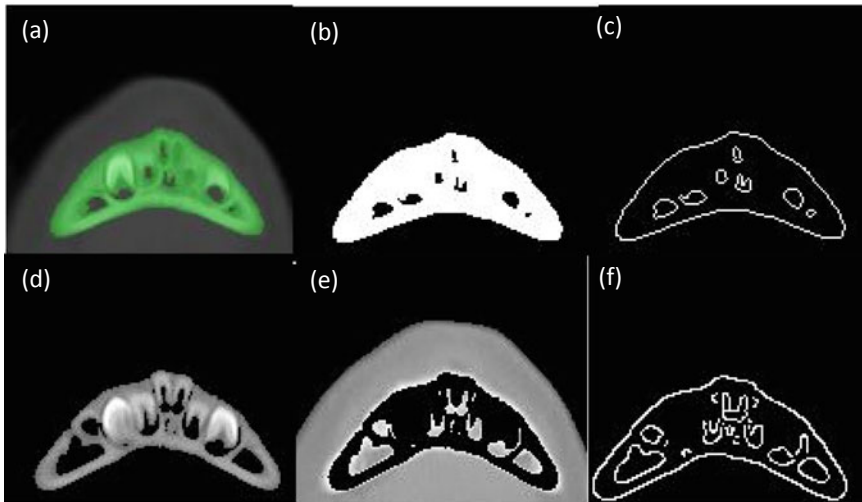


Fig. 16.5 **a** Cropped image of bone, **b** ROI of image, **c** edge detection of image, **d** original image for Otsu and Canny method, **e** Otsu thresholding, **f** Canny boundary

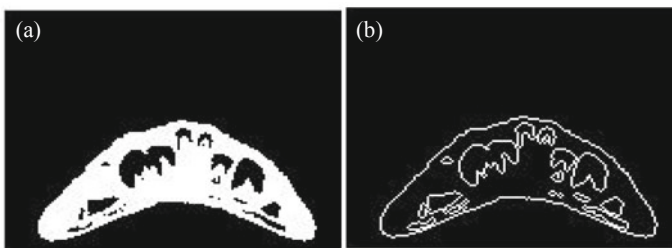


Fig. 16.6 **a** Simple thresholding, **b** Bwperi edge detection (images generated in MATLAB)

triangular patches between the pairs of contours so that the union is a closed bounding surface. It is a good approximation to the original surface.

Intermediate contours are created to achieve the interpolation between the contours of two slices. Linear interpolation is used to satisfy equal slice thickness and pixel size. The basic idea of the interpolation is to specify the plane height between the slices where the contours are desired. Once the plane is specified and described, the next objective is to interpolate the voxels on the basis of successive slice data.

The need for the reconstructing the 3D geometry by stacking up the DICOMS have always been essential for the biomedical applications. In bone cancer, Surgeries are done remove the cancerous area of bone. If the cancer is near a joint, then the whole joint must be removed and replaced with an artificial one. An implant generally called as prosthesis is assembled generally in the knee joint assembly or the hip point assembly. The correct implant is designed by the accurately choosing the region and

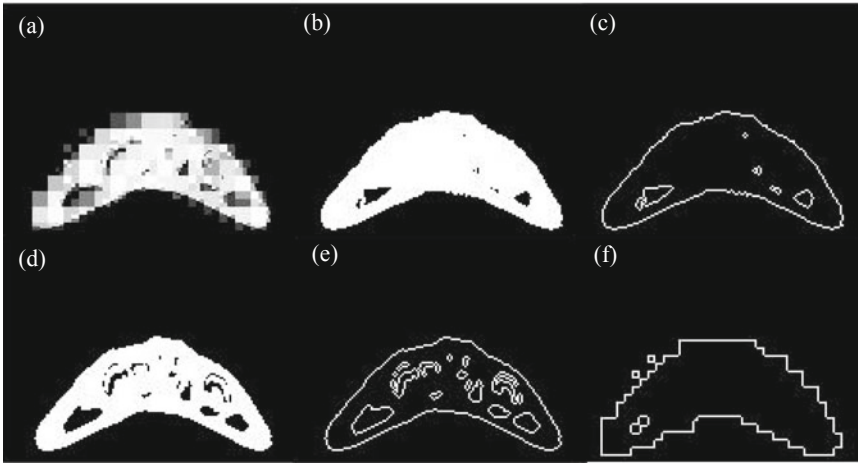


Fig. 16.7 a Image with salt and pepper noise, b Otsu thresholding, c number of blobs/contours, d multi thresholding, e wavelet decomposition and inverse wavelet decomposition, f Canny edge detection

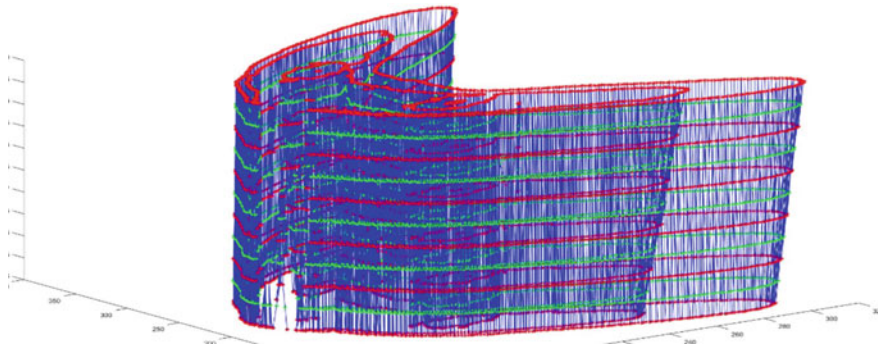


Fig. 16.8 Contours in slice by slice basis

describing its boundary in the corresponding slices. However, since the whole joint is removed, the CT scan of that area will be missing. One method to resolve the issue is to patch the surfaces homogeneously but accuracy is severely affected. Therefore, a much better alternative is to interpolate the contours in the missing region. Accurate interpolation leads to the exact reconstruction of the implant.

The treatment of mandible bone in case of jaw tumor treatment faces a very similar kind of problem. The jaw of a side is affected with tumor and has to be removed and reconstructed. There were many alternatives proposed initially for the reconstruction. The most popular option was to mirror the part of the non-defective side to the other side, using the CT-scans and create the whole jaw implant with at most symmetry. However, human body is not fully symmetrical and hence a mismatch is bound

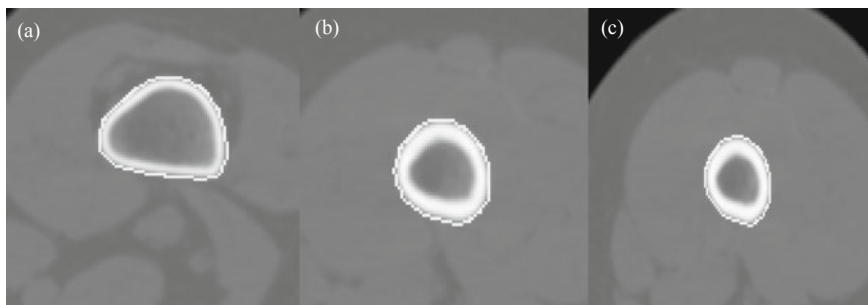


Fig. 16.9 a Start contour/slice no 132, b intermediate contour/slice no 180, c goal contour/slice no 189

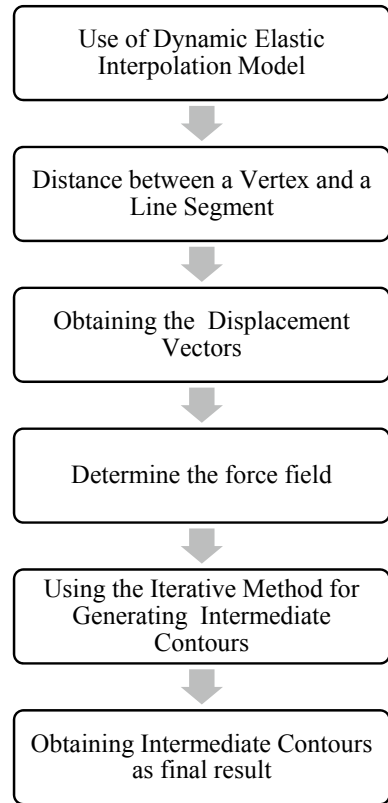
to happen. Therefore, interpolating the portion which was removed along with the tumor and then designing the implant results in better accuracy.

Two successive CT-scans of the femur bone region bone (226-1613 HU) were opened and read in MATLAB software. Our main interest was the region of the femur bone portion out of muscle, soft tissue, and bone marrow. The CT-scan was divided into 10 levels of thresholds using Otsu operator and that level is chosen which consists the threshold of the bone region. Canny operator was used to perform edge segmentation. The CT-scans were also processed in MIMICS software to fetch the bone area and imported to MATLAB and the coordinates of each contour of the corresponding slice were stored (Fig. 16.9).

16.12 Experimentation

Two successive slices are firstly processed to obtain the contours. A particular region of interest is selected using the Otsu segmentation. A modified canny edge detection is applied for creating the contours. The coordinates of contours are stored in the matrix. Once the slice height, slice number and slice thickness are specified, an intermediate height between two consecutive slices can be chosen. The algorithm for developing the contour is explained through the flow chart and the formulations are explained in Fig. 16.10.

A 3-D object is created by stacking all the contours. The model used to perform the interpolation between the start contour and goal contours. The contours points obtained from slices are sorted by head to tail method in an orderly fashion.

Fig. 16.10 Flow chart

16.13 Design

Now the interpolation is divided into four main steps:

- Overlapping the two contours and for each vertex in one contour the nearest line segment in another contour is determined based on Euclidean distance. Once the nearest distance is calculated, the orientation dissimilarity is calculated, and the total distance is thus calculated by combining positional difference and directional similarity.
- Determining the Displacement vector.
- Determining a “force field” based on the displacement vectors of the two contours.
- Formulate an iterative process to generate the intermediate contours from the start contour to the goal contour.

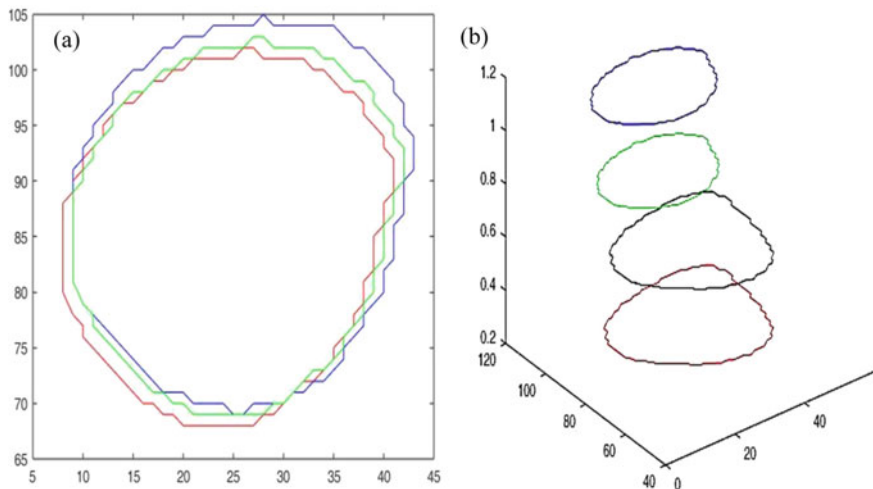


Fig. 16.11 Obtained result **a** generation of intermediate contour, **b** overlapping of intermediate contour with the original image

16.14 Analysis

The intermediate contour was created using the algorithm mentioned previously. The coordinates of the newly formed contour are saved in a matrix. The contour was compared with the original contours obtained from the slices that lie between these two contours for the similarity in orientation and it matched with the contour number—at a height between—from the initial contour. Moreover, the contour we obtained from the interpolation had a flexible centroid i.e. it can be shifted. The contour was overlapped with the contour of the image it resembled the most. In this case it resembled with Number. The percentage of area and perimeter overlapped with each other was calculated and the number of coordinates identical to each other was calculated (Fig. 16.11).

16.15 Results

The images obtained from the three algorithms, were overlapped respectively with the masked STL image derived from MIMICS. The overlapping area and the number of identical coordinates were calculated respectively. It was found that an improved Otsu and canny method was closest to the actual region of interest compared to the conventional segmentation and edge detection techniques (Table 16.1 and Fig. 16.12).

It was observed that 91.2% of the area was overlapped with the original image showing the similarity between the actual image and the generated image was large and the interpolation estimated the original contour with greater accuracy. The start

Table 16.1 Compressional study of area developed in three algorithms

S. No.	Method	Percentage overlapping area	Percentage overlapping perimeter
1.	Simple thresholding and perimeter	73.0091	16.534
2.	Otsu and Canny method	74.0862	8.6514
3.	Improvised Otsu and improved edge detection	82.0091	9.16

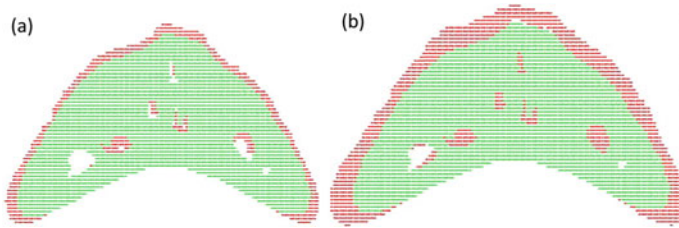


Fig. 16.12 Obtained result **a** overlapped area simple thresholding (green) with original image (red), **b** overlapped area in Otsu (green) in original image (red)

and the goal image have greater number of coordinates points compared to their original contours. Large coordinate points give refined image. Moreover, only the start and the goal contour are only needed to fill the hole region or generating the intermediate contours. Once the contours are generated, patching can be used to visualize as 3D model. Step size is used here to create the contours at user input heights. Step size can also be controlled to give the smoother images (Fig. 16.13).

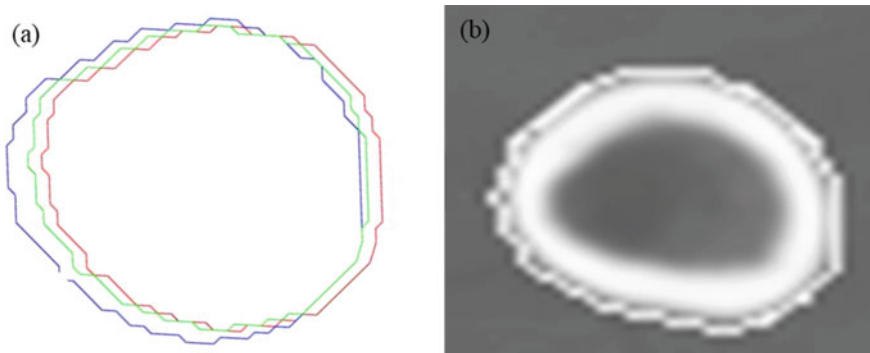


Fig. 16.13 **a** Interpolated contour and its actual image, **b** actual image

16.16 Discussion

Direct Slicing can generate precise slice contours from original CAD models and obviates the error-detection and repairing process of STL files. Segmentation and Edge Detection is applied on the CT-Scans to generate the region of interest after which the boundaries of ROI is detected. This iteration continues for the subsequent layers once the contour of one layer is defined. The 3d model is printed by assigning the contours as a tool path.

In this research work, contours from CT scans are developed, using the principle of direct slicing. Various algorithms are compared for fetching the region of interest and the boundary. Otsu thresholding automates the selection of global threshold value than any intermediate thresholding algorithm and hence an algorithm of its improvised version is used for segmentation. Further extraction of contour is done by selecting the most optimum edge detection technique out of Sobel, Robert, Prewitt and Canny. Canny edge detection produces sharper edges. Thus, an improvised algorithm of Canny is also used along with the Modified Otsu-Wavelet method.

The designed contour is compared to its STL [11–13], generated in MIMICS. The coordinates of the two images are superimposed at a given slice height and compared for the deviation of sliced area and perimeter of the two overlapped images. Results show that an improvised method of direct slicing with accurate segmentation and edge detection techniques can obtain the precise area, improve the shape and therefore overcome the inadequacies of the STL.

16.17 Conclusions

Advanced Segmentation techniques have been used lately to fetch the accurate region of interest. Algorithms are improvised by minimizing its drawbacks and inefficiency. Otsu, which is an automatic local thresholding, can be improvised by implementing condition of contour density prior to its application.

Canny edge detection, which is sensitive to the noise, can give better results when image is denoised completely. In this paper, an attempt to improvise the existing algorithm by rectifying its error was shown. In future, accurate methods can be proposed as a permanent solution to resolve the defects.

References

1. Sofia, A., Oliveira, C.M., Slud, R.: S s: a. *Int. J. Adv. Manuf. Technol.* **990**(2), 1–9 (2000)
2. Jamieson, R., Hacker, H.: Direct slicing of CAD models for rapid prototyping. *Rapid Prototyping J.* **1**(2), 4–12 (1995). <https://doi.org/10.1108/13552549510086826>
3. Varma, D.R.: Managing DICOM images: tips and tricks for the radiologist. *Indian J. Radiol. Imaging* **22**(1), 4–13 (2012). <https://doi.org/10.4103/0971-3026.95396>

4. Norouzi, A., et al.: Medical image segmentation methods, algorithms, and applications. *IETE Tech. Rev. (Institution Electron. Telecommun. Eng. India)* **31**(3), 199–213 (2014). <https://doi.org/10.1080/02564602.2014.906861>
5. Shuaib, K., Abdella, J.A., Barka, E., Sallabi, F.: *ICT Innovations 2012*, vol. 207, pp. 15–26 (2013). <https://doi.org/10.1007/978-3-642-37169-1>
6. Ganesan, P., Sajiv, G.: A comprehensive study of edge detection for image processing applications. In: *Proceedings 2017. International Conference on Innovations in Information, Embedded and Communication Systems (ICIIECS 2017)*, vol. 2018-January, pp. 1–6 (2018). <https://doi.org/10.1109/ICIIECS.2017.8275968>
7. Yuan, X., Martínez, J.F., Eckert, M., López-Santidrián, L.: An improved Otsu threshold segmentation method for underwater simultaneous localization and mapping-based navigation. *Sensors (Switzerland)* **16**(7) (2016). <https://doi.org/10.3390/s16071148>
8. Farhan, R.: A new method to improve canny edge detection on MRI brain affected by Rician Noise, May 2015, 2018
9. Kaur, S.: Noise types and various removal techniques. *Int. J. Adv. Res. Electron. Comput. Commun. Eng.* **4**(2), 226–230 (2015)
10. Comaneanu, R.M., Tarcolea, M., Vlasceanu, D., Cotrut, M.C.: Virtual 3D reconstruction, diagnosis and surgical planning with mimics software. *Int. J. Nano Biomater.* **4**(1), 69–77 (2012). <https://doi.org/10.1504/IJNB.2012.048212>
11. Nayak, A., Jain, P.K., Kankar, P.K.: Progress and issues related to designing and 3D printing of endodontic guide. In: *Innovative Design, Analysis and Development Practices in Aerospace and Automotive Engineering (I-DAD 2018)*, pp. 331–337. Springer, Singapore (2019)
12. Nayak, A., Jain, P.K., Kankar, P.K., Jain, N.: Computer-aided design-based guided endodontic: a novel approach for root canal access cavity preparation. *Proc. Inst. Mech. Eng. [H]* **232**(8), 787–795 (2018)
13. Nayak, A., Jain, P.K., Kankar, P.K., Jain, N.: Effect of volumetric shrinkage of restorative materials on tooth structure: a finite element analysis. *Proc. Inst. Mech. Eng. [H]* **235**(5), 493–499 (2021)

Chapter 17

Fatigue Analysis of FRP Laminate Composites



Nitin Johri and Bhaskar Chandra Kandpal

Abstract Fiber reinforced polymer (FRP) laminate composites display anisotropic behaviour on account of alternating phases of fiber and matrix in suitable weight fractions. Recent research has focussed on structural analysis of these composites pertaining to various strengths like tensile, compressive, flexural etc. This paper attempts to estimate fatigue life of these laminated composites on account of fatigue damage calculation using “Miner’s Rule”. Modelling of laminated composites is done in Ansys® Workbench (ACP) as per required weight/volume fraction. The structural response of modelled laminate is done by “Random Vibration Analysis” which utilises the standard deviation (1σ) of a stress, force or displacement to determine fatigue life of the laminated structure. The effect of fiber orientation and thickness of lamina is analyzed on fatigue life of epoxy E-glass laminated composite.

Keywords Fatigue · Standard deviation · FRP · Fiber orientation · Miner’s rule

17.1 Introduction

Degradation of a material’s mechanical properties or a mechanical component subjected to cyclic/intermittent loading is known as fatigue. Analyzing fatigue behaviour of laminated composites is of vital importance. Application of composite materials for commercial means may involve situations involving cyclic load widely, e.g., parts utilized in automobile, mass transit, and heavy vehicles. Comprehending the fatigue behaviour of laminated composites as compared to the determination of elastic stiffness or strength is rather difficult as the application of conventional fatigue approaches, like linear elastic fracture mechanics approach or stress versus cycles curve for laminated composites is not as straightforward. Presence of inherent heterogeneity and anisotropic nature in composites, being the primary reason for this

N. Johri (✉)

ME Department, Graphic Era (Deemed to be) University, Dehradun 248002, India

B. C. Kandpal

ME Department, Inderprastha Engineering College, Ghaziabad 201010, India

complexity. This result in different damage in composites on account of fatigue as compared to conventional materials.

Different damage modes characterizing fracture behaviour of composites with an early onset in fatigue life are fiber fracture, interfacial debonding and delamination, brittle matrix cracking, polymeric matrix crazing, matrix plasticity, multidirectional cracking and void growth. This leads to gradual stiffness loss during fatigue deterioration of a composite laminate. Varying zones of damage [1] formed in a fiber reinforced composite which behaves as anisotropic material and a conventional isotropic material on comparison are shown in Figs. 17.1 and 17.2, respectively.

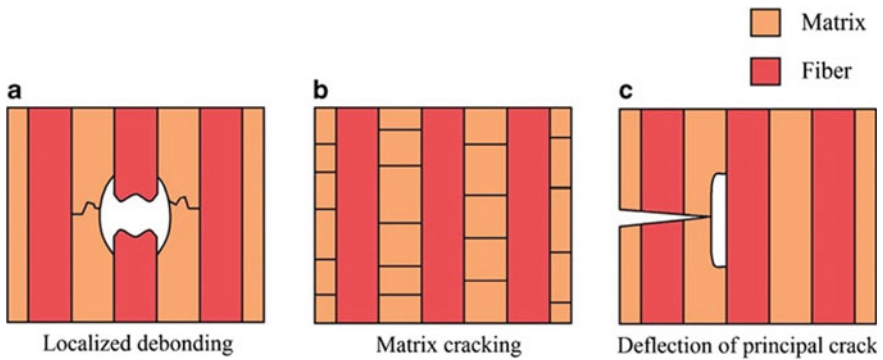
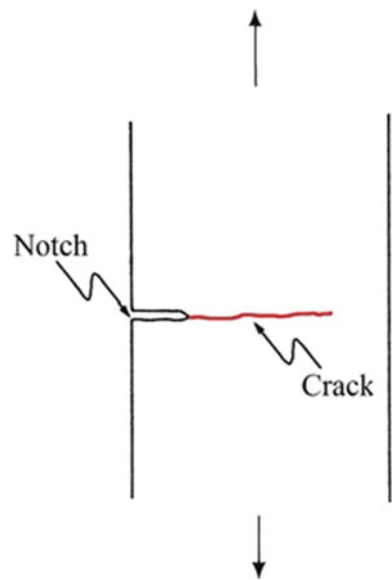


Fig. 17.1 Laminated FRP composite material damage zone: **a** fiber breakage and localized debonding; **b** matrix crack formation; **c** principal crack deflection along a weak fiber/matrix interface [1]

Fig. 17.2 Conventional (isotropic) material damage zone [1]



In case of the isotropic material, the cyclic loading results in initiation of a single crack propagating in a direction transverse to the axis of cyclic loading (mode I) whereas in the fiber reinforced composite (FRP) laminates, various damage mechanisms being subcritical (as shown) leads to a damage zone which is highly diffuse.

Various composite failure modes like delamination, fiber fracture, longitudinal and transverse matrix on account of being subjected to cyclic loading are visible in Fig. 17.3 on account of loading in a longitudinal and cross-ply laminated composite. The fracture of fiber and matrix accompanied by shear crack growth are seen in Fig. 17.4.

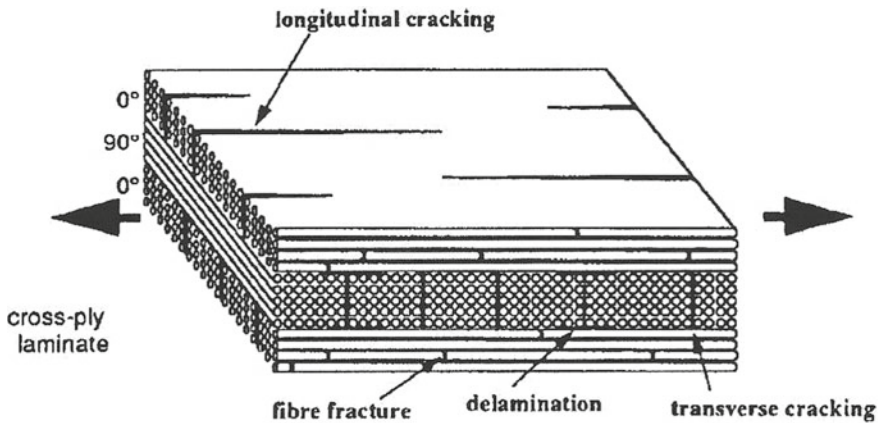


Fig. 17.3 Composite behaviour under cyclic loading [2]

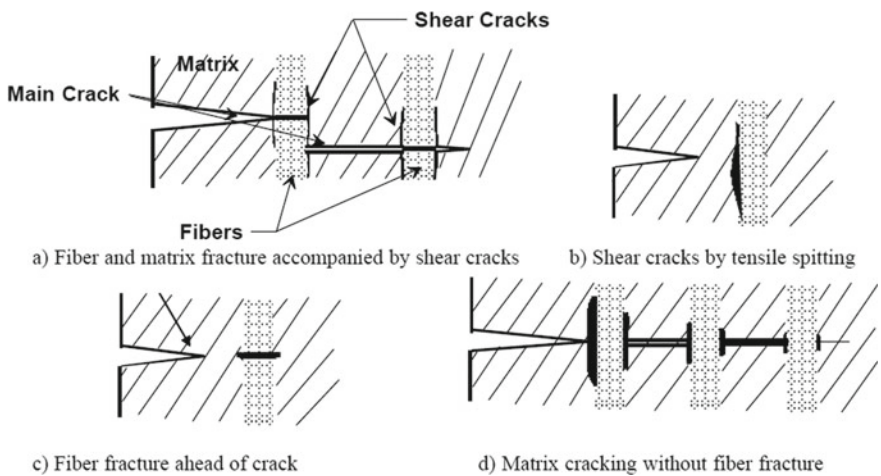


Fig. 17.4 Crack growth in composites subjected to fatigue loads [3]

A relative comparison of various composite failure modes like fiber fracture, delamination, matrix cracking and debonding in terms of stress amplitude versus cycle curve is seen in Fig. 17.5. This implies the fiber fracture being least affected, whereas fiber-matrix debonding being highly affected by fatigue loads.

Fiber orientation effect on fatigue failure in cross-ply roving and woven roving polymer composites is seen in Fig. 17.6. This emphasizes on highest fatigue resistance by longitudinal (0°) fibers in comparison to other fibers. Figure 17.7, illustrates a relative comparison of fiber volume fraction effect on fatigue damage in

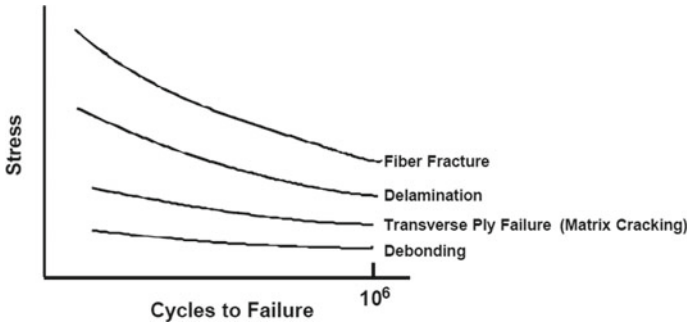


Fig. 17.5 Relative stress amplitude vs cycles curve for fatigue damage modes [3]

Fig. 17.6 Effect of fiber orientation on fatigue damage in polymer composites [3]

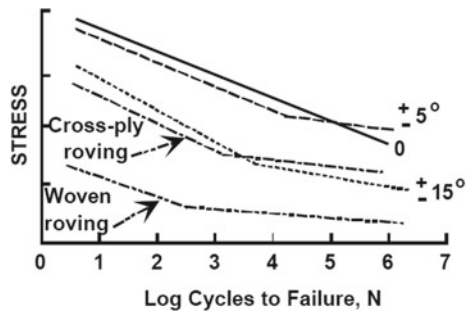
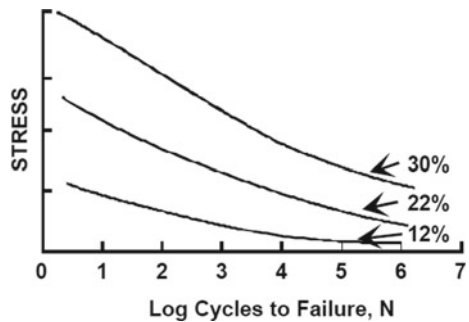


Fig. 17.7 Effect of fiber volume fraction on fatigue damage in polymer composites [3]



polymer composites, emphasizing reduced fatigue damage on account of increased fiber content. Various failure mechanisms like matrix cracking, interfacial debonding, delamination and fiber fracture in terms of percentage of fatigue life are shown in Fig. 17.8. Reduction in fatigue limit strain with increase in fiber orientation from 0° to 90° is shown in Fig. 17.9.

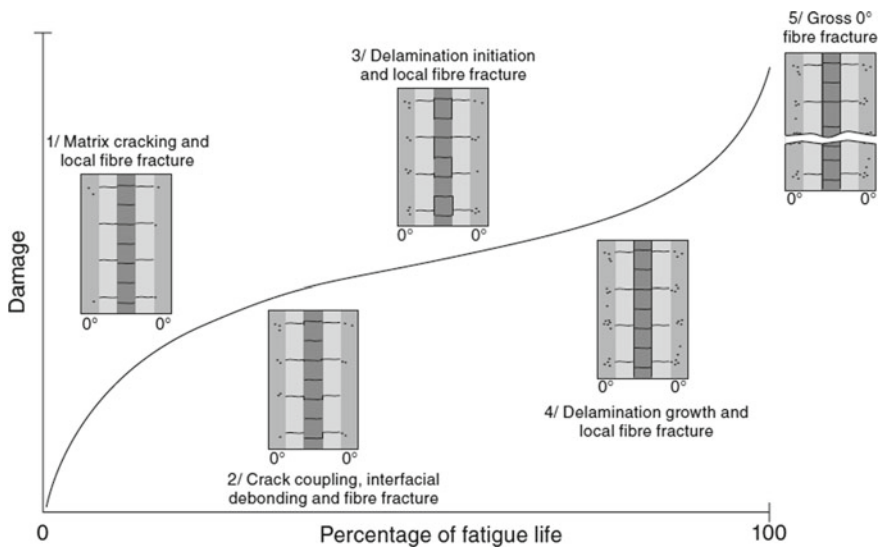


Fig. 17.8 Fatigue damage growth in a composite laminate under transverse loading [4]

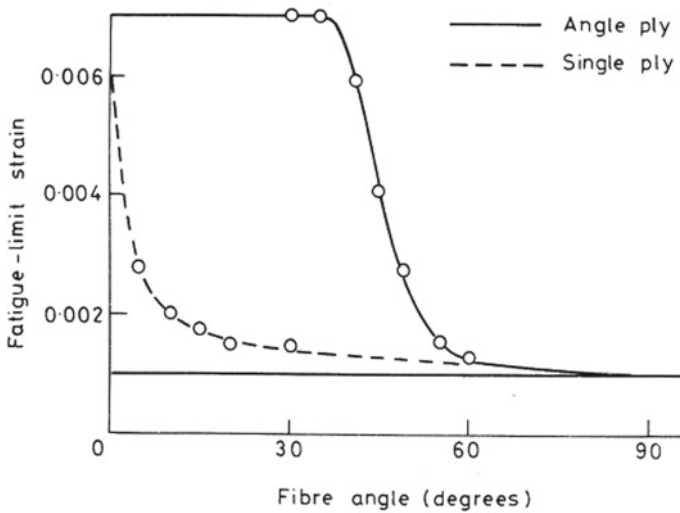


Fig. 17.9 Fiber orientation effect on fatigue limit strain [2]

17.2 Research Background

Ansari et al. [5], explored the effects of various parameters like fiber volume fraction, fiber orientation, fiber type etc. on the fatigue response of fiber-reinforced composites. In composite materials, the various types of fatigue damages are initiated on account of initiation of multiple micro-cracks in the initial stages of the fatigue growth. Fatigue strength is seen to increase with increasing fiber volume fraction till a certain level and then starts decreasing due to insufficient resin to grip the fibers. Fatigue behaviour of laminated composites is based on various factors, e.g., constituent materials, manufacturing process, fiber orientation, and type of loading. Degrieck and Van Paepegem [6], reviewed major fatigue patterns and methodology for life expectancy for fiber-reinforced polymer (FRP) composites subject to fatigue loads is presented. Samples are classified into three main categories: fatigue life models using SN curves and Goodman-type diagrams that take into account the actual attenuation mechanism, with the onset of some fatigue failure criteria, using one or more loss variables. Making progressive damage models related to measurable standards and damage—phenomenological model using transverse matrix cracks, contamination magnitude, etc. and finally residual hardness/strength. Kumar [7], calculated fatigue life of the components exposed to the sinusoidal periodic vibration using random vibration analysis, so that the damage content is analyzed by multiplying the stress amplitude of each cycle in the harmonic analysis by the actual number of cycles components experience in service. The miner's rule is seen to provide a very good assessment considering the complex evaluation of fatigue life in the random process. Irvine [8], utilized band pass filtering method to perform the power spectral density calculation in terms of (G^2/Hz) for the calculation of power spectral density functions, which can be used appropriately in random vibration analysis.

Belmonte et al. [9], investigated the effect of volume fraction of fiber on the fatigue deterioration mechanism in a small glass fiber reinforced polyamide composite. Tests for uniaxial fatigue were performed with different fiber content on the notched specimens. Field emission scanning electron microscopy has been performed for damage investigation. Mortazavian and Fatemi [10], assessed the mean stress effect on fatigue behaviour of two small glass fibers reinforced thermoplastic composites and stress concentration effect on the fatigue behaviour of an unreinforced and small glass fiber reinforced thermoplastics by experimental study. Several mean pressure parameters have been used to evaluate the ability to interact with average pressure data, including the revised Goodman, Walker, and Smith-Watson-Topper evaluation. Significance of effect of stress concentration was seen to be high with or without application of pressure in longitudinal as well as transverse directions. Vasiukov et al. [11], developed a method involving direct computation of life estimation for fiber reinforced polymers (FRP). This follows simplified direct method (SDM) approach, which allows estimation of life from a stabilized damage condition. Experimental verification of the method with different load ratios on standard fiberglass, angle ply and cross ply

laminate plates with fatigue loads was done. The effects of tension and compression load types and applied mean stress and quasi-static stress in testing of fatigue on damage mechanisms and mechanical behaviour in unidirectional carbon/epoxy laminates were studied in Brunbauer and Pinter [12], in addition with effect of fiber volume content.

Effect of fiber volume fraction on fatigue behaviour of carbon/epoxy laminate is investigated in Brunbauer et al. [13]. Unidirectional carbon/epoxy fiber and epoxy resin samples with varying fiber volume fractions were tested under tension-tension and quasi-static tensile fatigue loads. The results confirm the increase in strength and stiffness with increasing fiber content. The fatigue life of glass-fiber reinforced plastic (GFRP) used in wind turbine rotor blades is estimated by considering the fiber orientations in Huh et al. [14]. Fatigue limits were estimated and predicted for composites with linear Goodman and Gerber diagrams. The fatigue behaviour of GFRP alloys produced by the vacuum bagging process is evaluated by changing the fiber volume fraction by Mini et al. [15]. The constant-amplitude flexural fatigue tests were performed at zero mean stress, by variation in the frequency of the test machine.

The fatigue behaviour of various fiber reinforced polymer composites comprising fibers such as carbon, glass and basalt fibers, including hybrid such as carbon/glass and carbon/basalt is studied in Wu et al. [16]. Results suggest that progressive damage propagation can lead to fatigue failure of composites and that hybrid alloys of carbon/basalt significantly improve fatigue resistance compared to homogeneous basalt composites. Suppressed matrix cracking and a low crack propagation rate were observed in the hybrid-epoxy matrix, resulting on account of various toughening micro mechanisms induced by both rubber micro particles and silica nano particles. These factors are thought to contribute to a better fatigue life using the GFRP composite hybrid-epoxy matrix in Manjunatha et al. [17].

Fiber orientation distribution effect on the thickness of the specimen in determining the fatigue resistance of small glass fiber reinforced polyamide composites was investigated in Bernasconi et al. [18]. Stinchcomb and Bakis [19], presented the mechanics of stress redistribution on account of structural damage in the context of experimental evidence. The fatigue behaviour of many composite material systems in terms of strength, stiffness and life of composite laminates, both notched and without notch under different loading modes, are discussed.

The literature reviewed has largely focussed on damage assessment due to fatigue failure resulting due to cyclic repetitive loads. The vibrations caused due to lack of straightforward cyclic repetition can also lead to these types of failure and requires further research.

17.3 Research Methods

Fatigue analysis of a laminated composite Epoxy E-Glass with unidirectional fibers with a fiber volume fraction of around 50% is attempted with E-Glass fibers

as reinforcement and Resin Epoxy as matrix of Fiber reinforced polymer (FRP) composite. The methodology comprises of: creating composite tensile specimens with different ply thickness and ply orientation configurations (as per Table 17.1) in Ansys Workbench®, importing Composite model into modal analysis, finding mode shapes, applying boundary conditions and finally determining the fatigue behaviour of composite tensile specimen.

Modelling of a tensile test specimen as shown in (Fig. 17.10), is done using design modeller of Ansys Workbench®. Meshing of specimen is done taking ‘Quadrilateral Elements’ with an element size of 2 mm (Fig. 17.11). In setup mode of Ansys Composite Prepost (ACP) module, for a laminate for a constant thickness of 3 mm, the fabric for lamina is defined as “Epoxy E-Glass UD” with ply thickness as stipulated in (Table 17.1). Solid model (Fig. 17.12) of laminate is made by proper configuration of laminates as per the specified ply thickness and orientation. Fatigue Analysis

Table 17.1 Fatigue analysis of fiber reinforced polymer composite laminate

Ply orientation (all plies)	Ply thickness = 0.1 mm (30 plies)	Ply thickness = 0.3 mm (10 plies)	Ply thickness = 0.5 mm (6 plies)
	Fatigue life (days)	Fatigue life (days)	Fatigue life (days)
0	6.84	6.85	6.86
30	0	0	0
0/30	0.01	0.01	0.01
30/0	0.01	0.01	0.01
45	0	0	0
0/45	2.4	2.76	3.13
45/0	2.4	2.76	3.13
60	0.12	0.12	0.12
0/60	2.1	2.43	2.78
60/0	2.1	2.43	2.78
90	191.6	191.09	190.1
0/90	2.07	2.4	2.76
90/0	2.07	2.4	2.76

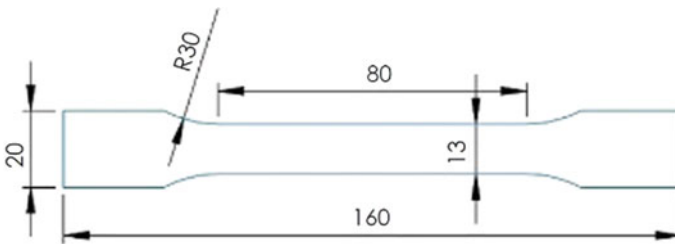


Fig. 17.10 Tensile test specimen

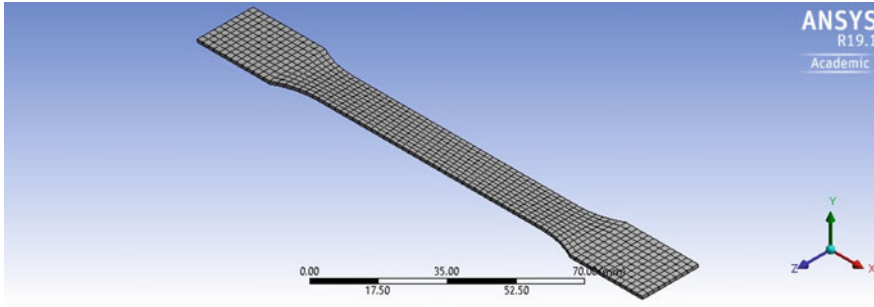


Fig. 17.11 Face meshed quadrilateral elements

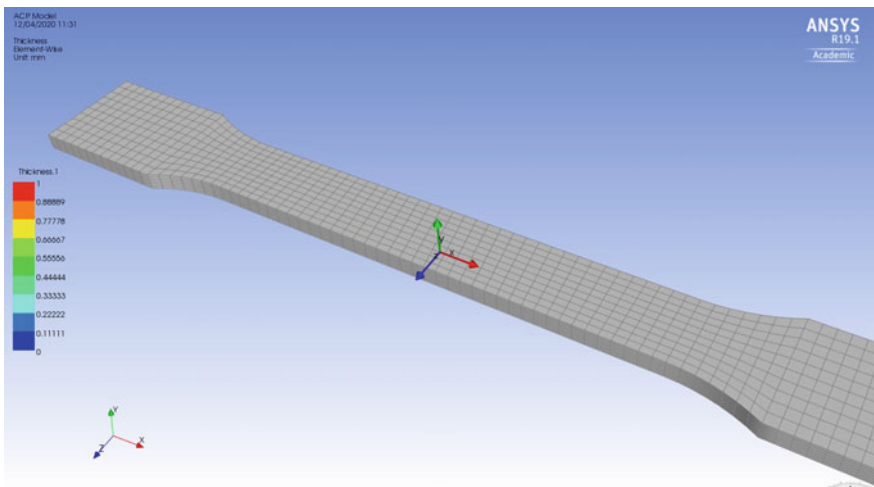


Fig. 17.12 Solid model of FRP composite laminate

of laminates on basis of ply thickness and ply orientation is done and analyzed using Miner’s fatigue damage criteria. Modal Analysis followed by random vibration analysis in Ansys Workbench® [7, 8] is employed for determining and comparing the fatigue life of the various FRP Composite laminates configurations.

17.3.1 Miner’s Fatigue Damage Criteria:

The stress amplitude (σ) versus cycles to failure (N) are shown on a logarithmic S-N curve, where these are related as:

$$\log \sigma = A \log N + B \tag{17.1}$$

Here 'A' refers to slope of the log—log S-N Curve and 'B' is the coefficient which refers to value of stress amplitude σ at $N = 1$ cycle.

As per Miner's fatigue damage criteria, the damage due to cyclic stresses resulting in fatigue failure in a mechanical component is given by:

$$D = \left(\frac{n_{1\sigma}}{N_{1\sigma}} + \frac{n_{2\sigma}}{N_{2\sigma}} + \frac{n_{3\sigma}}{N_{3\sigma}} \right) \quad (17.2)$$

Here

- $n_{1\sigma}$ actual no. of cycles at or below the 1σ level
- $n_{2\sigma}$ actual no. of cycles between 1σ and 2σ level
- $n_{3\sigma}$ actual no. of cycles between 2σ and 3σ level.

And $N_{1\sigma}, N_{2\sigma}, N_{3\sigma} =$ allowable number of cycles (from fatigue curve) at $1\sigma, 2\sigma, 3\sigma$ stress levels.

The values of $n_{1\sigma}, n_{2\sigma}$ and $n_{3\sigma}$ are obtained for $1\sigma, 2\sigma$ and 3σ levels respectively as:

$$\frac{1 \left(\text{Direction velocity in maximum node} \left(\frac{\text{mm}}{\text{s}} \right) \right)}{2\pi \left(\text{Directional deformation in maximum node} (\text{mm}) \right)} \quad (17.3)$$

In statistics the band of equivalent stress amplitude on account of modal analysis can be considered spread about mean value as $1\sigma, 2\sigma$ and 3σ (σ -Standard deviation) corresponding to the occurrence level as 68.3%, 27.2% and 4% respectively. Random vibration analysis is a spectral method which using results from modal analysis can determine some statistical properties of a structural response like standard deviation (1σ) of a displacement, force or stress. In this analysis standard deviation (1σ) is used to determine the fatigue life of structure.

17.4 Result Discussion

A comparative analysis of various laminate configurations of Epoxy-E Glass unidirectional laminate for fatigue life is done on basis of ply orientation, ply thickness and number of plies (Fig. 17.13). Following points can be inferred from the graph:

- The fiber orientation which can sustain fatigue for the longest duration is $[90]^\circ$ with a fatigue life of around 191 days.
- The fatigue life is increased hugely while changing the fiber orientation from $[60]^\circ$ to $[90]^\circ$ with variation being 0.12 days to 191 days.
- The fiber orientations which cannot sustain cyclic/intermittent loads leading to fatigue failure are $[30]^\circ$ and $[45]^\circ$ with a fatigue life of 0 days.
- Plies with fiber orientations of $[60]^\circ, [0/30]^\circ$ and $[30/0]^\circ$ are also having very weak response to fatigue with fatigue life of 0.12, and 0.01 days respectively.

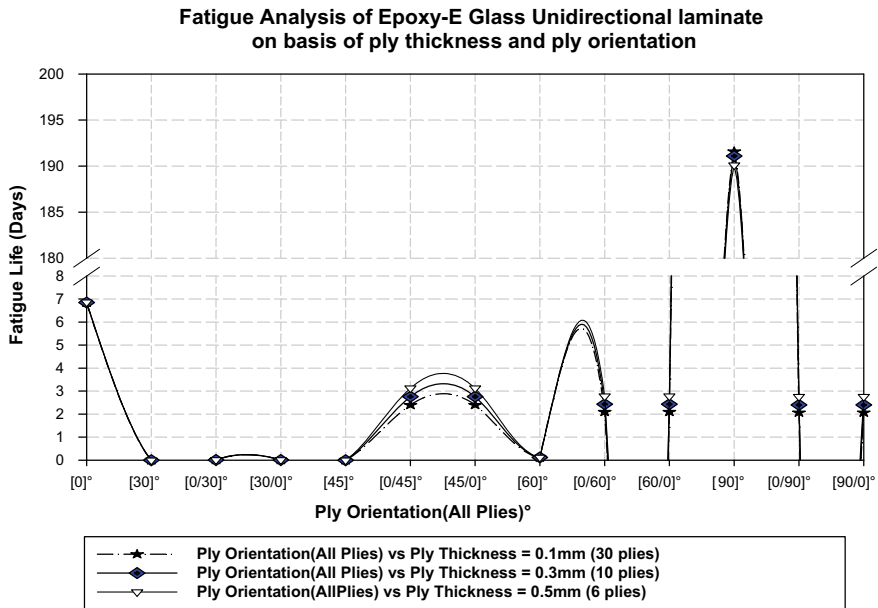


Fig. 17.13 Fatigue analysis of Epoxy-E Glass unidirectional laminate on basis of ply thickness and ply orientation

- Fatigue life is not affected by reversing the ply orientations in consecutive plies for e.g. $[0/45]^\circ$ to $[45/0]^\circ$
- For cross-ply laminate $[90]^\circ$ configuration, the increased number of plies seems to have a favourable effect on fatigue life.
- For ply configurations— $[0/45]^\circ$, $[0/60]^\circ$ and $[0/90]^\circ$ the reduced number of plies will have a favourable response to fatigue loads.
- For other ply configurations— $[0]^\circ$, $[0/30]^\circ$, $[45]^\circ$ and $[60]^\circ$ the response to fatigue failure seems not to be affected by increasing/decreasing number of plies/lamina.

17.5 Conclusion

Fatigue loads are responsible for unexpected failure of a wide variety of materials, which can fail at stresses well below the yield stress owing to cyclic/intermittent nature of these loads. Composite materials owing to their anisotropic nature responds to fatigue in a different way as compared to structures made from normal materials like steel, aluminium, copper etc. which behave in a isotropic manner. A modelling and simulation of a type of FRP composite laminate is suggested in Ansys Workbench® using Miner's fatigue damage criteria for prediction of fatigue life.

Fatigue analysis of FRP composite laminate subjected to cyclic loads is attempted with some important conclusions emphasizing the effect of fiber orientation in ply on

fatigue life. As per the simulation results the longitudinal plies with fiber orientation of 0° though good for static tensile or compressive loading are having extremely low fatigue resistance as compared to cross ply laminates with a ply fiber orientation of 90° . Also, the fatigue life is not affected by reversing the fiber orientation in a stackup for e.g. changing the fiber orientation of plies from $[0/30]^\circ$ to $[30/0]^\circ$ and vice versa.

Acknowledgements The authors acknowledge the support of the Coordination Committee of Scientific Research Projects of Mechanical Engineering Department, “Graphic Era (Deemed to be) University”, Dehradun, and “Inderprastha Engineering College”, Ghaziabad, India.

References

1. Chawla, K.K.: *Composite Materials: Science and Engineering*, 3rd edn (2012)
2. Bucinell, R.B.: *Composite Materials: Fatigue and Fracture*, vol. 7 (1998)
3. Salkind, M.: *Fatigue of Composites* (2009)
4. Hiley, M.: *Fatigue Failures of Polymer Composites* (2009)
5. Ansari, M.T.A., Singh, K.K., Azam, M.S.: Fatigue damage analysis of fiber-reinforced polymer composites—a review. *J. Reinf. Plast. Compos.* **37**, 636–654 (2018)
6. Degrieck, J., Van Paeppegem, W.: Fatigue damage modeling of fiber-reinforced composite materials: review. *Appl. Mech. Rev.* **54**, 279–300 (2001)
7. Kumar, S.M.: Analyzing random vibration fatigue. *ANSYS Adv.* **II**, 39–42 (2008)
8. Irvine, T.: Power Spectral Density Units: $[G^2/Hz]$ *Vibrationdata.com* [Online] (2007). Available: <https://vibrationdata.com/tutorials2/psd.pdf>
9. Belmonte, E., De Monte, M., Hoffmann, C.J., Quaresimin, M.: Damage initiation and evolution in short fiber reinforced polyamide under fatigue loading: influence of fiber volume fraction. *Compos. Part B Eng.* **113**, 331–341 (2017)
10. Mortazavian, S., Fatemi, A.: Effects of mean stress and stress concentration on fatigue behavior of short fiber reinforced polymer composites. *Fatigue Fract. Eng. Mater. Struct.* **39**, 149–166 (2016)
11. Vasiukov, D., Panier, S., Hachemi, A.: Direct method for life prediction of fiber reinforced polymer composites based on kinematic of damage potential. *Int. J. Fatigue* **70**, 289–296 (2015)
12. Brunbauer, J., Pinter, G.: Effects of mean stress and fiber volume content on the fatigue-induced damage mechanisms in CFRP. *Int. J. Fatigue* **75**, 28–38 (2015)
13. Brunbauer, J., Stadler, H., Pinter, G.: Mechanical properties, fatigue damage and microstructure of carbon/epoxy laminates depending on fiber volume content. *Int. J. Fatigue* **70**, 85–92 (2015)
14. Huh, Y.H., Lee, J.H., Kim, D.J., Lee, Y.S.: Effect of stress ratio on fatigue life of GFRP composites for WT blade. *J. Mech. Sci. Technol.* **26**, 2117–2120 (2012)
15. Mini, K.M., Lakshmanan, M., Mathew, L., Mukundan, M.: Effect of fiber volume fraction on fatigue behaviour of glass fiber reinforced composite. *Fatigue Fract. Eng. Mater. Struct.* **35**, 1160–1166 (2012)
16. Wu, Z., Wang, X., Iwashita, K., Sasaki, T., Hamaguchi, Y.: Tensile fatigue behaviour of FRP and hybrid FRP sheets. *Compos. Part B Eng.* **41**, 396–402 (2010)
17. Manjunatha, C.M., Sprenger, S., Taylor, A.C., Kinloch, A.J.: The tensile fatigue behavior of a glass-fiber reinforced plastic composite using a hybrid-toughened epoxy matrix. *J. Compos. Mater.* **44**, 2095–2109 (2010)
18. Bernasconi, A., Davoli, P., Basile, A., Filippi, A.: Effect of fiber orientation on the fatigue behaviour of a short glass fiber reinforced polyamide-6. *Int. J. Fatigue* **29**, 199–208 (2007)
19. Stinchcomb, W.W., Bakis, C.E.: *Fatigue Behavior of Composite Laminates*, vol. 4 (1991)

Chapter 18

Performance Enhancement of Electro-chemical Discharge Machining by Process Variants: A Review



Pankaj Kumar Gupta, Tapas Bajpai, Nikhil Jain, and Dharmendra Singh

Abstract Electro-Chemical Discharge Machining (ECDM) process has shown its potential over the other thermal and chemical energy based non-conventional methods due to its better capability in micro-feature generation on nonconductive, hard and brittle materials such as glass and ceramics. In this article, a comprehensive review had been carried out on different process variants which were used to enhance the process capability of ECDM. The process variants were classified into two groups based on level of hybridization or modification in the conventional ECDM. These variants were termed as primary and secondary variants. The article consists review of various process variants such as Electro-Chemical Discharge Trepanning (ECDTr), Electro-Chemical Discharge Dressing (ECDDr), Electro-Chemical Discharge Turning (ECDT), Die Sinking Electro-Chemical Discharge Machining (DS-ECDM), Wire Electro-Chemical Discharge Machining (W-ECDM), Electro-Chemical Discharge Milling (ECDMi), Powder Mixed Electro-Chemical Discharge Machining (PM-ECDM), Rotary Electro-Chemical Discharge Machining (R-ECDM), Electro Chemical Discharge Grinding (ECDG), Magnetic Field assisted Electro-Chemical Discharge Machining (MF-ECDM) Ultrasonic assisted Electro-Chemical Discharge Machining (US-ECDM), etc. These variants were used to enhance performance of ECDM in various aspects such as material removal rate, machining depth, surface quality, aspect ratio etc. In the end a possible multi-hybridization process variant has been proposed by combining of magnetic field and ultrasonic vibration assistances in ECDM.

Keywords ECDM · Process variant · Hybridization · Performance enhancement

P. K. Gupta (✉) · T. Bajpai · N. Jain

Department of Mechanical Engineering, Malaviya National Institute of Technology Jaipur, Jaipur, Rajasthan, India

e-mail: pankaj.mech@mnit.ac.in

D. Singh

Department of Mechanical Engineering, Government Engineering College Bikaner, Bikaner, Rajasthan, India

18.1 Introduction

In recent years, a lot of research had focused on advance materials due to their enhanced physical and chemical properties. These advance materials had shown their utility in the field of aerospace [1], medical [2] and in many other industrial applications [3]. The fabrications of micro-features on such materials are difficult with the use of unconventional machining methods. Electrical Discharge Machining (EDM), Laser Beam Machining (LBM) and Plasma Arc Machining (PAM). Electro-Chemical Discharge Machining (ECDM) had been emerged out as a possible solution to create micro features on advance materials such as glass and ceramics regardless of their properties. ECDM process has good capability to create micro-feature on glass [4], ceramics [5] and composite materials [6]. ECDM process is a hybrid machining process and uses the principles of ECM and EDM process [7]. ECDM process removes the material by chemical dissolution and melting [8, 9]. In ECDM process, tool electrode is partially immersed up to few millimetres in the electrolyte solution while the auxiliary anode is fully submerged in the electrolyte solution and situated at some distance away from the tool electrode [10]. The work-piece is suitably placed in the electrolyte chamber with the proper fixture on the worktable arrangement. The potential difference of about 50–60 V is used between electrodes through a suitable DC power supply [11] as shown in Fig. 18.1. The electrolysis process is occurred between two electrodes. Hydrogen and oxygen bubbles are formed at the surface of cathode and anode surface respectively [12]. However, after a certain time the generation rate of the hydrogen gas bubble near the tool electrode increases more rapidly and hydrogen gas film formed in the vicinity of the tool electrode [13]. The gas film behaves as an insulator. It ceases the flow of current and intensified the electric field around the tool electrode which results in arc discharge [12]. The bombardment of electrons from the tool electrode results in the melting of the work-piece [14, 15] and followed by subsequent high-temperature etching that removes the material. Basak and Ghosh [16] proposed a new mechanism of spark generation in the ECDM

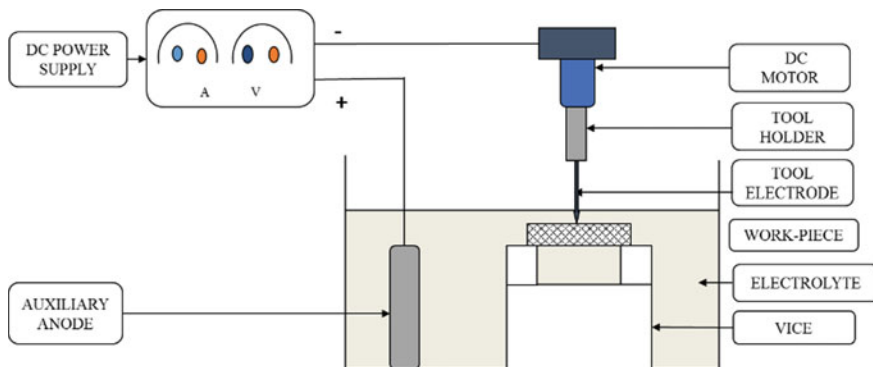


Fig. 18.1 Schematic diagram of ECDM set-up

process. It was found that the discharge location at the tool changes continuously with the period.

18.2 ECDM Variants

ECDM process has gained immense attention of several researchers due to its better capability in fabrication of micro-channel [17], micro-grooves [18], channel engraving and cylindrical hole [19]. ECDM process possess several limitations like overcut, hole taper, circulation of electrolyte in machining zone after certain depth [20] and poor MRR. In order to overcome above draw backs some change in process and experimental set-up are created. These modification or hybridizations are known as variants. The variants can be classified into two groups. The variants which include minor or major modification in existing system component of ECDM are classified as primary variants. On the other hand, the variants which include addition of other process mechanism while keeping existing system components intact are classified as secondary variants. Different types of variants are shown in Fig 18.2 according to their category.

18.2.1 Electro-chemical Discharge Trepanning (ECDTr)

In the ECDM process the drilling depth was difficult to control. Most of the heat evolved during increase in drilling depth is transferred to the electrolyte and only a small portion of heat conducted in the material. To overcome this limitation, ECDTr had been used as an alternative to achieve large drilling depth. In ECDTr process, the tool is offset by a small amount from the spindle rotation axis [21]. The orbital motion of the tool assists in the formation of a deep hole. However, crack propagation

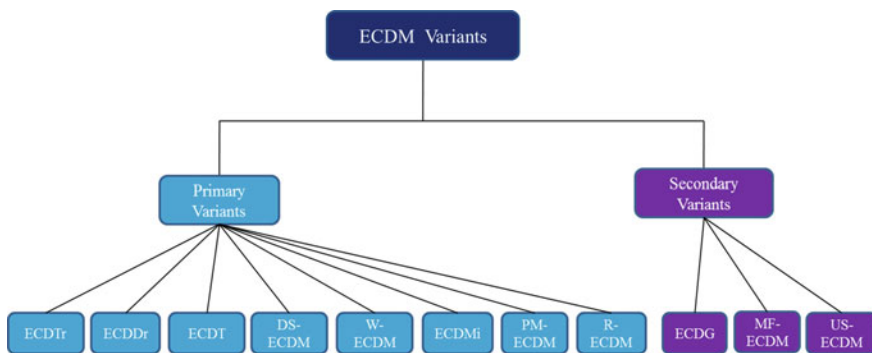


Fig. 18.2 Types of ECDM variants

in the material after achieving a certain depth diminishes the efficiency of the process [22]. To overcome the above drawbacks, [23] explored the effect of the abrasive tool electrode and pulsed power supply during ECDDr process. The abrading action of the abrasive particle helped in material removal with an increase in drilling depth. The pulsed power supply provides sufficient cooling around the work-piece during the pulse off period. Thus, it helped in improving the drilling depth and surface quality.

18.2.2 Electro-chemical Discharge Dressing (ECDDr)

ECDDr was used as an alternative for the efficient dressing of worn micro-grinding tool. The conventional method for dressing is grinding and rolling with the use of ultra-hard dresser. These methods are not very effective. In ECDDr, the electrolyte behaves as a dresser. The electrolysis process occurred between the micro-grinding tool and auxiliary anode. The grains protruded during the dressing do not damage the grinding face of the tool. Therefore, significant improvement in surface quality was observed [24].

18.2.3 Electro-chemical Discharge Turning (ECDT)

ECDT is a unique process variant to achieve deep grooves on cylindrical parts with the rotation of the work-piece. The remnants attached at the bottom of the tool electrode diminish the machining efficiency and restrict the electrolyte circulation in a deeper zone of machining. The rotation of the work-piece ensures the supply of fresh electrolyte in the narrower gap between tool and work-piece. Therefore, significant improvement in the debris removal was achieved, which leads to an increase in the machining depth. However, at a very high rotational speed, the stability of gas film was destroyed and a subsequent drop in the MRR was observed [25].

18.2.4 Die Sinking Electro-chemical Discharge Machining (DS-ECDM)

DS-ECDM process was used for the fabrication of a small shallow cavity with the use of a non-rotating tool. In DS-ECDM operation, the melted work-piece material re-solidified on the work-piece surface [26]. Therefore, efficient flushing of electrolyte was the major concern in the DS-ECDM process. The electrolyte concentration and duty factor were the most influencing parameters to get higher MRR during the DS-ECDM process [26]. An increase in the electrolyte concentration accelerates the electrolysis process, which leads to an increase in the MRR. However, beyond a

certain limit further increase in electrolyte concentration caused a decrease in the specific conductance of electrolyte, which leads to decrease in MRR. An increase in the duty factor ensures more amount of spark energy available for a longer period, which leads to an increase in the MRR.

18.2.5 Wire Electro-Chemical Discharge Machining (W-ECDM)

W-ECDM process was used for slicing large volumes of material during the fabrication of micro-grooves and other complicated surface profiles on non-conductive materials. The wire electrode behaves as a cutting tool and feeds toward the workpiece with the help of feed spool, takes up spool, pulley and stepper motor. Bhuyan and Yadva [27] explored the effect of pulse on-time and applied voltage on MRR and kerf width during the Travelling Wire ECDM (TW-ECDM) process. It was found that an increase in pulse on time and applied voltage increased the MRR and Kerf width due to more spark energy available for discharge. Yang et al. [28] explored the effect of mixing of SiC abrasive particles into the electrolyte on overcut and surface quality during the TW-ECDM process. It was observed that abrasive particles caused a significant increase in the critical voltage of the process and decrease in discharge energy. Thus, a significant reduction in the overcut was observed. The abrasive particles induced a lapping action in the process due to their relative motion. Thus, it helped in refining the micro-crack. Therefore, surface quality was improved.

18.2.6 Electro-chemical Discharge Milling (ECDMi)

ECDMi process was used to create 3D shaped profile structures, micro-grooves [29], micro-pyramid and micro-channel [30]. The rotating cylindrical shape wheel was used as a cutting tool. The tool travel rate and tool rotation rate played a major role in achieving a good quality surface profile. It was observed that higher tool rotation helped in electrolyte circulation which leads to the formation of a sharp edge micro-groove profile. An increase in the tool travel rate leads to increased depth of cut during formation of shallow micro-grooves. In order to achieve a good surface profile of micro-grooves, the material was removed layer by layer with very low depth of cut. This mechanism of material removal caused electrolyte flushing at deeper and narrower grooves. Thus, the surface quality of the micro-grooves was improved.

18.2.7 Powder Mixed Electro-chemical Discharge Machining (PM-ECDM)

In the PM-ECDM process the distribution of discharge energy around the machining zone plays a vital role to affect surface integrity and process repeatability. The addition of conductive powder particles assists in reducing the critical voltage and reduces the impact of discharge energy around the surface of the work-piece. Han et al. [31] used graphite powder mixed electrolyte. It was found that the addition of abrasive particles caused the intensification of the electric field around the tool electrode. The dynamic behaviour of particles helped in reducing the current density. Thus, surface quality was improved.

18.2.8 Rotary Electro-chemical Discharge Machining (R-ECDM)

In R-ECDM process rotary motion was provided to the tool with the help of DC motor. In R-ECDM process a gap was maintained between rotary tool electrode and work-piece. The rotary tool was positioned at the depth of cut while the work-piece is feed with constant velocity. The machining area was divided between Electro-chemical dissolution zone and electro-chemical discharge zone. The surface irregularity and cracks formed during the electric discharge process were removed by the electro-chemical dissolution. Therefore, this method was used to obtain crack-free smooth surface [32]. Harugade et al. [33] explored the effect of high speed tool rotation on overcut and hole taper during ECDM process. The high speed tool rotation assisted in reducing the contact area between the tool and work-piece. Moreover, better electrolyte circulation improved the heat conduction throughout the work-piece. Thus, considerable reduction in the overcut and hole taper were observed.

18.2.9 Electro-chemical Discharge Grinding (ECDG)

ECDG process was used to remove material by mechanical abrasion along with the assistance of ECDM principle. The abrasive particle embedded on rotary tool behaves as a grinding wheel [34]. The metallic bond is situated in between the abrasive particle layers. The metallic bond created spark while the abrasive particle induced cutting action during the ECDG process. In ECDG, the contact area between the tool and work-piece surface was kept very low so that the maximum abrasion was achieved by abrasive particles attached on tool. The abrasive particle provided maximum cutting action during the process which leads to increase in MRR. ECDG process was used to obtain micro-holes on alumina and borosilicate glass materials [35].

18.2.10 Magnetic Field Assisted Electro-chemical Discharge Machining (MF-ECDM)

In the MF-ECDM process, a permanent magnet was fixed at the tool holder. It caused upward and downward magnetic field action on the tool during the ECDM process. The magneto-hydrodynamic convection was induced in the process due to the magnetic field. The magneto-hydrodynamic convection helped in improving the electrolyte circulation. Thus, the machining efficiency of the process was improved [36]. Rattan and Mulik [37] studied the effect of the magnetic field on overcut and hole taper during the TW-ECDM process. It was found that magnetic field assistance helped in the removal of debris in the vicinity of the tool and work-piece. Moreover, the stable discharge during MF-ECDM increased the process efficiency. Therefore, the hole taper and overcut were significantly reduced in the case of the MF-ECDM process.

18.2.11 Ultra-sonic Assisted Electro-chemical Discharge Machining (US-ECDM)

The US-ECDM process consists of an ultrasonic generator and transducer to impart vibration to the tool. The ultrasonic assistance in the ECDM process provides the drag force on the bubbles. The drag force helps in thinner gas film formation. Thin gas film imparts small discharge and small micro-holes with good dimensional accuracy [38]. Rusli and Furtani [39] explored the effect of ultrasonic vibration and electrolyte level on MRR during ECDM process. At low electrolyte level the ultrasonic vibration improves the electrolyte circulation. Thus, the MRR was increased.

A summary of researchers who have worked on different ECDM process variant to improve the surface quality, MRR and dimensional accuracy for micro feature generation on non-conductive materials like glass, composite and ceramics is given in Table 18.1.

18.3 Proposed ECDM Variant

Characteristics of different process variants are studied to improve the performance of the ECDM process. A different type of process variants can be proposed based on the characteristics in preceding section. In this article, a variant is proposed by combining the ultrasonic assistance with magnetic field assistance which is shown in Fig 18.3 and named as Magnetic Field and Ultra Sonic assisted ECDM (MF-US-ECDM). The magnetic unit is attached to the tool holder and the tool is vibrated with the help of the transducer. The ultrasonic assistance increases the drag force on the bubbles and helps in the formation of the thinner gas film. The magnetic

Table 18.1 Summary of different type of process variants

S.No.	Author name	Process variant	Performance enhancement in term of
1	Pawariya et al. [21], Chak and Rao [23]	ECDDr	Drilling depth and surface quality
2	Wei et al. [24]	ECDDr	Surface quality
3	Furutani and Maeda [25]	ECDDr	Machining depth
4	Khairy and Mc-Geough [26]	DS-ECDDr	MRR
5	Bhuyan and Yadava [27], Yang et al. [28]	W-ECDDr/TW-ECDDr	Surface quality and MRR
6	Kuo et al. [29], Didar et al. [30]	ECDDr	Surface quality
7	Han et al. [31]	PM-ECDDr	Surface quality
8	Kozak and Zyburka [32], Harugade et al. [33]	R-ECDDr	Surface quality, dimensional accuracy
9	Chak and Rao [34], Jain et al. [35]	ECDDr	MRR
10	Cheng et al. [36], Rattan and Mulik [37]	MF-ECDDr	Machining efficiency and dimensional accuracy
11	Elhami and Razfar [38], Rusli and Furtani [39]	US-ECDDr	MRR and dimensional accuracy

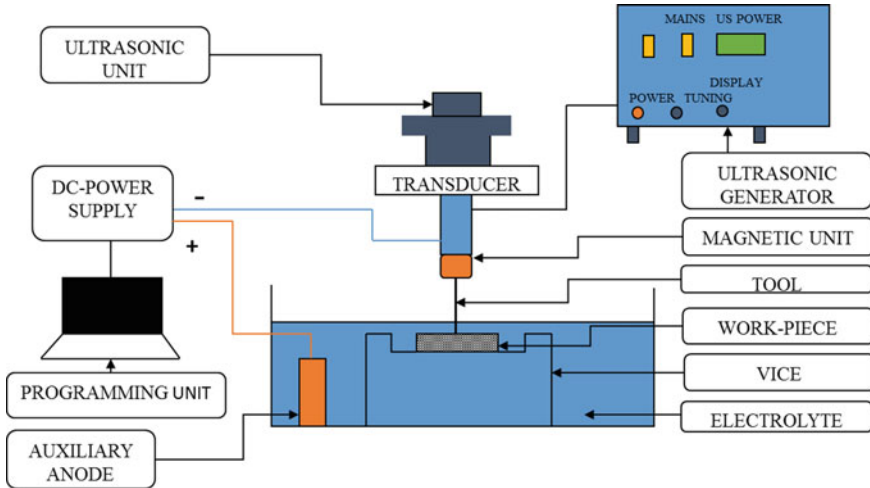


Fig. 18.3 Schematic diagram of MF-US-ECDDr set-up

field assistance caused magneto-hydrodynamic convection in the process. Thus, it helps in concentrating the spark around the machining zone. Therefore, MRR and dimensional accuracy may be improved.

18.4 Conclusion

A comprehensive literature review on different process variants results in following conclusions:

ECDTr is an emerging method for deep hole formation on alumina and quartz. ECDDr was used for dressing of worn micro-grinding tools. Thus, ECDDr was used to improve the surface quality. ECDDT involves the rotation of the work-piece. Therefore, fresh electrolyte removes the debris and deeper depth of cut was achieved. DS-ECDDM was proved as an efficient process variant for the small cavity formation and higher MRR was attained. W-ECDDM was used for slicing while TW-ECDDM achieved higher MRR. ECDDMi was very useful variant for fabrication of 3 D shaped structures. PM-ECDDM was an effective approach to attain good surface quality during micro-feature generation. MF-ECDDM improved the electrolyte circulation which results in lesser overcut and hole taper. US-ECDDM develops thinner gas film formation which leads to better dimensional accuracy and higher MRR. A proposed variant MF-US-ECDDM can be used to obtain advantages of individual process variant.

References

1. Ranganayakulu, J., Srihari, P.V.: Multi-objective optimization using Taguchi's loss function-based principal component analysis in electro-chemical discharge machining of micro-channels on borosilicate glass with direct and hybrid electrolytes. In: *Advances in Manufacturing Processes, Lecture Notes in Mechanical Engineering*, 349–60 (2018)
2. Jawalkar, C.S., Sharma, A.K., Kumar, P.: Investigations on performance of electro-chemical discharge machining process using NaOH and NaNO₃ electrolytes while micro machining soda lime glass. *Int. J. Manuf. Technol Manage.* **28**(1/2/3), 80–93 (2014)
3. Singh, T., Dvivedi, A.: Developments in electro-chemical discharge machining: a review on electro-chemical discharge machining. *Int. J. Mach. Tool Manuf.* **105**, 1–13 (2016)
4. Arab, J., Kannoja, H.K., Dixit, P.: Effect of tool electrode roughness on the geometric characteristics of through hole formed by ECDM. *Precis. Eng.* **60**, 437–447 (2019)
5. Dhanvijay, M.R., Ahuja, B.B.: Micro-machining of ceramic by electro-chemical discharge process considering stagnant and electrolyte flow method. *Procedia Eng.* **14**, 165–172 (2014)
6. Singh, M., Singh, S.: Machining of carbon fibre reinforced polymer composites by electro-chemical discharge machining process. *IOP Conf. Ser. Mater. Sci. Eng.* **521**, 1–6 (2019)
7. Ghosh, A.: Electro-chemical discharge machining: principle and possibilities. *Sadhana-Acad. Proc. Eng. Sci.* **22**, 435–447 (1997)
8. Gupta, P.K., Dvivedi, A., Kumar, P.: Developments on electro-chemical discharge machining: a review of experimental investigations on tool electrode process parameters. *Proc. Inst. Mech. Eng. Part B J. Eng. Manuf.* **229**, 920–930 (2014)
9. Gupta, P.K., Dvivedi, A., Kumar, P.: Effect of electrolytes on quality characteristics of glass during electro-chemical discharge machining. *Key Eng. Mater.* **658**, 141–145 (2014)

10. McGeough, J.A., Khayry, A.B.M., Munro, W., Crookall, J.R.: Theoretical and experimental investigation of the relative effects of spark erosion and electrochemical dissolution in electrochemical arc machining. *Ann. CIRP* **32**, 1–6 (1983)
11. Jain, V.K., Adhikary, S.: On the mechanism of material removal in electrochemical spark machining of quartz under different polarity conditions. *J. Mater. Process. Technol.* **200**, 460–470 (2008)
12. Gupta, P.K., Dvivedi, A., Kumar, P.: Effect of pulse duration on quality characteristics of blind hole drilled in glass by electro-chemical discharge machining. *Mater. Manuf. Process* **31**, 1740–1748 (2015)
13. Singh, M., Singh, S.: Electro-chemical discharge machining: a review on preceding and perspective research. *Proc. Inst. Mech. Eng. Part B J. Eng. Manuf.* **233**, 1425–1449 (2018)
14. Jain, V.K., Dixit, P.M., Pandey, P.M.: On the analysis of the electrochemical spark machining process. *Int. J. Mach. Tools Manuf* **39**, 165–186 (1999)
15. Kulkarni, A., Sharan, R., Lal, G.K.: An experimental study of discharge mechanism in electro-chemical discharge machining. *Int. J. Mach. Tool Manuf.* **42**, 1121–1127 (2002)
16. Basak, I., Ghosh, A.: Mechanism of spark generation during electro-chemical discharge machining: a theoretical model and experimental verification. *J. Mater. Manuf. Process* **62**, 46–53 (1996)
17. Cao, X.D., Kim, B.H., Chu, C.N.: Micro structuring of glass with feature less than 100 μm by electrochemical discharge machining. *Precision Eng.* **33**, 459–465 (2009)
18. Lu, C.J., Gu, A., Meng, L., Yang, S.Y.: The micro-milling machining of Pyrex glass using the electro-chemical discharge machining process. *Adv. Mater. Res.* **403**, 738–742 (2012)
19. Maillard, P., Despont, B., Bleuler, H., Wutrich, R.: Geometric characterization of micro hole drilled in glass by gravity-feed with spark assisted chemical engraving (SACE). *J. Micromech. Micro Eng.* **17**, 1343–1349 (2007)
20. Jui, S.K., Kamaraj, A.B., Sundaram, M.M.: High aspect ratio micromachining of glass by electrochemical discharge machining (ECDM). *J. Manuf. Process.* **15**, 460–466 (2013)
21. Pawariya, K., Dvivedi, A., Singh, T.: On performance enhancement of electro-chemical discharge trepanning (ECDT) process by sonication of tool electrode. *Precis. Eng.* **56**, 8–19 (2018)
22. Jain, V.K., Chak, S.K.: Electro-chemical spark trepanning of alumina and quartz. *Mach. Sci. Technol.* **4**(2), 277–290 (2000)
23. Chak, S.K., Rao, P.V.: Trepanning of Al_2O_3 by electro-chemical discharge machining (ECDM) process using abrasive electrode with pulsed DC supply. *Int. J. Mach. Tools Manuf.* **47**, 2061–2070 (2007)
24. Wei, C., Hu, D., Xu, K., Ni, J.: Electro-chemical discharge dressing of metal bond micro-grinding tools. *Int. J. Mach. Tools Manuf.* **51**, 165–168 (2011)
25. Furutani, K., Maeda, H.: Machining a glass rod with a lathe-type electro-chemical discharge machine. *J. Micromech. Microeng.* **18**(6), 1–6 (2007)
26. Khairy, A.B.E., McGeough, J.A.: Die-sinking by electro-erosion-dissolution machining. *Ann. CIRP* **39**, 1–5 (1989)
27. Bhuyan, B.K., Yadava, V.: Experimental study of travelling wire electrochemical spark machining of borosilicate glass. *Mater. Manuf. Process.* **29**, 298–304 (2014)
28. Yang, C.T., Song, S.L., Yan, B.H., Huang, F.Y.: Improving machining performance of wire electro-chemical discharge machining by adding SiC abrasive to electrolyte. *Int. J. Mach. Tools Manuf.* **46**, 2046–2050 (2006)
29. Kuo, K.Y., Wu, K.L., Yang, C.K., Yan, B.H.: Wire electrochemical discharge machining (WECDM) of quartz glass with titrated electrolyte flow. *Int. J. Mach. Tool Manuf.* **72**, 50–57 (2013)
30. Didar, T.F., Dolatabadi, A., Wutrich, R.: Characterization and modelling of 2D-glass micro-machining by spark assisted chemical engraving with constant velocity. *J. Micromech. Microeng.* **18**, 1–9 (2008)
31. Han, M.S., Min, B.K., Lee, S.J.: Improvement of surface integrity of electro-chemical discharge machining process using powder-mixed electrolyte. *J. Mater. Process. Technol.* **191**, 224–227 (2007)

32. Kojak, J., Zybur, M.: Mathematical modelling of rotary electro-chemical discharge machining. Proc. World Congr. Eng. Comput. Sci. **2012**, 1–6 (2012)
33. Harugade, M., Waigaonkar, S., Mane, N., Hargude, N.: Experimental investigation of high speed tool rotation on heat affected zone and over-cut in electro-chemical discharge machining. Mater. Today Proc. **18**, 1472–1478 (2019)
34. Chak, S.K., Rao, P.V.: The drilling of Al_2O_3 using a pulsed DC supply with rotary abrasive electrode by the electro chemical discharge process. Int. J. Adv. Manuf. Technol. **39**, 633–641 (2008)
35. Jain, V.K., Choudhury, S.K., Ramesh, K.M.: On the machining of alumina and glass. Int. J. Mach. Tools Manuf. **42**, 1269–1276 (2002)
36. Cheng, C.P., Wu, K.L., Mai, C.C., Hsu, Y.S., Yan, B.H.: Magnetic field-assisted electrochemical discharge machining. J. Micromech. Microeng. **20**, 1–8 (2010)
37. Rattan, N., Mullick, R.S.: Experimental set-up to improve machining performance of silicon dioxide quartz in magnetic field assisted TW-ECSM process. Silicon **10**, 2783–2791 (2018)
38. Elhami, S., Razfar, M.R.: Effect of ultrasonic vibration on the single discharge of electro-chemical discharge machining. Mater. Manuf. Process. **33**(4), 444–451 (2016)
39. Rusli, M., Furutani, K.: Performance of micro-hole drilling by ultrasonic assisted electro-chemical discharge machining. Adv. Mater. Res. **445**, 865–870 (2012)

Chapter 19

Behaviour of Voided Slab Utilizing Waste Materials



Maninder Singh, Babita Saini, Abhishek Kumar, Ronak Singh Poonia, and Katta Vinay Reddy

Abstract Slab is an essential structural member in any building and it also consumes highest amount of concrete. The major problem with concrete construction is that weight of slab increases with increase in length which limits the span. The use of cement results in emission of carbon dioxide gas to environment up to a certain extent. The objective of research is to minimize the possible weight of slab and utilization of waste material to reduce the consumption of cement. In the present investigation, plastic balls and thermocol balls were used as void formers and cement was replaced by industrial waste i.e. ground granulated blast-furnace slag. Five slabs were casted including one solid conventional slab. Two slabs were casted by replacing 25% of weight of cement with ground granulated blast-furnace slag (GGBFS). The main aim was to determine the load deflection and first crack. The results of voided slab with the void formers of both the materials (plastic balls and thermocol balls) were compared with conventional slab. It has been observed that reduction in weight of voided slab with thermocol balls and plastic balls was 11% and 14% respectively as compared to solid slab. The overall flexural performance of voided slab was found to be better than conventional slab.

Keywords Plastic balls · Voided · Thermocol · Slag · Flexural performance

19.1 Introduction

In the designing of reinforced concrete structures, the thickness of slab, span between the columns are very important aspects. Columns and slab are essential structural member in construction of any infrastructure which consume highest amount of concrete [1–5]. Therefore, to complete the demand of concrete the utilization of cement and aggregates also increase. Enormous research studies highlighted that the manufacturing process of cement adversely impact the environmental ecosystem [6–14]. On the other hand, the major problem with concrete constructions is that the

M. Singh (✉) · B. Saini · A. Kumar · R. S. Poonia · K. V. Reddy
Department of Civil Engineering, National Institute of Technology Kurukshetra, Kurukshetra, India

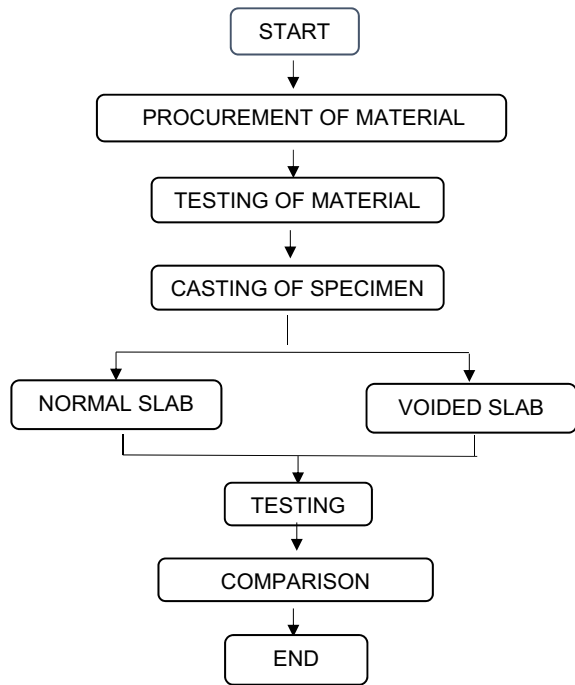
weight of slab increases with increase in length which limits the span. The deflection of slab increases, as the span is increased. Therefore, the slab thickness should be increased in order to compensate for high deflection. The increase in slab thickness increases the slab weight and leads to increased size of beam, column and foundation which results in increased usage of concrete and steel reinforcement. To avoid above disadvantages voided slab is suggested instead of conventional slab [15–17].

In last few decades, the one of emerging slab system was introduced in construction industry i.e. bubble deck slab to reduce the self-weight of the conventional slab. The middle part of the slab has been eliminated by void formers; because the concrete in the slab is not fully utilized and middle part of slab does not perform any structural function. Void forms in the middle of slab by means of plastic balls reduce the slab's self-weight up to 35%. In plastic voided slabs the amount of concrete required reduces by 30% or more. The flexible layout allows easy implementation to irregular and curved plan configurations [18–20]. It allows longer span with less expenses. Enormous researchers reported that bubble deck slab system has been better than conventional concrete slab system. However, shear and punching resistance of the bubble deck slab system is significantly lesser than conventional solid slab. The ratio of bubble diameter to slab thickness strongly influenced the performance of the bubble deck floor [21–25]. Void formers are placed in the slab system between the two meshes of reinforcement which have been arranged at the bottom and upper part of the internal structure of slab. After observing the issues associated with the conventional concrete and solid slab system, this study focuses on behaviour of voided slab with the utilization of industrial by products. The addition of waste products and void formers leads to reduction in cost and dead weight of the conventional solid slab system.

19.2 Methodology and Materials

The experimental study has been carried to compare the behaviour of voided slab with conventional solid slab. One normal slab and four voided slabs were casted with thickness 100 mm. Spherical, polystyrene and polyethylene balls were used to form voids in the slabs having diameter of 50 mm. Two slabs out of four voided slabs were casted by replacing 25% weight of cement with GGBFS waste which is a by-product of iron industry. The performance of the slabs was recorded after 28 days of curing to find their flexural capacities. Variation in load and deflection pattern has been compared for all the slabs. Reduction in weight of the slab has also been calculated for all the voided slabs.

Fig. 19.1 Flow chart of methodology used



19.2.1 Methodology

Step by step methodology used during this investigation has been illustrated in flow chart given in Fig. 19.1.

19.2.2 Materials

In this experimental analysis, 43 grade ordinary Portland cement (OPC) with specific gravity of 3.12 was used as per specifications of IS 8112:2013 [26]. Fine aggregate (10 mm) was selected as per IS 383:1970 [27] specifications with the specific gravity and fineness modulus of 2.6 and 3.26 respectively. Corresponding values for 20 mm coarse aggregates were 2.6 and 6.7. As per guidelines of IS 10262:2009 [28], M25 mix design was taken with proportion of 1:1.3:2.8. The calculated cement content and water cement ratio were 350 kg/m³ and 0.43 respectively. The polystyrene balls and low-density polyethylene balls (LDPE) were used in the form of solid spherical balls and hollow spherical balls, respectively.

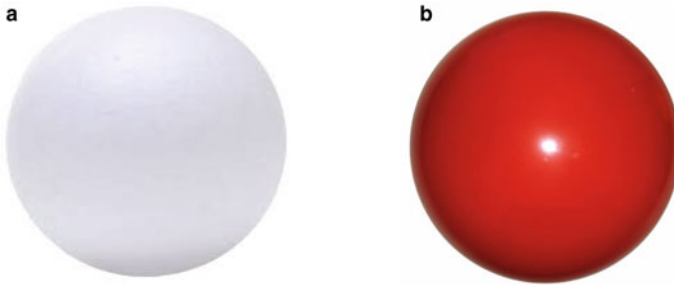


Fig. 19.2 a Spherical shaped polystyrene ball, b Spherical shaped polyethylene ball

19.2.3 Specimen Description

Total 5 voided slab specimens of 500 mm × 500 mm plan area and 100 mm thickness were casted. Polystyrene and polyethylene balls with 50 mm size were used as shown in Fig. 19.2. Volume of concrete was reduced by provision of void formers. Percentage of reduction of concrete was 4.18% for spherical shaped void formers of 100 mm thick slab. The steel wire mesh were placed over polystyrene and polyethylene balls to hold the void formers while pouring and compacting of concrete was done.

19.2.4 Casting of Specimens

Concrete slabs were casted in wooden moulds having length and breadth of 500 mm each and thickness 100 mm. One conventional slab and four voided slabs were casted for flexural testing as described in Table 19.1. Voids have been created in the slab by using thermocol and plastic balls of diameter 50 mm. The spacing between the balls was kept 92 mm centre to centre. The concrete can be easily placed and compacted in the space left between the balls. Clear cover of 20 mm was provided. The mixing was carried out in mixer to produce a homogenous, uniform in colour and consistence

Table 19.1 Description of specimens

S. No.	Description of specimens	Symbol
1	Solid Slab	SS
2	Polystyrene void former Slab	100VS50T
3	Polyethylene void former Slab	100VS50P
4	Polystyrene void former slab with 25% GGBS	100VS50TGGBS
5	Polyethylene void former slab with 25% GGBS	100VS50PGGBS

concrete. For compaction of concrete and to remove the entrapped air, needle vibrator was used. The specimens were kept under water for 28 day curing.

19.3 Experimental Setup

Two steel rollers were provided on the bed of testing machine to support slab. The center to center distance between the rollers was kept as 450 mm. The load was applied at the middle one third portion of the slab through two rollers mounted on the top surface of slab. Load was applied with the help of hydraulic jack and measured with the help of proving ring which was further calibrated to calculate the exact load applied. The deflection was measured using digital deflection gauge. The experiential setup of flexural testing has been shown in Fig. 19.3.



Fig. 19.3 Flexure testing of slab

19.4 Results and Discussion

In this study, flexure test on normal and voided slabs has been performed to find out the load and deflection pattern. The test has been performed after 28 days of curing. The performance of normal slab and voided slab was compared in terms of load-deflection performance and first crack pattern. The reduction in weight of the slab by using polystyrene and polyethylene balls has also been compared with the weight of solid conventional slab.

19.4.1 First Crack Load

The crack initiation load for all types of slabs has been recorded during flexural loading test as shown in Fig. 19.4. It has been observed that the first crack load of voided and GGBS included slabs were lesser as compared to solid slab. The first crack load of 100VS50T, 100VS50P, 100VS50TGGBS and 100VS50PGGBS slabs were decreased by 6.90%, 3.45%, 8.62% and 5.17% as compared to solid slab. The recorded values also depicted that the 25% utilization of GGBS as substitution of cement decreased the crack initiation load of the slabs. From all the designated slabs the minimum load for crack initiation was found for 100VS50TGGBS slab, while, maximum for SS slab.

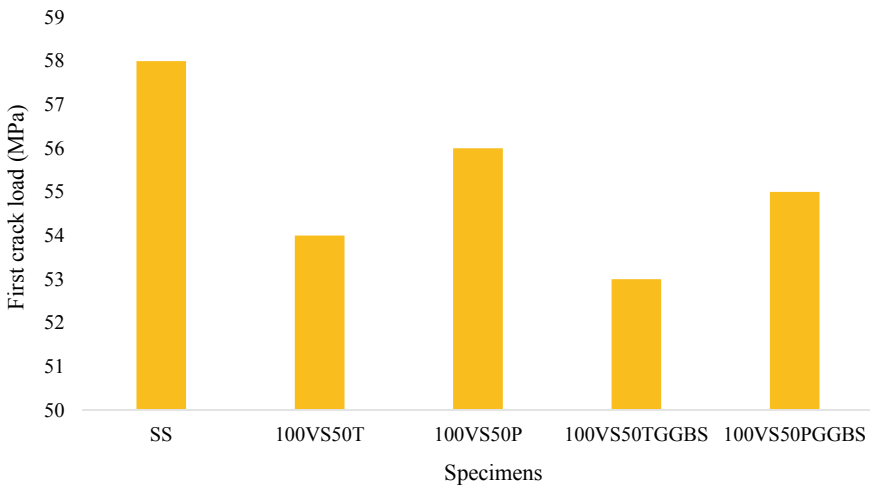


Fig. 19.4 First crack load for different types of slabs

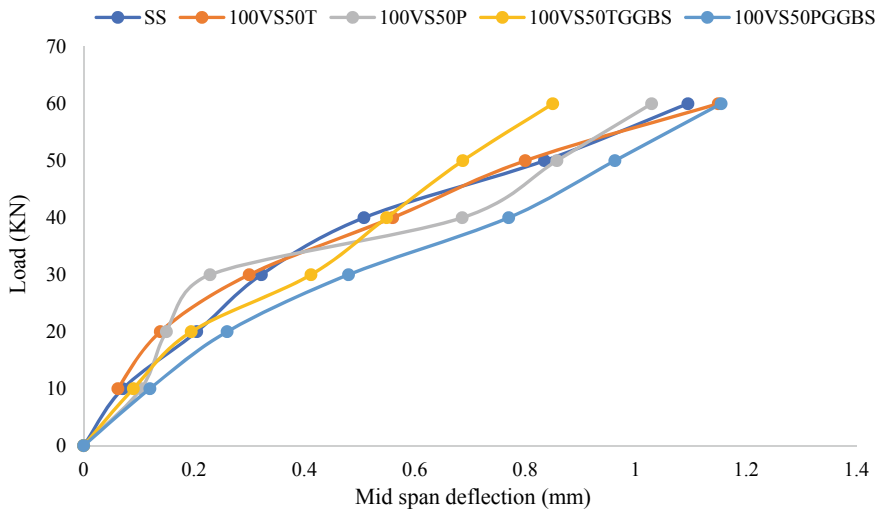


Fig. 19.5 load deflection performance of different types of slabs

19.4.2 Load Deflection Behaviour

The load deflection behaviour of different types of slabs has been recorded after 28 days of water curing as illustrated in Fig. 19.5. It has been observed that the deflection of voided and GGBS containing slabs were higher than solid slab. Figure 19.5 depicted that the deflection for plastic voided slab with 25% GGBS was more than other types of slabs. The recorded values depicted that void formers (thermocool and plastic balls) and GGBS contribute in increasing the deflection of the slabs.

19.4.3 Weight Analysis

Figure 19.6 depicts the comparison of weight for different types of slabs. It has been observed that void formers (thermocool and plastic balls) and GGBS reduced the overall weight of the concrete slab. Weight of the thermocool and plastic balls included slabs reduced by 11.11% and 14.28% as compared to conventional concrete slab. The inclusion of GGBS as replacement of cement, also contribute into reduction of weight of concrete slabs. GGBS is lighter in weight as compared to OPC due to which the reduction in weight was found with the inclusion of slag. The recorded values depicted that voided slab had maximum weight reduction of 16.66%.

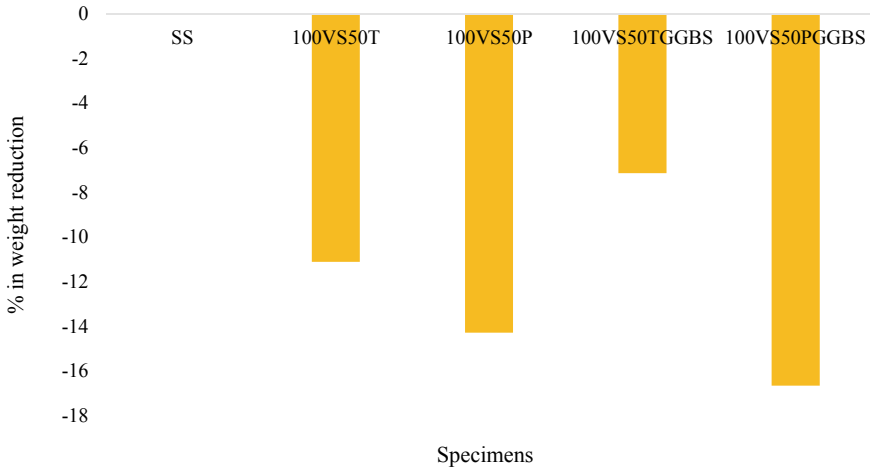


Fig. 19.6 Percentage of weight reduction as compared to solid slab

19.4.4 Crack Pattern

Figure 19.7 depicts the deflection pattern of conventional solid slab and voided slabs. It has been observed that most of the cracks were initiated from the outer one third portion of the slab.

19.4.5 Comparison of Solid Slab with Void Former Slab

The recorded results depicted that the void former slab decrease the toughness, first crack load and overall weight of the specimens. The deflection for voided slab was more than conventional solid slab. This may be attributed due to the reduction in overall fracture toughness. On the other side, the utilization of slag in production of cementitious matrix save the natural resources, environment ecosystem and reduce the carbon dioxide emissions.

19.5 Conclusions

In the present study, an experimental work has been carried out to compare the flexural performance, the first crack load and reduction in weight of voided slabs with conventional solid slab. The results of present study have been summarized as under.

1. Effect of void formers on performance of slabs

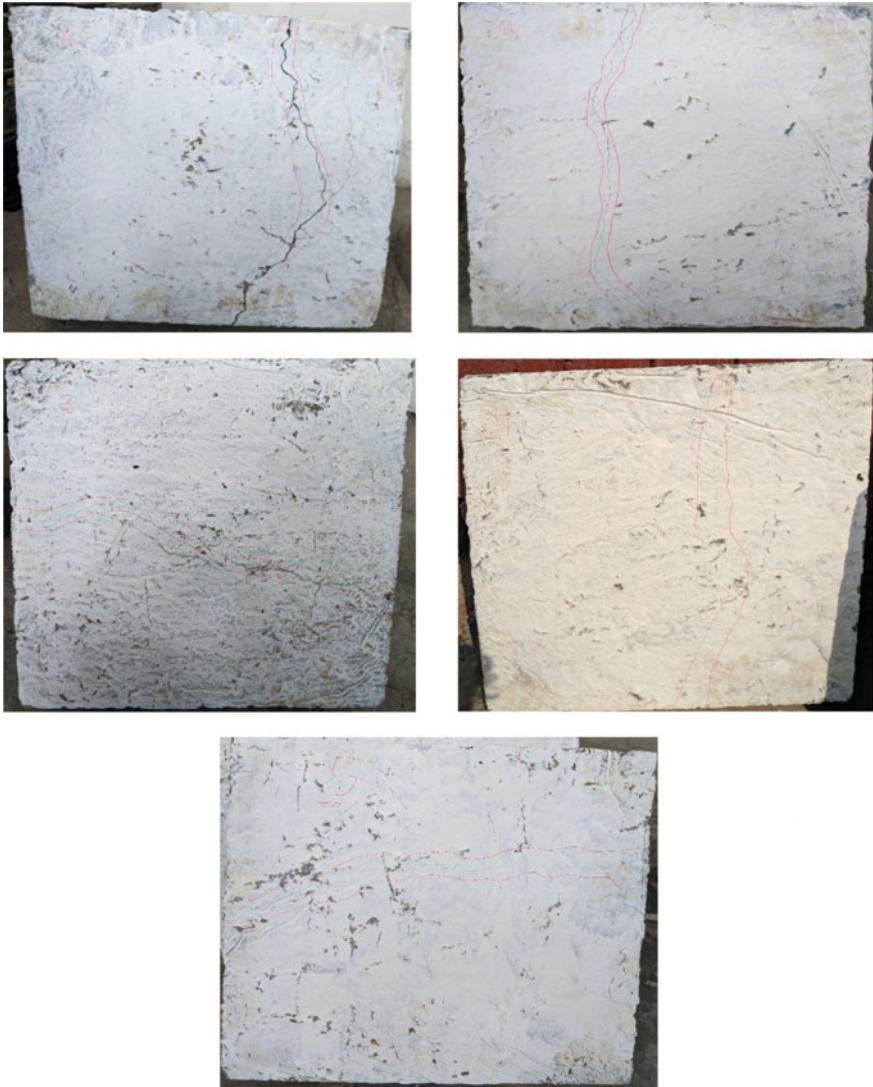


Fig. 19.7 Cracking pattern of slab specimens

- Maximum reduction in crack initiation load was found for thermocol voided slab as compared to other types of slabs. The first crack load of thermocol voided slabs decreased by 6.9% as compared to normal slab.
- Mid span deflection in plastic void former slab was found maximum as compared to other types of slabs. The deflection of plastic voided slab was higher by 5.48% as compared to conventional solid slab.

- The maximum reduction in weight of slab was found with plastic void formers (balls).
2. Impact of GGBS on performance of slabs
 - Inclusion of GGBS with void formers decreased the first crack load and weight of slab up to 8.62 and 16.66% as compared to solid slab.
 - The addition of GGBS as replacement of cement improved the load deflection performance of the slabs.
 - The utilization of GGBS waste as substitution of cement solve the problem of disposal and saves the natural resources and environmental ecosystem.

References

1. Saghafi, M.H., Shariatmadar, H.: Enhancement of seismic performance of beam-column joint connections using high performance fiber reinforced cementitious composites. *Constr. Build. Mater.* **180**, 665–680 (2018). <https://doi.org/10.1016/j.conbuildmat.2018.05.221>
2. Chidambaram, R.S., Agarwal, P.: Seismic behavior of hybrid fiber reinforced cementitious composite beam–column joints. *Mater. Des.* **86**, 771–781 (2015). <https://doi.org/10.1016/j.matdes.2015.07.164>
3. Dehghani, A., Mozafari, A.R., Aslani, F.: Evaluation of the efficacy of using engineered cementitious composites in RC beam-column joints. *Structures* **27**, 151–162 (2020). <https://doi.org/10.1016/j.istruc.2020.05.045>
4. Qudah, S., Maalej, M.: Application of engineered cementitious composites (ECC) in interior beam–column connections for enhanced seismic resistance. *Eng. Struct.* **69**, 235–245 (2014). <https://doi.org/10.1016/j.engstruct.2014.03.026>
5. Shannag, M.J., Barakat, S., Abdul-Kareem, M.: Cyclic behavior of HPFRC repaired reinforced concrete interior beam-column joints. *Mater. Struct.* **35**, 348–356 (2002). <https://doi.org/10.1007/BF02483154>
6. Gautam, N., Krishna, V., Srivastava, A.: Sustainability in the concrete construction. *Int. J. of Environ. Res. Dev.* **4**(1), 81–90 (2014). [https://doi.org/10.1061/\(ASCE\)1084-0680\(2008\)13:2\(98\)](https://doi.org/10.1061/(ASCE)1084-0680(2008)13:2(98))
7. Pathak, P.P.: Inclusion of Portland and pozzolona (fly ash waste) cement in specifications. *Ind. Highw.* **37**, 23–29 (2009)
8. Woodson, R.D.: Concrete materials. In: *Concrete Portable Handbook*, pp. 5–18. Elsevier Inc., Oxford (2012)
9. Singh, M., Saini, B., Chalak, H.D.: Flexural response and durability aspects of ECC containing stone slurry powder. *Asian J. Civ. Eng.* (2020). <https://doi.org/10.1007/s42107-020-00319-y>
10. Kumar, V., Kumar, A., Prasad, B.: Mechanical behavior of non-silicate based alkali-activated ground granulated blast furnace slag. *Constr. Build. Mater.* **198**, 494–500 (2019). <https://doi.org/10.1016/j.conbuildmat.2018.11.282>
11. Singh, N., Singh, S.P.: Electrical resistivity of self-consolidating concretes prepared with reused concrete aggregates and blended cements. *J. Build. Eng.* **25**, 100780 (2019). <https://doi.org/10.1016/j.jobbe.2019.100780>
12. Singh, M., Saini, B., Chalak, H.D.: An overview on waste materials used in engineered cementitious composite. In: *Smart Technologies for Sustainable Development*. LNCE, vol. 78 (2021). https://doi.org/10.1007/978-981-15-5001-0_17
13. Singh, M., Saini, B., Chalak, H.D.: An overview on utilization of stone waste in construction industry. In: *3rd International Conference on Innovative Technologies for clean and sustainable development, 2020* (2021). https://doi.org/10.1007/978-3-030-51485-3_38

14. Schepper, M.D., Heede, P.V.D., Driessche, I.V., Belie, N.D.: Life cycle assessment of completely recyclable concrete. *Materials* **7**(8), 6010–6027 (2014)
15. Sagadevan, B., Rao, N.: Experimental and analytical investigation of punching shear capacity of biaxial voided slabs. *Structures* **20**, 340–352 (2019). <https://doi.org/10.1016/j.istruc.2019.03.013>
16. Al-Gasham, T.S., Hilo Ali, N., Alawsi Manal, A.: Structural behavior of reinforced concrete one-way slabs voided by polystyrene balls. *Case Stud. Constr. Mater.* **11**, e00292 (2019). <https://doi.org/10.1016/j.cscm.2019.e00292>
17. Singh, M., Saini, B.: Experimental study on bubble deck slab: a review. In: International Conference on Environmental Geotechnology, Recycled Waste Materials and Sustainable Engineering. GNDEC, Ludhiana March 2018 (2018)
18. Chacko, I.J., Varghese, S.M.: Study on structural behavior of bubble deck slab using Indian Standards. *Int. J. Innov. Res. Technol.* **3**(4), 193–198 (2016)
19. Jamal, J., Jolly, J.: A study on structural behavior of bubble deck slab using spherical and elliptical balls. *Int. Res. J. Eng. Technol.* **4**(5), 2090–2095 (2017)
20. Dheepan, K.R., Saranya, S., Aswini, S.: Experimental study on bubble deck slab using polypropylene balls. *Int. J. Eng. Dev. Res.* **5**(4), 716–721 (2017)
21. Mushfiq, M.S., Saini, S., Rajoria, N.: Experimental study on bubble deck slab. *Int. Res. J. Eng. Technol. (IRJET)* **5**(5), 1000–1004 (2017)
22. Fatma, N.V.: To study comparison between conventional slab and bubble deck slab. *Int. Adv. Res. J. Sci., Eng. Technol.* **5**(1), 70–76 (2018)
23. Bhagat, S., Parikh, K.B.: Comparative study of voided flat plate slab and solid flat plate slab. *Int. J. Innov. Res. Dev.* **3**(3), 22–25 (2014)
24. Naik, S.R., Joshi, D.: A voided slab and conventional flat slab; a comparative study. *Int. J. Sci. Technol. Eng.* **4**(1), 44–50 (2017)
25. Harishma, K.R., Reshmi, K.N.: A study on Bubble Deck slab. *Int. J. Adv. Res. Trends Eng. Technol. (IJARTET)* **2**(10) (2015)
26. IS 8112:2013, Specification for 43 Grade ordinary Portland cement, 2nd Revision. Bureau of Indian Standard, New Delhi
27. IS 383:1970, Specification for coarse and fine Aggregates from natural Sources for concrete, 2nd Revision. Bureau of Indian Standard, New Delhi
28. IS 10269:2009, Guidelines for concrete mix design proportioning, 1st Revision. Bureau of Indian Standard, New Delhi

Chapter 20

Design Considerations for Body-Powered 3D Printed Prostheses with String Mechanism for Upper Limb Disarticulation



Abdul Dhiraj Hussain, Neeraj Radhakrishnan, Mohammed Sarfas, and Vishal Francis

Abstract In medical field, a prosthetic implant is an artificial device that replaces a missing body part/organ, which may be lost through trauma, disease, or a condition present at birth. Prostheses are intended to restore the normal functions of the missing body part therefore, it is essential to design and fabricate them as per the patient's specifications. This requirement of fabricating customized prostheses is an important issue that needs to be addressed. Moreover, In the case of children, there is a need for a periodical change of prosthetics due to the growth of their bones. These situations pose difficulty in adaptation of prostheses for the economically weak and rural area patient's. 3D printing technology provides a platform to fabricate any complex shaped polymeric parts economically with ease. This capability of the technology can be utilized to fabricate customized and patient-specific prostheses. The present paper discusses the process flow that can be adopted for designing and fabricating a patient-specific prosthetic hand using extrusion-based 3D printing technology. The design considerations for 3D printing of a body-powered prosthetic hand with all tolerances and clearances are discussed with the help of a case study. A provision for string and the elastic based mechanism is provided to deliver motion and action to the fingers. By appropriately applying the design considerations, 3D printing technology can be effectively utilized for the fabrication of economical prosthetic hands.

Keywords 3D printing · Prosthetic hand · Additive manufacturing · Design for additive manufacturing

20.1 Introduction

According to the International Health Organisation, around 0.5% of the total world population needs prostheses [1, 2]. This requirement is particularly crucial for developing countries' children, who over time outgrow the prostheses. Moreover, rural amputees have no access to the medical facilities and rarely go for maintenance. The

A. D. Hussain · N. Radhakrishnan · M. Sarfas · V. Francis (✉)
School of Mechanical Engineering, Lovely Professional University, Phagwara, Punjab, India
e-mail: vishal.24813@lpu.co.in

© The Author(s), under exclusive license to Springer Nature Switzerland AG 2022
R. Pratap Singh et al. (eds.), *Proceedings of the International Conference on Industrial and Manufacturing Systems (CIMS-2020)*, Lecture Notes on Multidisciplinary Industrial Engineering, https://doi.org/10.1007/978-3-030-73495-4_20

283

Table 20.1 Comparison of various types of prosthetic hand

Type	Functionality	Attributes
Passive prosthetic hand	<ul style="list-style-type: none"> • Aesthetic device • Simple carrying and balancing of things 	<ul style="list-style-type: none"> • Low cost • Limited functionality
Body powered prosthetic hand	<ul style="list-style-type: none"> • Gripping • Lifting • Manipulation 	<ul style="list-style-type: none"> • Low cost • Easy maintenance • Less weight • Limited degrees of freedom (DoFs)
External powered (Myoelectric) prosthetic hand	<ul style="list-style-type: none"> • Gripping • Lifting • Manipulation • Rotation 	<ul style="list-style-type: none"> • More DoFs • Intensive training required • High cost

creation of an inexpensive and durable prosthetic hand may be a potential option in this scenario. 3D printing offers great design flexibility and can help to develop any customized and complex shape geometry necessary for prosthetic development [3]. Speed, customization, and comfort are the few factors that can make 3D printing a key contender for prosthesis development. For growing children, the prosthesis has to be modified after a few years, in this respect the prosthesis should be economical. Affordable prosthesis may be a feasible alternative for many patients and families. Economical desktop 3D printers can be used to fabricate the prosthesis. The 3D printed prosthesis socket can be tailored to the anatomy of the patient's arm, thus providing greater comfort. The prosthetic hand can be broadly segregated into three categories namely, passive, body powered and external powdered. Table 20.1 shows a comparison between these categories along with their functionality and attributes. Each type of prosthetic hand has their own limitations and usages [4–9]. The selection of which entirely depends upon the patient and as advised by the surgeons. It can be seen that most of the functionality among the three types of prosthetic hand discussed is associated with externally powered devices. However, they require intensive training and are not economical. On the other hand, the body powered prosthetic hand are limited functionality and is much more economical compare to the externally powered devices. This type of prosthetic hand can be effectively utilised for promoting the usage of devices among rural areas and for growing children's [10].

20.2 Literature Review of Different Prostheses

The work done related to prostheses hand development is illustrated in Table 20.2.

Table 20.2 Literature review or State of art on deign and working of various types of prostheses

S. No.	Type of prosthetic	Objective	Design and working	References
1	Passive	<p>Helping a child for palmar grasp or hold and durability for this was tested by repeated bending Carrying entire weight of a child while crawling, sitting, pushing or pulling to stand and durability for this was tested by compression Children might use roughly while playing, for example banging toys on floor, which should be withstood by prosthetic which was tested for this by tension and repeated bending</p>	<p>The design was confined to sizes common to kids somewhere in the range of 3 and year and a half old enough and afterward tweaked in size to the customer being dealt with. Materials were chosen in view of execution and cosmesis</p>	[14]
2	Passive	<p>This work means to build up a minimal effort human hand prosthesis made through added substance producing. The technique utilized for the improvement of the prosthesis utilized moderate and cheap materials on the market. Malleable testing was performed to assess the mechanical properties to check the resistance of the printing material utilized. A short time later, the mechanical possibility study executed on the gadget was performed utilizing finite element technique</p>	<p>The material used was PETG (Polyethylene Glycol Terephthalate), obtained in filament form with 1.75 ± 0.5 mm in diameter Comparable display designs were used to plan a geometry close to a human hand to enhance the hand prosthesis, particularly corresponding to surface estimates and shapes. Based on simple (rectangular) geometries, the constituent parts of the gadget were constructed from the earlier and later renovated by the flexibility requires for flexion growth and hold rotation For the improvement of the from the earlier phalanges, the fingers were built utilizing a rectangular geometry as a base, and later renovated by the actual components of the phalanges bringing about the execution of flexion and rotation developments for the holding movement</p>	[15]

(continued)

Table 20.2 (continued)

S. No.	Type of prosthetic	Objective	Design and working	References
3	Passive	<p>This paper describes the mechanical features of an experimental, multi-finger, prosthetic hand intended for young people in the seven-year age range. There are standard prosthetic hands for these ages, but they have minimal mechanical ability. Passive adaptive grip, that is, the ability of the fingers to respond to the condition of an object held within the hand, may be achieved by the introduced test hand. The four fingers and thumb will flex inwards freely during holding, to adapt to the state of the article. This passive design is straightforward and upright, without sensors or electronic preparation necessary. The adaptive hold structure created here results in a hand that contrasts with other experimental hands with decreased size and weight, and has improved mechanical ability and cosmetic appearance compared to normal prosthetic hands</p>	<p>This paper describes an experimental prosthesis called the Toronto/Bloorview Mac-Millan Hand (TBM Hand) which uses passive adaptive grasp. For example, the hand can use a similar battery and engine regulator used by a conventional prosthesis, the VASI 7-II hand. The critical goal when modeling the four fingers (index, middle, ring and pinky) was to cause them to show up as natural as could reasonably be predicted. Since a human finger has three sections, known as phalanges, a three-section configuration has been chosen. At first, a cable-driven design was attempted to stimulate the fingers, but due to flimsiness problems, it was abandoned. Instead, using Working Model 2D software, a rigid linkage system was developed</p>	[16]

(continued)

Table 20.2 (continued)

S. No.	Type of prosthetic	Objective	Design and working	References
4	Body-powered	<p>The goal of this review was to find a productive energy transmission technique in a human underactuated body-powered (BP) prosthetic hand for use</p> <p>A pulley-cable finger and a hydraulic chamber finger were developed and attempted to contrast the transmission standard of the pulley-cable and the transmission standard of the hydraulic chamber</p>	<p>Two fingers, a pulley-cable finger and a hydraulic chamber finger, have been designed. Aside from the transmission standard, the fingers were indistinguishable. The two fingers had measurements that were identical</p> <p>A 1 mm thick cable made from steel was selected for the pulley-cable finger. As steel has a high elastic modulus (~200 GPa), the steel cable has a high stiffness. A cable's firmness depends on the stiffness of the material and the stiffness of the construction, which relies on the cable plait or interlace</p> <p>To motivate the high activation loads, the piston diameters of the hydraulic chamber finger were boosted. The distal chamber was amplified on the premise that there was only limited space within the finger to suit the distal chamber. The gap around was set at 7 mm, which was the largest width of the chamber that would fit into the human finger near the shape of the finger</p> <p>All were actuated unidirectionally. Helical springs were taken back to their original location following operation. For both fingers, similar springs in a similar configuration were used</p>	[17]

(continued)

Table 20.2 (continued)

S. No.	Type of prosthetic	Objective	Design and working	References
5	Body-powered	<p>A modern prosthetic hand style and upgrade that is lighter in weight, more affordable, and more useful than existing hands. The new prosthesis contains an endoskeleton inserted in self-skinning foam that gives the need for a separate cosmetic glove a functional look and aesthetics and deters it. Variable strength of grasp is provided by the voluntary closure scheme. The location of joints inside each of the four fingers in three places bears the expense of fair finger growth. The high-strength engineered cable attached to each finger's distal phalanx is used to cause flexion. Weight has been reduced by around half, relative to current hands, and cable performance needed by about half for maximum finger flexion</p>	<p>Voluntary closure is the feature of prosthesis. Until the belt cable is dislodged, the fingertips keep going out. Harness cord incitement induces flexion against the set thumb of each of the four fingers. The fingers stretch as the cord is released, opening the hold. This role assists in keeping a grasp on sensitive things. Full harness cable displacement of approximately 5 cm with 270 N is agreed to be available by bicipital abduction or likely glenohumeral bending</p>	[18]

(continued)

Table 20.2 (continued)

S. No.	Type of prosthetic	Objective	Design and working	References
6	Body-powered	<p>Ability to extend the concept to a mechanical hand created as a prosthetic terminal device by means of Shape Deposition Manufacturing (SDM)</p> <p>Hand test results have shown a degree of power, versatility, and other execution properties hidden in an artificial hand until now. Other than solid execution, the hand is rugged, delivered using a molding process that allows both inexpensive large-scale production as well as a functional appearance without a decorative glove requirement, and fuses a simple plan requiring only a solitary actuator for the eight DOFs. As a justification for either a body driven or remotely powered prosthetic terminal gadget that is sensible, utilitarian, powerful, and economical, these elements make it a good competitor</p>	<p>The SDM hand, as a terminal device, will be a 'activeclose' device, with springs that would open the hand in general. Every finger has a pre-extended, nylon-covered stainless-steel cable secured through the distal link for incitation, which goes to the base via low-erosion nylon tubing</p> <p>The ligament connection, which correlates to the cohesive joints, remains slack until activation and the finger is in its most relaxed state. This strategy facilitates the usage of non-drivable actuators and stops the actuator's inertial heap from expanding passive power.</p> <p>The strengthened ligament extracts a large portion of the relief from the fingertips after activation, bringing in a stiffer handle and more impressive stability</p>	[19]

(continued)

Table 20.2 (continued)

S. No.	Type of prosthetic	Objective	Design and working	References
7	External powered/Myoelectric	For a group of upper limb disabled children at far smaller ages to present electrically driven hands in comparison to standard activity. Implementing a powered prosthesis at a much younger age may be a more suitable alternative than preparing a body-powered prosthetic device while waiting by to achieve a more advanced age before accepting a powered prosthesis	To illustrate the introduction of a more powerful useful system, SCAMP hand was used to enable change in the independence required by age and to empower bimanual exercises that were not fulfilled by body-powered or cosmetic machines. Both sockets had an opening with the objective of using a get through 'stump sock' to provide a smoother use. For underneath elbow weakness, everyone had a solitary electrode sited over the parallel angle overlying the usual finger and wrist extensor muscle bunch to facilitate careful hand opening. The single electrode was mounted over the rear arm muscles for the child with a degree of insufficiency through the elbow. In these patients, myoelectric control was preferred over pull switches for use with SCAMP hands, as pull switches may have allowed the use of prohibitive working circles and unnatural activities to push the hand away from the body to perform the tasks of the hand	[20]

(continued)

Table 20.2 (continued)

S. No.	Type of prosthetic	Objective	Design and working	References
8	External powered/Myoelectric	<p>For a multi-degree prosthetic hand to set up a myoelectric segregation system</p> <p>Two surface electrodes are used by the separation framework to receive the electromyography (EMG) signal from the muscle of the flexor digitorum superficialis and the muscle of the extensor pollicis brevis</p>	<p>Eight kinds of hand technologies, which are the main developments used in the segregation framework, are frequently used in daily life. The procedures of variation, autoregressive model and spectral evaluation are used for preprocessing of highlights to identify such hand innovations. At that point, to segregate between the capabilities, an error feedback neural network is implemented. Finally, to validate the idea, a research interface structure based on the PC climate is established. Plus, to simulate the prosthetic creation of the NTU side, a practical 3-D interface program based on the hierarchical interactive graphic system (PHIGS) of the programmer is added. A success rate of 85% for offline testing and 71% for online testing can be reached through the separation system</p>	[21]

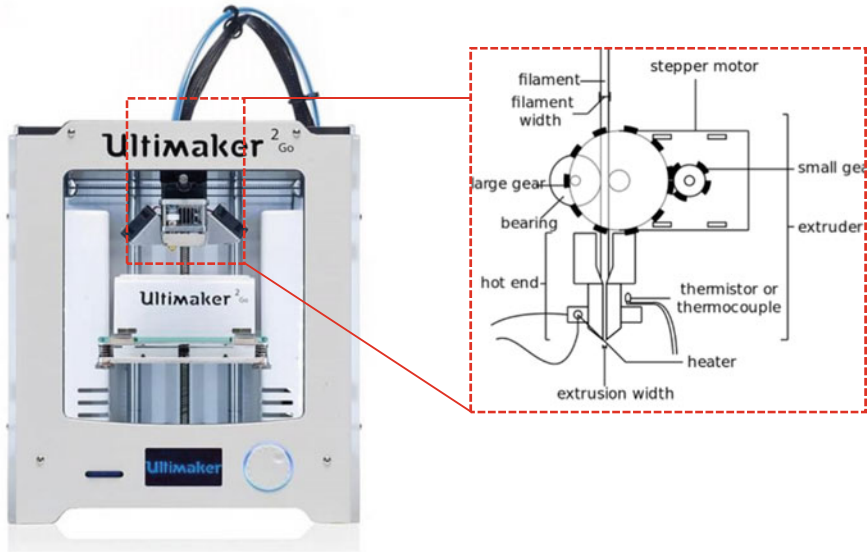


Fig. 20.1 Schematic diagram of FFF mechanism showing the internal details of a desktop 3D printer

20.3 The Extrusion-Based 3D Printing Technology for Upper Limb Prosthetic

Extrusion based 3D printing technology is one of the most economical one for fabrication of complex intricate features. The technology is also known as fused filament fabrication (FFF). The FFF is one of the most widely used 3D printing technologies due to its significant advantages. It involves placing the semi-molten material on a heated bed where it fuses with the adjacent deposited material. The part is built by depositing one layer at a time. Figure 20.1 shows the schematic of the FFF process and a desktop extrusion based 3D printer. One of the advantages of FFF above other 3D printing technology is that only the material needed to build the part is deposited which reduces material waste. The process is also cost-effective compared to other methods of processing polymers. Such attributes allow them an acceptable alternative for the manufacturing of specialized and economical upper limb prostheses for the user.

20.4 Design Considerations of Extrusion-Based 3D Printers for Upper Limb Prosthetic

When using the extrusion based 3D printers several design recommendations should be used to ensure proper prints. There is always difference between the developed CAD model and the 3D printed parts. This is because of the layer by layer

approach adopted by the technology. The CAD/STL model is sliced and the used to generate the path for the extruder. Therefore, the CAD model is approximated by the deposited 2D layers which after fusion resembles the CAD model. Moreover, there is always staircase errors over the periphery of the curved surface along the z direction. When designing for non-assembly functional parts there should be proper clearances provided at the surfaces which needs to be moving. This clearance may differ based on the type of the functionality however, at least 0.5 mm gap should be provided [11]. Another important aspect is the strength which is affected by the orientation and infill pattern and direction selected. It should be noted that the laying or deposition of the layers should be avoided along the direction of applied load. Surface finish of the mating parts, fingers, palm and socket needs to be smooth to provide proper functionality therefore the orientation of the parts should be accordingly selected. Contact of these surfaces with the support should be avoided. It is also important to provide the features in the CAD model for standard parts that have to be assembled after the prints. Since the accuracy in X and Y directions is more compared to the Z direction therefore, placing the model on the build platform should be appropriately selected. Next another very important decision is the selection of infill density of simply the density of the part. The parts that are subjected to loading should be printed with 70% to 100% [11]. However, the parts that are not directly subject to loading can be printed at much lower infill percentage such as 15% to 30%. Moreover, the material selected is also very crucial and should be selected as per the functionality [12, 13]. It has been reported that ABS (Acrylonitrile butadiene styrene) filaments have been utilized to fabricate the prosthetic hand using extrusion based 3D printing. However, on prolonged usage delamination and breakages can also occur. In this scenario composite filaments can be used such as ABS/CF (CF: carbon fiber). A prosthetic hand is modeled in Autodesk fusion 360 (Education license) keeping the average dimensions of a child. Figure 20.2 shows the orthographic views of the modeled hand. The dimensions taken for the design are illustrated in the figure. It can be seen from the figure that the amount of clearance provided is kept minimum as 0.5 mm to avoid any fusion of polymer layers while deposition and solidification process (refer the detailed view). It can also be seen that sufficient tolerance is provided between each fingers to ensure proper movement. In order to integrate the string mechanism for the functionality provisions are provided in each fingers to accommodate the same.

Figure 20.3 shows the three dimensional CAD model of the prosthetic hand. A lever has been provided at the bottom of the modeled hand for integration of the pulling mechanism that can be provided for integrating the functionality to the hand. It can also be seen that the provisions are provided to integrate the standardized parts such as bolts and screws to provide movement between the segments of the finger. Moreover, this can also be used to provide EMG sensors. The palm region of the modeled hand is shown in Fig. 20.4. The 2D detailed view provided in the figure shows the dimensions selected for the clearance between each segments of the finger and also between each fingers.

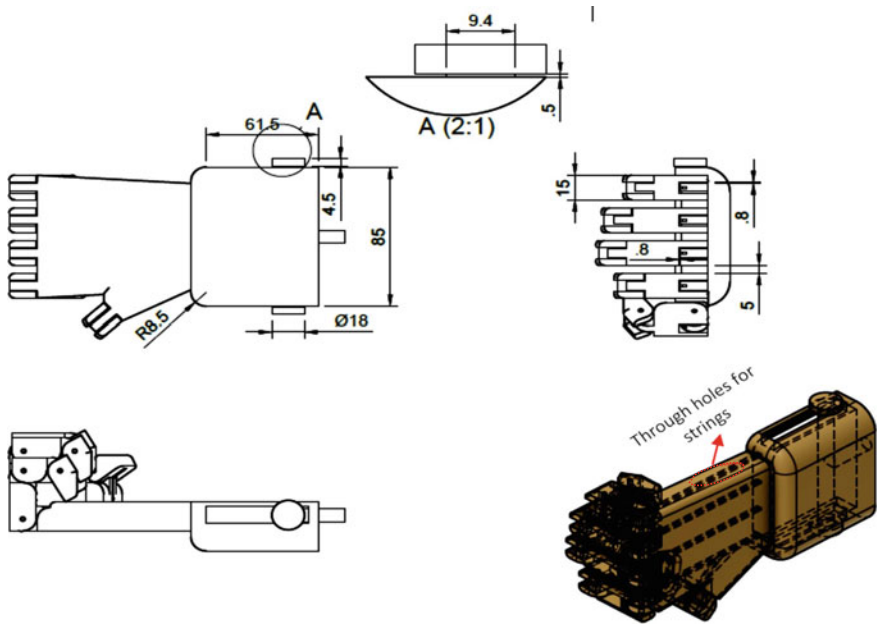


Fig. 20.2 Orthographic and isometric view of modelled prosthetic hand (All dimension are in mm)



Fig. 20.3 A 3D view of the modeled prosthetic hand in closed fist position

20.5 Working Mechanism of the Suggested Upper Limb Body-Powered Prosthetic

- From Fig. 20.5 given above we could see how the strings and lever arrangement is placed in a prosthetic hand in closed fist position.

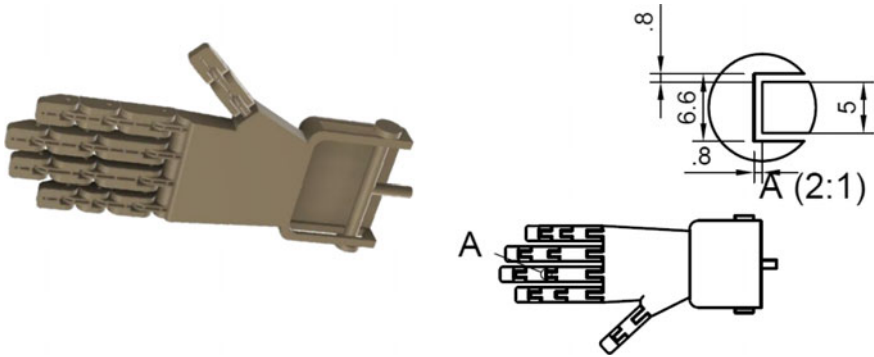


Fig. 20.4 A view showing the open palm region of the modelled prosthetic hand

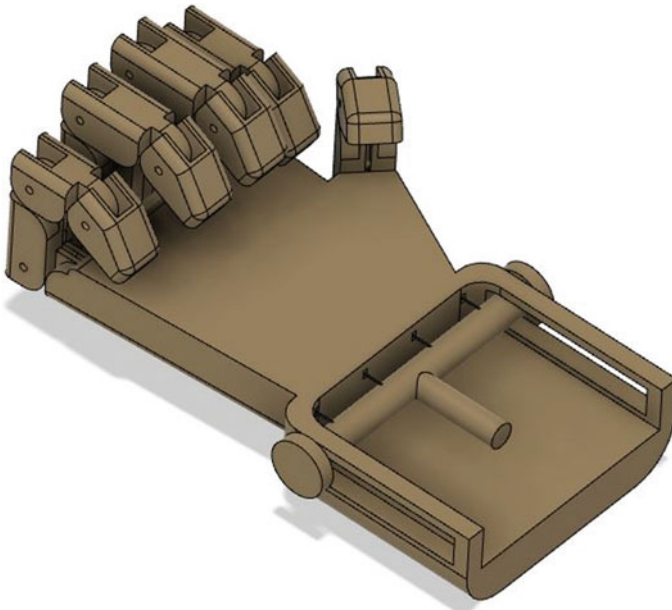


Fig. 20.5 Position of strings and lever arrangement in modeled prosthetic hand in closed fist position

- The above depicted position of the fist will be the initial or the actual position of the hand that will be attached to a patient’s hand.
- The position of the fist will be retained either with help of elastic strings or springs that is attached to the inner surface of the prosthetic hand fingers.
- The tension provided by the elastic will help in gripping the objects with the help of this hand.
- To open the fist the lever should be pulled out as shown in Fig. 20.6, as the lever moves out the string attached to the lever makes the finger opened.

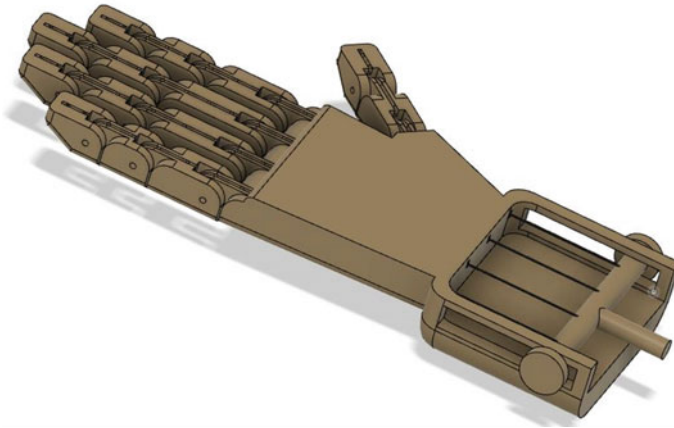


Fig. 20.6 Position of strings and lever arrangement in modeled prosthetic hand in open fist position

- This motion of the lever can be facilitated by the movement of the upper portion of hand or shoulder as the lever will be attached to the body via cables.
- As the shoulder or the hand get relaxed, the lever will move to its original position, that means the fist will get closed.
- In Fig. 20.7 we could see how an object will be held in the modeled hand due the

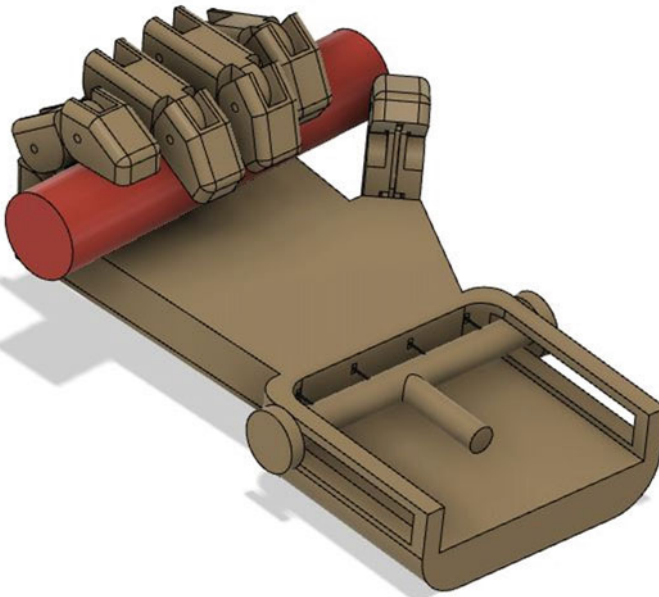


Fig. 20.7 Gripping action of prosthetic hand using string mechanism

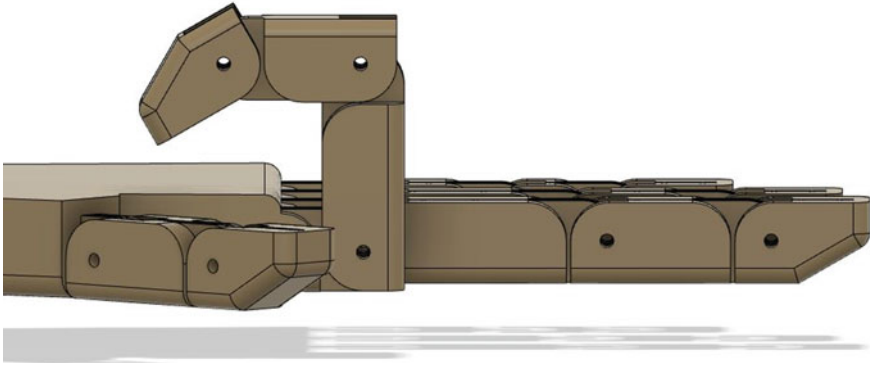


Fig. 20.8 Index finger in closed position

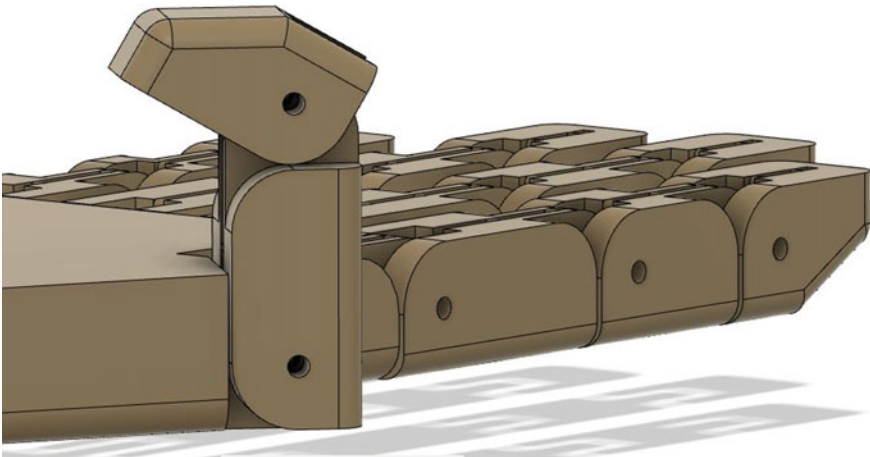


Fig. 20.9 Thumb in closed position

tension provided by the elastic and the string arrangement depicting the grasp.

- The bending motion of each finger can only be facilitated by providing proper tolerance between each element and that can be seen Figs. 20.8 and 20.9 where it shows the close-up view of the fingers when it is in a closed position.

20.6 Conclusions

- Low-cost body-powered prosthetic hands have many potential applications. This hand could be produced and dispersed in developing nations, where people with amputation who couldn't in any case bear the cost of a prosthesis may think that it's a welcome alternative. Furthermore, the prosthesis could be utilized by

developing kids who require a bigger size every 6 months or a year considering their body growth, it very well may be economically replaced. Grown-ups could likewise utilize this prosthesis as an expendable: whenever torn or stained, it very well may be replaced modestly [18].

- Important properties that should be taken into consideration while picking the polymeric FDM printing material, as they are straightforwardly identified with the chemical composition, are maximum stress, yield stress, modulus of elasticity, elongation, and hardness. Microstructural attributes and the capacity of the printed item to acquire great mechanical strength toward the finish of three-dimensional printing, which on account of prostheses is basic to join the low weight with the high mechanical strength of the device [15].
- The highlights of adaptive grasp, fingers curling inwards and a rotational thumb will build the mechanical utilization of a prosthetic hand, over that of traditional ones. The adaptive grasp of hand is accomplished threefold. Firstly, the fingers can curl as they flex, and also the string spring mechanism joined to the fingers permit the fingers to flex inwards freely of each other. Ultimately, the thumb can be passively turned by the capable hand of the client, along these lines giving additional grasping configurations [16].
- The initial objective was to study the feasibility of a cost-effective 3D printed prosthetic hand. However, in order to utilize the economical desktop 3D printer for fabrication of prosthetic hand several design recommendations need to be considered. This will provide the opportunity to fully utilize the 3D printing process for fabrication of economical prosthetic devices. Some areas, such as the wrist of the hand, are at high risk of failure if the system is exposed to forces. In the modern world, a functional prosthetic arm will be capable of sustaining abrupt shocks and bearing large loads without collapsing. Therefore, the material selection also plays an important role for better prostheses design. It can be stated that the 3D printing process can be adopted to fabricate patient specific prosthetic devices. sufficient room for the installation of electronics.

References

1. Johnson, D., Ritter, S., Mehta, K.: Characteristics of a 3D-printed prosthetic hand for use in developing countries. In: *Humanitarian Engineering and Social Entrepreneurship (HESE) Program School of Engineering Design, Technology, and Professional Programs, College of Engineering, The Pennsylvania State University Park, USA* (2015)
2. Baril, M., Gosselin, C., de Jesus Lima, E., Arabiam, A.: Development of a 3d printed prosthetic myoelectric hand driven by Dc actuators. *Technology Department State University of Feira de Santana, BA, Brazil*, 4 Oct 2017
3. Francis, V., Jain, P.K.: Experimental investigations on fused deposition modelling of polymer-layered silicate nanocomposite. *Virtual Phys. Prototyp.* **11**(2), 109–121 (2016)
4. Dombroski, C.E., Balsdon, M.E., Froats, A.: The use of a low cost 3D scanning and printing tool in the manufacture of custom-made foot orthoses: a preliminary study. *BMC Res Notes* **7**, 443 (2014)

5. Muilenburg, A.L., LeBlanc, M.A.: *Body-Powered Upper-Limb Components*, pp. 28–38. Springer, New York (1989)
6. Zuniga, J.M.: 3D printed antibacterial prostheses. *Appl. Sci.* **8**, 1651 (2018)
7. Zuniga, J.M., Peck, J.L., Srivastava, R., et al.: Functional changes through the usage of 3D-printed transitional prostheses in children. *Disabil. Rehabil. Assist. Technol.* **14**, 68–74 (2019)
8. Phillips, B., Zingalis, G., Ritter, S., et al.: A review of current upper-limb prostheses for resource constrained settings. In: *Proceedings of the Fifth IEEE Global Humanitarian Technology Conference (GHTC)*, Seattle, WA, 8–11 Oct 2015, pp. 52–58. IEEE, New York
9. Zuniga, J.: The Cyborg Beast, <https://www.unomaha.edu/college-of-education/biomechanics-core-facility/research/cyborg-beast/index.php>
10. e-NABLE: The raptor hand. Enabling the Future, 2014, <https://enablingthefuture.org/upper-limb-prosthetics/theraptor-hand/comment-page-1/>
11. Cuellar, J.S., Smit, G., Zadpoor, A., et al.: Ten guidelines for the design of non-assembly mechanisms: the case of 3D printed prosthetic hands. *Proc. IMechE, Part H: J. Eng. Med.* **232**, 962–971 (2018)
12. Francis, V., Jain, P.K.: Advances in nanocomposite materials for additive manufacturing. *Int. J. Rapid Manuf.* **5**, 215–233 (2015)
13. Francis, V., Jain, P.K.: Investigation on the effect of surface modification of 3D printed parts by nanoclay and dimethyl ketone. *Mater. Manuf. Process.* **33**(10), 1080–1092 (2018)
14. Eshraghi, A., Yoo, J., Klein, J., Mckenzie, I., Sebaldt, G., Leineweber, M., Artero, L., Ramdial, S., Andrysek, J.: A custom, functional and lifelike passive prosthetic hand for infants and small toddlers: clinical note. *Prosthet. Orthot. Int.* 0309364620909276 (2020)
15. da Silveira Romero, R.C., Machado, A.A., Costa, K.A., Rodrigues Guilherme Reis, P.H., Brito, P.P., Santos Vimieiro, C.B.: Development of a passive prosthetic hand that restores finger movements made by additive manufacturing. *Appl. Sci.* **10**(12), 4148 (2020)
16. Dechev, N., Cleghorn, W.L., Naumann, S.: Multiple finger, passive adaptive grasp prosthetic hand. *Mech. Mach. Theory* **36**(10), 1157–1173 (2001)
17. Smit, G., Plettenburg, D.H., van der Helm, F.C.: Design and evaluation of two different finger concepts for body-powered prosthetic hand. *J. Rehabil. Res. Dev.* **50**(9), 1253–1266 (2013)
18. Doshi, R., Yeh, C., LeBlanc, M.: The design and development of a gloveless endoskeletal prosthetic hand. *J. Rehabil. Res. Dev.* **35**, 388–395 (1998)
19. Dollar, A.M., Howe, R.D.: The SDM hand as a prosthetic terminal device: a feasibility study. In: *2007 IEEE 10th International Conference on Rehabilitation Robotics*, pp. 978–983, June 2007. IEEE
20. Datta, D., Ibbotson, V.: Powered prosthetic hands in very young children. *Prosthet. Orthot. Int.* **22**(2), 150–154 (1998)
21. Huang, H.P., Chen, C.Y.: Development of a myoelectric discrimination system for a multi-degree prosthetic hand. In: *Proceedings 1999 IEEE International Conference on Robotics and Automation (Cat. No. 99CH36288C)*, May 1999, vol. 3, pp. 2392–2397. IEEE

Chapter 21

Additive Manufacturing of Polymer-Based Bio-implants Using the Fused Filament Fabrication Process



Jasvir Singh and Vishal Francis

Abstract The additive manufacturing (AM) technology has proved its potential capability to fabricate complex anatomical geometrical customized parts for biomedical applications. One of the significant bottlenecks in restricting the widespread commercial acceptance of 3D printing in biomanufacturing is the availability of biocompatible, biodegradable, chemically inert biomaterial. The use of 3D additive manufacturing technology was initially limited to the fabrication of anatomical prototype models for product design consideration, showcasing and educational training purposes. This latest advancement in biomaterials leads to the exploration of technology in the development of novel biocompatible and biodegradable materials for the use in orthopedic, spine, maxilla-facial, cranial and others 3D printing manufactures complex design implants as per the customized requirement of a very complex three-dimensional physical model and prototype parts directly from computer of the patient with an exact match. The Fused filament fabrication technology enhancing the commercial use of various polymers and polymer-based composites in the medical field for the fabrication of Scaffolds structures and clinical devices tissue engineering systems. This manuscript focuses on the development of novel biomaterials, optimization of various critical fabrication printing process parameters to improve the surface quality, mechanical properties and improving the functionality of bioimplants.

Keywords Additive manufacturing · 3D printing · Biomedical · Implants · PEEK

J. Singh · V. Francis (✉)

School of Mechanical Engineering, Lovely Professional University, Jalandhar, India

e-mail: vishal.24813@lpu.co.in

21.1 Introduction

Additive manufacturing technology or 3D printing can be used for fabricating any complex shaped three-dimensional computer-aided design (CAD) models [1]. This commercial industrial system of layer by layer deposition [2] technique initiated during the early 1980s has improved the ability to fabricate the 3D physical model significantly with the more precise geometries from CAD, which has widely replaced the manufacturing [3] time for the production of 3D prototype models by conventional techniques. Further, it is very clear that the future scope and capabilities of this additive technology reached far beyond merely 3D prototyping [4].

The primary driver behind the development of the processes that enable to make the physical components quickly without the need for conventional manufacturing tooling is the evolution of this emerging technology [5]. Today's in the past decades it has been found that the number of cases reported for the replacement of the implants has been increasingly raising its demand for the research of novel biomaterials [6, 7].

AM Advantages

Design testing-Engineering Analysis, Product development, Product Planning, re-modification in the design.

- Design and development of medical devices and instrumentation.
- Execution of Planning and understanding the complexity level of the surgical operations.
- Exploring the teaching visual aids.
- Design and development of novel biocompatible and bioactive implants and tissue engineering.

Steps for generating a 3D physical model See Fig. 21.1.

Why a Rapid Prototyping (RP) is an emerging technology of today?

The importance of a RP techniques has exploded the thrust areas for

- To explore effective communication between manufacturer and customer.
- To reduce development time of the product.

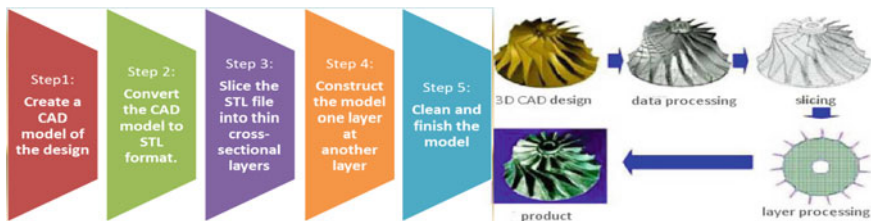
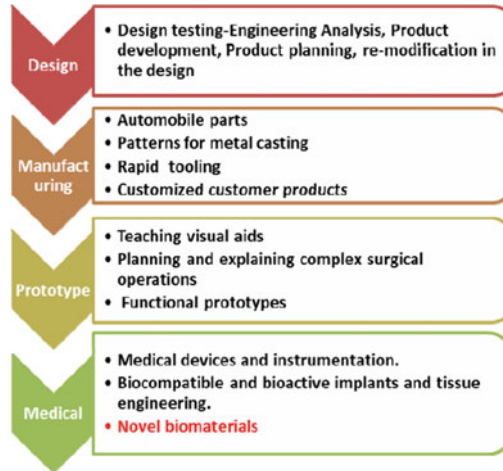


Fig. 21.1 Steps of 3D modeling

- To decrease costly mistakes and encourage sustainable design.

Applications of Additive manufacturing



Impact of Rapid Prototyping in the Medical Sector

The RP has significantly improved his ability to improve fabrication of the 3D physical models with highly precise geometries using CAD data from the medical imaging technologies [8]. One of the reasons for its application in the medical industry is its ability to fabricate any complex shaped geometry such as anatomical features. The CT scan data can be used to extract the region of interest in the development of the CAD model. These models provide better visualization compared to the virtual model and can further be used pre-surgical planning and development of surgical assistive devices [9]. The techniques can also be used to develop customized implants, prostheses and can also aid in communication between the patient and the surgeon [10–12] (Figs. 21.2, 21.3 and 22.4).

Liu et al. [15], Titanium and its alloys are extensively used in parts and medical implants, in particular as

- For the commercial replacement of hard tissue implantation in the cardiovascular and in cardiac parts for implantation.
- Modulus relatively weak, strong strength of fatigue, formability, machinability, resistance to corrosion, and bioactivity.
- In order to improve the biological, chemical, and mechanical properties undergoes surface modification.

From the biomedical engineering context, mechanical treatment, thermal spraying, sol-gel, chemical and electrochemical treatment, and ion implantation are used to maximize acceptable wear resistance, corrosion resistance, and biological properties.

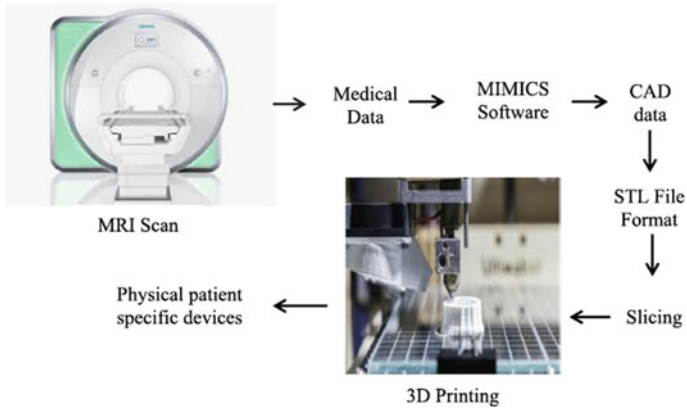


Fig. 21.2 Illustration of 3D printing [13] digitization in biomedical sector

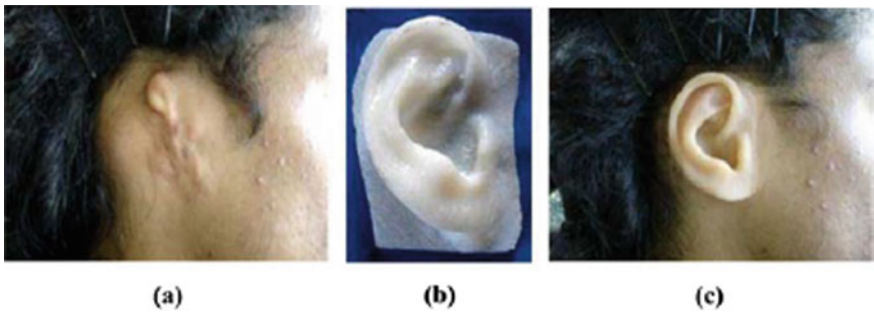


Fig. 21.3 a Patient (preoperative situation); b medical RP model; and c postoperative situation [14]

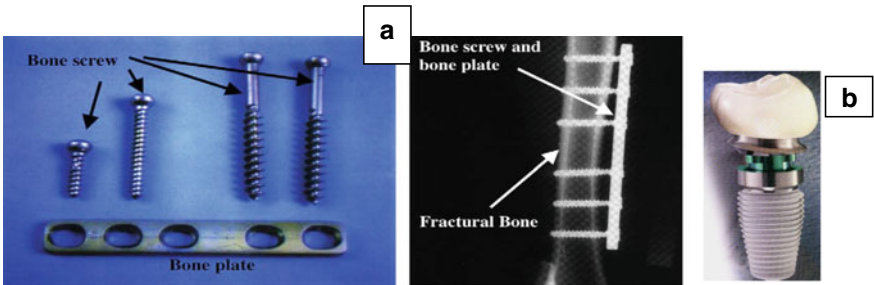


Fig. 21.4 a Titanium screw-shaped artificial tooth [15], b bone screw and bone plate for fracture bone implantation [15]

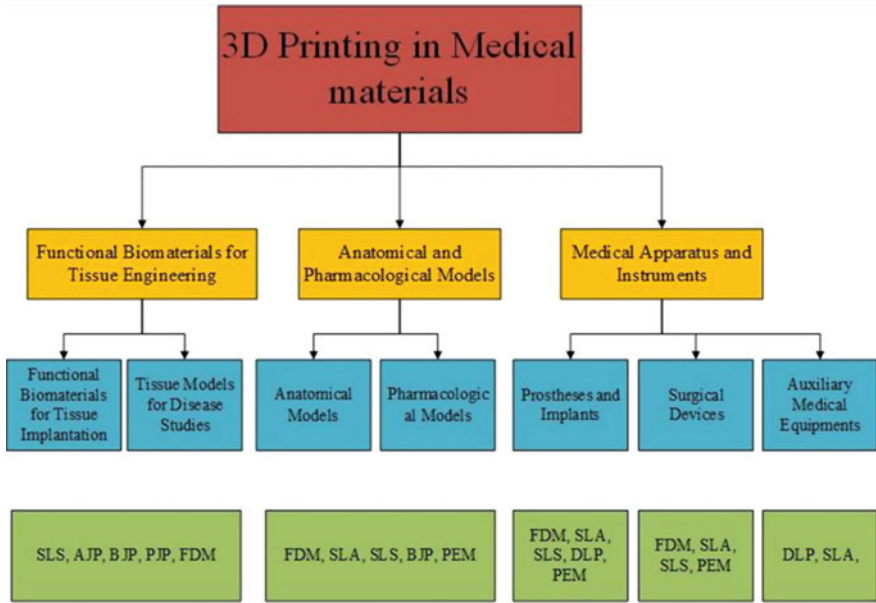


Fig. 21.5 Application of 3d printing in medical [16]

Figure 21.5 illustrates the various applications of 3D printing technology in biomedical sectors [16]. The technology can be used in tissue engineering, surgical device, anatomical models and for fabrication of implants.

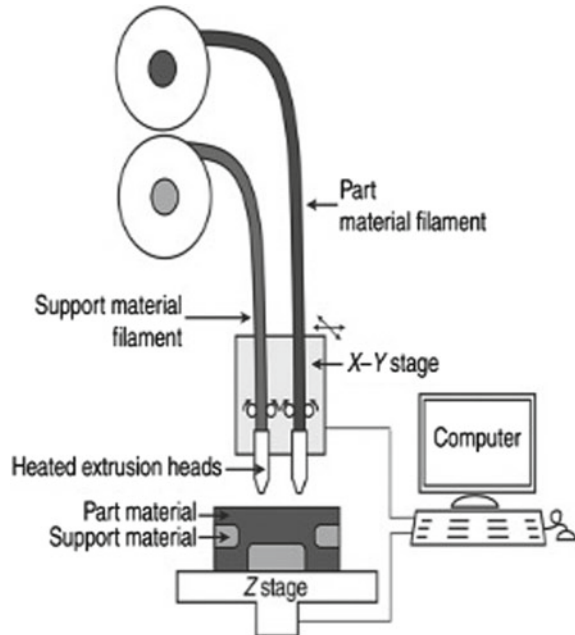
Fused Deposition Modeling for Biomedical applications

FDM is an extrusion-based process platform in which the polymer is melted and which get extruded through a nozzle head and is deposited on a machine build platform layer by layer [17–19]. The CAD model is used to generate the tool path for the extruder head by slicing the approximated CAD model (STL file). The material in the form of filament is feed through the nozzle and extruded to build the model [20].

The temperature of the extruder head is controlled as per the material used to maintain the flow of the material through the nozzle [21]. The schematic diagram of the FDM machine is given in Fig. 21.6.

In the FDM machine, the XY movement is provided to the head and z movement is given to the bed. The plastic material is heated above the level of its glass transition temperature and the bed is also heated to enhance the bonding between the deposited layers. Generally, two nozzles are used in the process. The build material is extruded from one of the nozzles and supporting material is laid on the bed from its second nozzle head. The Support material is required to build overhanging supporting features of a nozzle. The supporting material can be removed from the part by breaking away or by dissolving it with the chemical [22]. The density of the part can also be controlled by adjusting the infill ratio during the slicing procedure.

Fig. 21.6 Most commonly used 3D rapid prototyping technique: fused deposition modeling



Most of the FDM uses OEM based ABS P-400 is Stratasys Inc. manufactures and supplies ABS P-400 that costs approximately US\$260. This adds to the operating costs of the FDM technique which is one of the constraints to the merchandising of FDM technology for small and medium-sized industries.

Moreover, there has already been a deliberate effort amongst various researchers to create and improvement of an alternative FDM feedstock filament using multiple variations of Polymeric materials, abrasives, granulated powder metal, ceramic materials etc. [22–27].

Classification of Bio Materials

The biomaterials can be classified as illustrated in Fig. 21.7. Various bio-materials are utilized ranging from metals, ceramics, polymers and even composites.

One of the most promising polymer material for bio-medical applications is poly ether ether ketone (PEEK). It is known for its enhanced mechanical properties, chemical stability, biological chemical stability and biocompatibility, excellent chemical and biological inertness make it potential candidate suitable for highly complex 3D modeling of bones, customized modification of scaffolds and medical tooling and devices in biomedical implantations (Fig. 21.8) [28].

Due to the potential of PEEK material it has been considered as an alternative to metal which are used in bio-medical applications. Figure 21.8 shows the various applications of the material in clinical applications. The material can be used in cardiac surgery, orthopedic surgery, spine and dental surgeries [29].

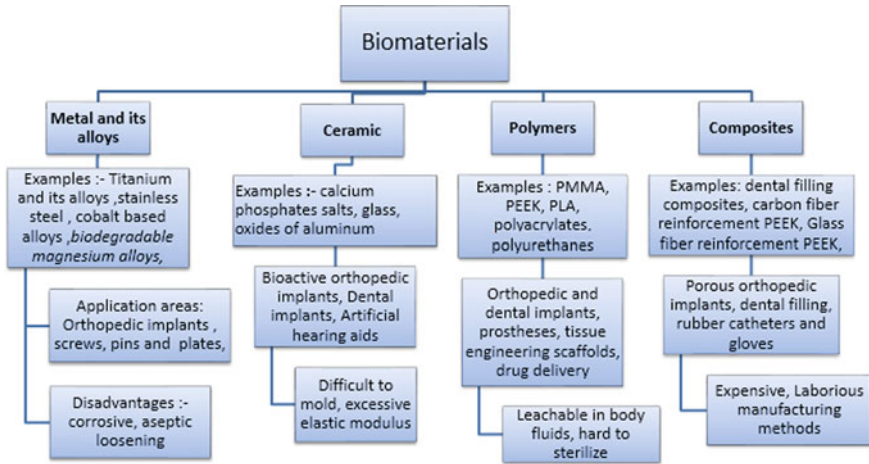
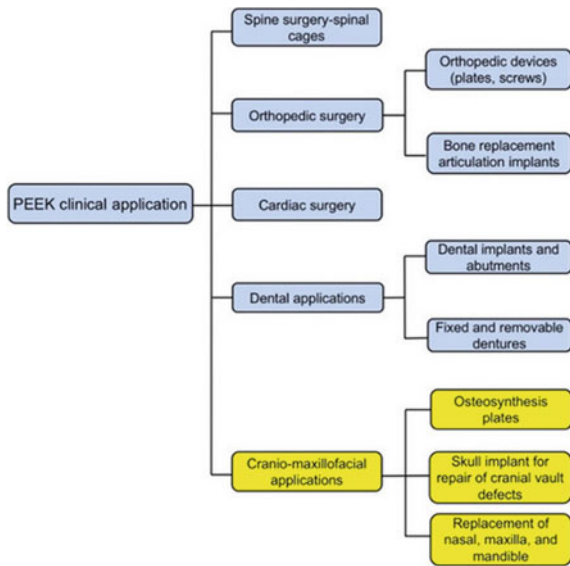


Fig. 21.7 Classification of bio-materials

Fig. 21.8 Medical applications of PEEK material [29]



Challenges with PEEK: High viscosity, low rate of the chemical affinity of PEEK with the bio-ceramics, Young’s Modulus, high processing temperature, high cost of PEEK feedstock filament, low integration to bone, wear rate failure of PEEK is very high. Standards for testing and validating are insufficient. The PEEK and its composites have been stated to be showing a promising future in the medical industry.

Ivan et al. [30] PEEK show semi-crystalline thermoplastic polymer with desirable mechanical characteristics for biomedical sciences applications. It has been

reported that the synthesis of PEEK composites is being used in different operational fields: spinal surgery, orthopedic surgery, maxillofacial surgery. The author has reported all structural modifications and surface improvements, alteration in mechanical and biocompatibility of PEEK and PEEK composites. The PEEK based biomedical implants is an improvement and it seems to prove a promising alternative for Titanium-based and ceramics implants [7].

Haleem et al. [31] 3D printing technologies are emerging in the production of PEEK implants to fulfill the customized demands of the biomedical field. PEEK material is often chosen to be printed on FDM printers.

Steinberg et al. [32] The author documented that Carbon fiber reinforced PEEK (CF-PEEK) is currently available in the orthopedic medical field. The investigator developed CF-PEEK nail, dynamic compression plate, proximal humeral plate volar plate were compared biomechanically-bending, static torsion of the nail, bending fatigue and wear/debris test were conducted. The paper explores the test results, provides recommended requirements for strength and wear for the safe and effective intended use of CF PEEK in humans.

Xiaoyong et al. [33], The author reported that the standard type of material used in the FDM 3D printer, for a Polylactic acid material nozzle head and ABS bipolymer print head temperature thresholds requirement is 190 degree to 230 degrees, the hotbed temperature is 110 degree, but PEEK material printing head temperature demands at least 340 degrees to 450 degrees. Through the experimental analysis, it is reported that the type of a semicrystalline polymer material, Printer head temperature and PEEK cooling temperature influence the mechanical properties and biological performance of the PEEK feedstock filament build.

Han et al. [34], Fused-filament fabrication (FFF) 3D printing method to fabricate PEEK implants which plays a major role in the repair of metallic implants and restoration of a prosthesis in facial orthopedic surgery, spine and craniomaxillofacial.

As the PEEK is bio-inert, which disrupts its potential ability for osseointegration and hampers its medical implementation in clinics.

The research work focuses on the study of bioactivity of FFF 3D printed PEEK. The author investigated a substantial increase in cell metabolic activity and enhanced osteoblast response with dense proliferation. The result revealed that the Fused Filament Fabrication technique produces highly rough densified surfaces and induce specially customized structures which were not attained using conventional grit blasting tools and techniques. Wettability adsorption plays a crucial role in the initial adhesion and proliferation of cells, surface morphology and roughness became favorable conditions for sound Osteoblast response.

Zhao et al. [35], Author found that the PEEK is a most demanding biomaterial with much exceptional functionality, potentially suitable for medical clinical legal applications. The material was investigated for its mechanical strength and vitro cytotoxicity. Two production methods namely SLS and FDM are available for high melting temperature materials such as for PEEK biomaterial. In recent years, FDM has been increasingly being tried for PEEK manufacturing for the economical processing of PEEK than SLS. The custom homemade FDM printer for PEEK is designed The L25 Orthogonal experiment examined the significant effect of the

thermal parameters on the mechanical strength. The temperature of nozzle heads, building platform and the ambient parameters were controlled during printing.

Vaezi et al. [36], PEEK shows magnificent bioactivity, combined strong strength-stiffness, elastic modulus similar to cortical bone, radiolucent which makes its an efficient, semi-crystalline alternative thermoplastic for biomedical implantation against metallic-ceramic materials. The researcher identified important critical parameters such as hot extrusion head design, extrusion temperature and ambient temperature conditions which have been focused on printing without warpage PEEK structures, delamination, degradation of polymers and nozzle clogging. The investigator compares syringe based and filament-based extrusion head designs suggested to utilize filament-based device which produces quite stable and productive PEEK interlayer bonded parts. The printed PEEK samples show significantly improved customized properties in comparison to resin-based on acrylate, ABS, polyamide, and alumni utilize different AM procedures.

Wang et al. [37], PEEK is an adaptable biomaterial that could be used in biomedical field applications to replace the traditional metal or ceramics parts. The researchers highlighted that the high melting temperature and high viscosity of PEEK is the challenge for manufacturing functional parts of complex PEEK structures. Using the FEA, PEEK's melting conditions and fluidity were simulated in a flow channel to print PEEK parts with reasonable surface quality and enhanced mechanical properties.

The investigators performed several FDM experiments investigating the effects of various printing parameters, including print temperature, print speed and layer thickness, mechanical behavior, microstructure and surface quality of PEEK printed 3D model parts.

The researcher proposed that the optimum parameters for PEEK printing were a heating temperature of 440 °C, a printing speed of 20 mm/s, and a printing layer thickness of 0.1 mm, respectively, that could ensure better mechanical properties and PEEK parts surface quality.

21.2 Conclusion

The present paper discusses the use of polymer-based materials for bio-medical applications using additive manufacturing technology. Extrusion-based AM technique such as FDM is discussed for fabrication of various medical applications. PEEK material potential is discussed with its applications and challenges.

References

1. Campbell, I., Bourell, D., Gibson, I.: Additive manufacturing: rapid prototyping comes of age. *Rapid Prototyp. J.* **18**(4), 255–258 (2012)

2. Negi, S., Dhiman, S., Sharma, R.K.: Basics and applications of rapid prototyping medical models. *Rapid Prototyp. J.* (2014)
3. Campbell, R.I., Dickens, P.M.: Rapid prototyping: a global view. In: Marcus, H.L., Beaman, J.J., Barlow, J.W., Bourell, D.L., Crawford, R.H. (eds.) *Solid Freeform Fabrication: An Advanced Manufacturing Approach*, 5th Solid Freeform Fabrication Symposium Proceedings. Center for Materials Science and Eng., Univ. of Texas, Austin, TX, pp. 110–117 (1994)
4. Milovanovic, Jelena, Trajanovic, Miroslav: Medical applications of rapid prototyping, *facta universitatis series. Mech. Eng.* **5**(1), 79–85 (2007)
5. Upcraft, S., Fletcher, R.: The rapid prototyping technologies. *Emeralds Assembly Autom.* **23**(4), 318–330 (2003)
6. Sun, Q., Rizvi, G.M., Bellehumeur, C.T., Gu, P.: Effect of processing conditions on the bonding quality of FDM polymer filaments. *Rapid Prototyp. J.* **14**(2), 72–80 (2008)
7. Liu, Q., Sui, G., Leu, M.C.: Experimental study on the ice pattern fabrication for the investment casting by rapid freeze prototyping. *Comput. Ind.* **48**, 181–197 (2002)
8. Melchels, F., Feijen, J., Grijpma, D.W.: A review on stereolithography and its applications in biomedical engineering. *Biomaterial* **31**(24), 6121–6120 (2010). Milovanovic, J., Trajanovic, M.: Medical applications of rapid prototyping. *Mech. Eng.* **5**(1), 79–85 (2007)
9. Kai, C.C., Meng, C.S., Ching, L.S., Hoe, E.K., Fah, L.K.: Rapid rototyping assisted surgery planning. *Int. J. Adv. Manuf. Technol.* **14**(9), 624–630 (1998)
10. Dhakshyani, R., Nukman, Y., Abu Osman, A.N.: Rapid prototyping models for dysplastic hip surgeries in Malaysia. *Eur. J. Orthopaedic Surg. Traumatol.* **22**(1), 41–46 (2012)
11. Singh, J.: A critical review on the recent applications of rapid prototyping in bio medical implantation. *Think India J.* **22**(17) (2019). ISSN: 0971-1260
12. Singh, Sunpreet, Prakash, Chander, Ramakrishna, Seeram: 3D printing of polyether-etherketonefor biomedical applications. *Eur. Polymer J.* **114**, 234–248 (2019)
13. *Three-Dimensional Microfabrication Using Two-Photon Polymerization 1st Edition*, Hardcover ISBN: 9780323353212, Micro and Nano Technologies (2015)
14. Negi, S., Dhiman, S., Sharma, R.K.: Basics and applications of rapid prototyping medical models. *Rapid Prototyp. J.* **20**(3), 256–267 (2014). ISSN 1355-2546
15. Liua, X., Chub, P.K., Ding, C.: Surface modification of titanium, titanium alloys and related materials for biomedical applications. *Mater. Sci. Eng. R* **47**, 49–121 (2004)
16. Daoyang, F., Yan, L., Xing, W., Tengjiao, Z., Qi, W., Hong, C., Weishi, L., Yun, T., Zhongjun, L.: Progressive 3D printing technology and its application in medical materials. *Front. Pharmacol.* **1663–9812**, 122 (2020)
17. Anitha, R., Arunachalam, S.: Critical parameters influencing the quality of prototypes in fused deposition modeling. *J. Mater. Process. Technol.* **113**(1–3), 385–388 (2001)
18. Choudhury, A., Chakraborty, D., Reddy, B.: Extruder path generation for curved layer fused deposition modeling. *Comput.-Aided Des. J.* **40**, 235–243 (2007)
19. Chhabra, M., Singh, R.: Rapid casting solutions a review. *Rapid Prototyp. J.* **17**, 328–350 (2011)
20. Masood, S.H.: Intelligent rapid prototyping with fused deposition modelling. *Rapid Prototyp. J.* **2**(1), 24–32 (1996)
21. Liu, T., Wang, M., Weizhi, W., Zhang, W.: Melt rheological properties of nylon 6/multi-walled carbon nano-tube composites. *Compos. Sci. Technol.* **68**, 2498–2502 (2008)
22. Singh, R., Singh, S.: Development of nylon based FDM filament for industrial applications. *J. Inst. Eng. (Ser.-C, Springer)* **92**(2), 103–108 (2014)
23. Van Weeren, R., Agarwala, M., Jamalabad, V.R., Bandyopadyay, A., Vaidyanathan, R., Langrana, N., Safari, A., Whalen, P., Danforth, S.C., Ballard, C.: Quality of parts processed by fused deposition. In: *Proceedings of the Solid Freeform Fabrication Symposium*, Austin, TX, pp. 314–321 (1995)
24. Kalita, S.J., Bose, S., Hosick, H.L., Bandyopadyay, A.: Development of controlled porosity polymer-ceramic composite scaffolds via fused deposition modeling. *Mater. Sci. Eng. C* **20**(5), 611–620 (2003)
25. Cheah, C.M., Chua, C.K., Lee, C.W., Feng, C., Totong, K.: Rapid prototyping and tooling techniques: a review of applications for rapid investment casting. *Int. J. Adv. Manuf. Technol.* **25**, 308–320 (2005)

26. Novakova, M.L., Novak, M.J., Barna, J., Torok, J.: Special materials used in FDM rapid prototyping technology applications. In: IEEE 16th International Conference on Intelligent Engineering Systems (INES), 12–15 June, pp. 73–76 (2012). E-ISBN: 978-1-4673-2693-3
27. Mireles, J., Kim, H.C., Lee, H., Espaln, L., Medna, D., MacDonald, F., Wicker, R.: Development of a fused deposition modelling system for low melting temperature metal alloy. *J. Electron. Packag. Trans. ASME* **134**(4) (2013). <https://doi.org/10.1115/1.4007160>
28. Singh, S., Prakasha, C., Ramakrishnabnggh, S.: 3D printing of polyether-ether-ketone for biomedical applications. *Eur. Polym. J.* **114**, 234–248 (2019)
29. Han, X., Yang, D., Yang, C., Spintzyk, S., Scheideler, L., Li, P., Li, D., Geis-Gerstorfer, J., Rupp, F.: Carbon fiber reinforced PEEK composites based on 3D-printing technology for orthopedic and dental applications. *J. Clin. Med.* **8**(2), 240 (2019). <https://doi.org/10.3390/jcm8020240>. PMID: 30759863; PMCID: PMC6406436
30. Panayotov, I.V., Orti, V., Cuisinier, F., Yachouh, J.: Polyetheretherketone (PEEK) for medical applications. *J. Mater. Sci. Mater. Med.* **27**, 118 (2016)
31. Haleem, A., Javaid, M.: Polyether ether ketone (PEEK) and its 3D printed implants applications in medical field: an overview. *Clin. Epidemiol. Glob. Health* **7**, 571–577 (2019)
32. Steinberg, E.L., Rath, E., Shlaifer, A., Chechik, O., Maman, E., Salai, M.: Carbon fiber reinforced PEEK Optima—A composite material biomechanical properties and wear/debris characteristics of CF PEEK composites for orthopedic trauma implants. *J. Mechanicalbehav. Biomed. Mater.* **17**, 221–228 (2013)
33. Xiaoyong, S., Liangcheng, C., Honglin, M., Peng, G., Zhanwei, B., Cheng, L.: Experimental analysis of high temperature PEEK materials on 3D printing. In: 9th International Conference on Measuring Technology and Mechatronics Automation (2017)
34. Han, X., Sharma, N., Zeqian, X., Scheideler, L., Geis-Gerstorfer, J., Rupp, F., Thieringer, F.M., Spintzyk, S.: An in vitro study of osteoblast response on fused-filament fabrication 3D printed PEEK for dental and cranio-maxillofacial implants. *J. Clin. Med.* **8**, 771 (2019)
35. Zhao, F., Li, D., Jin, Z.: Preliminary investigation of poly-ether-ether-ketone based on fused deposition modeling for medical applications. *Materials* **11**, 288 (2018)
36. Vaezi, M.R., Yang, S.: Extrusion-based additive manufacturing of PEEK for biomedical applications. *Virtual Phys. Prototyp.* (2015). ISSN: 1745-2759 (Print) 1745-2767
37. Wang, P., Zoua, B., Xiao, H., Ding, S., Huang, C.: Effects of printing parameters of fused deposition modeling on mechanical properties, surface quality, and microstructure of PEEK. *J. Mater. Process. Technol.* **271**(2019), 62–74 (2019)

Chapter 22

Design, Applications, and Challenges of 3D-Printed Custom Orthotics Aids: A Review



Ravi Kumar and Saroj Kumar Sarangi

Abstract 3D-printing technologies give better alternatives to improve on the functional abilities and traditional manufacturing technique of custom orthotics aids. The flexibility of design, mass customization, use of biodegradable materials and ability to build complex structures make it more popular over traditional methods. The traditional plaster of Paris method is bulky, breathless and fixed. The traditional method of fabrication may cause skin diseases, uneasiness and misalignment of joints. 3d printed orthotic aids overcome these problems. In this work recent advance in 3d-printed orthotics aids are presented. The design of fully customized 3d-printed orthotic aids is presented in a proper sequence. The geometrical data from patients affected parts are taken using photogrammetry software or 3-D scanner and data is imported in CAD modeler followed by modeling and topological optimization for stress analysis. The literature available on different 3d printing technologies used for printing orthotics aids is minutely reviewed. The selection of the right material for an orthotic aid is very important for its success. The physical properties of materials like strength, toughness, density, wear resistance and heat resistance are considered while selecting the materials for printing. The different types of polymers used for fabrication of orthotics are discussed in this paper in detail. Apart from this challenge for the fabrication of orthotics aids using 3d printing also reviewed.

Keywords 3D-printing · Orthotics aids · Photogrammetry

22.1 Introduction

The orthoses are assistive aids used to hold or correct the weakened muscles of the spine, arms, and legs. Orthotic aids allow physical or functional disable peoples to spend healthily and independent life. Each orthotics aids have particular function, like

R. Kumar

Department of Mechanical Engineering, Motihari College of Engineering, Motihari 845401, India

S. K. Sarangi (✉)

Department of Mechanical Engineering, National Institute of Technology Patna, Patna 800005, India

supporting or correcting the positioning of a body segment, improving its mobility, and relieving from pain. There is an estimation that around 0.5% of the human population would require prosthetics and orthotics aids globally of which more people will need orthotic aids [1]. In upcoming years, due increase in population and life expectancy there will be a need for these services. The large proportion of the aging population will have chance for developing functional disability [2], the demand for orthotics will increase accordingly. There are rapid increase in accidents, muscular misalignment [3] non-communicable diseases [4] like diabetes [5, 6] and stroke [7, 8], which will further increase the demand of orthotics aids. Thus, there is a need for continuous research in the orthotics field to make affordable treatment for every disabled person. Orthotics aids are classified according to the joint and the limb into three categories i.e. upper limb orthosis, spinal orthosis, and lower-limb orthosis. The classification for Orthotics aids is mentioned in Table 22.1 [9].

Upper limbs orthosis is broadly classified into wrist orthosis, wrist hand orthosis and elbow orthosis.

Wrist orthosis (shown in Fig. 22.1) is used to support the weakened or damaged part of forearm. Wrist hand orthosis (shown in Fig. 22.2) used to support the injured parts of forearm, wrist and hand. Elbows orthosis help in overcoming the injuries in elbows portion of the arm.

Table 22.1 Orthotics aids nomenclature [9]

Upper-limb orthosis		Lower-limb orthosis		Spinal orthosis	
WO	Wrist orthosis	AFO	Ankle-foot orthosis	CO	Cervical orthosis
				LO	Lumbar orthosis
WHO	Wrist Hand orthosis	FO	Foot orthosis	TO	Thoracic orthosis
EO	Elbow orthosis	KO	Knee orthosis	SIO	Sacroiliac orthosis

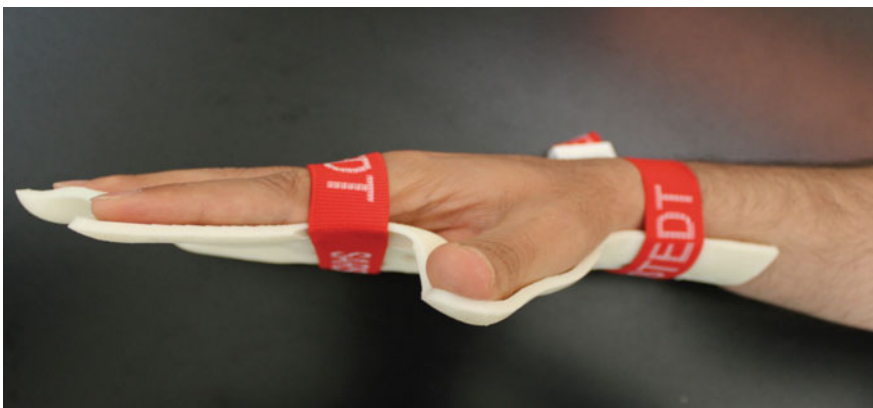


Fig. 22.1 Wrist orthosis [10]



Fig. 22.2 Wrist-hand orthosis [11]

Lower limb orthosis broadly classified into foot orthosis, ankle-foot orthosis and knee orthosis.

Foot Orthotic or orthotics insole are generally to used for offloading foot pressure reducing chance of foot ulcer in diabetics patients. Knee Orthosis (KO) relieve pressure from knee joint which is affected by stiffness in joint or underlying bones. Ankle Foot Orthosis (AFO) (as shown in Fig. 22.3) is an external wearable aids to hold ankle in the correct position by providing external mechanical support when there is some injuries or weakness in the muscular/skeletal system.



Fig. 22.3 Ankle-foot orthosis [12]

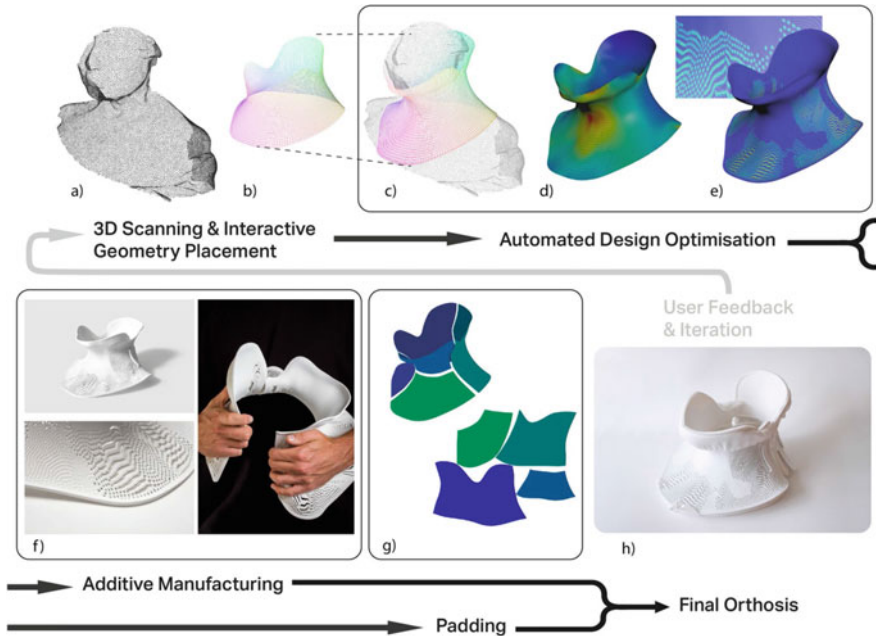


Fig. 22.4 Bespoke orthosis [13]

Spinal orthosis is classified into cervical orthosis, lumbar orthosis, thoracic orthosis and sacroiliac orthosis.

Cervical orthosis (as shown in Fig. 22.4) is used to stabilise the neck during neck pain; or provide support to head in neuromuscular injuries.

Orthotics aids can be fabricated either by using the traditional method or custom made using additive manufacturing methods. The traditional method uses plaster casts for orthotic treatment which are bulky, breathless, and fixed. The traditional moulds cause skin problems, discomfort, and joint and under laying bones injuries [14]. As per WHO, only 10% of people can afford orthotics aids, because of lack of awareness, availability, and high cost. 3-D printed orthotics aids would be better alternatives to the traditional method. Figure 22.5 compare the traditional method of orthotics fabrication with additive manufacturing.

The 3-D printed orthotics fabrications start with the design method followed by materials selections, choosing appropriate 3-D printing technologies to print the product and finally post-processing. This paper presents a systematic review of the design method, different 3-D printing technologies and materials selection for different orthotics aids. The first section discusses the design method for fully customized orthotics aids. In the next two sections, review the main 3-D printing technologies and material selections for these technologies to fabricate orthotics. Lastly, the applications and challenges are summarized.

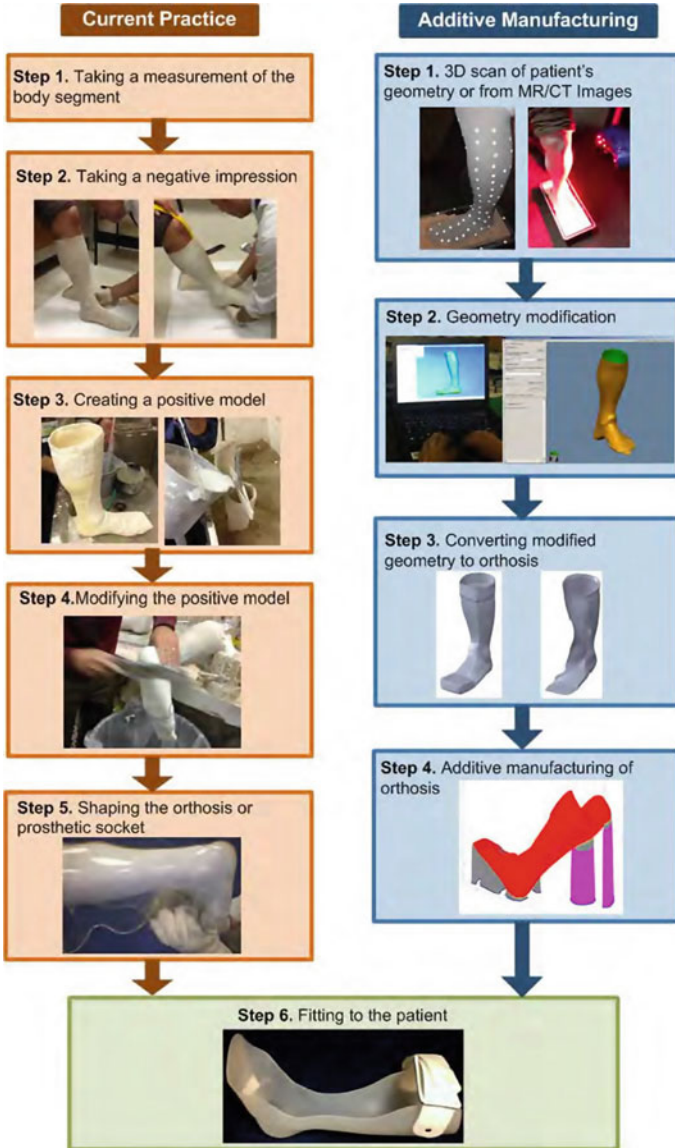


Fig. 22.5 Comparison of traditional method with additive manufacturing [3]

22.2 Design Method

The conventional method of orthosis fabrication is lengthy and time-consuming. They don't fulfil functional requirements of the patients. The design method used in 3d printing technologies are patients specific and less time consuming. The design



Fig. 22.6 Design process of the upper limb orthosis [11]

of orthotics aids is based on the 3d scanning or photogrammetry techniques without requiring preparation of individual mold for every patient. The custom-made insoles were compared with traditional pre-fabricated and off-the-shelf insoles by Caravaggi et al. [10]. In his case study, seventeen workers were selected and their feet were 3D scanned, concerning their plantar view, and these images were used to design 34 insoles. The study suggested that customized insoles are an effective solution for decreasing overloading and redistributing plantar pressure in workers' feet for different working activities. Surmen et al. n.d. created the 3D model of foot insole by taking multiple pictures from various angles and uploading these data to photogrammetry software technology. He next, transferred the 3D scan data to a CAD package and the model was altered for representing the geometric parameters of the subject's foot appropriately ready to 3D print [12].

The design process for orthotics aids is divided into the following steps (Fig. 22.6).

22.2.1 3-D Modeling: Acquisition of 3D Geometry

The 3-D model of orthotics aids can be taken using **photogrammetry** software or with a 3-D scanner. Photogrammetry is a technique of making a 3-D digital model of any subject by taking multiple images from all different angles. 150 images of patient's foot **[FO]** were captured at different angles and then uploaded on AgisoftPhotoScanPro™ software to obtain the 3D Model [15].

The 3D scanner captures human topography using light-based techniques to create 3D models. 3D scanner takes images to create a triangular mesh of the object. The software performs many functions like mesh generation, image cleaning, and exporting data [10].

22.2.2 *Importing DATA to CAD Modeller*

The next step in design method is to import photogrammetric or 3D scan data to CAD modeler. It allows building computer models of imported data. The mechanical CAD software SolidWorks™ was chosen to generate very well-parameterized ankle-foot orthosis [AFO] digital files, and also used for topological optimization [10]. The wrist orthosis model [WO] was exported to SolidWorks software, where 3 D model was built [11].

22.2.3 *Topological Optimization*

The finite element method is used to evaluate the mechanical properties under given conditions related to its function such as deformation, loading, temperatures resistance and bending. In AFO the *toe-off* and *heel-contact* phases of step are main area of interest and load is applied there during FEM simulation [10]. The calculated loading condition and the FEM can be used to design AFOs with a predetermined stiffness to match the patient's need and achieve desired biomechanical functions [12].

22.3 3-D Printing Technologies

3D printing is a rapid prototyping process that forms 3-D object from CAD or scan data by adding one layer over the adjacent layer. It consists of a microcontroller, motors and printer head. The motherboard of the 3-D printer read the uploaded design file and guides the printer head move along 3 axes to print objects either by the bottom up or the top-down approach.

As per ASTM Standard 3D printing technology are classified into 7 groups, these are binding jetting, directed energy deposition, material extrusion, material jetting, powder bed fusion, sheet lamination and vat photopolymerization.

22.3.1 *Binder Jetting*

In Binder jetting process (shown in Fig. 22.7) powder particles (metal, polymer, sand or ceramics) is first deposited on build platform. Liquid binding agent is spray by inkjet nozzle over it to bind the powdered particles together in layer by layer fashioned.

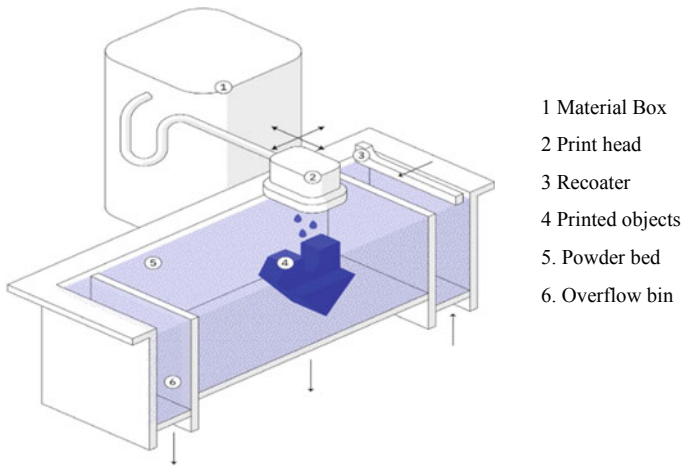


Fig. 22.7 Binder jetting Source from—what is 3 d printing? The definitive guide, 3D hubs

22.3.2 *Directed Energy Deposition*

Directed energy deposition is similar to material extrusion process where nozzle axis can move in multiple direction. This process is generally used for addition or repair work in already existing components.

22.3.3 *Materials Extrusion*

Material extrusion-based 3D printing technology is also known as Fused deposition modeling (FDM).

FDM (Fig. 22.8) is most commonly used 3D printing technology used to print objects in a layer by layer fashion by depositing melted filament through a nozzle moving along 3-axes. The layer height, wall thickness, infill density and printing orientation of filaments are the important processing parameters that decide the mechanical properties of the object [16].

FDM printers are capable of making plastics objects that have good but not great resolution. The layer thickness in FDM printing can be as low as 100 microns per layer so the object will strong but not have a good surface finish. One unique function of FDM technology is that the infill density of the object can be altered which greatly reduces the weight when compared to other techniques. Low cost, low weight, and easy to operate are the main advantages of FDM. On the other hand, anisotropic behavior, layer appearance, poor surface finish [17] high manufacturing time and unviability of thermoplastic materials with desirable properties are the main limitations of FDM [18]. The dimensional accuracy and resolution of FDM is minimum

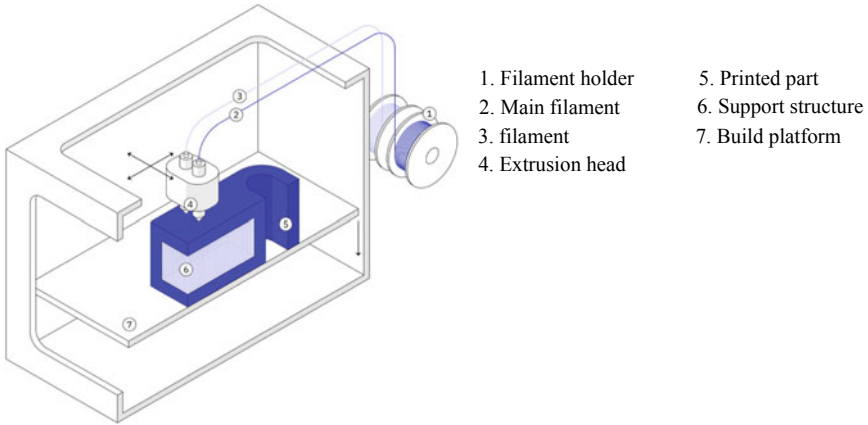


Fig. 22.8 FDM process Source from—what is 3 d printing? The definitive guide, 3D hubs

as compared with other 3D printing technologies, hence not good for printing parts with intricate details.

22.3.4 Materials Jetting

Material Jetting (shown in Fig. 22.9) working principle is similar to inkjet printing where droplets of photosensitive materials are deposited in layer by layer fashioned which solidified by UV light to form solid object. Wide varieties of materials such as polymers, composites, ceramics can be used in material jetting process.

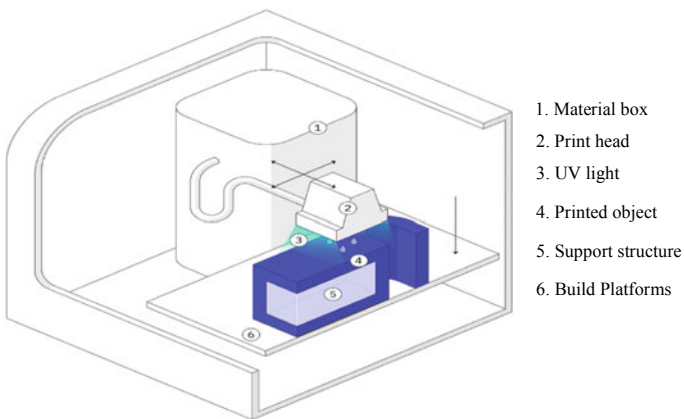


Fig. 22.9 Materials jetting. Source from—what is 3 d printing? The definitive guide, 3D hubs

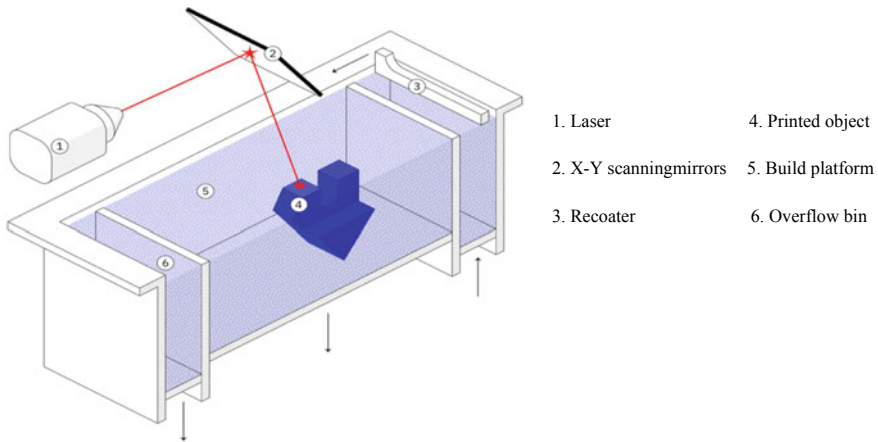


Fig. 22.10 SLS process Source from—what is 3 d printing? The definitive guide, 3D hubs

22.3.5 Powder Bed Fusion

The powder bed fusion process is also called selective laser sintering (SLS). Selective Laser Sintering (SLS) (Fig. 22.10) first introduced by DTM Corporation in the 90s [19] uses high-powered CO₂ laser to sinter powdered particles together to form 3-D objects. As per design data laser sintered the powder particles by moving along X&Y direction of a powder bed. The object is printed in a layer by layer form.

The key advantage of the SLS printer it works without support structures. The unsintered powder provides the desired support. For this reason, SLS is used to create freeform geometries that are not possible by other methods. It is capable of producing highly durable parts for real-world testing. The bond strength between layers is good in SLS printing. Also, SLS printed parts have isotropic in nature. However, the limitations of SLS technology are large production time, grainy surface finish and high porosity between fused powder particles.

22.3.6 Sheet Lamination

In Sheet lamination process sheet of materials are bond together with adhesive and cut to desired shaped by using laser.

22.3.7 Vat Photopolymerization

It is based on principle of photopolymerization, also called SLA 3d printing.

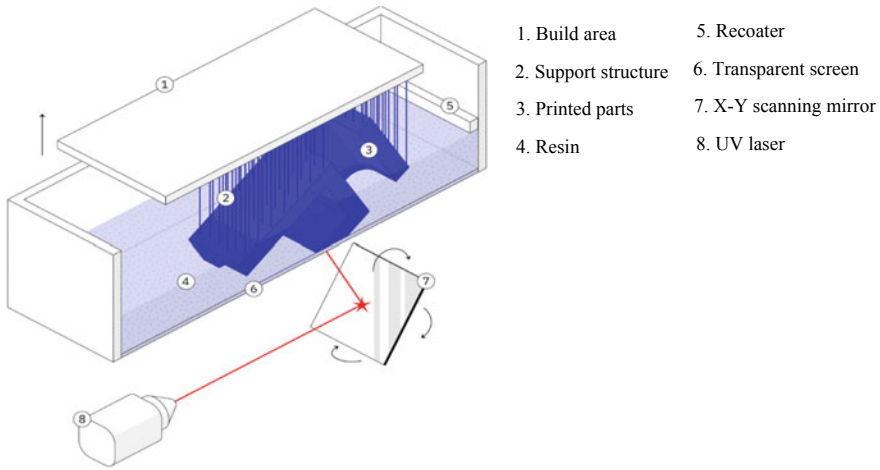


Fig. 22.11 SLA process Source from—what is 3 d printing? The definitive guide, 3D hubs

It was the first 3D printer created by Chuck Hall in 1986. He used a focused beam of ultraviolet light to harden a thin layer of a resin successively. He named this process stereolithography, also known as resin 3-D printing.

SLA (Fig. 22.11) creates objects by using a high-intensity light beam, such as a laser, to harden a soft resin. The materials used in SLA are photosensitive resin in a liquid form. The product with high resolution and smooth surface finish are created using the SLA technique. SLA can be used for fabrication of composites materials. However, objects made are not very strong. The process is very slow, costly and the materials available for printing are very limited. The kinetics reaction and the curing process is complex [20].

22.4 Materials Selections for Orthotics Aids

The selection of the right material for orthotic aids is very important for its success. There are specific types of material for each 3-D printing technology. Like photopolymers for SLA, powdered thermoplastics for SLS, thermoplastics filaments and metals for FDM. The desired physical properties of materials for orthotics fabrication comprises of flexibility, bending strength to weight ratio and durability [21]. Once you have determined the needs of your application Wizard allows you to filter through all of their available materials and determine which material fits the profile [22].

In SLA manufacturing technologies photopolymer i.e., resins are used as main printing materials. The resin used in SLA is generally viscous material in the form of plastics and glass or ceramic filled composite. The types of resin for 3-D printing are rigid resin, elastic resin, flexible resin, and high-temperature resin. There is not much literature available using resin as the material for making orthotics aids.

Photopolymer epoxy resin is used to make a prosthetic socket [23]. The prosthetic implant is constructed indirectly by SLA modeling of polymerizable or cross-linkage proteinaceous materials [24].

The most common material used in SLS printing is Nylon 12. Nylon powder can be reinforced with additives (such as carbon fibres, glass fibres or aluminium) to form composite material having desirable mechanical properties to print SLA products. However, such composite has certain limitations like anisotropic behaviour and brittleness. DuraForm EX natural plastic (3D system) nylon, is considered a durable material for manufacturing ankle-foot orthosis [25]. Mechanical damping characteristics of the SLS material for orthotics aids in Rilsan D80 is best, followed by DuraForm™ PA (nylon plastic), while DuraForm™ GF (glass-filled nylon) material has the worst damping property [26]. AFO is manufacture using the SLS technique by Nylon 11 material, having high ductility and low damping effect [27]. The foot orthotics [FO] produced in Nylon 12 on SLS machine which is biocompatible for orthotics fabrication [28].

For the FDM 3-D printer, the commonly available thermoplastics are PLA, ABS, PA, TPU, and PETG of which PLA and ABS are the 2 most frequently used materials. Table 22.2 compares the properties of these two materials.

PLA is the most popular biodegradable thermoplastic for the FDM 3-D printer made of starch prepared from grains of corn. It is very rigid, strong, and good visual quality but has brittleness property.

A PLA based material is used for custom made wrist orthosis (WO) due to it slow cost and also, the material is easily available and biodegradable [29]. PLA material have hydrophobic in nature, which degrade in the body affecting the PH

Table 22.2 Comparison between of PLA versus ABS properties

Properties ^a	ABS	PLA
Tensile strength ^b	27 MPa	37 MPa
Elongation	3.5–50%	6%
Flexural modulus	2.1–7.6 GPa	4 GPa
Density	1.0–1.4 g/cm ³	1.3 g/cm ³
Melting point	N/A (amorphous)	173 °C
Biodegradable	No	Yes, under the correct conditions
Glass transition temperature	105 °C	60 °C
Spool price ^c (1 kg, 1.75 mm, black)	\$USD 21.99	\$USD 22.99
Common products	LEGO, electronic housings	Cups, plastic bags, cutlery

^aSourced from MakeItFrom

^bSourced from Optimatter for a test specimen with 100% infill, 0.2 mm layer height printed in a linear pattern

^cSourced from Amazon ABS & PLA

of surrounding tissue; therefore, it must be replaced with polymers with a more hydrophilic properties [30]. The ankle-foot orthosis (AFO) with PLA (Poly-Lactic Acid) material is biocompatible and non-toxic, having maximum tensile stress and Young's modulus but is anisotropic [31].

ABS is usually preferred over PLA because of higher temperature resistance and higher toughness value. The orthosis is flexible and having more bending strength. Mechanical properties of ABS material calculated by tensile and bending test confirm that it is good for fabrication of wrist orthosis (WO) [11]. The FDM technology is capable of fabricating ankle-foot orthosis(AFO) with sufficient strength and stiffness using polycarbonate-acrylonitrile butadiene styrene (PC-ABS) materials as experimental results show that the FDM AFOs have lower strain during the subject's gait [12]. AFOs with PC-ABS materials were stiffer high strength to weight ratio [32].

Wang et al. [33] suggested PETG filament instead of PLA and ABS because of like moisture-bearing and more mechanical strength for customized insole fabrication. In his second experiment, Salles et al. [34] conducted the test using TPU material and suggested that the use and variability of their geometries favoured the modification of shock-absorption properties of the personalized insoles. Mogan et al. [35] printed the specimens by varying infill pattern percentages in TPU materials of two different make Filaflex and Ninjaflex. Hardness, tensile, and flexure test was performed on these specimens. They observed that tensile strength and hardness for Filaflex make filament is more compared to the Ninjaflex and based on result suggested that infill percentage of material could affect the hardness, tensile as well as flexural property materials can be suggested for applications in fabrication of orthotics insoles where flexibility and shock-absorbing are the desired properties.

From the literature review of polymers, it is observed that not a single polymer fulfils the desired mechanical properties for orthosis fabrication which includes properties like biocompatibility, flexibility, and good tensile and bending strength and there is a need to developed composite materials by reinforcing materials with desired into a polymer matrix, as they offer required mechanical properties. Tao et al. [36] prepared the TPU/PLA composite to compare with PLA filament. They found that the composite with 25% TPU give better toughness value than PLA filament without compromising the tensile strength. The insole was printed with TPU/PLA composite with the same tensile strength and better flexibility. Tekinalp et al. [37] prepared a composite by reinforcing the 3.5 mm carbon fiber by 10%, 20%, 30%, and 40% weight in ABS polymer matrix and observed that there is an increase in the tensile strength (up to 115%) and modulus (up to 700%) in the composite. Another experiment was carried out by Dul et al. [38] on the ABS matrix reinforced with graphene for 2, 4, and 8% weight fraction. Graphene reinforced composites have large value of elastic modulus and dynamic storage modulus; however, there is decrease in the maximum tensile strength and elongation at break point. Rimasauskas et al. [39] embedded 6.6 volume % continuous carbon fibre (CF) and 6.1 volume % jute fibre in the PLA polymer matrix and studied the reinforcement effect. PLA matrix reinforcement with 9.5 weight % continuous aramid fibre (8.6 volume %) has improved strength and modulus [40].

22.5 Other Applications

Besides WO, AFO 3-D printing technologies are also used in making other types of orthotics aids like orthotics insole, knee orthosis, and hand orthosis, cervical and thoracic orthosis. The detailed analysis of a hand orthosis is made using 3d printing process [10]. The customized knee orthosis is designed and developed using low-cost 3D printers [41]. The customized orthotics insole is printed using the FDM technique. The test is performed to compare plantar pressure of foot with insole to barefoot. The results suggest plantar pressure distribution in case of insole is more uniform which reduces the peak pressure to half from 218 to 109 kPa [42]. Tensile strength of PLA, ABS, Nylon and PETG materials are calculated and compared indicating PLA as a superior material followed by ABS, Nylon, and PETG and can be used in the development of a scoliosis brace [43].

22.6 Future Challenges

3-D printing technologies have great potential to change the traditional design and manufacturing process of orthotics products. It can fabricate custom-made **WO**, **AFO**, **HO**, **CO**, and other orthotics aids. However, studies clearly show that there is technological barrier on both design and manufacturing level that need to be overcome. The initial cost and printing cost are also too high as compared to traditional methods that need to be addressed [32]. High investment cost, large printing time, software barrier and limited availability of materials are the major challenges for these technologies. There is not a single software available today that can take the 3D scan data, modify the geometry of the 3D surface, convert the surface into a solid object, and create tramlines in a single shot. There is need to developed single software platform that can handle all these process [32]. PLA is an excellent material for FDM, but it is not the most mechanically resistance [31]. The manufacturing time using FDM for AFO using the current printer takes about a full day, which can be reduced by incorporating optimal topology geometry and sparse structure [12].

References

1. Rietmacher, G.: Report of a consensus conference on appropriate prosthetic technology for developing countries. Copenhagen: International Society for Prosthetics and Orthotics, Hanoi, Vietnam, 3–8 Apr 2006
2. Prosthetics and orthotics programme guide. Geneva, Landmine Survivors Network. http://www.ispoint.org/sites/default/files/img/programme_guide_final_version.pdf. Accessed 30 June 2016
3. Chen, R.K., Jin, Y., Wensman, J., Shih, A.: Additive manufacturing of custom orthosis and prostheses—a review. *Addit. Manuf.* **12**, 77–89 (2016)

4. Kate, J.T., Smit, G., Breedveld, P.: 3D-printed upper limb prostheses: a review. *Disabil. Rehabil. Assist. Technol.* **12**(3), 300–314 (2017)
5. Fisk, J.R., DeMuth, S., Campbell, J., DiBello, T., Esquenazi, A., Lin, R.S., et al.: Suggested guidelines for the prescription of orthotic services, device delivery, education, and follow-up care: a multidisciplinary whitepaper. *Mil Med* **181**(2 Supple), 11–17 (2016)
6. Priority assistive products list. Geneva, World Health Organization. http://www.who.int/phi/implementation/assistive_technology/global_survey-apl/en/. Accessed 30 Aug 2016
7. General terms for external limb prostheses and external orthoses. Geneva, International Organization for Standardization, ISO 8549-1, Prosthetics and orthotics, Vocabulary, Part 1
8. Terms relating to external limb prostheses and wearers of these prostheses. Geneva, International Organization for Standardization, ISO 8549-2, Prosthetics and orthotics, Vocabulary, Part 2
9. Shurr, D.G., Michael, J.W., Cook, T.M.: *Prosthetics and orthotics*. Prentice Hall (2002)
10. Baronio, G., Harran, S., Signoroni, A.: A critical analysis of a hand orthosis reverse engineering and 3D printing process. *Appl. Bionics Biomech.* Article ID 8347478, 7 (2016)
11. Palousek, D., Rosicky, J., Koutny, D., Stoklasek, P., Navrat, T.: Pilot study of the wrist orthosis design process. *Rapid Prototyp. J.* 27–32 (2014). ISSN 1355-2546
12. Chen, R.K., Chen, L., Tai, B.L., Wang, Y., Shih, A.J., Wensman, J.: Additive manufacturing of personalized ankle-foot orthosis. *Proc. NAMRI/SME* 42 (2014)
13. Hale, L., Linley, E., Kalaskar, D.: A digital workflow for design and fabrication of bespoke orthoses using 3D scanning and 3D printing, a patient-based case study. [www.nature.com/scientificreports/\(2020\)10:7028](http://www.nature.com/scientificreports/(2020)10:7028). <https://doi.org/10.1038/s41598-020-63937-1>
14. Kim, H., Jeong, S.: Case study: hybrid model for the customized wrist orthosis using 3D printing. *J. Mech. Sci. Technol.* **29**(12), 5151–5156 (2015)
15. Maso, A.D., Cosmi, F.: 3D-printed ankle-foot orthosis: a design method. *Mater. Today: Proc.* **12**, 252–261 (2019)
16. Mohamed, A., Masood, S.H., Bhowmik, J.L.: Optimization of fused deposition modeling process parameters: a review of current research and future prospects. *Adv. Manuf.* **3**(1), 42–53 (2015)
17. Chohan, J.S., Singh, R., Boparai, K.S., Penna, R., Fraternali, F.: Dimensional accuracy analysis of coupled fused deposition modeling and vapour smoothing operations for biomedical applications. *Compos. Part B* **117**, 138–149 (2017)
18. Wang, X., Jiang, M., Zhou, Z., Gou, J., Hui, D.: 3D printing of polymer matrix composites: a review and prospective. *Compos. Part B* **110**, 442–458 (2017)
19. Beaman, J., Deckard, C.: Selective laser sintering with assisted powder handling U.S. Patent No. 4,938,816, 3 July 1990
20. Melchels, F.P., Feijen, J., Grijpma, D.W.: A review on stereolithography and its applications in biomedical engineering. *Biomaterials* **31**(24), 6121–6130 (2010)
21. Vaish, A., Vaish, R.: 3D printing and its applications in Orthopedics. *J. Clin. Orthop. Trauma* **9**, S74–S75 (2018)
22. Material-wizard, Stratasysdirect
23. Donald, F., Wontorcik, L.: Stereolithography and prosthetic test socket Manufacture: a cost/benefit analysis. *JPO: J. Prosthet. Orthot.* 17–20 (1998)
24. D'urso, P.S.: Stereolithographic anatomical modelling process. US Patent, 5,741,215 (1998)
25. Schrank, E.S., Stanhope, S.J.: Dimensional accuracy of ankle-foot orthoses constructed by Rapid customization and manufacturing framework. *JRRD* **48**, 1 (2011)
26. Faustini, M.C., Neptune, R.R., Crawford, R.H., Stanhope, S.J.: Manufacture of passive dynamic ankle-foot orthoses using selective laser sintering. *IEEE Trans. Biomed. Eng.* **55**, 784–790 (2008)
27. Harper, N.G., Esposito, E.R., Wilken, J.M., Neptune, R.R.: The influence of ankle-foot orthosis Stiffness on walking performance in individuals with lower-limb impairments. *Clin. Biomech.* **29**, 877–884 (2014)
28. Pallari, J.H.P., D, K.W., Woodburn, J.: Mass customization of foot orthoses for rheumatoid arthritis using selective laser sintering. *IEEE Trans. Biomed. Eng.* **57**, 7 (2010)

29. De Souza, M.A., Schmitz, C., Pinhel, M.M., Setti, J.A.P., Nohama, P.: Proposal of Custom Made Wrist Orthoses Based on 3D Modeling and 3D Printing. *IEEE* (2017). 978-1-5090-2809-2/17/\$31.00
30. Miclaus, R., Repanovici, A., Roman, N.: Biomaterials: polylactic acid and 3D printing processes for orthosis and prosthesis. *Mater. Plastice* **54**, 1 (2017)
31. Maso, A.D., Cosmi, F.: 3D-printed ankle-foot orthosis: a design method. *Mater. Today: Proc.* **12**, 252–261 (2019)
32. Chen, R.K., Jin, Y., Wensman, J., Shih, A.: Additive manufacturing of custom orthoses and prostheses—a review. *Addit. Manuf.* 77–89 (2016)
33. Wang, J.C., Dommati, H., Cheng, J.: A Turnkey manufacturing solution for customized insoles using material extrusion process. In: *3D Printing and Additive Manufacturing Technologies*, pp. 203–216. Springer, Singapore (2018)
34. Salles, A.S., Gyi, D.E.: Delivering personalised insoles to the high street using additive manufacturing. *Int. J. Comput. Integr. Manuf.* **26**(5), 386–400 (2013). <https://doi.org/10.1080/0951192X.2012.717721>
35. Mogan, Y., Tun, U., Onn Malaysia, H., Periyasamy, R.: Thermoplastic elastomer infill pattern impact on mechanical properties 3D printed customized orthotic insole Development of Smart injection Molding Machine System View project Flexible filament feasibility study View project Mohd Halim Irwan Ibrahim, 2016
36. Tao, Y., Shao, J., Li, P., Shi, S.Q.: Application of a thermoplastic polyurethane/polylactic acid composite filament for 3D-printed personalized orthosis. *Mater. Tehnol.* **53**(1), 71–76 (2019). <https://doi.org/10.17222/MIT.2018.180>
37. Tekinalp, H., Kunc, V., Velaz-Garcia, G.M., Duty, C.E., Love, L.J., Naskar, A.K., Blue, C.A., Ozcan, S.: Highly oriented carbon fiber polymer composites via additive manufacturing. *Compos. Sci. Technol.* **105**, 144–150 (2014)
38. Dul, S., Fambri, L., Pegoretti, A.: Fused deposition modelling with ABS–graphene nanocomposites. *Compos. A Appl. Sci. Manuf.* **85**, 181–191 (2016). <https://doi.org/10.1016/j.compositesa.2016.03.013>
39. Matsuzaki, R., Ueda, M., Namiki, M., Jeong, T.K., Asahara, H., Horiguchi, K., Nakamura, T., Todoroki, A., Hirano, Y.: Three-dimensional printing of continuous-fiber composites by in-nozzle impregnation. *Sci. Rep.* **6**, 1–7 (2016). <https://doi.org/10.1038/srep23058>
40. Bettini, P., Alitta, G., Sala, G., Di Landro, L.: Fused deposition technique for continuous fiber reinforced thermoplastic. *J. Mater. Eng. Perform.* **26**, 843–848 (2017). <https://doi.org/10.1007/s11665-016-2459-8>
41. Santos, S., Soares, B., Leite, M., Jacinto, J.: Design and development of a customised knee positioning orthosis using low cost 3D printers. *Virtual Phys. Prototyp.* (2017). <https://doi.org/10.1080/17452759.2017.1350552>
42. Yarwindran, M., Ibrahim, M., Raveverma, P.: The feasibility study on fabrication customized orthotic insole using fused deposition modeling (FDM). *AIP Conf. Proc.* **1831**, (2017). <https://doi.org/10.1063/1.4981142>
43. Malik, R.: Tensile Testing of 3D Printed Materials for Scoliosis. *Brace*. <https://dspace.library.uvic.ca/handle/1828/8616>

Chapter 23

Analysis of Carbon Nanotubes Reinforced Functionally Graded Composite Beams by Finite Elements Method



Manish Kumar and Saroj Kumar Sarangi

Abstract This paper presents the static analysis of carbon nanotube reinforced composite (CNT) beams using the finite element method. Uniformly distributed CNT reinforced composite beams and FG-CNT reinforced composite beams are considered. Since the general mixing rule is not suitable for such beams, an extended mixing rule is used to calculate the material properties of the beams, taking into account the efficiency parameters of CNT, to include material properties depending on size. The finite elements model was developed for the beam in the ANSYS using the calculated properties of the material. The finite element model is first tested for validation, and then the results are shown for different load and boundary conditions. The influence of the volume fraction of CNT fibers in the composite beams on the bending analysis of beams has been investigated. It turns out that the deflection of the beam is strongly affected by the type of load and the grading of material properties. It is also detected that the bending deflection of the beams decreases with the increase in the volumetric fraction of CNT under different load conditions.

Keywords FEM · CNT reinforced · Functionally grade · Composite beams

23.1 Introduction

The carbon nanotube has unique mechanical, thermal and electrical properties and which are considered promising reinforcement for high performance structural and multifunctional composites with a variety of potential applications. The most important characteristics of the CNT are high rigidity with excellent elasticity. Han and Elliot [1] simulated the elastic properties of CNT composite, while Zhu et al. [2] showed the stress-strain curves of composite materials reinforced with CNT. These studies are very useful to demonstrate that the addition of a small amount of CNT significantly improves the properties of composites. These results are useful for analysing the overall response of CNT-reinforced composite in components. Wuite and Adali [3] worked on the deflection and the calculation of the stresses of beams

M. Kumar · S. K. Sarangi (✉)

Department of Mechanical Engineering, National Institute of Technology Patna, Patna, India

reinforced with nanocomposite by means of multiscale analysis. They found that a small portion of the carbon nanotube can significantly improve beam stiffness. Vodenitcharova and Zhang [4] investigated the pure local buckling and bending behavior of single wall CNT-reinforced composite beams. Earlier studies have shown that the use of CNT on nanocomposite was inhibited due to the weak bonding of the interface between CNT and the matrix. FGM materials have several advantages. It provided the multi functionality and the dynamic response, corrosion, wear and the capability to design for dissimilar complex environments of FGM materials used to eliminate stress concentration. FGM materials have provide the opportunity to enjoy the benefits of dissimilar material systems, e.g. metals and ceramics such a bonding capacity, oxidation resistance and toughness However, FGM materials present various challenges, for example mass production, production cost, production control, etc. Roque et al. [5] worked with the effect of scale parameters on the free vibration frequency of a functionally graded Tymoshenko beam. Differential evolution optimization is used to solve the optimization problem of minimizing the frequency of free vibrations of the beams. Wu et al. [6] study the nonlinear vibrational analysis of the reinforced composites beam by functionally graded carbon nanotubes with geometric defects. They concluded that the fundamental linear frequency of the beam increases due to the presence of initial defects, and this effect becomes more important as the amplitude of the rupture increases. Akbas et al. [7] studies the forced vibration of an FG beams with a porosity effect under harmonic load distributed according to the FEM method. In this article they saw that porosity plays a very vital role in the dynamics of deep FG beams. Kumar et al. [8] work with the influence of carbon nanotubes on CNT reinforced FGM nano sheets under their mechanical loading. CNTs have been confirmed to significant increase the strength of both FGMs and composites. It was specified that the CNT would lead to a resistance of the composite material under higher mechanical stress than the FGM. Though, under thermo mechanical loading, FGMs should have a higher strength than that of the composite material. Puneet et al. [9] work with bending, free vibration and buckling of FG-CNTRC beams. He concludes that increasing the number of wall in MWCNT, decreases dimensionless natural frequency and buckling load of the beams but increase bending deflection. The FGX-CNT distribution gives the largest frequency for all boundaries condition. Lin et al. [10] work with the linear oscillation of nanocomposite beams reinforced by SWCNT. Comparative studies between UD-CNT and FG-CNT based on the first and third order shear deformation theories come to the conclusion. Another study on the analysis of the free vibration of the FG-CNT beam has been developed [11–14]. As a result, FG materials are inhomogeneous composites that exhibit a continuous variation in material properties and these materials have been found to have many applications in the industry [11].

Studies of the free vibration characteristics of FG-CNT beams are available in the open literature. However a limited number of works are reported to investigate frequency of beams for FG-CNT. So, the tenacity of this study was to examine the free vibration performance of CNT reinforced FG nanocomposite beams. The material properties of the beam are assumed to varies along its thickness. These

material properties are obtained by the extended rule of mixture using with efficiencies parameters. The models of the FG beams are design in ANSYS. Results were obtained for UD-CNTRC beams for validation purposes. Detail parametric studies were performed to understand the special effects of nanotube volume fraction, end conditions in addition to CNT distribution on free vibration behaviour of FG-CNT reinforced beams.

23.1.1 Application of FGM

FGM is used for a variety of applications. It is now used in a number of industries. It has great potential for use in other applications. The current area of application includes defiance, biomedical, electrical, electronics, energy, aerospace, automobile, marine, thermoelectric, optoelectronics. It is also used for tough operating condition for thermoelectric generator, heat engine component, the rocket heat shield, the plasma facing for fusions reactors in nuclear reactors plants, electrical insulating application. The future demand of FGMS in such application, where unexpected thermal, chemical and mechanical properties are essential which is must be able to serve working environment. This potential will be used in future applications of nonlinear functions such as hardness, toughness, and so on.

The initial application is automobile industry. The present application include combustion chamber, for the leaf spring drive shaft, shock absorbers, flywheel, car body parts etc. FGM is used in automobiles for better bodybuilding. The application of FGMS in aerospace engineering is increased over the years. These included rocket engine component, turbine blade coating, nose caps, leading edge of missile; space craft truss structure, heat exchange panel, space shuttles, turbine wheel, solar panel and heat exchanger panel. FGM is also used to build walls that combine the heat and sound industries. The future use of FGM will be expanded as the production costs of these materials are reduced. Indeed, the production costs of FGMS are significant in many applications such as cutting tool, engine component and machine parts etc. so, the use of FGM materials are the most active and efficient material for sustainable growth in the industry.

23.2 Modelling of the Beam

Figure 23.1 shows a composite beam with length L , width b and thickness h . Three types of beams are considered, namely uniformly distributed CNT beams, functionally graded CNT beams of type X (FG-XCNT) and type Δ (FG- Δ CNT) in Figs. 23.2 and 23.3.

These CNT reinforced composite beams are deliberated to have comparable geometries and carry the similar total weight of CNTs m_{cnt} and with the total, volume fraction CNTs i.e. V_{cnt} .

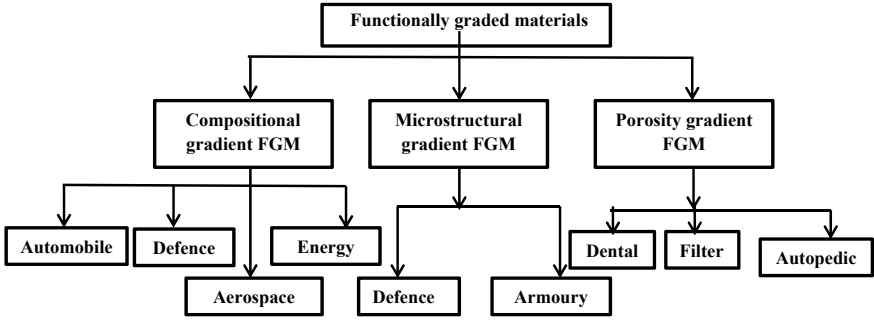


Fig. 23.1 Area of application for three types of FGMs

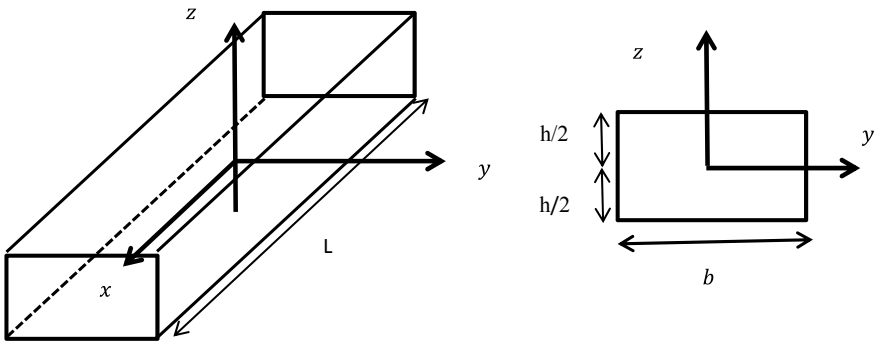


Fig. 23.2 Schematic diagram of beam

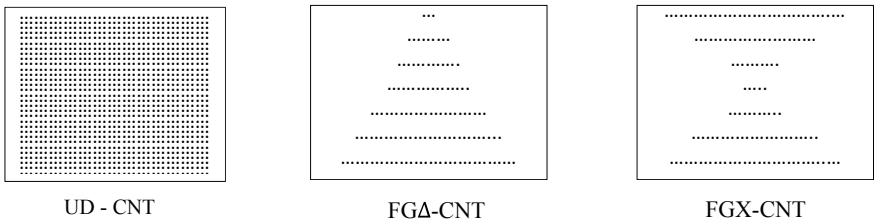


Fig. 23.3 Distribution of CNT

23.2.1 The Extended Rule of Mixture

According to the rule of mixture, FGM is assuming to vary smoothly along the direction as a function of material constituent and volume fraction. Since FGM beams consider the varying direction is thickness. The CNT volume fraction varies along z-axis direction which is explain as [6], (Only linear distribution is considered for practical purpose)

$$V_{CNT}(z) = \left(\frac{h - 2z}{2h} \right), \quad -\frac{h}{2} \leq z \leq \frac{h}{2}$$

The volume fraction of FG-XCNT is given by

$$V_{CNT}(z) = \left\{ \begin{array}{l} \frac{4z}{h} V_{tcnt}, \quad \left(0 \leq z \leq \frac{h}{2} \right) \\ -\frac{4z}{h} V_{tcnt}, \quad \left(-\frac{h}{2} \leq z \leq 0 \right) \end{array} \right\}$$

For an uniformly distributed CNT, the CNT is evenly distributed across the thickness of the beam, meaning that the CNT volume fraction varies along the z coordinate and is equal to the total CNT volume fraction [15].

$$V_{CNT}(z) = V_{tcnt} \left(-\frac{h}{2} \leq z \leq \frac{h}{2} \right)$$

Young’s modulus, shear modulus and density of the CNT composite beam were obtained based on the simulation results of existing molecular dynamics using the extended mixing rule. The expression is the following:

$$E_{11}(z) = \eta_1 V_{CNT}(z) E_{11}^{cnt} + V_m(z) E^m$$

$$v_{21}(z) = \frac{v_{12}(z)}{E_{11}(z)} E_{22}(z), \quad \rho(z) = V_{CNT}(z) \rho^{cnt} + V_m(z) \rho^m$$

$$v_{12}(z) = \eta_1 V_{CNT}(z) v_{12}^{cnt} + V_m(z) v^m$$

$$\frac{\eta_2}{E_{22}(z)} = \frac{V_{CNT}(z)}{E_{22}^{cnt}} + \frac{V_m(z)}{E^m}, \quad \frac{\eta_3}{G_{12}(z)} = \frac{V_{CNT}(z)}{G_{22}^{cnt}} + \frac{V_m(z)}{G^m}$$

$$V_m(z) = 1 - V_{CNT}(z)$$

$$E_{22} = E_{33}, G_{12} = G_{13}, G_{23} = 1.2G_{12}$$

where, $E^m, G^m, E_{11}^{cnt}, E_{22}^{cnt}$ and G_{22}^{cnt} are shear modulus and young’s modulus of matrix and CNT. v_{12}^{cnt} and v^m are Poisson’s ratio. η_1, η_2 are efficiency parameters of carbon nanotube and matrix, and ρ^m and ρ^{cnt} are mass densities of matrix and carbon nanotube respectively.

The Beam is considered to be made of various strips which are modelled separately using ANSYS package. The material properties in the strips are taken utilizing extended rule of mixture. All the strips are perfectly bonded to each other in the ANSYS (Fig. 23.4a, b).

The element type selected for the beam is solid 186. It has 6 nodes with higher solid element which has three degree of freedom per node. The three degrees of freedom

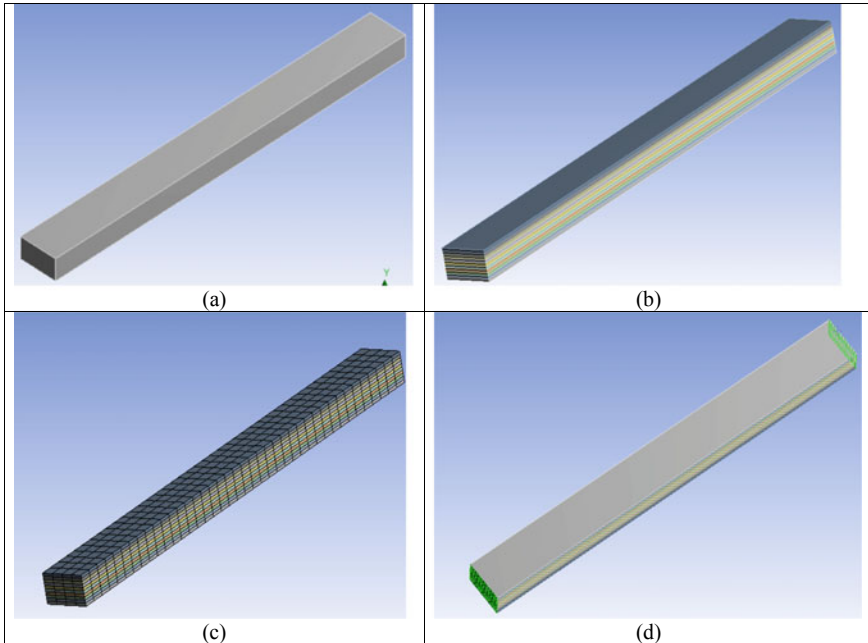


Fig. 23.4 **a** Functionally graded composite beam, **b** model of functionally graded composite beam with strips, **c** meshing of functionally graded composite beam, **d** HC-HC at the end of beam

are the nodes x , y and z . Solid 186 support great strain abilities, more deflection, hyper elasticity, stiffness with creep. CNT has great tensile strength, highly flexible (it can be bent without breaking). SOLID 186 have capability to simulate the beams of CNT reinforced composites.

Mesh:

The created 3D model is meshed by certain number of divisions or elements. A fine mesh is applied to achieve precise and accurate results than coarse mesh. An automated mesh is generated here on the created model as shown in Fig. 23.4c.

Boundary condition:

Four types of boundary conditions such as Pin (P), Hard clamped (HC), Free (F) and Soft Clamped (SC) condition are explained and current study takes into account each end of the beam. One boundary condition HC-HC is explained in Fig. 23.4d.

Table 23.1 Material properties of CNT and matrix

S. No.	Properties	Matrix	CNT
1	Densities (kg/m ³)	1190	2100
2	young's modulus (E_{11}) GPa	2.5	5646.6
3	young's modulus (E_{22}) GPa	2.5	7080
4	Passion ratio (ν_{12}^{CNT})	0.3	0.175
5	Shear modulus (G_{12}^{CNT}) GPa	0.7267	1944.5

Table 23.2 CNT efficiency parameters

CNT efficiency parameter	V_{icnt}	V_{icnt}	V_{icnt}
	0.12	0.17	0.28
η_1	0.137	0.142	0.141
η_2	1.022	1.626	1.585
η_3	0.715	1.138	1.109

23.3 Material Properties

CNTs are elastic, low thermal expansion co-efficient, high tensile strength. it is suitable for analysis of beam for using blade of turbine, cooling towers, radar bonnets and racing cars etc. The material property of the composite beams is explained in Table 23.1. The other required properties are calculated using extended rule of mixture (Table 23.2).

23.4 Results and Discussion

FG-CNT reinforced composite beam of different boundary condition is considered for detail exploration. The composites beams with three dissimilar types of FG distributed were tested for bending and free vibration characteristic. Present study aims to analyse firstly static analysis and secondly model analysis of FG-CNTRC beam. First the convergence study followed by validation is conducted for uniform distributed CNT beam and is presented. There are comparative studies of published results that were used to confirm the computational results that were used in this study.

Table 23.3 presents the maximum bending deflection for uniformly distributed CNT beams with total volume fraction 0.17. The L/h ratio of the beams is taken to be 10. The solution of this study fits well with Akbas et al. [7].

Now applying a static load 10 MPa on the beam, structural analysis is performed on the beam for three different volume fractions of CNT in ANSYS workbench to determine total deformation and von-misses stress (Figs. 23.5 and 23.6).

The dimensionless bending deflection is

Table 23.3 Effect of the V_{CNT} on maximum bending deflection (mm) of beams

CNT-distribution	Boundary condition	Current study	Ref. [7]
UD-CNT	SC-SC	1.01e-3	0.102e-2
FG-XCNT	SC-SC	0.98e-3	0.100e-2
FG Δ -CNT	SC-SC	1.27e-3	0.137e-2

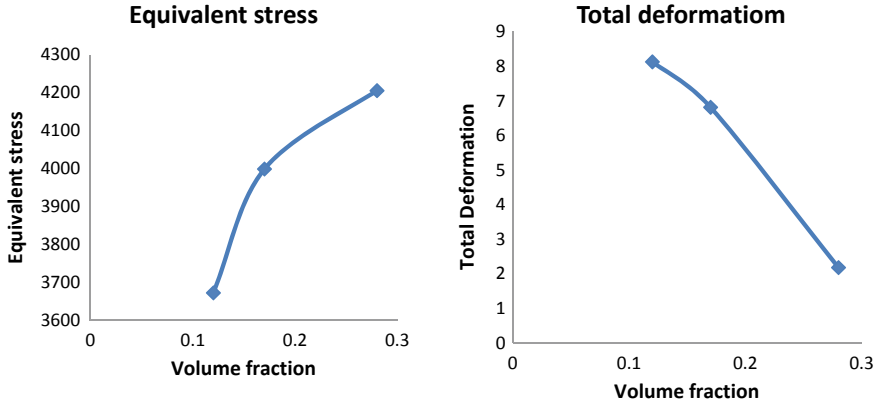


Fig. 23.5 a Equivalent stress with volume fraction, b total deformation with volume fraction

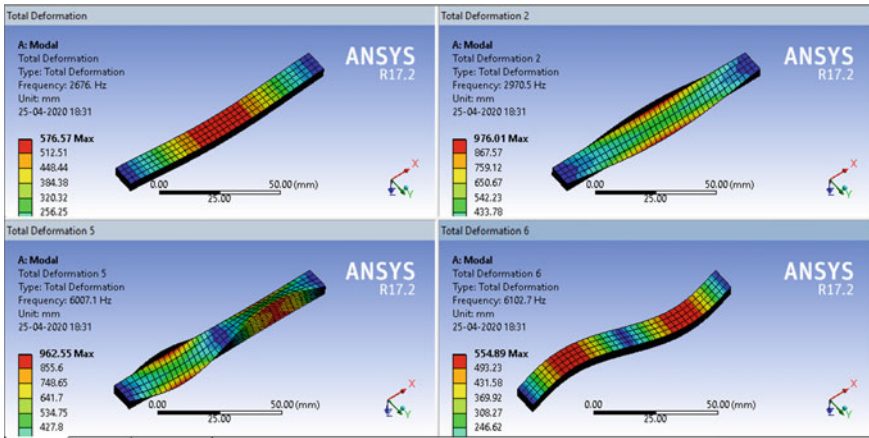


Fig. 23.6 The different mode of total deformation

$$\delta^* = \frac{100 * E^m * h^3 * \delta * (\frac{L}{2})}{q_0 L^4}$$

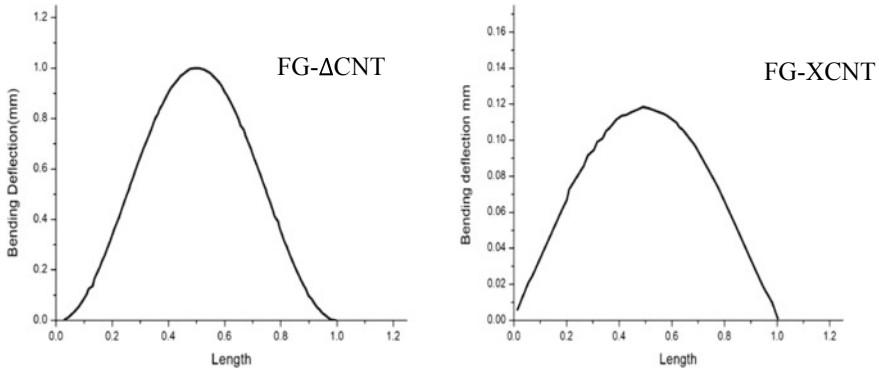


Fig. 23.7 Static non dimensionless bending deflection of the beams across the centre line through different length of the beam

Table 23.4 Non dimensional frequency parameters for evenly distributed CNT beams with V_{cnt} at 0.17 where L/h equal to 10

CNT-distribution	Boundary condition	Ref. [10]	Current study
Uniformly distributed CNT	P-P	1.56591	1.57640
	S C-P	1.84400	1.866990
	S C-S C	2.13310	2.16660

The static non dimensionless bending deflection of FGΔ-CNT and FGX-CNT beam for SC-SC boundary condition as shown in Fig. 23.7. FGΔ-CNT beam has greater bending deflection than FGX-CNT at all L/h ratio.

After performing static analysis by applying HC-HC boundary condition for UD-CNT beam, the different modes of total deformation is shown in Fig. 23.4. For finding the total deformation and natural frequency ANSYS 17.2 is used.

Table 23.4 present the fundamental frequency parameters for evenly distributed CNT. The L/h ration of the beams is taken to be 10. Frequency parameter is nondimensionalize as

$$\gamma = \frac{\omega l^2}{h} \sqrt{\frac{\rho_m}{E_m}}$$

Convergence studies and comparison confirmed the accuracy and reliability of the presently solution method to make the solution for FGΔ-CNT and FGX-CNT (Table 23.5).

In FGΔ-CNT, the CNT reinforced is continuously increasing from top to bottom. So, we see that in Fig. 23.8 if L/h ratio is increases the free vibration frequency continuously increases. Now, if total volume fraction of CNT is increases then free vibration frequency increases shown in Fig. 23.8.

In FGX-CNT, the CNT reinforced is continuously decreases at midpoint, after continuously increases from top to bottom. So, we see that in Fig. 23.9 if L/h ratio is

Table 23.5 Fundamental frequency parameters for functionally graded CNT beams with L/h ratio equal to 10

CNT distribution	Boundary condition	$V_{tcnt} = 0.17$	$V_{tcnt} = 0.28$
FG Δ -CNT	SC-F	0.5215	0.5353
	P-P	1.625	1.425
	HC-HC	1.7556	2.456
FG-XCNT	P-P	1.5324	1.7231
	SC-F	0.7234	0.7543
	HC-HC	1.870	2.145
UD-CNT	SC-F	0.5431	0.6256
	P-P	1.5764	1.524
	HC-HC	1.809	2.345

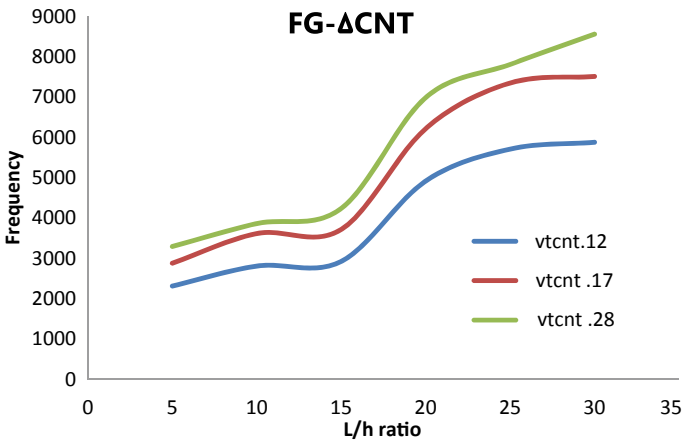


Fig. 23.8 Variation of natural frequency with different L/h ratio of FG Δ -CNT

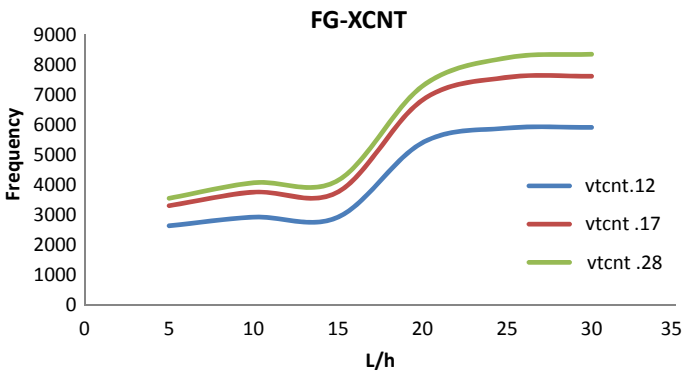


Fig. 23.9 Variation of natural frequency with different L/h ratio of FGX-CNT

increases the free vibration frequency continuously increases. Now, if total volume fraction of carbon nanotube is increases then free vibrational frequency increases shown in Fig. 23.9.

In UD-CNT, the CNT reinforced is distributed uniformly from top to bottom. So, we see that in Fig. 23.10 if L/h ratio is increases the free vibration frequency continuously increases. Now, if total volume fraction of CNT is increases then free vibration frequency increases but at 15 and 30 L/h ratio is same shown in Fig. 23.10.

In Fig. 23.11 show a comparison studies with different distribution of CNT reinforced beam at Simple clamp-simple clamp (SC-SC) boundary condition at

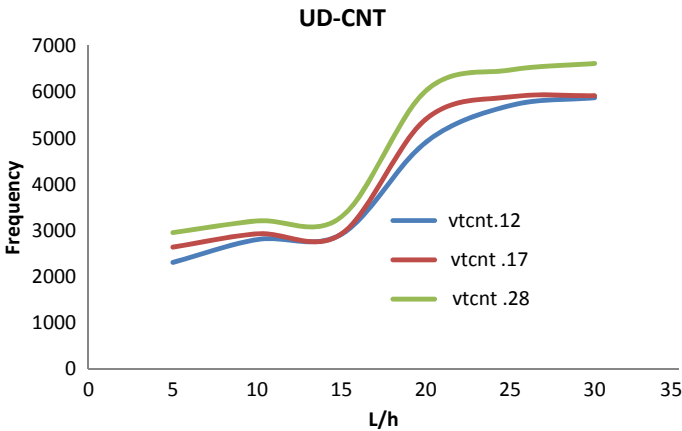


Fig. 23.10 Variation of natural frequency with different L/h ratio of UD-CNT

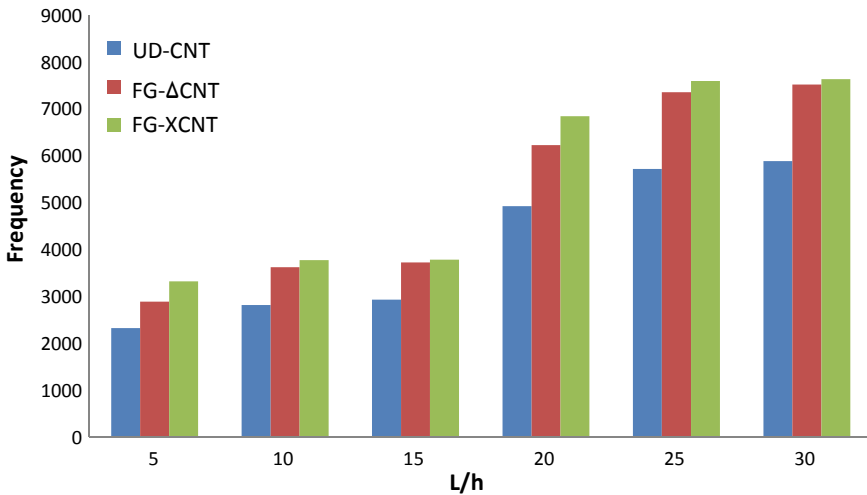


Fig. 23.11 Influence of L/h variation on frequency of various beams at 0.17 V_{cnt}

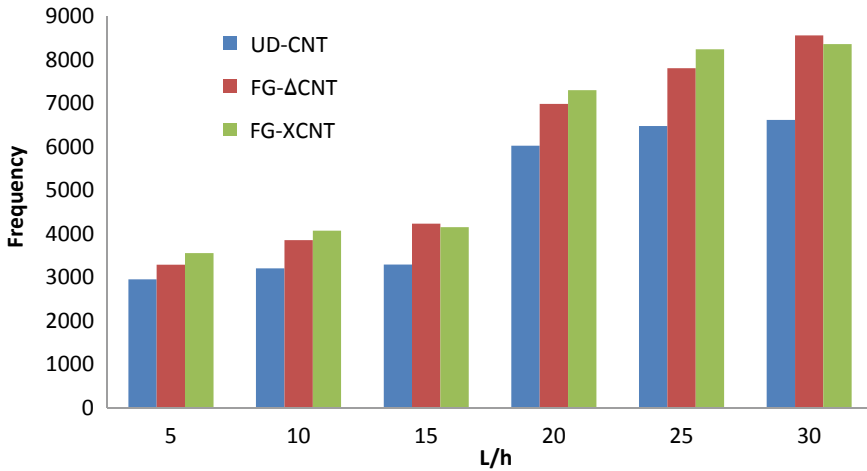


Fig. 23.12 Influence of L/h variation on frequency of various beams at $0.28 V_{tent}$

0.17 volume fraction of CNT. Figure show at all L/h ratio FGX-CNT higher free vibrational frequency.

In Fig. 23.12 show a comparison studies with different distribution of CNT reinforced beam at Simple clamp-simple clamp (SC-SC) boundary condition at 0.28 volume fraction of CNT. Figure show at some L/h ratio FGX-CNT higher free vibrational frequency but at 15 and 30 L/h ratio, free vibration frequency of FGX-CNT is less than that FGΔ-CNT.

23.5 Conclusions

This article looks at improved free vibration frequency of functionally graded CNT beams for different part of volume fraction. The FG beam model is developed in ANSYS environment. The results for UD-CNTRC beams are examined for validation purpose. A detailed study of the endpoint was evaluated to understand the influence of volume fraction the carbon nanotube of beams. Convergence studies and comparisons show the accuracy and reliability of the improved CNT reinforced beams model that is being developed. The comparison study also indicate the computed model to achieve the realistic response. The following conclusions are obtained from the present study.

1. It is observed that equivalent stress increases and total deformation decreases with increased volume fraction.
2. The natural frequency of beams increased with increased volume fraction of beams.
3. The FGX-CNT distribution gives the largest frequency though the UD-CNT distribution gives smallest frequency.

4. Boundary condition and L/h ratio intensely effect on frequency of FG-CNTRC beams.

References

1. Qian, D., Co Dickey, E., Andrews, R., Rantell, T.: Load transfer and deformation mechanisms in carbon nanotube-polystyrene composites. *Appl. Phys. Lett.* **76**(20), 2868–2870 (2000)
2. Han, Y., Elliott, J.: Molecular dynamics simulations of the elastic properties of polymer/carbon nanotube composites. *Comput. Mater. Sci.* **39**(2), 315–323 (2007)
3. Zhu, R., Pan, E., Roy, A.K.: Molecular dynamics study of the stress–strain behavior of carbon-nanotube reinforced Epon 862 composites. *Mater. Sci. Eng., A* **447**(1–2), 51–57 (2007)
4. Vodenitcharova, T., Zhang, L.C.: Bending and local buckling of a nanocomposite beam reinforced by a single-walled carbon nanotube. *Int. J. Solids Struct.* **43**(10), 3006–3024 (2006)
5. Roque, C.M.C., Martins, P.A.L.S., Ferreira, A.J.M., Jorge, R.M.N.: Differential evolution for free vibration optimization of functionally graded nano beams. *Compos. Struct.* **156**, 29–34 (2016)
6. Wu, H.L., Yang, J., Kitipornchai, S.: Nonlinear vibration of functionally graded carbon nanotube-reinforced composite beams with geometric imperfections. *Compos. B Eng.* **90**, 86–96 (2016)
7. Akbaş, Ş.D.: Forced vibration analysis of functionally graded porous deep beams. *Compos. Struct.* **186**, 293–302 (2018)
8. Kumar, L., Harsha, S.P.: Effect of carbon nanotubes on CNT reinforced FGM nano plate under thermo mechanical loading. *Procedia Technol.* **23**, 130–137 (2016)
9. Kumar, P., Srinivas, J.: Free vibration, bending and buckling of a FG-CNT reinforced composite beam. *Multidiscip. Model. Mater. Struct.* (2017)
10. Lin, F., Xiang, Y.: Vibration of carbon nanotube reinforced composite beams based on the first and third order beam theories. *Appl. Math. Model.* **38**(15–16), 3741–4375 (2014)
11. Ansari, R., Faghieh Shojaei, M., Mohammadi, V., Gholami, R., Sadeghi, F.: Nonlinear forced vibration analysis of functionally graded carbon nanotube-reinforced composite Timoshenko beams. *Compos. Struct.* **113**, 316–327 (2014)
12. Wu, H., Kitipornchai, S., Yang, J.: Free vibration and buckling analysis of sandwich beams with functionally graded carbon nanotube-reinforced composite face sheets. *Int. J. Struct. Stab. Dyn.* **15**(07), 1540011 (2015)
13. Alibeigloo, A.: Free vibration analysis of functionally graded carbon nanotube-reinforced composite cylindrical panel embedded in piezoelectric layers by using theory of elasticity. *Eur. J. Mech. A/Solids* **44**, 104–115 (2014)
14. Malekzadeh, P., Shojaei, M.: Buckling analysis of quadrilateral laminated plates with carbon nanotubes reinforced composite layers. *Thin-Walled Struct.* **71**, 108–118 (2013)
15. Kumar, M., Sarangi, S.K.: Harmonic response of carbon nanotube reinforced functionally graded beam by finite element method. *Mater. Today: Proc.* (2020)

Chapter 24

Studies on the Fatigue Performance of Wire and Arc Additive Manufactured SS 904L



Sharath Rajendran, A. Rajesh Kannan, B. Suresha, and N. Siva Shanmugam

Abstract To understand the complete potential of Wire Arc Additive Manufacturing (WAAM), it is required to explore the relationship between process, the resultant microstructure, and mechanical integrity of the components. WAAM process has achieved a significant attention because of the possibility of fabricating small-medium metal components. Most of the structures made by WAAM process are exposed to cyclic loads and the fatigue performance of WAAM components compared to wrought and cast alloys is far less understood. In the present work, single layered wall was produced via Gas metal arc welded (GMAW) based WAAM process. The wall dimensions were $200 \times 145 \times 6$ mm before machining and $180 \times 135 \times 3.5$ mm after machining, respectively. Fatigue specimens were prepared from the wall component along the built direction. The fatigue characteristics of the WAAM processed 904L samples were correlated to their microstructure as well as the mechanical properties. The fractographs were captured to reveal the fracture morphology. Recent works on WAAM process along with the several influencing parameters on the fatigue behaviour reveals the need for thorough understanding of the fatigue performance of steel structures by this technique. Based on this fact, some of the gaps are discussed in relation with microstructure and mechanical properties for future research in WAAM process.

Keywords ER904L · Wire arc additive manufacturing · Mechanical properties · Fatigue

S. Rajendran (✉) · B. Suresha
Department of Mechanical Engineering, The National Institute of Engineering, Mysuru,
Karnataka 570008, India
e-mail: sharathrajendran28@gmail.com

A. R. Kannan · N. S. Shanmugam
Department of Mechanical Engineering, National Institute of Technology Tiruchirappalli,
Tiruchirappalli, Tamil Nadu 620015, India
e-mail: rajesh.nitt88@gmail.com

24.1 Introduction

Austenitic stainless steels have been used in numerous industries due to their excellent corrosion performance and acceptable mechanical properties under elevated temperature. Super austenitic stainless steel (SS 904L) has excellent resistance to chloride attack, which makes it an ideal choice for application in the oil and gas refineries. The presence of copper in this grade of stainless steel makes it invulnerable to H_2SO_4 and other reducing agents, thus making it a good choice for chemical industries as well. SS 904L is considered as a best material to replace duplex stainless steel 2205 for certain applications.

Wire and Arc Additive Manufacturing (WAAM) can be a feasible option for medium to large scale products that have to be rapidly fabricated. This is because of the reason that WAAM using GMAW process with standard welding equipment is a very cost-effective method of manufacturing products which are otherwise very difficult to manufacture through conventional manufacturing methods. The buy-to-fly ratio of WAAM processed products are significantly lower than that of their counterparts from traditional machining.

Further, any advancements in the manufacturing aspect of engineering is to aid the use of the products in the industry. Most components in their applications are subjected to fatigue loads, rather than monotonic loads. This nature of loading decreases the life of the components used by a huge amount, as parts subjected to fatigue loading fail at stress levels far below the yield stress values of its material. Therefore, studying the behaviour of materials under such conditions is necessary to predict the fatigue life of the components.

24.2 Background of Research

Despite the noteworthy pros mentioned earlier, the fact remains that Additive Manufacturing, and WAAM is a comparatively unexplored area when austenitic stainless steels are taken into consideration in a research perspective, unlike the abundant research available for materials like Ti-6Al-4V, Inconel and similar alloys. Studies on fatigue behaviour of AM steels are usually on specimens manufactured through methods like Selective Laser Melting. Studies conducted by Lewandowski et al. [1] gives an insight that WAAM, a method of additive manufacturing of metals can be very cost effective as compared to conventional methods of production.

WAAM has been successfully demonstrated with many metals like Titanium, Aluminium, Steel, and Nickel based superalloys as discussed by Duraisamy et al. [2]. Various aspects like the cooling rate, process parameters, microstructure of the WAAM processed Titanium has been discussed by Martina et al. [3]. Gu et al. [4] have worked with cold metal transfer (CMT) process-based deposition and discussed the effects of post-deposition heat treatment on the CMT product. The influence of weld bead geometry for Aluminium-Copper alloys was also shown in the research.

In the research conducted by Cong et al. [5] the porosity issues that rise during the creation of the AM Al-Cu alloy wall was clearly explained. SS 347 was explored with WAAM process exhibited heterogenous microchemistry across the build direction and reported the presence of oxides at elevated temperatures (Fe_2O_3 and Fe_3O_4) during dry sliding wear test [6].

Considering various stainless steels, very little research has been carried out with SS 904L using WAAM process. Gordon et al. [7] conducted research on the fatigue behaviour of SS 304 and found that though the E value was lesser than its wrought counterpart, the WAAM processed specimens showed better σ_Y and σ_{UTS} values. It is also seen from the work of Grigorescu et al. [8] that among specimens taken from wrought SS 304L, 316L, and 904L, 904L displayed a higher number of life cycles due to its higher stability and slower α -martensite formation compared to the other two materials.

24.3 Experimentation

A single layered wall was constructed using GMAW based WAAM process with ER 904L consumable material (Fig. 24.1). The various stages during the fabrication of SS 904L plate via WAAM process as shown in fig. 24.2. The wall measured $200 \times 145 \times 6$ mm before machining and its final dimensions were measured to be $180 \times 135 \times 3.5$ mm. The welding parameters for the WAAM based deposition established through trial and error method and are given in Table 24.1.

The wall created was then machined to obtain a plate with necessary surface finish. Obtained plate was then subjected to Immersive type C Scan to reveal any defects if present. The parameters of the scan are provided in Table 24.2. Once cleared, specimens necessary for carrying out the fatigue analysis and tensile test were prepared according to ASTM E8/E8M-16a and ASTM E466-15 respectively. Fatigue

Table 24.1 Welding parameters for WAAM processing of SS 904L

Welding parameters	Welding current	Welding potential	Welding speed	No. of passes	Inter-pass delay	Initial plate dimensions	Final plate dimensions
Established Values	160 A	16.8 V	600 mm/min	90	60 s	$200 \times 145 \times 6$ mm	$180 \times 135 \times 3.5$ mm

Table 24.2 Parameters of Immersive Type C Scan performed of detection of faults

Scan parameters	Sampling frequency	Damp resistor	Gain	High pass filter	Low pass filter	Transducer mode	Pulse frequency	Pulse voltage and width
Established values	100 Hz	8.4 Ω	36 db	4.8 MHz	6.7 MHz	Pulse Echo	20 Hz	40, 20 db

testing samples were then mirror polished. Static tensile test of the sample showed that the Yield Stress σ_Y value for the material was found to be 302.11 MPa along the build direction and 279.32 MPa perpendicular to it. As seen, the minimum required mechanical properties for the material according to ASTM A240 was met, and further experiments were conducted. The microstructure of the material was analysed with specimens prepared according to ASTM E3-11, in the as-built condition. Based on the value of σ_Y , fatigue testing was carried out with different percentages (%) of σ_Y as the mean stress σ_M and corresponding stress amplitude σ_A and load ratio $R = 0.1$. Fatigue testing was conducted with the frequency of loading being 15 Hz. The fractured samples were examined using Scanning Electron Microscope (SEM) to reveal the fracture morphology (Figs. 24.1 and 24.2).



Fig. 24.1 WAAM setup

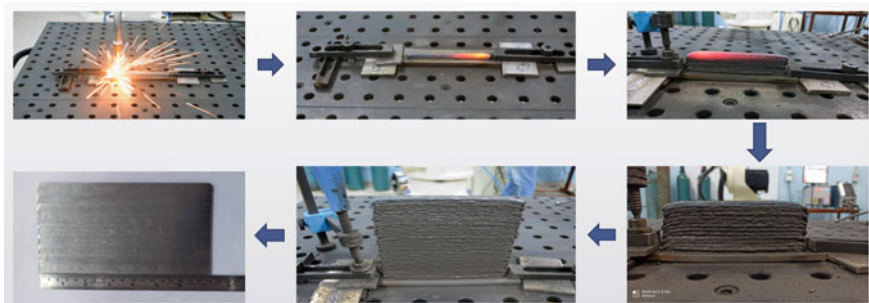


Fig. 24.2 Various stages of the creation of a single layer wall through WAAM and the final plate obtained

24.4 Results and Discussion

The C scan results of the plate which was scanned was studied. Waveform images from different points on the plate are shown in Fig. 24.3. as an example. Observing the absence of disturbance between the front-wall and the back-wall waveform clearly indicates the absence of macro defects in the material. Analysis of the microstructure of the material revealed that it was mostly dendritic in nature. The layers had majority of equiaxed grains with clusters of columnar and equiaxed grains near the boundary layers which were re-melted. Nucleation of the columnar dendrites was seen at the interface and then transitioning into equiaxed grains towards the middle, as shown in Fig. 24.4. The equiaxed dendrites closer to the boundary were found to have increased spacing due to the re-melting, and the observation was found to be in line with earlier

Fig. 24.3 Waveform results at various points across the fabricated SS 904L plate

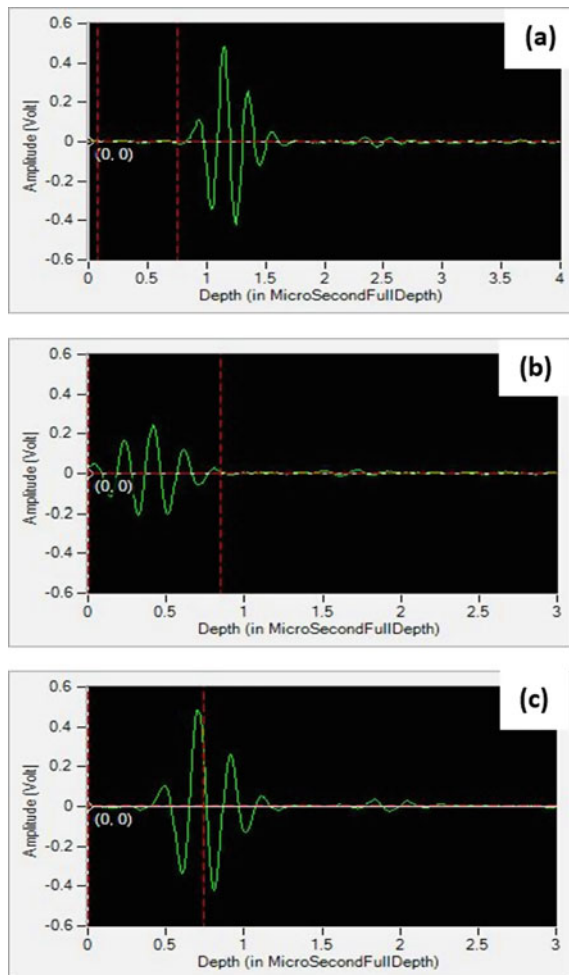
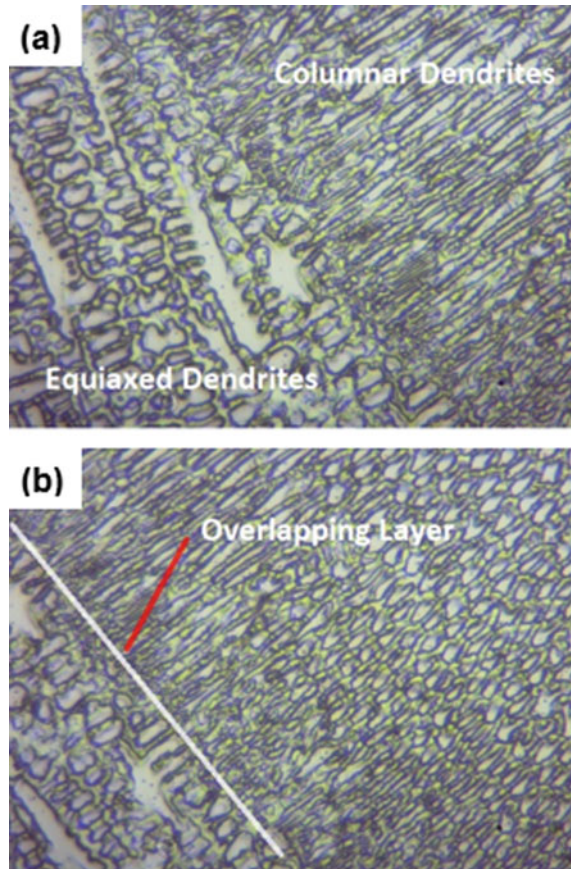


Fig. 24.4 Microstructure analysis images showing equiaxed and columnar dendrites and the overlapping layer in the SS 904L Plate



research [9]. The heterogeneous microstructure of the SS 904L is attributed to the complex cyclic thermal history (CCTH) [10]. Tensile tests were done on specimens prepared parallel and perpendicular to the build direction. The respective average σ_Y values were 302.15 MPa and 279.37 MPa, with the average σ_{UTS} values being 595.3 MPa and 483.79 MPa, respectively (Table 24.3). Ductile failure was observed for the specimens as shown in Fig. 24.5. The tensile properties meet the standard requirements for pressure vessel and general applications as mentioned in ASTM A240/A240M-18.

The fatigue test results and the S-N curve for the same are shown in Table 24.4 and Fig. 24.6, respectively. It is observed that there is a variation in the number of life cycles of the specimens for the same stress levels and alternating stresses. This leads us to attribute the variation to the difference in the microstructure at various points because of the CCTH. The S-N curve drawn can be seen with a right arrow indicating runout specimen at 2×10^6 cycles. As compared to its wrought counterpart whose life cycle count was 2×10^6 at a stress amplitude of 200 MPa, we can see

Table 24.3 Tensile test results

Specimen	Orientation w.r.t. building direction	σ_{UTS} (MPa)	σ_Y (MPa)	Elongation (%)
1	Horizontal	483.15	271.67	58.67
2		485.72	283.92	53.92
3		485.72	282.53	56.44
Average		483.79	279.37	56.34
Standard deviation		1.39	5.47	1.94
1	Vertical	593.27	297.41	46.23
2		597.74	305.69	47.38
3		594.89	303.37	45.41
Average		595.3	302.15	46.34
Standard deviation		1.85	3.48	0.81

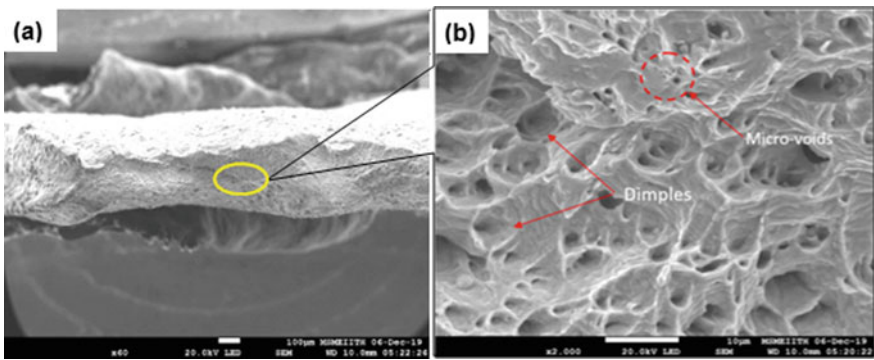


Fig. 24.5 SEM image of failed tensile test specimen showing the surface as having dimples and voids, indicative of ductile failure

Table 24.4 Fatigue test results

Specimen No.	Stress level (% of YS)	Alternating stress σ_A (MPa)	Cycles to failure (N)
1	80	241	63,799
2	80	241	65,389
3	70	211	150,671
4	70	211	165,423
5	60	181	417,836
6	60	181	439,725
7	50	151	2,000,000
8	50	151	2,000,000

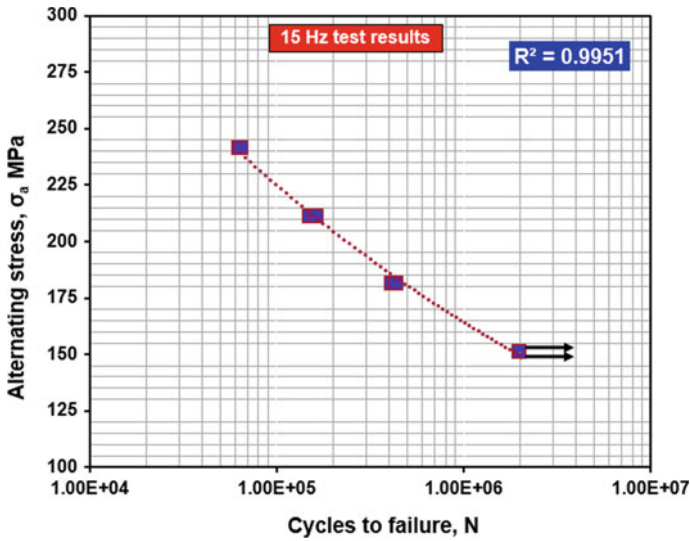


Fig. 24.6 Stress-life diagram for the fatigue test results of WAAM processed SS 904L

that the WAAM product has decreased fatigue strength and it can be associated with decreased ductility of the material. The R^2 value of 0.9951 shows the quality of the material.

Observing the fracture surfaces of the failed specimen, it was seen that the specimen which failed at the earlier part of the S-N curve, i.e. those having life cycles $<10^5$ had rough surfaces compared to those in the later part of the curve. The lower levels of stress experienced by the samples can be associated with the smooth fracture surfaces. The final ruptured surface, when observed, showed presence of voids and dimples, indicating ductile mode of fracture (Fig. 24.7), which was concurrent with earlier research [9]. Similar results can be seen in the work of Carneiro et al. [11] in

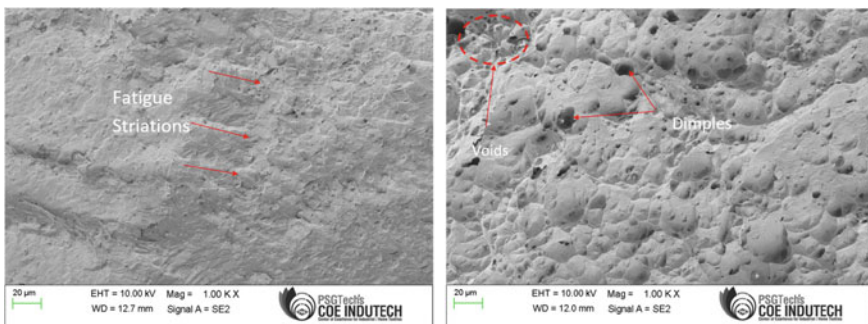


Fig. 24.7 Smooth fractured surface with fatigue striations observed for specimen at 70% YS ($>10^5$ cycles) and rupture surface showing presence of voids and dimples indicating ductile fracture

their research with Additive Manufactured 17–4 PH stainless steel, even though the manufacturing process was not WAAM, i.e. AM product showed a fatigue limit of 300 MPa compared to CM product, which had a fatigue limit of 640 MPa.

24.5 Conclusions

SS 904L is a viable material for WAAM with good weldability. The processed material has good quality with absence of any macro defects in it. The microstructure analysis showed the material to have equiaxed and columnar dendrites, with clusters of columnar dendrites towards the interlayer boundary. WAAM processed SS 904L showed better tensile strength than the wrought counterpart. However, the fatigue strength was comparatively a little low by approximately 25%. Specimens which failed at the earlier part of the S-N curve showed roughness whereas the ones in the later part of the curve was seen to have smooth surfaces.

References

1. Lewandowski, J.J., Seifi, M.: Metal additive manufacturing: a review of mechanical properties. *Annu. Rev. Mater. Res.* **46**, 151–186 (2016)
2. Duraisamy, R., Kannan, A.R., Kumar, S.M., Shanmugam, N.S., Sankaranarayanan, K.: Reliability and sustainability of wire arc additive manufactured plates using ER 347 wire-mechanical and metallurgical perspectives. *Proc. Inst. Mech. Eng., Part C: J. Mech. Eng. Sci.* (2019)
3. Martina, F., Mehnen, J., Williams, S., Colegrove, P., Wang, F.: Investigation of the benefits of plasma deposition for the additive layer manufacture of Ti-6Al-4V. *J. Mater. Process. Technol.* **212**, 1377–1386 (2012). <https://doi.org/10.1016/j.jmatprotec.2012.02.002>
4. Gu, J., Ding, J., Williams, S., Gu, H., Bai, J., Zhai, Y., Ma, P.: The strengthening effect of inter-layer cold working and post-deposition heat treatment on the additively manufactured Al-6.3Cu alloy. *Mater. Sci. Eng.: A* **651** (2015). <https://doi.org/10.1016/j.msea.2015.10.101>
5. Cong, B., Ouyang, R., Qi, B., Ding, J.: Influence of cold metal transfer process and its heat input on weld bead geometry and porosity of Aluminum-Copper alloy welds. *Rare Met. Mater. Eng.* **45**, 606–611 (2016). [https://doi.org/10.1016/S1875-5372\(16\)30080-7](https://doi.org/10.1016/S1875-5372(16)30080-7)
6. Duraisamy, R., Kannan, A.R., Kumar, S.M., Shanmugam, N.S., Sankaranarayanan, K., Ramesh, M.R.: Tribological performance of wire arc additive manufactured 347 austenitic stainless steel under unlubricated conditions at elevated temperatures. *J. Manuf. Process.* **56**(Part A), 306–321 (2020). ISSN 1526-6125
7. Gordon, J., Harlow, G.: Statistical modeling of wire and arc additive manufactured stainless steel 304: microstructure and fatigue. *Int. J. Reliab., Qual. Saf. Eng.* **26** (2019). <https://doi.org/10.1142/S0218539319500165>
8. Grigorescu, A., Hilgendorff, P.M., Zimmermann, M., Fritzen, C.P., Christ, H.J.: Fatigue behaviour of austenitic stainless steels in the VHCF regime. In: Christ, H.J. (eds.) *Fatigue of Materials at Very High Numbers of Loading Cycles*. Springer Spektrum, Wiesbaden (2018)
9. Kannan, A.R., Kumar, S.M., Kumar, N.P., Shanmugam, N.S., Vishnu, A.S., Palguna, Y.: Process-microstructural features for tailoring fatigue strength of wire arc additive manufactured functionally graded material of SS904L and Hastelloy C-276. *Mater. Lett.* **274**, 127968 (2020). ISSN 0167-577X

10. Kannan, A.R., Shanmugam, N.S., Rajkumar, V., Vishnukumar, M.: Insight into the microstructural features and corrosion properties of wire arc additive manufactured super duplex stainless steel (ER2594). *Mater. Lett.* **270**, 127680 (2020). ISSN 0167-577X
11. Carneiro Junior, L., Jalalahmadi, B., Ashtekar, A., Jiang, Y.: Cyclic deformation and fatigue behavior of additively manufactured 17-4 PH stainless steel. *Int. J. Fatigue* **123**, 22–30 (2019). <https://doi.org/10.1016/j.ijfatigue.2019.02.006>

Chapter 25

Heterogeneous Modeling for Fabrication of Anatomical Structure from DICOM Image Using Additive Manufacturing



Vivek Kumar Gupta, Ankit Nayak, Ujjwala Singh Thakur,
and Prashant Kumar Jain

Abstract In recent years, Additive Manufacturing (AM) unfolds its huge capability to fabricate an object in remarkable ways which either created directly from Computer Aided model and STL (Standard Tessellation Language) file or using Coordinate points and G codes. AM used in various field such as engineering, aerospace, biomedical, etc. Fused Filament Fabrication (FFF) is the most frequently used process for AM. It uses the technique of depositing a viscous material on the build platform to fabricate an object to use it for creating a mould for an industrial tool or developing models for preoperative planning for medical surgery or even Anatomical structure for demonstration purposes. FDM generally used to manufacture homogeneous object but when it comes to heterogeneous object it finds difficulty in altering desired process parameter in its software. The commercial FFF software generate toolpath whose parameters are selected by users but the choices are constrained and only limited number of variation of parameters such as raster angle, infill density, layer thickness toolpath pattern, etc. are available. Although this limitation does not affect the properties of homogenous material but fails to provide heterogeneity on a single layer. In AM certain techniques have been used in producing parts of various infill density. The optimization of infill parameter and multi contouring on a single layer gives a new method to model heterogeneous structure using FFF. A new approach has been used to obtain the density variation of human bone at its cross-section using digital image processing technique. The Developed algorithm is capable to extract useful data from an image based on density variation of bone and its variability is dependent on the value of grayscale for each pixel. Each pixel value is associated with the attenuation coefficient from the X-ray of the object which give the relative value of density at each pixel. The accumulated data correlates the heterogeneity and efficiency of the designed model with the actual bone. This single material modelling technique is more feasible and adaptable for biomedical application.

Keywords Additive manufacturing · Tool path · Fused filament fabrication · 3D printing · CT scan

V. K. Gupta · A. Nayak (✉) · U. S. Thakur · P. K. Jain
Mechanical Engineering Discipline, PDPM Indian Institute of Information Technology, Design & Manufacturing, Jabalpur, Madhya Pradesh 482005, India
e-mail: ankitnayak@iiitdmj.ac.in

25.1 Introduction

Over the past decades, Medical Image Processing has emerged as a promising technique for reconstruction of bone. This application can be used for bone replacement, modeling for crack removal of bone, scaffold generation and demonstration purpose as well. Various techniques have been developed to create artificial bone which can be done directly from STL (Standard Tessellation Language) file and its optimization. In Medical Diagnostic, computerized tomography (CT) scan plays an important and essential role in obtaining useful anatomical information. These diagnostic data are carried in different algorithms which are carried in the DICOM (Digital Imaging and Communications in Medicine) as input and kept in the encrypted format for storage purpose. CT scan gives the information about shape, orientation and density variation of the bone. Detecting the density variation is one important process in the image processing operation, this finding indicates that there is a significant genetic and density variation at the cross-sectional area in the femur bone [1, 2].

25.1.1 Additive Manufacturing

AM is a technology that uses sequential addition of material in a layered manner to develop a 3D object. It uses variety of material such as plastic, metal, human tissue and concrete etc., this idea of 3D technology came into knowledge in 1981 when Dr. Hideo Kodama from Japan put forward his idea of three-dimensional printing which was inspired from photo-hardening polymer technology but it couldn't due to lack of funding. After few years, MIT develop its first powder bed process which uses inkjet print heads and from there the term 3D printing were started using afterward.

Rapid Prototyping (RP) and AM can be used interchangeably but there is an exception i.e., RP is used produce a prototype of a new component whereas AM provides opportunities for both prototypes and final components. AM opens a world of design opportunities of new and complicated object without the limitations of subtractive manufacturing. AM is a technology that produces object with minimum waste and is very efficient for low-volume manufacturing [3].

25.1.1.1 Basic Steps Involved in AM Techniques

In AM, the first step is to create the cad model since the software related to part fabrication don't have features to prepare part model. This part model will then be converted into STL file and then sliced in multiple layers. These slicing will provide coordinates of each layer on which certain algorithm will be applied and these coordinates will get arranged in sequence. This gives the contour on which variable process parameter will be applied to fill the contour. After this process, a

toolpath is generated after which certain G&M codes is applied on these coordinates which will be compatible to FFF machine to generate parts and models.

25.1.2 Image Processing

It has been widely used for medical related image such as for finding Tumour or for locating Cancer in the MRI scan. It has also been used for generating boundary around a specified object. Scans such as Magnetic Resonance Imaging (MRI) and Computed Tomography (CT) scans are the most efficient source for obtaining visual information for analyzing anatomical part.

25.1.2.1 Uses of MRI and CT Scan

CT and MRIs are used to capture image within the body at the cross-section. The difference both of them is that MRIs uses radio waves and CT uses X-rays to scan the body. The rotating machines has been used to obtain e complete cross-sectional images in X-ray, which can generate single or multiple layers of slices whereas MRI provide extra details of each parts with respect to X-ray image, it is used to locate the soft tissues, blood vessels, and bones in various parts of the body. CT scan frequently used to examine and identify the following things such as:

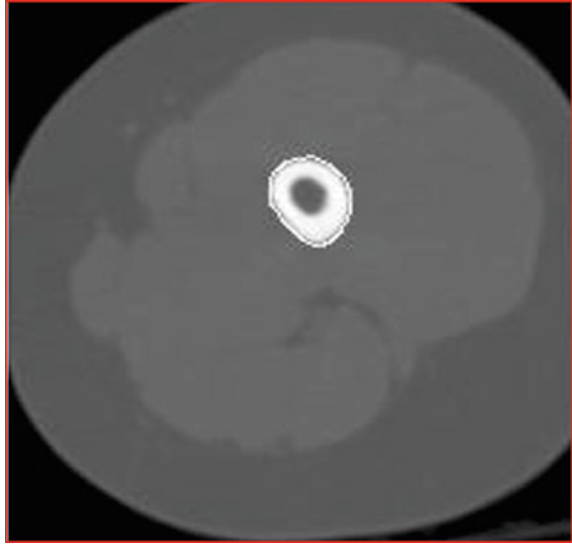
- Tumors
- Internal bleeding
- Bone fractures
- Cancer development

Whereas MRI scan has been used identifying things such as:

- ankles
- brain
- joints
- wrists
- blood vessels

CT and MRI image uses various format for transferring file so that there is no loss of data, its images are acquired in a special digital format, the DICOM Format (DCM). DICOM format ensures that the high quality of the images is retained. Each CT or MRI scan contains single or multiple images in the DICOM format that should be stored in a safe and secure.

Fig. 25.1 DICOM Image of Femur bone



25.1.3 DICOM Image and Its Importance

The Digital Imaging and Communications in Medicine (DICOM) is a standard format that was made under non-profitable protocol so that it can be used by any one which is used for data exchange, format and structure of images and its information. It was developed by the National Electrical Manufacturers Association (NEMA) for sharing and visualization of medical images (Fig. 25.1).

DICOM is an international standard for communicating and managing data related to medical images. Its mission is to ensure the safe and secure process of transmission of data. It is used for storing, exchanging and transmitting medical images all over the globe with its technique of integration of devices for medical imaging from different manufacturers [4, 5].

25.1.4 Grayscale

As the term defined, it scales the different variety of Gray colour which ranges from black to white in increasing order in terms of value which scales from 0 to 255. The RGB colour is a mixing model where a broad array of colours can be reproduced by mixing blue, green and red in certain proportionate to obtain various colour. The value of grayscale from any DICOM image describes the intensity of each pixel.

25.1.5 Fused Filament Fabrication (FFF) Process

Fused Filament Fabrication is one of the effective and popular AM techniques which is also known by fused deposition modeling, extruder-based printing, and filament freeform fabrication. In this process, the fabricating material a filament which is wound over the spool. The material is fed in the extruder where it is heated and converts into viscous form. Material is deposited bed or build platform through a nozzle as per the information of geometry feed into the machine called toolpath. After deposition of one layer, the build platform moves in positive direction of z-axis i.e., in downward direction, the next layer gets deposited upon the previous layer. The process is continued until the physical model gets completed. The main part of FFF machine is the nozzle head, moving along the x and y direction. It is controlled by a numerically controller system embedded in the FFF machine. In this process, the thermoplastic materials are used for part printing such as PLA, TPU etc.

25.2 Methodology

Medical Image Processing is a significant technique which has been used very frequently for reconstruction of bone. This application can be used for bone replacement, modeling for crack removal of bone, scaffold generation and demonstration purpose as well. Various techniques have been developed to create artificial bone which can be done directly from STL (Standard Tessellation Language) file and its optimization. In Medical Diagnostic, Computerized Tomography (CT) scan plays an important and essential role in obtaining useful anatomical information. These diagnostic data are carried in different algorithms which are carried in the DICOM as input for data storage. CT scan gives the information about shape, orientation and density variation of the bone. Detecting the density variation at the cross-sectional area in the femur is one important process in the image processing operation [6, 7] (Fig. 25.2).

25.2.1 Data Extraction from DICOM Image

The DICOM file (which is in DCM format) inserting in the software will give the information about the image in the form of greyscale. The value of the greyscale will vary from 0 to 255, the darker the region the more will be its greyscale value and vice versa. The value of the greyscale is obtained in the form of the pixel (Fig. 25.3).

DICOM file contains the sliced image of bone i.e., the cross-sectional area of femoral. The white area is showing the bone region which is having higher greyscale value as well as high density. The outer region of the bone, these are muscles and tissues and inner region from the white area is the bone marrow. The white region

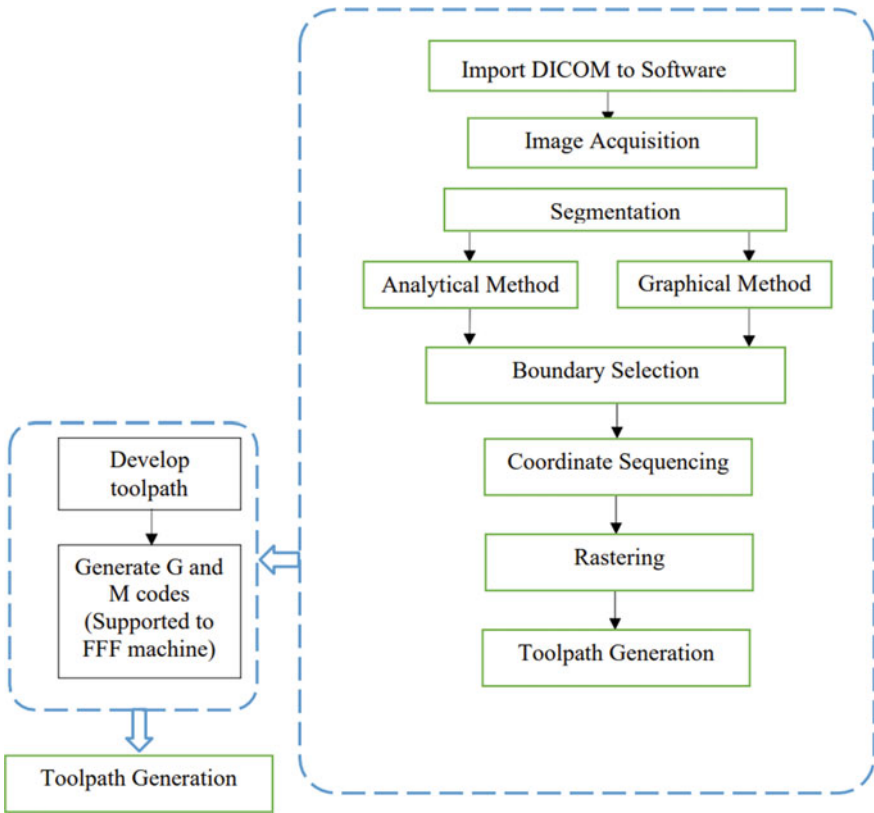


Fig. 25.2 Implementing procedure

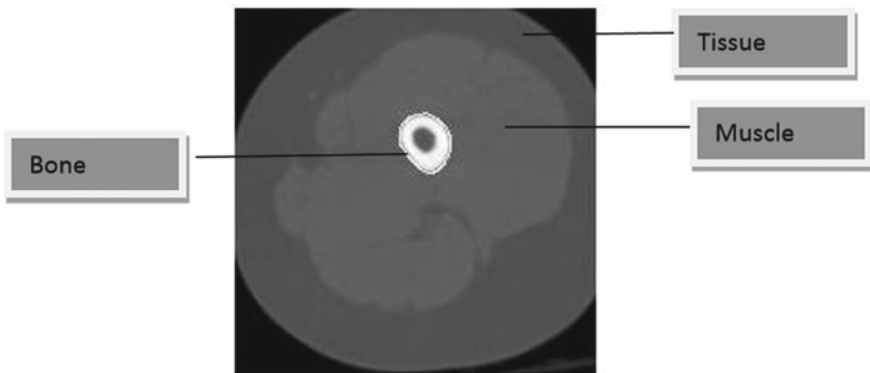


Fig. 25.3 CT Scan of cross-section of Femoral Bone

in the bone is the collection of high pixel values, these pixel values are varying from inside to outside which means there is variation in density of bone.

25.2.2 *Thresholding*

Two methods have been developed for find the threshold value for segmenting the multiple regions at the boundary point [8].

25.2.2.1 **The Analytical Method**

Segmented based on maximum difference method is used here to obtain the threshold value. The obtained threshold value is the value of boundary point at which regions get divided.

Maximum Difference Method

Moving radially outside to inside, there is pixel and its value in form of grayscale. Each pixel has its individual value,

$$\text{Threshold value} = P_2 - P_1$$

P_1 and P_2 are the consecutive pixel moving inside femur bone in the radial direction.

It's more like hit and trial method where there is multiple point outside the boundary of femur bone to move in a straight line, so the average is taken here. The density variation from maximum to minimum is red, blue, green and yellow respectively. The threshold value of grayscale for the region is 110 to 130 for crayon, 130 to 200 for yellow, 200–235 for green, 235–238 for blue and 238–255 for red (Fig. 25.4).

25.2.2.2 **The Graphical Method**

Segmented grayscale value obtained on the basis of graph is 112, 195, 235, 239 and 255 (Fig. 25.5).

Method used:

1. First find out the seed value from which bone region get separated from muscle and bone marrow. The seed value is obtained using maximum difference method and its value is 112.
2. Take all the grayscale value of each pixel in this region, arrange it in increasing order and put it on y-axis and on x-axis, the values are arranged according to its order relative to y-axis.

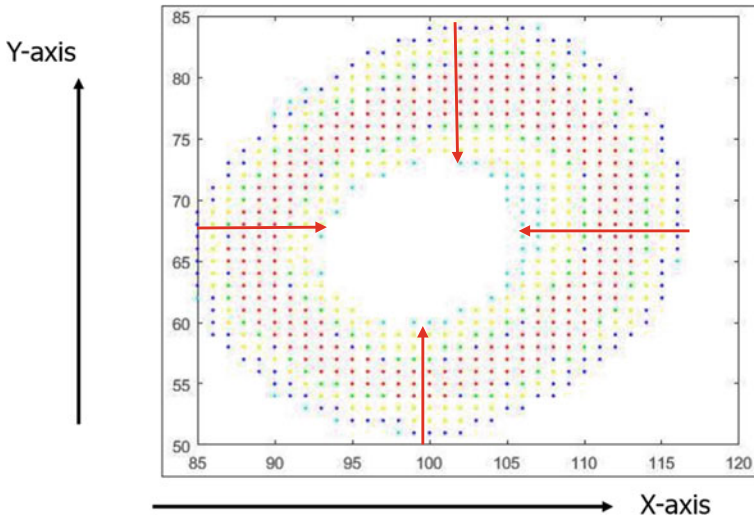


Fig. 25.4 Segmentation of region using analytical method

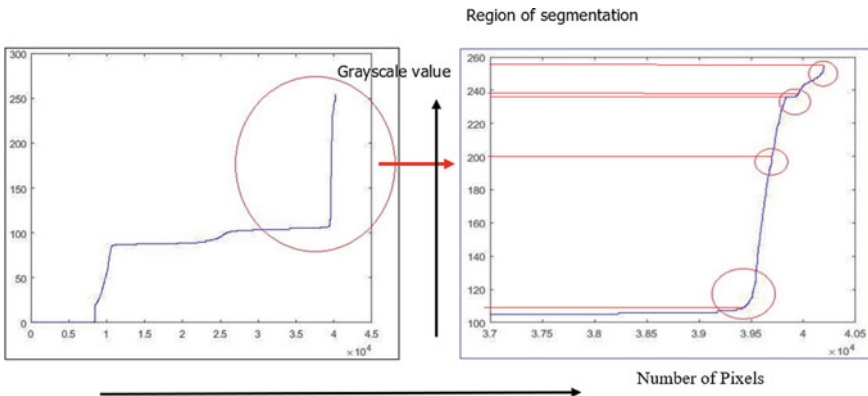


Fig. 25.5 Graphical analysis

Now the segmented value can be found as:

$$\theta = \tan^{-1}(\theta_2) - \tan^{-1}(\theta_1)$$

$$\theta_1 = \frac{B_{n-1} - B_{n-2}}{A_{n-1} - A_{n-2}}$$

$$\theta_2 = \frac{B_n - B_{n-1}}{A_n - A_{n-1}}$$

where,

θ	difference in angle of two consecutive point
θ_1	slope of 1st line
θ_2	slope of 2st line
A_1, B_1	coordinates of 1st point
A_2, B_2	coordinates of 2nd point
A_3, B_3	coordinates of 3rd point.

The maximum value of θ at each fluctuation of curve after the seed value is taken as threshold value for segmentation.

25.3 Development of an Algorithm for Heterogeneous Modelling

A programming software has been introduced for performing slicing and toolpath generation process. Two new approaches have been discussed for new boundaries insertion to obtain separate regions. In addition, different toolpath strategies have been discussed which shows uniform and non-uniform variation in parts fabrication.

25.3.1 Segmentation

Whenever there is data are values which is represent the same group or there is a similarity, these values need to be get separated from others. A method has been used which collect the coordinates of those values which get represented in certain range. These values store coordinates of each point which comes under certain range. In this Fig. 25.6, blue, green, red, yellow and crayon together represent the bone region. These values get separated from the whole region by using intensity of each pixel, which is in the form of grayscale. The higher the value of grayscale, higher is the density. The range of this segmentation is based on grayscale and the value is 110–255, 255 is the maximum value of grayscale.

25.3.2 Improved Segmentation

In Fig. 25.6, the number of segmented regions is 5 i.e., crayon, yellow, green, blue and red whose range of values are 110–130, 130–200, 200–235, 235–238 and 238–255 respectively. Segmented region such as yellow and green is very small and form a thin line, which will become irrelevant during fabrication due to the less accuracy of FFF machine. To overcome this, there is optimization of data which will be which is shown in Fig. 25.7. The crayon region is very small so it gets merged in yellow

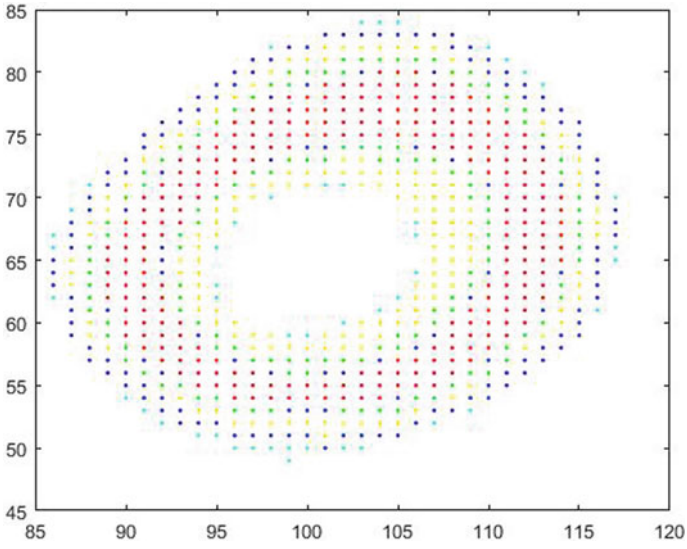


Fig. 25.6 Segmentation of femur bone

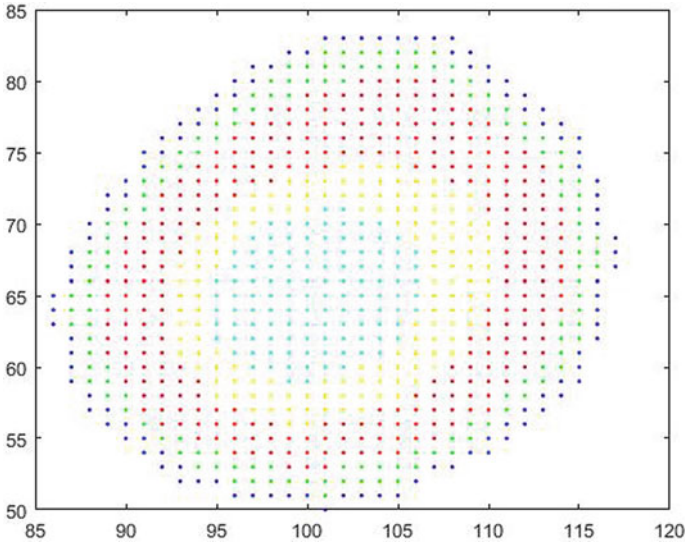


Fig. 25.7 Improved segmented region

region and the crayon region shown here is for the bone marrow which will be used form boundary generation.

25.3.3 Contour Approach

When points are randomly distributed and a contour has to be obtained then this approach is used. It uses minimum distance method to get the next coordinate. It is the simplest method to obtain contour yet become very difficult when a larger number of points are available and become difficult to choose next point then it gets left and get connected in random order to complete the loop. To prevent this a limiting value of distance should be given to that next point get prevent when it is far than limiting distance. The obtained contour will be in the form of group of connected line segments whose both ends are open which later connected to make it contour.

In Fig. 25.8, there is sequencing of point. These points are randomly distributed all over the region. To do this, first select a point then find the nearest point to it using minimum distance method. Now after finding this line segment use head to tail method, in this method heads are connected to tails and again minimum distance method is used in this to connect it. Similarly, this method has been used for multiple contours as shown in Fig. 25.9.

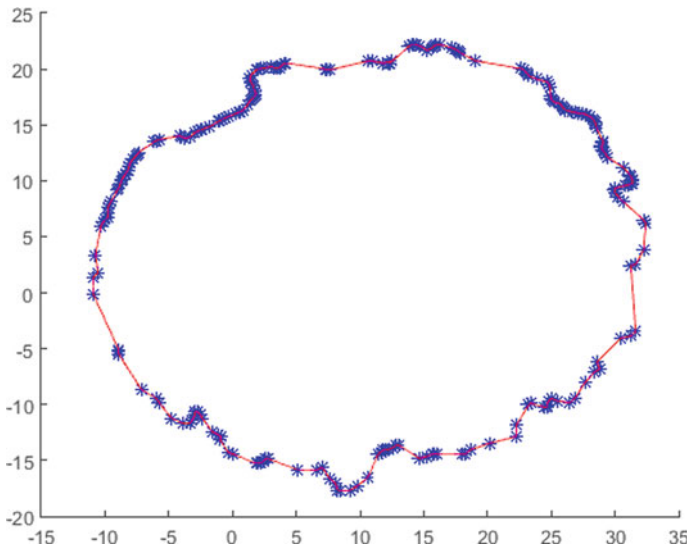


Fig. 25.8 Sequencing of coordinate points to generate contour

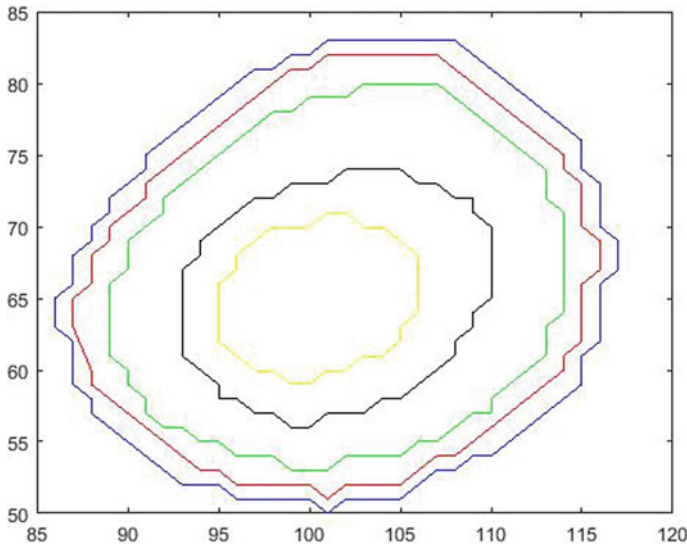


Fig. 25.9 Contour of multiple region

25.3.4 *Infill Parameter*

A standard FDM printing parameter is divided here in following categories. Each parameter has been altered to obtain the optimize design for part fabrication. The walls of the print that are exposed to the outside of the model. Here in this model, single layer of wall boundary is used so that the it shouldn't overlap with infill region. The thickness of each layer is uniform and each layer has a thickness of 0.4 mm. Each of the DICOM layer which are used here has a gap of 3 mm but the FFF machine i.e., Auto adobe duper XL 400 is used here for part fabrication have a maximum layer thickness of 0.4 mm so for fabrication process maximum limiting value of layer thickness is used here. The raster angle used here is 30, 60, 30 and 60 degree from outside to inside respectively as shown in Fig. 25.10. Although this raster angle is based on user input which can be easily changed based on requirement, similarly raster gap also used i.e., 0.7, 1.1, 0.5 and 1.5 from outside to inside can be changed based on the minimum difference in relative density of the model from the original object.

25.3.5 *Toolpath Generation*

Toolpath is used give direction of movement to extruder head in x, y and z direction in the cartesian coordinate form [9, 10]. Any toolpath can be generated by connecting all the raster line which is shown in Fig. 25.10. Most efficient toolpath is when the

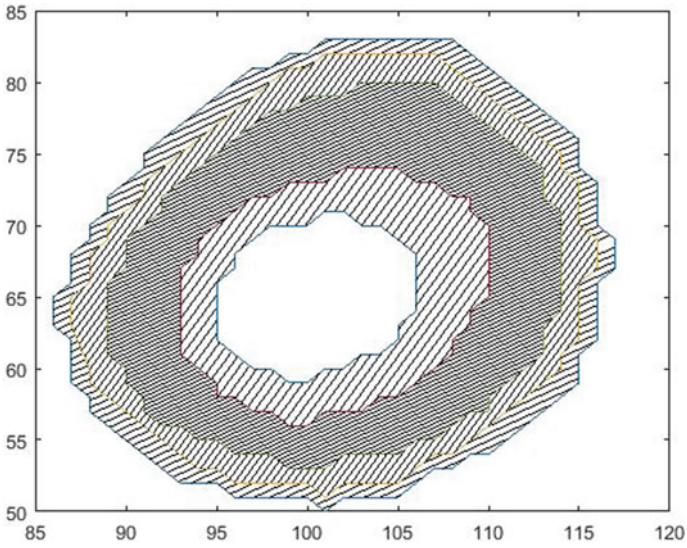


Fig. 25.10 Rastering using line pattern

extruder head takes minimum time to cover the of any layer. This can be done by one raster line to other which are nearest to it. The generated toolpath is shown in Fig. 25.11.

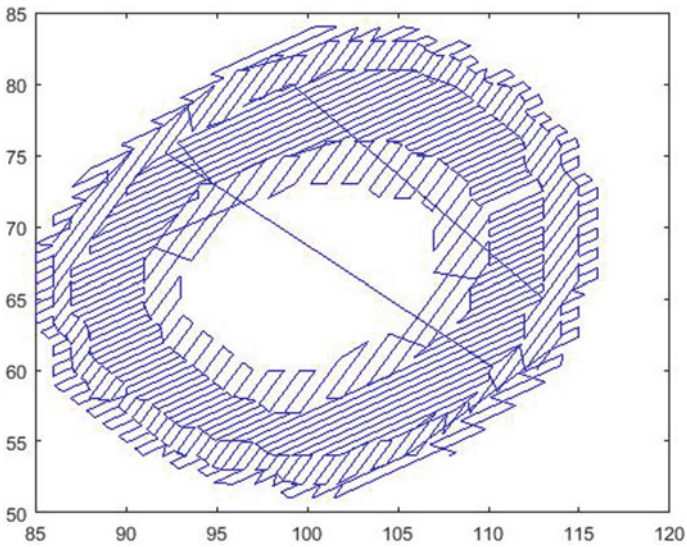


Fig. 25.11 Toolpath of single layer

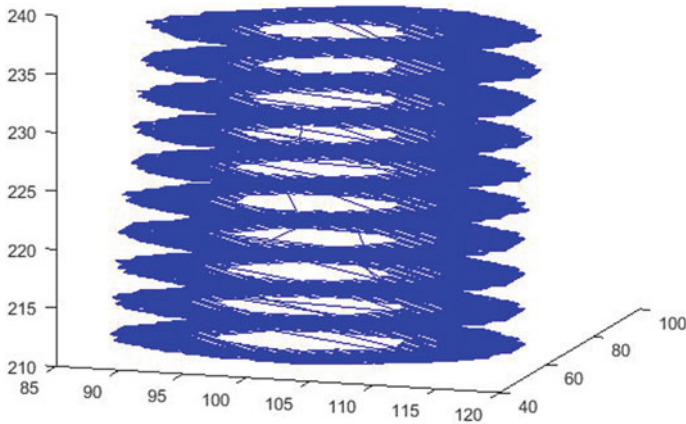


Fig. 25.12 Toolpath for 10 slices

When toolpath path is generated for single layer then z-axis can be neglected, but when it needs to generate for multiple layers than z axis should be included but this height along z axis will depends on layer thickness. In Fig. 25.12, the separation in between the two layer is 3 mm total number of 10 slices is used.

25.4 Result and Application

This model has been designed to fabricated heterogeneous object such as bone. There is various bone which is inside the human body which need to replace at an old age or under certain condition. These bones are hip joint, knee joint. Not only for these bones but this model has capability to fabricate any type of bone in heterogeneous form. Here, in this case femur bone is used as it has sufficient thickness to observe the heterogeneity within the bone.

25.4.1 Application

The capability of the proposed approaches has been demonstrated by considering heterogeneous model for Femur bone used in real world applications as described below. This model is capable of producing any heterogeneous object whose DICOM Image is available.

There is various application for which heterogeneous model can be used such as:

1. Hip joint replacement
2. Knee replacement
3. Demonstration purpose.

25.4.2 Fabrication of Heterogeneous Bone

Figure 25.13 shows the fabrication of different numbers of layer for different scale value. This shows that this model can be generalized for single and multiple layers for fabrication of any heterogeneous objects.

Figure 25.14 shows the heterogeneous model for multi-slices of DICOM image. Different orientation of the model is used to compare the similarity in between modelled image and fabricated image. This fabrication is done on FFF machine, the machine used is AUTOADOBE DUPER XL 400. The working volume of this machine is $200 \times 200 \times 200$ (in mm). The toolpath generated above is used to fabricate this femur bone as shown in Fig. 25.15. G and M code have been implemented on the coordinated of the toolpath.

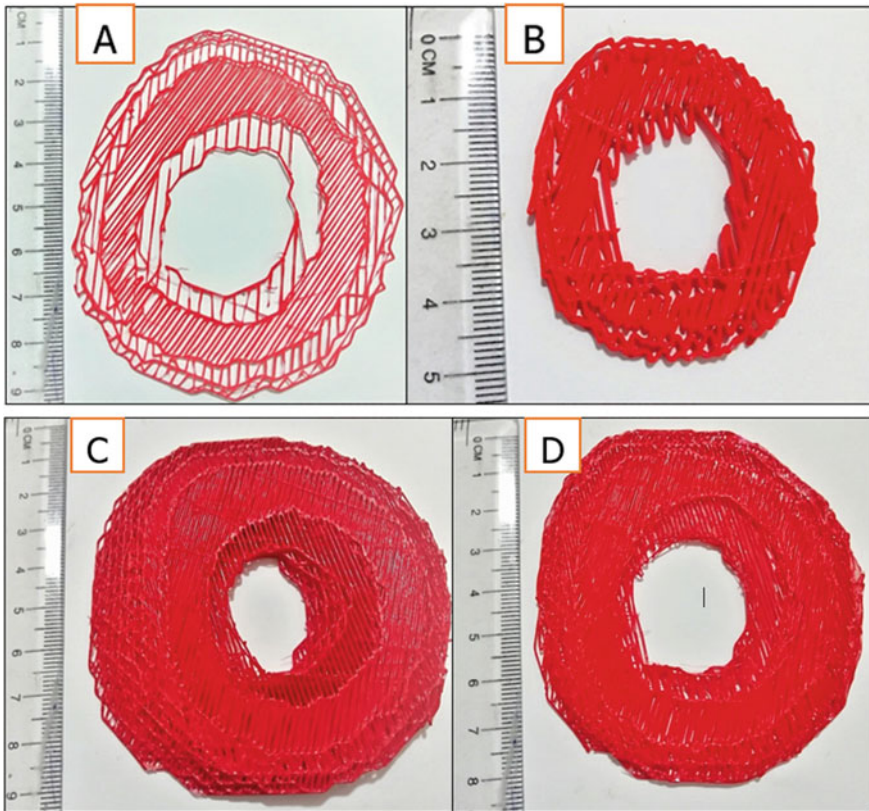


Fig. 25.13 a Single layer at 2.5 scaling, b 2 layers at scaling value of 2, c 5 layers at 2.5 scaling, d 3 layers at scaling value of 2.5

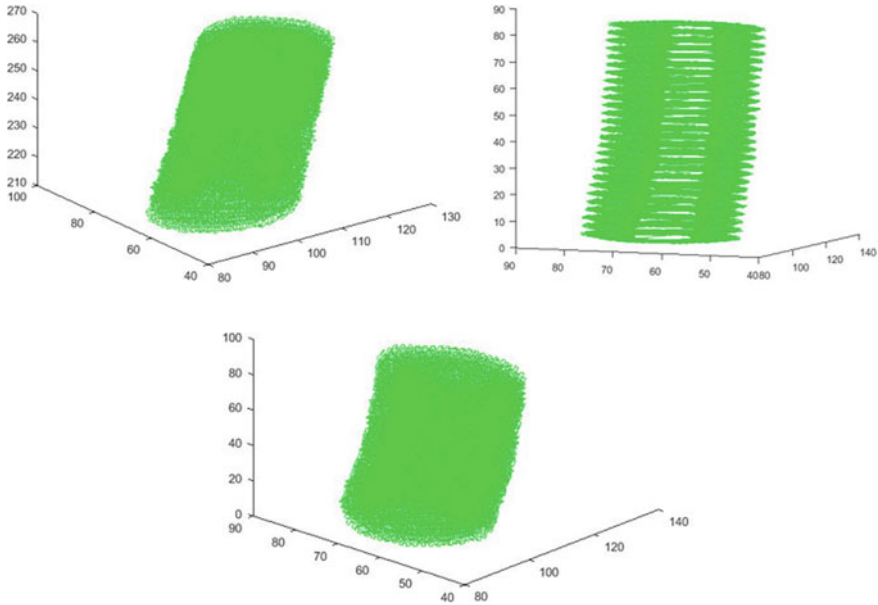


Fig. 25.14 Different orientation of heterogeneous model

25.5 Conclusions

The process of Additive Manufacturing, their benefits, limitations, and applications are explained in detail. Medical Image Processing Techniques have been explained. CT scan in DICOM format shows the cross-sectional image. This cross-section image is in the form of Grayscale whose value varies from 0 to 255. Higher the Greyscale value, higher is the density. FFF process is most commonly used in the AM process. The software used for density variation through FFF process and their limitations are explained. These software are not capable to provide localized variation in a part. Thus, a novel path planning tool has been developed for providing different set of process parameters in each layer as well as entire part. Two different methodology for obtaining threshold value has been explained. The obtained threshold value i.e., 110 in case of Analytical method and 113 in case of Graphical method has been obtained. The value then used to separate the region using segmentation method. Then segmented region then used for obtaining contour points at the boundary. Then these contours used for Rastering and toolpath generation. The detail explanation of segmentation, infill parameter and toolpath generation has been explained along with its algorithm. While segmentation, maximum difference method has been used to find the threshold value which comes under Analytical method and maximum difference in angle method has been used to find the threshold value in the Graphical method. Various infill parameter has been implemented on segmented region to obtain similar variation in density as in grayscale value of DICOM image. Then a toolpath is

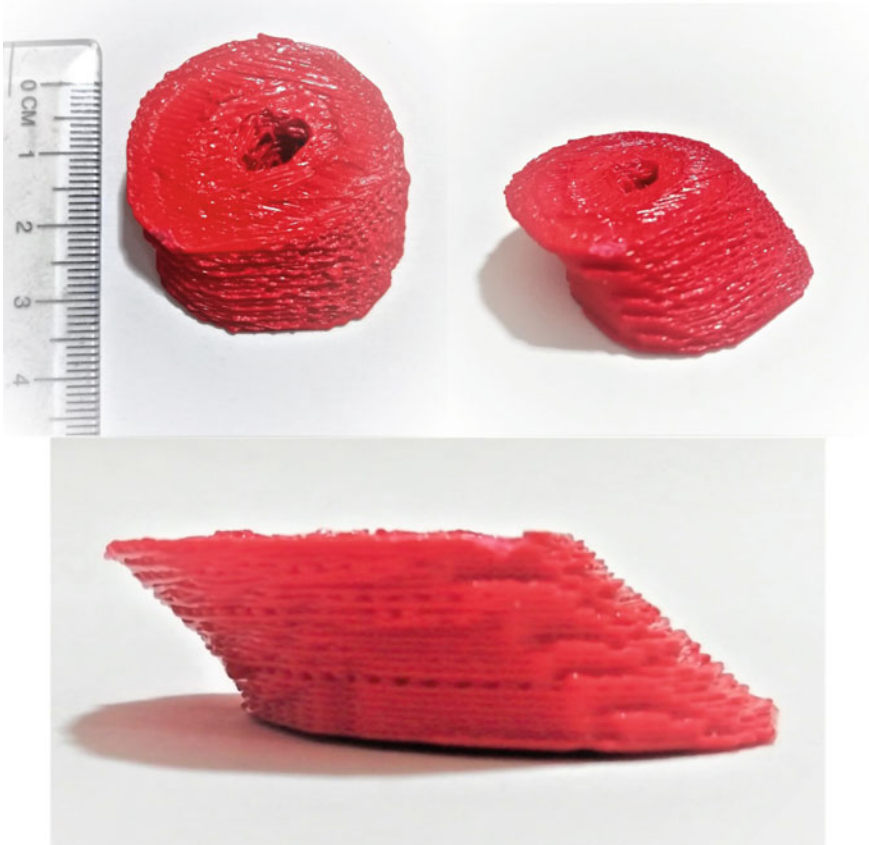


Fig. 25.15 Fabrication of femur bone for 20 slices of DICOM

generated then G & M codes has been implemented on it for part fabrication. Finally, this file is exported to FFF machine for implementation. The feasibility of proposed path planning tool has been discussed by considering a real-world application. The Printed model is a section of femur bone related to medical field. The cross section of femur bone has been segmented into four regions. Each region is filled with different set of process parameters which is relatively varied with respect to grayscale value. The region where grayscale value is high having higher density compare to remaining regions.

Concluding Remarks:

- A new approach of obtaining information about density variation at the cross-section of anatomical or any object has been obtained from CT scan in the form of DICOM image using Image Processing Technique.
- Two method, Analytical and Graphical method has been developed for obtaining threshold value for the segmentation of region.

- Improvisation in segmented region has been done to number and randomness in segmented region.
- Various process parameter has been introduced to obtain minimal difference in relative density of heterogeneous model with rest to original image across the region since the printing material is not same as of bone.
- Femur bone have been fabricated on FFF machine with non-uniform localized variations.

References

1. Hieu, L.C., Zlatov, N., Vander Sloten, J., Bohez, E., Khanh, L., Binh, P. H., Toshev, Y.: Medical rapid prototyping applications and methods. *Assem. Autom.* **25**(4), 84–292 (2005). <https://doi.org/10.1108/01445150510626415>
2. Navamani, T.M., Bharadwaja, A., Agrawala, R., Agarwala, U.: Secure transmission of DICOM images by comparing different cryptographic algorithms. *Mater. Today: Proc.* **15**, A1–A11 (2019). <https://doi.org/10.1016/j.matpr.2019.07.078>
3. Dave, J.K., Gingold, E.L.: Extraction of CT Dose information from DICOM metadata: automated Matlab-based approach. *Am. J. Roentgenol.* **200**, 142–145 (2013). <https://doi.org/10.2214/AJR.12.8501>
4. Nayak, A., Jain, P.K., Kankar, P.K., Jain, N.: Computer-aided design–based guided endodontic: a novel approach for root canal access cavity preparation. *Proc. Inst. Mech. Eng. [H]* **232**(8), 787–795 (2018)
5. Wergedala, J.E., Shenga, M.H.-C., Baylinka, D.J., Ackert-Bicknellb, C.L., Beamerb, W.G.: Genetic variation in femur extrinsic strength in 29 different inbred strains of mice is dependent on variations in femur cross-sectional geometry and bone density. *Bone* **36**(1), 111–122 (2005). <https://doi.org/10.1016/j.bone.2004.09.012>
6. Nayak, A., Jain, P.K., Kankar, P.K., Jain, N.: Image-based method for analysis of root canal geometry. In: *International Conference on ISMAC in Computational Vision and Bio-Engineering 2018 May 16*, pp. 1491–1497. Springer, Cham
7. Bhagat, A., Atique, M.: DICOM image retrieval using geometric moments and fuzzy connect-edness image segmentation algorithm. In: Satapathy, S., Avadhani, P., Udgata, S., Lakshmi-narayana, S. (eds.) *ICT and Critical Infrastructure: Proceedings of the 48th Annual Convention of Computer Society of India, vol. I. Advances in Intelligent Systems and Computing, vol. 248*. Springer, Cham (2014). https://doi.org/10.1007/978-3-319-03107-1_13
8. Kittler, J., Illingworth, J.: Minimum error thresholding. *Pattern Recogn.* **19**(1), 41–47 (1986). [https://doi.org/10.1016/0031-3203\(86\)90030-0](https://doi.org/10.1016/0031-3203(86)90030-0)
9. Castelino, K., D'Souza, R., Wright, P.K.: Toolpath optimization for minimizing airtime during machining. *J. Manuf. Syst.* **22**(3), 173–180 (2003). [https://doi.org/10.1016/s0278-6125\(03\)90018-5](https://doi.org/10.1016/s0278-6125(03)90018-5)
10. Wah, P.K., Murty, K.G., Joneja, A., Chiu, L.C.: Tool path optimization in layered manufacturing. *IIE Trans.* **34**(4), 335–347 (2002). <https://doi.org/10.1080/07408170208928874>

Chapter 26

Improved Local Search Based Grey Wolf Optimization for Feature Selection



Rahul Hans and Harjot Kaur

Abstract These days' technologies like machine learning have come into sight as promising areas of research, in which the system is trained using a dataset; that may comprise redundant and inappropriate features and may require more memory. Feature Selection aids to increase the accuracy during the process of classification while considering minimum number of features, that can be modeled as an optimization task. Currently, metaheuristic category of algorithms is being widely used by researchers to solve various optimization problems. In this context, this research proposes an improved variant of Grey Wolf optimization Algorithm using mutation based local search for getting into the bottom of the problem of selecting smallest set of features while increasing the accuracy. Moreover, the presented algorithm is weighed against several other algorithms for solving problem of selecting smallest set of features with increased accuracy.

Keywords Machine learning · Feature selection · Metaheuristic · Grey wolf optimization · K-nearest neighbours

26.1 Introduction

Machine learning has come out as a potential domain of research where an individual computable aspect of the process being experiential in acknowledged as feature [1]. In machine learning the larger sets of data can contain surplus features that are not significant [2] and which may require more storage. Thus, to get better accuracy in the classification whilst having minimum features, feature selection is the most needed task [1, 3]. Some of the recent applications of feature selection can be found in [4] for diagnosis in medical sphere, recognition of facial expression in [5, 6] contains the bronchitis diagnoses, [7] contains the selection of gene problem and classification of cancer.

R. Hans (✉) · H. Kaur

Department of Computer Science and Engineering, Guru Nanak Dev University, Regional Campus, Gurdaspur, Punjab, India

These days' metaheuristic algorithms have been regarded as more reliable for getting into the bottom of optimization problems [8] that generate acceptable results in a rational time [9].

The remaining paper is structured as: Sect. 26.2 puts forward some related research work, Grey Wolf Optimization Algorithm is discussed in Sect. 26.3 where as Sect. 26.4 puts forward an improved variant of the Grey Wolf Optimization Algorithm, Materials and Methods used are discussed in Sect. 26.5, Sect. 26.6 discusses the results and analyses them and lastly Sect. 26.7 concludes with some future direction.

26.2 Related Research Work

In recent times a lot of work has been done by various researchers for the improvement of the metaheuristic algorithms for solving various optimization problems including feature selection, some of the existing research works have been summarized in this section. Authors in [10] proposed the use of a metaheuristic algorithm known as Forest Optimization Algorithm (FOA) for selection of optimal number of features and evaluated them on 11 different datasets. In [11] versions of Bacterial foraging optimization have been proposed. In [12] the hybridization of GA and PSO is proposed and validated on Indian Pines Hyperspectral data set. In [13] feature selection is achieved by adaptively adjusting the parameters of ACO feature selection. In [14] author proposed the binary version GWO with PSO where position updating equation is modified using transformation function. The performance is tested on 18 UCI datasets and comparison is made with algorithms which are GWO, PSO, the GA and the WOASA. In [15] author proposed the binary variant of GWO for selection of optimal number of features. The two techniques are proposed in this paper. Firstly, crossover is performed on three initial binary solutions (grey wolves) to find the updated location. In second techniques sigmoid function is used find the updated location. In [16] author presented the improved binary version of grey wolf algorithm using crossover operator. This proposed technique is utilized on three Arabic datasets and results are obtained using three classifiers. Whale Optimization Algorithm is hybridized in [8] with simulated annealing which is used to improve solutions of WOA after iteration. The author proposed the two versions of this model using tournament selection. It is tested on 18 datasets form UCI and compared with ALO, PSO, and GA. It is superior to all of them. In [17] author proposed the improved sine cosine algorithm by using Elite strategy (ELM) for feature selection. This version is tested on 10 datasets (medical and non-medical) from UCI and comparison is made with Genetic algorithm, PSO, Basic SCA. The author claims that proposed version is giving the better results.

26.3 Grey Wolf Optimization

The GWO algorithm [18] is a metaheuristic algorithm inspired by the grey wolf's character of hunting. Grey wolves live in a pack and the leader of the pack called the alpha Wolf. Alpha wolf is followed by the entire pack and then there comes the Beta Wolves, they assist the Alpha Wolves in decision-making. At the third level Delta wolves work as a safeguard to protect the group also warned the pack in case of danger. Omegas are the last wolves following the instructions of senior wolves so using three best solutions and according to their position rest of all change their position. Firstly, grey wolves encircle the prey, shown in (26.1) and (26.2)

$$\vec{D} = |\vec{C} \cdot \vec{X}_p(t) - \vec{X}(t)| \quad (26.1)$$

$$\vec{X}(t+1) = |\vec{X}_p(t) - \vec{A} \cdot \vec{D}| \quad (26.2)$$

$$\vec{A} = 2 \cdot \vec{a} \cdot \vec{r}_1 - \vec{a} \quad (26.3)$$

$$\vec{C} = 2 \cdot \vec{r}_2 \quad (26.4)$$

where t indicates the current iteration \vec{A} and \vec{C} are the coefficient vectors, \vec{X}_p is the prey position and \vec{X} is the grey wolf position. The vector \vec{A} and \vec{C} can be calculate as shown in (26.3) and (26.4). Here the \vec{a} is linearly decreased from 2 to 0 over the course of iteration and r_1 and r_2 are the random vectors in $[0, 1]$. Where $\vec{X}_\alpha, \vec{X}_\beta$ and \vec{X}_δ are the first three best solutions at given iteration t where A is defined in Eq. (26.3) and D can be calculated as follows

$$\vec{D}_\alpha = |\vec{C}_1 \cdot \vec{X}_\alpha(t) - \vec{X}| \quad (26.5)$$

$$\vec{D}_\beta = |\vec{C}_2 \cdot \vec{X}_\beta(t) - \vec{X}| \quad (26.6)$$

$$\vec{D}_\delta = |\vec{C}_3 \cdot \vec{X}_\delta(t) - \vec{X}| \quad (26.7)$$

$$\vec{X}_1 = |\vec{X}_\alpha - \vec{A}_1 \cdot \vec{D}_\alpha| \quad (26.8)$$

$$\vec{X}_2 = |\vec{X}_\beta - \vec{A}_2 \cdot \vec{D}_\beta| \quad (26.9)$$

$$\vec{X}_3 = |\vec{X}_\delta - \vec{A}_3 \cdot \vec{D}_\delta| \quad (26.10)$$

Algorithm I: Grey Wolf Optimization Algorithm

Input: Search space, fitness function, Number of wolves, maximum number of iterations (Max_iter)

Outputs: The Best solution and its fitness value.

- 1) **Initialize** the population size (Wolves) randomly and A,C and a.
- 2) Evaluate the fitness of each search agent in the population and save the fitness alpha, beta and delta wolves.
- 3) $t=0$
- 4) **While** ($t < Max_iter$) do
 - Update the value of a (a decreases linearly from 2 to 0)
 - Generate randomly new values for r_2, r_3 .
 - for each** search agent X_i in the population **do**
 - Update the A and C for all the three wolves.
 - Compute the value of X_1, X_2 and X_3 using Eq. (8),(9),(10).
 - Update the population using equation Eq. (11).
 - end**
- 5) Calculate the fitness of each search agent and update the value of alpha, beta and delta.
- 6) Increment the iteration counter $t=t+1$
- 7) **end while**

$$\vec{X}(t+1) = \frac{\vec{X}_1 + \vec{X}_2 + \vec{X}_3}{3} \quad (26.11)$$

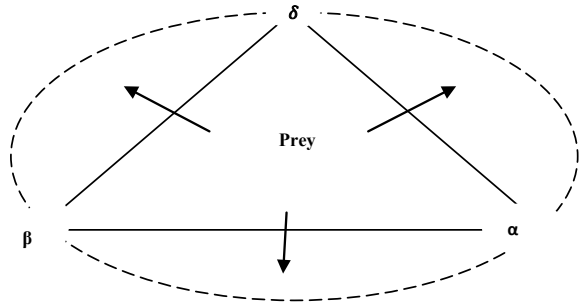
$$\vec{a} = 2 - t \frac{2}{MaxIteration} \quad (26.12)$$

The Position updating equation can be seen in (26.11). In every iteration \vec{a} is updated from 2 to 0 according to (26.12).

26.4 Proposed Grey Wolf Optimization

In literature various improved versions of metaheuristic algorithms have been proposed for solving various optimization problem, in [19] random walk is built-in with the grey wolf optimization algorithm in which leaders travels around by walking randomly and rest of the wolves modify their position by following them. Similarly, in [20] mutation is performed as a local search and also average is substituted by crossover operation. In the proposed version of improved grey wolf optimization, the position of the wolves is updated by performing local search around the top three best wolves' viz. Alpha, Beta and Delta wolves using mutation with as suitable mutation rate. The final position of the wolves is updated, by crossover of two leading wolves from the top three, depending upon the probability of the movement of the prey instead of the mean as in Eq. (26.11). The pseudo code of the proposed grey wolf can be seen in the Algorithm 2 (Fig. 26.1).

Fig. 26.1 Escaping behavior of the prey



Algorithm II: Improved Local Search Based Grey Wolf optimization(ILGWO)	
Input:	Search space, fitness function, population (habitats) , maximum number of iterations (Max_iter)
Outputs:	The Best solution and its fitness value.
1.	Initialize random solutions(wolfs) in the Population X
2.	$t=0$.
3.	while ($t < Max_iter$) do
4.	Weigh up the fitness of each wolf from X_i keep the fitness of alpha, beta and delta wolves. foreach X_i (wolf/search agent) do
	<ul style="list-style-type: none"> • Perform Local Search on the top three wolves to Form $LAlpha$, $LBeta$ and $LDelta$ using <i>mutation</i> in Eq. (13) • Update the remaining wolves using random number(r). <ul style="list-style-type: none"> if $r < \frac{1}{3}$ $X_i = Crossover(LAlpha, LBeta)$; else if $r < \frac{1}{3} \&\& r < \frac{2}{3}$ $X_i = Crossover(LAlpha, LDelta)$; else $X_i = Crossover(LBeta, LDelta)$; end if
	end
5.	Increment the iteration counter $t=t+1$
6.	end

In this research, the author assumes the escaping behavior of the prey as shown in Fig. 26.1. Considering this nature of the algorithm if the prey tries to escape from between α and β , then both the wolves will move locally to catch the prey.

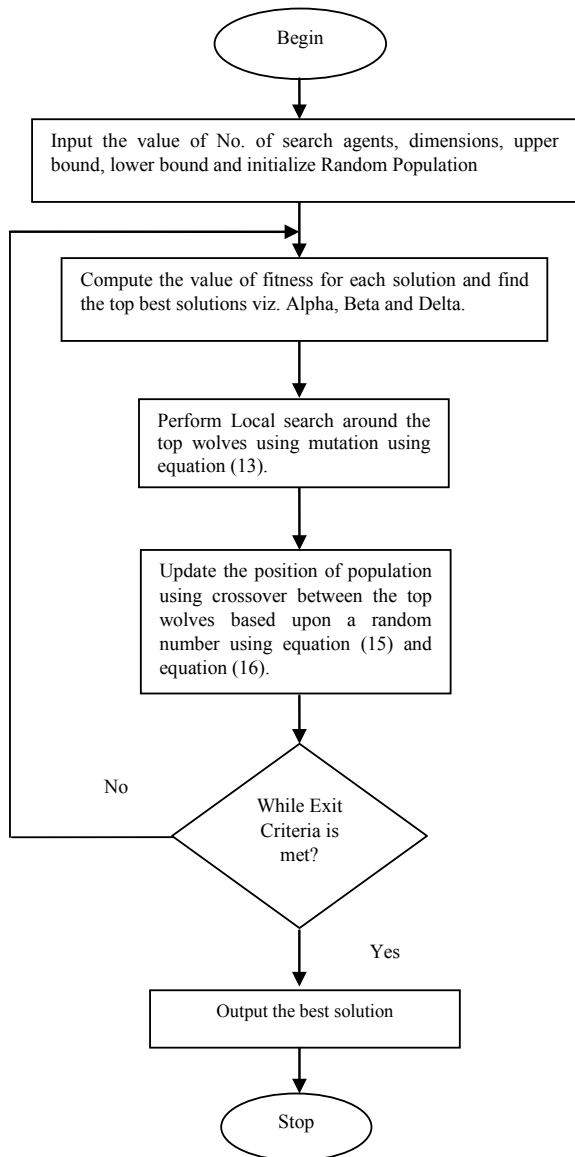
Local movement is modeled as mutation and catching behavior is modeled as crossover between the two wolves instead of mean as was in the standard grey wolf optimization algorithm the same process is repeated for the other two escaping options.

In the proposed version of improved grey wolf optimization, in every iteration the best solutions/ wolves are selected to attack the prey or in other words the top three best wolves participate in hunting process, as the prey tries to escape from the trap from any of the three directions, the corresponding wolves in that direction attacks the prey. The movement of the top best wolves is modeled by performing local search

around the top three best wolves' viz. *Alpha*, *Beta* and *Delta* wolves using mutation with as suitable mutation rate. The flow chart of the proposed algorithm is shown in Fig. 26.2.

Here *Alpha*, *Beta* and *Delta*, represent the fittest wolves that participate in hunting and *LAlpha*, *LBeta*, *LDelta* are the positions of the wolves after local movement to catch the escaping prey which is modeled by applying stochastic mutation around

Fig. 26.2 Flow chart of proposed ILGWO



Alpha, Beta and Delta in the binary mode [20]. The dm dimension value is depicted as I_{out}^{dm} for the vector as output after mutation, the input to be mutated is depicted as I_{in}^{dm} , the two uniform distribution based random numbers are depicted as $rand_1$, $rand_2$ in the range $[0, 1]$, and mr is the mutation rate.

$$I_{out}^{dm} = \begin{cases} I_{in}^{dm} & \text{if } rand_1 \geq r \\ rand_2 & \text{otherwise} \end{cases} \quad (26.13)$$

It worth mentioning that mr can be considered as to linearly decrement with iteration number ranging from 0.9 to 0 as seen in Eq. (26.14):

$$mr = 0.9 + \frac{-0.9 * (i - 1)}{Max_Iter - 1} \quad (26.14)$$

where mr is the mutation rate at iteration i and, Max_Iter is iterations in total considered. The final position of the wolves is updated, by crossover of two leading wolves from the top three, depending upon the probability of the movement of the prey instead of the mean. The position is updated as

$$X_i^{(t+1)} = \begin{cases} CrossOver(LAlpha, LBeta), & \text{If } mr < \frac{1}{3} \\ CrossOver(LBeta, LDelta), & \text{If } mr < \frac{1}{3} \ \&\& \ mr < \frac{2}{3} \\ CrossOver(LAlpha, LDelta), & \text{otherwise} \end{cases} \quad (26.15)$$

As per Emary et al. [20], $CrossOver(a, b)$ is appropriate crossover among vectors a and b , and $LAlpha$, $LBeta$ and $LDelta$ are solutions representing the effect of local search in $Alpha$, $Beta$ and $Delta$ using mutation.

$$I^{dm} = \begin{cases} I_1^{dm}, & \text{if } rand \geq 0.5 \\ I_2^{dm}, & \text{otherwise} \end{cases} \quad (26.16)$$

The mean operator is replaced by the crossover operator for position updating in basic grey wolf algorithm, which is implemented to get midway solution and is a stochastic crossover that shifts between the two input solutions with equal likelihood as shown in (26.16). The output from the crossover between two solutions I_1^{dm} and I_2^{dm} at dm dimension is seen as I^{dm} . The two evolutionary operators crossover and mutation brings diversity, where, crossover provides decent mingling, and its range is limited in the sub space while mutation can provide healthier variety. The proposed algorithm can be seen in the algorithm II.

26.5 Materials and Methods

The Smaller feature subset selection with maximum accuracy is modeled as an optimization problem with multiple objectives [8, 15] where two conflicting objectives accuracy of classification and selected feature subset size are considered and the fitness function is centered on the classifier k-NN [15] as shown in (26.17) above.

$$\text{Fitness} = L_1 \left| \frac{F_s}{N} \right| + L_2 * R(D) \quad (26.17)$$

where rate of error is shown by $R(D)$, Furthermore, $|F_s|$ feature subset size chosen and $|N|$ is the initial size of feature set, L_1 and L_2 presents worth of prominence of classification and subset dimension of features, where $L_1 \in [0, 1]$ and $L_2 = (1 - L_1)$ adopted from [15].

26.5.1 Parameter Settings and Dataset Description

To conduct the experiment a Core 2 Duo 2.00 GHz processor and 64-bit Operating system is considered. To conduct the experiments, 22 datasets were obtained from [21] summarized in Table 26.1 and also various parameter settings in Table 26.2.

26.5.2 Performance Criteria's

To measure the performance of the algorithms this research uses some performance criteria, as shown in Table 26.3.

1. **Average Accuracy**—Capability of the classification method in categorizing the dataset in all the runs or accuracy of classification when averaged on all the runs.
2. **Average fitness**—It is the mean of the fitness values in N runs.
3. **Feature Subset Size Selected**—It is mean of total features selected in N runs.
4. **Average time taken**—It is mean of running time of the algorithm in N runs.
5. **F-Measure**—It is mean of F-measure values of the algorithm in N runs.
6. **Standard Deviation**—The divergence of the finest solutions found averaged on N runs after running algorithm.

Table 26.1 Dataset Description

S. No.	Dataset	Instances	Attributes
1	Zoo	101	16
2	Statlog credit	1000	20
3	Lung cancer	32	56
4	Exactly	1000	13
5	Exactly2	1000	13
6	M-of-N	1000	13
7	Heart	294	13
8	Vote	300	16
9	Spect heart	267	22
10	Australian	690	14
11	Ionosphere	351	34
12	Water treatment	521	38
13	Wine	178	13
14	Indian Liver	583	10
15	Tic-Tac-Toe	958	9
16	Wavform	1000	21
17	Dermatology	366	34
18	Glass Identification	214	9
19	Breast cancer	699	9
20	Sonar	208	60
21	Vehicle	94	18
22	Vowel	990	13

26.6 Results and Analysis

The present section measures up to the ILGWO with Genetic Algorithm (GA), Particle Swarm Optimization (PSO), Grey Wolf Optimization (GWO) and Sine Cosine Algorithm (SCA). The results obviously specify that the proposed.

IGWO is superior than all the other algorithms when results were compared for average classification accuracy in Table 26.4, the IGWO outperforms on twenty one dataset out of twenty two datasets taken for comparison, moreover when results were compared on the basis of cumulative average of classification accuracies the results clearly indicate the outperformance of the proposed algorithm as shown in Fig. 26.3. A similar performance is observed in Table 26.5 when results were compared on the basis of average fitness values obtained, the results clearly indicate the outperformance of the proposed algorithm.

The proposed IGWO shows similar performance when results were compared on the basis of F-Measure and Average size of feature subset selected in Table 26.6. and Table 26.7. Furthermore the results also indicate the superior performance of the

Table 26.2 Parameter settings

Parameter	Value
Runs considered	10
Iterations considered	100
Search agents in the population	20
Lb (lower bound)	0
Ub (upper bound)	1
Dimensions	Total features in dataset
L ₂ parameter of the fitness function	0.99
L ₁ parameter of the fitness function	0.1
Crossover ratio in GA	0.9
Mechanism of selection in GA	Roulette wheel selection
Value of A in GWO	2 to 0
Cognitive constant (C ₁) in PSO	1
Social constant (C ₂) in PSO	1
Inertia constant (w) in PSO	0.3
Value of r1 in SCA	2 to 0

Table 26.3 Performance criteria

Evaluation criteria	Formula
Average classification accuracy	$Avg_Acc = \frac{1}{N} \sum_{t=1}^N Acc_t$
Average fitness	$Avg_fit = \frac{1}{N} \sum_{t=1}^N Fit_t$
Worst fitness	$Worst_fit = \max(Fit_1: Fit_N)$
Best fitness	$Best_fit = \min(Fit_1: Fit_N)$
Standard deviation	$St_dev = \sqrt{\frac{\sum_{t=1}^N (Fit_t - \bar{Fit})^2}{N-1}}$
Average size of feature subset	$Avg_FS = \frac{1}{N} \sum_{k=1}^N SizeFS_t$
F-measure	$F_Measure = \frac{2 \cdot Precision \cdot Recall}{(Precision + Recall)}$

proposed algorithm when results were compared on the basis of features selected averaged on all the datasets as shown in the Fig. 26.4.

Moving ahead, when IGWO is compared with other algorithms on the basis of cumulative sum of average computational time taken by the algorithms in the Fig. 26.5, the proposed IGWO performs better in terms of computational time also.

To summarize the performance of the proposed algorithm, it can be clearly seen that the performance of the algorithm increases by using evolutionary operators. Mutation based local search brings diversity and the solution generated by crossover

Table 26.4 Assessment of average accuracy

	GA	PSO	SCA	GWO	IGWO
Zoo	0.939	0.943	0.905	0.919	0.967
Statlog credit	0.720	0.710	0.716	0.717	0.759
Lung cancer	0.919	0.894	0.881	0.863	0.95
Exactly	0.784	0.723	0.718	0.703	0.989
Exactly2	0.753	0.755	0.748	0.754	0.762
M-of-N	0.976	0.900	0.831	0.880	0.999
Heart	0.830	0.817	0.816	0.805	0.846
Vote	0.955	0.931	0.939	0.943	0.966
Spect Heart	0.756	0.729	0.737	0.719	0.796
Australian	0.857	0.810	0.790	0.799	0.872
Ionosphere	0.872	0.854	0.870	0.866	0.923
Water treatment	0.847	0.807	0.815	0.815	0.891
Wine	0.982	0.979	0.978	0.974	0.997
Indian Liver	0.714	0.704	0.710	0.703	0.730
Tic-Tac-Toe	0.771	0.808	0.756	0.792	0.799
Wavform	0.826	0.830	0.801	0.823	0.851
Dermatology	0.982	0.974	0.948	0.962	0.992
Glass Identification	0.688	0.680	0.682	0.664	0.709
Breast cancer	0.972	0.975	0.965	0.971	0.978
Sonar	0.838	0.785	0.772	0.783	0.905
Vehicle	0.583	0.562	0.519	0.572	0.668
Vowel	0.838	0.823	0.790	0.820	0.861

has the features of both of the solutions used for crossover which aids to find better solution from a good solution.

When results were compared on the basis of average of accuracy to features selected ratio, the results clearly depict that the performance of the proposed ILGWO is better than the other algorithms considered for the comparison. The results clearly indicate the overall out performance of the proposed algorithms in terms of different parameters considered. The out performance of the proposed algorithms is due to the use of evolutionary operators viz. crossover and mutation and their simplicity of implementation. The results also indicate that apart from the proposed algorithm, the performance of the genetic algorithm is also better in terms of different parameters as compared to the other algorithms considered for the performance comparison. The bold values in the Tables 4 and 5 indicate the superior results.

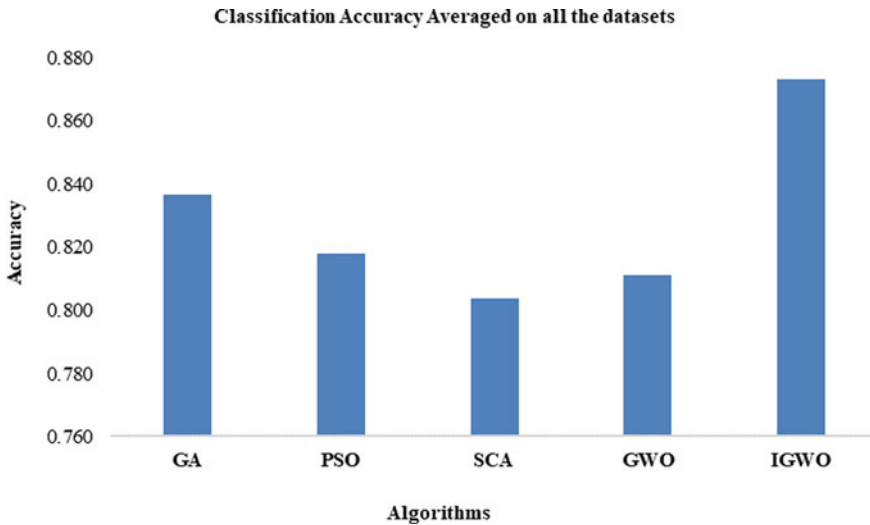


Fig. 26.3 Classification accuracy averaged on all the datasets

26.7 Conclusions and Future Work

This research work puts forward a superior edition of grey wolf optimization algorithm for selection of optimal feature subset, with the aim to maximize classification accuracy and while having minimum number of features. The proposed algorithm aims to model the position of top three grey wolves viz. alpha, beta and delta using a local search mechanism based on the mutation and instead of mean for updating the position, the proposed algorithm updates the position by taking the crossover of the top wolves positions (after applying local search) depending upon a random number. The results clearly indicate that the use of mutation and crossover operators in the grey wolf optimization algorithms aids to get better performance.

In future, work can be done to solve the feature selection problem for larger datasets or for any other real time application domain, the algorithms can be implemented to develop various computer aided diagnosis systems and for selection of optimal feature subset size in big data.

Table 26.5 Assessment of mean Fitness values

	GA	PSO	SCA	GWO	IGWO
Zoo	0.065	0.063	0.076	0.087	0.037
Statlog credit	0.282	0.293	0.281	0.286	0.242
Lung cancer	0.083	0.110	0.116	0.140	0.051
Exactly	0.219	0.282	0.255	0.302	0.016
Exactly2	0.248	0.247	0.252	0.249	0.238
M-of-N	0.029	0.107	0.100	0.127	0.006
Heart	0.172	0.186	0.184	0.197	0.155
Vote	0.049	0.074	0.062	0.062	0.037
Spect Heart	0.246	0.274	0.255	0.284	0.206
Australian	0.145	0.193	0.205	0.203	0.130
Ionosphere	0.131	0.150	0.129	0.137	0.078
Water treatment	0.155	0.197	0.182	0.189	0.111
Wine	0.023	0.028	0.019	0.031	0.008
Indian liver	0.287	0.297	0.289	0.298	0.271
Tic-Tac-Toe	0.232	0.199	0.206	0.216	0.207
Wavform	0.179	0.178	0.175	0.184	0.154
Dermatology	0.022	0.034	0.035	0.045	0.012
Glass identification	0.314	0.323	0.319	0.338	0.293
Breast cancer	0.033	0.030	0.037	0.035	0.028
Sonar	0.164	0.218	0.229	0.221	0.098
Vehicle	0.416	0.441	0.474	0.428	0.332
Vowel	0.166	0.182	0.186	0.185	0.143

Table 26.6 Assessment on the basis of mean F-Measure

	GA	PSO	SCA	GWO	IGWO
Zoo	0.963	0.963	0.959	0.980	0.943
Statlog credit	0.813	0.795	0.811	0.814	0.838
Lung cancer	0.809	0.552	0.721	0.705	0.906
Exactly	0.855	0.795	0.813	0.800	0.992
Exactly2	0.856	0.837	0.853	0.856	0.864
M-of-N	0.966	0.836	0.763	0.837	0.998
Heart	0.868	0.809	0.859	0.849	0.881♦
Vote	0.941	0.892	0.926	0.929	0.956
Spect heart	0.799	0.748	0.785	0.764	0.835
Australian	0.868	0.731	0.815	0.822	0.881
Ionosphere	0.908	0.883	0.907	0.904	0.942

(continued)

Table 26.6 (continued)

	GA	PSO	SCA	GWO	IGWO
Water treatment	0.910	0.859	0.892	0.891	0.935
Wine	0.987	0.979	0.980	0.980	0.996
Indian liver	0.815	0.786	0.809	0.806	0.824
Tic-Tac-Toe	0.836	0.861	0.827	0.856	0.857
Wavform	0.775	0.779	0.745	0.780	0.808
Dermatology	1.000	0.953	0.990	0.996	1.000
Glass identification	0.725	0.678	0.725	0.698	0.753
Breast cancer	0.979	0.976	0.973	0.978	0.983
Sonar	0.807	0.678	0.734	0.743	0.894
Vehicle	0.412	0.367	0.355	0.346	0.502
Vowel	0.934	0.903	0.892	0.918	0.929

Table 26.7 Assessment on the basis of average no. of features selected

	GA	PSO	SCA	GWO	IGWO
Zoo	6.8	10.5	11.3	10.3	5.6
Statlog credit	8.8	12.0	10.0	11.3	8.1
Lung cancer	14.3	27.0	27.2	24.0	8.8
Exactly	7.5	9.9	8.8	10.0	6.0
Exactly2	4.6	6.0	5.1	6.7	2.2
M-of-N	6.7	10.2	10.1	10.9	6.0
Heart	4.2	5.8	6.4	5.2	3.4
Vote	6.0	8.1	9.0	8.7	4.6
Spect heart	10.2	12.4	12.8	11.1	8.4
Australian	4.5	6.2	6.9	6.0	4.4
Ionosphere	12.3	18.9	19.0	13.9	7.9
Water treatment	13.2	20.7	21.4	19.0	13.1
Wine	6.3	9.1	9.3	7.4	5.5
Indian Liver	4.5	4.3	5.0	3.8	3.7
Tic-Tac-Toe	4.6	8.4	8.7	9.0	7.2
Wavform	13.8	19.0	17.5	19.5	14.5
Dermatology	14.7	26.4	26.2	26.6	13.9
Glass Identification	4.5	6.3	5.7	4.9	4.5
Breast cancer	4.7	5.5	6.2	6.0	5.5
Sonar	23.2	31.0	32.7	32.5	22.0
Vehicle	6.1	12.1	8.3	8.7	6.8
Vowel	7.6	9.5	8.7	9.4	7.5

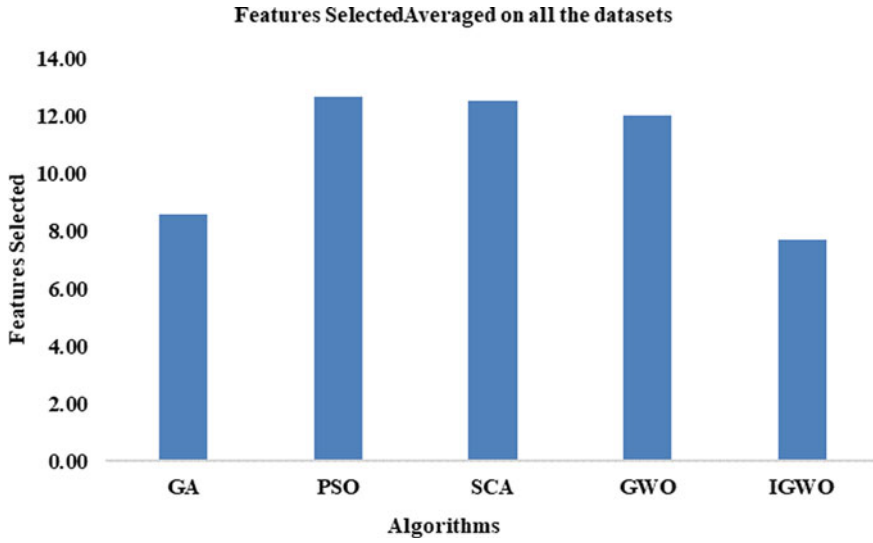


Fig. 26.4 Features selected averaged on all the datasets

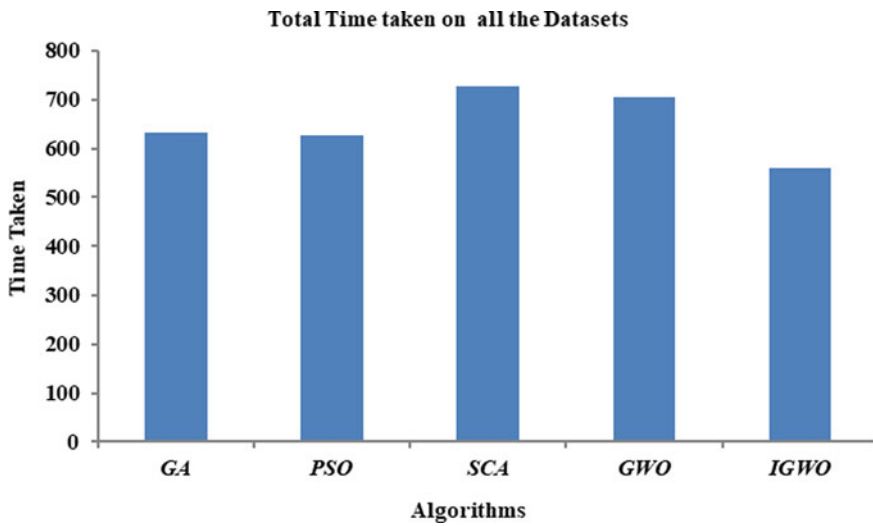


Fig. 26.5 Assessment for cumulative sum of mean computational time

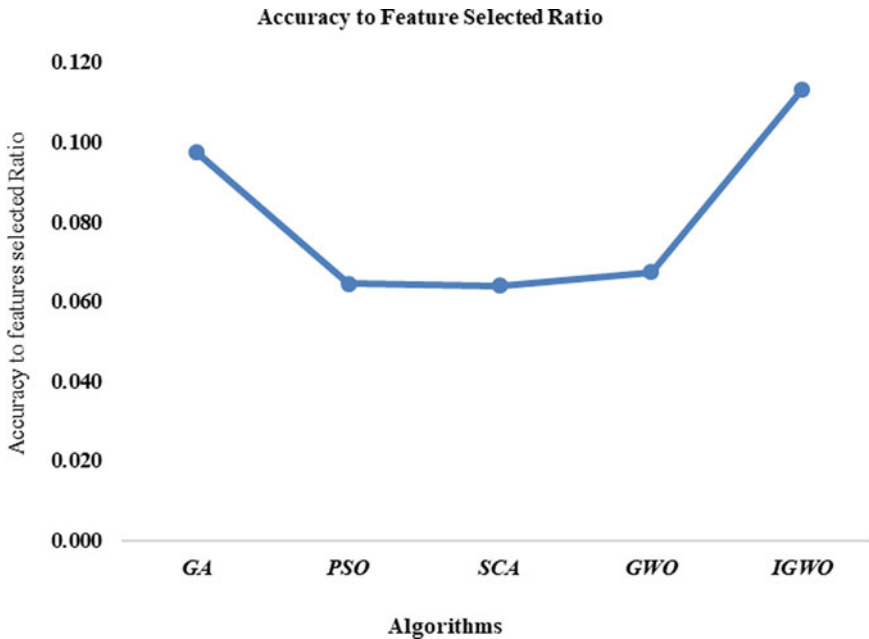


Fig. 26.6 Accuracy to features selected ratio for cumulative average on all the datasets

References

1. Chandrashekar, G., Sahin, F.: A survey on feature selection methods. *Comput. Electr. Eng.* **40**(1), 16–28 (2014)
2. Hancer, E., et al.: A modified binary ABC algorithm based on advanced similarity scheme for feature selection. *Appl. Soft Comput.* **36**, 334–348 (2015)
3. Sayed, G.I., Hassanien, A.E., Azar, A.T.: Feature selection via a novel chaotic crow search algorithm. *Neural Comput. Appl.* 1–18 (2017)
4. Inbarani, H.H., Azar, A.T., Jothi, G.: Supervised hybrid feature selection based on PSO and rough sets for medical diagnosis. *Comput. Methods Programs Biomed.* **113**(1), 175–185 (2014)
5. Mlakar, U., Fister, I., Brest, J., Potočnik, B.: Multi-objective differential evolution for feature selection in facial expression recognition systems. *Expert Syst. Appl.* **89**, 129–137 (2017)
6. Sweetlin, J.D., Nehemiah, H.K., Kannan, A.: Feature selection using ant colony optimization with tandem-run recruitment to diagnose bronchitis from CT scan images. *Comput. Methods Programs Biomed.* **145**, 115–125 (2017)
7. Jain, I., Jain, V.K., Jain, R.: Correlation feature selection based improved-binary particle swarm optimization for gene selection and cancer classification. *Appl. Soft Comput.* **62**, 203–215 (2018)
8. Mafarja, M.M., Mirjalili, S.: Hybrid whale optimization algorithm with simulated annealing for feature selection. *Neurocomputing* **260**, 302–312 (2017)
9. Yang, X.S., Deb, S., Fong, S.: Metaheuristic algorithms: optimal balance of intensification and diversification. *Appl. Math. Inf. Sci.* **8**(3), 977 (2014)
10. Ghaemi, M., Feizi-Derakhshi, M.R.: Feature selection using forest optimization algorithm. *Pattern Recogn.* **60**, 121–129 (2016)
11. Chen, Y.P., Li, Y., Wang, G., Zheng, Y.F., Xu, Q., Fan, J.H., Cui, X.T.: A novel bacterial foraging optimization algorithm for feature selection. *Expert Syst. Appl.* **83**, 1–17 (2017)

12. Ghamisi, P., Benediktsson, J.A.: Feature selection based on hybridization of genetic algorithm and particle swarm optimization. *IEEE Geosci. Remote Sens. Lett.* **12**(2), 309–313 (2015)
13. Wang, G., Chu, H.E., Zhang, Y., Chen, H., Hu, W., Li, Y., Peng, X.: Multiple parameter control for ant colony optimization applied to feature selection problem. *Neural Comput. Appl.* **26**(7), 1693–1708 (2015)
14. Al-Tashi, Q., Kadir, S.J.A., Rais, H.M., Mirjalili, S., Alhussian, H.: Binary optimization using hybrid grey wolf optimization for feature selection. *IEEE Access* **7**, 39496–39508 (2019)
15. Emary, E., Zawbaa, H.M., Hassanien, A.E.: Binary grey wolf optimization approaches for feature selection. *Neurocomputing* **172**, 371–381 (2016)
16. Chantar, H., Mafarja, M., Alsawalqah, H., Heidari, A.A., Aljarah, I., Faris, H.: Feature selection using binary grey wolf optimizer with elite-based crossover for Arabic text classification. *Neural Comput. Appl.* 1–20 (2019)
17. Sindhu, R., Ngadiran, R., Yacob, Y.M., Zahri, N.A.H., Hariharan, M.: Sine–cosine algorithm for feature selection with elitism strategy and new updating mechanism. *Neural Comput. Appl.* **28**(10), 2947–2958 (2017)
18. Mirjalili, S., Mirjalili, S.M., Lewis, A.: Grey wolf optimizer. *Adv. Eng. Softw.* **69**, 46–61 (2014)
19. Gupta, S., Deep, K.: A novel random walk grey wolf optimizer. *Swarm Evol. Comput.* (2018)
20. Emary, E., Zawbaa, H.M., Hassanien, A.E.: Binary ant lion approaches for feature selection. *Neurocomputing* **213**, 54–65 (2016)
21. Asuncion, A., Newman, D.: UCI machine learning repository (2007)

Chapter 27

Current Technologies on Electronics Cooling and Scope for Further Improvement: A Typical Review



K. R. Aglawe, R. K. Yadav, and S. B. Thool

Abstract The ongoing accentuation on laptops and PCs has resulted in a transformed enthusiasm for the improvement of higher performance cooling systems. The gigantic heat produced in laptops and PCs chip or enormous integrated circuit raises lots of exigent problems to be settled. The improvement within a cooling of electronic components needs the compact heat dissipation mechanism which gives higher performance. By the technological progression of several electronics equipment, liquid coolants were utilized progressively in PCs, servers, and super-computers. This review article covers the characteristics of heat transfer for several cooling technologies with its possible applicability to the field of electronics cooling. Several cooling technologies like conventional air cooling method, indirect liquid cooling by single/two-phase methods, and heat pipes have been examined in the study. The characteristics for performance evaluated based on values of heat flux, temperature and flow rate of coolant; which serve as pointers for limitations of various heat transfer and power prerequisites of individual cooling arrangement. An increase in the heating load, higher will be a decrement in the temperature occurred due to the cooling mechanism. In consideration of common computing methods, air cooling remains a reasonable choice as heat loads of every processor are limited to 190 W, albeit different factors like operational cost, reliability of device and recovery of waste heat might even now energize a utilization of liquid cooling. The liquid cooling is relied upon to be important into future thermal management of the laptop, where both proficient cooling and incredibly lower energy utilization are of significant role.

Keywords Electronics cooling technologies · Current cooling technology · Heat transfer · Thermal management · Air cooling · Liquid cooling · Heat pipes

K. R. Aglawe (✉) · R. K. Yadav

Department of Mechanical Engineering, National Institute of Technology, Raipur, India

S. B. Thool

Department of Mechanical Engineering, D. J. Sanghvi College of Engineering, Mumbai, India

27.1 Introduction

Electronics cooling technology is the developing concern for government and business engaged with electronics and IT industries like processing of data, storage, and media transmission. The fundamental reason behind the concern is expanding charge and multifaceted nature of thermal management into the electronics and IT industries. After the advancement of first, electronically operated digital PCs in the 1940s, productive evacuation of heat has assumed an important job while safeguarding the dependable activity of progressive PCs generations [24]. As the industries keep on embracing more current generations of processors that provide enhanced computational execution and capacities, an ascent into produced heat gets necessary [47].

The requirement of newer cooling answers for upcoming generation electronics is getting squeezed year by year. Various forecasts show the unbelievable heat fluxes expecting later on for elite computer devices [35] up to 250 W/cm^2 [7] and projected higher up to 1000 W/cm^2 in an upcoming decade [72]. The ITRS also echoes these expectations with a prediction of over 100 W/cm^2 between the years 2009–2010 [41]. Air cooling techniques will be getting overpowered by this heat fluxes as a coefficient of heat transfer related to higher forced convection techniques won't have the option to keep up working temperatures inside the dependable series. The temperature of chip and reliability connection is very much archived [4, 21, 38] and is a significant thought in the assurance of a cooling arrangement executed like a hardware substitution can provide a primary concern similarly as fast as energy utilization costs if not successfully oversaw [35].

Thermal management of electronic devices is one amongst the most significant challenge of the electronics and IT industries [32]. All heat produced due to electronics components must be expelled and dissolute into an atmosphere so as to keep up the temperature of components beneath adequate limits [47]. Air cooling has been recognized as the most actualized answer for accomplishing thermal management since the 1990s [34]. Even though it is an exceptionally advantageous and practical result, air cooling depends vigorously on vapor-compression methods at the facility level [102].

Also, producers of devices are consistently embracing newer processors generations that proffer enhanced computational execution and capacities; therefore creating heat at more noteworthy rates inside denser bundling [32, 93, 94]. This further compounds thermal management challenge by expanding the necessary cooling load, yet in addition by requiring a low temperature of air and high flow rates for dealing with the growing heat fluxes [47, 62]. Also, these patterns have persuaded immense measures of research managing alternative liquid cooling techniques planned for decreasing consumption of energy, and working expenses [47].

Two fundamental inefficiencies are prompting such tremendous energy prerequisites: the cooling necessities and IT hardware inefficiencies, both representing generally 40% of complete energy utilization, among an outcome that every kW h

of energy needs another kW h to cool. An energy proficient plan electronics and IT industries is an objectionable issue. IT load inefficiencies can be tended to by enhanced semiconductor advancements [18, 87], while electronics cooling can be accomplished in various manners, like by colder air, yet similar pattern to embrace direct liquid cooling [11] of a device is observed, like heat exchangers (tube and fin) joined to a rear server rack portion [2, 3].

The present review paper provides a comprehensive picture of several technologies accessible for thermal management in electronics and IT industries. In this paper, mechanisms for heat transfer of individual cooling arrangements are quickly explored whereas accentuation is set on their advantages, disadvantages, and limitations as found in industrial applications. The general aim is to give a valuable plan for thermal engineers engaged inside the electronics and IT sector cooling applications; especially as newer and advanced cooling innovations are rising.

27.2 Criteria for Assessment

In the present paper, solutions for cooling are assessed on the basis of the requirement of power and limitations for heat transfer and. Upcoming paragraphs provide the summary for inspiration and importance for the selection of these parameters.

27.2.1 Requirement of Power

Capital and working expenses of liquid-based cooling devices are represented in this paper. An indirect evaluation is feasible but during an assessment of coolant flow rates and temperatures; characteristics that are suitably recorded into experimentations. A high temperature of coolant encourages the utilization of free cooling, in this way decreasing the general working expense of vapor-compression cooling [49, 102]. Reduction in flow rates of coolant further reduces the working requirement of pump or fan for sufficient management of heat, in this way adding an additional decrease in working expenses [22]. One thought pursuers should remember is that a considerable number of variables important to perform such assessments are not introduced reasonably or successfully in numerous experimentation related publications. This is especially valid for variables identified with temperature and flow of coolants. Accordingly, the writers have endeavored as well as could be expected to evaluate these qualities dependent on accessible information.

27.2.2 Limitations for Heat Transfer

A limitation of heat transfer is the preeminent property of every cooling solution. This limitation of heat transfer is characterized like a most extreme rate during heat produced by the processor whereas the temperature of die working stays under suitable limits; ordinarily prescribed as 85 °C [22]. This description should likewise expect that the actual set of working situations applies. For instance, a limitation for heat transfer of an air cooling device might be expanded extensively by decreasing input air temperatures, but the provided methodology is rendered unconventional past the specific end because of enhanced vapor-compression cooling costs.

Even though regularly utilized up to rate the viability of the provided solution for cooling, these measurements neglect to give adequate data important to coordinate the correlation between different technologies [71]. The heat flux wall metric gives negative signs to the heat distribution zone needed for viable heat dissemination. Heat sink needs bigger bottom and fin surfaces corresponding to water block while processor cooling of indistinguishable size and power. The water block is subsequently an increasingly powerful cooling arrangement as it needs lesser space for parallel heat dissemination but can't be identified in the chip heat flux metric. Convective area for heat transfer, which represents expanded surfaces, doesn't legitimately describe the server space needed for the provided cooling arrangement.

27.3 Heat Loads in Electronics Components

Electronics equipment which generates a significant amount of heat mainly incorporates chipsets, memory modules, power supply, processors, and voltage controllers [19, 47, 88]. By considering the thermal management of the system, processors are considered as the most hazardous out of the mentioned equipment because of its higher heat flux. Processors consumed about 50% of total server power [19, 88]. Thus, most of the exploratory investigations found in review considered mostly heat loads and geometry of the processor.

American Society of Heating, Refrigerating and Air-Conditioning Engineers (ASHRAE) carried out the study for a limitations of heat transfer for various processors [19, 88]. The predicted values of limitations of heat transfer for various processors are shown in Table 27.1. The study predicts heat loads for a processor of high-performance computing (HPC) applications increasing up to 210–300 W [19, 88].

Table 27.1 Predictions for expected heat load of a processor by ASHRAE [19, 88]

S. No.	Component	No. of CPU's	Power (W) for year 2010	Power (W) for year 2015	Power (W) for year 2020
1	HPC processor (higher power)	1	250	300	300
2	HPC processor (lower power)	1	165	210	210
3	2S processor (general purpose)	1	140	140	140
4	4S processor (general purpose)	1	140	175	190

27.4 Electronics Cooling Solutions

The requirement of newer solutions electronics cooling for upcoming generations is squeezing constantly year by year. The requirement of a solution is mainly because of the predictions of heat fluxes in future years.

The various available electronics cooling solutions are shown in Fig. 27.1. Out of which critical review is mainly focused on air cooling and indirect liquid cooling methods.

27.4.1 Air Cooling

The air cooling method is still generally utilized and will consistently favor, over all other electronic cooling methods. Air cooling is usually achieved by a hot/cold aisle system as shown in Fig. 27.2 [28].

As air cooling requires speedily forced circulation due to its poor thermal transport properties, which approaches higher noise and vibration cut-off points. The maximum heat transfer coefficient ($150 \text{ W/m}^2 \text{ K}$, 1 W/cm^2 for $60 \text{ }^\circ\text{C}$ difference temperature) with acceptable noise levels can be achieved with a standard fan.

Because of the lack of sealing, air cooling is progressively flexible corresponding to liquid cooling methodologies [43, 91]. The extremely adaptable solution encourages the processes of installation and retrofitting [32, 85], additionally limiting the requirement of customization. Moreover, the nonexistence of liquid coolants minimizes the maintenance of a system and increases reliability [91]. These factors need to consider the highly simplified design and installation of the electronic cooling system.

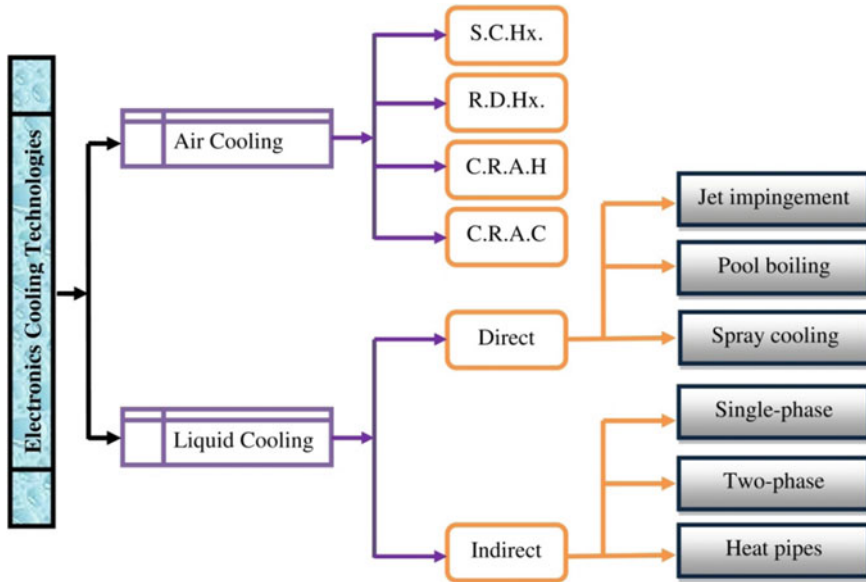


Fig. 27.1 Generalized electronics cooling solutions

27.4.1.1 Power Requirements and Heat Transfer Limitations of Air Cooling

Because of lower thermophysical characteristics of air cooling, it needs high flow rates and low temperature of coolant comparative with liquid cooling techniques; which results in increment in working costs. Temperature range of 16–25 °C and 30–45 °C can be achieved for cold aisle and hot aisle respectively [19, 34, 74, 88]. For feasible free cooling, cold aisle temperatures must be adequately high than outdoor air. This prerequisite of climate limits the cooling capacity of air cooling solutions into hotter areas. The heat exchanger (RDHx) or (SCHx) helps for reduction of power consumption in the air cooling technique [31, 36, 37]. The methodology of conveying cooling liquid towards singular racks eases the consumption of power by CRAH/CRAC fans and is evaluated to decrease working expenses up to 40% [37].

Air cooling operational properties of the heat sink on the basis of experimentation work are shown in Table 27.2. This studied a variety of domains of analysis exclusively for heat sinks. ASHRAE predicts the processor's rate of heat generation is as high as 140–190 Watts up to the year 2020 [19, 88]. The present limitations of heat transfer for air cooling are obviously not the hindering component inside the electronic cooling. In HPC, heat generation rates presently ranging from 210 to 300 W [19, 88], limitations of heat transfer don't allow further increment into densities of chip power. Limitations of heat transfer for air cooling might be increased with an increase in fin area and heat sink base, despite the fact that this is counter-productive for the industry to reduce spatial needs [32]. Limitations may likewise

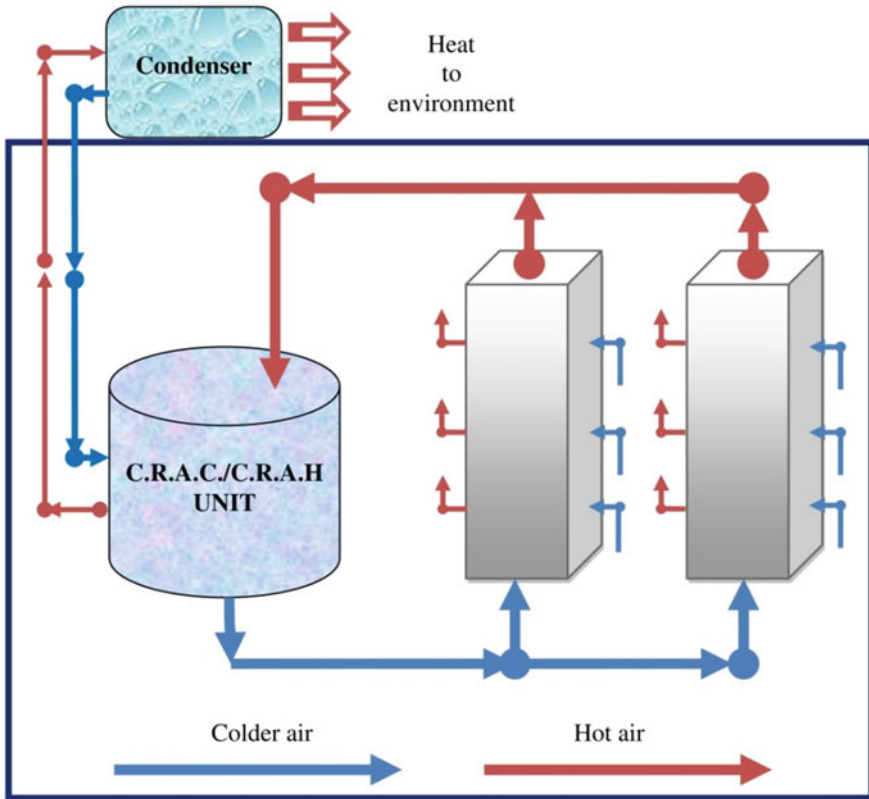


Fig. 27.2 Air cooling hot/cold aisle system

Table 27.2 Air cooling operational properties of the heat sink on the basis of experimentation work

References	q	h_{eff}	q''_{HS}	Q	A_{HS}	A_W	T_W	T_i	T_o
[83]	103	0.0463	1.62	12,000	64	2.56	70	35	42.1
[101]	110	–	1.33	7740	83	1.44	50	–	–
[40]	227	–	–	–	–	–	72	16	40.0
[99]	250	0.0417	2.50	24,000	100	4.00	90	30	38.6
[46]	300	0.0667	4.00	20,000	75	4.00	80	20	32.4

Note q—overall heat transfer rate (W); h_{eff} —($W/cm^2 \cdot K$); q''_{HS} —heat spreader heat flux (W/cm^2); Q—flow rate of air (cm^3/s); A_{HS} —heat sink base area (cm^2); A_W —heated surface area (cm^2); T_W , T_i and T_o —heated surface, inlet air and outlet air temperature ($^{\circ}C$)

be reached out by decreasing cold aisle air temperatures [48]. Working expenses in case of vapor-compression cooling increases by reducing cold aisle temperature.

Though the air cooling is mostly popular, limited studies have been performed on limitations of heat transfer. Limitations of heat transfer were recognized by the parametric investigation of fin geometry, material characteristics, and assembly configurations.

27.4.2 Indirect Liquid Cooling

This cooling process is a process of heat removal with indirect contact among a liquid/fluid heat source and coolant. This cooling technique is obtained by the replacement of conventional air-cooled heat sink by either liquid-cooled heat sinks or evaporators [34, 82, 93, 94]. The traditional indirect liquid cooling technique includes the utilization of colder plates and water-blocks. But currently, the research centered on the microchannel heat sinks and enhancement of its efficiency [5, 45].

Figure 27.3 shows the block diagram of indirect liquid-cooled DC. In this coolant distribution unit (CDU) exchange heat in form of close controlled chilled liquid from an externally cooled source towards an internally closed coolant loop which is joined thermally to electronic equipment [25].

Coolant is only supplied to processors as most of the heat generated there, whereas remaining ICT parts are air-cooled [91]. In spite of the fact that there exist scarcely any marketed arrangements that are stretched out to help liquid cooling for more server parts [25, 79].

As liquid cooling technique empowers the use of coolants through significantly predominant thermophysical characteristics than air. The liquid cooling technology is able to adequately broaden thermal hindrances and lessen the utilization of DC energy by means of permitting high temperature of the coolant and decreased flow rate of air [32, 92]. This issue can be set with speedy disengage fluidic connectors, in

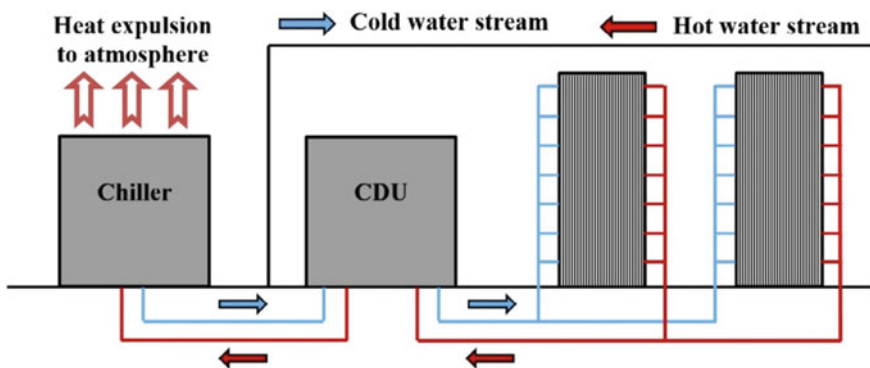


Fig. 27.3 Indirect liquid cooling system

any case, they signify additional dependability concerns because of expanding the leakage possibility [91].

27.4.2.1 Single-Phase Cooling

It is sensible heating of coolant circulation where change of phase not permitted to occurs. Water, amongst current dielectric liquids and refrigerants, is a preferable coolant because of higher boiling point and prevalent thermophysical characteristics. Though, because of the leakage danger, their uses have lower precedence and requirement in DCs industries [32]. This technique empowers the liquid cooling of different processors and improves the reliability of the server [6]. Most of the industries like Asetek [6], IBM [104, 105], and Cool IT Systems [17] have actualized this system in server level.

Table 27.3 shows the heat transfer properties of single-phase water cooling systems. These investigations have centered on chip-level thermal management by microchannel heat sinks (MCHS). The maximum heat transfer rate of (1150 W) has been gotten into a study [81] where performances were examined by utilizing MCHS. Maximum heat spreader heat fluxes (170 W/cm²) have been gotten in research [57] where diagonal fins were utilized. Overall, heat spreader heat fluxes have noticed between (2.68–170 W/cm²) that shows the considerable development comparative with air cooling.

Table 27.3 Single-phase water cooling operating properties of MCHS on the basis of experimentation work

References	q	h _{eff}	Q'' _{HS}	Q	A _{HS}	A _w	T _w	T _i	T _o	ΔP	P _{pump}
[14]	25	0.103	2.68	0.33	9.45	9.45	46	20	38	38.6	0.013
[89]	30	0.395	9.87	0.40	3.04	3.04	50	25	42.3	4.0	0.0016
[98]	36	4	100	6.40	0.36	0.36	45	20	33.6	115	0.75
[104, 105]	170	2.39	47.8	16.7	3.55	2.31	80	60	62	14	0.23
[12]	220	2.12	137	31.7	1.61	0.15	85	20	21.7	21	0.67
[80]	272	3.466	121	16.7	2.25	2.25	70	35	39	55.3	0.921
[57]	273	3.62	170	2.70	1.61	1.61	72	25	50	10	0.027
[20]	375	1.25	93.8	16.7	4	3.75	125	50	55	19.5	0.33
[78]	448	2.44	100	10.1	4.48	4.48	56	15	28	30	0.3
[56]	625	1.82	100	6.67	6.25	6.25	75	20	42	1.0	0.0067
[81]	1150	1.87	43	27	27	27	43	20	30	0.90	0.025

Note q—overall heat transfer rate (W); h_{eff}—(W/cm²·K); q''_{HS}—heat spreader heat flux (W/cm²); Q—flow rate of air (cm³/s); A_{HS}—heat sink base area (cm²); A_w—heated surface area (cm²); T_w, T_i and T_o—heated surface, inlet air and outlet air temperature (°C); ΔP—pressure drop (kPa) and P_{pump}—pumping power consumption (W)

The temperature of inlet water has ranged between 15 and 35 °C in an investigational study concerning MCHS; conversely, a noteworthy inlet temperature ranged between 45 and 60 °C has been seen in industrial usage [42, 75, 104, 105]. This expands the capability of waste heat recovery and free cooling at a higher temperature flowing air. The flow rates of water for single processor cooling have observed between 0.3 and 32 cm³/s. The basis of pressure drop measured along with different heat sinks, the power requirement for pumping has determined between 0.002 and 0.90 W per processor. The decrease into power utilization comparative with air cooling is obviously ascribed to expanded specific heat capacity and density of water [10], anyway enormous pressure drops produced along with MCHS yields considerable power requirements for pumping in specific cases [80].

27.4.2.2 Two-Phase Cooling

This type of cooling includes circling coolant latent heating; henceforth stage change of liquid-vapour is subjugated. Coolant selections usually include different dielectric liquids and refrigerants having low bubbling temperatures [84, 90]. Additional advantages of this solution incorporate decreased temperature gradients and improved rate of heat transfer [5, 45]. Significant worries with the system are identified with an unstable flow that initiates variations in temperature and pressure, inversion of flow, and few different practices which consequences in burning and superheated surfaces [45]. Two-phase cooling arrangements inside the industries are rare, a chose usage has been created with the author [23].

Table 27.4 shows the heat transfer properties of two-phase cooling systems. The greatest heat transfer rate about 2160 W has been noted by the study [77] and heat transfer qualities for flow bubbling inside graphite have been inspected. FC-72 (dielectric fluid) having 56 °C immersion temperature and none subcooling were passed by 48 cm² permeable heat sink of 85 °C temperature [1].

This examination additionally inspected the impact of changing a gap of evaporator over a permeable structure. Little gaps cause bubble restriction and development of the vapor layer on the bubble surface that fundamentally expanded the temperature of walls. Heat spreader heat flux found maximum (222 W/cm²) in the study by an author [1] where examination has been carried out on a 4 cm² microchannel heat sink using refrigerant R236fa.

In general, heat spreader heat flux values have observed (24.2–222 W/cm²) that shows an enhancement comparative with single-phase cooling.

The inlet temperature of coolant has observed in investigations about (0–63 °C) with immersion happening at temperatures between (25–63 °C). Flow rates have observed (0.66–12.2 cm³/s) and prerequisites of pumping power have been obtained per processor between the ranges (0.002–0.62 W). This demonstrates the decrease in siphoning power prerequisites comparative with water cooling that is ascribed for a latent heat transfer related to two-phase operating liquids [63].

Table 27.4 Two-phase cooling operating properties of MCHS on the basis of experimentation work

References	Coolant	q	h _{eff}	Q'' _{HS}	Q	A _{HS}	A _W	T _W	T _i	T _{sat}	ΔP	P _{pump}
[50, 51]	FC-72	250	0.721	40	2.1	6.25	6.25	85	29.5	56	5.0	0.0103
[50, 51]	FC-72	375	1.08	60	2.9	6.25	6.25	85	29.5	56	7.0	0.020
[69]	FC-72	84.9	1.72	24.2	0.663	3.5	3.5	68.1	54	56.1	—	—
[60, 61]	R134a	425	8.55	188	6.57	2.64	2.26	85	63	63	94	0.62
[76]	R134a	1080	2.05	180	12.2	6	4	110	22	25	—	—
[73]	R134a	61.9	1.96	27.5	2.07	2.25	2.25	34	20	25	—	—
[65]	R134a	1100	—	183	5.34	6	4	—	20	25	—	—
[9]	R134a	216	5.88	88.2	3.26	2.45	2.45	44.1	29.1	29.1	—	—
[65]	R236a	812	5.4	135	3.21	6	4	55	30	40	—	—
[9]	R245a	198	3.23	80.8	2.96	2.45	2.45	51	26	26	—	—
[65]	R245fa	860	—	143	2.30	6	4	—	25	40	—	—
[52]	R407C	64.7	1.85	28.75	2.20	2.25	2.25	35.5	20	25	—	—
[29]	HFE-7100	227	4.41	105.8	2.28	2.15	2.15	85	61	61	1.0	0.0023
[55]	HFE-7100	84.9	2.16	173	1.32	0.491	0.491	100	20	59.6	10	0.0132
[53, 54]	HFE-7100	98	2.5	200	1.32	0.49	0.49	80	0	60	10	0.0132

Note q—overall heat transfer rate(W); h_{eff}—(W/cm²·K); q''_{HS}- heat spreader heat flux (W/cm²); Q—flow rate of air (cm³/s); A_{HS}—heat sink base area (cm²); A_W—heated surface area (cm²); T_W, T_i and T_{sat}—heated surface, inlet air and saturation air temperature (°C); ΔP—pressure drop (kPa) and P_{pump}—pumping power consumption (W)

27.4.2.3 Heat Pipe Cooling

Heat pipes operation depends on a change of phase of operating liquid of the pipes, are capable methods for electronic system cooling, for example, PCs, laptop, and media transmission [13, 26, 27, 70]. Because of lower efficient thermal resistance and exceptionally higher viable thermal conductivity, it is a most feasible method for cooling higher heat flux creating electronic devices like CPUs.

Presently, there are numerous heat pipes industrial cooling applications and as a result of higher heat evacuation efficiency of this method has pulled in enormous enthusiasm by electronic industry which confirms the tremendous heat pipes production by industries. Mostly, heat pipes are produced monthly for CPUs, laptops, and PCs [26, 95, 96]. A Pentium processor of PCs uses the utmost volume of heat pipes for cooling [33]. Chen et al. [15], Mathew et al. [64], carried out the broad review on design, development, and investigation of smaller heat pipes in favor of electronics cooling. They additionally indicated a capability of smaller heat pipes for smaller electronic systems cooling.

As the heat pipe doesn't have moving parts therefore it is exceptionally reliable at lower maintenance cost. Heat pipes as well offer various significances like no utilization of external power, noiseless, expanded life span consequently lower working and overall expenses, improved adaptability, compact, flexible in direction, and fixed enclosure cooling thus no unfavorable impact to the atmosphere or electronic devices.

Figure 27.4 shows the different types of available heat pipes for application of electronics cooling.

The greatest advantage of heat pipe cooling is avoiding liquid leakage inside servers with the help of hermetically sealed devices [68]. Moreover, heat pipes passivity invalidates the prerequisites of chip-level pumping power whereas enhancing the reliability because of a nonappearance of moving components [68]. Xyber Technologies [100] has executed conventional heat pipe cooling in servers and replaced the server wall by finned heat sinks.

Fig. 27.4 Various types of heat pipes

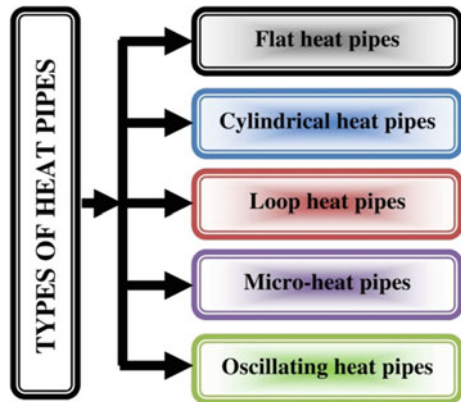


Table 27.5 Heat pipe cooling operating properties on the basis of experimentation work

References	Coolant	q	h_{eff}	q''_{HS}	C.C	Q	A_{HS}	A_W	T_W	T_i	T_o
[59]	Acetone	60	0.141	5	Air	–	12	12	52	16.5	–
[67]	Ammonia	130	0.163	8.13	Air	6040	16	16	70	20	37.94
[67]	Ammonia	230	0.288	14.38	Water	8.67	16	16	70	20	26.35
[67]	Ammonia	320	0.476	20	Water	8.67	16	16	62	20	29.83
[30]	Methanol	120	0.222	10	Air	–	12	12	65	20	–
[44]	Methanol	100	0.0463	3.7	Water	33.3	27	25	85	5	6.48
[66]	Methanol	175	0.202	12.5	Air	15,000	14	14	85	23	32.72
[97]	NF	150	0.242	12.5	Air	–	12	12	76.7	25	–
[66]	R141b	150	0.173	10.7	Air	15,000	14	14	85	23	31.3
[39]	SiO ₂ -H ₂ O	60	0.16	2.4	Air	–	25	25	60	45	–
[39]	Water	60	0.12	2.4	Air	–	25	25	70	50	–
[86]	Water	60	0.135	8.49	Air	–	7.07	6.25	85	22	–
[97]	Water	100	0.163	8.3	Air	–	12	12	75.8	25	–
[8]	Water	100	0.145	4.35	Water	38.9	23	16	85	55	55.62
[16]	Water	138	0.136	8.27	Air	–	16.62	9	85	24	–
[103]	Water	150	1.41	35.21	Air	–	4.26	4	80	55	–
[66]	Water	200	0.231	14.3	Air	15,000	10	10	85	23	34.1
[103]	Water	200	1.1	46.95	Air	–	4.26	4	65	22.5	–
[58]	Water	350	0.635	38.9	Air	22,300	9	6.25	85	23.7	36.78

Where, q—overall heat transfer rate (W); h_{eff} —(W/cm²·K); q''_{HS} —heat spreader heat flux (W/cm²); C.C—Condenser Coolant; Q—flow rate of air (cm³/s); A_{HS} —heat sink base area (cm²); A_W —heated surface area (cm²); T_W , T_i and T_o —heated surface, inlet air and outlet air temperature (°C)

Table 27.5 shows the heat transfer properties of heat pipe cooling systems. This table records the essential heat pipe coolant and medium (air or water) of heat transfer utilized for cooling of heat pipe condenser.

Maydanik, et al. acquired the largest heat transfer rate (700 W). Author has examined a compact heat pipe (copper-water loop) having 31 cm length through a 10.24 cm² flat-oval evaporator. Values heat spreader heat flux has observed between 2.4 and 68.4 W/cm² into heat pipe cooling systems. This shows a critical decrease in the limitations of heat transfer comparative with water cooling. In any case, this range of values surpasses the limitations of heat transfer for conventional air cooling and allows effectual thermal management.

27.5 Conclusions

The present review introduces the various properties of heat transfer for electronics cooling, more specifically for air cooling and indirect liquid cooling. The solutions provided by liquid cooling displayed a critical enhancement as compared with conventional air-cooling especially for the variables like limitations of heat transfer, coolant temperatures, and flow rates. This ascribed the predominant mechanisms for heat transfer as related to liquid cooling.

Air cooling limitation isn't a hindering element to thermal management as concerned with all-purpose computing. So, the execution of liquid cooling techniques ought to be encouraged by different variables like decrements of working expenses, and enhanced chip performance. Waste heat recovery is not as functional and even impractical by conventional air-cooling techniques.

The conclusions mentioned in the above paragraphs are not applicable in high-performance computing because, heat generation rate of the chip have approached air cooling limitation. In these types of situations, this variable must be assuming a bigger job while designing the processes. The current review promisingly allows effectual thermal management with proper heat spreading to higher performance processors available till the 2020 year. Subsequently, optional variables must be viewed as while choosing a perfect liquid cooling solution; which incorporates flexibility, dependability, hot-swap ability, various financial expenditures, and maintenance necessities.

References

1. Agostini, B., Revellin, R., Thome, J.R., Fabbri, M., Michel, B., Calmi, D., Kloter, U.: High heat flux flow boiling in silicon multi-microchannels—Part III: saturated critical heat flux of R236fa and two-phase pressure drops. *Int. J. Heat Mass Transf.* **51**(21–22), 5426–5442 (2008). <https://doi.org/10.1016/j.ijheatmasstransfer.2008.03.005>
2. Almoli, A., Thompson, A., Kapur, N., Summers, J., Thompson, H., Hannah, G.: Computational fluid dynamic investigation of liquid rack cooling in data centres. *Appl. Energy* **89**(1), 150–155 (2012). <https://doi.org/10.1016/j.apenergy.2011.02.003>
3. Anandan, S.S., Ramalingam, V.: Thermal management of electronics: a review of literature. *Therm. Sci.* **12**(2), 5–25 (2008). <https://doi.org/10.2298/TSCI0802005A>
4. Anthes, G.: Power Play: The Search for Energy-Efficient Chips, from https://www.computerworld.com/s/article/104017/Power_Play (2005)
5. Asadi, M., Xie, G., Sunden, B.: A review of heat transfer and pressure drop characteristics of single and two-phase microchannels. *Int. J. Heat Mass Transf.* **79**, 34–53 (2014). <https://doi.org/10.1016/j.ijheatmasstransfer.2014.07.090>
6. Asetek: 2019. <https://www.asetek.com>
7. Bar-Cohen, A.: Needs and future trends for enhanced phase change heat transfer-DARPA, PowerPoint presentation, International Workshop on Micro and Nano Structures for Phase Change Heat Transfer, Needham, MA, from <https://micronano.mit.edu/presentations/Bar-Cohen.pdf> (2013)

8. Becker, S., Vershinin, S., Sartre, V., Laurien, E., Bonjour, J., Maydanik, Y.F.: Steady state operation of a copper-water LHP with a flat-oval evaporator. *Appl. Therm. Eng.* **31**, 686–695 (2011). <https://doi.org/10.1016/j.applthermaleng.2010.02.005>
9. Bertsch, S.S., Groll, E.A., Garimella, S.V.: Effects of heat flux, mass flux, vapor quality, and saturation temperature on flow boiling heat transfer in microchannels. *Int. J. Multiph. Flow* **35**(2), 142–154 (2009). <https://doi.org/10.1016/j.ijmultiphaseflow.2008.10.004>
10. Borgnakke, C., Sonntag, R.E.: *Fundamentals of thermodynamics*, 7th edn. Wiley, New Jersey (2008)
11. Cader, T., Westra, L., Sorel, V., Marquez, A.: Liquid cooling in data centers. *ASHRAE Trans.* **115**(pt 1), 231–241 (2009)
12. Calame, J.P., Myers, R.E., Binari, S.C., Wood, F.N., Garven, M.: Experimental investigation of microchannel coolers for the high heat flux thermal management of GaN-on-SiC semiconductor devices. *Int. J. Heat Mass Transf.* **50**(23–24), 4767–4779 (2007). <https://doi.org/10.1016/j.ijheatmasstransfer.2007.03.013>
13. Chang, Y.W., Cheng, C.H., Wang, J.C., Chen, S.L.: Heat pipe for cooling of electronic equipment. *Energy Convers. Manage.* **49**(11), 3398–3404 (2008). <https://doi.org/10.1016/j.enconman.2008.05.002>
14. Chein, R., Chuang, J.: Experimental microchannel heat sink performance studies using nanofluids. *Int. J. Therm. Sci.* **46**(1), 57–66 (2007). <https://doi.org/10.1016/j.ijthermalsci.2006.03.009>
15. Chen, X., Ye, H., Fan, X., Ren, T., Zhang, G.: A review of small heat pipes for electronics. *Appl. Therm. Eng.* (2016). <https://doi.org/10.1016/j.applthermaleng.2015.11.048>
16. Choi, J., Sung, B., Kim, C., Borca-Tasciuc, D.A.: Interface engineering to enhance thermal contact conductance of evaporators in miniature loop heat pipe systems. *Appl. Therm. Eng.* **60**(1–2), 371–378 (2013). <https://doi.org/10.1016/j.applthermaleng.2013.06.060>
17. Coolit systems: 2019. <https://www.coolitsystems.com/>
18. Cushing, R., Doherty, J.: *Next generation data centres*. MSC Business Development Ltd. (2009)
19. *Datacom equipment power trends and cooling applications*, 2nd edn., American Society of Heating, Refrigerating and Air-Conditioning Engineers, Inc. (2012)
20. Dede, E.M., Liu, Y.: Experimental and numerical investigation of a multi-pass branching microchannel heat sink. *Appl. Therm. Eng.* **55**(1–2), 51–60 (2013). <https://doi.org/10.1016/j.applthermaleng.2013.02.038>
21. Dhande, H.K., Shelare, S.D., Khope, P.B.: Developing a mixed solar drier for improved postharvest handling of food grains. *Agric. Eng. Int.: CIGR J.* **22**(4), 17–24 (2020)
22. Ebrahimi, K., Jones, G.F., Fleischer, A.S.: A review of data center cooling technology, operating conditions and the corresponding low-grade waste heat recovery opportunities. *Renew. Sustain. Energy Rev.* **31**, 622–638 (2014). <https://doi.org/10.1016/j.rser.2013.12.007>
23. Ebullient: 2020. <https://www.ebullientcooling.com/product/>
24. Ellsworth, M.J., Campbell, L.A., Simons, R.E., Iyengar, M.K., Schmidt, R.R., Chu, R.C.: The evolution of water cooling for IBM large server systems: Back to the future. In: 2008 11th IEEE Intersociety Conference on Thermal and Thermomechanical Phenomena in Electronic Systems, I-THERM, pp. 266–274 (2008). <https://doi.org/10.1109/I-THERM.2008.4544279>
25. Ellsworth, M.J., Goth, G.F., Zoodsma, R.J., Arvelo, A., Campbell, L.A., Anderl, W.J.: An overview of the IBM Power 775 supercomputer water cooling system. *J. Electron. Packag., Trans. ASME* **134**(2), 1–9 (2012). <https://doi.org/10.1115/1.4006140>
26. Faghri, A.: Review and advances in heat pipe science and technology. *J. Heat Transfer* (2012). <https://doi.org/10.1115/1.4007407>
27. Faghri, A.: Heat pipes: review, opportunities and challenges. *Front. Heat Pipes* **5**(1) (2014). <https://doi.org/10.5098/fhp.5.1>
28. Fakhim, B., Behnia, M., Armfield, S.W., Srinarayana, N.: Cooling solutions in an operational data centre: a case study. *Appl. Therm. Eng.* **31**(14–15), 2279–2291 (2011). <https://doi.org/10.1016/j.applthermaleng.2011.03.025>

29. Fu, B., Lee, C., Pan, C.: The effect of aspect ratio on flow boiling heat transfer of HFE-7100 in a microchannel heat sink. *Int. J. Heat Mass Transf.* **58**(1–2), 53–61 (2013). <https://doi.org/10.1016/j.ijheatmasstransfer.2012.11.050>
30. Gai, D., Liu, Z., Liu, W., Yang, J.: Operational characteristics of miniature loop heat pipe with flat evaporator. *Heat Mass Transf.* **46**(2), 267–275 (2009). <https://doi.org/10.1007/s00231-009-0563-0>
31. Gao, T., David, M., Geer, J., Schmidt, R., Sammakia, B.: Experimental and numerical dynamic investigation of an energy efficient liquid cooled chiller-less data center test facility. *Energy Build.* **91**, 83–96 (2015). <https://doi.org/10.1016/j.enbuild.2015.01.028>
32. Garimella, S.V., Yeh, L.T., Persoons, T.: Thermal management challenges in telecommunication systems and data centers. *IEEE Trans. Comp., Packag. Manuf. Technol.* **2**(8), 1307–1316 (2012). <https://doi.org/10.1109/TCPMT.2012.2185797>
33. Garner, S.D.: Heat pipes for electronics cooling applications. *Electron Cool* **2**(3) (1996)
34. Geng, H.: *Data center handbook*. Wiley, New Jersey (2015)
35. Gess, J., Dreher, T., Bhavnani, S., Johnson, W.: Effect of flow guide integration on the thermal performance of high performance liquid cooled immersion server modules. In: ASME 2015 International Technical Conference and Exhibition on Packaging and Integration of Electronic and Photonic Microsystems, InterPACK 2015, collocated with the ASME 2015 13th International Conference on Nanochannels, Microchannels, and Minichannels, 1, 1–10 (2015). <https://doi.org/10.1115/IPACK2015-48771>
36. Goth, G.F.: An overview of the IBM power 775 supercomputer water cooling system. *J. Electron. Packag.* **134**, 020906 (2012)
37. Grimshaw, J., McSweeney, M., Novotny, S., Gagnon, M.: Data center rack level cooling utilizing water-cooled, passive rear door heat exchangers (RDHX) as a cost effective alternative to CRAH air cooling, (December), 10 p (2011)
38. Gu, J.: Health assessment and prognostics for electronics products: an alternative to traditional reliability prediction methods, from <https://www.electronics-cooling.com/2009/05/health-assessment-and-prognostics-of-electronic-products-an-alternative-to-traditional-reliability-prediction-methods/> (2009)
39. Gunnasegaran, P., Abdullah, M.Z., Shuaib, N.H.: Influence of nanofluid on heat transfer in a loop heat pipe. *Int. Commun. Heat Mass Transfer* **47**, 82–91 (2013). <https://doi.org/10.1016/j.icheatmasstransfer.2013.07.003>
40. Ham, S.W., Kim, M.H., Choi, B.N., Jeong, J.W.: Simplified server model to simulate data center cooling energy consumption. *Energy Build.* **86**, 328–339 (2015). <https://doi.org/10.1016/j.enbuild.2014.10.058>
41. ITRS: 2009 ITRS, from <https://www.itrs.net/Links/2009ITRS/Home2009.htm> (2011)
42. Iyengar, M., David, M., Parida, P., Kamath, V., Kochuparambil, B., Graybill, D., Chainer, T.: Server liquid cooling with chiller-less data center design to enable significant energy savings. In: Annual IEEE Semiconductor Thermal Measurement and Management Symposium, vol. 1, pp. 212–223 (2012). <https://doi.org/10.1109/STHERM.2012.6188851>
43. Jawalekar, S.B., Shelare, S.D.: Development and performance analysis of low cost combined harvester for rabi crops. *Agric. Eng. Int.: CIGR J.* **22**(1), 197–201 (2020)
44. Joung, W., Gam, K., Park, K., Ma, S., Lee, J.: Transient responses of the flat evaporator loop heat pipe. *Int. J. Heat Mass Transf.* **57**(1), 131–141 (2013). <https://doi.org/10.1016/j.ijheatmasstransfer.2012.10.025>
45. Kadam, S.T., Kumar, R.: Twenty first century cooling solution: microchannel heat sinks. *Int. J. Therm. Sci.* **85**, 73–92 (2014). <https://doi.org/10.1016/j.ijthermalsci.2014.06.013>
46. Katoh, T., Xu, G., Vogel, M., Novotny, S.: New attempt of forced-air cooling for high heat-flux applications. *Thermo Mech. Phenomena Electron. Syst.-Proc. Intersoc. Conf.* **2**, 34–39 (2004). <https://doi.org/10.1109/itherm.2004.1318249>
47. Kheirabadi, A.C., Groulx, D.: Cooling of server electronics: a design review of existing technology. *Appl. Therm. Eng.* **105**, 62–638 (2016). <https://doi.org/10.1016/j.applthermaleng.2016.03.056>

48. Kovar, J.F.: Power, environmental concerns driving data center design, 2012, <https://www.crn.com/news/data-center/232600187/power-environmental-concerns-driving-data-center-design.htm>. Accessed 20 Jan 2020
49. Kumbhare, H., Shelare, S.: Innovative advancement in drone technology for water sample collections—a review. *Int. J. Sci. Technol. Res.* **9**(03), 7266–7269 (2020)
50. Law, M., Lee, P.S.: A comparative study of experimental flow boiling heat transfer and pressure characteristics in straight- and oblique-finned microchannels. *Int. J. Heat Mass Transf.* **85**, 797–810 (2015). <https://doi.org/10.1016/j.ijheatmasstransfer.2015.01.137>
51. Law, M., Lee, P.S., Balasubramanian, K.: Experimental investigation of flow boiling heat transfer in novel oblique-finned microchannels. *Int. J. Heat Mass Transf.* **76**, 419–431 (2014). <https://doi.org/10.1016/j.ijheatmasstransfer.2014.04.045>
52. Leão, H.L.S.L., do Nascimento, F.J., Ribatski, G.: Flow boiling heat transfer of R407C in a microchannels based heat spreader. *Exp. Therm. Fluid Sci.* **59**, 140–151 (2014). <https://doi.org/10.1016/j.expthermflusci.2014.03.014>
53. Lee, J., Mudawar, I.: Fluid flow and heat transfer characteristics of low temperature two-phase micro-channel heat sinks—Part 1: experimental methods and flow visualization results. *Int. J. Heat Mass Transf.* **51**(17–18), 4315–4326 (2008). <https://doi.org/10.1016/j.ijheatmasstransfer.2008.02.012>
54. Lee, J., Mudawar, I.: Fluid flow and heat transfer characteristics of low temperature two-phase micro-channel heat sinks—Part 2. Subcooled boiling pressure drop and heat transfer. *Int. J. Heat Mass Transf.* **51**(17–18), 4327–4341 (2008b). <https://doi.org/10.1016/j.ijheatmasstransfer.2008.02.013>
55. Lee, J., Mudawar, I.: Critical heat flux for subcooled flow boiling in micro-channel heat sinks. *Int. J. Heat Mass Transf.* **52**(13–14), 3341–3352 (2009). <https://doi.org/10.1016/j.ijheatmasstransfer.2008.12.019>
56. Lee, Y.J., Lee, P.S., Chou, S.K.: Experimental investigation of silicon-based oblique finned microchannel heat sinks. In: 2010 14th International Heat Transfer Conference, IHTC 14, vol. 6, pp. 283–291 (2010). <https://doi.org/10.1115/IHTC14-23413>
57. Lee, Y.J., Singh, P.K., Lee, P.S.: Fluid flow and heat transfer investigations on enhanced microchannel heat sink using oblique fins with parametric study. *Int. J. Heat Mass Transf.* **81**, 325–336 (2015). <https://doi.org/10.1016/j.ijheatmasstransfer.2014.10.018>
58. Li, J., Wang, D., Peterson, G.P.: Experimental studies on a high performance compact loop heat pipe with a square flat evaporator. *Appl. Therm. Eng.* **30**(6–7), 741–752 (2010). <https://doi.org/10.1016/j.applthermaleng.2009.12.004>
59. Liu, Z., Gai, D., Li, H., Liu, W., Yang, J., Liu, M.: Investigation of impact of different working fluids on the operational characteristics of miniature LHP with flat evaporator. *Appl. Therm. Eng.* **31**(16), 3387–3392 (2011). <https://doi.org/10.1016/j.applthermaleng.2011.06.023>
60. Madhour, Y., Olivier, J., Costa-Patry, E., Paredes, S., Michel, B., Thome, J.R.: Flow boiling of R134a in a multi-microchannel heat sink with hotspot heaters for energy-efficient microelectronic CPU cooling applications. *IEEE Trans. Comp., Packag. Manuf. Technol.* **1**(6), 873–883 (2011). <https://doi.org/10.1109/TCPMT.2011.2123895>
61. Madhour, Y., Olivier, J., Costa-Patry, E., Paredes, S., Michel, B., Thome, J.R.: Two-phase flow boiling of R134a in a multi-microchannel heat sink for microprocessor cooling. In: 16th International Workshop on Thermal Investigations of ICs and Systems (THERMINIC) (2010), pp. 1–6
62. Mali, P.K., Sakhale, C.N., Shelare, S.D.: A literature review on design and development of maize thresher. *Int. J. Pure Appl. Res. Eng. Technol.* **3**(9), 9–14 (2015)
63. Marcinichen, J.B., Olivier, J.A., Thome, J.R.: On-chip two-phase cooling of datacenters: cooling system and energy recovery evaluation. *Appl. Therm. Eng.* **41**, 36–51 (2012). <https://doi.org/10.1016/j.applthermaleng.2011.12.008>
64. Mathew, J.J., Sakhale, C.N., Shelare, S.D.: Latest trends in sheet metal components and its processes—a literature review. In: Algorithms for Intelligent Systems, pp. 565–574 (2020). https://doi.org/10.1007/978-981-15-0222-4_54

65. Mauro, A.W., Thome, J.R., Toto, D., Vanoli, G.P.: Saturated critical heat flux in a multi-microchannel heat sink fed by a split flow system. *Exp. Thermal Fluid Sci.* **34**(1), 81–92 (2010). <https://doi.org/10.1016/j.expthermflusci.2009.09.005>
66. Maydanik, Y.F., Dmitrin, V.I., Pastukhov, V.G.: Compact cooler for electronics on the basis of a pulsating heat pipe. *Appl. Therm. Eng.* **29**(17–18), 3511–3517 (2009). <https://doi.org/10.1016/j.applthermaleng.2009.06.005>
67. Maydanik, Y.F., Vershinin, S.V., Pastukhov, V.G., Fried, S.S.: Loop heat pipes for cooling systems of servers. *IEEE Trans. Compon. Packag. Technol.* **33**(2), 416–423 (2010). <https://doi.org/10.1109/TCAPT.2009.2035514>
68. McGlen, R.J., Jachuck, R., Lin, S.: Integrated thermal management techniques for high power electronic devices. *Appl. Therm. Eng.* **24**, 1143–1156 (2004). <https://doi.org/10.1016/j.applthermaleng.2003.12.029>
69. Megahed, A.: Local flow boiling heat transfer characteristics in silicon microchannel heat sinks using liquid crystal thermography. *Int. J. Multiph. Flow* **39**, 55–65 (2012). <https://doi.org/10.1016/j.ijmultiphaseflow.2011.09.003>
70. Mochizuki, M., Nguyen, T., Mashiko, K., Saito, Y., Nguyen, T., Wuttijumnong, V.: A review of heat pipe application including new opportunities. *Front Heat Pipe* **2**, 013001 (2011)
71. Mowade, S., Waghmare, S., Shelare, S., Tembhurkar, C.: Mathematical model for convective heat transfer coefficient during solar drying process of green herbs. In: *Computing in Engineering and Technology*, pp. 867–877 (2019). https://doi.org/10.1007/978-981-32-9515-5_81
72. Nakayama, W.: Heat in computers: applied heat transfer in information technology. *J. Heat Transf.* **136**(1) (2014)
73. Nascimento, F.J., Leão, H.L.S.L., Ribatski, G.: An experimental study on flow boiling heat transfer of R134a in a microchannel-based heat sink. *Exp. Thermal Fluid Sci.* **45**, 117–127 (2013). <https://doi.org/10.1016/j.expthermflusci.2012.10.014>
74. Oró, E., Depoorter, V., Garcia, A., Salom, J.: Energy efficiency and renewable energy integration in data centres. Strategies and modelling review. *Renew. Sustain. Energy Rev.* **42**, 429–445 (2015). <https://doi.org/10.1016/j.rser.2014.10.035>
75. Parida, P.R., David, M., Iyengar, M., Schultz, M., Gaynes, M., Kamath, V., Chainer, T.: Experimental investigation of water cooled server microprocessors and memory devices in an energy efficient chiller-less data center. In: *Annual IEEE Semiconductor Thermal Measurement and Management Symposium*, pp. 224–231 (2012). <https://doi.org/10.1109/STHERM.2012.6188852>
76. Park, J.E., Thome, J.R.: Critical heat flux in multi-microchannel copper elements with low pressure refrigerants. *Int. J. Heat Mass Transf.* **53**(1–3), 110–122 (2010). <https://doi.org/10.1016/j.ijheatmasstransfer.2009.09.047>
77. Pranoto, I., Leong, K.C.: An experimental study of flow boiling heat transfer from porous foam structures in a channel. *Appl. Therm. Eng.* **70**(1), 100–114 (2014). <https://doi.org/10.1016/j.applthermaleng.2014.04.027>
78. Qu, W., Mudawar, I.: Experimental and numerical study of pressure drop and heat transfer in a single-phase micro-channel heat sink. *Int. J. Heat Mass Transf.* **45**(12), 2549–2565 (2002). [https://doi.org/10.1016/S0017-9310\(01\)00337-4](https://doi.org/10.1016/S0017-9310(01)00337-4)
79. Rackcdu d2c liquid cooling, asetek; 2017. <https://www.asetek.com/data-center/oem-data-center-coolers/rackcdu-d2c/>
80. Reyes, M., Arias, J.R., Velazquez, A., Vega, J.M.: Experimental study of heat transfer and pressure drop in micro-channel based heat sinks with tip clearance. *Appl. Therm. Eng.* **31**(5), 887–893 (2011). <https://doi.org/10.1016/j.applthermaleng.2010.11.011>
81. Rimbault, B., Nguyen, C.T., Galanis, N.: Experimental investigation of CuO-water nanofluid flow and heat transfer inside a microchannel heat sink. *Int. J. Therm. Sci.* **84**, 275–292 (2014). <https://doi.org/10.1016/j.ijthermalsci.2014.05.025>
82. Sahu, P., Shelare, S., Sakhale, C.: Smart cities waste management and disposal system by smart system: a review. *Int. J. Sci. Technol. Res.* **9**(03), 4467–4470 (2020)

83. Saini, M., Webb, R.L.: Heat rejection limits of air cooled plane fin heat sinks for computer cooling. In: Inter Society Conference on Thermal and Thermomechanical Phenomena in Electronic Systems, IThERM, 1–8 Jan 2002 (2002). <https://doi.org/10.1109/ITHERM.2002.1012431>
84. Shelare, S.D., Thakare, P.S., Handa, C.C.: Computer aided modelling and position analysis of crank and slotted lever mechanism. *Int. J. Mech. Eng. Prod. Eng. Res. Dev.* **2**(2), 47–52 (2012)
85. Shelare, S.D., Kumar, R., Khope, P.B.: Formulation of a mathematical model for quantity of deshelled nut in charoli nut deshelling machine. In: *Advances in Metrology and Measurement of Engineering Surfaces*, pp. 89–97 (2020). https://doi.org/10.1007/978-981-15-5151-2_9
86. Singh, R., Akbarzadeh, A., Dixon, C., Mochizuki, M., Riehl, R.R.: Miniature loop heat pipe with flat evaporator for cooling computer CPU. *IEEE Trans. Compon. Packag. Technol.* **30**(1), 42–49 (2007). <https://doi.org/10.1109/TCAPT.2007.892066>
87. Tembhurkar, C., Kataria, R., Ambade, S., Verma, J.: Transient Analysis of GTA-Welded Austenitic and Ferritic Stainless Steel. In: *Advances in Materials Processing*, pp. 59–65 (2020). https://doi.org/10.1007/978-981-15-4748-5_6
88. *Thermal guidelines for data processing environments*, 3rd edn. American Society of Heating, Refrigerating and Air-Conditioning Engineers, Inc., 2012
89. Tran, N., Zhang, C., Dang, T., Teng, J.T.: Numerical and experimental studies on pressure drop and performance index of an aluminum microchannel heat sink. In: *Proceedings of 2012 International Symposium on Computer, Consumer and Control, IS3C 2012*, pp. 252–257 (2012). <https://doi.org/10.1109/IS3C.2012.71>
90. Tuma, P.E.: Fluoroketone C2F5C(O)CF(CF3)2 as a heat transfer fluid for passive and pumped 2-phase applications. In: *Annual IEEE Semiconductor Thermal Measurement and Management Symposium*, (4), pp. 173–179 (2008). <https://doi.org/10.1109/STHERM.2008.4509386>
91. Tuma, P.E.: The merits of open bath immersion cooling of datacom equipment. In: *Annual IEEE Semiconductor Thermal Measurement and Management Symposium*, pp. 123–131 (2010). <https://doi.org/10.1109/STHERM.2010.5444305>
92. Waghmare, S., Sirsat, P., Sakhale, C., Shelare, S., Awatade, S.: A case study on improvement of plant layout for effective production. *Int. J. Mech. Prod. Eng. Res. Dev.* **7**(5), 155–160 (2017). <https://doi.org/10.24247/ijmperdoct201716>
93. Waghmare, S.N., Sakhale, C.N., Tembhurkar, C.K., Shelare, S.D.: Assessment of average resistive torque for human-powered stirrup making process. In: *Computing in Engineering and Technology*, pp. 845–853 (2019). https://doi.org/10.1007/978-981-32-9515-5_79
94. Waghmare, S., Mungle, N., Tembhurkar, C., Shelare, S., Sirsat, P., Pathare, N.: Design and analysis of power screw for manhole cover lifter. *Int. J. Recent Technol. Eng.* **8**(2), 2782–2786 (2019). <https://doi.org/10.35940/ijrte.B2628.078219>
95. Waghmare, S.N., Shelare, S.D., Tembhurkar, C.K., Jawalekar, S.B.: Development of a model for the number of bends during stirrup making process. In: *Advances in Metrology and Measurement of Engineering Surfaces*, pp. 69–78 (2020). https://doi.org/10.1007/978-981-15-5151-2_7
96. Waghmare, S., Shelare, S., Sirsat, P., Pathare, N., Awatade, S.: Development of an innovative multi-operational furnace. *Int. J. Sci. Technol. Res.* **9**(04), 885–889 (2020)
97. Wan, Z., Deng, J., Li, B., Xu, Y., Wang, X., Tang, Y.: Thermal performance of a miniature loop heat pipe using water-copper nanofluid. *Appl. Therm. Eng.* **78**, 712–719 (2015). <https://doi.org/10.1016/j.applthermaleng.2014.11.010>
98. Wang, G., Niu, D., Xie, F., Wang, Y., Zhao, X., Ding, G.: Experimental and numerical investigation of a microchannel heat sink (MCHS) with micro-scale ribs and grooves for chip cooling. *Appl. Therm. Eng.* **85**, 61–70 (2015). <https://doi.org/10.1016/j.applthermaleng.2015.04.009>
99. Xu, G., Guenin, B., Vogel, M.: Extension of air cooling for high power processors. *Thermomech. Phenom. Electron. Syst. Proc. Intersoc. Conf.* **1**(858), 186–193 (2004). <https://doi.org/10.1109/itherm.2004.1319172>
100. Xyber Technologies, <https://www.xybertechologies.com/>

101. Zhang, H.Y., Pinjala, D., Teo, P.S.: Thermal management of high power dissipation electronic packages: from air cooling to liquid cooling. In: Proceedings of 5th Electronics Packaging Technology Conference, EPTC 2003, (11), 620–625 (2003). <https://doi.org/10.1109/EPTC.2003.1271593>
102. Zhang, H., Shao, S., Xu, H., Zou, H., Tian, C.: Free cooling of data centers: a review. *Renew. Sustain. Energy Rev.* **35**, 171–182 (2014). <https://doi.org/10.1016/j.rser.2014.04.017>
103. Zimbeck, W., Slavik, G., Cennamo, J., Kang, S., Yun, J., Krociczek, E.: Loop heat pipe technology for cooling computer servers. In: 2008 11th IEEE Intersociety Conference on Thermal and Thermomechanical Phenomena in Electronic Systems, I-THERM, pp. 19–25 (2008). <https://doi.org/10.1109/ITHERM.2008.4544248>
104. Zimmermann, S., Meijer, I., Tiwari, M.K., Paredes, S., Michel, B., Poulikakos, D.: Aquasar: a hot water cooled data center with direct energy reuse. *Energy* **43**(1), 237–245 (2012). <https://doi.org/10.1016/j.energy.2012.04.037>
105. Zimmermann, S., Tiwari, M.K., Meijer, I., Paredes, S., Michel, B., Poulikakos, D.: Hot water cooled electronics: exergy analysis and waste heat reuse feasibility. *Int. J. Heat Mass Transf.* **55**(23–24), 6391–6399 (2012). <https://doi.org/10.1016/j.ijheatmasstransfer.2012.06.027>

Chapter 28

Numerical Optimization of ZnMgO/CIGS Based Heterojunction Solar Cells via Change of Buffer and BSF Layer



Raushan Kumar, Akhilesh Kumar, and Kumar Saurabh

Abstract In this work, the scientific community has presented acceptable physical properties of ZnMgO semiconductor which is among the buffer materials that later used for better consideration solar cell fabrication. In our effort, AFROS-HET version 2.5 one dimensional simulator is applied to the optimization of ZnMgO buffer and ZnSe BSFC (Back Surface Field Contact) layer-based solar cells. The buffer and BSFC layer are introduced in the conventional experimental device Grid AR/ITO/ZnO/CdS/CIGS/Mo/Na glass solar structure to improve the performance of the electrical parameters of the device and which is used in the field of renewable energy. We have introduced ZnMgO material in the portion of the buffer layer for improvement of efficiency from 13.8 to 37.39%. Several physical parameters optimization (i.e. doping density, thickness and EQE) of the buffer, absorber and BSFC layer has been done. The performance of the electrical parameters of the proposed structure is achieved ($V_{oc} = 898.1$ mV, $J_{sc} = 52.94$ mA/cm², FF = 78.64 and $\eta = 37.39\%$) keeping the fixed value of doping density and thickness of ZnMgO about $N_d = 4 \times 10^{19}$ cm⁻³ and $W = 50$ nm. These results are optimized of AM1.5G irradiance ($1\text{sun} = 100$ mW/cm²) and the temperature was kept constant at 300 K.

Keywords Heterojunction · BSF · AFROS-HET · CIGS · ZnMgO

28.1 Introduction

Power utilization of the world increases day by day for the reason behind increases in energy consumption and a decrease in conventional fossil fuel demand. Renewable energy is a sustainable, non-pollute, high-efficient and cost-effective alternative source of the world. Solar energy consumption is one of the most active parts of

R. Kumar · A. Kumar

Department of Electronics and Communication Engineering, National Institute of Technology, Jamshedpur, India

K. Saurabh (✉)

Department of Electronics and Communication Engineering, Dr. B. R. Ambedkar National Institute of Technology, Jalandhar, India

power utilization among available renewable energy sources [1]. The solar energy consist of outstanding power efficiency given by silicon solar cell technology has the upper hand, but it is too costly, and it has limited source [2]. Thin film-based solar cell (TFBSC) technologies such as CdTe, CdMnTe, CZTS, CZTSe, CZTSSe, etc. [3] have materialized as a potential replacement and are carefully accessible with balanced performance. In respect to heterojunction solar cells, Cu(In,Ga)Se₂ (CIGS) as the most favorable materials for high-efficiency TFBSC paid attention [4]. CIGS is a direct bandgap semiconductor consist of chalcopyrite compounds with superior optical properties, long term stability, high absorption coefficient and high radiation acceptance [5]. Moreover, the chalcopyrite semiconductor's bandgap can be concocted by the partial substitution of indium with gallium.

Several researchers has reported in the field of absorber layer CIGS material with a combination of different type of buffer layer materials. The primary purpose of the use of CIGS materials is due to its lower band energy and high absorption of a photon. In 1994 oh take has been designed ZnSe/CIGS buffer and absorber layer solar cell, and he has 11.6% record efficiency [6]. After that, Minemoto has design 16.2% efficient solar cells with the use of the ZnMgO buffer layer 2000 [7, 8], designed 18.1% efficiency with used of ZnS material. In regards the combination of several buffer layer materials to increase the efficiency, these materials are CdS (experimental), In₂S₃, ZnOS, CdZnS, ZnMgO, ZnSo and CdS based solar cells achieved the efficiency of 13.8%, 16.4%, 18.5%, 19.52%, 23.35%, 23.82% and 36.11% [9–15]. While the CdS/CIGS heterojunction solar cell has less expansive but poor efficiency (η %), J_{sc} and V_{oc} which is not better than ZnMgO/CIGS based solar cell.

The decreasing of electrical parameters of CdS buffer layer solar cells is due to lower energy bandgap and less absorption of a photon. In our proposed structure to optimize the cell model with the use of the Mg-doped Mg_xZn_{1-x}O buffer layer for altered doping concentration 'x', which is better than CdS and ZnSo buffer layer solar cells [15]. The bandgap of 3.20–3.9 eV for MgZnO (can be changed for the different values of x (0–40%). In this paper, all the electrical parameters find with a 40% doping concentration of Mg. In the 40% [16, 17] of the doping concentration of Mg, the energy bandgap has founded (3.9 eV) [15]. In this paper, only two things, we have modified buffer and BSF layer materials for conventional experimental structure (Grid AR/ITO/ZnO/CdS/CIGS/Mo/Na glass) solar cell [9]. The newly modified structure (SLG/Al/i-ZnO/ZnMgO/CIGS/MoSe2/Al) solar cell has been optimizations several physical parameters that are (doping density, thickness and EQE) of buffer, absorber and BSF layer. The performance of the electrical parameters of the proposed structure achieved $V_{oc} = 898.1$ mV, $J_{sc} = 52.94$ mA/cm², FF = 78.64 and $\eta = 37.39\%$ keeping the fixed value of doping density and thickness of ZnMgO about $N_d = 4 \times 10^{19}$ cm⁻³ and W = 50 nm.

28.2 Design and Numerical Optimization of ZnMgO/CIGS Solar Cell Structure

28.2.1 Structure of Proposed ZnMgO/CIGS Heterojunction Cell

The design modelling of new arrangements has been explained into two phases. The first phase of the design modeling of conventional experimental structure, which is a design by CdS based buffer layer (Grid AR/ITO/ZnO/CdS/CIGS/Mo/NA Glass) shown in Fig. 28.1b. The fabrication of CIGS based solar cells, CdS is the most common buffer layer material. But, the use of CdS is antagonistic because of poisonousness and lower energy band gap about 2.4 eV.

In the second phase, we have elaborate on the new structure, which is substituted by buffer and BSF layer with 40% Mg-doped ZnO (SLG/Al/i-ZnO/ZnMgO/CIGS/MoSe₂/Al) solar cell. The region behind the change of buffer layer material, we have non toxicity and wide energy gap 3.9 eV. The new modeling consists of the four-layer window, buffer, absorber and BSF layer as shown in Fig. 28.1a. All the layers are deliberate with the numerical value of optical and electronics parameters which is given to the input of the software simulator. Table 28.1 gives a summary of the material properties of all layers [15, 18–21]. The value of the refractive index and the extraction constant of ZnMgO is 2.12 and 0.17 [16]. The wide bandgap of ZnMgO falls in the range of 3.20–3.9 eV, depending upon the

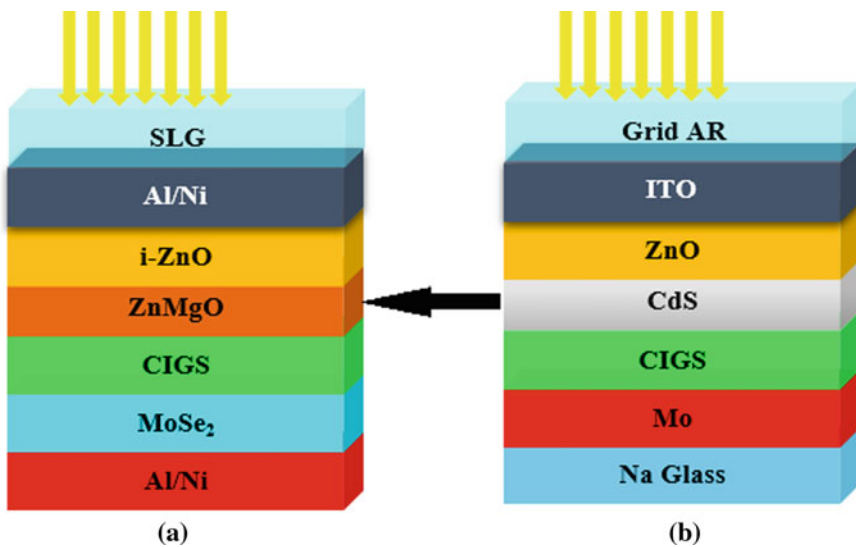


Fig. 28.1 Modelling architecture of **a** new structure (ZnMgO) and **b** conventional structure (CdS) based solar cell

concentration of Mg. In this structure, the tuning of donor density of the buffer layer in between 1.5×10^{19} and $1 \times 10^{20} \text{ cm}^{-3}$ with 50 nm thickness, respectively. The highest performance we have observed $V_{oc} = 898.1 \text{ mV}$, $J_{sc} = 52.94 \text{ mA/cm}^2$, $FF = 78.64$ and $\eta = 37.39\%$ with $N_d = 4 \times 10^{19} \text{ cm}^{-3}$ and $W = 50 \text{ nm}$.

28.2.2 Simulation Platform

Numerical analysis of new ZnMgO buffer layer solar cells is done by use of hetero-junction solar cells known as Automat (AFORS-HET) with version 2.5 [22]. The one-dimensional numerical analysis simulator tool built-up by Helmholtz-Zentrum Berlin fur Materialien und Energie institute of berlin, Germany [23]. AFORS-HET is a dominant device simulation software and its simulation of AC as well as DC measurement of electrical and optical parameters of the solar cells. AFORS-HET simulator gives several electrical and optical results that are short circuit current density (J_{sc}), open-circuit voltage (V_{oc}), fill factor (FF) photo conversion efficiency (PCE), external quantum efficiency (EQE) and spectral response (SP) by using of visible sunlight. This tool has another feature to reduce individual defects introduced in each layer of the bulk materials. These defects in the intrinsic level initiated and it has closed to the mid bandgap, which helps in further compensation. The overall discontinuity parameters of the band neglected. The work function, series and shunt resistance magnitudes are work of 300 K with default set temperature. In our device, we have used AM (air mass) 1.5G irradiance ($1\text{sun} = 100 \text{ mW/cm}^2$) for all simulation reported in this proposed work.

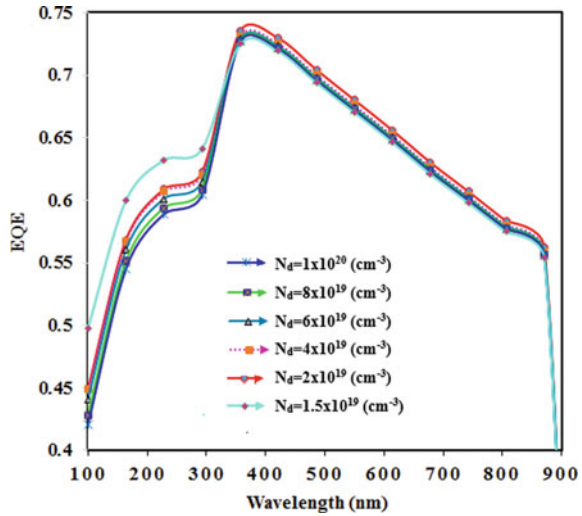
28.3 Results Discussion

In this section we have found several physical electrical parameters of proposed structure i.e. EQE, spectral response, J_{sc} , V_{oc} , FF and efficiency of the solar cell. All the parameters optimized for the tuning of donor and acceptor density of buffer and absorber of ZnMgO/CIGS based solar cell.

28.3.1 Effects of Quantum Efficiency (QE) and J-V Characteristics with the Change of the Donor Doping Concentration of ZnMgO

It is observed in the given Fig. 28.2 the deviation of EQE due to the variation of donor doping concentration from 1.5×10^{19} to $1 \times 10^{20} \text{ cm}^{-3}$ of the ZnMgO buffer layer. When the value of donor density less than $1.5 \times 10^{19} \text{ cm}^{-3}$, the cell performance

Fig. 28.2 Deviation of EQE for different donor density of the ZnMgO buffer layer



of EQE is lower. When the N_d of the buffer layer increased, about $2 \times 10^{19} \text{ cm}^{-3}$ performance of EQE will decrease. Due to maximum number of photons absorbed by the buffer cell and minimum number of photons reaching to the CIGS absorber layer. The highest performance of wavelength versus EQE characteristics we have found that the donor density about $2 \times 10^{19} \text{ cm}^{-3}$ with 400 nm wavelength. The variation of donor density of the ZnMgO layer. The doping crucial parameters of the buffer layer in Fig. 28.3 the J-V characteristics for the different value of N_d concentration of ZnMgO buffer layer with 50 nm thickness of buffer layer and 250 μm of the absorber layer and all other numerical parameters are unaffected. However, the value of donor density is lower ($<10^{18} \text{ cm}^{-3}$) values of electrical parameters like V_{oc} , J_{sc} , FF and η are too small. That's why values of donor density taken from the greater than ($>10^{19} \text{ cm}^{-3}$) if the increases in doping concentration of the ZnMgO buffer layer would

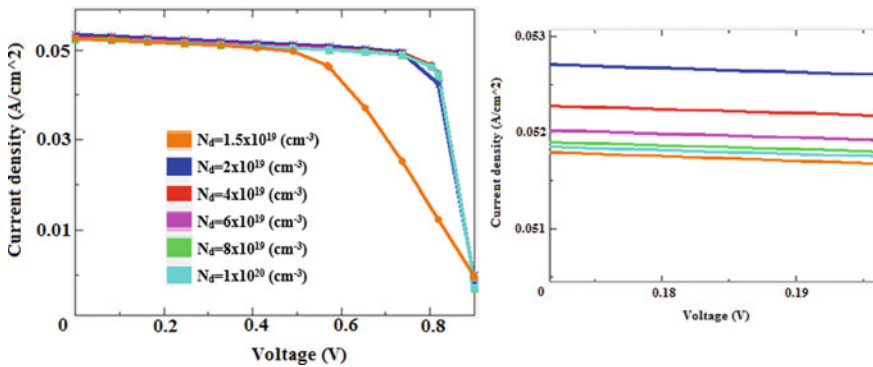


Fig. 28.3 J-V characteristic with different ZnMgO buffer layer donor density

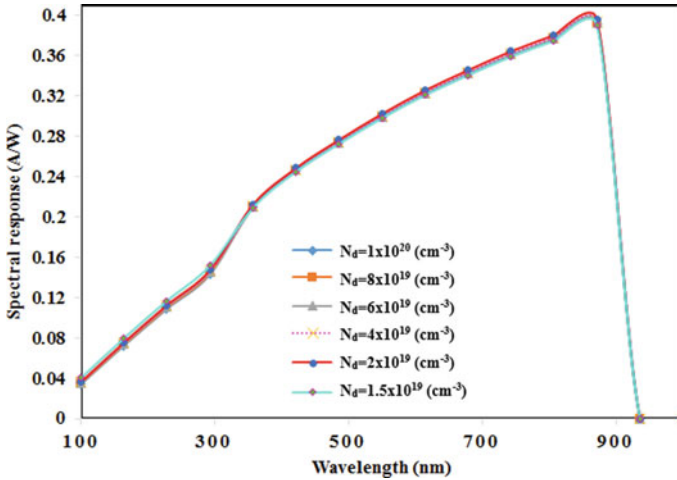


Fig. 28.4 Deviation of spectral response for different donor density of the ZnMgO buffer layer

increase the electric field in the heterojunction. That’s why the collection of photo-generated electron–hole pairs grew at the end of the junction. However, the donor density of the buffer layer is above $4 \times 10^{19} \text{ cm}^{-3}$, J_{sc} will decrease. It seems that the carrier recombination in bulk increases when the N_d is higher. Thus the preferable donor density of the ZnMgO buffer layer is fixed $4 \times 10^{19} \text{ cm}^{-3}$.

It observed in the given Fig. 28.4 wavelength verse spectral response of the ZnMgO based solar cell. The variation of donor density of buffer layer about 1.5×10^{19} to $1 \times 10^{20} \text{ cm}^{-3}$ the highest, the peak we have observed at $2 \times 10^{19} \text{ cm}^{-3}$ with 800 nm wavelength.

28.3.2 Effects of Quantum Efficiency and J-V Characteristics with Changed of the Acceptor Doping Concentration of CIGS

Impacts of acceptor density of the absorber layer by changing the N_a of the CIGS absorber layer from 1×10^{15} to $1 \times 10^{17} \text{ cm}^{-3}$ and set 250 μm thickness and another input parameter of the simulator kept constant, which shown in Table 28.1. The enhancement of cell performance analysed by the AFROS-HET simulation tool. Figure 28.5 shows the effects of short circuit current density with change of acceptor density. It can be clearly absorb that all the cell parameter increases with CIGS acceptor density.

The performance of EQE shown in Fig. 28.6 of the CIGS absorber layer based photovoltaic cell with a variable acceptor concentration of the absorber layer. If the thickness of the CIGS layer decreases, more and more photons can collect in the

Table 28.1 Numerical analysis of electronics parameters used in different materials

Electrical parameters	i-ZnO	ZnMgO	CIGS	MoSe ₂
Thickness (nm)	60	50	250 μm	10
E _g (eV)	3.3	3.9	1.4	1.1
χ (eV)	4.3	3.67	4.2	4.14
ε _r	9	10.5	10	8.6
N _C (cm ⁻³)	2.2 × 10 ¹⁸	2.5 × 10 ¹⁹	2 × 10 ¹⁸	5.66 × 10 ¹⁷
N _V (cm ⁻³)	1.8 × 10 ¹⁹	4.2 × 10 ¹⁹	1.5 × 10 ¹⁹	2.41 × 10 ¹⁸
V _e (cm ² s ⁻¹)	2.4 × 10 ⁷	3 × 10 ⁶	3.9 × 10 ⁷	4.13 × 10 ⁷
V _h (cm ² s ⁻¹)	1.3 × 10 ⁷	1.5 × 10 ⁶	1.4 × 10 ⁷	2.55 × 10 ⁷
μ _e (cm ² V ⁻¹ s ⁻¹)	100	50	400	30
μ _h (cm ² V ⁻¹ s ⁻¹)	20	10	25	10
N _d (cm ⁻³)	1 × 10 ²⁰	4 × 10 ¹⁹ (variable)	0	0
N _a (cm ⁻³)	0	0	5 × 10 ¹⁶ (variable)	1.2 × 10 ¹⁶
Auger coefficient of electron (cm ⁶ s ⁻¹)	1.12 × 10 ¹³	2.8 × 10 ⁻³⁴	2.4 × 10 ⁻³⁰	0
Auger coefficient of hole (cm ⁶ s ⁻¹)	1.12 × 10 ¹³	1.5 × 10 ⁻³⁴	1.1 × 10 ⁻³⁰	1.2 × 10 ¹³
Band to band recombination coefficient (cm ³ s ⁻¹)	1.2 × 10 ⁻¹²	2 × 10 ⁻¹¹	1.1 × 10 ⁻¹⁰	1.2 × 10 ¹³
σ _e (cm ²)	1 × 10 ⁻¹⁵	3 × 10 ⁻¹⁴	1 × 10 ⁻¹⁵	0
σ _h (cm ²)	1 × 10 ⁻¹³	3 × 10 ⁻¹⁵	1 × 10 ⁻¹³	0
N _t (cm ⁻³)	7 × 10 ¹⁶	5.6 × 10 ¹⁸	3.12 × 10 ¹³	0

Fig. 28.5 J-V characteristic with different CIGS absorber layer acceptor density

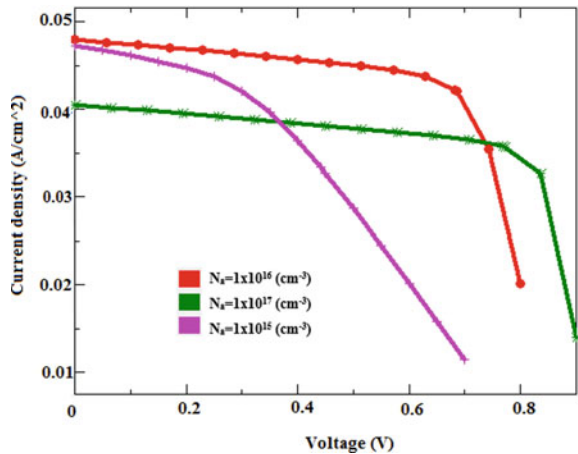
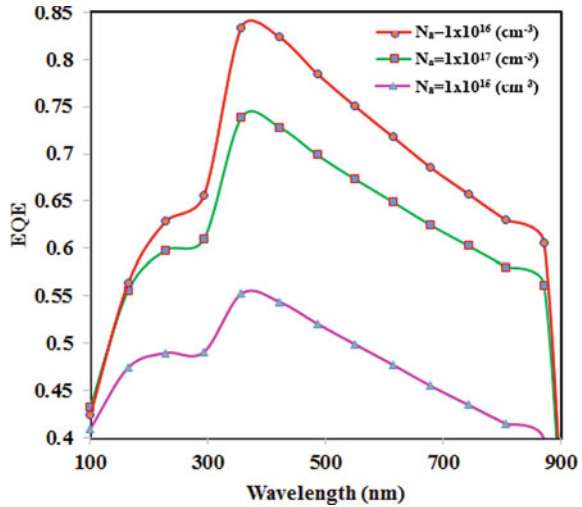


Fig. 28.6 Deviation of EQE for different acceptor density of the CIGS absorber layer



absorber layer. That is why more and more electron-hole pair generation and meeting of the longer wavelength photons can be absorbed in the portions of heterojunction and finally, efficiency will increase. However, when the thickness of the CIGS layer decreases below 250 μm , the cell performance cannot be enhanced appropriately. It has been seen that the electron-hole pairs fashioned from the junction and most of the photons combine at a longer wavelength before reaching the depletion region.

28.3.3 Change of Electrical Parameter (J_{sc} , V_{oc} , FF , η) with Changes of N_d and N_a of ZnMgO and CIGS Layer

The doping concentration of the an essential parameter of the ZnMgO buffer layer based solar cell for the analysis of electrical parameters of the device. In Table 28.2 shows the changes of parameters due to changes in donor density of about 1.5×10^{19} to 1×10^{20} cm^{-3} . The highest value of electrical parameters, we observed at 4×10^{19}

Table 28.2 Performance of electrical parameters with changes of donor density

Electrical parameters	$N_d = 1.5 \times 10^{19}$	$N_d = 2 \times 10^{19}$	$N_d = 4 \times 10^{19}$	$N_d = 6 \times 10^{19}$	$N_d = 8 \times 10^{19}$	$N_d = 1 \times 10^{20}$
V_{OC} (mV)	898.1	898.1	898.1	898.1	898.1	898.1
J_{SC} (mA/cm 2)	52.55	53.4	52.94	52.68	52.56	52.51
FF (%)	55.94	75.54	78.64	78.76	78.79	78.81
H (%)	26.4	36.22	37.39	37.26	37.19	37.16

Table 28.3 Performance of electrical parameters with changes of acceptor density

Electrical parameters	$N_a = 1 \times 10^{15}$	$N_a = 1 \times 10^{16}$	$N_a = 5 \times 10^{16}$	$N_a = 1 \times 10^{17}$
V_{OC} (mV)	858.5	860.5	898.1	921.2
J_{SC} (mA/cm ²)	47.28	47.97	52.94	40.51
FF (%)	36.01	69.44	78.64	74.98
H (%)	14.62	28.66	37.39	27.98

cm⁻³ of the donor density of the absorber layer. Table 28.3 shows that the variation of electrical parameters due to changes in acceptors density of CIGS absorber layer about $N_a = 1 \times 10^{15}$ to 1×10^{17} cm⁻³. The better performance of V_{oc} , J_{sc} , FF and % η absorb $N_a = 5 \times 10^{16}$ cm⁻³ and all other parameters kept constant, as display in Table 28.1.

28.3.4 Performance of CdS/CIGS, ZnSo/CIGS and ZnMgO/CIGS Based Solar Cells

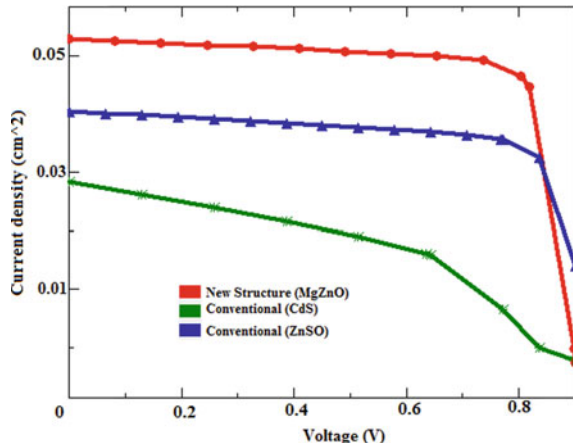
Numerical optimizations of the ZnMgO/CIGS buffer and absorber layer solar cell. The thickness of the ZnMgO/CIGS layers is fixed to 50 nm and 250 μm individually. The donor density of the ZnMgO layer and acceptor density of the absorber layer is fixed of 4×10^{19} and 5×10^{16} cm⁻³, respectively. Other parameters of the device kept constant, as display in Table 28.1.

After simulation of the photovoltaic conversion efficiencies for CdS, ZnSo and new ZnMgO layer are about 13.8, 23.82 and 37.93% separately, which shown in Table 28.4. The short circuit current density for J-V characteristics for CdS, ZnSo and new ZnMgO buffer layer, found 28.4, 40.163 and 56.82 mA/cm² respectively shown in Fig. 28.7. The given table has clearly shown that the performance of ZnMgO buffer layer based solar cell is better than other buffer layer materials.

Table 28.4 Comparison ZnMgO/CIGS buffer and absorber layer based hetrojunction solar cell

Electrical parameters	CdS/CIGS, based solar cell [9]	ZnSo/CIGS, based solar cell [14]	New MgZnO/CIGS/ZnSe, based solar cell
V_{oc} (mV)	670	707.5	916.3
J_{sc} (mA/cm ²)	28.4	40.163	56.82
FF (%)	72.4	83.832	72.85
η (%)	13.8	23.82	37.93

Fig. 28.7 Comparison of J-V characteristic conventional CdS, ZnSo, and new ZnMgO buffer layer based solar cell



28.4 Conclusion

The CdS-free buffer layer, ZnMgO can be apply into the CIGS photovoltaic cell. In this article, a comprehensive mathematical simulation of CIGS absorber layer solar cell with ZnMgO buffer layer, whose 40% deposited concentration is investigated by AFROS-HET software. The effects of the ZnMgO buffer layer, donor concentration, acceptor concentration and thickness of the proposed solar cell presentation is considered. The appropriate doping density of ZnMgO, CIGS and ZnSe₂ about 4×10^{19} , 5×10^{16} and 1.2×10^{16} cm⁻³ separately. In respect of the entire doping density of materials, we have found that the conversion efficiency is 37.93% with $J_{sc} = 56.82$ mA/cm², FF = 72.85 and $V_{oc} = 916.3$ mV. The numerical investigation of enhanced ZnMgO buffer layer based solar cells is done to improve power conversion efficiency, EQE and spectral response with the change of donor density and thickness.

References

1. Mesquita, I., Andrade, L., Mendes, A.: *Renew. Sust. Energy Rev.* **82**, 2471–2489 (2018)
2. Chander, S., Dhaka, M.S.: *Exploration of CdMnTe thin-film solar cells. Solar Energy* **183**(December 2018), 544–550 (2019)
3. Mishra, S., Bhargava, K., Deb, D.: *Numerical simulation of potential induced degradation (PID) in different thin-film solar cells using SCAPS-1D. Solar Energy* (2019)
4. Sharbati, S., Gharibshahian, I., Orouji, A.A.: *Designing of Al_xGa_{1-x}As/CIGS tandem solar cells by the analytical model. Sol. Energy* **188**(February), 1–9 (2019)
5. Mezher, M., Garris, R., Mansfield, L.M., Horsley, K., Weinhardt, L., Duncan, D.A., et al.: *Electronic structure of the Zn(O, S)/Cu(In, Ga)Se₂ thin-film solar cell interface. Prog. Photovoltaics Res. Appl.* **24**, 1142–1148 (2016)

6. Ohtake, Y., Kushiya, K., Yamada, A., Konagai, M.: Development of ZnO/ZnSe/CuIn_{1-x}Ga_xSe₂ thin-film solar cells with bandgap of 1.3 to 1.5 eV. In: Proceedings of the 24th IEEE Photovoltaic Specialist Conference, vol. 1, Waikoloa, HI, pp. 218–221 (1994)
7. Minemoto, T., Takakura, H., Hamakawa, Y., Hashimoto, Y., Nishiwaki, S., Nigami, T.: Highly efficient Cd-free Cu(In,Ga)Se₂ solar cells using novel window layer of (Zn, Mg)O films. In: Proceedings of the 28th European Photovoltaic Solar Energy Conference, Paris, vol. 1, pp. 686–689 (2000)
8. Nakada, T., Mizutani, M.: 18% efficiency Cd-Free Cu(In,Ga)Se₂ thin-film solar cells. *Jpn. J. Appl. Phys. Part 2 Lett.* **41**, L165–L167 (2002)
9. Eeles, A., Arnou, P., Bowers, J.W., Walls, J.M., Whitelegg, S., Kirkham, P., Allen, C., Stubbs, S., Liu, Z., Masala, O., Newman, C., Pickett, N.: High-efficiency CIGS solar cell. *Nanoparticle Solut.-Process.* **8**(1), 288–292 (2018)
10. Hariskos, D., Spiering, S., Powalla, M.: Buffer layers in Cu(In, Ga)Se₂ solar cells and modules. *Thin Solid Films* **480**, 99–109 (2005)
11. Zimmermann, U., Ruth, M., Edoff, M.: Cadmium-free CIGS minimodules with ALD-grown Zn (O, S)-based buffer layers. In: Proceedings of the 21st European Photovoltaic Solar Energy Conference, Dresden, pp. 1831–1834 (2006)
12. Bhattacharya, R.N., Contreras, M.A., Egaas, B., Noufi, R.N., Kanevce, A., Sites, J.R.: High-efficiency thin-film CuIn_{1-x}Ga_xSe₂ photovoltaic cells using a Cd_{1-x}Zn_xS buffer layer. *Appl. Phys. Lett.* **89**, 253503–253505 (2006)
13. Nakamura, M., Yamaguchi, K., Kimoto, Y., Yasaki, Y., Kato, T., Sugimoto, H.: Cd-Free Cu(In,Ga)(Se,S)₂ thin-film solar cell with a record efficiency of 23.35%. *IEEE J. Photovoltaic's* **9**(6), 1863–1867 (2019)
14. Alqahtani, S.M., Baloch, A.A.B., Ahmed, S.S., Alharbi, F.H.: Dilute oxygen alloys of ZnS as a promising toxic-free buffer layer for Cu(In, Ga)Se₂ thin-film solar cells. *IEEE Trans. Electron Devices* **67**(4), 1–8 (2020)
15. Muchahary, D., Maity, S.: High-efficiency thin-film ZnMgO/ZnO solar cell simulation approach: temperature dependency, BSF and efficient small-signal analysis. *Superlattices Microstruct.* **109**, 209–216 (2017)
16. Othman, Z.J., Matoussi, A.: Morphological and optical studies of zinc oxide doped MgO. *J. Alloy. Compd.* **671**, 366–371 (2016)
17. Rouchdi, M., Salmani, E., Fares, B., Hassanain, N., Mzard, A.: Synthesis and characteristics of Mg-doped ZnO thin films: experimental and ab-initio study. *Results Phys.* **7**, 620–627 (2017)
18. Jackson, P., Wuerz, R., Hariskos, D., Lotter, E., Witte, W., Powalla, M.: Effects of heavy alkali elements in Cu(In, Ga)Se₂ solar cells with efficiencies up to 22.6%. *Phys. Status Solidi R* **10**, 583–586 (2016)
19. Bauer, A., Sharbati, S., Powalla, M.: A systematic survey of suitable buffer and high resistive window layer materials in CuIn_{1-x}Ga_xSe₂ solar cells by numerical simulations. *Sol. Energy Mater. Sol. Cells* **165**, 119–127 (2017)
20. Lee, S., Price, K.J., Saucedo, E., Giraldo, S.: Engineering of the effective back-contact barrier of CZTSe: Nanoscale Ge solar cells—MoSe₂ defects implication. *Sol. Energy* **194**(October), 114–120 (2019)
21. Paul, S., Swartz, C., Sohal, S., Grice, C., Bista, S.S., Li, D.B., Yan, Y., Holtz, M., Li, J.V.: Buffer/absorber interface recombination reduction and improvement of back-contact barrier height in CdTe solar cells. *Thin Solid Films* **685**(June), 385–392 (2019)
22. Stangl, R., Kriegel, M., Schmidt, M.: AFORS-HET, version 2.2, a numerical computer program for simulation of heterojunction solar cells and measurements. In: Conference Record of the 2006 IEEE 4th World Conference on Photovoltaic Energy Conversion, WCPEC-4, vol. 2, pp. 1350–1353 (2006)
23. Froitzheim, A., Stangl, R., Elstner, L., Kriegel, M., Fuhs, W.: AFORS-HET: a computer program for the simulation of heterojunction solar cells to be distributed for public use. In: Proceedings of the 3rd World Conference on Photovoltaic Energy Conversion, A (6), pp. 279–282 (2003)

Chapter 29

Additive Manufacturing of Large Size Parts Through Retrofitment of Three-Axes CNC Machining Centre



Sagar Kailas Gawali, Narendra Kumar, and Prashant Kumar Jain

Abstract The size of the additive manufactured parts limits their use in prototyping and small functional applications. Additive Manufacturing (AM) systems with large build volume are relatively costly as compared to small ones. However, the use of existing three-axis CNC machining centres could provide an alternative for large-size parts fabrication at a minimal cost. Therefore, the present paper investigates the possibilities for the additive manufacturing of large-size parts using retrofitted three-axis CNC machining centre. A CNC-assisted extrusion deposition based AM system has been used. The setup consists of a material processing tool (MPT) and large-size build platform. Initial experiments have been conducted to check the feasibility of the developed setup for large-size parts. Large parts with different cross-sections were fabricated by processing ABS material in pellet form. Moreover, characterization was carried out to analyse the quality of fabricated parts. The observed results show that developed setup has potential to fabricates large-size parts in future.

Keywords Additive manufacturing · Retrofitment · ABS pellets · 3D printing · Large-size parts · Hybrid process · Big area additive manufacturing · BAAM

29.1 Introduction

With the advent of modern technologies, designing the products have become much more convenient. A huge number of CAD tools are available in the market which makes a design process better all in all, and the designers are investigating much more with design and development of different products than ever before. This revolution in Information Technology (IT) enabled design-manufacturing has also been accompanied by a subsequent demand for flexible manufacturing processes. Additive

S. K. Gawali · P. K. Jain

Mechanical Engineering Discipline, PDPM Indian Institute of Information Technology, Design and Manufacturing, Jabalpur 482005, MP, India

N. Kumar (✉)

Department of Industrial and Production Engineering, Dr B R Ambedkar National Institute of Technology, Jalandhar 144011, Punjab, India

e-mail: kumarn@nitj.ac.in

Manufacturing (AM) is based on the concept of IT-enabled design-manufacturing technology which has been accepted by technologists and designers across the world.

Additive Manufacturing (AM) is a process that fabricates 3D objects by deposition of material in the layer-by-layer method, unlike subtractive manufacturing. The part fabrication capabilities of AM with any complexity offers the significant saving of cost and materials, unlike time-consuming conventional manufacturing processes like machining, casting, forming, etc. AM process works as a rapid and flexible manufacturing process. As per ASTM F42 standard, AM has been classified into seven classes based on different working principles as material extrusion, vat photopolymerization, direct energy deposition, binder jetting, powder bed fusion, material jetting, sheet lamination, etc. (Fig. 29.1).

Among these working principles, material extrusion process has become most used due to its design simplicity and low cost. Fused Filament Fabrication (FFF) is one of the processes in which material in the form of filament is processed through extruder based on material extrusion principle to fabricate parts. The processed material in semi-molten state extrudes through nozzle and deposit on moving build platform in a layer-by-layer manner and built the part as shown in Fig. 29.2b. Nozzle extrudes material in a predefined toolpath in the X–Y plane and deposits the layer to

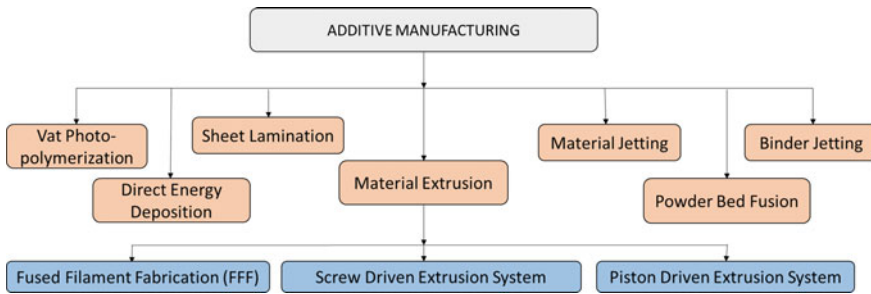


Fig. 29.1 Categorization of AM

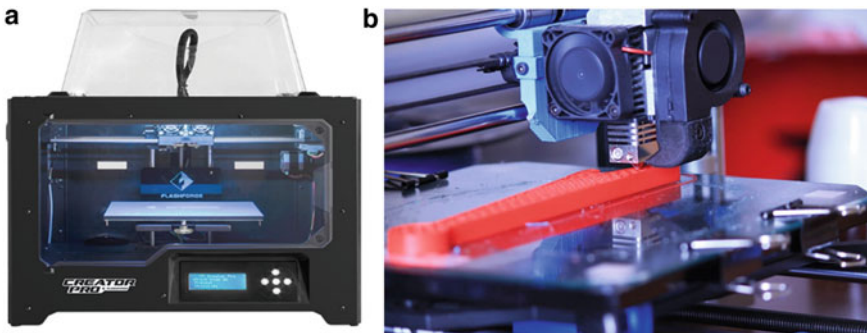


Fig. 29.2 a Flashforge 3D printer (Source <https://www.flashforge.com>). b Small size part on FFF (Source <https://www.sculpteo.com>)

build the base for the parts. After the deposition of first layer, build platform moves downward by the value of layer thickness for deposition of subsequent layer over the previously deposited layer and the process continues until the complete part was fabricated. In FFF process, most commonly used thermoplastic polymer material are ABS, Polyethylene (PE), and Polylactic acid (PLA), etc. FFF process mostly used for fabrication of parts among other AM processes because of simplicity in processing, minimum material wastage and easy material handling. Although, FFF process has various advantages but, there are certain limitations associated with this process which restrict its application domain [1–3]. Currently, part fabrication with small size is one of them which limits its use only for rapid prototyping (RP) and some end-use functional applications. The part size can be enlarged by adding large size build platform underneath of the extruder. Consequently, bigger gantry system would be required to build the parts with large-size on the large build platform.

Since the last five decades, manufacturing industries have used the CNC machining centre to fabricate the parts of metal with high precision. In these industries, large-size of CNC machining centre is used to serve the purpose which has larger gantry system as compare to existing FFF machines. In industries, the gantry system of the existing CNC machining centre could assist in the additive manufacturing of parts with large-size at a nominal cost. To achieve this goal, a material deposition tool could be developed compatible to CNC machining centre. This tool would be attached or detached with CNC machining centre similar to milling cutter. Moreover, a large build platform can also be designed and developed which can be kept on machining workspace.

Therefore, the present paper aims to perform additive manufacturing of large-size parts by developing a material deposition system compatible to CNC machining centre. The developed system is made up of three components: three-axis CNC machining centre, Material Processing Tool (MPT), heated large-size build platform. Three-axes CNC machining centre is used as a gantry system with a positional accuracy of 1 μm . MPT is attached to the spindle of machining centre for extruding material, while the heated build platform is placed on the machining workspace to utilize complete workspace. The method involves an approach of the material extrusion process and then building the 3D parts through the use of an MPT on the three-axes CNC machining centre. Thus, the development of the new system presents a major hope for the implementation of low-cost, large-size product development technique in manufacturing industries.

29.2 Literature Review

Many researchers have explored the fabrication of large-size parts through additive manufacturing by developing indigenous experimental setups. Wang et al. developed the Fused Pellet Modeling (FPM) system using a big size robotic arm for the fabrication of the large-size part. Different shapes of filament were investigated to minimize the formation of the voids in fabricated parts using multiphysics software.

Moreover, deformation was recorded within the part with an increase in size [4]. Liu et al. developed the double-stage-screw extruder to fabricate large-size part of composite material prepared using Acrylonitrile Butadiene Styrene (ABS) and 10 wt% of Glass Fibers (GF) (Fig. 29.3). The effect of screw speed and pressure were studied on the melt flow rate, print speed and layer thickness. Also, surface finish and bonding strength were examined under the variation in spacing between deposited roads [5].

Nieto et al. developed a pellet based AM process in which the functional prototypes with a volume of 2000 mm³ were fabricated using PLA and ABS materials for the use in the naval industry. Thermomechanical deformation and behaviour were studied. Based on observations, weight was reduced by 64.4 and 55.5% for PLA and ABS prototypes respectively [6]. Felsch et al. have presented a study in which a combination of industrial robots was employed with additive manufacturing technologies for enabling the fabrication of complex and large parts [7]. Jun et al. developed a setup to fabricate large-size thin-walled parts using modified FDM process. An infrared laser was installed on the existing FDM machine to preheat the surface just before the deposition of material. Due to the preheating of surface, enhancement in the mechanical properties was observed [8]. Vijay et al. developed a direct ink writing based AM system using an industrial six-axis robot. Large-scale objects were fabricated using natural bio-composite materials. Improvement in tensile strength with minimum shrinkage was the main highlight of the study [9].

Apart from academia, the industries have also shown their interest in the additive manufacturing of large parts for the use in some functional applications. Cincinnati incorporation developed a Big Area Additive Manufacturing (BAAM) machine in collaboration with oak ridge national laboratory. It offers the material extrusion and deposition via screw extrusion principle. An open environment gantry system of unbounded size was utilized to fabricate large parts. In comparison to conventional FDM machine, part fabrication with large volume was offered by BAAM. The developed setup of BAAM had capabilities of fabricating ten times large volume parts than that of FDM [10]. Similarly, Thermwood company was collaborated with oak ridge national laboratory to develop a Large Size Additive Manufacturing (LSAM). A build platform of large size of 2540 × 254 × 508 mm³ was developed for fabricating parts like a boat hull, concrete mould etc.

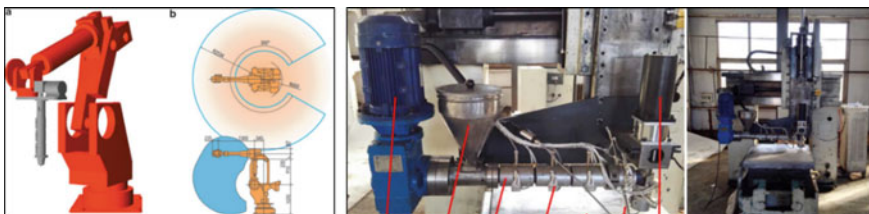


Fig. 29.3 a Big size robotic arm. b Double-stage-screw extruder

29.3 Methodology

Additive manufacturing of large-size parts requires not only the material processing unit but also require the large-size build platform. This has been achieved by developing a Material Processing Tool (MPT) and a large-size build platform for material processing and deposition respectively.

MPT works on the screw-driven material extrusion-based principle to process the pellet form of material. In this method, the material is processed through screw rotation. The required rotation to screw is provided by three-axis CNC machining centre. Apart from providing screw rotation, the CNC machining centre also offers the necessary movements to the tool for material deposition in X, Y and Z directions. Firstly, the CAD model of the part is prepared in 'Solidworks' software which is exported in Standard Tessellation Language (STL) file format. This STL file is further used for pre-processing purpose through toolpath generation software. Since current study explores the use of 3-axes CNC machining centre, the commercially available Computer-Aided Manufacturing (CAM) software can not generate a required toolpath for material deposition as they are intended to generate code for machining purpose only. Therefore, an in-house developed software has been used in the current study to fulfil above requirements related to toolpath generation. Full details about this software can be found elsewhere [11, 12]. The tasks such as slicing and toolpath generation are performed using the aforementioned software. The file containing generated toolpath is then fed into CNC machining centre (Fig. 29.4).

29.4 Fabrication of Additive Manufacturing Large-Size Parts (AMLSP)

29.4.1 *Material Processing Tool (MPT)*

Material Processing Tool (MPT) is used for extruding material in continuous and uniform manner. Part quality may be affected greatly by the performance of MPT. In the current study, the modified version of a deposition tool is used as MPT which was earlier developed by Kumar et al. to fabricate flexible parts of EVA (Ethylene Vinyl Acetate) material. More details about MPT can be found elsewhere [13]. In this version, assembly of hopper, barrel, and nozzle was modified to fabricate large-size parts comparatively at a faster rate. The different diameter of nozzles were taken to perform the current study. 2.5 and 3 mm diameter nozzles were considered initially for performing preliminary experiments. Material in the viscous/semi-molten form was extruded from these nozzles in the form of continuous extrudates which is deposited on the developed build platform to fabricate large-size parts.

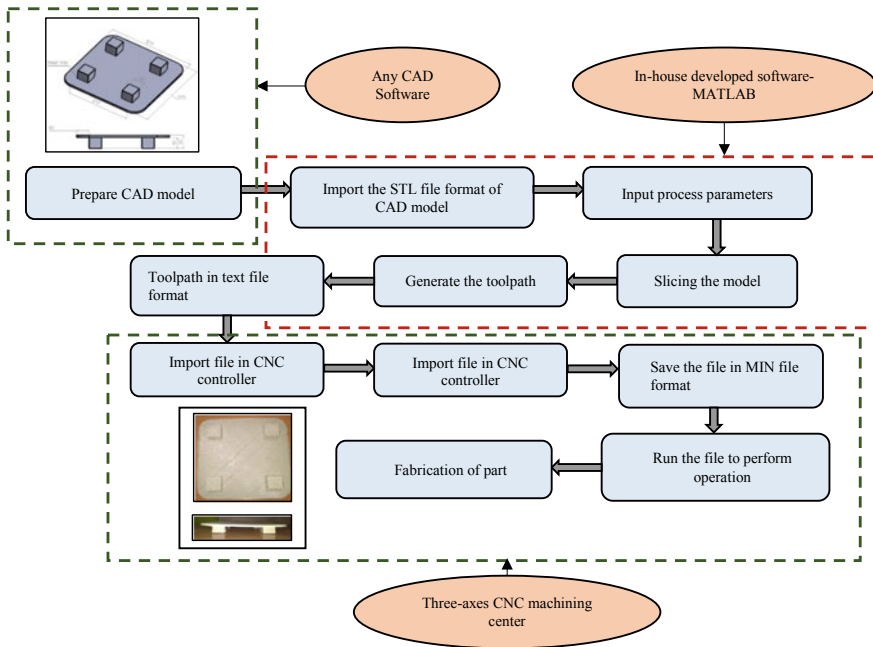


Fig. 29.4 Process flowchart of CNC-assisted extrusion deposition based AM system

29.4.2 Large-Size Build Platform

The build platform plays an important role during part fabrication as the material is deposited onto it in prespecified manner. It is eminent that warpage may occur within the fabricated part as a result of induced thermal stresses. When the surface area of part increases with an increase in the size of part, may lead to rapid transfer of heat which results in warpage. As a result of warpage, the part may be failed as lowermost layers of the part may get curled and peeled off from the build platform. Build platform provides the required temperature to the part during the fabrication process to avoid failure because of warpage. Build platform allows the fabricated part to stay warm during the fabrication and may prevent any damage to part tempted due to uneven heat transfer. Moreover, the build platform is helpful to stick the first layer of part strongly on its surface [14–17].

In the current study, large-size build platform has been developed. Heating elements are provided to preheat the build platform surface at the appropriate temperature for avoiding any possible warpage problem. The developed platform consists of a 5 mm thick aluminium plate, a 230 W AC operated silicon pad heater (AC supply), PID (Proportional-Integral-Derivative) temperature controller as the main elements. Moreover, the type-k thermocouple is also attached to monitor and maintain the given temperature value. Similar to the commercial 3D printer build plate, threaded bolts with adjustable nuts has been provided to fix the developed platform

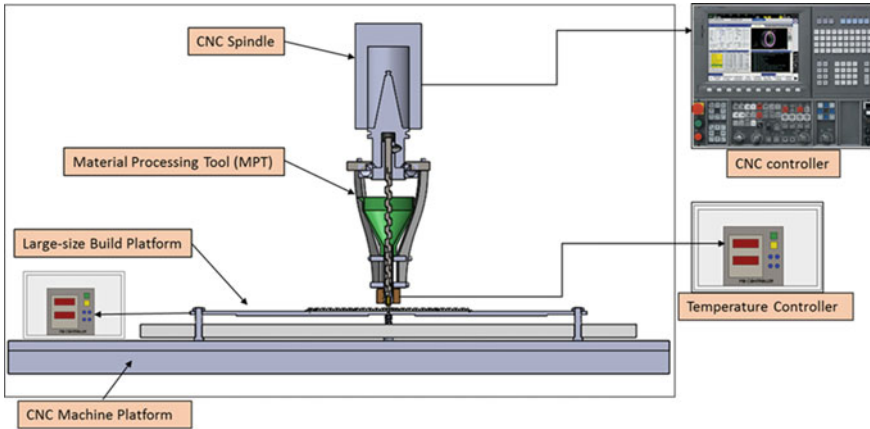


Fig. 29.5 Proposed experimental setup

on CNC machining centre bed to adjust the gap between the nozzle and build platform [18]. The developed build platform has been placed on the CNC machining centre bed with the help of jigs and fixtures. The CNC machining centre used in the current study has a maximum travel range of 750, 450 and 400 mm in X-, Y- and Z-axis respectively. Because of design constraints of developed platform, part of size 600 mm × 450 mm × 400 mm can be fabricated. Schematic diagram of the proposed experimental setup consists of a material processing unit and build platform is shown in Fig. 29.5.

29.5 Feasibility Testing, Part Fabrication and Characterization

Acrylonitrile Butadiene Styrene (ABS-M204) is used as a raw material in form of pellets because of ease in availability at a cheap rate. The robust rheological behaviour of ABS material provides extrusion at a continuous rate which may help in fabricating robust parts. Moreover, ABS material has been recognized as the standard material in additive manufacturing, that's why the ABS material is selected in the current study. The properties of ABS considered in current research work is shown in Table 29.1 (Fig. 29.6).

Figure 29.7 shown in-below is a developed experimental set-up on a three-axis CNC machining centre that consists of MPT and build platform.

For fabrication of the large-size parts, the nozzle of diameter 2.5 mm was used in the present study. To fabricate the part in the initial studies, process parameters is been chosen based on the literature study as MPT temperature (220 °C), material deposition speed (700 mm/min), screw speed (60 RPM), build platform temperature

Table 29.1 Properties of ABS material

Properties	ASTM test method	Test conditions	Units	Value
Melt flow index	ISO 1133	220 °C/10 kg	gms/10 min	35
Vicat softening temperature	D 1525	Cond. B-50 N	°C	97
Co-efficient of linear thermal expansion	D 696	23–55 °C	10E-4/°C	0.7–1.0
Rockwell hardness	D 785	23 °C	R-scale	103
Tensile strength at yield	D 638	50 mm/min	kg/cm ²	500
Tensile modulus	D 638	50 mm/min	kg/cm ²	27,000
Flexural strength	D 790	5 mm/min	kg/cm ²	750

Fig. 29.6 ABS material pellet form

(110 °C). Preliminary experiments have been conducted using these process parameters and carried out a feasibility study of the developed system by fabricating some primitive shapes of large-size. Some primitive shapes is been presented along with their dimensions in Fig. 29.8.

Figure 29.9 shows that parts with smooth and curvy edges successfully fabricated using developed setup. Also, internal contour features in the fabricated parts were shows the capability of setup. The fabricated parts have been characterized to analyze the structure and quality of parts visually. Various issues were encountered in fabricated parts which are to be discussed in the next section.

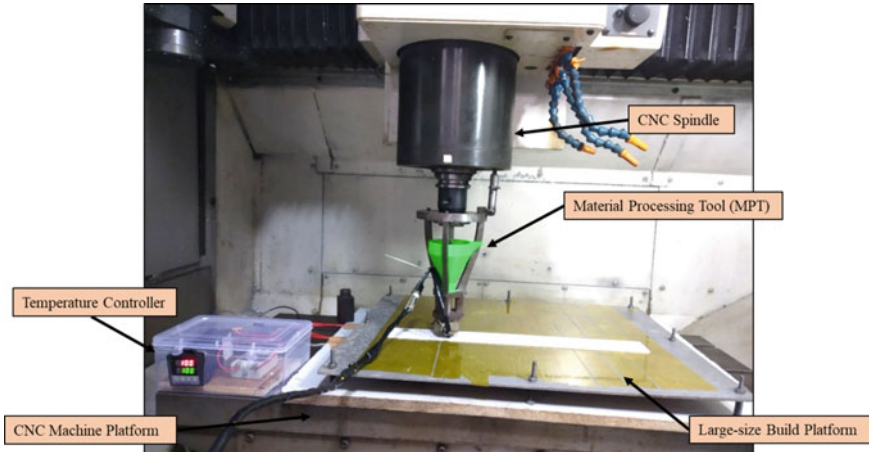


Fig. 29.7 Developed experimental setup

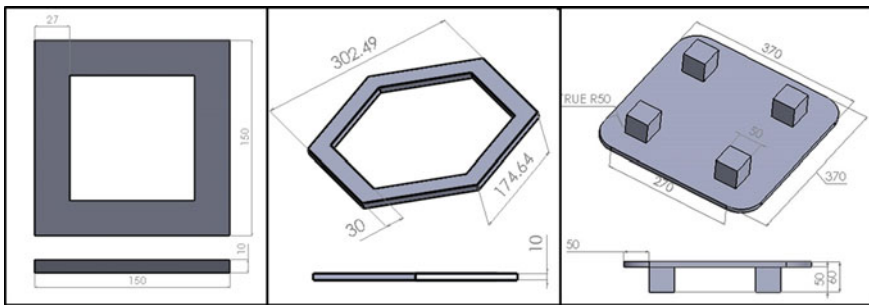


Fig. 29.8 Different primitive shapes

29.6 Characterization Results and Discussion

In the developed system, parts are fabricated similar to the commercial extrusion-based AM systems, using different material processing technique. In AM, the quality of the parts fabricated through extrusion-based AM depends on various factors. The changes in processing method, nozzle diameter and build platform may cause a change in the quality of parts. In order to observe and study the effect of these changes, characterization is done by taking the images of parts structure. The characterization study includes an effect of modified system and values of process parameters on dimensional accuracy, surface quality and structure of fabricated parts. There were various issues found during and after the fabrication process, which are compiled and enlisted.

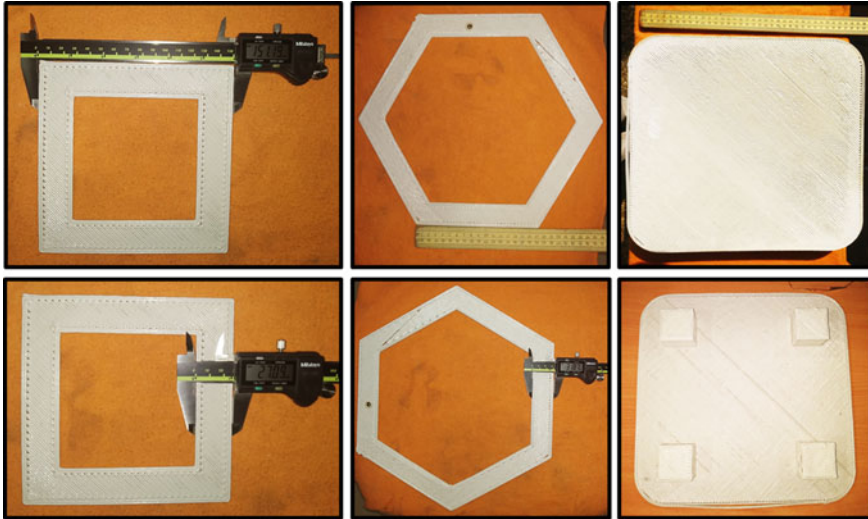


Fig. 29.9 Fabricated parts of the different primitive shapes




29.6.1 Dimensional Accuracy

In AM, dimensional accuracy always been a major concern, in the pre-processing stage maybe some CAD information lose during slicing and toolpath generation. In the fabrication of large-size parts issue of dimensional accuracy mainly observed, because of factors such as thermal contraction, under or over-extrusion, pellets quality, and even the standoff distance of first layer nozzle. In the present study, the fabricated parts were equated with CAD model dimensions to estimate deviations from actual dimensions. The results showed significant changes between dimensions of the fabricated parts and CAD model in all three directions. Results are reported in Table 29.2. The reason behind the obtained deviation can be related to thermal shrinkage during the cooling period. The filament extruded through MPT is varying its uniformity with time while depositing onto the build platform. Because of this reason, more change in deposited filament road width was observed than the filament thickness.

29.6.2 Surface Texture

Surface texture, also known as surface roughness is measuring the unevenness of the surface. The quality of surface of fabricated parts in AM become a more vital being used for end-use applications. The surface finish of parts is important not only to improve functionality and appearance but also for cost-effective processing and reduction of processing time. Surface roughness can be characterized in two different

Table 29.2 Dimensions of different cross sectional shapes

S. No.	Part	Dimensions	Actual (mm)	Measured (mm)	% Difference
1		Length	150.00	151.19	0.79
		Width	150.00	151.19	0.79
		Thickness	10.00	9.85	1.50
2		Length	302.49	300.00	0.82
		Width	174.64	172.00	1.51
		Thickness	10.00	8.90	0.11
3		Length	370.00	350.00	5.40
		Width	370.00	350.00	5.40
		Thickness	42.00	41.80	0.47

planes one is along with the build orientation and another one is perpendicular to build orientation.

In the present study, the surface roughness of the fabricated parts was measured using contact-type Mitutoyo Surftest SJ-500 surface roughness tester. In order to study surface roughness of fabricated part cutoff length considered 1 mm. The obtained surface roughness profiles of parts shown in Fig. 29.10. The profiles signify that in third cross-section (Table 29.2, Sr. No. 3) measured the height of roughness in both along and perpendicular to build orientation deviates more from its mean position. The parameters affect behind deviation of height mainly initial selected values of a parameter such as layer thickness and deposition speed. In order to enhanced surface roughness ultimately the quality of parts have to optimize the parameters accordingly.

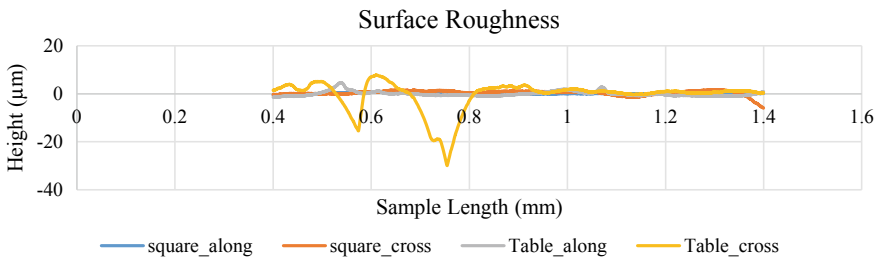


Fig. 29.10 Surface roughness measurement of different cross-sections

29.6.3 Structural Analysis

The mechanical properties and surface quality of any part largely depend on its microstructure. These qualities and properties of fabricated parts can be predicted with the help of microstructure or internal structure and bonding between the layers. In the present study, ABS pellet is processed using CNC-assisted extrusion deposition based AM system. Therefore, it is necessary to analyse the structural changes within the part. The issues related to analysis is been discussed in the section.

29.6.3.1 Gaps Between Infill and Internal–External Contours

In additive manufacturing, each layer is formed when the material is deposited within and along the contours. Contours represent the boundary of a part that guides material deposition tools in the filling of area inside the boundary. In the fabricated parts through the system, there were some gaps between infill and contours observed. Since the current study was the initial investigation in which part fabrication has been done initially with randomly chosen process parameters based on user experience. It is well-known that process parameters such as infill percentage, deposition speed and raster angle play a vital role during part fabrication. In this way, the observed gaps between infill and contours can be attributed to the fabrication with unoptimized process parameters. As compared to the other two parameters, deposition speed may affect the deposition rate of material within contour which may lead to the formation of irregular shape voids. As a result of higher deposition speed, the road does not get sufficient time to bond with contours. In the present study, material is deposited at a raster angle of 45° which is different than the orientation of the contour. This may also generate voids between infill and contours. To eliminate or minimize the gaps between infill and contours decreases or optimizes deposition speed (Fig. 29.11).

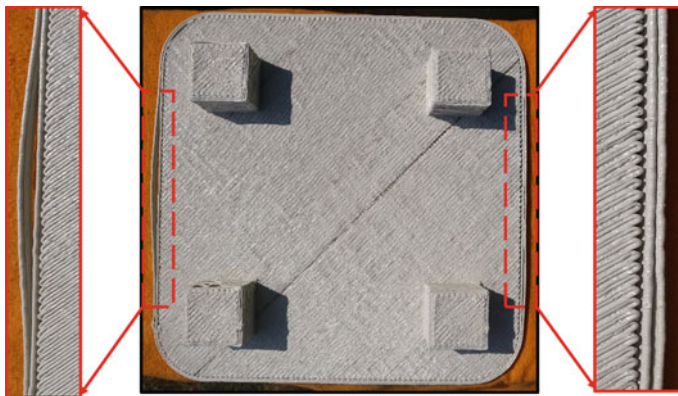


Fig. 29.11 Gaps between infill roads and contours

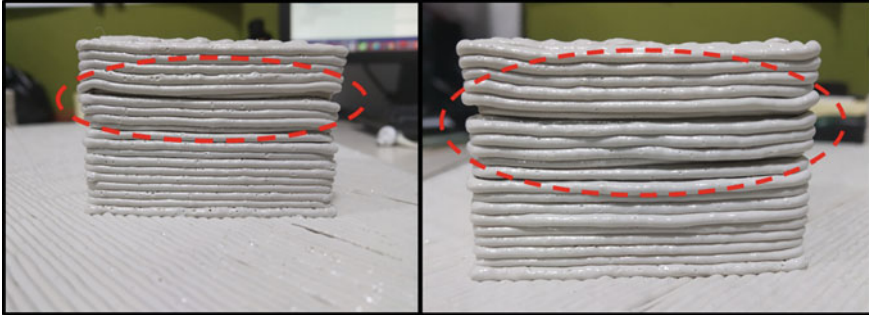


Fig. 29.12 Delamination

29.6.3.2 Layer Separation/ Delamination

AM is the process that builds the parts by layer-by-layer manner to create a desired 3D shape. However, for the build parts to be strong and reliable, need to assure that the deposited layer adequately bond with the previous layer. If bonding between the layers is not enough, then the part may split or layer gets separate. Parameters such as layer thickness, barrel temperature and deposition speed affect mainly bonding of layer. In the present study, these parameters values are considered as follows, layer height is been selected same as the diameter of nozzle, barrel temperature set nearer to the value of melting point of the material. After selecting the value of parameters fabricate part using system, during fabriaction issues like layer separation occurred, as shown in Fig. 29.12. This issue may be minimized with the selection of layer thickness lesser than the diameter of the nozzle. In this manner, a new layer would press the layer below it so that the two layers may bond strongly. Moreover, other process parameters related to temperature and speed could also be controlled to avoid layer separation.

29.6.3.3 Warpage

It is found that the heat transfer rate is increased with the increase in surface area of the part. Due to this, deposited roads cool and solidify fastly as a result, first few deposited layers of build part solidify quickly and lead to curl and deform edges of parts, that is known as warpage. Its effect can be severe which can separate out the part from the build platform. In the present study, the same issue was observed due to the large surface area of the parts (Fig. 29.13).

Warpage may be eliminated by incorporating a closed heated chamber across the build parts which is not the easy task as a developed system uses a CNC machining centre a gantry system. This constraint does not allow to build a closed chamber. Therefore, only the heated build platform was incorporated instead of the closed build chamber which may help to avoid the warpage issue through gradual increase

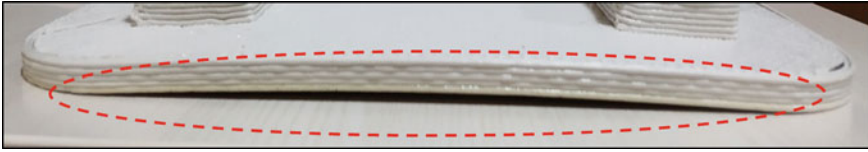


Fig. 29.13 Warpage

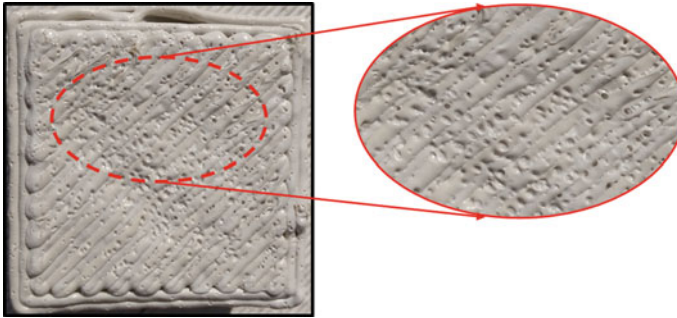


Fig. 29.14 Holes on top layers

or decrease in build platform temperature. Heated build platform helps to keep the bottom layers of part warm throughout the fabrication process. The heated build platform temperature was kept at 110 °C, which significantly reduced the amount of warpage in these layers. Problem with a thermoplastic material such as ABS is that it tends to warp during cooling. To avoid this, the fabricated parts were cooled down slowly at a gradual temperature interval.

29.6.3.4 Holes in the Top Layers

Blowholes were observed within deposited layers due to the hygroscopic nature of ABS and air entrapment during material processing in the barrel of MPT as shown in Fig. 29.14. Preheating of ABS and proper feeding of pellets into the barrel can be useful to overcome these issues.

29.6.3.5 Under-Extrusion/ Over-Extrusion

The material extrusion process does not provide any feedback about how much material extrudes through the nozzle. Due to this, sometimes less or more amount of material (under-extrusion or over-extrusion) is extruded through nozzle than that of expectation. The developed system consists of Material Processing Tool (MPT) that does not have any response unit to control the flow of extruded material through the

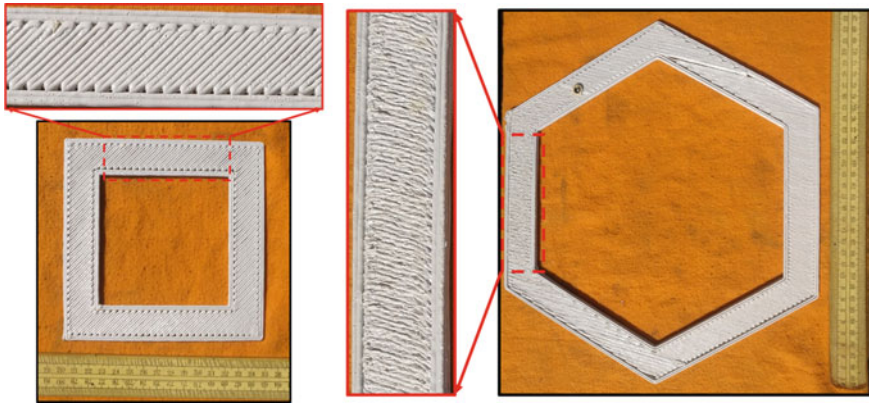


Fig. 29.15 Under-extrusion/over-extrusion

nozzle. Therefore, some issues are noticed such as gaps between the contours and layers due to under-extrusion, overlapping of layers due to over-extrusion as shown in Fig. 29.15. In order to overcome these issues, further experimentation is required to determine the optimum value of screw speed, deposition speed.

29.7 Conclusion

The purpose of large part fabrication was achieved by successful retrofit of existing three-axis CNC machining centre. The detailed study of the Material Processing Tool (MPT) was presented in this research work. The feasibility of experimental setup has been validated through the fabrication of large-size parts of the different cross-sections. The characterization study of fabricated parts and fabrication related issues have also been presented. The effect of process parameters, such as layer thickness, screw speed, deposition speed on the surface quality, dimensional accuracy and structural analysis of fabricated parts has also been discussed. The results revealed that layer thickness and deposition speed had a great influence on the structure of fabricated parts. Also, the surface quality was highly affected with larger layer thickness and higher deposition speed. Apart from these parameters, the influence of build platform temperature during and after the fabrication of parts was more significant for the quality of parts. The observations showed that the fabricated part gets warped or deformed due to inappropriate build temperature, thermal contraction, and environmental conditions. Overall characterization results suggest that further improvements are required in order to get large parts with desired dimensional and surface quality. Optimized values of different process parameters need to be determined. It can also be concluded that the developed setup has potential and could be used to fabricate large-size parts in forthcoming after incorporating some improvements in the existing setup.

References

1. Ngo, T.D., Kashani, A., Imbalzano, G., Nguyen, K.T.Q., Hui, D.: Additive manufacturing (3D printing): a review of materials, methods, applications and challenges. *Compos. Part B* **143**, 172–196 (2018). <https://doi.org/10.1016/j.compositesb.2018.02.012>
2. Mohan, N., Senthil, P., Vinodh, S., Jayanth, N.: A review on composite materials and process parameters optimisation for the fused deposition modelling process. *Virtual Phys. Prototyp.* **12**, 47–59 (2017). <https://doi.org/10.1080/17452759.2016.1274490>
3. Singh, S., Singh, G., Prakash, C., Ramakrishna, S.: Current status and future directions of fused filament fabrication. *J. Manuf. Process.* **55**, 288–306 (2020). <https://doi.org/10.1016/j.jmapro.2020.04.049>
4. Wang, Z., Liu, R., Sparks, T., Liou, F.: Large-scale deposition system by an industrial robot (I): design of fused pellet modeling system and extrusion process analysis. *3D Print. Addit. Manuf.* **3**, 39–47 (2016). <https://doi.org/10.1089/3dp.2015.0029>
5. Liu, X., Chi, B., Jiao, Z., Tan, J., Liu, F., Yang, W.: A large-scale double-stage-screw 3D printer for fused deposition of plastic pellets. *J. Appl. Polym. Sci.* **45147**, 1–9 (2017). <https://doi.org/10.1002/app.45147>
6. Moreno Nieto, D., Casal López, V., Molina, S.I.: Large-format polymeric pellet-based additive manufacturing for the naval industry. *Addit. Manuf.* **23**, 79–85 (2018). <https://doi.org/10.1016/j.addma.2018.07.012>
7. Felsch, T., Klaeger, U., Steuer, J., Schmidt, L., Schilling, M.: Robotic system for additive manufacturing of large and complex parts. *IEEE International Conference on Emerging Technologies and Factory Automation. ETFA*, pp. 1–4 (2017). <https://doi.org/10.1109/ETFA.2017.8247739>
8. Du, J., Wei, Z., Wang, X., Wang, J., Chen, Z.: An improved fused deposition modeling process for forming large-size thin-walled parts. *J. Mater. Process. Technol.* **234**, 332–341 (2016). <https://doi.org/10.1016/j.jmatprotec.2016.04.005>
9. Sanandiya, N.D., Vijay, Y., Dimopoulou, M., Dritsas, S., Fernandez, J.G.: Large-scale additive manufacturing with bioinspired cellulosic materials. *Sci. Rep.* **8**, 1–8 (2018). <https://doi.org/10.1038/s41598-018-26985-2>
10. Duty, C.E., Kunc, V., Compton, B., Post, B., Erdman, D., Smith, R., Lind, R., Lloyd, P., Love, L.: Structure and mechanical behavior of big area additive manufacturing (BAAM) materials. *Rapid Prototyp. J.* **23**, 181–189 (2017). <https://doi.org/10.1108/RPJ-12-2015-0183>
11. Vispute, M., Kumar, N., Jain, P.K., Tandon, P., Pandey, P.M.: Shrinkage compensation study for performing machining on additive manufactured parts. *Mater. Today Proc.* **5**, 18544–18551 (2018). <https://doi.org/10.1016/j.matpr.2018.06.197>
12. Kumar, N., Jain, P.K., Tandon, P., Pandey, P.M.: Extrusion-based additive manufacturing process for producing flexible parts. *J. Brazilian Soc. Mech. Sci. Eng.* **40**, 1–12 (2018). <https://doi.org/10.1007/s40430-018-1068-x>
13. Kumar, N., Jain, P.K., Tandon, P., Pandey, P.M.: Additive manufacturing of flexible electrically conductive polymer composites via CNC-assisted fused layer modeling process. *J. Brazilian Soc. Mech. Sci. Eng.* **40**, 175 (2018). <https://doi.org/10.1007/s40430-018-1116-6>
14. Rictor, A., Riley, B.: Optimization of a heated platform based on statistical annealing of critical design parameters in a 3D printing application. *Procedia Comput. Sci.* **83**, 712–716 (2016). <https://doi.org/10.1016/j.procs.2016.04.157>
15. Messimer, S.L., Patterson, A.E., Muna, N., Deshpande, A.P., Rocha Pereira, T.: Characterization and processing behavior of heated aluminum-polycarbonate composite build plates for the FDM additive manufacturing process. *J. Manuf. Mater. Process.* **2**, 12 (2018). <https://doi.org/10.3390/jmmp2010012>
16. Spoerk, M., Gonzalez-Gutierrez, J., Sapkota, J., Schuschnigg, S., Holzer, C.: Effect of the printing bed temperature on the adhesion of parts produced by fused filament fabrication. *Plast. Rubber Compos.* **47**, 17–24 (2018). <https://doi.org/10.1080/14658011.2017.1399531>

17. Choi, Y.-H., Kim, C.-M., Jeong, H.-S., Youn, J.-H.: Influence of bed temperature on heat shrinkage shape error in FDM additive manufacturing of the ABS-engineering plastic. *World J. Eng. Technol.* **04**, 186–192 (2016). <https://doi.org/10.4236/wjet.2016.43D022>
18. Gawali, S.K., Kumar, N., Jain, P.K.: Investigations on the development of heated build platform for additive manufacturing of large-size parts. In: *Manufacturing Engineering*, pp. 1–17. Springer, Singapore (2020)

Chapter 30

Investigation of Machining Rate and Tool Wear in Processing of Fe-Based-SMA Through Sinking EDM



Ranjit Singh, Ravi Pratap Singh, and Rajeev Trehan

Abstract Shape memory alloys (SMAs) is one of the category of advanced materials which have the ability to memorize their shape when treated upto particular conditions of temperature. SMAs have numerous applications in the field of biomedical, automotive, aerospace, robotics and industrial sector. SMAs have spotted to be the alloys having superior and unique properties having commercial applications. SMAs are basically classified into three types Ni-based, Cu-based and Fe-based. Fe-based SMAs is an important class of shape memory alloys having applications in pipe joint for steel pipes, fishplate for crane rail and in other structural materials. It is an inexpensive alloy as compare to other SMAs, due to this these alloys are used as commercial production of stainless steel in industry. The non-conventional machining of Fe-based SMA is an area of future concern which is going to be explore in this paper. In this article the effect of various process parameters on material removal and tool wear rate has been studied while performing Electrical discharge machining operation on Fe-based SMA. Pulse on time and Pulse off time are the major influential process parameters impacting the MRR and TWR than the other two parameters i.e. peak current and gap voltage.

Keywords SMA · SME · EDM · MRR · TWR · RSM

30.1 Introduction

In today's era of advancement in technology, the need for smart materials is continuously rising due to their exceptional and inimitable properties, and applications in distinct sectors from biomedical to manufacturing industry. Shape Memory Alloys (SMAs) is a major class of advanced materials which have the capability to recover their original form when exposed to the alterations in the magnetic and temperature conditions [1]. This behavior of returning back to its previous form is broadly known as shape memory effect (SME). The SMAs was firstly discovered by the Arne

R. Singh · R. P. Singh (✉) · R. Trehan
Department of Industrial and Production Engineering, Dr B R Ambedkar National Institute of Technology, Jalandhar 144011, Punjab, India
e-mail: singhrp@nitj.ac.in

© The Author(s), under exclusive license to Springer Nature Switzerland AG 2022
R. Pratap Singh et al. (eds.), *Proceedings of the International Conference on Industrial and Manufacturing Systems (CIMS-2020)*, Lecture Notes on Multidisciplinary Industrial Engineering, https://doi.org/10.1007/978-3-030-73495-4_30

439

Olander in 1932 [2]. Among all of them, there are three SMA major classifications i.e. Ni–Ti based, Cu-based and Fe-based. Fe-based SMA is an important category of SMA alloy system, which have numerous applications in the manufacturing sector. Sato [3] discovered the Fe-30Mn-1Si alloy and subsequently the Fe-Mn alloy SME, which led to lower production costs. In addition, compared to the other SMAs i.e. Ni-based and Cu-based, Fe-SMAs have a large transformation hysteresis and high rigidity and strength. Kajiwara et al. [4] and Farjami et al. [5] revealed the presence of fine VN and NbC precipitates in the microstructure that heightened the SME of Fe-SMAs without any training process. Dong et al. [6] and Leinenbach et al. [7] enhanced the SME of Fe-16Mn-5Si-10Cr-4Ni-1(V, N) and Fe-17Mn-5Si-10Cr-4Ni-1(V, C) by mass fraction. Established SMEs, high rigidity, high strength and low cost of production of these Fe-SMAs have led international research into their application in civil engineering fields such as damping, active control and pre-or post-stress tensioning of structures. Iron-based SMAs are the third projecting group of SMAs to be preceded by NiTi and Copper-based SMAs. This SMA class has been economically viable over the NiTi alloy system due to its relatively low alloy part & easy production [8]. Iron-based SMAs are often known as shape memory steel (SMS) and consist of various alloys; i.e. Fe–Pt, Fe–Pd, Fe–Mn–Si, Fe–Mn–Al, Fe–Ni–C, Fe–Ni–Co–Ti [8]. The production rate of SMS must be as high as that of carbon steel for an economically viable operation. The machining of Fe-based SMA with the non-conventional machining operations is an area of future concern. Machining of Fe-based SMA with the EDM process is an area of future explorations for studying the impact of various process parameters on machining responses. The study of EDM process on Fe-based SMA brings up new machining concepts and helps in commercially uplifting this process for the industrial growth. The optimization based studies have also been attempted while processing advanced materials with newest machining processes [9–12].

Electrical discharge machining is a type of thermo-erosive process in which spatially and temporally controlled separated pulsed discharges are utilized to machine electrically conductive materials irrespective of their chemical, mechanical and thermo-physical properties [10, 13–16]. In the 1940s, the EDM method was discovered [17]. EDM exists as one of the modern machining operations productively used for machining tough to cut materials [18, 19]. The overall concept of EDM process is to utilize thermos-electric energy to erode the material from a workpiece with the help of periodic electrical sparks between the uncontacted electrode and the workpiece [20–23]. The tool and the workpiece are immersed in a dielectric fluid [8, 11]. The spark formation results into the formation of electrons and positive ions which results into the formation of conductive channel [24, 25]. Due to the collision of the ions there is a formation of high temperature plasma channel [26]. The high temperature region results into removal of workpiece due to instantaneous melting and evaporation [27–30] (Fig. 30.1).

The objective of this paper is to study the effect of various process parameters i.e. Pulse on time, Pulse off time, Peak current, Gap voltage on the material removal rate and tool wear rate of the work material and tool used for machining purpose in EDM operations. The study focused on the variation of MRR and TWR while

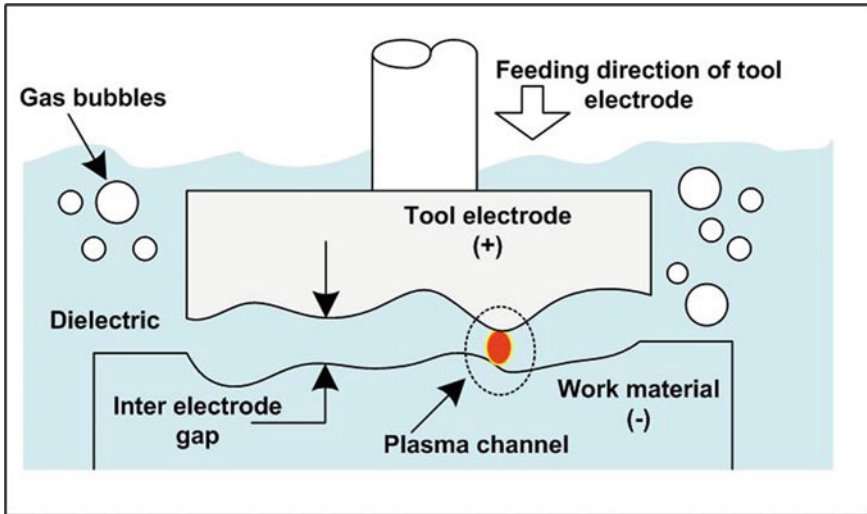


Fig. 30.1 Basic working mechanism of EDM process

performing experiment work at different process parameter setting. The behavior of the parameters has been studied graphically to explore the MRR and TWR during the experiment work and different results and discussions has been provided for studying the concept of machining of Fe- based SMA with EDM operations.

30.2 Materials and Methods

The Fe-based SMA has been used as workpiece and Cu-based electrode is used as a tool in EDM operations. Fe–Mn–Si–Cr–Ni has been used as work material in the EDM operations. The workpiece is in disc form having dimensions 110 × 15 mm and 20 mm height. The diameter of Cu electrode used in EDM operations is 10 mm. The process parameters taken in the EDM process are pulse on time, pulse off time, peak current and gap voltage. The response parameters which are measured with the variation of process parameters are MRR and TWR (Figs. 30.2 and 30.3).

The process parameters chosen for the experiment are pulse on time, pulse off time, peak current and gap voltage. The response parameters selected for studying the impact of process parameters are Material Removal Rate (MRR) and Tool Wear Rate (TWR) (Tables 30.1, 30.2, 30.3, 30.4, 30.5, 30.6, 30.7 and 30.8).



Fig. 30.2 EDM machine set-up

Fig. 30.3 Fe-based SMA disc



30.3 Results and Discussions

The experiments have been performed on CNC EDM machine set-up at CIHT Maqsdan Jalandhar. The four process parameters are varied and their effect on

Table 30.1 MRR values at different Pulse on time values

S. No.	Pulse on time (μ s)	Act. diameter (mm)	Actual depth (mm)	MRR (mm^3/min)
1	30	10.02	6.81	536.7255
2	45	10.04	5.6	443.1238
3	60	10.05	5.9	467.7931
4	90	10.07	6.2	493.5376
5	120	10.09	6.82	545.05
6	150	10.12	7.13	573.2185
7	250	10.16	6.15	498.3474
8	300	10.19	7.25	590.9572
9	400	10.21	7.24	592.4609

Table 30.2 TWR values at different pulse on time values

S. No.	Pulse on time (μ s)	Time in minutes	Int. wt. of tool (g)	Final wt. of tool (g)	TWR (g/min)
1	30	47.66	34.5	33.85	0.013638271
2	45	25.66	32.66	31.75	0.035463757
3	60	20.71	33.85	32.7	0.05552873
4	90	17	31.75	30.7	0.061764706
5	120	16.16	33.77	32.72	0.064975248
6	150	17.13	32.9	31.84	0.061879743
7	250	16.9	30.44	29.3	0.067455621
8	300	16.8	32.72	31.5	0.072619048
9	400	17.43	31.66	30.41	0.071715433

Table 30.3 MRR values at different Pulse off time values

S. No.	Pulse off time (μ s)	Act. diameter (mm)	Actual depth (mm)	MRR (mm^3/min)
1	20	10.15	7.01	566.9174
2	45	10.12	6.82	548.296
3	60	10.11	6.32	507.0947
4	90	10.09	6.2	495.5
5	120	10.07	6.12	487.1694
6	200	10.05	7.05	558.9731
7	250	10.03	6.26	494.3629
8	300	10.02	6.15	484.708

Table 30.4 TWR values at different Pulse off time values

S. No.	Pulse off time (μ s)	Time in minutes	Int. wt. of tool (g)	Final wt. of tool (g)	TWR (g/min)
1	20	21.43	31.65	30.9	0.034997667
2	45	16.56	29.75	28.85	0.054347826
3	60	15.78	30.5	29.6	0.057034221
4	90	16.53	31.23	30.2	0.06231095
5	120	18.71	29.41	28.38	0.055050775
6	200	34.26	34.9	33.94	0.028021016
7	250	32.91	33.8	32.83	0.029474324
8	300	35.78	32.7	31.67	0.028787032

Table 30.5 MRR values at different Peak current values

S. No.	Peak current (A)	Act. diameter (mm)	Actual depth (mm)	MRR (mm^3/min)
1	8	10.02	7.16	564.3105
2	14	10.04	7.02	555.4874
3	20	10.05	6.17	489.2006
4	24	10.07	6.12	487.1694
5	30	10.1	6.59	527.713
6	40	10.12	6.33	508.9023
7	50	10.15	5.88	475.5313

Table 30.6 TWR values at different Peak current values

S. No.	Peak current (A)	Time in minutes	Int. wt. of tool (g)	Final wt. of tool (g)	TWR (g/min)
1	8	79	29.72	29.58	0.001772152
2	14	41.9	37.64	37.47	0.004057279
3	20	22.13	33.94	32.6	0.060551288
4	24	17.9	32.81	31.84	0.054189944
5	30	18	31.69	30.77	0.051111111
6	40	11.26	29.57	28.48	0.096802842
7	50	9.1	37.46	36.35	0.121978022

MRR and TWR are recorded as numerical values in tabular form. The effect of process parameters on MRR and TWR are studied with the help of graphical charts (Fig. 30.4).

The plot of MRR versus Pulse on time reveals that the MRR increases with the increase in pulse on time. With the rise in pulse on time there is a less time lag between the pulses, due to which the spark formation is more and it results into high

Table 30.7 MRR values at different Gap voltage values

S. No.	Gap voltage (V)	Act. Diameter (mm)	Actual depth (mm)	MRR (mm ³ /min)
1	30	10.08	6.54	521.6371
2	40	10.06	6.05	480.6412
3	50	10.04	6.51	515.1315
4	60	10.03	6.04	476.9891
5	70	10.03	6.42	506.9984
6	80	10.02	6.39	503.6235

Table 30.8 TWR values at different gap voltage values

S. No.	Gap voltage (V)	Time in minutes	Int. wt. of tool (g)	Final wt. of tool (g)	TWR (g/min)
1	30	21.2	32.16	31.32	0.039622642
2	40	18.05	28.85	27.85	0.055401662
3	50	22.68	27.26	26.45	0.035714286
4	60	18.86	30.28	29.27	0.053552492
5	70	18.23	27.84	26.98	0.047174986
6	80	21.35	31.33	30.47	0.04028103

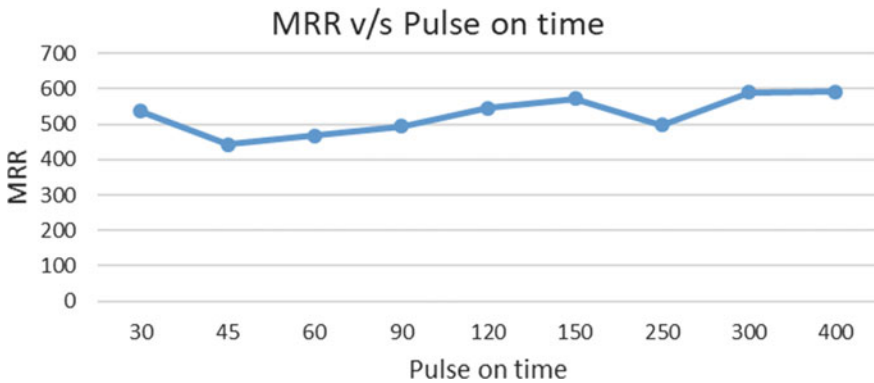


Fig. 30.4 Plot for MRR versus pulse on time

temperature formation which leads in more material removal. The pulse on time has been varied from 30 to 400 μs. The maximum MRR reported is 592.4609 mm³/min at 400 μs pulse on time (Fig. 30.5).

Another important machining performance parameter is Tool wear rate. As depicted from the plot, the effect of pulse on time on TWR is clearly visible. There is continuous rise in TWR as the rise in pulse on time value. The main reason behind the increase in TWR value is more spark formation due to less rest time between

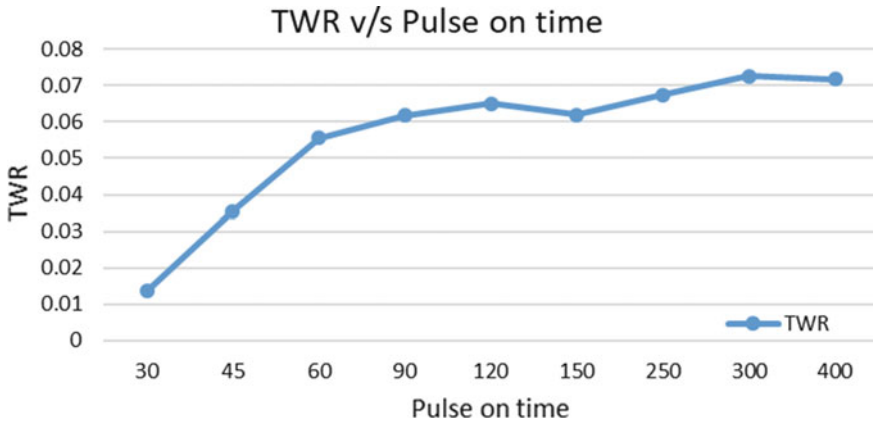


Fig. 30.5 Plot for TWR versus pulse on time

pulses. The pulses arriving fast with the increase in pulse on time, which leads to high temperature generation due to more spark formation. The high temperature zone results into more tool wear, tool gets eradicated with the rise in pulse on time. The maximum TWR is 0.072619048 at pulse on time of 300 μ s (Figs. 30.6 and 30.7).

The effect of pulse off time on MRR and TWR has been studied with the help of graphical plots presented above. The MRR versus Pulse off time plot clear depicts the decrease in material removal rate with the increase in pulse off time. The rise in pulse off time brings more lag time between corresponding pulses due to which the spark formation occurrence becomes less which ultimately leads to less temperature formation which further going to decline the MRR. TWR also follows the same trend as MRR with the rise in pulse off time (Figs. 30.8 and 30.9).

The graphical plot of peak current versus the MRR and TWR reveals the behavior of material removal and tool wear with the variation of peak current. The MRR value is 564.3105 mm^3/min i.e. maximum MRR at 8 A peak current and minimum i.e. 475.5313 mm^3/min . The TWR value is maximum i.e. 0.121978022 g/min at 50 A peak current (Figs. 30.10 and 30.11).

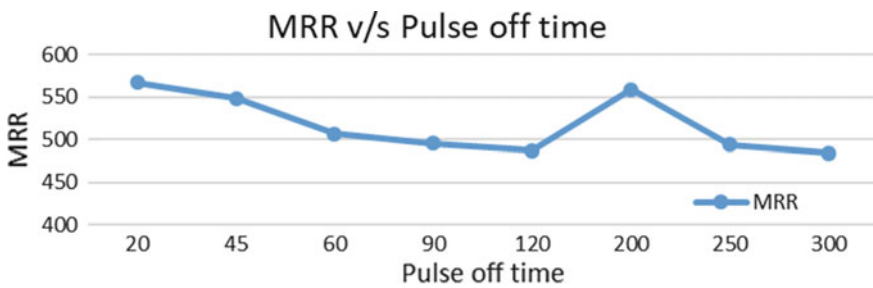


Fig. 30.6 MRR versus pulse off time plot

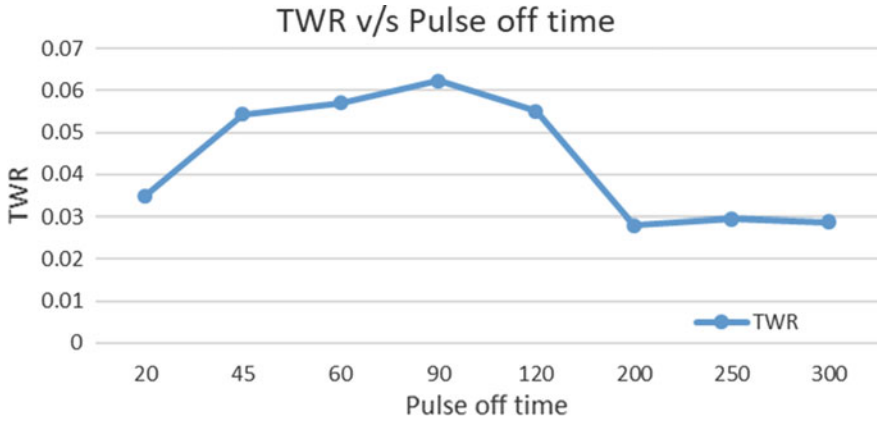


Fig. 30.7 Plot between TWR and pulse off time

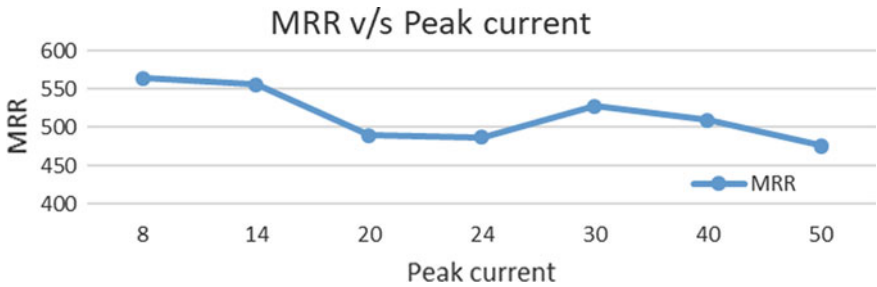


Fig. 30.8 Plot between peak current and MRR

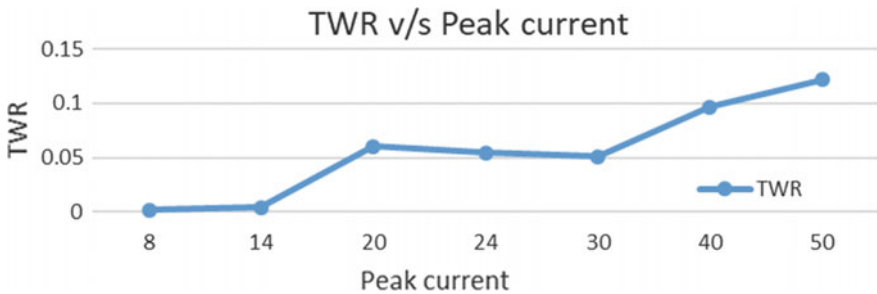


Fig. 30.9 Peak current versus TWR plot

The plot of Gap voltage versus the MRR and TWR reveals the effect of gap voltage on material removal and tool wear rate. The maximum MRR is 521.6371 mm³/min at 30 V and maximum TWR is 0.055401662 g/min at gap voltage of 40 V.

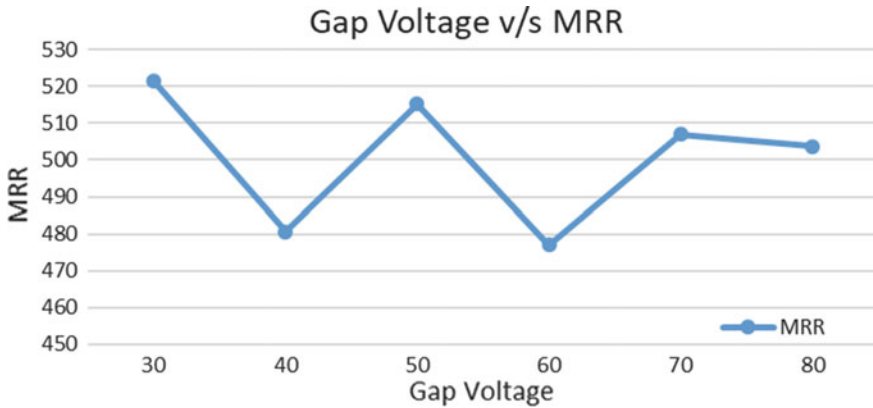


Fig. 30.10 Plot between MRR and gap voltage

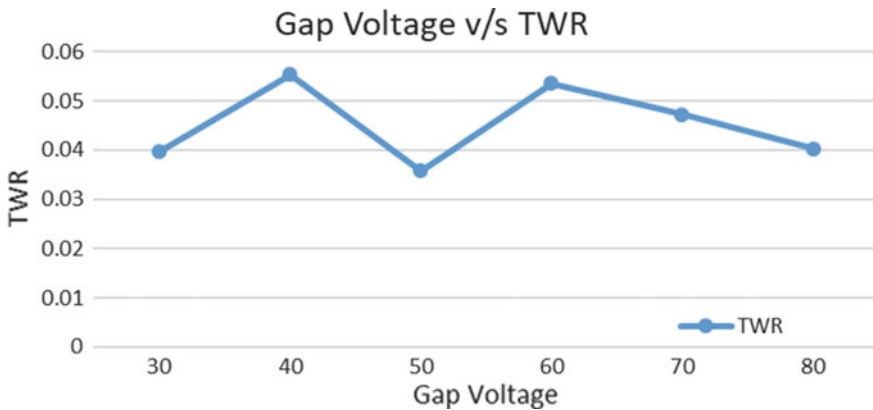


Fig. 30.11 TWR versus gap voltage plot

30.4 Conclusions

The following insinuations have been observed after performing the experimental operations on the Fe-based SMA in CNC EDM process:

1. The major parameters which have a crucial and major impact on the MRR and TWR are Pulse on time and Pulse off time.
2. MRR increases with increase in Pulse on time as no lag between corresponding pulses results into more discharge formation which results into higher temperature formation which ultimately results into more MRR. MRR maximum value is 592.4609 mm³/min at 400 μs pulse on time. Minimum value of MRR is 443.1238 mm³/min at 45 μs pulse on time.

3. Pulse on time also has a significant impact on the TWR. Tool wear increases with rise in pulse on time, as it leads to high temperature region formation which results into high eradication of tool, ultimately more TWR. The maximum value of TWR is 0.072619048 g/min at 300 μ s pulse on time.
4. Pulse off time is another major influential parameter for the MRR and TWR. With the increase in pulse off time the MRR decreases. The reason for decrease in the MRR is large time lag between the pulses that leads to less spark formation which results into low temperature formation that leads to less MRR. TWR gets decreased with increase in pulse off time, as it leads to less spark formation which results into low temperature formation that results into less TWR. MRR maximum and minimum value is 566.9174 and 484.708 mm³/min. The TWR maximum and minimum value is 0.06231095 g/min and 0.028021016 g/min.
5. MRR and TWR increases with the increase in peak current. The peak current results in passage of more current that results into more spark formation leading to high temperature formation that results into more material removal and deterioration of the tool. Maximum and minimum values of MRR is 564.3105 mm³/min and 475.5313 mm³/min at peak current of 8 and 50 A. The TWR maximum and minimum value is 0.121978022 g/min and 0.001772152 g/min.
6. The maximum MRR is 521.6371 mm³/min at gap voltage of 30 V and minimum value of MRR is 476.9891 at 60 V. The maximum and minimum value for the TWR is 0.0554 g/min and 0.0357 g/min at gap voltage of 40 V and 50 V.

References

1. Jani, J.M., Leary, M., Subic, A., Gibson, M.A.: A review of shape memory alloy research, applications and opportunities. *Mater. Des.* (1980–2015) **56**, 1078–1113 (2014)
2. Ölander, A.: An electrochemical investigation of solid cadmium-gold alloys. *J. Am. Chem. Soc.* **54**(10), 3819–3833 (1932)
3. Sato, A., Chishima, E., Soma, K., Mori, T.: Shape memory effect in α transformation in Fe-30Mn-1Si alloy single crystals. *Acta Metall.* **30**, 1177–1183 (1982)
4. Kajiwara, S., Liu, D., Kikuchi, T., Shinya, N.: Remarkable improvement of shape memory effect in Fe-Mn-Si based shape memory alloys by producing NbC precipitates. *Scripta Mater.* **44**, 2809–2814 (2001)
5. Farjami, S., Hiraga, K., Kubo, H.: Shape memory effect and crystallographic investigation in VN containing Fe-Mn-Si-Cr alloys. *Mater. Trans.* **45**, 930–935 (2004)
6. Dong, Z., Klotz, U.E., Leinenbach, C., Bergamini, A., Czaderski, C., Motavalli, M.A.: Novel Fe-Mn-Si shape memory alloy with improved shape recovery properties by VC precipitation. *Adv. Eng. Mater.* **11**, 40–44 (2009)
7. Leinenbach, C., Kramer, H., Bernhard, C., Eifler, D.: Thermo-mechanical properties of an Fe-Mn-Si-Cr-Ni-VC shape memory alloy with low transformation temperature. *Adv. Eng. Mater.* **14**, 62–67 (2012)
8. Wen, Y.H., Peng, H.B., Raabe, D., Gutiérrez-Urrutia, I., Chen, J., Du, Y.Y.: Large recovery strain in Fe-Mn-Si-based shape memory steels obtained by engineering annealing twin boundaries. *Nat. Commun.* **5**, 4964 (2014)

9. Singh, R.P., Singhal, S.: Rotary ultrasonic machining: a review. *Mater. Manuf. Process.* **31**, 1795–1824 (2016)
10. Singh, R.P., Singhal, S.: Investigation of machining characteristics in rotary ultrasonic machining of alumina ceramic. *Mater. Manuf. Process.* **32**, 309–326 (2017)
11. Singh, R.P., Singhal, S.: Experimental investigation of machining characteristics in rotary ultrasonic machining of quartz ceramic. *J. Mater. Des. Appl.* **232**, 870–889 (2018)
12. Singh, R.P., Singhal, S.: Rotary ultrasonic machining of alumina ceramic: experimental study and optimization of machining responses. *J. Eng. Res.* **6**, 01–24 (2018)
13. Singh, R.P., Singhal, S.: Rotary ultrasonic machining of macor ceramic: an experimental investigation and microstructure analysis. *Mater. Manuf. Process.* **32**, 927–939 (2017)
14. Vernon, L.B., & Vernon, H.M., 1941. U.S. Patent No. 2,234,993. U.S. Patent and Trademark Office, Washington, DC.
15. Singh, R.P., Singhal, S.: An experimental study on rotary ultrasonic machining of macor ceramic. *J. Eng. Manuf.* **232**, 1221–1234 (2018)
16. Kulkarni, V.N., Gaitonde, V.N., Aiholi, V., Hadimani, V.: Multi performance characteristics optimization in wire electric discharge machining of nitinol superelastic alloy. *Mater. Today: Proc.* **5**(9), 18857–18866 (2018)
17. Singh, S., Maheshwari, S., Pandey, P.C.: Some investigations into the electric discharge machining of hardened tool steel using different electrode materials. *J. Mater. Process. Technol.* **149**(1–3), 272–277 (2004)
18. Kumar, A., Kumar, V., Kumar, J.: Prediction of surface roughness in wire electric discharge machining (WEDM) process based on response surface methodology. *Int. J. Eng. Technol.* **2**(4), 708–719 (2012)
19. Datt, M., Singh, D.: Optimization of WEDM parameters using Taguchi and ANOVA method. *J. Curr. Eng. Technol.* **5**(6), 3843–3847 (2015)
20. Singh, R.P., Tyagi, M., Kataria, R.: Selection of the optimum hole quality conditions in manufacturing environment using MCDM approach: a case study. *Operations management and systems engineering*, pp. 133–152. Springer, Singapore (2019)
21. Cladera, A., Weber, B., Leinenbach, C., Czaderski, C., Shahverdi, M., Motavalli, M.: Iron-based shape memory alloys for civil engineering structures: an overview. *Constr. Build. Mater.* **63**, 281–293 (2014)
22. Singh, R.P., Kataria, R., Singhal, S.: Decision-making in real-life industrial environment through graph theory approach. In *Computer Architecture in Industrial, Biomechanical and Biomedical Engineering*. IntechOpen (2019). <https://doi.org/10.5772/intechopen.82011>
23. Daneshmand, S., Hessami, R., Esfandiari, H.: Investigation of wire electro discharge machining of Nickel-Titanium shape memory alloys on surface roughness and MRR. *Life Sci. J.* **9**(4), 2904–2909 (2012)
24. Baruj, A., Kikuchi, T., Kajiwara, S., Shinya, N.: Improved shape memory properties and internal structures in Fe-Mn-Si-based alloys containing Nb and C. In: *Journal de Physique IV (Proceedings)*, Vol. 112, pp. 373–376. EDP Sciences (2003)
25. Liu, J.F., Guo, Y.B., Butler, T.M., Weaver, M.L.: Crystallography, compositions, and properties of white layer by wire electrical discharge machining of nitinol shape memory alloy. *Mater. Des.* **109**, 1–9 (2016)
26. Tanaka, Y., Himuro, Y., Kainuma, R., Sutou, Y., Omori, T., Ishida, K.: Ferrous polycrystalline shape-memory alloy showing huge superelasticity. *Science* **327**(5972), 1488–1490 (2010)
27. Singh, R.P., Kumar, J., Kataria, R., Singhal, S.: Investigation of the machinability of commercially pure titanium in ultrasonic machining using graph theory and matrix method. *J. Eng. Res.* **3**, 75–94 (2015)
28. Tyagi, M., Panchal, D., Singh, R.P., Sachdeva, A.: Modeling and analysis of critical success factors for implementing the IT-based supply-chain performance system. In *Operations Management and Systems Engineering*, pp. 51–67. Springer, Singapore (2019)
29. Singh, R., Singh, R.P., Trehan, R.: State of the art in processing of shape memory alloys with electrical discharge machining: a review. In: *Proceedings of the Institution of Mechanical Engineers, Part B: Journal of Engineering Manufacture* (2020), 0954405420958771

30. Singh, R., Singh, R.P., Tyagi, M., Kataria, R.: Investigation of dimensional deviation in wire EDM of M42 HSS using cryogenically treated brass wire. In: *Materials Today: Proceedings* (2019)
31. Singh, R.P., Kataria, R., Kumar, J., Verma, J.: Multi-response optimization of machining characteristics in ultrasonic machining of WC-Co composite through Taguchi method and grey-fuzzy logic. *AIMS Mater. Sci.* **5**, 75–92 (2018)
32. Singh, R., Singla, V.K.: Surface characterization of M42 HSS treated with cryogenic and non-cryogenated brass wire in WEDM process. *IMRF Biannual Peer Rev. Int. Res. J.* **5**, 28–32 (2017)
33. Singh, R., Singla, V.K.: Parametric modeling for wire electrical discharge machining of M42 HSS using untreated and cryogenated treated brass wire by using RSM. *Int. J. Mechan. Prod. Eng.* **5**, 63–67 (2018)

Chapter 31

Study of Microstructure, Mechanical and Fracture Properties of Bagasse Ash Powder Strengthened Aluminium Matrix Composites



Vaibhav Singh, Satpal Sharma, and Bhaskar Chandra Kandpal

Abstract The present research work focused on Al 6061-Bagasse ash metal matrix composites are produced with stir casting process. The different mass fractions of bagasse ash particles (1, 3, 5 and 7%) under speed of 300 r/min. different mechanical properties such as hardness, tensile strength and toughness of fabricated aluminium metal matrix composites are tested. It was found that the mechanical properties were greatly affected with increasing percentage volume of reinforcement. The optical microscopy results affirmed the uniform conveyance of reinforced particles in the metal matrix combination.

Keywords Bagasse ash · Stir casting · Vicker hardness test · Toughness

31.1 Introduction

Composites are delivered by mix of at least two materials one of which is a metal where desired and unique combination of engineering properties are achieved like high specific strength, wear resistance, strength to weight, thermal conductivities, friction coefficient, wear resistance, damping properties etc. Composite materials with matrices of Al alloys are the most important type of composite materials. Such types of composites have wide applications in automotive and aerospace industries. Since MMC's are the combination of metallic alloys and ceramic reinforcements they combine the properties of metallic alloys such as toughness and ductility with properties of ceramic reinforcements like improved strength as well as modulus. With the use of certain ceramic reinforcements such as SiC, Al₂O₃ and Graphite in defined volumetric share improvement of mechanical as well as tribological properties take place. Composite materials also occur in nature and they can be made by humans as well. Such type of composites can be produced by solid state processing and liquid route processing.

V. Singh · S. Sharma

Department of Mechanical Engineering, Gautam Buddha University, Greater Noida, India

B. C. Kandpal (✉)

Department of Mechanical Engineering, Inderprastha Engineering College, Ghaziabad, India

31.1.1 Composite Materials

Composite materials are comprised of at least two materials which vary in physical properties and chemical composition and are insoluble in one another. In the composite, each segment has its own personality and displays its extraordinary structure and properties. The properties of composite material are generally relying on properties of reinforcement and matrix phases. Each component imparts its own properties so that the result and properties are superior to either component alone. Composite materials also occur in nature as well as are made by humans.

Composite materials are on the basis of geometry of the reinforcement in matrix phase can be characterized into particle-reinforced, fibre-reinforced or structural composites.

31.1.2 Metal Matrix Composites

These composites comprise of metal as matrix stage while reinforcement might be a different material or another metal. Different sorts of reinforcement phase, for example, strands, hairs or particles are utilized in metal matrix composites. The metal matrix composites have numerous favourable circumstances over different kinds of materials like progressed mechanical, synthetic and actual properties.

31.1.3 Manufacturing of Metal Matrix Composites

The composites have many superior features compared to metals as discussed above so their applications are increasing day by day in various engineering fields. Different processes are used to manufacture MMCs. Primary processing of metal matrix composites are classified into three processes namely vapour state processing, solid state processing and liquid state processing. It is very economical to produce metal matrix composites with stir casting. The stir casting parameters are to be controlled to maintain the quality of samples. The stirring speed and time are very important in the process. The pouring temperature factor also played important role in the process of impeller. Properties like wettability and porosity in cast metal matrix composites can be improved by controlling these boundaries.

31.2 Literature Review

Aigbodion et al. [1] found that there was improvement in mechanical properties with the expansion in weight level of SiC they saw the maturing conduct in Al-Cu-Mg/Bagasse ash particulate composite. The processing parameters were controlled to improve the quality. The effect of percentage of reinforcement on the properties of MMC was reported. The hardness and impact strength were enhanced as we increased the percentage of reinforcement. It was also found that the advanced method is successful to obtain uniform mixing of reinforcement in the matrix. Srinivasan et al. [2] produced Sugar Cane- Bagasse Ash, which contains silica and aluminium, in concrete with cement by weight of 0, 5, 10, 15, 20 and 25%. They found that cement can be replaced with bagasse ash in concrete to reduce cost. The properties of composites were seen to be profoundly influenced by the distribution of reinforcement particulates in the framework and the morphology of the secondary matrix. The properties of mix cast MMCs were inspected at various strides of the castings. Sharanabasappa et al. [3] found that rice husk fly ash can be used as reinforcement to produce composite. It was observed that use of rice husk ash with high silica content which not only improved the mechanical properties of aluminium but also minimised the industrial waste thereby making it beneficial for the environment. They investigated the effects of processing parameters and selection of matrix and reinforcements on properties of MMCs. The mechanical properties, for example, hardness and tensile strength were accounted for to be improved.

31.3 Experimental Work

31.3.1 Material Selection

Matrix and reinforcement phase: For the matrix phase of our composite material we have selected Aluminium alloy 6061. Aluminium 6061 alloy is the most affordable of all the Aluminium alloys.

Reinforcement Phase: Bagasse Ash was obtained from Mansurpur Sugar Mill, Muzaffarnagar as an industrial waste.

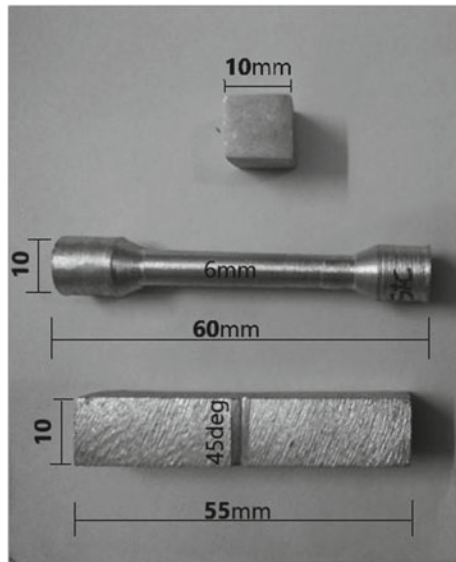
31.3.2 Experimental Set Up

Stir casting method was used because it is very economical process for making metal matrix composites. The process started with the determination of quantities of Bagasse ash required to produce 1, 3, 5 and 7 wt.% reinforcement (Figs. 31.1 and 31.2).



Fig. 31.1 Stir casting setup

Fig. 31.2 Hardness test, tensile test and impact test specimens



31.3.3 Mechanical Testing

The samples were manufactured for mechanical testing of samples. The samples were manufactured as per ASTM standards. The samples were polished for optical microscopy.

31.4 Results and Discussion

31.4.1 Microstructural Examination

The samples for optical microscopy were polished using various emery papers. The polishing machine was used for final polishing. The etchant was used properly for seeing grain boundaries in microscope. It was observed the bagasse particles were uniformly distributed in the mixture. The optical photographs were shown here for various percentages as shown in figures here (Figs. 31.3, 31.4, 31.5, 31.6; Tables 31.1, 31.2).

It was found from the experimental results that the tensile strength of the MMCs was enhanced the results of tensile test were tabulated here. It can be noted that the increase percentage of reinforcement particles enhances the tensile strength of the MMCs. It was found that there was increase in UTS of cast composite samples due to presence of hard ceramic particles. It was maximum in case of 20% Al_2O_3 and minimum in case of 5% Al_2O_3 . The increment in UTS was due to increase in dislocation density in the melt mixture. It was also due to difference of thermal properties of both the phases in cast samples. The hardness of samples was measured using vicker hardness testing. It was found that hardness of samples enhances due to reinforcement of bagasse particles. It was found that there was a decrease in elongation

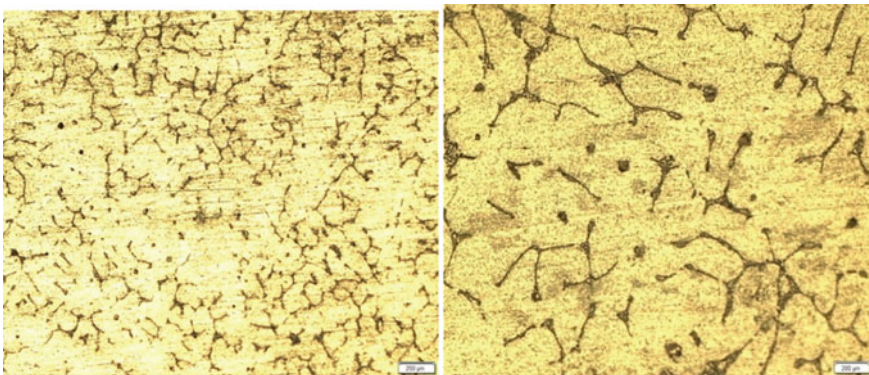


Fig. 31.3 Microscopic view of 1% Bagasse Ash reinforced Al at 100X and 200X

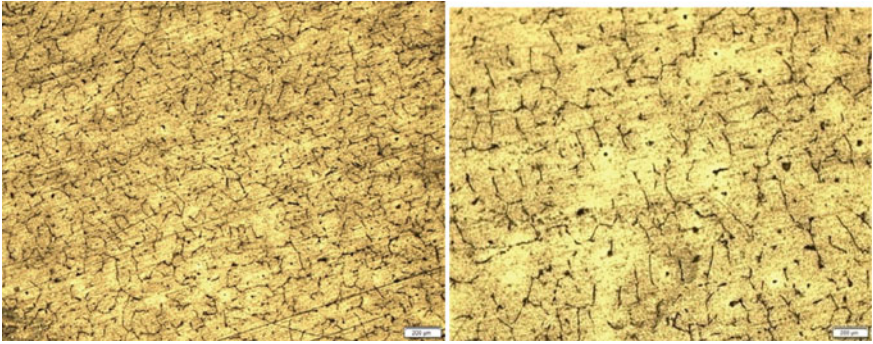


Fig. 31.4 Microscopic view of 3% Bagasse Ash in Al at 100X and 200X

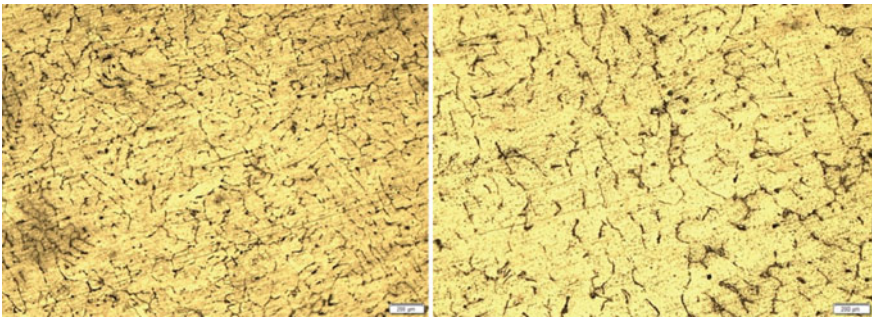


Fig. 31.5 Microscopic view of 5% Bagasse Ash reinforced in Al at 100X and 200X

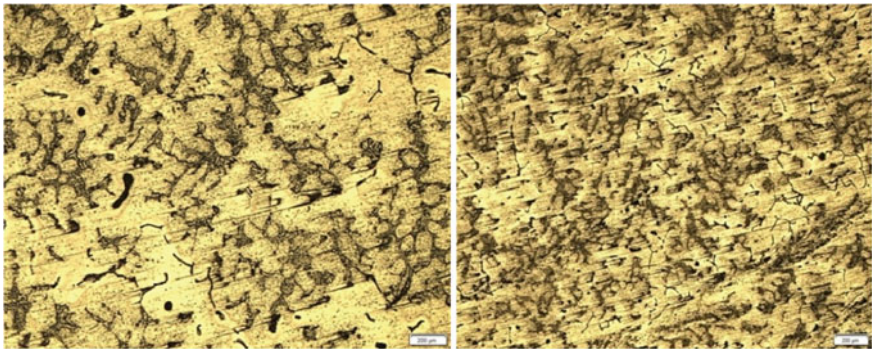


Fig. 31.6 Microscopic view of 7% Bagasse Ash reinforced in Al at 100X and 200X

Table 31.1 Hardness and tensile test results

Sample no	Reinforcement (%)	Hardness (VHN)	UTS (N/mm ²)	Yield stress	Elongation (%)
1	1	77	118	96.5	9.5
2	3	86	129	101	9.7
3	5	94	70.5	53.9	2.8
4	7	115	56	42	1.6

Table 31.2 Impact toughness test results

Sample no	Sample name (%age reinforcement)	Impact energy (J)
1	1% Bagasse Ash	150
2	3% Bagasse Ash	166
3	5% Bagasse Ash	140
4	7% Bagasse Ash	120

which is due to brittle nature of Bagasse Ash particles. The toughness of samples were improved initially but then decreased due to brittle nature of reinforcement particles.

31.5 Conclusions

The ends drawn from the current examination are:

- The Hardness of MMCs samples were more than the matrix phases. As we increased the percentage composition of our Bagasse Ash component hardness of the metal matrix composite increased.
- Tensile strength of our MMC increased as we introduced the Bagasse Ash reinforcement and kept on increasing till 3% but it dropped substantially as it went past 3%.
- The toughness of the MMC reduced as we kept on increasing the Bagasse Ash content.
- The micro structural observations confirmed the presence of bagasse particles in mixture. It was observed that as the percentage of Bagasse ash increases in our MMC, it lead to agglomeration effect.

References

1. Aigbodion, V.S., Hassan, S.B., Dauda, E.T., Mohammed, R.A.: Experimental study of ageing behaviour of Al-Cu-Mg/bagasse ash particulate composites. *J. Tribol. Indus.* **33**(1), 28–35 (2011)
2. Srinivasan, R., Sathiya, K.: Experimental study on Bagasse ash in concrete. *Int. J. Serv. Learn. Eng.* **5**, 60–66 (2010)
3. Patil, S.R., Motgi, B.S.: A study on mechanical properties of fly ash and alumina reinforced aluminium alloy (LM25) composites. *IOSR J. Mechan. Civil Eng. (IOSR-JMCE)* **7**(6), 41–46 (2013)

Chapter 32

Analysis of the Surface Roughness Characteristics of EDMed Components Using GRA Method



Vidyapati Kumar and Shankar Chakraborty

Abstract The mechanical efficiency of two mating surfaces is significantly affected by the values of their surface roughness, which is also related to increased friction and their tribological performance. In this paper, during generation of holes on D3 tool steel material, the machining capability of an electrical discharge machining (EDM) process is investigated, while considering pulse-on time, pulse-off time and peak current as the controllable parameters. Various surface roughness characteristics, like Rt, Ra, Rq, Rsk, Rz, Rku, Rk, Mr1 and Mr2 are contemplated here as the process outputs because achievement of better tribological properties with low wear significantly depends on those responses. During the experimental trials, pulse-on time is varied from 90 to 250 μs , whereas, the values of pulse-off time and peak current are altered from 45 to 150 μs and 14 to 22 A respectively. Multi-objective optimization of the considered EDM process is accomplished using grey relational analysis (GRA) technique. Confirmation experiment is also carried out to confirm the betterness of the optimal parametric intermix for the said EDM process. It is observed that almost all the surface roughness properties of the EDMed components are mainly influenced by pulse-on time, followed by peak current.

Keywords EDM process · Surface roughness · Central composite design · Optimization

32.1 Introduction

Electrical discharge machining (EDM) is an extensively utilized unconventional machining process for difficult-to-cut materials and alloys which are hard to machine using the conventional material removal techniques with excellent surface finish and dimensional accuracy. It is a thermal and electrical energy-based process where material is removed from the workpiece due to erosive effects caused by a series

V. Kumar (✉)

Central Institute of Mining and Fuel Research, Dhanbad, Jharkhand, India

S. Chakraborty

Department of Production Engineering, Jadavpur University, Kolkata, India

of sparks produced between the work material and tool submerged in a dielectric fluid. Generally, deionized water or kerosene is utilized as the dielectric medium. The sparks produce the impulsive pressure by dielectric explosion which generates a high temperature of around 10,000 °C, resulting in melting as well as vaporization of the work material [5]. With the help of dielectric liquid, the eroded debris from the spark gap is rinsed away. This paper deals with the study of the influences of various controllable factors of an EDM process on its responses (outputs) while machining D3 grade tool steel material. For this EDM process, pulse-on time, pulse-off time and peak current are considered as the controllable parameters, whereas, various surface roughness characteristics of the machined components are treated as the responses.

In the EDM process, a perfect replication of the tool shape is generated on the work material. It is especially appropriate for generating intricate shape profiles on electrically conductive materials with low machinability. Since there is no direct contact between the tool and the work material, this operation is free from any mechanical stress generation, chatter/burr formation and vibration problem. Its machining performance is also uninfluenced by the hardness of the work material because the removal of material occurs due to melting at elevated localized heat generation. Since no cutting force is involved in this process, extremely deep narrow holes having higher aspect ratio can be machined with minimum tool wear. It can even generate intricate cavities in a single operation. But, this process suffers from several drawbacks, like generation of recast layer, low material removal rate, high machining time along with the related cost, low flexibility, capability of machining only electrically conductive materials etc.

For machining a particular material, there is a large pool of input variables that can be controlled during the EDM operation. During actual machining operation, it is quite difficult to examine all the EDM process parameters, because the experimental time as well as the related cost would proportionately increase with the number of input parameters. It has been noticed that the machining performance of an EDM operation with respect to material removal rate, surface roughness, tool wear rate, radial overcut etc. is significantly affected by different electrical controllable factors (peak current, pulse-on time, pulse-off time, polarity, gap voltage etc.) and non-electric controllable factors (electrode material, type of the dielectric used, dielectric pressure, rotation of the electrode etc.). Thus, to fulfil the requirements of better response values, it is always preferred to operate an EDM set-up while maintaining the settings of its different input parameters as their optimal levels. It would also lead to higher production rate with reduced machining time. The literature analysis, however, reveals that three main input parameters in the form peak current, pulse-on time and pulse-off time typically control the machining performance of the EDM operation. Keeping in mind the basic objective of this paper, it endeavours to apply grey relational analysis (GRA) technique to explore the influences of these three controllable EDM parameters on various surface roughness characteristics of the machined components while machining D3 grade tool steel material. The adoption of this technique also helps in searching out the optimal parametric intermix of the considered EDM process for attaining the best possible values of the responses (outputs).

Thus, in this paper, pulse-on time, pulse-off time and peak current are considered as the process parameters, whereas, nine most important surface roughness characteristics, i.e. maximum magnitude of surface roughness (R_t), arithmetic average deviation of the profile (R_a), root-mean-square deviation of the profile (R_q), skewness of the amplitude distribution (R_{sk}), average maximum height of the profile (R_z), kurtosis of the amplitude distribution (R_{ku}), depth of the core roughness (R_k), material components of the peaks (Mr_1) and material components of the valleys (Mr_2) are treated as the responses. Finally, the computed grey relation grade (GRG) values measured would assist the concerned process planners to evaluate the most appropriate configuration of the NTM process parameters as well as optimize all the competing performance measures. Therefore, implementation of this multi-objective optimization tool would enhance the operational efficiency of the EDM processes.

32.2 Review of the Literature

Lee and Li [10] analyzed the significance of different input parameters of an EDM process while machining tungsten carbide work material and attempted to correlate them with the achieved surface finish of the machined components. Özdemir and Özek [12] studied the machining potential of a wire EDM process during machining of cast iron material, and adopted regression analysis coupled with statistical simulation to explore the relationships between various input parameters and surface roughness properties. Tomadi et al. [18] developed the corresponding mathematical models for identification of the most influential EDM process parameters and modelled surface roughness with respect to those parameters during machining of tungsten carbide work material. Kumar and Hariharan [7] explored the machining capability of an EDM process on ductile iron material and modelled surface finish based on variations of different input parameters. It can thus be propounded that there is always a need to propose new models for investigating the surface quality on the machined components for varying combinations of the process parameters or new workpiece-tool combination. Hence, for prediction of surface finish of the EDMed components, new models need to be developed. Surface roughness is also perceived to be an indicator of product consistency [16]. Different machining processes were studied by Benardos and Vosniakos [1], and it was concluded that varying surface roughness parameters could be considered to describe mechanical properties of the mating surfaces. Petropoulos et al. [13] also evaluated and characterized surface texture related to various machining processes. De Chiffre et al. [2] pointed out that despite the wide application of 2D surface parameters, it would not be enough for the explanation of the functionality of the mating surfaces because they would also interact in three dimensions rather than only in two dimensions.

Ramasawmy and Blunt [14] reported that the functional characteristics of the surfaces of the machined components would significantly depend on various combinations of the corresponding surface roughness parameters. Deleanu et al. [3]

attempted to analyze surface texture parameters, and stated that if the initial magnitudes of those parameters, such as arithmetic mean deviation of the surface, RMS deviation of the height difference of the surface and surface segment etc. were high, wear generated in a machined surface would also be higher. Sedlaček et al. [15] studied the influences of surface quality in lubricated and dry conditions. It was reported that during dry wear test, friction coefficient would be low at higher surface roughness. On the other hand, during lubricated case, friction coefficient would also be low at smaller surface roughness. An increase in kurtosis topographic height distribution would also result to an increase in friction during lubrication and a reduction in friction at dry state. When skewness of the amplitude distribution would approach to be more negative in lubricated samples, lower value of friction could be achieved. Input process parameter optimization is thus a critical process and can serve as a guide to define the set of the most influential EDM process parameters influencing the machining performance.

Based on Taguchi's design strategy, Mazarbhuiya et al. [11] carried out eight experimental runs in an EDM set-up, and employed GRA technique to decide the optimal settings of discharge current, flushing pressure, pulse-on time and polarity of the tool to accomplish the targeted values of material removal rate and surface roughness. While treating peak current, polarity of the tool, pulse-on time, gap voltage and tool spindle speed as the input variables of an EDM operation, Gohil and Puri [6] adopted Taguchi-GRA technique to maximize material removal rate and minimize surface roughness during machining of titanium alloys. Tharian et al. [17] conducted simultaneous optimization of material removal rate and surface roughness during EDM operation of Al7075 alloy based on GRA technique. Kumar and Kumar [8] utilized GRA methodology to find out the desired operating levels for various EDM process parameters, i.e. electrode setting, discharge current, pulse-on time and gap voltage, while treating material removal rate, electrode wear rate and surface roughness as the critical responses. Material removal rate and tool wear rate were viewed by Laxman and Guru Raj [9] as the two major respondents during EDM operation, and GRA technique was later utilized to single out the optimal settings of various input variables of the said process. Multi-response optimization of different unconventional machining operation has always remained a subject of immense research interest since the past few years and GRA technique has been efficiently deployed by the previous researchers for this purpose. It has already established itself as a popular tool for deriving the best possible combinations of different controllable parameters of diverse machining processes in order to achieve the targeted response values.

32.3 GRA Technique

Deng [4] first proposed the principle of grey system, in which grey means the rudimentary data in a system that is underprivileged, incomplete and indeterminate. Grey relation describes the insufficient relationship of knowledge within a given dataset. The GRA technique performs a comparative analysis between quantitative

data sequences, thus determining the degree of relationship between the ideal order and an empirical order (response values). The calculated degree of sequence similarity is referred to as the grey relational coefficient (GRC). If two values of the components considered seem to be of similar significance, the subsequent GRC value would be 1. Thus, in GRA technique, multi-response variables can be mapped to a single GRG value while considering the average GRC values for every data series (response). When the GRG value for an alternative is observed to be higher than that of the others, it can be identified to be the most preferred choice.

The Taguchi approach was historically adopted to evaluate the most relevant process parameters for a single quality characteristic. It was thus specifically aimed at maximizing a single quality characteristic. However, products have multiple quality characteristics in order to satisfy customers' requirements. The Taguchi approach employs engineering intuition to single out the optimal factor levels for achieving targeted response values, which may often lead to uncertainty during the decision making process. This drawback can be efficiently overcome by the principle of grey system theory. This approach transforms the defined multiple quality characteristics into single GRG values. In order to derive the optimal operating levels of various process variables, the calculated GRG values are contrasted so as to meet the requirements of attaining the most favoured response values.

In GRA technique, the earliest phase starts with the development of a decision matrix comprising n criteria (responses) and m alternatives (experimental trials). The steps used in GRA technique are presented as follows:

32.3.1 Step 1: Normalization

The values in the decision matrix are initially normalized to bring them within a range of 0 to 1 in order to minimize variance and make them dimensionless. Based on the type of the quality attribute under consideration, the following equations for normalization can be employed.

For higher-the-better characteristic:

$$p_i^*(j) = \frac{p_i(j) - \min p_i(j)}{\max p_i(j) - \min p_i(j)} \quad i = 1, 2, \dots, m \text{ and } j = 1, 2, \dots, n \quad (32.1)$$

For lower-the-better characteristic:

$$p_i^*(j) = \frac{\max(j) - p_i(j)}{\max p_i(j) - \min p_i(j)} \quad (32.2)$$

where $p_i(j)$ and $p_i^*(j)$ are the measured and normalized values for i^{th} alternative with respect to j^{th} criterion respectively.

32.3.2 Step 2: Computation of Grey Relational Coefficient

For each response, the corresponding GRC values are computed using Eq. (32.3) from the normalized data. The association between the best and the normalized values is represented using these GRC values.

$$\xi_i(j) = \frac{\delta_{\min} + \eta\delta_{\max}}{\delta_{0i}(j) + \eta\delta_{\max}} \quad (32.3)$$

where $\delta_{0i}(j)$ is the deviation between the values, $p_i^0(j)$ (ideal order) and $p_i^*(j)$, and η is the distinguishing coefficient which takes a value between 0 and 1 ($\eta = 0.5$ is usually preferred). It is mainly responsible for expansion or compression of the range for GRC values. Moreover, $\delta_{\min} = \forall j^{\min} \in i \forall j^{\min} \|p_0(j) - p_j(j)\|$ is the minimum value of δ_{0i} , and $\delta_{\max} = \forall j^{\max} \in i \forall j^{\max} \|p_0(j) - p_j(j)\|$ is the maximum value of δ_{0i} . Higher value of GRC indicates an alternative to be closer to the desired solution with regard to a particular criterion.

32.3.3 Step 3: Computation of Grey Relational Grade

The GRG values are finally computed while taking into account the average GRC values of the considered criteria for each of the alternatives.

$$G_i = \frac{1}{n} \sum_{j=1}^n \xi_i(j) \quad (32.4)$$

The experimental trial with the highest GRG value is recognized to be the most favoured alternative revealing its dominance over the others for a said machining application. The procedural steps for the application of GRA technique are portrayed in Fig. 32.1.

32.4 Experimental Details

Keeping in mind the basic objective of this paper, experimental trials are conducted for generating holes on D3 grade tool steel material using an EDM set-up, considering pulse-on time, pulse-off time and peak current as the controllable process parameters. This work material has high carbon and chromium contents, exhibiting excellent resistance to abrasion. It has found wide-ranging applications in plastic moulds, brick and tile mould liners, punches etc. It can also be used in the blanking process

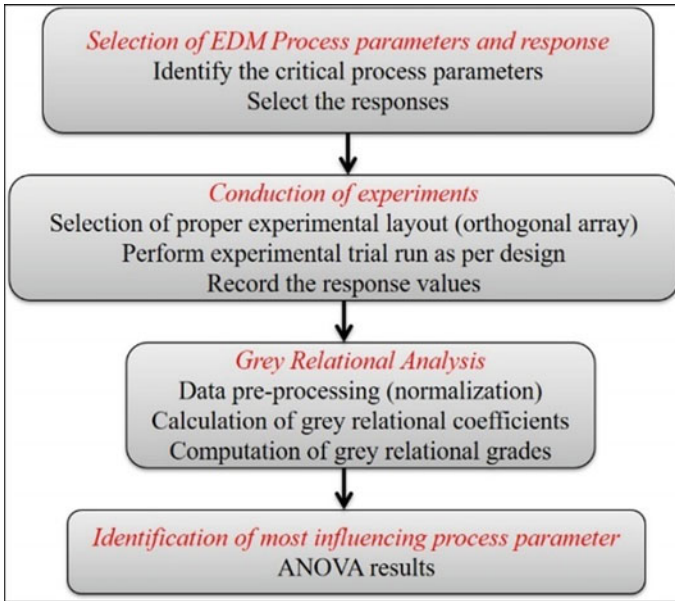


Fig. 32.1 GRA technique for parametric optimization of the EDM Process

for complex applications. Its chemical composition and mechanical properties are presented in Tables 32.1 and 32.2 respectively.

During the EDM operation on D3 grade tool steel material, values of each of the considered parameters are varied at five different operating levels, as provided in Table 32.3. According to the three-factor five-level central composite design plan, 20 experiments are conducted in an Oscar Max EDM machine. The technical specifications of this set-up are provided in Table 32.4 and its photograph is shown in Fig. 32.2. During the machining operation, Castrol SE 180 EDM fluid is used as the

Table 32.1 Chemical composition of D3 grade tool steel material

Element	C	Si	Mn	P	S	Cr	Ni	Mo	V	Cu	Al	Others
%	2.1	0.29	0.21	0.03	0.04	11.35	0.16	0.08	0.06	0	0.002	85.678

Table 32.2 Mechanical properties of D3 grade tool steel

Mechanical property	Value
Tensile strength	970 MPa
Yield strength	850 MPa
Hardness	28 HRC
Density	7.86 gm/cm ³
Heat conductivity	20 W/m K

Table 32.3 Process Parameters of the EDM with their operating levels

Process parameter	Symbol	Unit	Level				
			-2	-1	0	1	2
Pulse-on time	T _{on}	Ms	90	120	150	200	250
Pulse-off time	T _{off}	Ms	45	60	90	120	150
Peak current	I	A	14	16	18	20	22

Table 32.4 Oscar Max EDM specifications

Make	Taiwan
Model	Oscar S 430
Travel	[X400 Y300 Z300] mm
Accuracy	0.02 mm/300 mm



Fig. 32.2 EDM set-up

dielectric fluid because of its various advantageous properties, like low odour, higher stability with extended life, low viscosity, high flash point, increased reliability and safe use. The specimen size is taken as 15 × 40 mm.

It is worthwhile to mention here that all the 20 experiment runs are performed here in random order to minimize the machining error. Nine most important surface roughness characteristics, i.e. Rt, Ra, Rq, Rsk, Rz, Rku, Rk, Mr1 and Mr2 are treated as the responses. A profilometer (Mitutoyo make) with skid-less stylus having cut-off length 2.5 mm is utilized for measurement of those surface roughness parameters. Table 32.5 displays the experimental layout along with the measured values of the considered responses. In Fig. 32.3, the photographs of the copper electrode utilized during EDM operation and the machined component are provided (5 mm depth and 20 mm diameter).

Table 32.5 Details of the experimental results

Exp. No.	T _{on}	T _{off}	I	Rt (μm)	Ra (μm)	Rq (μm)	Rsk (μm)	Rz (μm)	Rku (μm)	Rk (μm)	Mr1 (%)	Mr2 (%)
1	150	90	18	79.4790	11.4527	12.7630	0.5203	56.5120	3.9010	42.2465	16.7500	80.1400
2	120	120	20	23.2890	11.0620	14.3190	0.5374	58.3090	3.1520	35.0080	8.0700	86.5600
3	150	90	18	88.1110	10.9770	13.0470	0.1671	47.7420	3.0218	41.3840	17.4800	88.4200
4	200	120	20	82.2390	11.0910	13.7320	0.2987	50.5170	3.0667	31.8520	7.1400	82.8500
5	120	60	20	72.0470	12.3540	15.9090	0.2121	50.1080	2.3092	36.8560	8.0400	93.1400
6	150	90	18	66.7890	12.1270	15.3580	0.6021	62.9110	3.1329	49.9200	12.2600	97.3400
7	120	120	16	57.3340	14.5480	17.6160	0.2273	61.8780	2.7097	40.4960	5.8000	90.2300
8	200	120	16	107.6330	12.0530	16.3460	0.8099	57.3600	5.3160	36.8240	8.8900	82.1100
9	150	90	18	73.8150	14.8140	18.1380	0.0738	57.5510	2.3045	43.9840	12.0000	87.4500
10	200	60	16	65.2480	13.3480	17.2210	0.5625	68.8870	3.3903	43.6640	8.4500	88.2400
11	200	60	20	54.9390	9.4060	11.9320	0.7935	45.5290	3.2486	30.6400	12.4500	94.9100
12	90	90	18	88.7300	10.6620	14.6460	0.7293	50.3080	4.9092	32.1440	11.2400	86.7900
13	250	90	18	75.1110	9.6120	12.3820	0.3062	48.7120	3.0777	25.7760	9.0000	76.6700
14	150	150	18	82.0410	13.0040	16.5580	0.1183	61.8710	2.7973	40.5520	5.0400	88.4600
15	150	90	18	79.7720	12.4560	15.8250	0.1929	56.1150	2.3483	36.7360	9.6500	86.3000
16	120	60	16	88.0080	11.3370	14.5130	0.4315	56.5120	2.5710	36.0960	10.7200	88.4100
17	150	90	22	67.5810	11.5410	15.2230	0.1239	61.3470	2.7821	37.5600	9.4100	88.3400
18	150	90	14	82.4020	11.9170	14.7570	0.2091	57.3570	2.7288	39.4240	8.1500	88.3900
19	150	45	18	80.4265	11.8149	13.6247	0.4278	56.5789	3.2465	40.1278	9.1245	84.2314
20	150	90	18	83.1282	12.1269	13.7945	0.5249	56.1783	3.5287	42.6515	13.1487	86.1785



Fig. 32.3 Round copper tool and the machined component

32.5 Results and Discussions

The GRA technique is now applied to search out for the most favourable combination of the EDM process parameters which is responsible for simultaneous minimization of all the considered surface roughness characteristics. As all the surface roughness characteristics are ‘lower-the-better’ type attributes, the experimental values of Table 32.5 are pre-processed using Eq. (32.2) to convert them to a normalized range between 0 and 1. Based on these normalized data, the corresponding GRC and GRG values are subsequently estimated in Table 32.6. It can be noticed that experimental trial number 13 with the maximum GRG value gives the optimal parametric mix for this EDM operation for simultaneous optimization of all the surface roughness characteristics under consideration. Figure 32.4 provides the calculated GRG values for all the 20 experimental trials. The response table for these GRG values is presented in Table 32.7, developed based on averaging the GRG values at the corresponding operating levels of the EDM process parameters. In this table, boldface highlights the highest GRG value for each of the process variables. It can be observed from Table 32.7 that in order to achieve the most favoured values of all the surface roughness characteristics, the corresponding input variables of the EDM process need to be set at $T_{on} = 250 \mu s$, $T_{off} = 60 \mu s$ and $I = 20 A$.

In Table 32.7, the difference between the highest and lowest GRG values signifies the influence of each of the EDM process parameters on the responses. Thus, it can be observed that for the said EDM operation, the surface roughness characteristics are primarily affected by pulse-on time, followed by peak current. The derived optimal settings of the EDM process parameters can also be validated based on the response graph, as shown in Fig. 32.5. The maximum steepness of pulse-on time identifies it as the most prominent EDM process variable. The analysis of variance (ANOVA) results based on GRG values, exhibited in Table 32.8, also ensure the maximum

Table 32.6 GRG values for the experimental trials

Exp. No.	Rt	Ra	Rq	Rsk	Rz	Rku	Rk	Mr1	Mr2	GRG	TOPSIS score
1	0.4287	0.5692	0.7888	0.4518	0.5154	0.4854	0.4229	0.3469	0.7486	0.5286	0.5648
2	1.0000	0.6202	0.5652	0.4425	0.4775	0.6399	0.5667	0.6724	0.5110	0.6106	0.6455
3	0.3942	0.6325	0.7357	0.7976	0.8407	0.6773	0.4361	0.3333	0.4680	0.5906	0.4611
4	0.4170	0.6161	0.6329	0.6206	0.7007	0.6639	0.6652	0.7476	0.6258	0.6322	0.6534
5	0.4638	0.4784	0.4383	0.7268	0.7184	0.9969	0.5214	0.6746	0.3856	0.6005	0.5941
6	0.4922	0.4984	0.4753	0.4106	0.4019	0.6451	0.3333	0.4628	0.3333	0.4503	0.4011
7	0.5533	0.3446	0.3531	0.7056	0.4167	0.7880	0.4506	0.8911	0.4325	0.5484	0.5450
8	0.3333	0.5053	0.4128	0.3333	0.4968	0.3333	0.5221	0.6177	0.6552	0.4678	0.4600
9	0.4549	0.3333	0.3333	0.9997	0.4928	1.0000	0.3987	0.4719	0.4895	0.5527	0.5950
10	0.5013	0.4069	0.3698	0.4296	0.3333	0.5810	0.4029	0.6459	0.4718	0.4603	0.4640
11	0.5713	1.0000	1.0000	0.3384	1.0000	0.6146	0.7128	0.4563	0.3617	0.6728	0.6620
12	0.3919	0.6828	0.5334	0.3596	0.7096	0.3663	0.6547	0.5008	0.5053	0.5227	0.5521
13	0.4487	0.9292	0.8733	0.6129	0.7858	0.6607	1.0000	0.6110	1.0000	0.7691	0.7421
14	0.4179	0.4291	0.4015	0.8919	0.4168	0.7534	0.4496	1.0000	0.4671	0.5808	0.5912
15	0.4275	0.4699	0.4435	0.7554	0.5245	0.9717	0.5241	0.5743	0.5177	0.5787	0.5647
16	0.3945	0.5834	0.5459	0.5071	0.5154	0.8496	0.5391	0.5227	0.4682	0.5473	0.5246
17	0.4877	0.5588	0.4853	0.8800	0.4247	0.7592	0.5060	0.5873	0.4697	0.5732	0.6081
18	0.4164	0.5185	0.5234	0.7311	0.4968	0.7802	0.4694	0.6667	0.4686	0.5634	0.5578
19	0.4247	0.5289	0.6470	0.5097	0.5138	0.6152	0.4569	0.6036	0.5775	0.5419	0.5341
20	0.4134	0.4984	0.6249	0.4493	0.5231	0.5516	0.4170	0.4341	0.5208	0.4925	0.4032

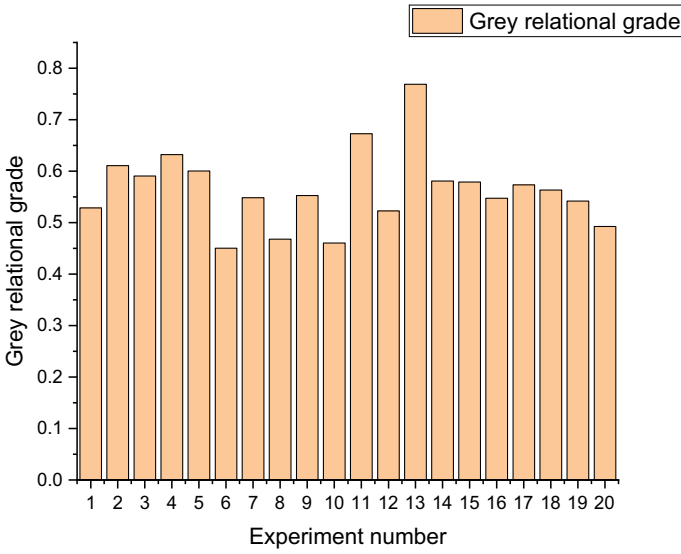


Fig. 32.4 GRG values for the experiment trials

Table 32.7 Response table for GRG values

Process parameter	Level					Max–Min	Rank
	–2	–1	0	1	2		
Pulse-on Time	0.5227	0.5767	0.5416	0.5583	0.7691	0.2464	1
Pulse-off Time	0.5419	0.5702	0.5659	0.5647	0.5808	0.0389	3
Peak current	0.5634	0.5059	0.5608	0.6290	0.5732	0.1231	2

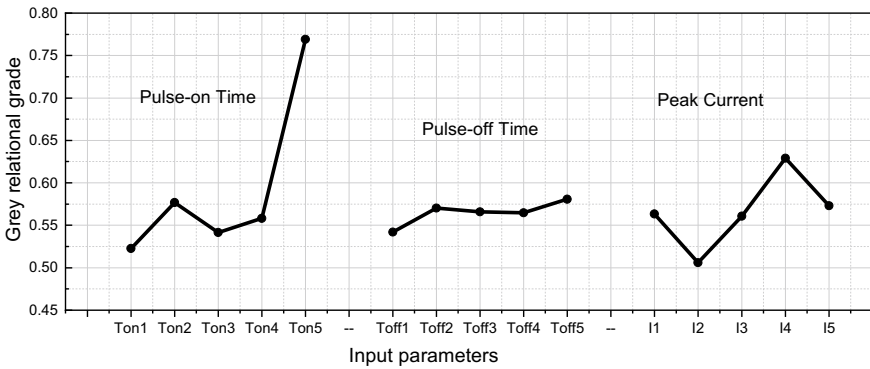


Fig. 32.5 Response graph for GRG values

Table 32.8 ANOVA results for EDM process

Source	DF	Seq SS	Adj SS	Adj MS	F	% Contribution
T _{on}	2	0.045679	0.045679	0.022840	6.46	55.98
T _{off}	2	0.013672	0.013672	0.006836	1.93	16.75
I	2	0.015181	0.015181	0.007591	2.15	18.60
Error	2	0.007072	0.007072	0.003536		8.67
Total	8	0.081605				

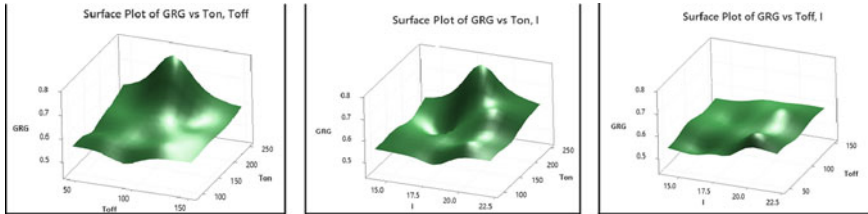


Fig. 32.6 Surface plots indicating the effects of various EDM process variables on GRG value

contribution of pulse-on time in dominating the measured surface roughness values. The related surface plots are also developed, as depicted in Fig. 32.6, displaying the impacts of different EDM process parameters on the estimated GRG values.

32.5.1 Effect of Pulse-On Time

It is noticed from the ANOVA table that pulse-on time plays the pivotal role in influencing all the considered surface roughness characteristics of the EDMed components. As in EDM process, material is removed due to formation of craters resulted from the sparks, greater crater sizes lead to rough surfaces. Thus, the dimension of the crater, which primarily relies on the energy per spark, controls the consistency of the machined surface. The surface roughness increases as pulse energy increases. In other words, surface roughness characteristics are significantly affected by higher pulse energy available during higher pulse-on time. Based on the distance between the highest peak and the lowest valley located along the evaluation length, Rt is the maximum profiler height across the surface profile. Its value also drastically increases due to rise in pulse-on time. It has been noticed that a discharge channel is developed during the EDM operation that contributes to material removal. When pulse-on time increases, discharges are formed on the surface more rapidly resulting in higher roughness due to excessive erosion. The Ra is the profile’s arithmetic average deviation which also increases with increased pulse-on time. The estimated maximum profiler height Rz is estimated along the cut-off lengths as the gap between the highest

peak and the lowest valley, which shows an increasing trend with higher pulse-on time.

The depth of core roughness, R_k is obtained from the ISO 13,565-2:1996 standard bearing area curve [14]. The bearing area curve is developed for each surface profile while simulating a horizontal line passing from the top-down across the profile, assessing the percentage of contact that the line would make with the surface at each step. Since an increase in pulse-on time contributes to an increase in the width of the discharge channel, the depth of core roughness is thereby increased. The root-mean-square deviation from the mean line (R_q) depends on the peaks and valleys of the profile, which would again rise with an increase in pulse-on time.

The third central moment of the probability density function of the profile amplitude, also referred to as the skewness of amplitude distribution (R_{sk}), usually varies between 0 and 1. It also increases when pulse-on time increases. The fourth central moment of the probability density function of the profile amplitude intensity or kurtosis of the 3D surface texture's amplitude distribution (R_{ku}), exhibits an increasing trend with increase in pulse-on time as the deviation from the ideal standard profile distribution also changes. The fractions of a line that slice through the material at a given height above and below the mean line while sectioning a profile are popularly referred to as material components of the peaks (Mr_1) and material components of the valleys (Mr_2) respectively. If the distance of the peak from the mean line increases, the value of Mr_1 would rise with reduction in pulse-on time. Higher pulse-on time results in an increase in Mr_2 value.

32.5.2 Effect of Pulse-Off Time

Pulse-off time is the time gap between successive sparks during EDM operation when current is not supplied to the electrodes and thus, dielectric deionization takes place. As the dielectric flushes the debris from the machining gap during the pulse-off time, it also plays a crucial role in controlling the surface roughness parameters, although it has only 16.75% contribution, as noticed from the ANOVA results. Flushing of debris can properly take place when pulse-off time is longer. At higher pulse-off time, R_t value would be smaller. As the distances between peaks and valleys decrease at higher pulse-off time, lower values of both R_a and R_z can be obtained. It can be unveiled that the value of R_k does not significantly vary with changing values of pulse-off time, as it depends on the bearing area curve developed by simulating a horizontal line passing through the surface profile. As the R_q also depends on the peaks and valleys of the profile, its lower value can be attained at higher pulse-off time. In the similar direction, higher pulse-off time would be responsible for lower values of both R_{sk} and R_{ku} . With rise in pulse-off time, Mr_1 value decreases as the distances of the peaks from the mean line are reduced due to proper flushing of the eroded material. On the other hand, as a rise in pulse-off time increases the valley size, Mr_2 value of the machined surface is supposed to decrease.

32.5.3 Effect of Peak Current

In EDM operation, peak current is the amount of energy effectively utilized for material removal. It is the highest amount of current available from the power supply at each pulse. It can be revealed that all the values of Rt, Ra and Rz increase with higher peak current due to formation of more crater on the machined surface. Similarly, higher peak current is accountable for poor quality of the machined surface with respect to higher values of Rk, Rq, Rsk and Rku. As a rise in peak current results in pulse's high energy, the peak length decreases and the valley length rises from the mean line, resulting in decrease of Mr1 and increase of Mr2.

32.5.4 Confirmation Test

The TOPSIS (technique for order of preference by similarity to ideal solution) approach is a well accepted multi-criteria decision making tool which recognizes the optimal solution based on the longest distance from the anti-ideal solution and shortest distance from the ideal solution [19]. A validation test based on TOPSIS exhibits that experiment number 13 (shown in Table 32.6) provides the optimal parametric combination for multi-response optimization of the EDM operation, as depicted in Fig. 32.7.

The predicted GRG (GRG_p) value at the optimal parametric combination is estimated using Eq. (32.5) to justify the applicability and potentiality of GRA technique in improving the machining performance of the said EDM process.

$$GRG_p = GRG_m + \sum_{i=1}^n (\overline{GRG}_i - GRG_m) \quad (32.5)$$

where GRG_m is the average GRG value calculated for all the observational trials performed, n is the number of input parameters and \overline{GRG}_i is the mean value of GRG with respect to the i^{th} optimal level of a process parameter. From Table 32.9, it can be revealed that the GRG value predicted at the derived optimal parametric intermix is better than that calculated at the initial experimental trial ($T_{\text{on}} = 150 \mu\text{s}$, $T_{\text{off}} = 90 \mu\text{s}$ and $I = 18 \text{ A}$). A confirmatory test run is also performed at the optimal combination of $T_{\text{on}} = 250 \mu\text{s}$, $T_{\text{off}} = 150 \mu\text{s}$ and $I = 20 \text{ A}$, and the corresponding values of all the surface roughness characteristics under consideration are measured. It can be confirmed from Table 32.9 that the derived optimal parametric mix causes improvements in Rt, Ra, Rq, Rsk, Rz, Rku, Rk, Mr1 and Mr2 by 6.74, 20.33, 5.03, 76.75, 68.40, 48.42, 48.42, 44.80, 69.07, and 4.49% respectively, with an overall increment in GRG value by 45.48%.

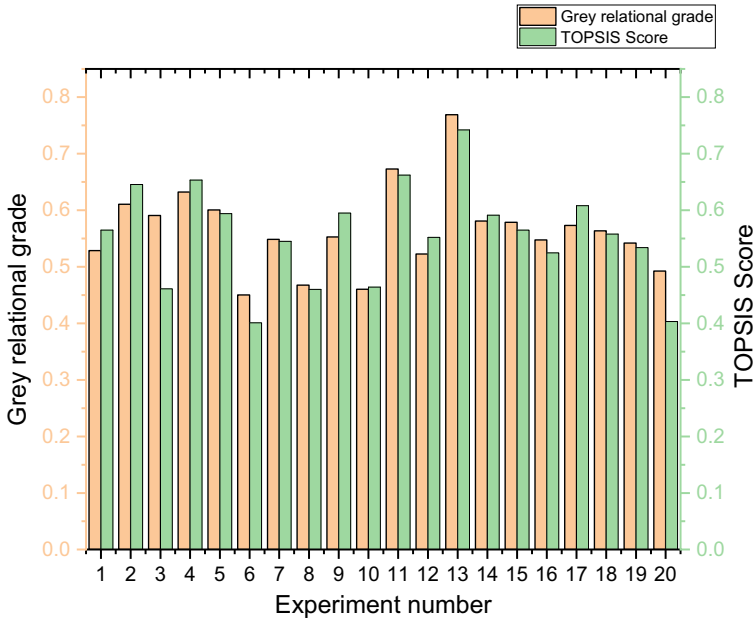


Fig. 32.7 Comparison between GRG and TOPSIS scores

Table 32.9 Comparison of the response values

Response	Initial parametric combination	Optimal parametric combination		% Improvement
	$T_{on} = 150 \mu s, T_{off} = 90 \mu s, I = 18 A$	$T_{on} = 250 \mu s, T_{off} = 150 \mu s, I = 20 A$		
		Predicted	Experimental	
$R_t (\mu m)$	79.4790		74.12	6.74
$R_a (\mu m)$	11.4527		9.124	20.33
$R_q (\mu m)$	12.7630		12.121	5.03
$R_{sk} (\mu m)$	0.5203		0.1644	76.75
$R_z (\mu m)$	56.5120		48.517	68.40
$R_{ku} (\mu m)$	3.9010		2.0123	48.42
$R_k (\mu m)$	42.2465		23.321	44.80
$Mr_1 (\%)$	16.7500		5.18	69.07
$Mr_2 (\%)$	80.1400		76.54	4.49
GRG	0.5286	0.7698	0.7690	45.48

32.6 Conclusions

This paper investigates the effects of pulse-on time, pulse-off time and peak current on Rt, Ra, Rq, Rsk, Rz, Rku, Rk, Mr1 and Mr2 during EDM operation on D3 tool steel material. A multi-objective optimization tool in the form of GRA technique is employed for identifying the best parametric intermix for the said process. Based on this experimental study, the following inferences can be drawn:

- (a) The corresponding EDM process parameters must be set at pulse-on time = 250 μ s, pulse-off time = 150 μ s and peak current = 20 A to obtain the most favourable response values.
- (b) With a contribution of 55.98% in deciding the GRG values, pulse-on time appears out as the most vital EDM process parameter, accompanied by peak current with a contribution of 18.60%.
- (c) The confirmatory tests demonstrate that the values of Rt, Ra, Rq, Rsk, Rz, Rku, Rk, Mr1 and Mr2 can be improved by 6.74, 20.33, 5.03, 76.75, 68.40, 48.42, 44.80, 69.07 and 4.49% respectively at this optimal parametric combination.
- (d) The GRG value is also enhanced by 45.48% at this combination as compared to the initial machining condition.

It can thus be concluded that in obtaining the optimal parametric combination of the considered EDM operation, GRA approach with a sound mathematical foundation can be effectively deployed.

References

1. Benardos, P.G., Vosniakos, G.C.: Predicting surface roughness in machining: a review. *Int. J. Mach. Tools Manuf.* **43**(8), 833–844 (2003)
2. De Chiffre, L., Lonardo, P., Trumpold, H., Lucca, D.A., Gosh, G., Brown, C.A., Raja, J., Hansen, H.N.: Quantitative characterization of surface texture. *CIRP Ann.* **49**(2), 635–652 (2000)
3. Deleanu, L., Georgescu, C., Suci, C.: A comparison between 2D And 3D surface parameters for evaluating the quality of surfaces. *Ann. “Dunarea De Jos” Univ. Galati* **5**, 5–12 (2012)
4. Deng, J.L.: Introduction to grey system theory. *J. Grey Syst.* **1**(1), 1–24 (1989)
5. Faisal, N., Kumar, K.: Optimization of machine process parameters in EDM for EN 31 using evolutionary optimization techniques. *Technologies* **6**(2), 1–16 (2018)
6. Gohil, V., Puri, Y.M.: Multi-objective optimization of material removal rate and surface roughness in electrical discharge turning of titanium alloy (Ti-6Al-V). *Indian J. Eng. Mater. Sci.* **24**(6), 429–436 (2017)
7. Kumar, K.M., Hariharan, P.: Experimental determination of machining responses in machining austempered ductile iron (ADI). *Procedia Eng.* **64**, 1495–1504 (2013)
8. Kumar, S.V., Kumar, M.P.: Optimization of cryogenic cooled EDM process parameters using grey relational analysis. *J. Mech. Sci. Technol.* **28**(9), 3777–3784 (2014)
9. Laxman, J., Guru Raj, K.: Optimization of EDM process parameters on titanium super alloys based on the grey relational analysis. *Int. J. Eng. Res.* **3**(5), 344–348 (2014)
10. Lee, S.H., Li, X.P.: Study of the effect of machining parameters on the machining characteristics in electrical discharge machining of tungsten carbide. *J. Mater. Process. Technol.* **115**(3), 344–358 (2001)

11. Mazarbhuiya, R.M., Choudhury, P.K., Rahang, M.: Taguchi-grey relational based multi-objective optimization of process parameters in electric discharge machining of aluminium with copper electrode. *J. Basic Appl. Eng. Res.* **3**(13), 1169–1171 (2016)
12. Özdemir, N., Özek, C.: An investigation on machinability of nodular cast iron by WEDM. *Int. J. Adv. Manuf. Technol.* **28**(9–10), 869–872 (2006)
13. Petropoulos, G.P., Pandazaras, C.N., Davim, J.P.: Surface texture characterization and evaluation related to machining. In: *Surface Integrity in Machining*, pp. 37–66. Springer, London (2010)
14. Ramasawmy, H., Blunt, L.: 3D surface topology assessment of the effect of different electrolytes during electrochemical polishing of EDM surfaces. *Int. J. Mach. Tools Manuf.* **42**, 567–574 (2002)
15. Sedlaček, M., Podgornik, B., Vižintin, J.: Influence of surface preparation on roughness parameters, friction and wear. *Wear* **266**, 482–487 (2009)
16. Smith, S.: *Machining, Polishing & Grinding : Precision Metalsmiths Handbook*, pp. 1–95. Industrial Press, USA (2015)
17. Tharian, B.K., Jacob, E., Johnson, J., Hari, V.: Multi-objective parametric optimization in EDM using grey relational analysis. *Mater. Today Proc.* **16**(2), 1013–1019 (2019)
18. Tomadi, S.H., Hassan, M.A., Hamedon, Z., Daud, R., Khalid, A.G.: Analysis of the influence of EDM parameters on surface quality, material removal rate and electrode wear of tungsten carbide. In: *Proceedings of International Multiconference of Engineers and Computer Scientists, Hong Kong*, vol. 2, pp. 18–20 (2009)
19. Tripathy, S., Tripathy, D.K.: Multi-attribute optimization of machining process parameters in powder mixed electro-discharge machining using TOPSIS and grey relational analysis. *Eng. Sci. Technol. Int. J.* **19**(1), 62–70 (2016)

Chapter 33

Smart Materials for 4-D Printing: A Comprehensive Review



Amit Gupta, P. Sudhakar Rao, and Mohd. Yunus Khan

Abstract 4-D printing is an exciting new technology that combines the concept of multi-material 3-D printing and smart materials to form a printable material that has an additional dimension of time. The process of 4-D printing employs programmable matter such that the printer product reacts with external stimuli and changes its shape. These kinds of materials find their application in the carious fields such as self-construction structures, medicinal devices, smart pipes and soft robotics. In this paper, review of smart materials and their possible applications has been conducted.

Keywords 4-D printing · Smart materials · External stimuli · 3D printing

33.1 Introduction

4-D printing is one of the hot topics of research and is some of the most common methods of Additive Manufacturing (AM). The idea of 4-D printing was first put forward by Tibbit [1], which redefined the definition of 3-D printed structures which can change their state in terms of shape or properties due to the influence of external stimuli, thereby giving a 4-D printed section which is time-reliant yet expectable [2]. The process of 4-D printing is quite similar to that of 3-D printing except for the fact that in the case of 3-D printing [3], the printed material is static in nature, while for 4-D printing the printed product has another dimension of time [4]. The characteristic of printing static structures of 3-D printing fall short for applications that demand exhibiting dynamic capabilities from printed materials such as soft grippers for surgery [5], self-folding packages [6] and adaptive wind turbines [7]. 4-D printing advances from 3-D printing in terms of smart materials and smart design [8].

Apart from this, there are many differences noticed in comparing 3-D printing and 4-D printing. The materials used for 3-D printing are commonly thermoplastics,

A. Gupta (✉) · P. Sudhakar Rao · Mohd. Yunus Khan
Department of Mechanical Engineering, National Institute of Technical Teachers'
Training and Research (NITTTR), Chandigarh, India
e-mail: amit.mech19@nitttrchd.ac.in

metals, ceramics or biomaterials. While for 4-D printing, the materials include self-assembly materials, multilateral etc. For 3-D printing technology, the design requirements include scanning or drawings. While for 4-D printing, the design requirements are 3-D digital information for change/deformation. The 3-D printed materials don't show any change with respect to time, while 4-D printed materials exhibit change in printed material in the form of shape, color, function etc. [4]. 4-D printing exhibits many advantages over traditional AM in terms of basic factors such as association time, net cost and failure rate [9]. Other major differences between 4-D printing and traditional AM are highlighted in [10]. 4-D printed parts show changing aspects in shapes, properties and functionality [11, 12], these parts exhibit two states, which undergo a change on exposure to stimuli [13].

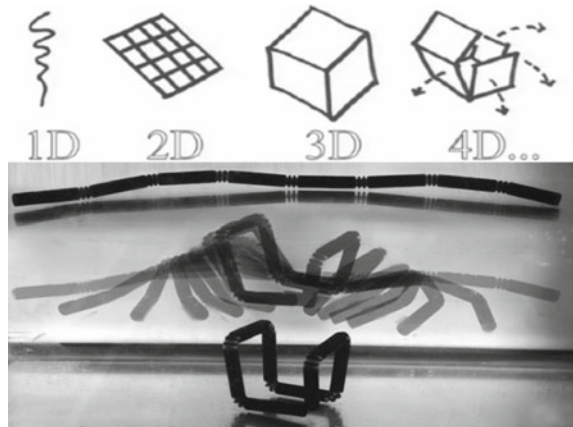
The whole process of 4-D printing comprises of five features namely, the AM method, the type of stimulus- responsive solid, the kind of stimuli, interaction mechanism between material and stimuli, and mathematical modeling. Mathematical modeling is needed to calculate the time required and the sequence of stimuli actions on the stimuli-responsive content. Mathematical modeling is carried out as a combination of geometric programming and finite element analysis [14]. One such illustration of 4-D printing is shown in Fig. 33.1.

The major aspects behind 4-D printing include:

1. Smart materials (which depict the change in shape on action by external stimuli)
2. 3-D printing using smart materials and
3. Self-assembly of micro-sized smart particles [16].

Common methods of 4-D printing include laser-assisted bio-printing [17], Fused Deposition Modeling (FDM) [18, 19], Stereolithography (SLA) [19], Direct inkjet cure [20–22], Selective Laser Melting (SLM) [23]. Commonly available 4-D printers are discussed in [24, 25]. The research aspects of 4-D printing begin with a basic idea of manipulating the materials at Nano and Micro levels to produce 3-D printed products which can modify their structures at macro levels over time. Such kind of

Fig. 33.1 Illustration of 4-D printing [15]



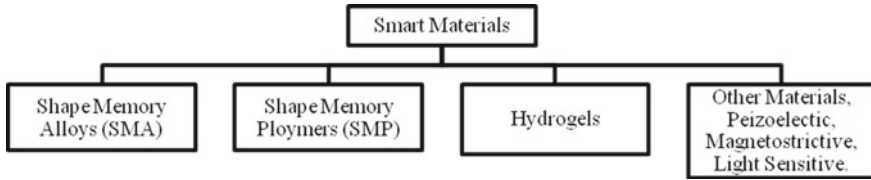


Fig. 33.2 General classification of smart materials

manipulated materials are termed as Smart Materials. In 4-D printing, the commonly used smart materials include Shape Memory Polymers (SMP) and Shape Memory Alloys (SMA). Apart from these self-assembled materials, hydrophilic polymers, biomaterials and plant oils are also used. The applications of 4-D printed structures have major applications in healthcare, from nano-particle design to human scale biomaterials [3, 4, 11]. Other important applications of 4-D printed structures include self-assembling origami [26]. 4-D printed products are found suitable for creating artificial muscles that could be subjected to a stress range of 40–80 MPa due to their low mechanical strength and durability [27]. In this paper, review of some common smart materials for 4-D printing and their possible applications has been carried out.

33.2 Smart Materials for 4-D Printing

For created 4-D printed products, the special kind of materials employed is Smart Materials. These Smart materials have special properties due to which they exhibit a change on application of external stimuli including young's modulus, stiffness and resistance [28]. These stimulus-responsive materials based on their ability to change their physical assets are classified these are Shape Change Material and Shape Memory Material. Shape change materials change their shape on response to stimuli and returns to their original shape on the elimination of stimuli. Shape memory materials possess the skill to remember and mend to original form from short-term shape on the application of a stimulus, due to Shape Memory Effect (SME) [14].

A general classification of smart materials is shown in Fig. 33.2, while the classification of methods of stimuli is shown in Fig. 33.3.

Commonly used printing technologies for 4-D printing along with the material type and types of stimuli are discussed in Table 33.1.

33.3 Shape Memory Alloys

SMA's are metal systems which are capable of existing in multiple exclusive phases when subjected to stimuli and can retain their unique shape after severe distortion

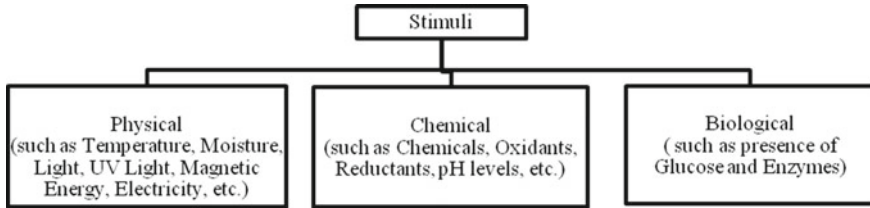


Fig. 33.3 Methods of stimuli

Table 33.1 Commonly used 4-D printing technologies [29]

Printing technology	Material type used	Driving mechanism	Stimuli	Physical change observed
Polyjet	Shape memory polymer (SMP)	Shape memory effect (SME)	Heat	Strain
	Hydrophilic polymer	Swelling	Moisture	Strain
SLA	Shape memory polymer (SMP)	Shape memory effect (SME)	Heat	Strain
	Piezoelectric material	Change of state of energy	Voltage	Strain
SLM	Shape memory alloy (SMA)	Shape memory effect (SME)	Heat	Strain
Extrusion based	Hydrogel	Expansion/contraction	Heat	Strain

[29, 30]. The two phases of SMA are namely, Martensite phase (Low Temperature) and the Austenite phase (High Temperature). Transformation of SMA has a forward phase, also referred as austenitic-martensitic transformation, and reverse-phase referred as martensite-austenite transformation [31]. These changes of phases have shown an impact on strength of SMA; the forward transformation had a decrease in strength, while reverse transformation has a negligible impact as discussed in [32].

Applications of SMA can be found in engineering and medical sectors [33, 34], like repair of structures [35], automotive applications [36] and aerospace applications [30]. Various industrial and commercial applications of SMA are discussed in [37]. One such application of SMA in aerospace applications is discussed, where Ni-Mn based SMA systems are used for the production of actuators and sensors [38].

33.4 Shape Memory Polymers

SMP's are majorly polymeric resources with an ability to return back to its pre-programmed shape from the temporary structure on exposure to stimuli [39]. SMP's shows a combination of polymers and programming [40]. Polymer is deformed into an irregular shape, which then regains its final form on the application of external energy predominantly heat [41, 42]. SMP's responding to thermal stimuli have a typical changeover temperature, such as glass transition temperature (T_g) which demands the retrieval force to be harnessed for material activation [28]. Time series of shape memory tube formed using polymethacrylate polymer is shown in Fig. 33.4.

Applications of SMP's in biomedical is seen inform of creating a shape memory airway stent [43], which then recovers to its original shape to match the target anatomy. Another important SMP is Mitsubishi Heavy Industries (MHI) polyurethane SMP [44], which showed a wide series of transition temperatures making it ideal for several scenarios. Thermal and moisture properties of MHI

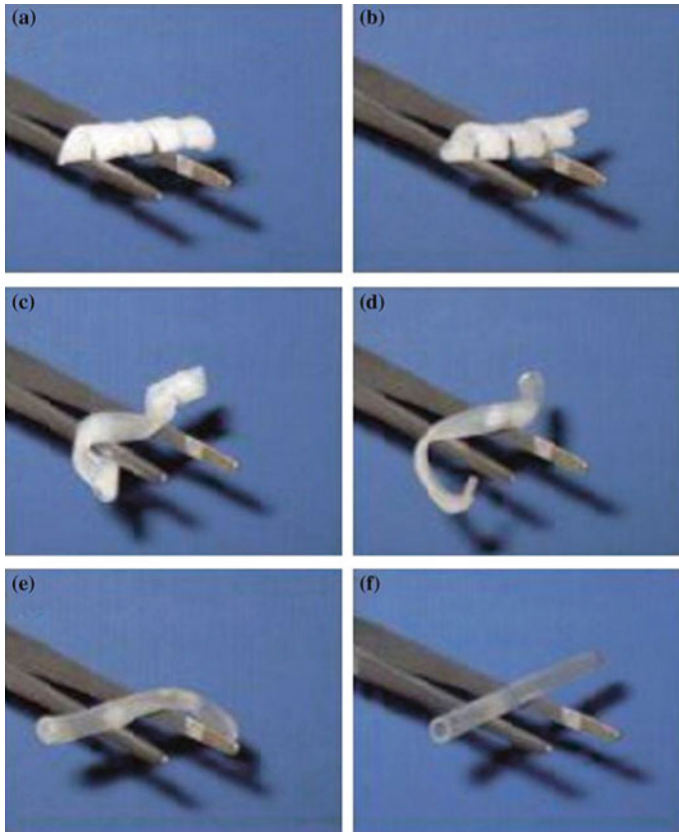


Fig. 33.4 Time series of shape memory tube forms using Polymethacrylyate polymer [41]

polyurethane SMP are discussed in [45]. Some of the applications of MHI polyurethane SMP's include thermal responsive Braille Pen and moisture responsive SMP stents. Multilateral gripper was constructed with cross-linked polymers using projection micro stereolithography that has a resolution of a few microns [46].

Apart from SMP's which exhibit two primary shapes on exposure to stimuli, Triple SMP's exhibit a tertiary shape consisting of covalent cross links [47]. A detailed comparison between SMP's and SMA's are discussed in [48].

33.5 Hydrogels

Hydrogels, also referred to as Hydrophilic polymeric materials, show a change in volume in response to stimuli [49]. Structures made up of hydrogels tend to be frail and brittle, so they are permeated with secondary polymeric networks are shown in Fig. 33.5. Hydrogels are normally operated in aqueous atmosphere, which causes them to absorb moisture till moisture saturation point of hydrogel. The control of hydrogel working can be achieved by controlling the temperature of the environment. One such example is interpenetrating network hydrogels made up of ionic and covalently bonded cross-linked polymeric networks [50]. Hinges with optimized bending characteristics are made up of hybrid hydrogel inks that are discussed in [51]. Hydrogels find applications in biomedicine [52, 53], such as creating cellular constructs like kidney cells [54], wound healing medicines [52, 55]. Temperature responsive valve was designed hydrogels with actuating temperature oscillating from 20 to 60 °C [49]. The very demonstration of the hydrophilic polymer was a multi-material 1D strand used to form the abbreviation 'MIT' in water [56] as shown in Fig. 33.5. Moisture actuated 3D printed objects were designed in [57] using natural occurrences such as dispersal of seeds and hygroscopicity of wood fiber. The Smart valve which controlled flow rate in response to the pressure of liquid flow is designed using polydimethylsiloxane hydrogel [58]. Hydrogels have an additional advantage of biocompatible and easiness of printing with direct-ink [59]. Micro gripper joints are fabricated using pNIPAM-AAC soft hydrogels, which are gradient cross-linked [5].

Fig. 33.5 Multi-material 1-D strand made up of hydrogel [56]



33.6 Other Materials

Other kinds of smart materials include piezoelectric materials, magnetostrictive materials and light-sensitive materials which change/undergo deformation on the application of electromotive force (emf), magnetic field or light respectively. Piezoelectric material show change in force with respect to change in voltage. A 4-D part was created using piezoelectric composite slurry using mask image projection based stereolithography technology [60]. Piezoelectric ink was created to manufacture thick films by piezoelectric inkjet printing [61]. A printed soft artificial muscle, comprise of silicone elastomer and ethanol. This structure acted on the application of minute current which caused ethanol to evaporate, expanding the whole matrix [62].

Magneto responsive materials form a 4-D printed structure that responds to magnetic fields. This kind of materials shows change is mechanical energy on the use of stimuli in the procedure of magnetic energy, like Terbium, Iron and Dysporium, with an application in telephone receivers, oscillators, sonar scanning, damping systems and positioning equipment. Micro gripper printed from hydrogels and remotely controlled by magnetic fields was discussed in this study [5].

Smart polymers which are activated by light are created using hinges of pre-stressed polystyrene sheets, with black ink. The Stimulus used in infrared light to create a temperature change, to change the geometry of the material [63]. The bending of 4-D printed structures was achieved by projecting weak UV light on liquid resin [64].

A comprehensive review of various industries and 4-D printed products are defined in Table 33.2.

Table 33.2 Various industries and 4-D printed products

Industry	4-D printed products	References
Electronics industry	Smart Sensors	[38]
	Smart Valves	[58]
Healthcare	Airway Stents	[43]
	Kidney Cells	[54]
	Wound healing structures	[52]
	Micro-grippers	[5]
Industrial Machinery	Grippers	[46]
	Actuators	[38]

33.7 Conclusions

4-D printing is the future of research in AM, where the studies focus on using smart materials to develop time-dependent yet predictable products. From the first demonstration of SLA machine in 1983, to Tibbits self-assembly lab, material research has proved its contribution towards societal development. 4-D printing opened up paths to develop printed products for a wide range of solicitations such as home appliances and health care. SMA's, SMP's, Hydrogels prove to be commonly used smart materials used for 4-D printing. A comprehensive review of these smart materials along with some applications was discussed in depth in this paper. Being a hot topic of research, many new printed products using new materials is expected in the near future, which will continue driving further, the research in AM.

References

1. https://www.ted.com/talks/skylar_tibbits_the_emergence_of_4d_printing. Accessed 25 Mar 2020
2. Momeni, F., Hassani, N., Liu, X., Ni, J.: A Review of 4D printing. *Mater* **122**, 42–79 (2017)
3. Gao, W., Zhang, Y., Ramanujan, D., Ramani, K., Chen, Y., Williams, C.B., Wang, C.C., Shin, Y.C., Zhang, S., Zavattieri, P.D.: The status, challenges, and future of additive manufacturing in engineering. *Comput. Aided Des.* **69**, 65–89 (2015)
4. Choi, J., Kwon, O.C., Jo, W., Lee, H.J., Moon, M.W.: 4D printing technology: a review. *3D Print. Addit. Manuf.* **2**(4), 159–167 (2015)
5. Breger, J.C., Yoon, C., Xiao, R., Kwag, H.R., Wang, M.O., Fisher, J.P., Nguyen, T.D., Gracias, D.H.: Self-folding thermo-magnetically responsive soft microgrippers. *ACS Appl. Mater. Interf.* **7**(5), 3398–3405 (2015)
6. Ge, Q., Qi, H.J., Dunn, M.L.: Active materials by four-dimension printing. *Appl. Phys. Lett.* **103**(13), 131901 (2013)
7. Momeni, F., Sabzpooshan, S., Valizadeh, R., Morad, M.R., Liu, X., Ni, J.: Plant leaf-mimetic smart wind turbine blades by 4D printing. *Renew. Energy* **130**, 329–351 (2019)
8. Sharma, A., Singholi, A.K.: A Comprehensive Review of Materials Used for 4D Printing. In: *Advances in Engineering Design*, pp. 747–754. Springer, Singapore (2019)
9. Tibbits, S., McKnelly, C., Olguin, C., Dikovskiy, D., Hirsch, S.: 4D Printing and Universal Transformation, pp. 539–548 (2014)
10. Gurung, D.: Technological Comparison of 3D and 4D Printing: Analytical Study (2017)
11. Ge, Q., Dunn, C.K., Qi, H.J., Dunn, M.L.: Active origami by 4D printing. *Smart Mater. Struct.* **23**(9), 094007 (2014)
12. Campbell, T.A., Tibbits, S., Garrett, B.: The next wave: 4D printing programming the material world, pp. 1–15. The Atlantic Council, Washington, DC (2014)
13. Leist, S.K., Zhou, J.: Current status of 4D printing technology and the potential of light-reactive smart materials as 4D printable materials. *Virt. Phys. Prototyp.* **11**(4), 249–262 (2016)
14. Pei, E., Loh, G.H.: Technological considerations for 4D printing: an overview. *Progr. Addit. Manuf.* **3**(1–2), 95–107 (2018)
15. <https://futurism.com/forget-3d-printed-constructs-4d-printing-is-becoming-all-the-rage>. Accessed on 27 Mar 2020
16. Koch, L., Deiwick, A., Chichkov, B.: Laser-Based Cell Printing. In: *3D Printing and Biofabrication*, pp. 303–329. Springer International Publishing, Cham (2018)

17. Wang, G., Do, Y., Cheng, T., Yang, H., Tao, Y., Gu, J., An, B., Yao, L.: Demonstrating printed paper actuator: a low-cost reversible actuation and sensing method for shape changing interfaces. In: *Extended Abstracts of the 2018 CHI Conference on Human Factors in Computing Systems*, pp. 1–4 (2018)
18. Miao, S., Cui, H., Nowicki, M., Xia, L., Zhou, X., Lee, S.J., Zhu, W., Sarkar, K., Zhang, Z., Zhang, L.G.: Stereolithographic 4D bioprinting of multiresponsive architectures for neural engineering. *Adv. Biosyst.* **2**(9), 1800101 (2018)
19. Liu, Y., Shaw, B., Dickey, M.D., Genzer, J.: Sequential self-folding of polymer sheets. *Sci. Adv.* **3**(3), 602417 (2017)
20. Zolfagharian, A., Kaynak, A., Khoo, S.Y., Kouzani, A.: Pattern-driven 4D printing. *Sens. Actuat. A* **274**, 231–243 (2018)
21. Akbari, S., Sakhaei, A.H., Kowsari, K., Yang, B., Serjouei, A., Yuanfang, Z., Ge, Q.: Enhanced multimaterial 4D printing with active hinges. *Smart Mater. Struct.* **27**(6), 065027 (2018)
22. Dadbakhsh, S., Speirs, M., Kruth, J.P., Schrooten, J., Luyten, J., Van Humbeeck, J.: Effect of SLM parameters on transformation temperatures of shape memory nickel titanium parts. *Adv. Eng. Mater.* **16**(9), 1140–1146 (2014)
23. <https://www.slideshare.net/Funk98/4d-printing-with-smart-materials>. Accessed 25 Mar 2020
24. <https://shop.prusa3d.com/en/31-printer-upgrades>. Accessed 25 Mar 2020
25. Pati, F., Jang, J., Ha, D.H., Kim, S.W., Rhie, J.W., Shim, J.H., Kim, D.H., Cho, D.W.: Printing three-dimensional tissue analogues with decellularized extracellular matrix bioink. *Nat. Commun.* **5**(1), 1–11 (2014)
26. Ramakrishna, S., Mayer, J., Wintermantel, E., Leong, K.W.: Biomedical applications of polymer-composite materials: a review. *Compos. Sci. Technol.* **61**(9), 1189–1224 (2001)
27. Lee, V.K., Dias, A., Ozturk, M.S., Chen, K., Tricomi, B., Corr, D.T., Intes, X., Dai, G.: 3D bioprinting and 3D imaging for stem cell engineering. In: *Bioprinting in Regenerative Medicine*, pp. 33–66. Springer, Cham (2015)
28. Shin, D.G., Kim, T.H., Kim, D.E.: Review of 4D printing materials and their properties. *Int. J. Precis. Eng. Manuf. Green Technol.* **4**(3), 349–357 (2017)
29. Sossou, G., Demoly, F., Montavon, G., Gomes, S.: Design for 4D printing: rapidly exploring the design space around smart materials. *Procedia CIRP* **70**, 120–125 (2018)
30. Cipollo, P., Surrusco, B.: An Electrically Actuated Pin-Puller for Space Application using Nickel-Titanium Memory Alloy (2004)
31. Wang, G.Z.: Effect of martensite transformation on fracture behavior of shape memory alloy NiTi in a notched specimen. *Int. J. Fract.* **146**(1–2), 93–104 (2007)
32. Yan, W., Wang, C.H., Zhang, X.P., Mai, Y.W.: Effect of transformation volume contraction on the toughness of superelastic shape memory alloys. *Smart Mater. Struct.* **11**(6), 947 (2002)
33. Loh, C.S., Yokoi, H., Arai, T.: New shape memory alloy actuator: design and application in the prosthetic hand. In: *2005 IEEE Engineering in Medicine and Biology 27th Annual Conference*. IEEE, pp. 6900–6903 (2006)
34. Haga, Y., Esashi, M.: Small diameter active catheter using shape memory alloy coils. *IEEJ Trans. Sens. Micromach.* **120**(11), 509–514 (2000)
35. Cladera, A., Weber, B., Leinenbach, C., Czaderski, C., Shahverdi, M., Motavalli, M.: Iron-based shape memory alloys for civil engineering structures: an overview. *Constr. Build. Mater.* **63**, 281–293 (2014)
36. Saghaian, S.M., Karaca, H.E., Souri, M., Turabi, A.S., Noebe, R.D.: Tensile shape memory behavior of Ni50. 3Ti29. 7Hf20 high temperature shape memory alloys. *Mater. Des.* **101**, 340–345 (2016)
37. Jani, J.M., Leary, M., Subic, A., Gibson, M.A.: A review of shape memory alloy research, applications and opportunities. *Mater. Des.* (1980–2015) **56**, 1078–1113 (2014)
38. Umetsu, R.Y., Xu, X., Kainuma, R.: NiMn-based metamagnetic shape memory alloys. *Scripta Mater.* **116**, 1–6 (2016)
39. Monzón, M.D., Paz, R., Pei, E., Ortega, F., Suárez, L.A., Ortega, Z., Alemán, M.E., Plucinski, T., Clow, N.: 4D printing: processability and measurement of recovery force in shape memory polymers. *Int. J. Adv. Manuf. Technol.* **89**(5–8), 1827–1836 (2017)

40. Mather, P.T., Luo, X., Rousseau, I.A.: Shape memory polymer research. *Annu. Rev. Mater. Res.* **39**, 445–471 (2009)
41. Langer, R., Tirrell, D.A.: Designing materials for biology and medicine. *Nature* **428**(6982), 487–492 (2004)
42. Behl, M., Lendlein, A.: Shape-memory polymers. *Kirk-Othmer Encyclopedia of Chemical Technology*, pp. 1–16 (2000)
43. Zarek, M., Mansour, N., Shapira, S., Cohn, D.: 4D printing of shape memory-based personalized endoluminal medical devices. *Macromol. Rapid Commun.* **38**(2), 1600628 (2017)
44. Liang, C., Rogers, C.A., Malafeev, E.: Investigation of shape memory polymers and their hybrid composites. *J. Intell. Mater. Syst. Struct.* **8**(4), 380–386 (1997)
45. Huang, W.M., Yang, B., Zhao, Y., Ding, Z.: Thermo-moisture responsive polyurethane shape-memory polymer and composites: a review. *J. Mater. Chem.* **20**(17), 3367–3381 (2010)
46. Ge, Q., Sakhaei, A.H., Lee, H., Dunn, C.K., Fang, N.X., Dunn, M.L.: Multimaterial 4D printing with tailorable shape memory polymers. *Sci. Rep.* **6**, 31110 (2016)
47. Moon, S., Rao, I.J., Chester, S.A.: Triple shape memory polymers: constitutive modeling and numerical simulation. *J. Appl. Mech.* **83**(7) (2016)
48. Liu, C., Qin, H., Mather, P.T.: Review of progress in shape-memory polymers. *J. Mater. Chem.* **17**(16), 1543–1558 (2007)
49. Bakarich, S.E., Gorkin, R., III., Panhuis, M.I.H., Spinks, G.M.: 4D printing with mechanically robust, thermally actuating hydrogels. *Macromol. Rapid Commun.* **36**(12), 1211–1217 (2015)
50. Sun, J.Y., Zhao, X., Illeperuma, W.R., Chaudhuri, O., Oh, K.H., Mooney, D.J., Vlassak, J.J., Suo, Z.: Highly stretchable and tough hydrogels. *Nature* **489**(7414), 133–136 (2012)
51. Naficy, S., Gately, R., Gorkin, R., III., Xin, H., Spinks, G.M.: 4D printing of reversible shape morphing hydrogel structures. *Macromol. Mater. Eng.* **302**(1), 1600212 (2017)
52. Thakur, S., Chaudhary, J., Kumar, V., Thakur, V.K.: Progress in pectin based hydrogels for water purification: trends and challenges. *J. Environ. Manage.* **238**, 210–223 (2019)
53. Mohammadinejad, R., Maleki, H., Larrañeta, E., Fajardo, A.R., Nik, A.B., Shavandi, A., Sheikhi, A., Ghorbanpour, M., Farokhi, M., Govindh, P., Cabane, E.: Status and future scope of plant-based green hydrogels in biomedical engineering. *Appl. Mater. Today* **16**, 213–246 (2019)
54. Hong, S., Sycks, D., Chan, H.F., Lin, S., Lopez, G.P., Guilak, F., Leong, K.W., Zhao, X.: 3D printing of highly stretchable and tough hydrogels into complex, cellularized structures. *Adv. Mater.* **27**(27), 4035–4040 (2015)
55. Murphy, S.V., Skardal, A., Atala, A.: Evaluation of hydrogels for bio-printing applications. *J. Biomed. Mater. Res., Part A* **101**(1), 272–284 (2013)
56. Tibbitts, S.: 4D printing: multi-material shape change. *Architect. Des.* **84**(1), 116–121 (2014)
57. Le Duigou, A., Castro, M., Bevan, R., Martin, N.: 3D printing of wood fibre biocomposites: from mechanical to actuation functionality. *Mater. Des.* **96**, 106–114 (2016)
58. Zhang, Y.S., Yue, K., Aleman, J., Mollazadeh-Moghaddam, K., Bakht, S.M., Yang, J., Jia, W., Dell’Erba, V., Assawes, P., Shin, S.R., Dokmeci, M.R.: 3D bioprinting for tissue and organ fabrication. *Ann. Biomed. Eng.* **45**(1), 148–163 (2017)
59. Au, A.K., Bhattacharjee, N., Horowitz, L.F., Chang, T.C., Folch, A.: 3D-printed microfluidic automation. *Lab Chip* **15**(8), 1934–1941 (2015)
60. Chen, Z., Song, X., Lei, L., Chen, X., Fei, C., Chiu, C.T., Qian, X., Ma, T., Yang, Y., Shung, K., Chen, Y.: 3D printing of piezoelectric element for energy focusing and ultrasonic sensing. *Nano Energy* **27**, 78–86 (2016)
61. Kuscer, D., Noshchenko, O., Uršič, H., Malič, B.: Piezoelectric properties of Ink-Jet-Printed lead zirconate titanate thick films confirmed by piezoresponse force microscopy. *J. Am. Ceram. Soc.* **96**(9), 2714–2717 (2013)

62. Miriyev, A., Stack, K., Lipson, H.: Soft material for soft actuators. *Nat. Commun.* **8**(1), 1–8 (2017)
63. Liu, Y., Boyles, J.K., Genzer, J., Dickey, M.D.: Self-folding of polymer sheets using local light absorption. *Soft Matter* **8**(6), 1764–1769 (2012)
64. Wu, J., Zhao, Z., Kuang, X., Hamel, C.M., Fang, D., Qi, H.J.: Reversible shape change structures by grayscale pattern 4D printing. *Multifunct. Mater.* **1**(1), 015002 (2018)

Chapter 34

Composites in Context to Additive Manufacturing



Mohd Shoeb, Lokesh Kumar, Abid Haleem, and Mohd Javaid

Abstract The very first application in the Additive Manufacturing (AM) is the development of prototypes, that too by using plastic in fused deposition modeling (FDM) 3D printing processes, Stereolithography, SLS and others. Apart from printing ordinary shaped objects, Additive Manufacturing is also able to produce composites by using different materials on a single production platform. Continuous research and development has improved Additive manufacturing capability to develop various composite materials including fiber-reinforced composite, Biocomposite, Nanocomposites, Polymer matrix composites and Polymers. The primary purpose of this work is the literature-based study on FDM printed composite materials. For this purpose, the keyword “FDM Composites” is used in SCOPUS search and research papers from reputed publishers and Journals were identified and studied. Further, discussed the methods for the development of composite using FDM, and different composite materials with their types which can be printed by using FDM are discussed in a tabular form. It is learned that FDM provides an extraordinary chance to develop typical AM parts with the use of composite materials. Exploration, expansion and commercialization of AM materials are a significant extent of the study in the field of a composite at present.

Keywords Additive manufacturing (AM) · Composites · Fused deposition modeling (FDM) 3D printing

34.1 Introduction

3D Printing is the rapid production technology for making 3D parts directly from CAD files [1]. This process can produce 3D parts without using the conventional technique. It made layer by layer deposition of materials. There are different ways to produce a layer by using different 3D printers which may be with the help of binders [2] or by using 3D lithographic method [3] or by sintering using laser [4] or by plastic

M. Shoeb (✉) · L. Kumar · A. Haleem · M. Javaid
Department of Mechanical Engineering, Jamia Millia Islamia, New Delhi 110025, India
e-mail: mshoeb1@jmi.ac.in

© The Author(s), under exclusive license to Springer Nature Switzerland AG 2022
R. Pratap Singh et al. (eds.), *Proceedings of the International Conference on Industrial and Manufacturing Systems (CIMS-2020)*, Lecture Notes on Multidisciplinary Industrial Engineering, https://doi.org/10.1007/978-3-030-73495-4_34

filament deposition [5] or by the electron beam [6]. It observed that the FDM is most economic and suitable technology [7]. The broad dissemination of Additive Manufacturing and innovative performance necessities required advanced composite and multimaterial solutions [8]. Properties of composites generally depends on comparative quantities, production technique, geometry such as shape and size, distribution and positioning of reinforcement phase, phases properties and interfacial boundaries strength [9]. This work comprises the study of composite material printing with help of Fused Deposition Modeling method. In FDM 3D printing the thermoplastic filament is used for deposition in a reel form which passes through a hot head. The temperature in head is maintained above the filaments melting point and the melted filament is deposited in XY plane developing a solid material layers on build platform [10]. The Fused Deposition Modeling is found most commonly used method due to their advantages such as economical, reliable, dimensionally stable, high-quality resolution [8], customization of a variety of materials [9] easy fabrication method [10] and capability to develop common geometrical objects in friendly environment conditions. The highly flexible process simply incorporated with CAD packages. Researchers are working on the process parameters optimization and concentrate on the study to inter-relate the various parameters and their response to the final developed product [11].

The most common classification of the 3DP process is based on the initial state of materials and working principle [12] (Kindly see Table 34.1).

34.2 Reason to Embrace 3D Printing for Composites

The main reason for AM implementation and its industrial applications are Geometrical independence, Part functionality, economic and environmental sustainability [13]. The critical application of AM are in the field of energy, aerospace, biomedical, automotive and others [14, 15].

Composites are used in making light structures in different medical and industrial applications. In automobile sector, since 2015, it is observed that there is 5% increase in composites use [16].

34.3 Materials Used in 3D Printing Technologies

3D printing is considered as an important technology in the manufacturing sector worldwide. Its success mainly depends on the enhancement of the materials for the requirement of different applications. This enhancement includes the class, strength, cost and types of materials. There is a variety of materials that can be used in 3D printing according to the requirements of the market. The different types of materials used in 3D Printing are briefly discussed here [17]: *Nylon (Polyamide)*—Flexible, strong and durable. *Resin*—Delicate but rigid. *ABS*—Created by filament-like

Table 34.1 3DP process based on the initial state of materials and working principle

Materials initial state	Distinctive materials	Preparation of material	Process	Method of layer formation	Uses
Solid sheet	Metal, plastic, paper	Laser cutting	LOM	Sheets binding and feeding with the help of adhesives	Models casting and prototypes
Liquid	UV curable resin, ceramic suspension Ceramic paste	The resin in a vat Paste in nozzle	SLA Robocasting	Laser scanning Continuous extrusion	Casting patterns, Prototypes Functional parts
Powder	Polymer, ceramic powders Metal	Powder in bed Powder in bed Powder in bed	3DP SLM EBM	Drop-on-demand binder printing Laser scanning Electron beams scanning	Casting shells, Prototypes Tooling, functional parts Tooling, functional parts
Filament	Thermoplastics, waxes	Melted in nozzle	FDM	Continuous extrusion and deposition	Casting patterns, prototypes

spaghetti and many colour options. *Silver and Gold*—In the category of Strong materials. *Titanium*—In the category of strongest materials. *Gypsum*—Fragile and rigid known as rainbow ceramics or sandstone. *Ceramics*—Found in rigid form but delicate, obtained by printing and glazing the surface. *VisiJet CF-BK*—Black rubber-like material, appeared in rubber form, highly flexible good ability to absorbs impacts and shocks. *VisiJet FTX Materials*—Parts are micro-manufactured generally used for Jewelry items. *VisiJet CR-WT*—Rigid white ABS-like material, high-temperature resistance greater rigidity highly durable.

34.4 Methods Used for Composites Creation Using FDM

The following methods are briefly discussed here for composite creation using FDM technique:

34.4.1 Multi-Material Structures Creation Using an Element

By this method, multi-material structures are created by printing polymer material layers on wood, metal, ceramic or polymer materials surfaces. The elements obtained by this method have few materials, and built-in material inhabits much of total volume [18]. The main limitation is to break the prototype in parts alienated by comparable planes, successive printing stages to be identified and to resume printing without interrupting the steadiness of material.

34.4.2 Composite Structure Creation Using a Single Nozzle with Reinforcement Material

A composite structure is created by printing using a single nozzle on reinforcement material. The method is same as of multi-material structures creation. The multi-stage method used for composite creation, the amount of stages corresponds to reinforcement layers of the final element. Each stage is planned by the required division plate to enable discontinuing the printing and reinforcement phase deposition on print. Composite may reinforce with cloth and the fibre [19]. The restriction for reinforcement of material layers thickness is the disadvantage of this method. The approximately 0.5 mm layer thickness of reinforcement is generally found.

34.4.3 Composite Structure Creation Using a Single Nozzle with Specific Filament

This method creates composite structure by using different filament with the help of conventional 3D printing method, in addition to polymeric material has additives like microspheres, carbon fiber, wood flour, particles of glass etc. [20]. The limitation of this method is printing material availability.

34.4.4 Composite Creation Using Two Different Materials Alternatively

The process of printing by two materials alternatively is considered as modern and most commonly used 3D printing process. In this method, a head with two nozzles or a nozzle with changeable filament system is used. Alternate layers of different materials are possible in one printing step [21]. Disadvantages of this method are contamination due to problem of transition in filaments and fragments.

34.4.5 Layered Composite Creation Using Two Different Materials

This method is similar to the method using two materials method only they differ by way of deposition of materials [21]. In this method first, apply one material layer then apply the layer of other material.

34.4.6 Skeletal Composite Creation Using Two Different Materials

This method is similar to the method of creating a layered composite the only difference is that the material is a skeletal structure instead of solid. Reducing infills algorithm is used, which reduces materials consumption and time in the printing process. Commonly known skeletal structures are honeycomb, square cells, hexagonal cells and other self-designed structure can be used.

34.4.7 Layered Composite Creation Using a Special Nozzle for Continuous Fiber Introduction

The filaments used as matrix material and reinforcing fibers provided independently to the nozzle. The fiber is heated to increase the mixing capacity to thermoplastic materials and reinforcement phase before entering the nozzle [21]. Fibers supplied to printer head by filament motion automatically, and in printer head the plasticized filament is linked to reinforcement phase. The other stages of printing are the same as the standard 3D printing method.

34.5 Various Composites Printed by FDM 3D Printing

The various composite materials printed by FDM are arranged in tabular form (Table 34.2) based on types, constituents, findings and references.

34.6 Implications of This Study

The present state of manufacturing methods generally depends on composite, plastics and polymer because of high strength corresponding to weight ratio, lightweight and low cost. Various kinds of composites which are commonly used for research are

discussed here. Researchers mainly focused on mechanical properties, rheological properties, process parameters optimization, stability, and finding new areas like dimensional accuracy and tissue engineering. Various composite materials for FDM use are studied and a brief discussion is arranged in tabular form based on types, constituents, findings and references.

Table 34.2 Composites by using FDM based on types, Constituents, findings and references

S. No.	Types of composites	Constituents	Findings	References
1	Fiber-reinforced composites	Fiber-reinforced thermoplastic composites	UTS 165 MPa for isotropic layers of carbon fiber and better fatigue performance	Alberto et al. [22]
		Carbon fiber—Nylon Glass fiber—Nylon Kevlar fiber—Nylon	Impact strength 82.26 kJ/m ² Impact strength 280.95 kJ/m ² Impact strength 184.76 kJ/m ²	Caminero et al. [23]
		Carbon fibers—Epoxy resin	792 MPa UTS and 161 GPa Young’s modulus were found	Hao et al. [24]
		PLA—Carbon fiber	Impregnation advances on increasing melting temperature, mechanical properties increases, above 240 ⁰ C surface accuracy decreases	Tian et al. [25]
		PLA—Carbon fiber	Ellipsoid shaped holes observed by SEM. the orientation of extrusion coincide with a major axis and thus decreasing tensile strength	Hofstatter et al. [26]
		PLA—Bamboo fiber	At 160 °C, 273 MPa flexural strength and 6.8 GPa modulus are found. Strength increases at 160 °C and decreases after 180 °C while modulus increases at 140 °C	Ochi [27]

(continued)

Table 34.2 (continued)

S. No.	Types of composites	Constituents	Findings	References
2	Bio-composites	Woven cotton fabric—PLA	Fabrics with pore sizes 0.5 mm, 1.0 mm, 1.5 mm and concentrations of PLA, 0.01 g/mL, 0.03 g/mL, and 0.06 g/mL used to develop woven cotton fabric—PLA composite	Macha et al. [28]
		Cow Dung (CD)—Poly lactic acid (PLA)	Improvement in flexural properties and drop in tensile and impact strength with increasing CD loading	Yusef et al. [29]
		Wood bio-composite	Mechanical behaviour observed by changing the printing width, porosity increases by increasing the printing width	Duigou et al. [30]
		Blended TPS—ABS Biomass Alloys	Filaments flowing capability, organic emissions, mechanical, thermal and physical properties are found better than that of commercial ABS	Kuo et al. [31]
		Polyester scaffolds with PCL and PLA	Biocompatibility found increases by proliferation and adhesion on their surfaces	Sabino et al. [32]
		TCP-PLA	TCP morphology depends on the process temperature and affects the biodegradability. Superior compactness and dimensional accuracy affect mechanical performance	Drummer et al. [33]

(continued)

Table 34.2 (continued)

S. No.	Types of composites	Constituents	Findings	References
3	Nano-composites	ABS-Carbon Nanotubes (CNT)	Optimal CNT content in the filament at 6 wt%, thermal, mechanical and electrical properties investigated	Dul et al. [34]
		Graphene-ABS	A significant reduction in deformation at tensile and breaking strength in the Z direction and small in X and Y directions. Filler content optimized to 4%, reduction in creep compliance and thermal coefficient	Dul et al. [35]
		Nano clay—ABS	Tensile strength and modulus increases with increase in loading weight from 5 to 10% but decreases if increases to 15%. For batch-loading, 5% to 10% hardness increases to 60.5% and compressive strength increases to 24.6% as compared to ABS material	Francis and Jain [36]
		CNT-PLA	Observed UTS—80 MPa Young's Modulus—1.99 GPa	Melenka et al. [37]
		Graphene in ABS and PLA	Higher mechanical strength achieved	Wei et al. [38]
4	Polymer matrix composites	Al ₂ O ₃ powder with Nylon	Al ₂ O ₃ significantly increases the wear resistance and length of the part greatly affects the dimensional accuracy	Singh et al. [39]

(continued)

Table 34.2 (continued)

S. No.	Types of composites	Constituents	Findings	References
		Fe-Nylon	Nearly alike influence of three parameters, extrusion temperature 20%, filler materials shares 25% and extrusion load 45%	Garg and Singh [40]
		Copper and Iron micro-scale in ABS	Observed UTS—15 MPa Young's modulus—0.23 GPa	Nikzad et al. [41]
		PA6-TiO ₂	Excellent mechanical properties of PA6 at 30 weight per cent of TiO ₂ obtained while 10 and 20 weight percentage shows reasonable. 30%TiO ₂ shows minimum wear of PA6 at load 20 N and 10 min run time	Soundararajan et al. [42]
		Fe ₃ O ₄ in P301 Nylon	UTS—4 MPa & Young's modulus—0.054 GPa	Masood [43]
5	Polymers	ABS	For impact loading, the tensile test shows brittle nature with moderate Elasticity Modulus	Owolabi et al. [44]
		PEEK	Comparatively best results are possible at 300 μm layer thickness and 0°/90° raster angle	Wu et al. [45]
		Nylon	Tensile strength increased at 77 °K	Cruz et al. [46]
		ABS-TPE, ABS-TiO ₂ , ABS-Jute fibre and Pure-ABS	Improvement in the surface finishes with TPE, improvement in ultimate tensile strength for ABS with TiO ₂ in comparison to pure ABS, high roughness for ABS with jute fiber	Perez et al. [47]

(continued)

Table 34.2 (continued)

S. No.	Types of composites	Constituents	Findings	References
		ABS	Elastic behaviour of ABS parts is affected by the parameters like an air gap, raster angle and layer thickness	Lee et al. [48]

34.7 Future Opportunities

The developments in 3D printing have a greater impact on medical and industrial engineering field with different ink designs, enhanced depiction and ink assets modelling in deposition and improved ink deposition and better robotic control for smarter précised 3D printing. The capability of locally specify for both structure and composition is permitting better mechanism concluded the functionality and possessions of the subsequently developed materials.

34.8 Conclusions

This work presents a literature-based study on composite development with FDM technology. This has been done to identify the suitability of FDM for the development of different composite applications. For this research papers from reputed journals are selected and studied. Identified 3DP processes based on the initial state of materials and working principles. Also presents in tabular format the types of composites based on types, constituents and research findings with references. In this study, various materials like Fiber-reinforced composite, Biocomposites, Nanocomposites, Polymer matrix composites and Polymers have been studied and found that FDM seems most suitable for manufacturing parts with composites. Finally attaining challenges, prospects and future aspects of FDM provides a compelling way to blowout smooth technique in various areas like building construction, farming and biomedical fields.

References

1. Chua, K., Leong, F., Lim, S.: Rapid Prototyping: Principles and Applications 2nd edn. World Scientific (2003)
2. Upcraft, S., Fletcher, R.: The rapid prototyping technologies. *Assembly Autom.* **23**, 318–330 (2003)

3. Williams, M., Adewunmi, A., Schek, M., Flanagan, L., Krebsbach, H.: Bone tissue engineering using polycaprolactone scaffolds fabricated via selective laser sintering. *Biomaterials* **26**, 4817–4827 (2005)
4. Li, X., Wang, T., Zhang, G., Li, C.: Fabrication and characterization of porous Ti6Al4V parts for biomedical applications using electron beam melting process. *Mater. Lett.* **63**, 403–405 (2009)
5. Zhang, X., Jiang, N., Sun, C.: Micro-stereolithography of polymeric and ceramic microstructures. *Sens. Actuat.* **77**, 149–156 (1999)
6. Zein, I., Hutmacher, W., Tan, C., Teoh, H.: Fused deposition modeling of novel scaffold architectures for tissue engineering applications. *Biomaterials* **23**, 1169–1185 (2002)
7. Jones, R., Haufe, P., Sells, E., Irvani, P., Oliver, V.: RepRap—the replicating rapid prototype. *Robotica* **29**, 177–191 (2011)
8. Harun, W., Sharif, S., Idris, H., Kadirgama, K.: Characteristic studies of collapsibility of ABS patterns produced from FDM for investment casting. *Mater. Res. Innov.* **13**(3), 340–343 (2009)
9. Plymill, A., Minneci, R., Greeley, A., Gritton, J.: Graphene and carbon nano-tube PLA composite feedstock development for fused deposition modeling. University of Tennessee Honors Thesis Projects (2016)
10. Masood, H., Song, Q.: Development of new metal/ polymer materials for rapid tooling using fused deposition modeling. *Mater. Des.* **25**, 587–594 (2004)
11. Kruth, P.: Material increase manufacturing by rapid prototyping techniques. *CIRP Ann. Manuf. Technol.* **40**, 603–614 (1991)
12. Kruth, P., Leu, C., Nakagawa, T.: Progress in additive manufacturing and rapid prototyping. *CIRP Ann. Manuf. Technol.* **47**, 525–540 (1998)
13. Horn, J., Harrysson, L.: Overview of current additive manufacturing technologies and selected applications. *Sci. Prog.* **95**, 255–282 (2012)
14. Guo, N., Leu, C.: Additive manufacturing: technology, applications and research needs. *Front. Mechan. Eng.* **8**, 215–243 (2013)
15. Mellor, S., Hao, L., Zhang, D.: Additive manufacturing: a framework for implementation. *Int. J. Prod. Econ.* **149**, 194–201 (2014)
16. Yakout, M., Elbestawi, M.: Additive manufacturing of composite materials: an overview. In: 6th International Conference on Virtual Machining Process Technology (VMPT), Montréal, May 29th–June 2nd (2017)
17. Lipson, H., Kurman, M.: *Fabricated: The New World of 3D Printing*. Wiley, Indianapolis (2013)
18. Dudek, P.: FDM 3D printing technology in manufacturing composite elements. *Arch. Metall. Mater.* **58**(4), 1415–1418 (2013)
19. Katarzyna, B., Elźbieta, P., Paweł, S., Wojciech, Ś., Marek, P.: Polymer Composite Manufacturing by FDM 3D Printing Technology. MATEC Web of Conferences 237. <https://doi.org/10.1051/mateconf/201823702006>
20. Ning, W., Cong, W., Qiu, J., Wei, J., Wang, S.: Additive manufacturing of carbon fiber reinforced thermoplastic composites using fused deposition modeling. *Compos. B Eng.* **80**, 369–378 (2015)
21. Kumar, S., Kruth, P.: Composites by rapid prototyping technology. *Mater. Des.* **31**, 850–856 (2010)
22. Pertuz, A.D. et al.: Static and fatigue behaviour of continuous fibre reinforced thermoplastic composites manufactured by fused deposition modelling technique. *Int. J. Fatig.* **130**, 105275 (2020)
23. Caminero, A., Chac, J., Moreno, I., Rodriguez, G.: Impact damage resistance of 3D printed continuous fibre reinforced thermoplastic composites using fused deposition modeling. *Compos. B Eng.* **148**, 93–103 (2018)
24. Hao, W., Liu, Y., Zhou, H., Chen, H., Fang, D.: Preparation and characterization of 3D printed continuous carbon fiber reinforced thermosetting composites. *Polym. Test.* **65**, 29–34 (2018)
25. Tian, X., Liu, T., Yang, C., Wang, Q., Li, D.: Interface and performance of 3D printed continuous carbon fibre reinforced PLA composites. *Compos. Part A: Appl. Sci. Manuf.* **88**, 198–205 (2016)

26. Hofstätter, T., Gutmann, I., Koch, T., David, B.: Distribution and orientation of carbon fibres in polylactic acid parts produced by fused deposition modeling. In: Proceedings of ASPE summer topical meeting 2016: dimensional accuracy and surface finish in additive manufacturing. APSE—The American Society for Precision Engineering
27. Ochi, S.: Flexural properties of long bamboo fibre/PLA composites. *Open J. Compos. Mater.* **5**, 70–78 (2015). <https://doi.org/10.4236/ojcm.2015.53010>
28. Macha, J., Medard, M., Josephat, L.: In vitro study and characterization of cotton fabric PLA composite as a slow antibiotic delivery device for biomedical applications. *J. Drug Deliv. Sci. Technol.* **43**, 172–177 (2018)
29. Yusef, M., Khalid, M., Yasin, M.: Physico-mechanical properties of poly(lactic acid) biocomposites reinforced with cow dung. *Mater. Res. Exp.* **4**(2) (2017). <https://doi.org/10.1088/2053-1591/aa5cdb>
30. Duigou, A.L., Castro, M., Bevan, R., Martin, N.: 3D printing of wood fibre biocomposites: from mechanical to actuation functionality. *Mater. Des.* **96**, 110–114 (2016)
31. Kuo, C., Liu, C., Teng, W., Chang, H.: Preparation of starch/Acrylonitrile-Butadiene-Styrene copolymers (ABS) biomass alloys and their feasible evaluation for 3D printing applications. *Compos. B Eng.* **86**, 36–39 (2016)
32. Sabino, M., Fermín, Z., Marielys, L., Moret, J.: In vitro biocompatibility study of biodegradable polyester scaffolds constructed using fused deposition modeling. In: The International Federation of Automatic Control, Fortaleza, Brazil (2013)
33. Drummer, D., Cuellar, S.C., Rietzel, D.: Suitability of PLA/TCP for fused deposition modeling. *Rapid Prototyp. J.* **18**(6), 500–507 (2012). <https://doi.org/10.1108/13552541211272045>
34. Dul, S., Fambri, L., Pegoretti, A.: Filaments production and fused deposition modelling of ABS/carbon nanotubes composites. *Nanomaterials* **8**, 49 (2018). <https://doi.org/10.3390/nan8010049>
35. Dul, S., Fambri, L., Pegoretti, A.: Fused deposition modelling with ABS-graphene nanocomposites. *Compos. Part A: Appl. Sci. Manuf.* **85**, 181–191 (2016)
36. Francis, V., Jain, P.K.: Experimental investigations on fused deposition modelling of polymer-layered silicate nanocomposite. *Virt. Phys. Prototyp.* **11**(2), 109–121 (2016)
37. Melenka, W., Cheung, K., Schofield, J., Dawson, M., Carey, J.: Evaluation and prediction of the tensile properties of continuous fibre-reinforced 3D printed structures. *Compos. Struct.* **153**, 866–875 (2016)
38. Wei, X., Li, D., Jiang, W., Gu, Z., Wang, X., Zhang, Z., Sun, Z.: 3D printable graphene composite. *Sci. Rep.* **11**181 (2015)
39. Singh, R., Singh, S., Fraternali, F.: Development of in-house composite wire-based feedstock filaments of fused deposition modelling for wear-resistant materials and structures. *Compos. B Eng.* **98**, 244–249 (2016)
40. Garg, H., Singh, R.: Investigations for melt flow index of Nylon6-Fe composite based hybrid FDM filament. *Rapid Prototyp. J.* **22**(2), 338–343 (2016)
41. Nikzad, M., Masood, H., Sbarski, I.: Thermo-mechanical properties of a highly filled polymeric composites for fused deposition modeling. *Mater. Des.* **32**(6), 3448–3456 (2011)
42. Soundararajan, R., Jayasuriya, N., Vishnu, R., Prasad, B., Pradeep, C.: Appraisal of mechanical and tribological properties on PA6-TiO₂ composites through fused deposition modelling. *ICMPC-2019 Materials Today: Proceedings* (2019). <https://doi.org/10.1016/j.ijfatigue.2019.105275>
43. Masood, H., Song, Q.: Development of new metal/ polymer materials for rapid tooling using fused deposition modelling. *Mater. Des.* **25**, 587–594 (2004)
44. Owolabi, G., Peterson, A., Habtour, E., Riddick, J., Coatney, M.: Dynamic response of Acrylonitrile butadiene styrene under impact loading. *Int. J. Mechan. Mater. Eng.* **11**(1), 1–8 (2016)
45. Wu, W., Geng, P., Li, G., Zhao, D., Zhang, H.: Influence of layer thickness and raster angle on the mechanical properties of 3D-printed PEEK and a comparative mechanical study between PEEK and ABS. *Materials* **8**(9), 5834–5846 (2015)

46. Cruz, P., Shoemaker, E., Adam, P., Leachman, J.: Tensile strengths of polyamide-based 3D printed polymers in liquid nitrogen. *IOP Publishing* **102**(1), 1–6 (2015)
47. Perez, T., Roberson, A., Wicker, R.: Fracture surface analysis of 3D-Printed tensile specimens of novel ABS-based materials. *J. Fail. Anal. Prev.* **14**, 343–353 (2014)
48. Lee, H., Abdullah, J., Khan, Z.: Optimization of rapid prototyping parameters for production of flexible ABS object. *J. Mater. Process. Technol.* **169**, 54–61 (2005)

Chapter 35

A Critical Review on Dissimilar Joining of ASS and FSS



Chetan Tembhurkar, Ravinder Kataria, Sachin P. Ambade,
and Jagesvar Verma

Abstract Austenitic stainless steel used worldwide in various major industries like chemical, petrochemical and shipbuilding industries but the cost of material is high and it highly affects the producers and end-users. But, Ni price is the prime concerned for various industries as there is a shortage of nickel and nickel price increasing day by day according to the London Metal Exchange (LME). So, the demand for low nickel alloy which might be welded with austenitic stainless steel will be used worldwide in industries that need higher heat input, correct choice of filler material and defect-free joints for high production rate. However various welding techniques like Tungsten Inert Gas (TIG)/Metal Inert Gas (MIG)/Electron beam (EBW)/Shielded metal arc (SMAW)/Submerged arc (SAW)/Electron Beam Melting (EBM)/Resistance Spot/Laser and friction welding are used for welding austenitic with ferritic stainless steel. Apart from different techniques used for welding, the dissimilar welding is advantageous proving beneficial and more popular. However dissimilar welding is not so easy and information regarding this is dispersedly available. In view of this, systematic information for better understanding of this process is needed. This paper attempts a critical review of the process of joining the fundamental difference between ferritic and austenitic stainless steel, effect on a microstructure, mechanical properties and resistance to corrosion in various combinations.

Keywords Austenitic stainless steel · Dissimilar welding · Different welding conditions · Heat input and ferritic stainless steel

C. Tembhurkar (✉) · R. Kataria
School of Mechanical Engineering, LPU, Jalandhar, Punjab, India

S. P. Ambade
Department of Mechanical Engineering, YCCE, Nagpur, Maharashtra, India

J. Verma
Department of Manufacturing Engineering, NIFFT, Ranchi, Jharkhand, India

35.1 Introduction

An austenitic stainless steel (ASS) is employed worldwide as a result of its higher strength and higher corrosion resistance. But due to the high nickel price which is increasing day by day the whole replacement of 300 series austenitic stainless steel is not possible but welding with ferritic stainless steel (FSS) 400 series is possible as this steel has higher property than ASS. The deformation is limited to the FSS exclusively in stainless steel joint of austenitic-ferritic [1]. Welding techniques such as electron beam (EBW)/tungsten inert gas (TIG), and friction welding is used to join dissimilar material [2]. For joining the two materials there are different parameters which are current, voltage, welding speed, energy input and types of filler materials used in welding. The optimum parametric combination can be determined by Taguchi-Desirability analysis for optimization of process parameters [3].

35.2 Problem During Welding

For different industrial applications 316L ASS is widely used in industrial applications are completely different on different leading temperature for exceptional mechanical properties and better resistance against corrosion [4]. An addition of nickel into bit contributes to develop the mechanical strength and creep resistance of the material [5]. During welding, FSS would be difficult to weld due to excessive growth of grains, coarse grains into heating affected zone (HAZ) and welding zone of fusion welding. But according to the various authors of the low heat input reduces the formation of coarse grains into a material [6]. A sensitization and mechanical properties of FSS can be eliminated by adding carbide and nitride [7]. Teker and Kurşun [8] investigated ferritic stainless steel (AISI 430) which showed higher tensile strength, minimum heat affected zone (HAZ) and less grain growth in GMAW-P joints compared with GMAW joints due to minor heating input, better hardness of fusion, and better fusion zone grain. Mallaiah et al. [9] improve the percentage of weight of titanium(Ti), copper(Cu), and aluminum(Al) for operation of mechanical properties and substance of austenite within the welding region for AISI 430 FSS by Taguchi Method. Sarkari Khorrami et al. [10] used GTAW for welding plain carbon steel and AISI 430 FSS by using ER309L filler metal, the ultimate tensile strength, absorbed energy and hardness increases by the addition of filler metal.

35.3 Process Selection

Tjong et al. [11] investigated in 316L ASS and the same two metals are joined by utilizing electron beam welding (EBW) and laser technology. The joint failed in the parting and the HAZ regions of the weld due to creep. Reddy et al. [12] used friction

and electron beam welding for a same and different from ferritic stainless steel (AISI 430), austenitic stainless steel (AISI304), and duplex stainless steel (AISI 2205). Steel welding duplex stainless-steel highest observed tensile strength while friction welding shows better resistance to impact and notch tensile strength of welding by electron beam. Martins et al. [13] replaced AISI 316L ASS with Cr-Mn Stainless Steel having less pitting corrosion resistance by TIG Welding process and by analysing the fatigue crack propagation in the exhaust system of a naval gas turbine. Sarkari Khorrami et al. [10] found ductile fracture in specimen welded with ER 309 L filler metal though in autogenous weld, plain carbon steel welded with AISI 430FSS by GTAW the cleavage fracture occurs. Reddy et al. [14] welded AISI 4140 and AISI 316, using a TIG welding method with and without filler and found that the weld strength is judged to be higher and comparable. Hara et al. [15], used Ferritic/Martensitic and 316L austenitic steel. Electron beam welding is used to locate the mechanical properties and better by optimizing the position of the electron beam welding. Ravikumar et al. [16], found that higher tensile strength obtained at a 75° groove angle, 120 A current, and 15 LPM gas flow rate. The range of hardness for the weld zone is 153–172 BHN for 304 ASS by TIG welding. Singh et al. [17] found that 5-weld pass technique caused greater impact toughness than the 3-weld pass technique by using 316 ASS compared with GTAW and GMAW process. Ghasemi et al. [18] found that grain growth phenomenon was accompanied by the martensite formation in HAZ of FSS therefore this region was the weakest zone in all specimens by welding 304 with 430 FSS by GTAW process. Verma et al. [19] welded dissimilar joints AISI 430 and UNS 32,205 of stainless steel with arc welding technique and found that UNS 32,205 provides better charge transfer resistance which indicates that the sample shows the optimum corrosion resistance than others. The filler E309LMo and duplex E2209 electrodes shows better weld joints. Jeraldnavinsavio et al. [20] welded dissimilar metals of AISI 316L ASS and 430FSS with TIG welding process and with two types of fillers ER310 and ER2594 and found that the ER2594 weld shows greater mechanical properties than ER310 filler weld.

35.4 Dissimilar Welding of 316L ASS and 430FSS with Other Alloys

The different researches have welded the austenitic and ferritic stainless steel with different types of fillers and there has been a change in the microstructure, mechanical and corrosion properties of the welded plates. Table 35.1 represents the fillers used for similar and dissimilar combination used by different researchers.

In the friction welding of 304 ASS and 430 FSS steel, the toughness and strength properties are greater than the base material of ferritic stainless steel [1]. Impacts of different welding process like FW, GTAW, and EBW upon a microstructure, the toughness and strength of ferritic stainless steels and austenitic similar to the combination of different metals are found. Resistance welding of dissimilar metals

Table 35.1 Fillers used for similar and dissimilar combination used by different researchers

Grades	316 L ASS	430 FSS	409 FSS	304 ASS	Carbon steel/low carbon steel	Duplex stainless steel
316 L ASS	316 L, Inconel 182, Inconel 82, 430L and 2209	E309L and E2209 Duplex SS	AISI 308	Without filler material	ER 309L	E2209
430 FSS	E309L and E2209	–	–	ER 430, 316 L, 2594 L	316 L, ER309 L	

is intermediate into a gas tungsten arc, electron beam, and friction welding shows improved toughness into all dissimilar welds [2].

There are different welding processes for Ferritic and Austenitic Stainless Steel such as Electron Beam/Friction/Gas Tungsten Arc/Resistance Spot/Gas Metal Arc/Laser Beam/Arc/Electron Beam Machining/Laser Beam Machining/and Spot Welding.

X-ray diffraction (XRD), energy dispersive spectroscopy (EDS) and scanning electron microscope (SEM) techniques can be utilized for analyse the welding evaluation of two dissimilar joints. Using SEM–EDS to analyse the friction welding performance of carbon steel in 304 ASS and AISI 1040, the results show that the increment of percentage of chromium combined with a concentration of carbon and nickel is sufficient for forming of several type of nickel-based intermetallic compound within a reduced range of carbide precipitation at an interface [21]. SEM/EDAX analysis of weldments in the heat-affected zone of AISI 4140 and AISI 316 showed that large amounts of iron and carbon and trace amounts of nickel, chromium and manganese [22]. According to EDAX analysis, it has been observed that in autogenously weldments form carbides into a heating affected zone of AISI 316, and the high percentage of C and Cr are present in the weldments [23]. X-ray diffraction (XRD) is utilized for analyse EBM manufactured by 316L ASS, in which a large proportion of delta ferrite is transformed into XRD spectrum located in the precursor and manufactured 316L stainless steel product [24].

35.5 Aspects of Mechanical Properties Due to Welding Parameters

The different welding parameters impact on microstructure, mechanical and corrosion properties of the welded metals. Tjong et al. [11] welded similar two plates of 316L ASS with electron beam welding process and found that the mechanical properties are virtuous for the parameters used and microstructural observation shows equiaxed and cellular structured grains. Reddy et al. [12] used GTAW to weld 304ASS

and 430FSS and found poor toughness compared to other welding processes due to the formation of columnar grains in the direction of crack. Martins et al. [13] welded 316L ASS and Cr Mn ASS by TIG welding process and found that the yield strength values found to be higher for Cr Mn ASS than 316L ASS at 24, 350 and 500 °C which leads to be an important factor to obtain shock resistance. Sarkari Khorrani et al. [10] revealed that the ER309L filler weld of AISI 430 and Plain Carbon Steel have greater hardness and tensile properties due to the higher absorbed energy with higher strength and ductility due to the presence of martensite and ferrite and strengthening elements. Reddy et al. [14] found that the tensile strength is reduced for the ER309L filler weld than autogenous weld due to the decrease in hardness value in 316L ASS side which results in fracture of 316L ASS side in tensile test. Hara et al. [15] used electron beam dissimilar welded F82HIEA and SUS 316L ASS and revealed that the tensile, hardness and toughness properties were improved due to the optimization of electron beam position. Singh et al. [17] compared 3-weld pass welding with 5-weld pass welding of 316L ASS and found that the impact toughness value for 5-pass weld were found to be higher than 3-pass weld due to the thermal aging techniques conducted at various time and temperatures. Verma et al. [25] used shielded metal arc welding to weld 316L ASS and 2205DSS with E2209 and E309L fillers and found that the ultimate tensile strength, hardness and toughness were found to be higher for E2209 filler weld than E309L filler weld. Jeraldnavinsavio et al. [20]. TIG welded 316L and 430 with fillers ER2594 and ER310 and found that the ER2594 weld have better mechanical properties (tensile and toughness) than ER310 filler weld. Table 35.2 represents the different suggested welding parameters by different researchers.

35.6 Corrosion Properties

The welded joints are more susceptible to corrosion attack in the heat affected zone region of the welded joints. Figures 35.1 and 35.2 show the cyclic potentiodynamic polarization (CPDP) curve for 316L ASS and 430 FSS in sodium chloride (NaCl) solution. The different researchers have predicted the intergranular and pitting corrosion attack on the weldments. The Chromium carbide formation predicts the presence of intergranular corrosion in the weld joint. The intergranular corrosion were found in the autogenous weld of 316L ASS and 430 FSS were found to be highest than the ER309L and ER316L filler weld and found that the 430 FSS base metal found greater degree of sensitization than 316L ASS base metal [41]. The E2209 weld shows higher degree of sensitisation (Cr-C formation) than the E309LMo and E309L weld due to the more perception nature of the austenite. The highest pitting corrosion resistance were found with E2209 weld than other two filler welds due to the increased amount of nitrogen present in the duplex filler materials [26]. The dissimilar metal of AISI304L ASS and AISI430 FSS welded by GTAW with 316L and 2594L fillers with two different heat treatment temperatures 860 and 960 °C and found that the pitting corrosion resistance were found to be less for 860 °C than 960 °C due to the residual stress and presence of precipitation in grain boundaries due

Table 35.2 Different suggested welding parameters by different researchers

Welding processes	Welded material	Fillers used	Current (A)	Voltage (V)	Welding speed (mm/s)
EBW	316L ASS	–	0.042	60,000	20
GTAW	304ASS and 430 FSS	ER430	170	10	1.16
GTAW	430FSS and plain carbon steel	ER309L	85	12	2
GTAW	316ASS and 4140	ER309L	150–170	16–18	–
EBW	F82H IEA and SUS316L ASS	–	0.02	150,000	16.67
GTAW	316L ASS	–	120	18–20	4
GMAW	316L ASS	–	180–230	22–27	3–4
Arc welding	32,205 and 430	E309L Mo and E2209	120	21–29	4.6
SMAW	316L ASS and 2205DSS	E2209 and E309L	120	25–26	3.1–3.3
TIG	316L ASS and 430FSS	ER310 and ER2594	50–70	10–12	–

Fig. 35.1 CPDP curve for 316L ASS in 3.5 wt% NaCl [30]

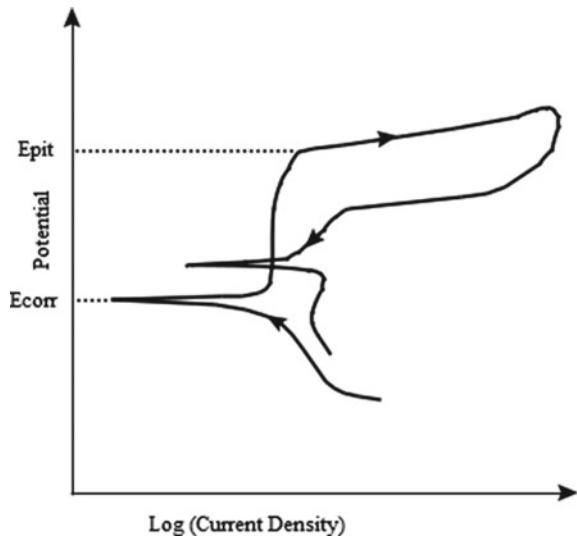
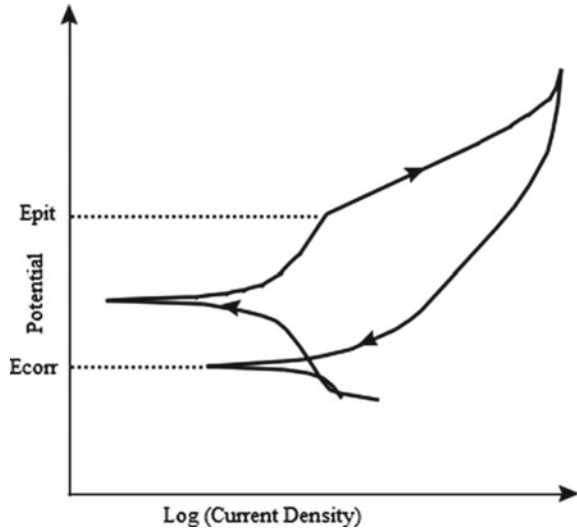


Fig. 35.2 CPDP curve for 430 FSS in 3 wt% NaCl [30]



to quenching [27]. Figure 35.3 shows the SEM/EDS images of the chromium carbide concentration for E309L, E309L Mo and E2209 filler weld. Figure 35.4 shows the SEM images of the pitting corrosion of base metal 430 and 304 L and HAZ area of ferritic and austenitic stainless steel at 860 and 960 °C. The variation in the heat input in GTAW varies the corrosion rate of 409 M ferritic stainless steel. The corrosion rate were found to be less for GTAW as compared to GMAW and SMAW [28]. As for higher heat input the corrosion rate is less as compared to low heat input due to the presence of grain boundary austenite (GBA) and windmanstatten austenite (WA) with high nickel content which increases the corrosion resistance of the weld joint [29].

In the presence of aggressive ions, the breakdown of the passivation film will produce corrosion similar to pitting corrosion. The special type potentiometer is used for electrochemical measurement. The cyclic potentiodynamic polarization (CPDP) is employed for beginning of passivity, breakdown of oxide film, susceptibility to repassivation and calculation of the rate of pitting corrosion due to the extensive variety of scanning potential [30]. ASTM G61 and F2129 standards are used to conduct the CPDP test for iron, nickel or cobalt based alloys [30]. Record the steady-state potential after immersing the sample within the electrolyte for 10 min, and use a scanning potentiostat to increase the potential at scanning rate of 2 mV/s [31]. A current potential increase suddenly after passive zone is pitting potential (E_{pit}). Samples showing a large number of positive potentials are considered to have superior pitting resistance [32]. As comparing with the parent metal, the resistance to pitting corrosion of the weld has been greatly improved, which can be because of a presence of the dynamic recrystallization microstructure and the consistency of the composition due to the increased cooling rate fast, which does not favour the separation of the element [1, 33].

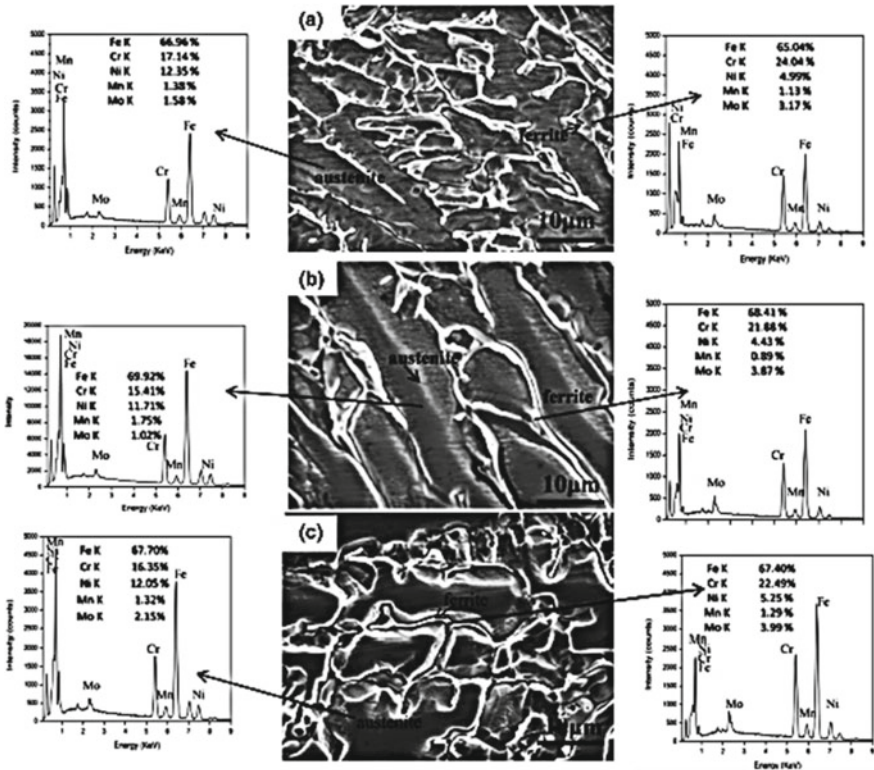


Fig. 35.3 SEM /EDS images of Chromium carbide precipitation for fillers E309L, E309L Mo and E2209 [26]

35.7 Temperature Distribution in the Weld Region

The temperature distribution in the weld region is given by the various advanced software such as ANSYS it helps to analyse the temperature fields and stress distribution in the weld joint, beam, etc. [34, 35]. The temperature distribution of the weld region for filler ER309L, ER316L and without filler are compared and found that the temperature distribution for without filler weld were found to be higher than other two types of fillers [36]. Two carbon steel plates were welded with manual metal arc welding process and the residual stresses and magnitude in the axial direction were obtained. The results shows that the experimental residual stresses values are very much noble with the simulation results [37]. The FEM simulation of similar 304 ASS by adapting constant heat flux analysis shows that the transient thermal temperature and residual stresses. The thermal temperature distributions at weld zone were found to be higher than the heat affected zone and base metal region [38]. The TIG and Laser welding techniques were used to weld two dissimilar Inconel 625 and AISI 316ASS and different mechanical properties are recorded such as yield strength, tensile strength

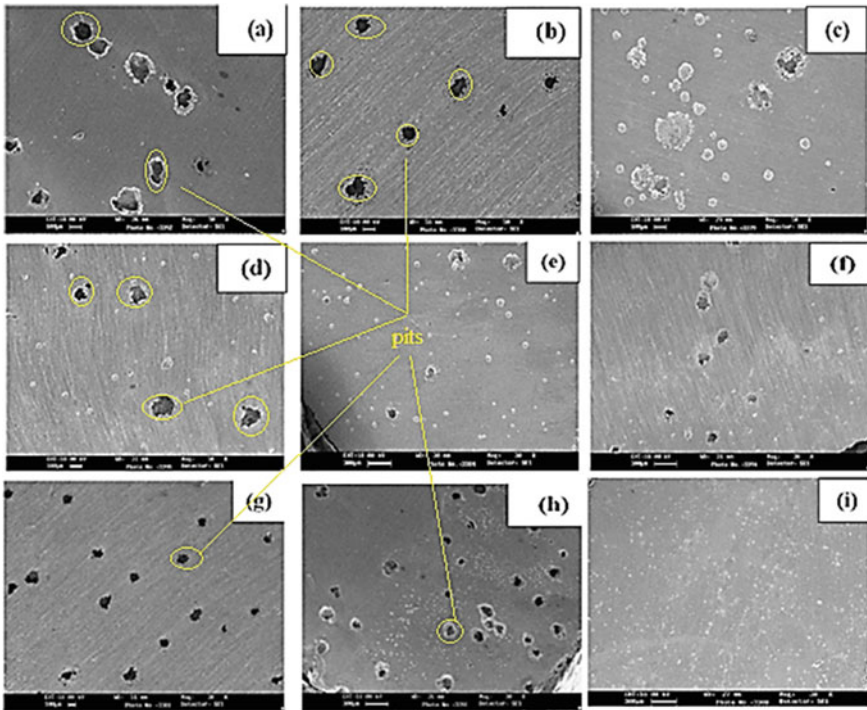


Fig. 35.4 SEM images of Pitting corrosion of base metal 430 and 304 L and HAZ area of ferritic and austenitic stainless steel at 860 °C and 960 °C [27]

and elastic modulus for different temperatures. The pseudo-linear approach was used to estimate the final stresses developed in the joint [39]. Figures 35.5, 35.6 and 35.7 show the temperature distribution across the weld region ER309L, ER316L (fillers) and autogenous weld.

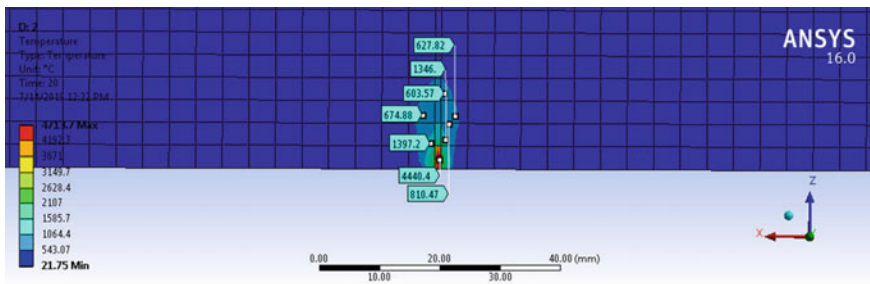


Fig. 35.5 Temperature distribution across the weld region for ER309L filler weld [36]

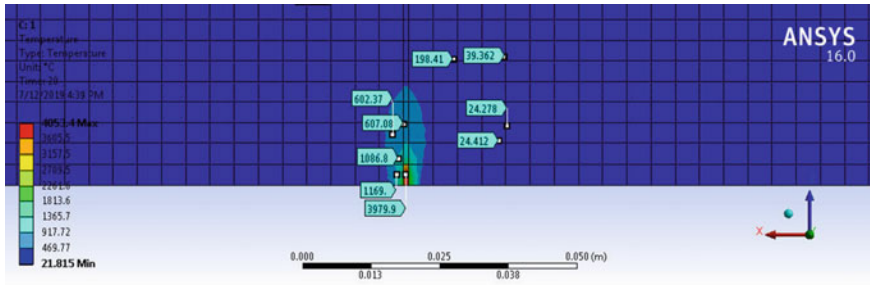


Fig. 35.6 Temperature distribution across the weld region for ER316L filler weld [36]

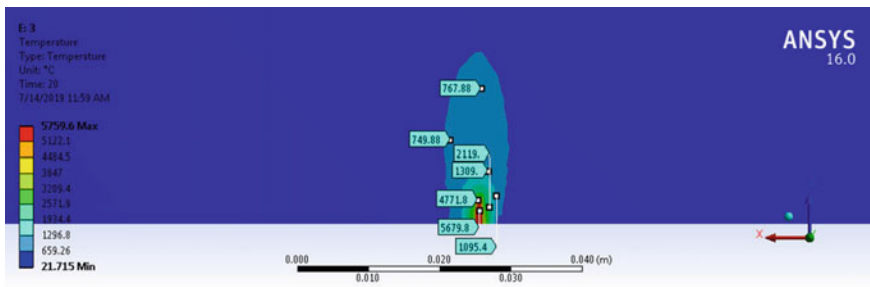


Fig. 35.7 Temperature distribution across the weld region for Autogenous weld [36]

35.8 Recent Trends and Future Perspectives

Many countries are being utilized several materials in a single industry to reduce the maintenance cost and increase the life span of the components such as chemical industries in the UK, petrochemical industries in USA & Japan and oil industries in Saudi Arabia which opens the wide space for the constructions with reliability or sustainability of the material. Irrespective of the extensive work by the researchers still there are many other issues.

Recent Trends

Currently, industries around the world need to fully own materials with higher strength and corrosion resistance composed of 316L ASS. The production has been significantly modified to find materials with the same strength and compatibility as 316L ASS. In some engineering applications that require the use of different materials for welding, outstanding and widely used grades require additional analysis in this space.

Welding of 316L ASS through different alloys (like ferrite, martensite and carbon steel) still clearly selects filler materials. In processes such as GTA, GMA, SMA welding, undesirable precipitates formed, and the increasing rate of deformation

in multi-pass welding is still a problem [40]. The high residual stresses obtained in friction welding resulted within the deformation of the material. Recently, the formation of welds and defects within the weld region due to the multi-pass welding process are some of the main issues in industries.

Future Perspective

The advanced techniques such as hybrid welding to join dissimilar metal still an issue and should be developed in the future. The main and foremost issue is the corrosion behaviour of dissimilar welding for other advanced processes. The development of a cost-efficient electrode is the need an hour for industries. It is a challenge for several sorts of analysis to seek out the heat distribution across the weld zone and analyse which parameter affects the foremost by analysing the heat distribution phenomenon.

35.9 Conclusions

- (1) The friction welding and fusion welding processes are well adequate for similar and dissimilar joining processes. But still, there is a scope in this area for a few materials of austenitic and ferritic grades.
- (2) The high heat rate when ferritic stainless steel is welded to other metals converts it to martensitic grade, hence they are prone to corrosion.
- (3) Advanced laser hybrid technique is required to weld thick materials as multi-pass welding increases the distortion of material.
- (4) The dissimilar welding of austenitic-ferritic steel by friction welding has higher strength and toughness than the base material of ferritic stainless steel.
- (5) Since an influence of carbides into a microstructure is smaller as comparing with similar welding processes (GTAW and EBW like), friction welding of the dissimilar weld has greater resistance to pitting corrosion.

References

1. Satyanarayana, V.V., Reddy, G.M., Mohandas, T.: Dissimilar metal friction welding of austenitic-ferritic stainless steels. *J. Mater. Process. Technol.* **160**(2), 128–137 (2005). <https://doi.org/10.1016/j.jmatprotec.2004.05.017>
2. Reddy, G.M., Mohandas, T., Rao, A.S., Satyanarayana, Y.V.: Influence of welding processes on microstructure and mechanical properties of dissimilar austenitic-ferritic stainless steel welds. *Mater. Manuf. Process.* **20**(2), 147–173 (2005). <https://doi.org/10.1081/AMP-200041844>
3. Ghosh, N., Pal, P.K., Nandi, G.: GMAW dissimilar welding of AISI 409 ferritic stainless steel to AISI 316L austenitic stainless steel by using AISI 308 filler wire. *Eng. Sci. Technol. Int. J.* **20**(4), 1334–1341 (2017). <https://doi.org/10.1016/j.jestch.2017.08.002>
4. Weiss, B., Stickler, R.: Phase instabilities during high temperature exposure of 316 austenitic stainless steel. *Met. Trans.* **3**(4), 851–866 (1972). <https://doi.org/10.1007/bf02647659>

5. Ganesan, V., Ganesh Kumar, J., Laha, K., Mathew, MD.: Notch creep rupture strength of 316LN SS and its variation with nitrogen content. *Nucl. Eng. Des.* **254**, 179–184 (2013). <https://doi.org/10.1016/j.nucengdes.2012.10.001>
6. Ramkumar, K.D., et al.: Comparative studies on the weldability, microstructure and tensile properties of autogeneous TIG welded AISI 430 ferritic stainless steel with and without flux. *J. Manuf. Process.* **20**, 54–69 (2015). <https://doi.org/10.1016/j.jmapro.2015.09.008>
7. van Warmelo, M., Nolan, D., Norrish, J.: Mitigation of sensitisation effects in unstabilised 12%Cr ferritic stainless steel welds. *Mater. Sci. Eng. A* **464**(1–2), 157–169 (2007). <https://doi.org/10.1016/j.msea.2007.02.113>
8. Teker, T., Kurşun, T.: Weldability of AISI 430/AISI 1030 steel couples via the synergic controlled pulsed (GMAW-P) and manual gas metal arc (GMAW) welding techniques. *Mater. Manuf. Process.* **26**(7), 926–932 (2011). <https://doi.org/10.1080/10426914.2011.551909>
9. Mallaiah, G., Kumar, A., Ravinder Reddy, P., Madhusudhan Reddy, G.: Influence of grain refining elements on mechanical properties of AISI 430 ferritic stainless steel weldments—Taguchi approach. *Mater. Des.* **36**, 443–450 (2012). <https://doi.org/10.1016/j.matdes.2011.11.063>
10. Sarkari Khorrami, M., Mostafaei, M.A., Pouraliakbar, H., Kokabi, A.H.: Study on microstructure and mechanical characteristics of low-carbon steel and ferritic stainless steel joints. *Mater. Sci. Eng. A* **608**, 35–45 (2014). <https://doi.org/10.1016/j.msea.2014.04.065>
11. Tjong, S.C., Zhu, S.M., Ho, N.J., Ku, J.S.: Microstructural characteristics and creep rupture behavior of electron beam and laser welded AISI 316L stainless steel. *J. Nucl. Mater.* **227**, 24–31 (1995)
12. Reddy, G.M., Rao, K.S.: Microstructure and mechanical properties of similar and dissimilar stainless steel electron beam and friction welds. *Int. J. Adv. Manuf. Technol.* 875–888 (2019). <https://doi.org/10.1007/s00170-009-2019-6>
13. Martins, R.F., Matos, J.B., Branco, C.M.: On the use of a new ultrahigh-strength Cr-Mn austenitic stainless steel in gas turbine's exhaust systems. *Procedia Eng.* **10**, 2554–2559 (2011). <https://doi.org/10.1016/j.proeng.2011.04.421>
14. Reddy, M.P., et al.: Assessment of mechanical properties of AISI 4140 and AISI 316 dissimilar weldments. *Procedia Eng.* **75**, 29–33 (2014). <https://doi.org/10.1016/j.proeng.2013.11.006>
15. Hara, N., et al.: Mechanical Property Changes and Irradiation Hardening Due to Dissimilar Metal Welding with Reduced Activation Ferritic/Martensitic Steel and 316L Stainless Steel, vol. 1055 (July 2017)
16. Ravikumar, J., Acharya, G.D., Kikani, P.: Experimental Investigation of Welding Process Parameters on Mechanical Properties for TIG Welded Austenitic Stainless Steel 30, vol. 8, pp. 13–16 (2017)
17. Singh, R.: Influence of Multipass Welding Procedures and Thermal Aging Conditions on the Impact Toughness of AISI 316 Austenitic Stainless Steel Butt Welded Joints, vol. 13, no. 11, pp. 9283–9287 (2018)
18. Ghasemi, R., Beidokhti, B., Fazel-Najafabadi, M.: Effect of delta ferrite on the mechanical properties of dissimilar ferritic-austenitic stainless steel welds. *Arch. Metall. Mater.* **63**(1), 437–443 (2018). <https://doi.org/10.24425/118958>
19. Verma, J., Taiwade, R.V., Kataria, R., Kumar, A.: Welding and electrochemical behavior of ferritic AISI 430 and austeno-ferritic UNS 32205 dissimilar welds. *J. Manuf. Process.* **34**(April), 292–302 (2018). <https://doi.org/10.1016/j.jmapro.2018.06.019>
20. Jeraldnavinsavio, D., Farid, A.M., Ramanamurthy, E.V.V., Porchilamban, S., Ravikumar, S.: Science direct evaluation of mechanical properties and micro structural characterization of dissimilar TIG welded AISI 316L and AISI 430 plates using ER310 and ER2594 filler. *Mater. Today Proc.* **16**, 1212–1218 (2019). <https://doi.org/10.1016/j.matpr.2019.05.216>
21. James, J.A., Sudhish, R.: Study on effect of interlayer in friction welding for dissimilar steels: SS 304 and AISI 1040. *Procedia Technol.* **25**, 1191–1198 (2016). <https://doi.org/10.1016/j.protcy.2016.08.238>
22. Reddy, M.P., William, A.A.S., Prashanth, M.M., Kumar, S.N.S., Ramkumar, K.D., Arivazhagan, N.: Assessment of mechanical properties of AISI 4140 and AISI 316 dissimilar weldments. *Procedia Eng.* **75**, 29–33 (2014). <https://doi.org/10.1016/j.proeng.2013.11.006>

23. Khan, M.M.A., Romoli, L., Dini, G.: Optics and laser technology laser beam welding of dissimilar ferritic / martensitic stainless steels in a butt joint configuration. *Opt. Laser Technol.* **49**, 125–136 (2013). <https://doi.org/10.1016/j.optlastec.2012.12.025>
24. Segura, I.A., et al.: Characterization and mechanical properties of clad stainless steel 316L with nuclear applications fabricated using electron beam melting. *J. Nucl. Mater.* **507**, 164–176 (2018). <https://doi.org/10.1016/j.jnucmat.2018.04.026>
25. Verma, J., Taiwade, R.V., Khatirkar, R.K., Kumar, A.: A comparative study on the effect of electrode on microstructure and mechanical properties of dissimilar welds of 2205 austeno-ferritic and 316L austenitic stainless steel. *Mater. Trans.* **57**(4), 494–500 (2016). <https://doi.org/10.2320/matertrans.M2015321>
26. Verma, J., Taiwade, R.V.: Effect of austenitic and Austeno-ferritic electrodes on 2205 Duplex and 316L austenitic stainless steel dissimilar welds. *J. Mater. Eng. Perform.* (2016). <https://doi.org/10.1007/s11665-016-2329-4>
27. Ghorbani, S., Ghasemi, R., Ebrahimi-Kahrizangi, R., Hojjati-Najafabadi, A.: Effect of post weld heat treatment (PWHT) on the microstructure, mechanical properties, and corrosion resistance of dissimilar stainless steels. *Mater. Sci. Eng. A* **688**, 470–479 (2017). <https://doi.org/10.1016/j.msea.2017.02.020>
28. Ambade, S., Sharma, A., Patil, A., Puri, Y.: Effect of welding processes and heat input on corrosion behaviour of Ferritic stainless steel 409M. *Mater. Today Proc.* **xxxx** (2020). <https://doi.org/10.1016/j.matpr.2020.06.251>
29. Verma, J., Taiwade, R.V., Khatirkar, R.K., Sapate, S.G., Gaikwad, A.D.: Microstructure, Mechanical and Intergranular Corrosion Behavior of Dissimilar DSS 2205 and ASS 316L Shielded Metal Arc Welds. *Trans. Indian Inst. Met.* **70**(1), 225–237 (2017). <https://doi.org/10.1007/s12666-016-0878-8>
30. Esmailzadeh, S., Aliofkhaezai, M., Sarlak, H.: Interpretation of cyclic potentiodynamic polarization test results for study of corrosion behavior of metals: a review. *Prot. Met. Phys. Chem. Surf.* **54**(5), 976–989 (2018). <https://doi.org/10.1134/S207020511805026X>
31. Oldfield, J.W.: Test techniques for pitting and crevice corrosion resistance of stainless steels and nickel-base alloys in chloride-containing environments. *Int. Mater. Rev.* **32**(1), 292–306 (1987). <https://doi.org/10.1179/095066087790150313>
32. Reddy, G.M., Rao, K.S., Sekhar, T.: Microstructure and pitting corrosion of similar and dissimilar stainless steel welds. *Sci. Technol. Weld. Join.* **13**(4), 363–377 (2008). <https://doi.org/10.1179/174329308X299968>
33. Lakshminarayanan, A.K., Balasubramanian, V.: An assessment of microstructure, hardness, tensile and impact strength of friction stir welded ferritic stainless steel joints. *Mater. Des.* **31**(10), 4592–4600 (2010). <https://doi.org/10.1016/j.matdes.2010.05.049>
34. Deogade, S.R., Ambade, P.S.P., Patil, A.: Finite Element Analysis of Residual Stresses on Ferritic Stainless Steel using Shield Metal Arc Welding, vol. 3, no. 2, pp. 1131–1137 (2015)
35. Waghmare, S., Mungle, N., Tembhurkar, C., Shelare, S., Pathare, N.: Design and analysis of power screw for manhole cover lifter. *Int. J. Recent Technol. Eng.* **8**(2), 2782–2786 (2019). <https://doi.org/10.35940/ijrte.B2628.078219>
36. Tembhurkar, C., Kataria, R., Ambade, S., Verma, J.: Transient analysis of gta-welded austenitic and ferritic stainless steel. *Lect. Notes Mech. Eng.* 59–65 (2020). https://doi.org/10.1007/978-981-15-4748-5_6
37. Review, S.T.: Finite element analysis of residual stress in butt welding two similar plates. *Computer (Long. Beach. Calif)* **1**, 57–60 (2009)
38. Vemanaboina, H., Akella, S., Buddu, R.K.: Welding process simulation model for temperature and residual stress analysis. *Procedia Mater. Sci.* **6**, 1539–1546 (2014). <https://doi.org/10.1016/j.mspro.2014.07.135>
39. Capriccioli, A., Frosi, P.: Multipurpose ANSYS FE procedure for welding processes simulation. *Fusion Eng. Des.* **84**(2–6), 546–553 (2009). <https://doi.org/10.1016/j.fusengdes.2009.01.039>
40. Verma, J., Taiwade, R.V.: Effect of welding processes and conditions on the microstructure, mechanical properties and corrosion resistance of duplex stainless steel weldments—a review. *J. Manuf. Process.* **25**, 134–152 (2017). <https://doi.org/10.1016/j.jmapro.2016.11.003>

41. Tembhurkar, C., Kataria, R., Ambade, S., Verma, J., Sharma, A., Sarkar, S.: Effect of fillers and autogenous welding on dissimilar welded 316L austenitic and 430 ferritic stainless steels. *J. Mater. Eng. Perform.* <https://doi.org/10.1007/s11665-020-05395-4>

Chapter 36

Industrial Waste Management in Portugal for Environmental Development



**Mayank, Vaibhav Chaturvedi, Tmana Mahajan, Ravi Pratap Singh,
Parampreet Kaur, and Amit Arora**

Abstract Portugal received 330,915 tons of waste and out of which 57,740 tons of waste has already been exported according to the 2018 Transboundary Waste Movement Survey. Shortly, Portugal is preparing to reduce this import. Physical, chemical, high temperature, and biological approaches are utilized for the handling of hazardous waste. Hazardous waste which cannot be treated by incineration or other chemical methods is landfilled. Disposing radioactive wastes in lagoons is risky. It is advised to get a form of engineering studies before any remedial action. The current research has systematically examined the numerous kinds of hazardous waste produced in Portugal and its management.

Keywords Environment · Hazardous waste · Industrial · Portugal

36.1 Introduction

As more and more industries and companies emerge, waste generation from factories and societies in industrialized and developing countries has continued to increase, together with rising urbanization rates and global population. Consequently, proper management of waste is required at all levels of society. Waste management is the behaviour and practices necessary, including mitigation measures for the treatment

Mayank (✉) · V. Chaturvedi · T. Mahajan
Department of Civil Engineering, Dr B R Ambedkar National Institute of Technology (NIT),
Jalandhar, Punjab, India

R. P. Singh
Department of Industrial and Production Engineering, Dr B R Ambedkar National Institute of
Technology (NIT), Jalandhar, Punjab, India

P. Kaur
Department of Civil Engineering, Shaheed Bhagat Singh State University Campus, Ferozepur,
Punjab, India

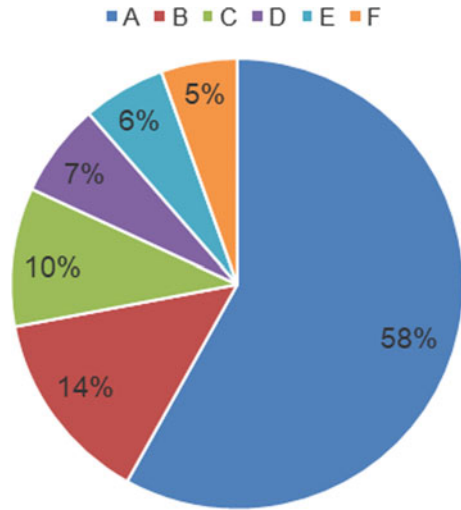
A. Arora
Department of Chemical Engineering, Shaheed Bhagat Singh State University Campus,
Ferozepur, Punjab, India

or recycling of waste from source to the final disposal. Waste may be liquid, solid or gas, and with each form of destruction, there are various management and disposal methods. In certain situations, waste can pose a danger to human health. Waste is often generated by human operations, such as refining and mining of raw materials. Waste management is proposed to reduce the unfriendly health, environmental or aesthetic effects of waste and enhance hygiene. Waste management acts are not universal among all developed- and developing-country countries; regions (urban and rural) and residential and industrial areas can follow different strategies. The enormous waste management system handles municipal solid waste (MSW) and wastes, comprised of the heft of the waste created by agricultural, domestic and commercial operations.

Outside the development of large quantities of liquid and solid waste, rapid industrialization has culminated in sugar, pulp and paper, fruit and food processing, Amylum, distillery, livestock, tannery, slaughterhouses, poultry, etc. Such pollutants are usually discarded on land or dumped onto water sources, given the criteria for emission control measures, though. Portugal Industry was put together in several large urban areas: South Focal Lisbon-Setubal and North Porto-Aveiro-Braga. Overall, they produced almost three-fourths of both of the total manufacturing production in Portugal. The territories of Lisbon contained significant undertakings like iron and steel; development and maintenance of transport; oil processing, equipment, mineral, cement and electronics, liquor and fruit. Setubal, some 80 km south-east of Lisbon, also had an immense shipyard and vehicle assembly and machine production facility, an amendment, wood pulp, plug and fish handling plants. Sines, which is centred 40 km Lisbon, was the locate Deepwater port and large industrial complex. Started under Caetano, Sines installed an oil refinery, petrochemical facilities, and a coal-fired power plant of 1200 megawatts. Mainly a centre of light manufacture centre Porto contained textiles, shoes, wine, and food handling. Porto was also the region with the most significant oil refinery in the world. The other one was based in Lisbon. Portimao became a fishing place. Aveiro invested much time not only in wood pulp and other wood products but also in boots and machinery. Braga trades in textiles, cutlery, chairs, and accessories. Covilha was a textiles region, too [1]. All industrial installation sector in percentages shown Fig. 36.1.

Waste management is a significant component in a business or an industrial ability to retain ISO14001 accreditation. The ISO14001 standard helps companies to expand their waste by eliminating waste through resource recovery procedures, management and environmental efficiencies each year. Implementing resource recovery procedures such as recycling products such as food scraps, paper and cardboard, glass, metals, and plastic bottles is one way to do this. It is possible to supply recycled materials to the building industry [4]. Many inorganic waste sources may be used to produce construction materials.

Fig. 36.1 Number of Industrial emissions directive (IED) industrial installations by sector, Portugal (2015) [2, 3]. **A** = Food, drink, textiles, surface treatment, pulp, paper, wood, intensive rearing of poultry or pigs and other activities. **B** = Non-hazardous waste and hazardous waste. **C** = Mineral and other. **D** = Metals (Iron and steel), Non-ferrous. **E** = Chemical. **F** = Energy and Power



36.2 Methodology

Industrial waste generated by the inventory of data relating to industrial waste generation was developed by conducting a list of Academic surveys and accompanied by data verification field visits. It is essential to verify the data obtained from the previous secondary data options (either published data or available for another industry producing similar products). The estimated rates of industrial waste generation from plant capacity in the Portuguese industry are available and will help recognise any inaccurate data and corrections in the database. The key search engines used were: ScienceDirect, PubMed, and ResearchGate. These are the primary sources of academic information on managing waste and threats to the environment and public health. A search was also carried out on the Ministry of the Environment's website, the central government agency responsible for Portugal's environmental management. Investigations were also carried out on the websites of critical newspapers and industry sources. 'Portugal', 'Industrial waste management' were the principal terms used. To ensure that the content was as recent as possible, articles that were more than five years old were excluded from the search. Focusing on only reliable and verifiable sources is (e.g., Government sources).

36.3 Hazardous Industrial Waste in Portugal

Every year the European Union generates about 3 billion tons of waste, out of which 90 million tons are hazardous waste, these wastes are very harmful to the Environment. In the early 90s in Europe, there was an increase in production of 10% waste.

To deal with this problem, some part of the waste was dumped into the incinerator. This caused extreme damage to the Environment. This condition is very harmful to human health as well as plants and animals. Considering it as a severe problem, the European Union and the Portuguese made a policy. The main objective of this policy was to reduce the rate of increase in waste produced every year. In 1997 Strategic Plan (PERSUI) was created in Portugal. So that the amount of solid waste can be reduced [5]. The most significant and most rancorous environmental dispute in the nation's history, which occurred in Portugal, was the decontamination of hazardous industrial waste in cement kilns by the co-incineration method. There was a controversy where between government and experts over dangerous industrial waste management. Their behaviour exposed the false premise that a decontextualized technical and science policy focused solely on mathematical likelihood equations might take the place of the political order, societal needs and values.

The main reason for the origin of hazardous waste is industrial waste. It is found in solid, liquid and gaseous state. Various agencies have defined dangerous waste in their ways. Thus, no uniformly accepted international definition has been created so far. According to the National Institute of Waste, Portugal generated around 13 million tons of industrial waste in 2001, 1.4% of which was hazardous. In this, South Region (Lisbon, Setubal) and North Region (Porto, Aveiro, Braga) dangerous toxic waste production added much. The mining sector, manufacturing industry and energy have contributed to the enormous amount of pollution. The production of industrial waste increased by about 50% in the middle of 1998 until 2007. Portugal sent 193,928 tons of hazardous waste for recycling and disposal in 2008 [6] (Table 36.1).

Table 36.1 Hazardous industrial waste in Portugal (2000), [7]

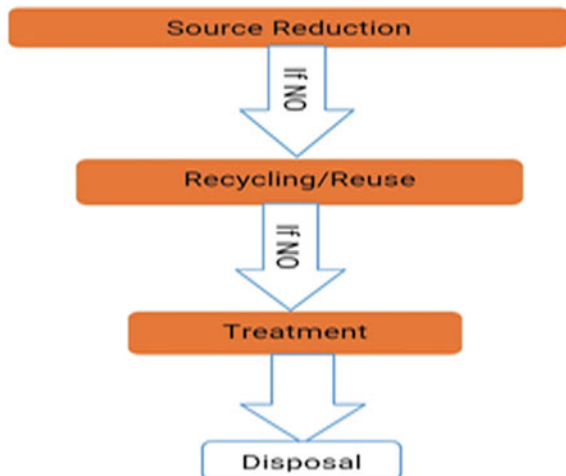
S.No	Hazardous industrial waste	Percentages
1	Oil refinement and used oils	51.0
2	Solvents, ink, polish and enamel	13.1
3	Organic	12.8
4	Treatment of metal, water treatment and plastic surfaces	6.2
5	Inorganic material from the thermal process and inorganic material with metals	6.1
6	Inorganic chemist	4.3
7	Non specified and other	6.5

36.4 General Principles of Waste Management

36.4.1 Waste Hierarchy

The waste hierarchy explains that about EUR 0.033 has been decreased, processed and re-used to identify waste management methods according to their suitability in waste minimization. The hierarchy of waste is the reason for most waste minimization strategies. The goal of the waste hierarchy is to increase the goods' functional utility and produce minimal volumes of end waste. Provided that the rudimentary waste hierarchy is a pyramid, the idea is that strategies would encourage attempts to prevent the creation of waste. The next or preferred step is to search for alternate uses for waste already created (i.e., reuse). Next is recycling, like composting. This process is accompanied by resource recycling and waste-to-energy. The final action is recycling, incineration and waste disposal, without energy recovery. This last step is not to prevent, redirect or recover waste from the final resort. While complete and absolute waste prevention is almost impossible, the most effective way of waste management is to avoid waste generation at least it reduces waste generation. The waste hierarchy reflects the progression through sequential phases of the waste management pyramid of a material or product. This plan's main objective was to reduce waste and promote recovery and recycling centres with technology. To manage this plan, the European Union approved the management of waste by the hierarchy waste management principles (Fig. 36.2), which was included in the (PESGRI99) Act [7, 8].

Fig. 36.2 Hierarchy waste management principle [8]



36.4.2 *Polluter-Pays Principle*

The polluter pays theory allows the polluting group to compensate for the effect on the climate. Regarding waste control, this is generally related to the requirement for waste generators to compensate for the effective disposal of unrecoverable content.

36.4.3 *Resource Efficiency*

The efficiency for resources reflects the fundamental understanding that the existing production and consumption patterns cannot maintain world economic growth and development. Universally, humans extract more energy than the earth can replenish to generate products and services. Energy efficiency is the elimination of the environmental effects of these products' manufacture and consumption, from the final production of raw materials to the last use and then disposal.

36.5 Waste Transport and Handling Practices

Methods for waste disposal vary significantly between different countries. Domestic waste disposal systems are supplied regularly by municipal councils or commercial waste collection services. Companies of commercial and industrial waste. There is no structured waste collection system in some areas and regions, particularly in less developed countries. Curbside collection is the most common disposal method in most of Canada, New Zealand, the US, Europe and many other areas of the developed world, where waste is gathered regularly at intervals by specialist vehicles. This is generally related to the isolation of curb-side waste. Waste will have to be carried to the rural transfer station. The waste obtained is then transferred to appropriate treatment facilities. Vacuum collection is used in several areas, where waste is intrigued by vacuum along some small-scale tubes from ho companies. Systems are in operation in Europe and North America. Unsegregated garbage is processed and converted into unusable waste and recyclables in different jurisdictions at the curb-or waste collection stations. These machines will sort large amounts of solid waste, conserve recyclable materials and turn the remains into biogas and soil conditioners. In San Francisco, with its zero-wash goal by 2020, the city government (LG) set up the Obligatory Recycling and Composting Ordinance (MRCO), which required everyone to keep compostable recyclables from the waste site. The Wonderful three-bin curbside device collects the three streams. Black for waste-fill materials, blue for recyclables and green for compostable commodities sponsored and serviced for businesses and people by Recology (San Francisco's only reject carrier). "The City "Pay-As-you-Throw" programme taxes consumers by volume of waste products; this offers cash rewards for sorting other discards from compostable materials and

recyclables [4]. The City's Environment Department's zero waste plan has driven the City to reach 80 per cent diversion, North America's highest diversion rate.

36.6 Common Waste Disposal and Management Methods

36.6.1 Incineration

Incineration is a waste management process in which agricultural solid waste is combusted to be converted into both contaminants and gases. Incineration is effective in eliminating all solid residues from wastewater treatment and commercial solid waste. It lowers the quantity of solid waste by 80–95%. High-temperature waste incineration and other treatment systems are also defined as thermal treatment. Waste is transformed into fire, gas, ash and steam by incinerators. Individuals conduct small-scale incineration and companies or governments on a large scale. Any toxic waste is regarded as a realistic type of disposal (e.g., biological and medical wastes). Incineration is a problematic waste management method owing to concerns such as the leakage of gaseous contaminants. Combustion is not always perfect in an incinerator, and chemicals in gas waste stacks are of concern. Some organic compounds, such as furans, PAHs, and dioxins that are incredibly persistent and may have broader environmental consequences, have been of particular concern.

36.6.2 Landfill

A landfill site is a site whereas typically seen in most parts of the world. Waste materials are disposed of by burial. Although the burying of waste is modern, the landfill is the oldest method of waste treatment; traditionally, the refuse was simply dumped in pits or left in piles.

36.6.3 Recycling

Recycling is a resource recycling method that refers to waste products such as plastic containers and empty beverage containers being collected and reused. It is possible to reprocess materials from which the items are produced into new products. Through some dedicated bins and vans, kerbside disposal may be taken, recycling separately from the general waste. In most cultures, the waste owner is expected to separate the waste. Materials to be recycled before recycling in various bins (e.g. for metals, paper, plastics); whereas in other cultures, all recyclable materials are placed in a single container for collection. Collection and sorting are handled at the central facility later

on. The latter mechanism is known as single-stream recycling. Due to the additional dismantling and the separation necessary, recycling complex items (such as electronic equipment, computers) is more complicated. The materials approved for recycling differ according to city and country. To manage the various types of recyclable materials, each city and country has different recycling programs. However, some differences in acceptance are expressed in products' resale value after they have been reprocessed. The Chinese government declared in July 2017 that the ban on imports of 24 categories of recyclables and solid waste, including plastic, mixed paper and textiles, has had a tremendous effect on developing countries worldwide that have exported directly or indirectly to China.

36.6.4 Pyrolysis

Pyrolysis is the thermochemical oxidation by heat in the absence of stoichiometric oxygen concentrations; various hydrocarbon gases are produced by decomposition. Pyrolysis is typically used for transforming different forms of manufacturing and household residues into recycled fuels. Other conditions of waste materials in the pyrolysis procedure (e.g. agricultural waste, pneumatic waste, food waste) are likely to provide alternate fossil fuels sources. During pyrolysis, the object's molecules vibrate at high speeds such that the molecules are breaking down. The rate of pyrolysis rises with the temperature. Temperatures in commercial applications are over 430 °C. Slow pyrolysis produces reliable charcoal and gases. Pyrolysis has the promise to turn waste biomass into usable liquid fuel. Some pyrolysis methods yield less chlorine, alkaline metal and sulphur-containing by-products than the incineration system. However, pyrolysis of this waste creates gases like SO₂ and HCl that impact the atmosphere.

36.6.5 Reuse

36.6.5.1 Energy Recovery

Waste energy recycling is the processing of non-recyclable waste materials to useful heat, power or electricity by different methods: combustion, pyrolysis, anaerobic digestion, gasification, and waste filling. In general, the technique is known as waste-to-energy. Energy waste recycling is part of non-hazardous waste disposal treatment Structure. The use of energy regeneration to turn non-recyclable wastes into heat and electricity will create green energy supplies and reduce CO₂ pollution by balancing the demand for fossil fuel energy and reducing methane output from sites. Globally, 16% of waste disposal is replaced from waste to electricity.

36.6.5.2 Biological Reprocessing

To decompose organic matter, recoverable organic materials, such as food waste, paper products and plant material, can be recovered by digestion and composting processes. For landscaping or agricultural purposes, the resulting organic materials are then recycled as mulch or compost. Also, waste gas from the process, such as methane, can be collected and used to increase electricity and heat generation efficiency. The purpose of biological processing in waste management is to monitor and accelerate organic matter decomposition's natural process.

36.7 Health Consequences of Poor Industrial Waste Disposal

Many chemicals are contained in the solid waste produced from industrial sources, some of which are toxic. If the concentration of the ingredients exceeds the specified value, the waste is known as harmful. Although the quantities of individual components that sometimes exceed the acceptable limit, only if the ingredients' overall value reaches the toxicity level can the waste be deemed toxic. To assess a given substance's toxicity, various standards and tests have been established by multiple agencies. Determining whether unchecked release into the Environment causes adverse effects on people or other living species in the ecosystem, the properties of the waste should be identified. Criteria such as toxicity, phytotoxicity, genetic activity and bio-concentration are used to carry out this assessment. The quantity of the toxic constituents also depends on the possible harmful effects. Depending on the dosage, exposure, and duration of exposure, substances are categorised as hazardous or otherwise dependent. It needs to contact or penetrate the human body for a chemical to affect human health. There are many ways that this can occur.

36.7.1 Skin Contact

Normally, chemicals that cause dermatitis do so by directly contacting the skin contact. The skin can be affected by certain chemicals like corrosive acids by a single connection, while others can cause harm, such as organic solvent, by exposure repeatedly.

36.7.2 Inhalation

Inhalation is the most common cause of exposure to chemicals in the workplace and the hardest to manage. Air emissions may be directly affected by harm to the respiratory tract or are absorbed by the lung and cause it to system/systemic implications. An adult male is about to breathe 10 cubic metres the air on a regular day of work.

36.7.3 Ingestion

contamination of groundwater and subsoil water from leachates Ingestion may result from waste dumps and poorly maintained landfill sites—toxic compounds from communities of people residing far from the plant Sites and decades after garbage was processed.

36.8 Industrial Waste Management

Today the entire world is struggling with the amount of industrial waste. Its quantity is increasing at a rate of 100 million tons per year. If we look at the Portugal system, then in July 1995, the national project plan added industrial waste with solid waste. The project calculated that Portugal produced 4.4 million tones, of which 1,37 million were dangerous, during 1994. According to this project's objective, about 82.9% of hazardous industrial waste was to be treated locally, and out of this, only 17.09% was to be an integrated system of industrial waste treatment. One incinerator, one physical–chemical treatment and two landfill units were also included in this plan. In 1997, in industrial waste management, the European Union made a new rule whose primary purpose was to treat and manage the hazardous waste [4–9]. Subsequently, a strategic industrial waste plan was formed at the end of 1999 (Table 36.2).

Article 278 (damage against nature), Article 279 (pollution), and Article 279-A (dangerous activities to the Environment) are classified as criminal penalties. About 87 waste management industrial installations in Portugal (2015) must have a permit based on the Industrial emissions directive (IED). A lot of effort is being made by the Portugal government for the management of hazardous waste to meet the objective set by the government in this field [10–12]. There are strict legislation and regulations in this direction, and the nation even decreases the manufacture of this waste to achieve its targets.

Table 36.2 Event details of co-incineration conflict [5]

S. No.	Year	Events details
1	1998	The Environmental impact statement was submitted for a public inquiry. The result is hundreds of opinion, criticism and requests. The EIS is presented for a public examination
2	2000 (December)	In consideration of co-incineration the Scientific Committee study states
3	2001	The Environment Ministry receives nearly 12,000 positive reviews. General discussion on the findings of the two independent committees of experts
4	2001 (May)	It is released the results of a government-class stock of (ordinary and hazardous) waste forms and amounts collected in Portugal. This inventory suggests no co-incineration alternative in terms of the amount of dangerous industrial waste generated globally
5	2003	The PSD-CDS government reveals a modern way of handling hazardous industrial waste—CIRVER

36.9 Management in Other Countries

36.9.1 *The United States*

The 1976 Resource Management and Recovery Act (RCRA) establishes government oversight of solid waste in the United States. The United States has released national guidelines on the storage, storage and recycling of waste. Committee for Environmental Conservation (EPA). The EPA has allowed individual State environmental agencies to enforce and implement the RCRA legislation by licenced waste management programmes. The EPA presently treats 2.96 million tonnes of solid, toxic and industrial waste. The RCRA policy has improved since it was implemented, as inefficiencies grow and waste management advances. One of the earliest efforts to enact environmental emission regulations was the Clean Air Act in 1963 and the Air Quality Act in 1967. There has since been a tighter control of interstate air emissions. The Clean Air Act of 1970 extended pollution restriction rules. The government watched, for example, mobile sources such as cars, vehicles and manufacturing sources. This intervention aimed to monitor the spread of ozone, nitrogen dioxide, plum, monoxide, and sulphur dioxide. According to the EPA, these six pollutants were the most common (the United States Environmental Protection Agency). The 1977 Clean Air Act Amendments: Air quality regions under national guidelines for environmental quality management have improved attention to prevent PSD (Prevention of Significant Deterioration). Clean Water Act: The 1972 CWA safeguards certain places against contamination. Industrial firms in these areas are

not allowed to dump until CWA protects them [4]. This is situated where the consistency of the water is regulated. In the United States, these two actions led to pollution control, but several improvements remain. With proposals in motion, emissions preservation would not be cheap in the United States.

36.9.2 China

The amount of water contamination has risen, triggering diarrhoea in children. Chinese air and water quality have been covered by around \$100 billion. However, if China ignores China's quality, it would accentuate water pollution. One of China's biggest air contamination sources is carbon combustion, which causes people to wear facial masks. Problems of emissions occur in manufacturing and power plants. Residents who aim to push the State to engage in this study. The government did not deal with the heavy industry. There are many common ways of treating hazardous waste. Stricter rules for hazardous waste firms often have to be enforced. Waste heat is sometimes produced and dumped into the field, according to an article. Water evaporation in the sector produces excess heat. If businesses utilise extra heat to their gain, fossil fuels may be reduced. Many attempts to eliminate industrial waste are attributed to improvements in human lifestyle and better environmental control.

36.9.3 London

There has been a 20 million pound fund to boost air quality in London. The above comes from our Mayor's Air Quality Fund (MAQF). 12 Emission Low Bus Areas were implemented in London. It helps to eliminate harmful fumes that are released from cars. London is in the same condition as in The United States when it comes to handling waste.

36.10 Factors Affecting Industrial Waste

36.10.1 Environmental Impact

Since vast quantities of water are required for production or cooling of equipment, factories and power stations are typically situated in water sources. Several regions with industrialised resources or technologies already have little resources or technology accessible for disposing of waste that is less environmentally-friendly. Wastewater, both untreated and partially handled, is regularly expressed in an almost lying body of water. Sea ecosystems and the wellbeing of those that depend on water

as food or drinking water supplies are specifically influenced by water resources emitted from metals, chemicals and waste. Depending on marine organisms, wastewater pollutants can destroy marine life or trigger different disease degrees for those that use a pollutant for these marine animals. Metals and chemicals influence water habitats in water bodies.

36.10.2 Air Pollution

Another clear consequence of industrial waste is the release of air from the burning of fossil fuels. As they do not have the money to tackle this particular issue, many environmental issues have disastrous consequences on third world countries. Nitrogen dioxide is also a natural air contaminant present in the air. Air pollutants are devastating to humans because they trigger many diseases, while others involve carbon monoxide and also causes death when significant amounts reach the body limit; there have been many instances in which individuals and even whole families have unintentionally been killed due to severe mortality, in Nigeria and other parts of the world. Ammonia is often the source of several lung conditions and may be acquired from the environment. Air exposure disorders include inflammation of the eye, skin, mouth or nose. There is also the risk of severe bronchitis and pneumonia. Citizens have also mentioned headache, dizziness and nausea from air emissions. The WHO has said that air contamination is the worst threat to human health. Air contamination has been around for a long time. Indoor air quality is also a possibility for humans. This kind of air emission is induced by burning solid fuel, mostly through cooking or heating.

36.10.3 Water Pollution

One of the most damaging effects of hazardous waste is water contamination. For specific processing methods, heavy volumes of water that come into contact with harmful substances are used. There usually are metals or toxic products. When the majority of trash ends in oceans, lakes or waterways, the environment is impaired. As a result, water gets polluted, creating a danger to everyone's wellbeing. Farmers depend on this water, so it can pollute the planted crops if the water is polluted. This affects communities' wellbeing, so industrial firms cannot clean up their pollution because it affects people's life and livestock. The wellbeing of aquatic organisms is impaired by the chance of life from this polluted water.

36.11 International Waste Movement

Although waste transport is subject to national regulations in a given region, the transportation of waste across frontiers is often regulated by international treaties. For several nations, it's a huge concern. Dangerous pollution persisted. The Basel Convention, signed by 172 nations, denounces radioactive waste from advanced to less developed countries. The provisions of the Convention have been incorporated into the European Union's laws on waste shipping in Basel. While dangerous, radioactive waste does not come under the control of the Basel Convention.

36.12 Waste Challenges in Developing Countries

In addition to inadequately unregulated and maintained dumpsites, areas with developing economies typically experience depleted waste collection systems. The issues are worsening. Governance issues exacerbate circumstances. Waste management in the field of owing to poor institutions, rapid population growth, and chronic under-resourcing, these developing countries and cities face an ongoing challenge. Many of these challenges, along with the absence of awareness of multiple factors related to the waste management hierarchy, influence waste treatment.

36.13 Focus on Developing Countries

Mobilize humanitarian assistance and climate and conservation assets to support the most impoverished nations. Increase the level of funding on waste management by a factor of 10, from the 0.3% achieved since 2020 to an average of 3 of total international aid funding in the period from 2015 to 2030.

- As a first stage, the target is:
- hit 100 per cent coverage in all cities with more than 1 million inhabitants;
- Prevent free combustion of industrial and related solid waste;
- close, wide open dumps and substitute them with managed waste installations.
- Establish a systematic approach to all residues treatment. Establish convergence of wastewater services and solid waste management services in particular.
- Draw on current recycling programmes, thus removing toxic waste recovery activities for safe livelihoods and city costs.
- Safe handling of radioactive waste. Enforce and adequately fund the Basel Convention's domestic implementation and guarantee that waste is sufficient for developed countries' sound infrastructure.
- Encourage production responsibility initiatives to guarantee that foreign businesses assume full responsibility for their commodity and waste disposal in developed countries.

- Create/strengthen diverse capacity-building initiatives in the institutional, technological and market sectors. Involve existing communities and encourage cooperation by twinning.

36.14 Focus on All Countries

Both countries also have a path to accomplish their 2030 objectives:

- Improved access to support for and activities of adequate waste treatment systems.
- Removes waste at root, includes residents, businesses and other players—from linear to circular waste management.
- Increase the availability and reliability of waste and resource control data—you cannot handle it if you don't calculate it.

36.15 Conclusions

In recent decades, the world's excessive human growth and the ecosystem change have shown a drastic increase in waste production. To that end, the Portuguese Government has introduced substantial improvements to the treatment of this form of waste. The hazardous waste collection and management software in Portugal is more effective. The Portuguese Government is operating in this direction dynamically. More recently, reforms have been introduced in legislation pertaining to the import of this form of waste. Your nation is increasingly heading in this direction and will soon reach the goal set here.

References

1. Solsten, E.: Portugal: A Country Study. Washington: GPO for the Library of Congress, 1993. <https://countrystudies.us/portugal/69.htm>
2. European Commission: The EU Environmental Implementation Review 2019 Country Report—Portugal, 2019
3. Scarbrough, T., Menadue, H., Zettl, E., Doktorova, J.: Industrial emissions policy country profiles—Methodology Paper. Ricardo Energy & Environment, Issue-5 (2018)
4. Chinaza, A., et al.: Industrial and community waste management: global perspective. *Am. J. Phys. Sci.* 1(1), 1–16 (2020)
5. Ribeiro, A., Castro, F., Macedo, M., Carvalho, J.: Waste management in Portugal and Europe: an overview of the past, present and future. *WASTES: Solutions, Treatments and Opportunities* (2011)
6. Jerónimo, H.M., Garcia, J.L.: Risks, alternative knowledge strategies and democratic legitimacy: the conflict over co-incineration of hazardous industrial waste in Portugal. *J. Risk Res.* 14(8), 951–967 (2011). <https://doi.org/10.1080/13669877.2011.571783>
7. Couto, N., Silva, V., Monteiro, E., Rouboa, A.: Hazardous waste management in Portugal: an overview. *Energy Procedia* 36, 607–611 (2013). <https://doi.org/10.1016/j.egypro.2013.07.069>

8. EPA's Guide for Industrial Waste Management, Chapter-Integrating Pollution Prevention, pp. 1–18
9. Portugal: Governmental order 205/1997 (1995a). Last access December 2020
10. Portugal: Ministers Resolution No 98/1997 (1995b). Last access December 2020
11. Portugal: Decree-Law 239/1997 (1997). Last access December 2020
12. Portugal: Decree-Law 516/1999 (1999). Last access December 2020

Chapter 37

Designing a Mechanism to Paint a Conical Shaped Part



Rufus R. Thomas, C. N. Sakhale, M. S. Giripunje, and Sagar D. Shelare

Abstract Many manufacturers desire for automating their painting processes for improvement in quality, reduction in the time, reduction in coating, and reduction in labor content. Automation into paint systems is a sustainable solution to overcome the above mentioned drawback but initial cost of automation is quite higher for small scale industry. Therefore this paper presents design of a mechanisms made by raw material available into the industry for conical part painting. The mechanism will function via motor for rotation, fixture for mounting of work piece and cam follower principle etc. The simple controls for the painting were provided with ON/OFF knob. Proposed mechanism contains of numerous mechanical parts which assembled together for carrying out a specific task. Mainly the synchronized movement between the rotating motor with work piece and spraying spray from automatic spray gun is the key factor for this assembly model. Through the present mechanization speed of the motor as well as paint flow can be controlled which results in enhanced finishing and reduction in processing time.

Keywords Conical shaped part · Production technology · Fixture development · Synchronize movement

37.1 Introduction

In this competitive world we are tending towards automation which will replace all manual efforts to automation [1]. The functions will remain same as far as the mechanism and objectives are concerned. Automation can be classified into two major sections as complete automatic and semi-automatic. In semi-automation the joint effort of manual efforts and mechanical mechanism is required where as in full automation human interference is neglected [2, 3]. The purpose of this project is to understand the design and fabrication of the mechanism which ease the painting task efficiently. The knowledge of this mechanism was very important so as to carry out the task efficiently.

R. R. Thomas · C. N. Sakhale (✉) · M. S. Giripunje · S. D. Shelare
Department of Mechanical Engineering, Priyadarshini College of Engineering, Nagpur, India

Previously the painting task was carried out by the worker manually by actually making the use of paint brush, paint etc. [4, 5]. Because of this the amount of the paint used was uneven and there was the issue of wastage of the paint from the paint brush and spills around the surrounding work place making it untidy. By the use of this old and conventional manual method the production achieved was very less and hardly we have to limit our production requirement to a minimum numbers [6]. Thus the need of manual method has to be brought into existence. Thus it gave birth to the idea of doing such innovative task. This manual method not only gave us limited production but also it has certain limitation within it. After working on this task worker starts feeling the fatigue which also leads an indirect reduction in production.

In this project we are simply going to design and fabricate a mechanism which is going to ease the efforts taken by the worker to accomplish this task. It also enables the management to get readily available components for the next process [7, 8]. By making use of this mechanism one can minimise the usage of the following things like time, efforts, paint etc. Today in this competitive world we cannot afford in getting minimum production instead we have to make something innovative which eases almost all hardships etc.

Hence the objective to carrying out the research was

- To reduce the time utilised for painting work piece via. Electrically operated spray gun.
- To gain the work done efficiently by an automation of mechanism without having much interference of human being.
- To reduce the wastage of the paint, since we are making use of the spray gun.
- To reduce human efforts since the mechanism is designed in such a way so that the work done is much more intense.
- To gain smooth spraying on the surface.

37.2 Overview of the Problem

The title statement starts in this way “DESIGNING A MECHANISM TO PAINT A CONICAL PART” means that particular component was earlier painted manually by an operator. The total production comes out to be 250–280 nos per 8 h shift. In complete machining of this component, the most important steps as it is the base for finishing the product that is painting and it plays important role in durability and the life of the components [9, 10]. The problem which was faced in priming process was mainly production is mainly the amount of efforts required which are in terms of Technical skills, Labor, time and cost [11, 12]. Secondly the major parameter is quality and consistency of work. So we can come to a point that is we need to work on these problems and give valid solutions. For giving vital solution extensive study and efforts are required [13, 14]. The solutions can be in terms of design of some automation which can standardize the whole process of priming on the sheet metal components.

37.3 Designing the Mechanism for the Model

In this project we will be proceeding further on the left over work done as mentioned in previous stages. It is a continuous and never-ending practice of a human being towards the simplification of their critical task in the companies gave the birth of automation in the manufacturing companies [15]. Automation in the manufacturing companies has become an important objective to built or invent those ideas which later on will takes the phase of model, whereas the culture of getting more and more production in an manufacturing companies has emerged a lot during this age [16]. Let's talk about how the automatic paint spilling device will help companies to increase more production and how practical exercises will lead to overcome the paint usage. This automatic technique is followed by many sections such domestic, household, factories and companies etc. Following are the components used in the making of the mechanism:

37.3.1 0.5 HP CNC Lathe m/c Chips Conveyor Motor

Generally this motor is attached to the conveyor which drags away the chips generated by the cutting operation inside the machine. With the gear ratio of 270:10 and maximum of 20 rpm within build worm and worm gear. Figure 37.1 shows the conveyor motor.



Fig. 37.1 Conveyor motor

Fig. 37.2 Electrically operated paint gun



37.3.2 Electrically Operated Paint Spray Gun

This is electrically operated paint gun which after proper setting will discharge the jet of the paint on the decided area of the conical component. Electrically operated means it actually compresses the air with in it and mixes with the paint to form amalgam and discharges it out [17, 18]. This gun have a 0.8 L paint holding capacity. Figure 37.2 shows the electrically operated paint gun.

37.4 Fabrication and Working of Model

Once the design has been decided or framed, we have to work on model making. While the model is been prepared we have to consider all the aspect like model size that the size of the model should not be the as large as it consumes lot of space. The performance should be based on the trial and error parameters until it has been set to a particular parameters. In this all the components should be tagged with label. The main motto of preparing this model is to make prototype and it can be used in a very simple way, with a low expenses and without taking much efforts. Taking the reference of the previous work done. Following are the list of the components which are used in model making: (1) CNC chips conveyor motor, (2) Electrically operated automatic paint spray gun, (3) Base platform, (4) Electric cable etc. Figure 37.3 shows the actual set up of the mechanism.

The working of the actual set up is explained step by step below:

- First the base plate is fixes and isolated so that we can make use of it.



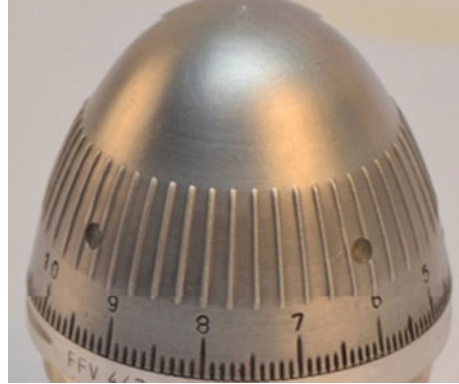
Fig. 37.3 Actual set up of the mechanism

- Now mount the motor on the base plate platform and make alignment of it so that it can carry the entire weight of the assembly.
- Mount the electrically operated automatic spray gun just in front of the motor in a aligned way.
- Mount fixture on the spindle shaft of the motor.
- Mount the work piece on the fixture.
- Adjust the length of the flow of the paint from the paint gun.
- Care should be taken that the length should not be too long or not too short.
- Hit the ON button, by which the cycle starts and the process of painting goes on.
- Soon after the completion of one rotation, automatically the cycle gets stops. And we get the work piece painted.
- The construction of this mechanism is bifurcated into the following path lines.
- First of all when the on button is switched on the current passes through motor leading to the rotation of the shaft attached to it on which a holding fixture is fixed which will rotate the conical component on it in a desire rpm.
- At the same time the trigger of the spray gun also gets pressed via a attachment attached on it. Specifies arrangements are made that will enable the paint to spray on a desired spot with the accuracy.
- Now, there is a attachment of the limit switch which will enable the mechanism to open the spraying port for the require time and for the particular duration.
- The main motto of the limit switch is to on start and stops the trigger for paint flow thru the nozzle.
- That can be utilised on particular shaped work piece say conical shaped one.

37.5 Experimentation

Figure 37.4 shows the conical model which need to be painted with the help of

Fig. 37.4 Conical part to be painted



designed mechanism. For checking the suitability of the mechanism, this conical shaped part was painted manually and the overall production was noted for continuous ten days. Time required for painting and consumption of the paint was also calculated. On the similar line, painting operation was done with the help of developed mechanism and time required for painting and consumption of the paint was calculated.

Figure 37.5 shows the conical model after painting on the designed mechanism.

37.6 Result and Discussion

Table 37.1 shows the result obtained for manual painting of the conical part. While calculating the total times following factors were considered.

- Time required painting single component = 50 s
- Handling time = 17 s
- Allowances include 0.5 h. Lunch/dinner time + Non value added time (like washroom, drinking water, fatigue feeling).

Figure 37.6 shows the graph of comparative results for the comparison between the theoretical and actual output per hour and per day when the process carried out manually.

Table 37.2 shows the result obtained for automated painting of the conical part with the help of developed mechanism. While calculating the total times following factors were considered.

- Time required painting twenty component (twenty component mounted simultaneously) = 480 s
- Machine setting time = 30 min.
- Allowances includes 0.5 h. Lunch/dinner time + Non value added time (like washroom, drinking water, fatigue feeling) of the operating worker.

Fig. 37.5 Conical part after painting



Table 37.1 Result for manual painting

Day	Theoretical output per hour	Theoretical output per day (8 h)	Actual output per hour	Actual output per day	Total paint consumption	Paint consumption per component
1	53	424	52	390	4290	11
2	53	424	51	408	4773.6	11.7
3	53	424	50	400	4760	11.9
4	53	424	52	416	4451.2	10.7
5	53	424	53	424	4960.8	11.7
6	53	424	51	408	4528.8	11.1
7	53	424	51	408	4120.8	10.1
8	53	424	50	400	3880	9.7
9	53	424	52	416	4867.2	11.7
10	53	424	53	424	4282.4	10.1

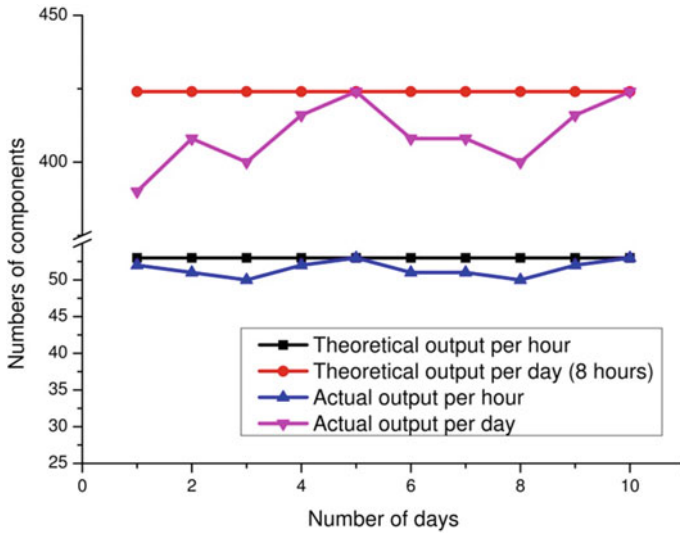


Fig. 37.6 Comparative results for the manual painting process

Table 37.2 Result for automated painting with developed mechanism

Day	Theoretical output per hour	Theoretical output per day (8 h)	Actual output per hour	Actual output per day	Total paint consumption	Paint consumption per component
1	150	1200	140	1120	7952	7.1
2	150	1200	140	1120	8176	7.3
3	150	1200	140	1120	7280	6.5
4	150	1200	160	1280	8832	6.9
5	150	1200	160	1280	9216	7.2
6	150	1200	160	1280	8704	6.8
7	150	1200	120	960	6720	7
8	150	1200	120	960	6336	6.6
9	150	1200	140	1120	8176	7.3
10	150	1200	120	960	6432	6.7

Figure 37.7 shows the graph of comparative results for the comparison between the theoretical and actual output per hour and per day when the process carried out with the help of automated mechanism.

Figure 37.8 shows the graph of comparative results for the comparison between the actual output per hour and per day when the process carried out manually and with the help of automated mechanism.

Figure 37.9 shows the graph of consumption of the paint when the paintings were

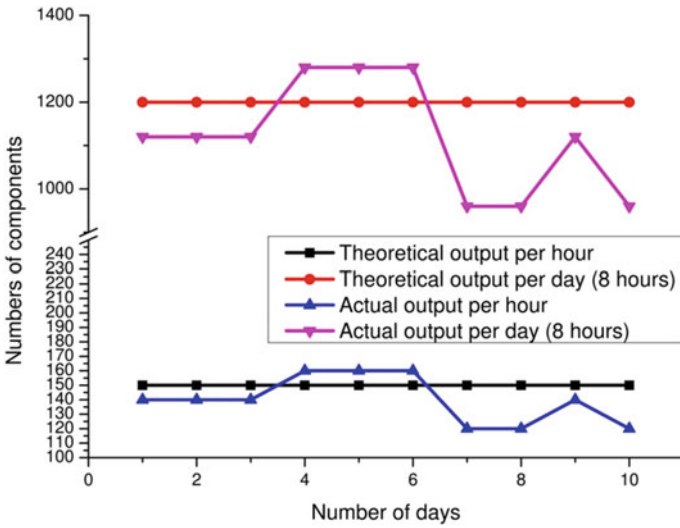


Fig. 37.7 Comparative results for automated painting with developed mechanism

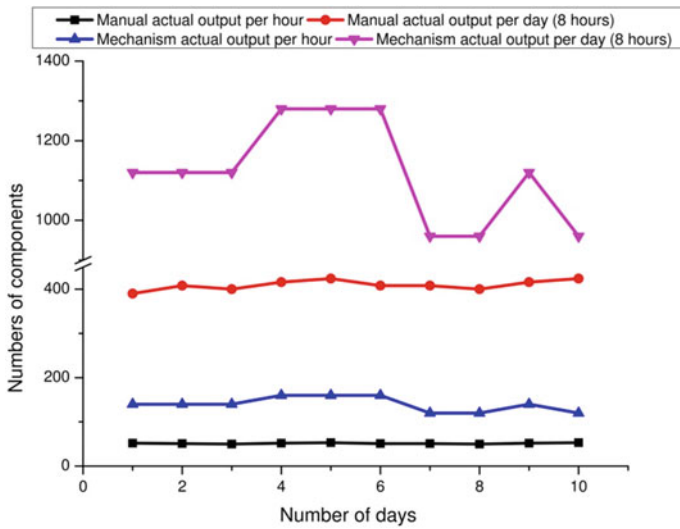


Fig. 37.8 Comparative results for manual and automated painting with developed mechanism

carried out manually and with the help of automated mechanism.

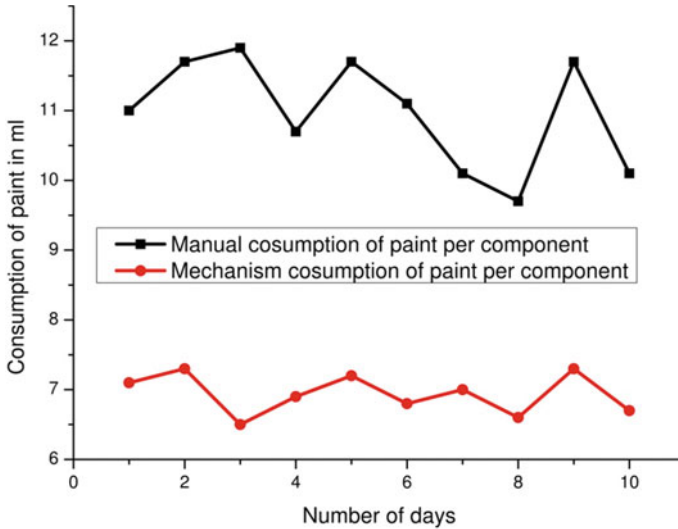


Fig. 37.9 Consumption of the paint when the paintings were carried out manually and with the help of automated mechanism

37.7 Conclusion

A mechanism was successfully developed and tested for painting a conical shaped part. Following major conclusions can be drawn from this research:

1. With the help of developed mechanism production rate was increased significantly with minimised consumption of paint.
2. The surface finish obtained is much superior to the manual painting.
3. Developed model is useful for the small scale industry having manual painting operation.

References

1. Plesniak, M.W., Sojka, P.E., Singh, A.K.: Transfer efficiency for airless painting systems. *JCT Res.* **1**(2) (2004)
2. Ye, Q., Domnick, J., Scheibe, A.: Numerical simulation of spray painting in the automotive industry. In: *Proceedings of the 1st European Automotive CFD Conference Bingen, Germany, June 2003*
3. Domnick, J., Scheibe, A., Ye, Q.: The simulation of the electrostatic spray painting process with high-speed rotary bell atomizers. Part I: Direct charging, Part. Part. Syst. Charact. **22**, 141–150 (2005)
4. Domnick, J., Scheibe, A., Ye, Q.: The simulation of the electrostatic spray painting process with high-speed rotary bell atomizers. Part II: external charging. Part. Part. Syst. Charact. **23**, 408–416 (2006)

5. Shelare, S.D., Thakare, P.S., Handa, C.C.: (2012) Computer aided modelling and position analysis of crank and slotted lever mechanism. *Int. J. Mech. Eng. Prod. Eng. Res. Dev.* **2**(2), 47–52 (2012)
6. Ye, Q., Domnick, J., Khalifa, E.: Simulation of the spray coating process using a pneumatic atomizer. ILASS-Europe, September 2002, Zaragoza Azadivar, F., Shu, V., 1999. Maintenance policy selection for JIT production systems. *Int. J. Prod. Res.* **37**(16), 3725–738
7. Waghmare, S.N., Sakhale, C.N., Tembhurkar, C.K., Shelare, S.D.: Assessment of average resistive torque for human-powered stirrup making process. In: *Computing in Engineering and Technology*, pp. 845–853 (2019). https://doi.org/10.1007/978-981-32-9515-5_79
8. Jennerjohn, P.: Unique aspects involved in the robotic painting of commercial aircraft structures. SAE Technical Paper 2011-01-2790, 2011. <https://doi.org/10.4271/2011-01-2790>
9. Milojevic, D.: High performance robotics for aerospace paint finishing operations. Presented at the Wichita Aviation Technology Congress & Exhibition, Wichita, Kansas, 19–21 Aug 2008
10. Dhande, H.K., Shelare, S.D., Khope, P.B.: Developing a mixed solar drier for improved postharvest handling of food grains. *Agric. Eng. Int.: CIGR J.* **22**(4), 17–24 (2020)
11. Mowade, S., Waghmare, S., Shelare, S., Tembhurkar, C.: Mathematical model for convective heat transfer coefficient during solar drying process of green herbs. In: *Computing in Engineering and Technology*, pp. 867–877 (2019). https://doi.org/10.1007/978-981-32-9515-5_81
12. Jawalekar, S.B., Shelare, S.D.: Development and performance analysis of low cost combined harvester for rabi crops. *Agric. Eng. Int.: CIGR J.* **22**(1), 197–201 (2020)
13. Kumbhare, H., Shelare, S.: Innovative advancement in drone technology for water sample collections—a review. *Int. J. Sci. Technol. Res.* **9**(03), 7266–7269 (2020)
14. Mali, P.K., Sakhale, C.N., Shelare, S.D.: A literature review on design and development of maize thresher. *Int. J. Pure Appl. Res. Eng. Technol.* **3**(9), 9–14 (2015)
15. Mathew, J.J., Sakhale, C.N., Shelare, S.D.: Latest trends in sheet metal components and its processes—a literature review. In: *Algorithms for Intelligent Systems*, pp. 565–574 (2020). https://doi.org/10.1007/978-981-15-0222-4_54
16. Sahu, P., Shelare, S., Sakhale, C.: Smart cities waste management and disposal system by smart system: a review. *Int. J. Sci. Technol. Res.* **9**(03), 4467–4470 (2020)
17. Shelare, S.D., Kumar, R., Khope, P.B.: Formulation of a mathematical model for quantity of deshelled nut in charoli nut deshelling machine. In: *Advances in Metrology and Measurement of Engineering Surfaces*, pp. 89–97 (2020). Available at: https://doi.org/10.1007/978-981-15-5151-2_9
18. Waghmare, S.N., Shelare, S.D., Tembhurkar, C.K., Jawalekar, S.B.: Development of a model for the number of bends during stirrup making process. In: *Advances in Metrology and Measurement of Engineering Surfaces*, pp. 69–78 (2020). https://doi.org/10.1007/978-981-15-5151-2_7

Chapter 38

Designing of an Anti Roll Bar to Adjust the Balance and Stability of a Formula Student Car



Ankit Kumar Singh, Ekansh Prasad, and Pradeep Kumar Jain

Abstract This paper focuses on the designing procedure of an adjustable anti-roll bar (ARB) for a Formula Student Car. ARB is a component in suspension assembly which can provide a specific understeering effect to the vehicle depending on its roll stiffness. Different drivers prefer different understeering effects on the car depending on their driving style. For this project, Adjustability in ARB leads to 4 roll rate distribution and 3 roll gradients in the car hence overall 12 settings from one ARB assembly. The ARB has been designed using software like MATLAB and MS Excel to obtain the geometric dimensions and specific orientation of the ARB blade pertaining to different balance and stability. This paper also demonstrates the effect of ARB on suspension travel. The proposed method can help drivers to choose the vehicle dynamics according to their driving style in different tracks.

Keywords Anti roll bar · FSAE · Roll gradient · Roll rate distribution · Suspension travel · MATLAB

38.1 Introduction

FSAE cars are developed with independent Double A-arm suspension but since FSAE racetracks are smooth and the merits of adding ARB, certainly overpower the inherent dependence on left-right suspension that it creates. Anti-Roll Bar can be placed both at the front-rear end of the car which can lead to a specific balance of the car. But Anti Roll Bar can also be designed such that the roll rate is adjustable providing driver specific understeering and oversteering effect. It is important to fix the roll rate distribution and roll gradient according to the driver's preference and is specific to the racetrack. But due to different nature of racetracks in different competitions, it is a good choice to develop an Adjustable anti roll bar which can provide variable roll rate distribution (Front-Rear) and variable roll gradient up to a certain range.

A. K. Singh (✉) · E. Prasad · P. K. Jain
Department of Mechanical Engineering, Delhi Technological University, New Delhi, India

Bhanage and Padmanabhan [1] suggests that an important parameter which affects the design of an anti-roll bar is choosing the stabilizer bar rate correctly. This paper presents the reliability of an anti roll bar using AISI 1020, SAE 4340, SAE 5160 and SAE 9262 materials under constant amplitude loading before ductile to brittle transition temperature, which leads to failure. It concludes that SAE 5160 has higher fatigue life compared to others in similar conditions using ANSYS n code Design life software. Reimpell et al. [2] use of the stabilizer bar gives different characteristics to the vehicle. Using an Anti-roll Bar enables to increase the understeering in front suspension and to improve the manoeuvre attribute while changing the direction and, for rear suspension, using an-roll bar enables to increase the oversteering. Tuysuz et al. [3] aims to correlate the results of test rig and FE model for the design of ARB of a vehicle. According to their calculation and FE Analysis results for different diameters of ARB tubes, while doing new design of An-roll bar, FEA analysis results can be found by multiplying the calculation result with 0.97 which is roll rate factor without applying FEA analysis. Sharma et al. [4] in his paper analyse stiffness of anti-roll bars by varying the various geometric conditions of the anti-roll bar. This paper shows that the lowest value of the roll angle is obtained with the bar having minimum length of arm. He also concluded that the distance between the bushes should be greater as less portions of the bar will be subjected to bending thereby improving the stiffness of the anti-roll bar.

From the above references it is evident that limited work has been done in designing an adjustable ARB which can be used by the driver to choose the vehicle dynamics according to the track manoeuvrability and driving preference. The ARB is designed such that it has the adjustability to achieve the required ARB percentages for different settings from single assembly only. The MATLAB software is used to quickly set the Blade angles, geometric dimensions of the ARB and simulate it. This process saves time considering the number of dimensions that can be altered to achieve the required rate.

38.2 Design Methodology

38.2.1 Desired ARB Rate Calculation

Roll rate distribution and Roll gradient are the input parameters used in the designing process. As we know, these parameters decide the overall performance of the car on track given the engine parameters, track characteristics are constant. If the track profile is known and the driver preference is known beforehand the designing of the suspension system, it is preferred to fix the two parameters to minimize the complexity. Otherwise, adjustability is incorporated so that one can change the two parameters in real time to tune the car according to the driver's preference.

After studying several research papers and Vehicle Dynamics books the preferred range of roll rate (r) distribution is 0.4–0.625 and roll gradient (R) is 0.5–0.7. The

Table 38.1 Range of roll balance and roll gradient

S. No.	r	R (deg/g)
1	0.5	0.45
2	0.55	0.45
3	0.6	0.45
4	0.65	0.45
5	0.5	0.53
6	0.55	0.53
7	0.6	0.53
8	0.65	0.53
9	0.5	0.6
10	0.55	0.6
11	0.6	0.6
12	0.65	0.6

roll rate distribution is divided into 4 steps and roll gradient is divided into 3 steps which gives overall 12 cases of unique parameters which is presented in Table 38.1.

Several input parameters that are decided by taking into consideration the FSAE rulebook and the trends in FSAE cars like Weight, State of the vehicle, Dimensions, roll axis heights above ground, Spring Rates etc. are defined below:

Vehicle State:

Cornering acceleration (A_y) = 1.5 g m/s²

Longitudinal acceleration (A_x) = 0 m/s²

Track curve radius = 914 mm

Yaw velocity = 2.21 rad/s

Longitudinal velocity (V_x) ~ 40 m/s¹.

Vehicle Parameters:

Total weight of vehicle (W_T) = 258.54 kg

Front vehicle track (t_f) = 1524 mm

Rear vehicle track (t_r) = 1524 mm

Vehicle Wheelbase (l) = 2895 mm

Centre of Gravity height (h) = 457 mm

CG to Roll Axis height (H) = 335 mm

Distance front track to CG (a) = 789 mm

Distance rear track to CG (b) = 759 mm

Table 38.2 Net load on wheels after load transfer

S. No.	Wfo	Wfi	Wro	Wri
	N	N	N	N
1	1116.66	302.364	1201.02	269.064

Front Roll centre height (z_{rf}) = 76 mm

Rear Roll centre height (z_{rr}) = 190 mm

Tire stiffness (K_t) = 117 N/mm

Actual spring rate front ($K_{s\ rate\ f}$) = 26.27 N/mm

Actual spring rate rear ($K_{s\ rate\ r}$) = 26.37 N/mm

Weight Distribution = 49%.

Using the above State and Geometry of the vehicle, we can calculate the effective load on each wheel i.e. Front-Outer, Front-Inner, Rear-Outer, Rear-Inner. The load transfer calculation has been shown in [4–8]. The effect of gyroscopic moments on a wheel is illustrated in [9]. The load transfer equation for this paper is elaborated in (Appendix 1) (Table 38.2).

FSAE race cars usually run on frequencies around 3 to 4 Hz. The frequency for front (ω_f) and rear (ω_r) section is chosen in such a way that the ARB percentage comes out to be positive or approximately zero. The chosen frequency for first is tabulated in Table 38.3. Similarly, other 11 cases can be obtained. After choosing the appropriate frequencies, the ride rate can be calculated using formulae:

$$\omega_f = \frac{1}{2\pi} \sqrt{\frac{Krf \times 12 \times 32.2}{W_2}}; \quad \omega_r = \frac{1}{2\pi} \sqrt{\frac{Krr \times 12 \times 32.2}{W_4}} \tag{38.1}$$

Assuming the stiffness of tire and ride rate to be as K_t and K_r respectively, we can calculate the Wheel Rate (Kw) using Eq. 38.2. The ride rates (Front/Rear) and wheel rates (Front/Rear) abbreviated as (K_{rf}/K_{rr}) and (K_{wf}/K_{wr}) are calculated using Eqs. 38.1 and 38.2 respectively are presented in Table 38.3.

$$K_w = K_r K_t / K_t - K_r \tag{38.2}$$

Table 38.3 Frequency and wheel rates front/rear

S. No.	ω_f (new)	ω_r (new)	Krf (new)	Krr (new)	Kwf (new)	Kwr (new)
	Hz	Hz	N/mm	N/mm	N/mm	N/mm
1	3.55	3.51	31.6	32.1	43.2	44.2

The overall roll rate (K_{ϕ}) required to satisfy the initial chosen roll gradient at given lateral acceleration (A_y) and total sprung mass (W_{tsp} W_{tsp}) is derived using the formula

$$K_{\phi} = \frac{W_{tsp} \times H}{R} \tag{38.3}$$

According to the roll rate distribution, the obtained roll rate is divided into front ($K_{\phi f}$) and rear ($K_{\phi r}$) roll rates using:

$$K_{\phi f} = r \times K_{\phi}; \quad K_{\phi r} = (1 - r) \times K_{\phi} \tag{38.4}$$

The desired roll rate front ($K_{\phi af}$) and rear ($K_{\phi ar}$) through ARB from Front and Rear can be further calculated using:

$$K_{\phi af} = \frac{K_{\phi f} \times 6 \times Kt \times Tf^2}{(6 \times Kt \times Tf^2 - K_{\phi f})} - 6 \times K_{wr} \times T_r^2;$$

$$K_{\phi ar} = \frac{K_{\phi r} \times 6 \times Kt \times Tr^2}{(6 \times Kt \times Tr^2) - K_{\phi r}} - 6 \times K_{wr} \times T_r^2 \tag{38.5}$$

The percentage of ARB for Front (ARB % F) and Rear (ARB % R) is obtained using:

$$ARB\%F = K_{\phi af}/K_{\phi f} \times 100; \quad ARB\%R = K_{\phi ar}/K_{\phi r} \times 100; \tag{38.6}$$

Equations 38.1–38.6 has been obtained from [7]. The numerical value of each parameter in Eqs. 38.3, 38.4, 38.5 and 38.6 has been tabulated in Table 38.4. In the ARB%F and ARB%R column of Table 38.4, we can see that each of the 12 cases requires a different percentage of ARB (Front and Rear) to satisfy the initial condition of Roll Gradient and Roll Rate Distribution. Therefore, it is essential to design an Adjustable ARB to satisfy these cases.

Table 38.4 Desired arb rate and percentage front/rear

S. No.	$K_{\phi f}$ (N-m/rad)	$K_{\phi r}$ (N-m/rad)	$K_{\phi af}$ (N-m/rad)	$K_{\phi ar}$ (N-m/rad)	ARB % F	ARB % R
1	27,692.456	27,692.456	9943.504	11,835.4	35.9	42.7

38.2.2 Proposition to Derive Suspension Travel w.r.t. Wheel Centre

Now, as we know that the ARB makes the suspension system dependent, therefore the suspension travel of the inner wheel should affect the respective travel of the outer wheel and vice versa. Let us assume,

\mathbf{x}_{inner} = deflection of inner wheel centre; \mathbf{x}_{outer} = deflection of outer wheel centre

$$\begin{aligned} \text{Net load transfer(outer)} &= (Fsdo - Wfstst); \\ \text{Net load transfer(inner)} &= (Wfstst - Fsdil) \end{aligned}$$

The proposed governing equation for deflection calculation at wheel centre is

$$\text{Net load transfer(outer)} = [\mathbf{x}_{outer}] [K\omega_{outer} + K_{arb}] + [\mathbf{x}_{inner}] [K_{arb}] \quad (38.7)$$

$$\text{Net load transfer(inner)} = [\mathbf{x}_{inner}] [K\omega_{outer} + K_{arb}] + [\mathbf{x}_{outer}] [K_{arb}] \quad (38.8)$$

$$\text{ARB ride stiffness WC Front } (K_{arb}) = \left(\frac{K\phi af}{12Tf^2} \right) \quad (38.9)$$

Solving the above Eqs. 38.7, 38.8 and 38.9, we get the expression of \mathbf{x}_{outer} and \mathbf{x}_{inner} as shown in Eq. 38.10.

$$\begin{aligned} \mathbf{x}_{inner} &= \frac{(Wfstst - Fsdil) \left(Kw f + \frac{K\phi af}{12Tf^2} \right) - (Fsdo - Wfstst) \left(\frac{K\phi af}{12Tf^2} \right)}{\left(Kw f + \frac{K\phi af}{12Tf^2} \right)^2 - \left(\frac{K\phi af}{12Tf^2} \right)^2}; \\ \mathbf{x}_{outer} &= \frac{(Fsdo - Wfstst) \left(kw f + \frac{K\phi af}{12Tf^2} \right) - (Wfstst - Fsdil) \left(\frac{K\phi af}{12Tf^2} \right)}{\left(Kw f + \frac{K\phi af}{12Tf^2} \right)^2 - \left(\frac{K\phi af}{12Tf^2} \right)^2} \quad (38.10) \end{aligned}$$

38.2.3 Calculation of Force Versus Deflection for ARB

Using the deflections obtained in from Eq. 38.10, we can calculate the force due to ARB at wheel centre (Front and Rear) using:

$$\text{ARB Force at WC Front} = \left(\frac{K\phi af}{12Tf^2} \right) (\mathbf{x}_{inner} + \mathbf{x}_{outer}) \quad (38.11)$$

Table 38.5 Force versus deflection of ARB

S. No.	Front		Rear	
	ARB force at WC	ARB droop link relative travel at WC	ARB force at WC	ARB droop link relative travel at WC
	N	mm	N	mm
1	74.52	13.74	84.33	9.78

Now, the force on the ARB w.r.t wheel centre and its deflection has been determined using Eqs. 38.10 and 38.11. It is tabulated below in Table 38.5 for the first case. Similarly other 11 cases can be obtained.

We will use the above force vs deflection table to determine the geometry of the ARB, and the angular orientation of left and right blade independently.

38.2.4 Calculation of Geometric Dimensions of Blade and Tube

The deflection of cantilever beam (Y) with uniform cross section as shown in [10] is given below,

$$Y = wl^3/3EI \tag{38.12}$$

But, if the cross-section of the beam changes continuously along the length of the blade, the Moment of Inertia becomes variable. Also, the taper angle of the blade as shown in Fig. 38.3 can be defined by the equation of line given by Eq. 38.16 (Figs. 38.1 and 38.2).

Equation of line in Fig. 38.3,

$$Z = mx + c \tag{38.13}$$

Fig. 38.1 Side view of ARB blade

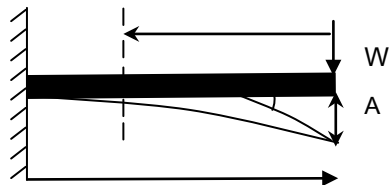


Fig. 38.2 Front view of ARB blade

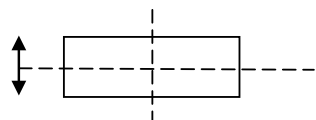
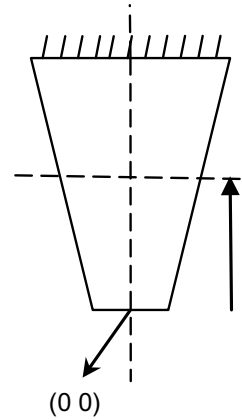


Fig. 38.3 Top view of ARB blade



Now, Moment of Inertia along required axis,

$$I_z = \frac{2z(t^2)}{12}; \quad I_y = \frac{(t)(2z)^3}{12} \tag{38.14}$$

$$I_z = (I_x + I_y)/2 + (I_z - I_y)/2 \times \cos(2a) \tag{38.15}$$

Now, the modified bending equation for cantilever beam with variable cross section as shown in Fig. 38.3. Equation 38.16 is integrated twice and the constants of integration are obtained using the following boundary conditions given in Eq. 38.17. Also the origin point is defined in Fig. 38.3.

$$\frac{d^2y}{dx^2} = \frac{Wx}{E(I_z)} \tag{38.16}$$

$$y = 0 \text{ at } x = 1; \quad \frac{dy}{dx} = 0 \text{ at } x = 1 \tag{38.17}$$

The deflection of the ARB when the left and right blade are rotated by an angle ‘a’ and ‘b’ respectively is obtained using the MATLAB script shown in Appendix 2.

38.2.5 Procedure of Using MATLAB Script

The script file has a designated section where geometric dimensions of the ARB tube and blades can be provided. The various dimensions which is controlled by the designer are as follows:

- Material property—Young’s Modulus of Elasticity

- Thickness of the blade
- Taper angle of the blade
- Length of ARB tube
- Outer diameter of ARB tube
- Inner Diameter of ARB tube.

Once the geometric dimensions are defined, our aim is to find the appropriate angle for left and right blade such that the input Force leads to the deflection which matches the deflection column of Table 38.5 respectively.

38.3 Result and Discussion

The deflection of the inner and outer wheel centre comes out to be different due to the presence of ARB in the suspension system. After solving the governing Eqs. 38.7 and 38.8, the obtained deflection is shown in Eqs. 38.9 and 38.10. Numerical results of deflection in mm for the first case is tabulated in Table 38.6.

The results in Table 38.6 supports that the ARB creates dependency in the suspension system. Also, it has been shown how to calculate the deflection using Eqs. 38.9 and 38.10.

The second result is determining the geometric dimensions of the ARB such that all the 12 cases can be satisfied from one blade angle or the other. The geometric parameters of ARB are tabulated in Table 38.7.

Table 38.6 Suspension travel due to presence of ARB

S. No.	Inner_WheelCenter_Travel (mm)	Outer_WheelCenter_Travel (mm)
1	5.69	8.05

Table 38.7 Geometric parameters of ARB

S. No.	Property name	Symbol	a	b
1	Shear modulus	G	78×10^9	Pascal
2	Young's modulus of elasticity	E	193×10^3	N/mm ²
3	Thickness of the blade	t	4.75	mm
4	Taper angle of the blade	m	0.05	–
5	Length of ARB tube	q	521	–
6	Length of blade	l	84	mm
7	Outer diameter of ARB tube	D	19	mm
8	Inner diameter of ARB tube	d	15	mm
9	Motion ratio of ARB	MRarb	0.31	–

Table 38.8 Blade angle left/right for corresponding setting of “r” and “R”

S. No.	r	R (deg/g)	a (radian)	b (radian)
1	0.5	0.45	$\pi/36$	$\pi/36$
2	0.55	0.45	$\pi/9$	$\pi/9$
3	0.6	0.45	$\pi/4$	$\pi/10$
4	0.65	0.45	$\pi/20$	$\pi/2$
5	0.5	0.53	$\pi/15$	$\pi/15$
6	0.55	0.53	$\pi/120$	$\pi/180$
7	0.6	0.53	$\pi/18$	$\pi/18$
8	0.65	0.53	$\pi/5$	$\pi/10$
9	0.5	0.6	N/A	N/A
10	0.55	0.6	$\pi/20$	$\pi/27$
11	0.6	0.6	$\pi/2$	$\pi/20$
12	0.65	0.6	$\pi/23$	$\pi/20$

The third result is the calculation of appropriate angle for the left and right blade of the arb to satisfy the corresponding condition of Roll gradient and Roll rate distribution. It has been tabulated below in Table 38.8. We recommend to use matlab code in Appendix 2, to calculate a and b respectively. It is to be noted that setting 9 which corresponds to $r = 0.5$ and $R = 0.6$ deg/g requires the ARB to be removed completely.

38.4 Conclusion

This paper demonstrates the use of in-depth load transfer calculation by treating sprung- unsprung mass separately and by including the effect of Gyroscopic moment and Overturning moment. The ride frequency has been chosen in such a way to obtain a positive contribution of ARB on total Roll rate. The dependency created by the presence of ARB in the suspension system has been taken into account to calculate the suspension travel, and it has been found that the suspension travel of inner and outer wheel is unequal due to presence of ARB.

The MATLAB script is used to obtain the geometric dimensions of ARB such that it satisfies all the given cases. Also the specific angle of blade can be noted to achieve a specific setting. The proposed method saves a significant amount of time when it is compared with respect to designing the ARB using Ansys simulation Software. The simulation software needs to update the CAD model of ARB for geometric dimensions and blade angle. However on the other hand, the proposed MATLAB script allows us to change the dimensions and angle by just updating the corresponding value in the script.

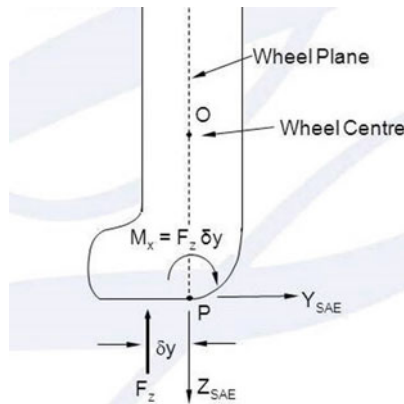
The proposed design methodology shows that an ARB can be designed to provide different driving experiences. The driver can choose the best possible setting according to his driving style on a specific track.

Appendix 1: Weight Transfer Equations

1. **Gyroscopic Load transfer**

$$\text{Gyroscopic Moment} = 2 \times (I_x \times \omega_y \times \omega_z) / 1.35$$

$$\text{Gyroscopic Load transfer} = (2 \times (I_x \times \omega_y \times \omega_z) / 1.35) / T_f = \mathbf{6.88 \text{ pounds}}$$



where, $\omega_y = \sqrt{\frac{A_y R_c}{R}}$ $\omega_z = \sqrt{\frac{A_y}{R_c}}$

R Radius of wheel = **0.228 m.**

Rc Radius of track curvature = **3 m.**

I_x Area MOI of wheel = **0.278 kg m².**

ω_y Angular velocity of wheel about lateral y-axis = **29.13 rad/s.**

ω_z Yawing velocity of wheel about vertical z-axis = **2.214 rad/s.**

Note: Gyroscopic Load transfer is positive for outer wheel and negative for inner wheel.

2. **Load Transfer Due To Overturning Moment**

The equivalency has been drawn overturning moment at wheel center patch and a force has been assumed at wheel center on its behalf, which is formulated as: $F_f = \frac{M_x r}{R}$

$$F_r = \frac{M_x r}{R}$$

where,

Mx = Overturning Moment.

The weight transfer due to F has been taken into similar fashion as for un-sprung mass.

Total Load Transfer = Sprung mass Load transfer + Unsprung Mass Load Transfer + Direct load transfer of Front and Rear + Gyroscopic Load transfer + Load transfer due to overturning moment.

W = Weight of Car	b = Distance of CG from rear axle
W_{fu} = Front Un-sprung mass	L = wheelbase
A_y = Cornering Acceleration	H_s = sprung cg height
W_s = total sprung weight	T_f = Front Track
W_{RU} = Rear un-sprung Mass	Z_{ub} = Height of Rear un-sprung mass
r = Roll Rate Distribution	W_{sb} = Sprung mass rear
T_r = Rear Track	a = distance of CG from front axle
W_{sa} = Sprung Mass Front	K_ϕ = Roll rate
Z_{rf} = Height Of front roll centre	Z_{rr} = Height of Rear roll centre
Z_{ua} = Height of front unsprung mass	

$$\begin{aligned}
 \therefore \text{Load Transfer} = & \frac{W_{fu} \times Z_{ua} \times A_y}{T_f} + \frac{W_{ru} \times Z_{ub} \times A_y}{T_r} \\
 & + \frac{W_{sa} \times Z_{rf} \times A_y}{T_f} + \frac{W_{sb} \times Z_{rr} \times A_y}{T_r} \\
 & + \frac{W_s \times H_s \times A_y}{T_f} \left[\frac{K_\phi r + \frac{b}{l} W_s H_s}{K_\phi - W_s H_s} \right] \\
 & + \frac{W_s \times H_s \times A_y}{T_r} \left[\frac{K_\phi(1-r) + \frac{a}{l} W_s H_s}{K_\phi - W_s H_s} \right] \\
 & + (2 \times (l_x \times w_y \times w_z)/1.35)/T_f \\
 & + (2 \times (l_x \times w_y \times w_z)/1.35)/T_r + \frac{F_f \times Z_{ua}}{T_f} \\
 & + \frac{F_r \times Z_{ub}}{T_f}
 \end{aligned}$$

Here,

$$H_s = \frac{W \times h - Z_{fu} \times W_{tu}}{W_{ts}}$$

For the start, spring of 26 N/mm was used for both front and rear respectively.
Where, Aero load on the car = 78.6 lbs = W_{haero} .

$$\begin{aligned} W_{fo} &= W_{fst} + W_f + W_{haero}/4 & W_{fi} &= W_{fst} - W_f + W_{haero}/4 \\ W_{ro} &= W_{rst} + W_r + W_{haero}/4 & W_{ri} &= W_{rst} - W_r + W_{haero}/4 \end{aligned}$$

Appendix 2: MATLAB Code to Determine the Geometric Dimensions of ARB

% Input force at droop link from Table 38.5

Fwc = 96.542; % Force at Wheel Centre, N

% Blade angle adjustment to get the desired deflection from ARB

a = pi/62.3; % Angle in radian for left blade

b = pi/62.3; % Angle in radian for right blade

% User defined parameters, they can be tweaked to get the desired deflection for a given input % force

```

E = 193 * 103; % Young's Modulus in (N/mm2)
G = 78 * 109; % Shear Modulus Pascal
l = 84; % Length of blade, mm
q = 521; % Length of tube, mm
g = 5; % Thickness of gear blade, mm
m = 0.05; % Slope term of spline equation
c = 7.5; % Constant term of spline equation
t = 4.75; % Thickness of blade
MRarb = 0.31; % Motion Ratio of arb
w = Fwc/MRarb; % Force at ARB droop link, N
% Calculating the deflection at ARB droop link due to right ARB blade
D = 0.019; % Outer Diameter, m
z = (m*x)+c; % Here "z" corresponds to half width of the blade

Iz(x) = (2*z*(t3))/12; % Moment of Inertia about Z-axis
Iy(x) = (t*((2*z)3))/12; % Moment of Inertia about Y-axis
Iz2(x) = (Iz + Iy)/2 + (Iz-Iy)*cos(2*b)/2 ; % Transformed MOI for 'a' angle of
rotation
sy(x) = w*x/(E*Iz2); % Modified equation of Bending
fy(x) = int(sy(x),x); % First integration
cy(x) = fy + -fy(l);
c1 = -fy(l) ; % Value of first Integration Constant
y(x) = int(cy(x),x);
yc(x) = y + -y(l);
c2 = -y(l); % Value of second Integration constant
yc(x); % Deflection at x = 0
(yc(0)); % Final deflection value of the blade
Iarb(x) = (1*(int(int(w*x/(E*Iz2),x) + -fy(l),x) + -y(l)));
Travel(1)=(Iarb(0));

```

% Calculating the deflection at ARB droop link due to left ARB blade

```

z = (m*x)+c; % Here "z" corresponds to half width of the blade
Iz(x) = (2*z*(t3)/12; % Moment of Inertia about Z-axis
Iy(x) = (t*((2*z)3)/12); % Moment of Inertia about Y-axis
Iz1(x) = (Iz + Iy)/2 + (Iz-Iy)*cos(2*a)/2; % Transformed MOI for 'a' angle of
rotation
sy(x) = w*x/(E*Iz1); % Modified equation of Bending
fy(x) = int(sy(x),x); % First integration
cy(x) = fy + -fy(l);
c1 = -fy(l); % Value of first Integration Constant
y(x) = int(cy(x),x);
yc(x) = y + -y(l);
c2 = -y(l); % Value of second Integration constant
yc(x); % Deflection at x = 0
Travel(2) = (yc(0)); % Final deflection value of the blade

```

% Calculating the deflection at ARB droop link due to twist of ARB tube

```

Tube_Rate = (G * 1000* J*pi)/(q*180); %Tube Rate in N-m/deg
Theta = Moment/Tube_Rate; %Twist angle of arb, Degree
td = (Theta*pi/180)*(1+((D*1000)/2)+g); %Droop link travel due to tube deflection
Travel(3) = td;

```

% Total deflection of ARB droop link due to individual deflection of 2 blades and 1 hollow tube

$$T_{wc} = ((Travel(1) + Travel(2) + Travel(3))/MR_{arb})$$

References

1. Bhanage, A., PADmanabhan, K.: Static and fatigue simulation of automotive anti roll bar before DBTT. *10*(71) (2015). ISSN 0973-4562

2. Reimpell, J., Stoll, H., Betzler, J.W.: *The Automotive Chassis: Engineering Principles*, 2nd edn. ISBN 0 7680 06570
3. Tuysuz, C., Pasaoglu, A., Durus, M., Ceyhan, A., Tutuk, E., Ozkardesler, B.C., Hatik Ford Otosan, G.: DOE study on ARB to understand contribution of disturbances and FEA correlation (2014)
4. Tripathi, S., Tiwary, A., Rai, S.: Design of a formula sae chassis according to lateral load transfer distribution. *Int. J. Res. Eng. Technol.* **06**(07) (2017). eISSN: 2319-1163 | pISSN: 2321-7308
5. Bortoluzzi, L.I., Schommer, A., Martins, M., Buenos, A.A.: Formula SAE chassis design to improve suspension tuning. SAE Paper No. 2016-36-0239 (2016). ISSN 0148-7191
6. Schommer, A., Soliman, P., Farias, L.T., Martins, M.: Analysis of a formula SAE vehicle suspension: chassis tuning. Society of Automotive Engineers. SAE Paper No. 2015-36-0275 (2015). ISSN 0148-7191
7. Milliken, W., Milliken, D.: *Race car vehicle dynamics*. Society of Automotive Engineers (1995). ISBN 978-1-56091-526-3
8. de Oliveira Santos, R.: A discussion on steady-state lateral weight transfer and how to use it in setup. <https://racingcardynamics.com/weight-transfer/> (2015)
9. Kaplan, H., Hirsch, A.: Gyroscopic motion: show me the forces! *Phys. Teacher* **52** (2014). <https://doi.org/10.1119/1.4849150>
10. Samal, A.K., Eswara Rao, T.: Analysis of stress and deflection of cantilever beam and its validation using ANSYS. **6**(1), (Part-4), 119–126 (2016). ISSN: 2248-9622

Chapter 39

Study and Comparison of Initial Populations on the Performance of Modified Differential Evolution Algorithm



I. R. Gawai and D. I. Lalwani

Abstract In nature, based on the survival of the fittest principle, the individual with better fitness has more chance to survive and produce a competitive offspring with inherited traits of the parent. Similarly, in evolutionary algorithms, individuals or solutions with better fitness can generate better offspring with higher survival rate. In evolutionary algorithms, the offspring are usually produced by variation operations (mutation and crossover). The generated offspring are compared with parents and better one either from the offspring or parent is selected in the next generation. The quality of initial population (group of individuals or solutions) can affect the performance of evolutionary algorithm. The present work aims to study the effect of initial population on the performance of modified Differential Evolution (DE) algorithm. Four types of initial population, generated by different techniques, are studied and compared for some standard benchmark functions. Four population-generation techniques, namely, random population, random population using the concept of design of experiments, population using symmetric Latin hypercube design and opposition-based learning population, are considered. The results are compared based on the performance measure such as success rate, feasibility rate, success performance, average number of evaluations to a solution, quality measure, fitness and population measure.

Keywords ADEA · DE · Random population · Grid wise population · Performance evaluation measures

39.1 Introduction

The optimization algorithms which are inspired by the nature are called as evolutionary optimization algorithms. In the evolutionary algorithm, a sample of individuals is created which is called as population. The procedure of creating population is named as initialization. The population creation procedures are also known as

I. R. Gawai (✉) · D. I. Lalwani
Mechanical Engineering Department, Sardar Vallabhbhai National Institute of Technology, Surat,
Gujarat, India

space filling design. This population undergoes variation operations to find global optimum. The efforts (Number of function evaluations) to reach global optimum is based on this initial population. In evolutionary algorithms the initial population is generated using techniques like random population generation technique, grid wise population generation technique, univariate method and many others. The study in this paper is focused on random population generation technique and grid wise population generation technique.

Usually the initial population in evolutionary algorithm is randomly generated according to uniform distribution. Tizhoosh [2] proposed the opposition based learning (OBL) algorithm to generate initial population, which was used by Rahnamayan et al. [8] to modify differential algorithm, named as opposition based differential algorithm (ODE). McKay et al. [6] proposed a Latin Hypercube Sampling (LHS) that divides the parameter bound using equal marginal probability. Fang et al. [4] explained the use of Latin Hypercube Design, properties of orthogonal array and the concept of SLHD (Symmetric Latin Hypercube Design) in the population generation. Regis and Shoemaker [10] used SLHD as population generation technique in optimization of costly functions. Antony [1] explained the use of design of experiments (DOE) in several engineering problems. Rana and Lalwani [9] used the concept of DOE to generate population in modified DE algorithm, ADEA.

To test the population generation techniques, amended differential evolution algorithm (ADEA) proposed by Rana and Lalwani [9], was used. Liang et al. [11] gave performance parameters like successful rate (SR), feasible rate (FR) and success performance (SP) to test the algorithm. Average number of evaluation to solutions (AES) was adopted from Eiben et al. [3] to study the results of population generation techniques in this paper. Feoktistov [5] listed some modern performance evaluation measures like quality measure (Q_m), Enes, population measure. These performance evaluation measures are used to perform current study.

The structure of the paper is as follows: The 2nd section explains the population generation techniques. The 3rd section explains ADEA, in 4th section performance measures are listed with their respective formula. The results are listed in 5th section and the paper is concluded in 6th section.

39.2 Population Generation Techniques

In this section, the population mentioned above are explained. The population generation is also called as sampling or space filling. The Individual in the population is made up of the variables.

39.2.1 Random Population Generation Technique

39.2.1.1 Random Population

Random population creates an array of random points within the boundaries of search space. In the current study, the random numbers are generated by the `rand()` command in the Matlab 2016b. This command generates uniformly distributed random numbers between interval (0, 1). Using following Matlab code creates a matrix X, of uniformly distributed random numbers is obtained.

$$X = lb + rand(NP, D) .* (ub - lb) \quad (39.1)$$

where NP is the population size, D is the number of decision variables and lb and ub are the lower and upper bound of respective decision variable. The `rand(NP, D)` will generate a random matrix of size (NP,D) between (0,1).

The uniform distribution ensures that every individual in the population has same probability. Figure 39.1 shows the uniform random population between interval (0, 1).

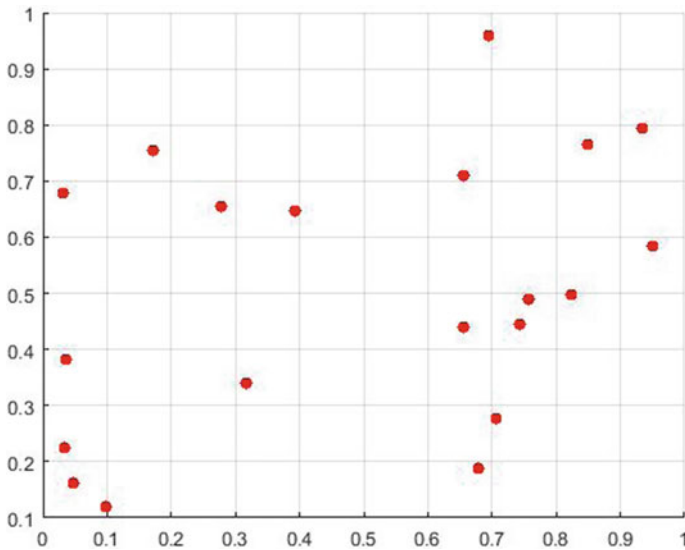


Fig. 39.1 Plot of random points between intervals (0, 1)

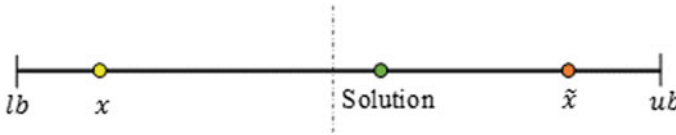


Fig. 39.2 Arbitrary representation of Opposition based population

39.2.1.2 Random Population Using Opposition Based Learning

Opposition based learning was introduced by Tizhoosh [12]. His concept is to create the opposite of the existing population. Then compare them with each other and select top individuals as population. To create the opposite of each individual in the population having size NP, following equation is used:

$$\tilde{x} = lb + ub - x \quad (39.2)$$

where, \tilde{x} is the opposite population, x is the existing population and lb and ub are the lower and upper bound of the decision variable respectively. Therefore, the sample space of the population after the creation of the opposite population will be twice the initial population size and top NP individuals are selected from new population for further processes. In Fig. 39.2, the x represents the existing individual and the \tilde{x} stands for opposition based individual and the dash dotted line shows the centre of the line extended from lower bound to the upper bound. Considering the one-dimensional problem shown in Fig. 39.2, the opposition-based individual \tilde{x} is nearer to the solution, hence \tilde{x} will be selected for the final population instead of x .

39.2.2 Gridwise Population Generation

In this study, two grid wise population generation techniques discussed, they are design of experiments and symmetric latin hypercube design. In grid search the factors represents the controllable variables, the search space is known as experimental domain or input variable space. It is the space where factors take values. The search space is bound by the user defined boundaries. In search space the factors are tested at some specified values. These values are known as levels. The combination of the levels for the factors is called as the level combination. A run or trial is the implementation of a level-combination in the experimental environment [4].

39.2.2.1 Symmetric Latin Hypercube Design

McKay et al. [6] considered LHD as designs for computer experiment. The advantage of these designs over other designs is that they are well spread over search space

without replication of coordinate values. Also, LHDs are computationally cheap to construct. Fang et al. [4], defined LHD with n runs and s input variables, denoted by $LHD(n, s)$, as an $n \times s$ matrix, in which each column is a random permutation of $\{1, 2, \dots, n\}$.

For example, LHD for 5 runs and 2 input variables can be given as shown below.

$$LHD(5, 2) = \begin{bmatrix} 1 & 5 \\ 4 & 4 \\ 3 & 3 \\ 2 & 1 \\ 5 & 2 \end{bmatrix}$$

To create a sample using LHDs which is also called as latin hypercube sampling, an algorithm is listed in Fang et al. [4].

Step 1: Generate an $LHD(n, s)$ where each element is denoted by $\pi_j(1), \dots, \pi_j(n)$ for $j = 1, \dots, s$.

Step 2: Take ns random numbers $U_k^j \sim U(0, 1), k = 1, \dots, n, j = 1, \dots, s$, which are mutually independent. Let $x_k = (x_k^1, \dots, x_k^s)$, where

$$x_k^j = \frac{\pi_j(k) - U_k^j}{n}, \quad k = 1, \dots, n, \quad j = 1, \dots, s. \tag{39.3}$$

The experimental points $D_n = \{x_1, \dots, x_n\}$ is a LHS (Latin Hypercube Sample). The term $\pi_j(k)$ in Eq. (39.3) determines in which cell x_k is located and U_k^j determines where it is located. If we replace U_k^j by 0.5 then the point will locate in the centre of the cell. Figures 39.3 and 39.4 shows the difference between both. This design is called as midpoint latin hypercube sampling (MLHS) or centred latin hypercube sampling. As both are LHDs, there will be only one point is allotted for each pair of row and column, i.e., there are no replication of coordinate values. This phenomenon holds true also for higher number of factors or input variables.

A midpoint LHD is called a symmetric latin hypercube design, denoted by SLHD(n, s), if it has the reflection property: for any row x_k of the matrix there exist another row such that it is the reflection of x_k through the centre $\frac{n+1}{2}$ [4].

The reflection property can be explained as; if (a_1, \dots, a_s) is k th row in an MLHD(n, s) then there will be a row in the matrix whose value is $(n+1-a_1, \dots, n+1-a_s)$ and its position will be $(n-k+1)$. Also, the summation of these rows is $(n+1, \dots, n+1)$. For example consider following matrix M, an MLHD(11,2).

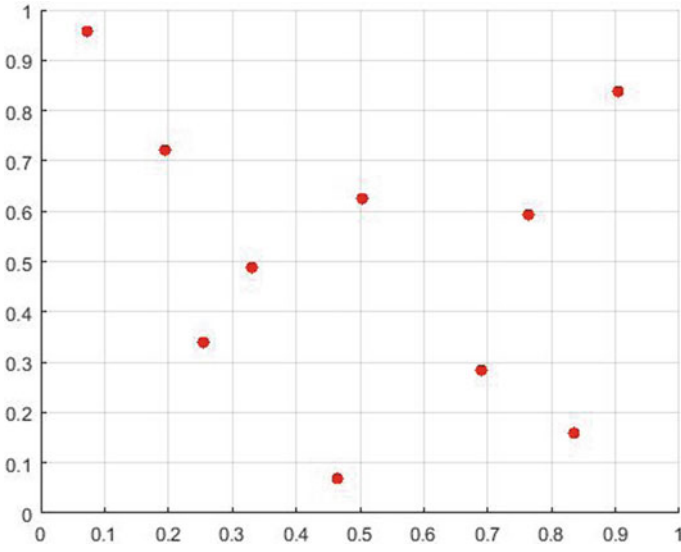


Fig. 39.3 LHS (10, 2)

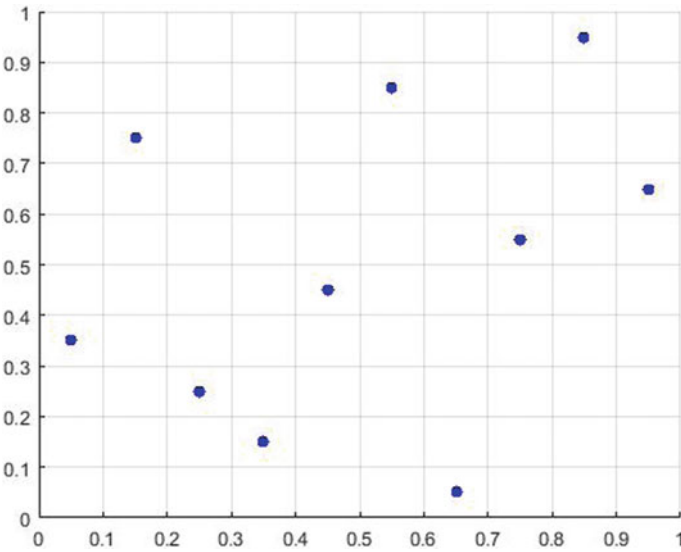


Fig. 39.4 MLHS (10, 2)

$$M = \begin{bmatrix} 1 & 5 \\ 2 & 8 \\ 8 & 2 \\ 5 & 3 \\ 9 & 11 \\ 6 & 6 \\ 3 & 1 \\ 7 & 9 \\ 4 & 10 \\ 10 & 4 \\ 11 & 7 \end{bmatrix}$$

In matrix M, the reflection of 1st row is $(n + 1 - a_1, n + 1 - a_2) = (11 + 1 - 1, 11 + 1 - 5) = (11, 7)$. These values can be spotted in row 11 whose position happens to be $(n - k + 1) = (11 - 1 + 1) = 11$ and the sum of rows 1 and 11 is equal to $(n + 1, n + 1) = (12, 12)$. This holds true for rows 2 and 10, 3 and 9, 4 and 8, 5 and 7 and as the 6th row is the middle row its reflection will be itself. Therefore, the matrix M, an MLHD(11, 2), is an SLHD(11, 2).

Regis and Shoemaker [10] gave an algorithm to construct an SLHD, it is as follows:

1. Initialize an array M of size $\times D$, where NP is population size and D is the number of input variables (factors).
2. If M is odd, set $M((NP + 1)/2, j) = (NP + 1)/2$ for $j = 1, \dots, D$.
3. Define $k = (NP - 1)/2$
4. For each $j = 1, \dots, d$, randomly select a permutation of $1, \dots, k$ and denote it by ψ_j .
5. For each pair (i, j) , where $i = 1, \dots, k$ and $j = 1, \dots, d$,
 - (a) Generate a uniform random number $\omega_{i,j} \in [0, 1]$.
 - (b) If $\omega_{i,j} \leq 0.5$, set $M(i, j) = \psi_j(i)$ and $M(NP + 1 - i, j) = NP + 1 - \phi_j(i)$.

Otherwise, set $M(i, j) = NP + 1 - \phi_j(i)$ and $M(NP + 1 - i, j) = \phi_j(i)$.
6. For each $j = 1, \dots, d$, let π_j be the j th column of M .
7. For each $j = 1, \dots, d$, partition the interval (variable bound) $[a_j, b_j]$ into NP subintervals of equal length and let $c_j^{(i)}$ denote the midpoint of the i th subinterval of $[a_j, b_j]$.
8. Now, for each $i = 1, \dots, NP$, the i th SLHD point is given by $(c_1^{(\pi_1(i))}, c_2^{(\pi_2(i))}, \dots, c_d^{(\pi_d(i))})$.

In above algorithm after step 5, a random SLHD has formed. The steps after step 5 are carried out to create SLHD within the variable bounds. Figure 39.5 given below shows the SLHD within bounds.

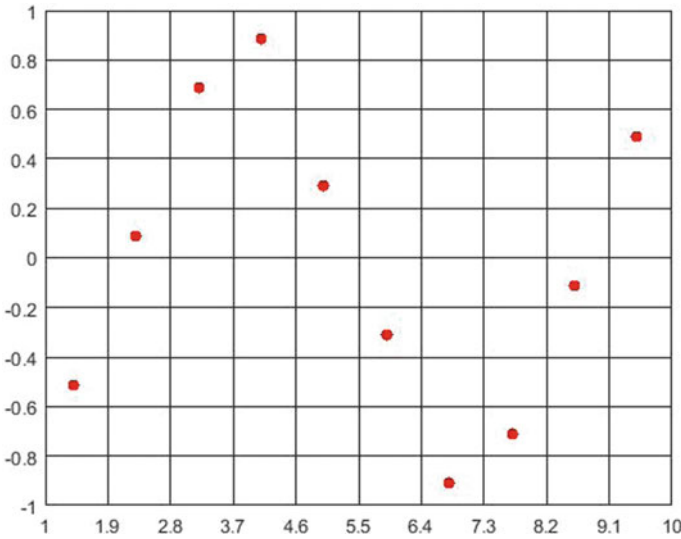


Fig. 39.5 SLHD(10, 2) within bounds

39.2.2.2 Population Using Design of Experiments

Various designs are available in DOE to study the system by performing experimental dependency upon objective of study. In this study a face centred central composite design (FCCD) is adopted [9] to create a matrix of level combinations of factors. This matrix is converted into subspaces and a subpopulation, whose size is decided by the user, is created within that subspace.

To create subspaces in the search space, the range of search space i.e. $(l_b - u_b)$ is divided into three equal parts, where l_b and u_b are lower and upper bound of the search space. The points which divide the range into subrange are named as x_{mb1} and x_{mb2} . The suffix *mb1* stands for middle bound for factor one. Equations (39.4) and (39.5) give the formula for determining the values of x_{mb1} and x_{mb2} respectively. The subranges formed after division are coded as -1 , 0 and 1 , where -1 stands for low range, 0 for middle and 1 for high range. These subranges create subspace. The number of subspaces can be determined by Eq. (39.6).

$$x_{mb1} = lb + \left(\frac{ub - lb}{3} \right) \tag{39.4}$$

$$x_{mb2} = lb + 2 \times \left(\frac{ub - lb}{3} \right) \tag{39.5}$$

$$\text{Number of subspaces} = 2^D + (2 \times D) + 1 \tag{39.6}$$

The subspaces are given names they are corner region (CR), axial region (AR) and centre region (C_nR). In Eq. (39.4) the 2^D gives the number of corner region, $(2 \times D)$ gives the number of axial region and one axial region. For $D = 2$, nine regions are created within the search space. As per the codes allotted to the region their respective lower bounds and upper bounds are changed. For example for the axial region whose codes are $(0, -1)$, its lower bound will be $[7, 3]$ and upper bound will be $[12, 8]$ as shown in Fig. 39.6. A random population is generated within their respective updated bounds. The user can decide how many random points should be generated in each subspace. Therefore, the individuals will spread all over the search space and after function evaluation, top NP individuals are selected further optimization process. In Fig. 39.7 two points are generated in each subspace and in central region four points are generated. Hence, in total 20 points or individuals are generated. In the following example the procedure for generating population using DOE is explained.

There are two input variables $X_1[2, 17]$ and $X_2[3, 18]$, $D = 2$.

1. Number of regions = $2^D + (2 \times D) + C_R = 2^2 + (2 \times 2) + 1 = 9$
 2^D : Number of corner regions, $(2 \times p)$: Number of axial regions and C_R : Number of centre regions (number of centre regions can be decided by the user, it would be one or more than one depending upon the requirement of centre points).
2. The sub-ranges of X_1 and X_2 are given as below.

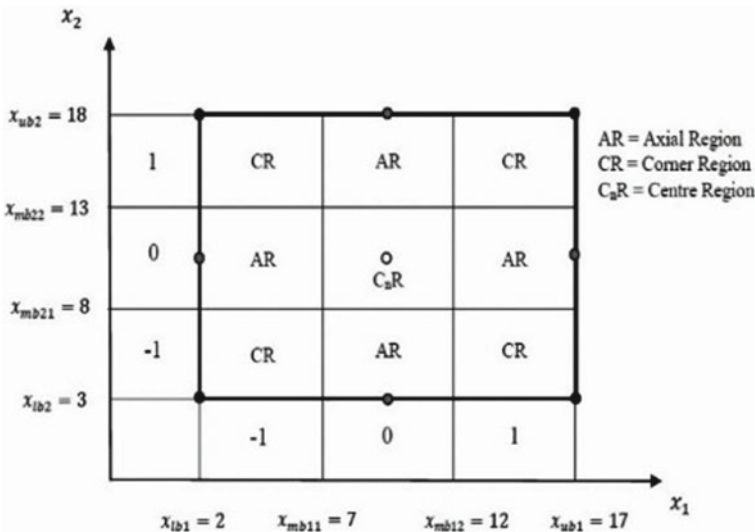


Fig. 39.6 Two factor, face centred composite design [9]

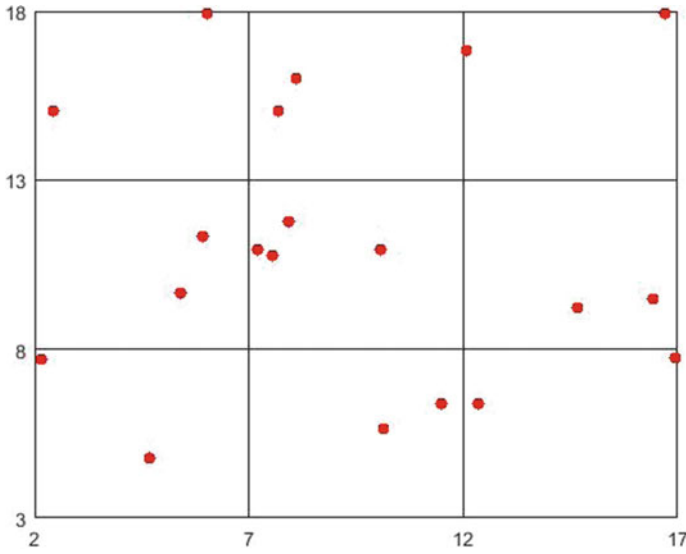


Fig. 39.7 Distribution of points in the search space generated by DOE technique

Middle Values	$X_{mb1} = lb + \left(\frac{ub-lb}{3}\right)$	$X_{mb2} = lb + 2\left(\frac{ub-lb}{3}\right)$
X_{mb1}	5	12
X_{mb2}	8	13

Sub-ranges	-1 [lb, X_{mb1}]	0 [X_{mb1} , X_{mb2}]	1 [X_{mb2} , ub]
X_1	[2, 7]	[7, 12]	[12, 17]
X_2	[3, 8]	[8, 13]	[13, 18]

Face Centered Central Composite Design (FCCD) for two process parameters ($\times 1$ and $\times 2$) as per the code and sub-population ($n = 2$) from each parameter range is given in Table 39.1.

Table 39.1 Decoding the FCCD codes to get parameter range and subpopulation

Region No	FCCD(code)		Parameter sub-bounds as per codes		Sub-population, n = 2		Total population
	X ₁	X ₂	X ₁	X ₂	X ₁	X ₂	
1	-1	-1	[2, 7]	[3, 8]	3.312	7.426	1
					2.428	3.189	1
2	-1	1	[2, 7]	[13,18]	2.146	16.98	1
					6.005	17.57	1
3	1	-1	[12, 17]	[3, 8]	15.650	4.309	1
					16.640	3.494	1
4	1	1	[12,17]	[13,18]	14.890	16.400	1
					14.440	14.680	1
5	0	-1	[7, 12]	[3, 8]	8.158	6.895	1
					9.606	5.471	1
6	0	1	[7, 12]	[13, 18]	10.120	17.520	1
					9.444	16.580	1
7	-1	0	[2, 7]	[8,13]	4.294	11.610	1
					3.186	8.534	1
8	1	0	[12,17]	[8,13]	14.730	12.450	1
					16.820	11.490	1
9	0	0	[7, 12]	[8,13]	10.400	9.671	1
					8.837	8.989	1
10 ^a	0	0	[7, 12]	[8,13]	8.978	11.270	1
					11.940	8.534	1
Total Population						20	

^aTaking an extra centre point (0, 0) to generate extra 2 individual. Hence, there are four points in the centre region. Figure 39.7 shows how the points are distributed. Out of 20 individuals top NP individuals are selected based on their fitness value

39.3 ADEA

The original DE algorithm was proposed to solve the unconstrained optimization problems, to solve the constrained optimization problems Rana and Lalwani [9] made some changes in the original algorithm and named the algorithm as ADEA. ADEA stands for amended differential evolution algorithm. The ADEA algorithm proposed the \sum -constrained handling technique to solve the constrained problem. Other modifications or amendments made in original DE [7] are listed below:

1. Initialization of population using the concept of design of experiments.
2. Selection of scale factor (F) and crossover rate (CR) based on the rank of the individual.
3. Mutant vector selection.

4. Constraint handling technique.
5. Selection operation.

39.3.1 Population Generation Technique

The importance of good initial population is described in earlier chapters. In ADEA, the initial random population is generated using DOE algorithm and it is named as RPDoe. The DOE algorithm is explained with example in Sect. 39.2.2.2 of this paper.

39.3.2 Range of Parameters and Ranking

In DE algorithm, the parameters mutation factor (F) and crossover ratio (Cr) have a high influence on the optimization process. The parameter decides the scale of exploration of search space and an individual's probability of getting selected. In classical DE there is a static value for F and Cr. When the population is converging, the value of F and Cr remains same and hence its amount exploration and probability of selection remains same. Therefore, it takes more generations to reach optimum. But in ADEA the values of F and Cr changes according to the fitness of the individual. The fitness is the measure of individual's distance from optimum. To change the values of F and Cr, all the NP individuals in population are ranked based on their fitness. Also, a range is allotted to the parameters whose boundaries for mutation factor F are F_{\min} and F_{\max} and for crossover ratio Cr are Cr_{\min} and Cr_{\max} . Equations (39.7) and (39.8) gives formula for changing the value of parameters for each individual according its fitness.

$$F_i^G = F_{\min} + (F_{\max} - F_{\min}) \left(\frac{R_i^G - 1}{NP - 1} \right) \quad (39.7)$$

$$Cr_i^G = Cr_{\max} - (Cr_{\max} - Cr_{\min}) \left(\frac{R_i^G - 1}{NP - 1} \right) \quad (39.8)$$

where R_i^G is the rank for each individual that varies from 1 to NP (Population Size) for G^{th} generation. According above equations, the individual which is ranked first, will have minimum value of mutation factor i.e. F_{\min} and maximum value of crossover ratio i.e., Cr_{\max} . Therefore, that individual will have least exploration and high probability of selection.

39.3.3 Mutation Strategy

In classical DE there is one mutation vector whereas in ADEA creates two mutation vectors and selects one which has best fitness. Therefore in each generation twice the exploration takes place. The one mutation vector generated in classical DE is denoted by DE/rand/1. It stands for Differential evolution with mutation using random individuals and one difference vector. In ADEA two mutation vectors are generated using Eqs. (39.9) and (39.10).

$$M_1^G = X_a + F(X_b - X_c) \tag{39.9}$$

$$M_2^G = X_a - F(X_b - X_c) \tag{39.10}$$

where suffix a, b and c are three different index of individual which are also not equal to current index and X_a , X_b and X_c are their respective individuals. M_1 and M_2 are the mutation vectors for each individual at G^{th} generation and F is the mutation factor. The fitness of both mutant vector is determined and the mutant vector with best fitness is selected. Figure 39.8 shows the graphical representation of ADEA mutation strategy.

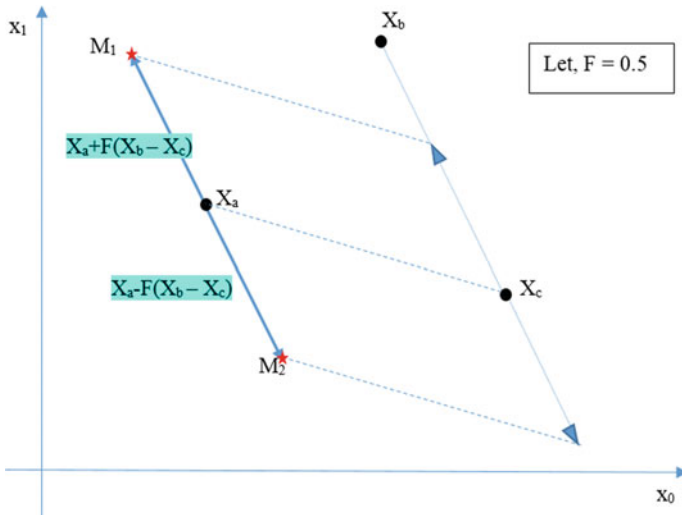


Fig. 39.8 Two mutant vectors strategy for mutation factor $F = 0.5$

39.3.4 Constraint Handling Technique

There are two types of constraints, i.e., equality constraints and inequality constraints. The equality constraints are converted into inequality constraints, because the algorithm requires some space before convergence. By converting the equality constraint into inequality the search space is widened and algorithm can run. To convert equality constraint into inequality, the technique given by Coello [2] is used. The technique is given in Eq. (39.11).

$$|h_m^g| - \varepsilon \leq 0 \tag{39.11}$$

where h_m^g the equality constraint and m is the number of equality constraint. ε is a very small value. For present work $\varepsilon = 0.001$ ($1e-3$) is taken [2].

In ADEA Σ -constraint handling technique is introduced. In this technique constraints violation for an individual are summed up. This sum is added with objective function value for that individual and a value lambda (λ) is also added to it. This total is named as combined function (Ψ). The combined for each infeasible individual is shown below in Eq. (39.12).

$$\Psi = fx + \sum_{i=1}^{NOC} (Violation_i) + \lambda \tag{39.12}$$

where NOC is the number of constraints to an objective function, the λ is the maximum of $|f_{max}|$ and $|f_{min}|$ and fx is the objective function value for the individual. The combined function is calculated only for infeasible solution.

39.3.5 Selection Operation

In ADEA instead of comparing the solution based on its combined function, the solution is compared with respect to its objective function value and total constraint violation value separately or total constraint violation value only. Equation (39.13) shows the selection strategy.

$$x_{i,g+1} = \begin{cases} u_{i,g} & \left[\begin{array}{l} \text{if } f(C_{i,g}) \leq f(x_{i,g}) \text{ and } \Sigma_{const}(C_{i,g}) \leq \Sigma_{const}(x_{i,g}) \\ \Sigma_{const}(C_{i,g}) \leq \Sigma_{const}(x_{i,g}) \end{array} \right] \text{ or} \\ x_{i,g} & \text{Otherwise} \end{cases} \tag{39.13}$$

where $C_{i,g}$ is the trial vector obtained after crossover operation in generation g for solution i . If the objective function value of Fig. 39.9 shows the flowchart of the

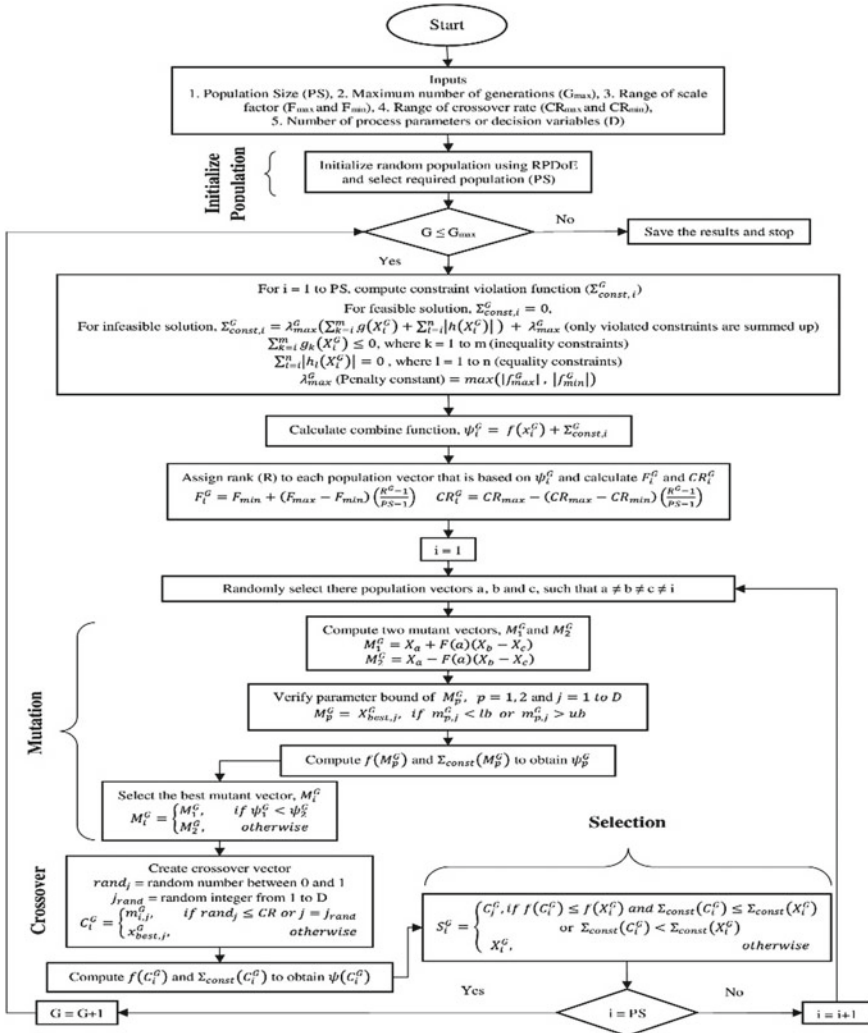


Fig. 39.9 Flowchart for ADEA [9]

ADEA algorithm.

39.4 Performance Evaluation Measures

The maximum number of function evaluations are set to 500,000. Within the maximum function evaluation the solution must satisfy criteria for minimization problem given in Eq. (39.14). The solutions which satisfies all the constraints are

Table 39.2 Performance measures

Performance measure	Expression
Feasibility rate, FR [11]	$FR = \frac{\text{(number of feasible run)}}{\text{(total runs)}}$
Success rate, SR [11]	$SR = \frac{\text{(number of successful run)}}{\text{(total runs)}}$
Success Performance, SP [11]	$SP = \frac{\text{mean}(FEs \text{ for successful runs})}{\text{(number of successful runs)}} \times \frac{\text{(number of total runs)}}{\text{(number of successful runs)}}$
Q-measure [5]	$Q_m = \left(\sum_{j=1}^{n_c} FE_j \right) / n_c / n_c / n_t \%$
Enes [5]	$Enes = \left(\sum_{i=1}^{n_t} FE_i \right) / n_c$
P-measure [5]	$P_m = \max_i \text{indi} - \left(\frac{\sum_{i=1}^{NP} \text{indi}}{NP} \right)_E, \quad i = 1, \dots, NP$
Average number of evaluation to a solution, AES [3]	$AES = \frac{\text{sum of function evaluation for successful trials}}{\text{successful trials}}$

known as feasible solutions and if at least one solution is feasible in a run, then run is called as feasible run. In a run if Eq. (39.14) is satisfied then run is called as successful run.

$$f(x) - f(x^*) \leq 0.0001. \tag{39.14}$$

where $f(x)$ is the feasible optimized objective function value determined by the algorithm and $f(x^*)$ is the solution listed in CEC 2006 [11]. There are several performance evaluation measures used in this study and they are listed in Table 39.2 given. In table FE stands for function evaluations, n_c is number of successful runs, n_t is number of total runs, ind stands for individual or solution and NP is population size.

On contemplating the performance measures SP , Q_m , $Enes$ and AES , it can be seen that if number of successful run is equal to number of total runs, i.e., $n_c = n_t$ then $SP = Q_m = Enes = AES$. Also it is observed that, lower the values of SP , Q_m , $Enes$ and AES , better is the algorithm.

39.5 Results and Discussion

13 benchmark problems from CEC 2006 [11] and ADEA [9] are used to calculate FR, SR, SP, AES, Q_m and Enes, time required to generate population, population measure, grand sum of constraint violation and number of feasible individual in

initial population. FR, SR, SP, AES, Q_m and Enes are given in Table 39.3 and the characteristics of initial population are given in Table 39.4. The best obtained values are represented in bold letters in Tables 39.3 and 39.4.

The system used for solving the problems is HP Pavilion 15 Notebook with Intel i5 1.6 GHz processor and 8 GB RAM. In ADEA, the size of initial population is set to 50, the range of mutation factor is set between $F_{\min} = 0.5$ and $F_{\max} = 0.85$, the range of crossover ratio is set between $Cr_{\min} = 0.8$ and $Cr_{\max} = 0.95$. The maximum generations are set to 5000 and each problem has undergone 20 trials. The best, worst and standard deviation of 20 solutions obtained after 20 trials are given in Table 39.3.

From the results shown in Table 39.3 it can be observed that OBL showed better performance in 5 problems, namely g02, g03, g04, g06, g08, DOEPOP showed excellence in 4 problems, g01, g07, g09, g12, SLHD and RANDPOP showed better result in one problem each and they are g11 and g10 respectively. None of the population generation techniques were able to find a successful run for problems g05 and g13, therefore none of the performance measuring parameters could not be calculated. But best feasible answer was reported by DOEPOP for g13 and solution with least constraint violation was reported by SLHD for g05.

From Table 39.4 it is observed that RANDPOP takes least amount of time to generate initial population, as built in function of MATLAB was used, and DOEPOP took maximum amount of time among four population generation techniques. Also, DOEPOP wasn't able to generate population for g02 benchmark function because g02 has 20 variables and the system was inadequate to spend the required computational expense. But, DOEPOP has the least amount of constraint violation for 11 benchmark functions and for the remaining two, g06 and g08, OBL showed least amount of constraint violation. The more densely the population is better is the convergence [5]. Therefore, population generation technique with least amount of P-measure might have better convergence. The farthest point in DOEPOP was reported closer to mean for g01, g03, g07, g09, g12 and g13, than other population generation techniques. OBL has least amount of P-measure in g04, g06, g08 and g11. SLHD has least amount of P-measure for g02, g05 and g10, whereas RANDPOP has more scattered population. Amount of feasible solutions in the initial population can decrease the efforts required for achieving optimum solution. The DOEPOP showed maximum number of feasible solutions in initial population for g01, g04 and g09. OBL showed maximum feasible solutions in initial population for g02. The population size for given study is 50 and OBL gave 100 feasible solutions, so top 50 solutions were selected for optimization process.

39.6 Conclusion

From results and discussion it can be concluded that the overall performance of the OBL population generation technique is better than other techniques. DOEPOP showed good quality of initial population but for problems with large number of variables, the computational cost of DOEPOP is higher. It is not advisable to use

Table 39.3 Results for 13 benchmark problems given in CEC 2006 [11]

	Best	Worst	Mean	Std. Dev	FR	SR	SP	AES	Trials	Avg. Gen	Avg. time(min.)	Quality Measure	Enes
g01	Randpop	-14.9999	-14.9999	4.54E-06	1	1	16,497.5	16,497.5	20	330	1.194149	16,497.5	16,497.5
	DOEPOP	-14.9999	-14.9999	2.81E-06	1	1	16,142.5	16,142.5	20	323	1.711871	16,142.5	16,142.5
	SLHD	-14.9999	-14.9999	4.75E-06	1	1	16,182.5	16,182.5	20	324	1.312252	16,182.5	16,182.5
g02	OBL	-15	-15	0	1	1	16,592.5	16,592.5	20	332	20.45737	16,592.5	16,592.5
	Randpop	-0.80352	-0.74934	-0.78149	0.018808	1	779,900	779,900	20	3900	20.52722	3,119,600	779,900
	DOEPOP	-	-	-	-	-	-	-	-	-	-	-	-
g03	SLHD	-0.80353	-0.71562	-0.77605	0.026228	1	1,454,950	1,454,950	20	4365	19.96821	9,699,667	1,454,950
	OBL	-0.80352	-0.71032	-0.77592	0.027516	1	617,750	617,750	20	3707	18.49021	2,059,167	617,750
	Randpop	-1.0004	-0.26548	-0.6427	0.197475	1	4,946,900	4,946,900	20	4947	11.45874	98,938,000	4,946,900
g04	DOEPOP	-1.00039	-0.26168	-0.57572	0.254302	1	65,535	65,535	20	5000	11.44058	0	0
	SLHD	-1.00036	-0.21211	-0.66637	0.233216	1	65,535	65,535	20	5000	13.21805	0	0
	OBL	-1.0004	-0.27374	-0.59966	0.186256	1	4,940,850	4,940,850	20	4941	11.51231	98,817,000	4,940,850
g05	Randpop	-30.665.7	-30.665.5	-30.665.6	0.037597	1	3255	3255	20	66	0.277357	3255	3255
	DOEPOP	-30.665.7	-30.665.5	-30.665.6	0.045049	1	3280	3280	20	66	0.279758	3280	3280
	SLHD	-30.665.6	-30.665.5	-30.665.6	0.025946	1	3232.5	3232.5	20	65	3.743115	3232.5	3232.5
g05	OBL	-30.665.7	-30.665.5	-30.665.6	0.053128	1	3197.5	3197.5	20	64	0.273302	3197.5	3197.5
	Randpop	5004.358	5124.588	5085.227	37.69218	0	INF	INF	20	5000	19.31823	INF	INF
	DOEPOP	5056.096	5121.633	5099.837	19.403	0	INF	INF	20	5000	17.94758	INF	INF
SLHD	5056.539	5125.13	5104.761	17.20109	0	INF	INF	20	5000	17.73326	INF	INF	

(continued)

Table 39.3 (continued)

	Best	Worst	Mean	Std. Dev	FR	SR	SP	AES	Trials	Avg. Gen	Avg. time(min.)	Quality Measure	Enes
g06	OBL	4705.405	5073.468	91.34417	0	0	INF	INF	20	5000	18.48417	INF	INF
	Randpop	-6961.81	-6949.25	56.19116	1	0.95	16,044.73684	16,044.74	20	305	1.007023	16,889.2	16,044.74
	DOEPOP	-6961.81	-6945.28	56.04682	1	0.9	30,725	30,725	20	554	1.488335	34,138.89	30,725
	SILD	-6961.81	-6961.81	2.27E-05	1	1	2845	2845	20	57	0.253169	2845	2845
g07	OBL	-6961.81	-6961.81	2.57E-05	1	1	2820	2820	20	57	0.242241	2820	2820
	Randpop	24.30629	24.3063	6.75E-06	1	1	25.655	25.655	20	257	1.468059	25.655	25.655
	DOEPOP	24.30629	24.3063	5.85E-06	1	1	25,270	25,270	20	253	1.650115	25,270	25,270
	SILD	24.30629	24.3063	4.48E-06	1	1	26,080	26,080	20	261	1.612723	26,080	26,080
g08	OBL	24.30628	24.3063	6.28E-06	1	1	25.605	25.605	20	257	1.575061	25.605	25.605
	Randpop	-0.09582	-0.09573	2.98E-05	1	1	855	855	20	9	0.10648	855	855
	DOEPOP	-0.09582	-0.09574	2.51E-05	1	1	447.5	447.5	20	9	0.646873	447.5	447.5
	SILD	-0.09582	-0.09573	3.25E-05	1	1	427.5	427.5	20	9	0.077524	427.5	427.5
g09	OBL	-0.09582	-0.09574	2.59E-05	1	1	422.5	422.5	20	9	0.095354	422.5	422.5
	Randpop	680.6301	680.6302	1.65E-05	1	1	4862.5	4862.5	20	98	0.428213	4862.5	4862.5
	DOEPOP	680.6301	680.6302	9.89E-06	1	1	4452.5	4452.5	20	90	0.411835	4452.5	4452.5
	SILD	680.6301	680.6302	1.8E-05	1	1	4822.5	4822.5	20	97	0.419679	4822.5	4822.5
g10	OBL	680.6301	680.6302	1.42E-05	1	1	4967.5	4967.5	20	100	0.43175	4967.5	4967.5
	Randpop	7049.248	7049.25	0.000391	1	0.85	94,202.94118	94,202.94	20	1602	4.748212	110,827	94,202.94
	DOEPOP	7049.248	7049.248	2.81E-05	1	0.85	142,741.1765	142,741.2	20	2427	8.382054	167,930.8	142,741.2
	SILD	7049.248	7049.249	0.00012	1	0.75	144,886.6667	144,886.7	20	2174	6.743685	193,182.2	144,886.7
OBL	7049.248	7049.248	8.88E-05	1	0.85	109,802.9412	109,802.9	20	1867	6.161445	129,179.9	109,802.9	

(continued)

Table 39.3 (continued)

	Best	Worst	Mean	Std. Dev	FR	SR	SP	AES	Trials	Avg. Gen	Avg. time(min.)	Quality Measure	Enes
g11	Randpop	0.749905	0.750024	0.000188	1	0.8	65,803.125	65,803.13	20	1053	2.779763	82,253.91	65,803.13
	DOEPOP	0.749902	0.753925	0.013505	1	0.8	65,509.375	65,509.38	20	1049	2.755187	81,886.72	65,509.38
	SILHD	0.749902	0.749944	3.19E-05	1	1	2772.5	2772.5	20	56	0.251129	2772.5	2772.5
	OBL	0.749903	0.749979	0.749928	1	1	3187.5	3187.5	20	64	0.260008	3187.5	3187.5
g12	Randpop	-0.99999	-0.99996	2.73E-05	1	1	275	275	20	6	0.051984	275	275
	DOEPOP	-0.99999	-0.99994	2.83E-05	1	1	250	250	20	5	0.051244	250	250
	SILHD	-1	-0.99991	2.68E-05	1	1	272.5	272.5	20	6	0.055653	272.5	272.5
	OBL	-1	-0.99999	3.28E-05	1	1	257.5	257.5	20	6	0.050422	257.5	257.5
g13	Randpop	0.151857	0.611737	0.227063	1	0	INF	INF	20	5000	14.7956	INF	INF
	DOEPOP	0.336132	0.999791	0.227685	1	0	INF	INF	20	5000	14.31045	INF	INF
	SILHD	0.438803	0.995848	0.198469	1	0	INF	INF	20	5000	14.64811	INF	INF
	OBL	0.209112	0.996501	0.226287	1	0	INF	INF	20	5000	14.86366	INF	INF

Table 39.4 Initial population characteristics for 13 benchmark functions form CEC 2006 [11]

Problems	Time required for generation				Sum of violation			
	Randpop	DOEPOP	SLHD	OBL	Randpop	DOEPOP	SLHD	OBL
g01	0.000772	0.28585	0.022818	0.001951	29,977.67	912.5742	27,934.11	20,798.84
g02	0.000784	-	0.02504	0.00296	0	-	0	0
g03	0.000767	0.092476	0.038698	0.003109	111.1892	37.16628	116.0901	78.51319
g04	0.000751	0.08404	0.026692	0.002481	33.76069	0.709482	45.37136	9.433672
g05	0.000749	0.087893	0.026169	0.002477	97,689.59	44,819.4	98,815.37	68,414.21
g06	0.000768	0.094862	0.030491	0.003064	315,982.1	184,388.1	296,809.8	139,631.9
g07	0.000751	0.116361	0.038351	0.003458	93,464.27	32,188.6	100,274.3	83,889.39
g08	0.000814	0.073794	0.022341	0.002326	2072.337	975.6943	1845.073	828.32
g09	0.000768	0.099409	0.031016	0.003092	278,961.3	1173.448	329,530.5	119,326.2
g10	0.000808	0.092293	0.03102	0.002358	87,060.412	10,434,850	69,039,950	38,053,064
g11	0.00089	0.109463	0.036485	0.003657	26.43891	7.394346	31.07233	13.07816
g12	0.000771	0.074377	0.022565	0.002317	1296.818	129.1535	1246.394	841.3298
g13	0.000758	0.087669	0.024544	0.002337	1185.04	430.5609	1117.791	564.0062

(continued)

Table 39.4 (continued)

Problems	Population measure (P-measure)				Number of feasible solutions			
	Randpop	DOEPOP	SLHD	OBL	Randpop	DOEPOP	SLHD	OBL
g01	76.82358277	7.890853397	66.36185199	73.77381947	0	1	0	0
g02	15.20566309	-	14.54235194	15.96790294	50	-	50	100
g03	1.214978637	1.068565473	1.10788086	1.09037088	0	0	0	0
g04	16.53909821	16.40901814	16.21454902	15.40082882	19	42	15	28
g05	800.7110288	763.6247143	722.5953514	789.6415465	0	0	0	0
g06	57.85590392	50.2548788	59.00295671	42.66466404	0	0	0	0
g07	21.1584037	19.22161033	22.91025971	22.45064275	0	0	0	0
g08	6.762314605	4.585975691	6.370243323	4.399950348	0	0	0	0
g09	19.06002703	10.10323241	20.28496981	17.35881588	0	27	1	1
g10	6727.039034	7054.413691	6539.800132	7264.789042	0	0	0	0
g11	1.368824652	1.268869912	1.277810628	1.153922408	0	0	0	0
g12	8.237138305	2.38230913	6.339558344	5.141272453	0	0	0	0
g13	5.013451099	3.528015937	5.42989429	4.189578422	0	0	0	0

SLHD and RANDPOP for the generation of initial population as both were not able to produce competitive results.

References

1. Antony, J.: Design of Experiments for Engineers and Scientists: Second Edition. Design of Experiments for Engineers and Scientists: Second Edition (2014). <https://doi.org/10.1016/C2012-0-03558-2>
2. Coello, C.A.C., Van Veldhuizen, D.A., Lamont, G.B.: Evolutionary Algorithms for Solving Multi-Objective Problems (Genetic and Evolutionary Computation) (2002). <https://doi.org/10.1007/978-4757-5184-0>
3. Eiben, A.E., Marchiori, E., Valkó, V.A.: Evolutionary algorithms with on-the-fly population size adjustment. Lecture Notes in Computer Science (Including Subseries Lecture Notes in Artificial Intelligence and Lecture Notes in Bioinformatics), vol. 3242, pp. 41–50 (2004)
4. Fang, K.-T., Li, R., Sudjianto, A.: Design and modeling for computer experiments. Des. Model. Comput. Exp. (2005). <https://doi.org/10.1201/9781420034899>
5. Feoktistov, V.: Differential evolution in search of solutions. In: Optimization and Its Applications, vol. 5 (2006). <https://doi.org/10.1002/j.1551-8833.2004.tb10728.x>
6. McKay, M.D., Beckman, R.J., Conover, W.J.: A comparison of three methods for selecting values of input variables in the analysis of output from a computer code. Technometrics **42**(1), 55–61 (2000)
7. Price, K.V., Storn, R.M., Lampinen, J.A.: Differential evolution a practical approach to global optimization (2005). Retrieved from www.springer.com/series/4190
8. Rahnamayan, S., Tizhoosh, H.R., Salama, M.M.A., Evolutionary, A.: Oppos.-Based Different. Evol. **12**(1), 64–79 (2008)
9. Rana, P.B., Lalwani, D.I.: Optimization of turning process using amended differential evolution algorithm. Eng. Sci. Technol., Int. J. **20**(4), 1285–1301 (2017)
10. Regis, R.G., Shoemaker, C.A.: Local function approximation in evolutionary algorithms for the optimization of costly functions. IEEE Trans. Evol. Comput. **8**(5), 490–505 (2004)
11. Runarsson, T.P., Liang, J.J., Mezura-Montez, E., Clerc, M., Suganhtan, P.N., Coello Coello, C.A., Deb, K.: Problem definitions and evaluation criteria for the CEC 2006 special session on constrained real-parameter optimization. In: Problem Definitions and Evaluation Criteria for the CEC 2006 Special Session on Constrained Real-Parameter Optimization, (January) (2006)
12. Tizhoosh, H.R.: Opposition-based learning: a new scheme for machine intelligence. In: Proceedings of International Conference on Computational Intelligence for Modelling, Control and Automation, CIMCA 2005 and International Conference on Intelligent Agents, Web Technologies and Internet, vol. 1, pp. 695–701 (2005)

Chapter 40

Evaluation of Smart Bio-materials in Orthopedics and Tissue Engineering



Pravin S. Nerkar, Sanket J. Tawale, Shailesh M. Saoji, and Akshay D. Doye

Abstract Bio-materials are used to create bio-mimetic models with same characteristics as biological entity to be operated. Far from these materials, new class of smart bio-materials has been developed, and these materials are highly react to minute changes in their environment. Smart bio-materials are classified on basis of piezo-electric material, shape memory alloys, self healing materials, thermo-electric materials etc. The development of smart materials for various medical applications has become centre of attention for research interest. Smart materials are growing interest as model in research to understand complex bio-materials in medical applications. The study of smart materials in orthopedics, tissue engineering and introduction of advanced smart materials in current practice is necessary. In this paper recent smart materials in orthopedics and tissue engineering were discussed. Different advanced smart materials in orthopedics and tissue engineering were proposed to introduced in actual practice. This paper focuses on advancement and new smart materials to be introduced in biomedical applications. The information provided in this paper may be beneficial for the future development of biomedical devices and their clinical applications thus improving standard of patient life and advancement in biomedical sector.

Keywords Smart bio-materials · Orthopedics · Tissue engineering · Advancement in materials

40.1 Introduction

Bio materials are natural or synthetic materials which can be able to permit absolutely or quick with the useful resource of the human body. Bio materials are classified into natural bio-materials and synthetic bio-materials. Synthetic bio-materials are further classified into bio inert, bio reasonable and bio active materials [1]. Bio inert are those materials which react minimum without surrounding tissue once located

P. S. Nerkar (✉) · S. J. Tawale · S. M. Saoji · A. D. Doye
Mechanical Engineering Department, St Vincent Pallotti College of Engineering & Technology,
Nagpur, Maharashtra 441108, India

in human body. Stainless steel, alumina, platinum are most commonly used for surgical equipment which include dental implant. Bio active materials react with their surrounding bone and with smooth tissue in some instances. Glass ceramic and hydroxyapatite are most commonly used. Bio active materials are commonly used in hip joint surgery. Bio reasonable materials dissolve with nearby human body changing injury with new joint. Such a material are used for cancer treatment. These materials include gypsum, calcium oxide and calcium carbonate [2]. Loss of useful integration is largest obstacle in fulfillment of bio medical industry. A new class of smart bio materials has been developed and these materials notably react to minute adjustment of their surroundings. Smart bio materials quick deliver curative action to intended site of body. It is very tough to categorize smart bio materials because of its different approach. Due to their active fixed properties smart materials allow smart bio material to be developed. Smart bio-materials are classified on basis of piezoelectric material, shape memory alloys or polymers, self healing materials, thermo-electric materials etc. The development of smart materials for various medical applications has become centre of attention for research interest. Smart materials are growing interest as model in research to understand complex bio-materials in medical applications [3]. Due to their dynamically alterable properties, smart materials allows smart bio-materials to be developed.

The bone and joint disorder are leads to degeneration of the mechanical properties. Over few years revision surgical procedure of hip and knee implants has been extremely increased. For this reason it is anticipated that there will be more demand for new and advanced implants materials in in coming years. At present the materials used for implants are 316L stainless steel, Co-Cr alloys and titanium based alloys [4]. But this material possesses tendencies to fail after long-term because of high modulus in comparison to that of bone low strength, low wear and absence of bio compatibility. Thus it is expected that implant should survive for longer period or until lifetime without failure or revision surgery. Hence development of suitable materials with the highest strength and good bio compatibility is essential.

The smart orthopedics and tissue engineering techniques based on bio-materials have interesting potential to meet these urgent needs. Bio-materials in orthopedics are those materials which are used to repair or rebuild bone disorder. The main requirement of bio-material in orthopedics is to use those implant material which can resist the effect of repeated stress mostly metals ceramics and composites satisfy this requirement. The implant material should have high strength, high resistance to fatigue and corrosion resistance. Tissue engineering involve use of dwelling cells or entire endogenous cells to resource tissue formation for regeneration and thereby way of manner of produce therapeutic or diagnostic benefits. New generation intelligent bio materials offer exciting potential and provide promising opportunity to significantly increase the efficiency of hard tissue engineering and regenerative medicine [5]. The study of smart materials in orthopedics, tissue engineering and introduction of advanced smart materials in current practice is necessary. In this paper, recently developed titanium alloy as a smart materials and smart derivatives of calcium phosphate for bone tissue engineering is discussed. The main focus of this paper is on advancement and new smart materials to be introduced in biomedical applications.

The information provided in this paper may be beneficial for the future development of biomedical devices and their clinical applications.

40.2 Bio-materials in Orthopedics and Tissue Engineering

Orthopaedics implants are commonly made of metal, ceramics, Polymers and composites. Commonly used metallic bio-materials consists of the stainless steel, Cobalt (Co)-Chromium (Cr) alloys and the pure Titanium and its alloy. Stainless Steels and Co-Cr alloys was firstly metallic materials used for orthopedics applications. At present stainless steel with chromium content of the 20% and the high nickel content of 0.3–0.4% has been used for joint prosthesis [6]. Earlier, Stainless steel consists minor amount of chromium iron and nickel was used for the artificial hip joint, but due to the poor strength, unable to the support under the high stress, this material is replaced by the CO-Cr-Mo alloys. Steel with the high carbon proportion has most commonly used in fracture plate, screws and medullary nail. Currently Stainless steel (316L), Ti-6Al-4V and Ti-6Al-7Nb used for medullary nail. Co-Cr alloys are always have excellent corrosion resistance and can sustain under load more than of stainless steel. Co-Cr alloy shows the high elastic modulus i.e. 230GPa which is much higher than the cortical bone. Co-Cr alloys are commonly used for the making prosthetic femoral head. Higher hardness, corrosion resistance causes due to the pitting in Co-Cr alloys can obtained by introducing molybdenum (Mo) thus, Co-Cr-Mo alloy was used for the hip prostheses. Pure Titanium and its alloys especially Ti-6Al-4V alloys are widely used in the current Orthopaedics applications. Table 40.1 shows detailed materials used in the orthopedics application. Porous tantalum have also been successfully used for the many orthopedics purpose [7]. Due to its high bulk density, low modulus of elasticity and good friction properties, tantalum foam used for the load bearing applications such as total joint orthoplasty.

Ceramics are those materials which are ionic and covalent bonded brittle in nature and shows good corrosion resistance they are normally used in the bone cement and tissue engineering application. The commonly used ceramics material uses can be categorized as Bio active glass (BGs), glass-ceramics and Calcium phosphate (CaP). β -tricalcium phosphate (TCP) and the hydroxyapatite (HA) and their derivatives which are very similar to bones are widely used as bio ceramic. HA Indicates desirable reactive properties and HA remain into the regenerate bone tissue after implantation. High density and pure Alumina was used for the acetabular cups and femoral head showing good wear, corrosion resistance, high strength and excellent bio compatibility. Zirconia shows highest strength in ceramics thus well suited for the orthopedics application. Due to low wear of zirconia femoral head was inserted with alumina for hip prosthesis. High hardness of Zirconia shows good mechanical properties for hip replacement [8]. CaP are infectable, harden inside the broken bone tissue and generate low heat transfer thus avoids the ultimately demise of surrounding cell. Glasses, glass-ceramics and ceramics that take specific organic reaction at the interface among the fabric and the bone tissue which ends within the formation of

Table. 40.1 Materials used in the orthopedics application

Orthopedics implants	Bulk bio material used	Types of system used
Bone attachment devices and stabilizers	Stainless steel, titanium and alloys, cobalt-chromium alloys, carbon fibre reinforces PEEK, PLLA	Intramedullary nail systems Plate systems Screw systems Pins and wire systems Other fastening devices
Artificial joints	Stainless steel, titanium and alloys, cobalt-chromium alloys, tantalum, zirconia-toughened alumina, pyrocarbon, UHMWPE, silicone	Hip replacement systems Knee replacement systems Shoulder replacement systems Elbow replacement systems Hand and foot joint replacement systems
Artificial ligaments and tendons	Stainless steel, titanium and alloys, PEEK, carbon fibre-reinforced PEEK, PLLA, UHMWPE, PET, nylon, absorbable composites	Non-absorbable sutures Bone and suture anchor systems
Artificial spine devices	Titanium, titanium alloys, cobalt-chromium alloys, tantalum, silicon nitride, UHMWPE, PEEK	Inter-vertebral disc systems Vertebral body replacement systems Inter-body fusion devices Interspinous process fusion devices Spinal support devices
Biologic and tissue engineering inducers	Calcium phosphate composites, autografts, allografts, collagen, PMMA, BMP-2 and other growth factors	Bone grafts and fillers Cartilage and osteochondral grafts Osteogenic inducers

a bond between them. CaP based ceramics has commonly used for orthopedics and tissue engineering due to their similar mechanical properties as that of the bone. Silicon as bio ceramics improves bio activity by forming Si-OH group on the surface [9]. The Si-OH involve in nucleation and formation of apatite layer on the surface thus, improving material bone bonding.

Polymethylmethacrylate (PMMA) widely used as bone cement. Due to better properties of PMMA bone cement, it provides good primary fixation of the prosthesis. Polyetheretherketone (PE) and especially ultra high molecular weight polythene (UHMWPE) are very attractive for the application such as the acetabular layer for general hip replacement tibial inserts for the knee, orthoplasty as well as patella components and intervertebral disc replacement. Polymers such as Poly lactic acid (PLA), Polyglycolide (PGA), poly(ϵ -caprolactone) (PCL), Poly (2-hydroxy-ethyl-methacrylate) (PHEMA) are all biodegradable polymers. Biodegradable implants reduces effect against stress, eliminate the follow up that may be required to remove metal implant and allow post operative diagnostic imaging to present metal artifacts [10]. PLA, PGA, PCL are widely used. PLA clamps are used for foot surgery fixation of the gaps. PLA arrows and plugs are also used to repair damage to knee

joint and Shoulder dislocation. Chitosan, PHEMA, polyethylene glycol (PEG) and hyaluronic acid are some of the most suitable hydrogels used widely. Polymers of these types are mainly used in the repair of the cartilage, ligaments, tendons and the discs. PLA, PCL and poly hydroxybutyrate (PHB) are preferred for the bone tissue engineering purpose. Biodegradable Complex scaffold with the biological activity offer unique advantage in tissue engineering. Silicate Bio-ceramics, Biphasic Calcium Phosphate (BCP), Bio active Glass and Glass-Ceramics, Calcium Phosphates are used widely for bone tissue engineering.

40.3 Titanium Alloys as Smart Bio-materials for Bone Implants

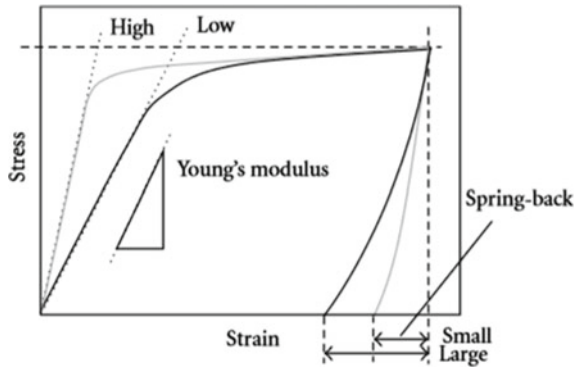
Titanium alloys are most commonly used as bio-materials because of their better mechanical properties such as as high strength, low density, resistance to corrosion, and bio-compatibility behaviour. Different Titanium alloys and various surface modification techniques to achieve bio-compatibility, higher wear and corrosion resistance was discussed in detail [11–13]. Titanium alloys provides high strength and comparatively low Young's modulus. The titanium materials are classified on a basis of structure at equilibrium state such as alloys of α , $\alpha + \beta$ and β structure. β structure alloys are most commonly used, due to their high bio-compatibility and lowest Young's modulus [14, 15]. This make alloys close to that of human bone and reduces stress shielding effect. Ti-6Al-4V mostly used for construction of implant devices. But due to high Young's modulus i.e. 108 GPa and released of aluminium ions from implant and toxic nature of vanadium causes serious health problems. In orthopedic applications, implant materials should have high strength and low Young's modulus. Hence, low Young's modulus titanium alloys can be anticipated in practical applications as a implant material. Other properties such as small spring back, is essential for maintaining the bending shape of the implant in the body, and simultaneously low yielding stress and high ultimate strength. Schematic explanation of relationship between Young's modulus and spring back shown in Fig. 40.1.

Practical methods to improve the static and dynamic strength along with low Young's modulus for β -type titanium alloys was discussed [16]. Recent developed Ti-based bio materials their properties and application demonstrate the latest advances in Ti-based materials [17]. Following are the smart Ti-based alloys that are developed over recent year can satisfy to be use in actual applications.

40.3.1 *Smart Ti-Zr-Mo Alloys*

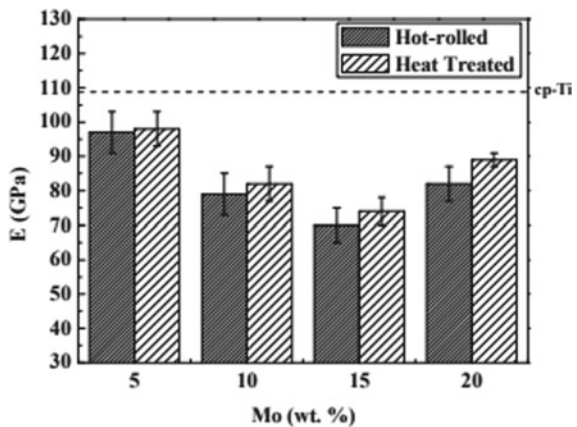
This alloy has low Young's modulus of <70GPa. The tensile strength of is >700 MPa. It was found that tensile strength increases in this alloy after cold rolling. In an

Fig. 40.1 Schematic explanation of relationship between Young's modulus and spring back [16]



Ti-30Zr-Cr and Ti-30Zr-Cr-Mo alloys elongation decreases with increasing Mo content. Elongation of the Ti-30Zr-Cr alloys was found to be <10% and further elongation of the Ti-30Zr-Cr-Mo alloys was found much larger than that of Ti-30Zr-Cr alloys. Therefore, Mo is considered an important element to improve the elongation of Ti-Zr alloy series. The crystal structure and micro structure are sensitive to the concentration of molybdenum and shows β phase the in this alloys with addition of 5 wt% and 10 wt% molybdenum. The Ti-15Mo-15Zr provides best results, making it an excellent material for analytical and biomedical applications. Vickers micro hardness for Ti-15Zr-Mo alloy shown in Fig. 40.2 which proves Mo content plays an effective role in this alloy series [18]. It was proved experimentally that adding Mo into Zr improved its corrosion resistance which effects in increasing the thermodynamic stability and passivity of zirconium [19]. During cold rolling process a deformation- induced phase transformation was seen in this alloy series. In this alloy series Ti-30Zr-3Cr-3Mo (3Cr3Mo) exhibits excellent tensile properties. The transmission electron microscope and X-ray diffraction technique of phase constitution alloys is greatly depend on Mo content. Mo content effect on shape

Fig. 40.2 Vickers micro hardness for Ti-15Zr-Mo alloy [18]



memory recovery ratio, η first increases and then decreases with the increasing of Mo content was experimentally proved [20]. Laser manufacturing methods proved effective for manufacture Ti–Zr–Mo implants and it can eliminate certain drawback [21]. Moreover Young’s modulus and hardness of Ti–8Mo–19Zr alloys is low and elastic modulus was found to be 78 GPa which is close to that of bone, thus it is efficient to use for implant applications.

40.3.2 Smart Ti-29Nb-13Ta-4.6Zr (TNTZ) Alloy

The strength of TNTZ alloy can increase by adding alloying element such as Fe, Si and O [22]. It was found strength increases by 20% and elastic modulus decreases by 20% was achieved in TNTZ-Fe-Si-O alloys when compared with Ti-6Al-4V alloy. The Stress–strain curves with addition of alloying element was shown in Fig. 40.3a. It was also seen that yield strength and ultimate strength doubles by addition of 0.7 wt% of oxygen. Although Fe and Si provides additional strengthening, TNTZ alloy with 0.7 wt% of oxygen alloy shows better mechanical properties and suitable for load-bearing orthopaedics implants manufacturing. Moreover this alloying element provides good effect on the modulus of elasticity which is maintained at 75GPa approx, yield strength values is 1000 MPa, and ductility [23]. The appearance of TNTZ-(O) films has highly depend on oxygen addition [24]. With an addition oxygen the mechanical properties and grain refinement of TNTZ-(O) film increases. Moreover, hardness increase of grain refinement and compressive stress increases. Deposition of super elastic thin film under a appropriate quantity of oxygen was recommended and leads to improve mechanical properties. It was proved that oxygen added β -type Ti-29Nb-13Ta-4.6Zr alloy to increase strength, while keeping Young’s modulus low. It was found that single β phase structure gives the excellent super elastic behavior with pseudo elastic strain ratio (S) of 20% in TNTZ alloys [25]. The super elasticity decreases as the micro structure consist of α precipitates was assign to

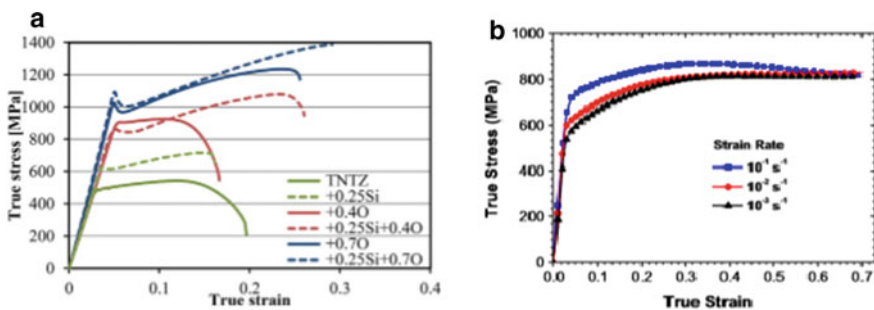


Fig. 40.3 a Stress-strain curves with alloy addition of alloying element [22], b True stress-strain curves of TNTZ [27]

a higher stability of β phase due to the mechanical and chemical stabilization. Generally, with an increase in the oxygen content, an alloy's tensile strength increases, but its tensile elongation failure decreases. In order to prove this a series of TNTZ-(0.1, 0.3, and 0.7 mass pct) O alloy samples was prepared and solution treated. This samples are named as 0.1ST, 0.3ST, and 0.7ST [26]. It was observed that because of higher work-hardening rate and higher resistance to local stress concentration, 0.1ST and 0.7ST elongation to failure was larger and increased monotonically, while their elongation to failure decreased in 0.3ST. Hence, it is recommended to use TNTZ alloy with 0.3ST for better mechanical properties. The TNTZ alloy generally shows high strain-rate reactivity which results to increase the yield strength with an increase in strain rate shown in Fig. 40.3b. The yield strength increases as strain rate increases at 10^{-3} , 10^{-2} , 10^{-1} s^{-1} , respectively which is shown in fig [27]. It was also observed that with increase of impact velocity, the exothermic chemical reaction was highly increase in TNTZ alloys.

40.3.3 Smart Ti-Nb Alloys

Ti-8.34Nb alloys, with water quenching exhibit shape memory effect. This is due to the reorientation of existing martensites. Stress-induced martensitic transformation during compression was seen in Ti-25.57Nb alloys [28]. From an transmission X-ray diffraction technique it was observed that initial β -phase transforms into martensitic phase with deformation. Furthermore, with increase in compressive strain, super elasticity becomes imperfect. It was also observed that water quenching of Ti-Nb shows lower Young's modulus seen from Fig. 40.4a. Super elasticity strain recovery rate with an addition of alloying element such as Ta, Si, Fe, Zr, Mo and Sn increases in Ti-22Nb alloy. Among alloying element, the Ti-22Nb-Fe alloy shows the highest strain recovery rate up to 70% [29]. The elastic modulus of Ti16Nb50SH and Ti16Nb70SH alloys is found to be 35 and 15GPa. Compressive and transverse fracture strength is found to be 300–100 MPa and 264–97 for both the alloys. Higher the amounts of

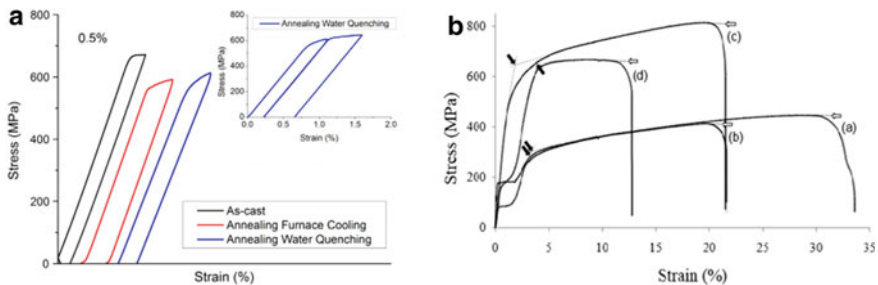


Fig. 40.4 **a** Stress–Strain curve of water quench TiNi alloy [28], **b** Stress–strain curves of Ti–24Nb (a), Ti–26Nb (b), Ti–24Nb–0.5O (c), and Ti–24Nb–0.5 N (d) alloys at room temperature [31]

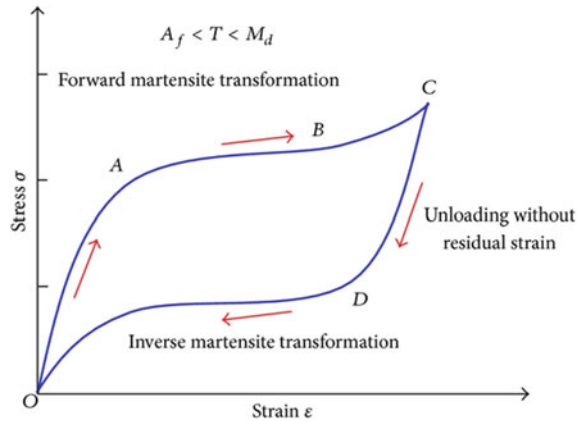
the NH_4HCO_3 as space holder causes mechanical properties more close to cortical bone [30]. Therefore, the danger of the stress shielding effect was also reduced. It was found that the Ti16Nb50SH and Ti16Nb70SH alloy caused the formation of 23.38%, 41.87%, 60.79% porosity addition of the 30%, 50%, 70% space holder.

It is possible that the properties such as porosity size ($>100 \mu\text{m}$) and porosity ratio (40%) of the Ti16Nb50SH and Ti16Nb70SH alloys comfort for new cell of bone development. The density of the produced Ti16Nb70SH alloy which is 1.91 g/cm^3 was close to density of cortical bone i.e. 1.85 g/cm^3 . Thus, it was concluded that Ti16Nb50SH and Ti16Nb70SH alloys may meet the requirements for implant manufacture in future. Elastic limit value and young's modulus values of Ti-24Nb-0.5O and Ti-24Nb-0.5N is found to be 665 MPa and 50GPa. Tensile test result shows high mechanical strength, low modulus and magnificent ductility in both the alloys [31]. It was also notice that elastic modulus ratio for Ti-24Nb-0.5O was 0.012 which was much higher than Ti-6Al-4V alloy i.e. 0.007. With an addition of O and N the mechanical properties improved which is shown in Fig. 40.4b. Some properties of the Ti-24Nb-0.5O alloys are based on O content in the medium, which does not completely impede the SIM transformation, which mean that this transformation can be reversed when the tensile strength of the curve is reached [32]. The elastic deformation in both alloys of the α'' martensite due to the initial structure in the β -phase is mainly carried out by the parameter $b_{\alpha''}$. It is recommended to be used super elastic Ti-24Nb-0.5N and Ti-24Nb-0.5O as implants or prostheses in a compare with Ti-6Al-4V alloy.

40.3.4 Smart NiTi Alloys

Shape memory effect is an capability of materials to deform in cold and get better its unique shape when heated. NiTi alloys are used widely as shape memory materials for biomedical application. The density of NiTi alloys is 6.45 g/cm^3 . NiTi shows good elastic modulus 75–83 GPa. Yield strength is found to be 195–690 MPa and poisson's ratio is 0.33. The stress-strain curve of TiNi alloy is shown in Fig. 40.5 which shows this alloys can recover it's shape at an instant without producing strain. But due to release of Ni ion from the surface of NiTi implant results in wear debris above a certain limit, furthermore causes some allergic reaction and bio-compatibility problems. It has been found that NiTi alloys exhibit different oxidation characteristics at temperature below $500 \text{ }^\circ\text{C}$ Ni-free region for oxidation temperature at 500 and $600 \text{ }^\circ\text{C}$ are found in oxide layer [33]. Oxidation of $500 \text{ }^\circ\text{C}$ creates a thin nickel-free oxide protective layer containing a relative small amount of Ni at the air/oxide interface, which indicates the good bio-compatibility for a NiTi implant. Furthermore thermal treatment of NiTi alloys at $3 \times 10^2 \text{ mbar}$ at 400°C for 2 h 30 min results in stoichiometric TiO_2 formation with a small Ni content [34]. Thermal treatment along with a bath in boiling water for 1 h, reduces 100% of release of Ni after 24 h of dip. Although thermal treatment reduces allergic reaction and bio-compatibility

Fig. 40.5 Stress-strain curve of TiNi alloy



at greater extent but also provides good corrosion resistance and improves toxicity of NiTi alloys. With an addition of Cr to $\text{Ti}_{50}\text{Ni}_{50}$ shape memory alloy (SMA), martensite transformation temperature decreases which make it effective for biomedical applications. It was experimentally proved that surface hardness improved by manufacturing $\text{Ti}_{50}\text{Ni}_{50}$ implant using Electron Beam Machining, thus retaining its good shape recovery ability [35]. A highly porous $\text{Ti}_{49.5}\text{Ni}_{50.5}$ shows better mechanical properties for implant [36]. The elastic modulus is found to be 0.95GPa and super elasticity is found to be 5.9% after heating. The stress strain curves changes at 7 MPa and shows 8% elongation with stress-induced $\text{B}_2\text{-B}_{19}'$ transformation. TiNi alloys with Ta coatings effectively increase corrosion resistance, while DLC coatings improves the mechanical properties and blood compatibility [37].

40.4 Smart Bio Ceramics for Bone Tissue Engineering

These intelligent bio materials can transmit and control stem cells to improve tissue regeneration provide control space and suitable time for the release of drugs and biologically active substances and to regulate bio films and infections in wound control zones. The development of ceramics better controls the process of bone resorption and replacement. It was found that the BCP ratio at the ectopic site can affect the rate of bone formation and in order to achieve bone formation, it is necessary to achieve an optimal balance between a more stable and more soluble phase [38]. More recently mesenchymal stem have been cultured by BCP for a period of time to promote bone formation as a layer of tissue in the implant prior to implantation. BCP ceramics have been demonstrated to be bio compatible biological active osteoconductive safe and predictable capable of delivering and inducing stem cell differentiation. In terms of cost, effectiveness, unlimited supply and lack of disease transmission these traits can replace autograft, allografts and other implants. BCP

is a versatile matrix simple in chemistry, size and shape allowing developing strategies for bone formation. Bio mimetic composite scaffolds of collagen and biphasic calcium phosphate nanoparticles (BCP NPs) was developed with a controlled release of dexamethasone (DEX) and the control pore structure. The excellent performance of this scaffolds proved to be useful for bone tissue engineering. The DEX BCP NPs were distributed homogeneously on the walls of the scaffolds, thus improving the mechanical property and hardness of the scaffolds. The DEX BCP NPs scaffolds with different DEX loading amount had good biocompatibility and restoring osteogenic differentiation of hMSCs and promote new bone tissue regeneration in vitro culture and vivo implantation. The DEX BCP NPs composite scaffold with the highest DEX loading amount proved to be use for bone tissue engineering [39].

Micro macro porous biphasic CaP dissolves in the body creating new bones when Ca and P ions are released into the biological environment [40]. Based on the concept of optimal balance between the most stable HA phase and soluble TCP. (MBCP⁺™) shows high porosity of 73%, contain micro porous off less than 100 μm and micro pore off more than 10 μm. The crystal size of MBCP⁺™ is from 0.5 to 1 μm and of specific area was around 6 m²/g. MBCP⁺™ shows higher colonization than bone cells which is suitable for tissue engineering matrix. The HA/TCP, 20/80 ratio is also more effective in combination with complete cultivation and expansion of bone marrow or stem cells before transplantation. Advanced techniques for tissue engineering include strong matrix effects on other appropriate surgical techniques. New absorbent porous bio active silicon composition based on calcium phosphate able to absorb large amount of serum protein and stimulate rapid bone formation [41]. The highly porous silica calcium phosphate composition increases cell colonies and bone formation inside the graft. The effect of bone conduction and absorption capacity of SCPC are better than bio active glasses. Crystallization of amorphous silicon in L-quartz significantly inhibits the absorption of serum proteins but the conversation of L-quartz into a crystalline solid solution significantly increases protein absorption. Pyro- and ti-calcium phosphates are converted to β-rhenanite during thermal treatment significantly increased protein absorption.

Bone defects grafted with SCPC enriched silica were detected as new bones and contained minimal graft residue. Thermal treatment results for iron substitution caused by SCPC and solid solution formation at remarkable low temperature. SCPC contains NaCaPO₄ which increases bone regeneration and improves the absorption of the material than Ca₂P₂O₇. The excellent biological activity and high porosity of SCPC show that this material can be used as a cell and drug delivery agent. In addition the material can be e applied to metal implants to improve fixation of the implant that can be mixed with polymers to increase biological activity. Highly effective bio ceramics that combine bone inducing that is Silicon and bio active that is wallastonite elements using additive manufacturing with selective laser melting shows better Mechanical properties [42]. The diameter of circular cross is about 400 μm and porosity level of 35%. The density is around 1.4 g/cm³ compressive strength is 110 MPa and modulus of elasticity is 2.9 GPa, which is suitable for bone tissue engineering. Compressive strength is decreased after two weeks of impression in tris buffer it decreased slightly by 90 MPa. Pore size increase biological activity

and compressive strength shows potential to use Silicon Wallastonite scaffolds manufacture by SLM process in bone repair application. Wallastonite and hydroxyapatite, and combination of wallastonite-hydroxyapatite composite group developed more blood vessels after 12 weeks of surgery. The wallastonite-hydroxyapatite composite biomaterial enhance the formation and growth of new bone in the defect area and it provides effective results [43].

40.5 Conclusion

Most of problems in orthopedics device have not fundamentally changed. However, innovation devices are developed using new materials, so the choice of solution is greatly expanded. Ti-6Al-4V alloys widely used in orthopedics application. Certain drawback Ti-6Al-4V alloys i.e. high Young's modulus, release of aluminium ions from implant and toxic nature of vanadium causes serious health problems. Hence development of smart titanium alloys is essential. The recent developed titanium alloy describe in this paper shows good mechanical properties close to bone, corrosion resistance and bio-compatibility. Hence this smart alloys proves effective to be used in orthopedics application. Moreover this smart alloys can successfully eliminates drawback of Ti-6Al-4V alloys and shows dual properties. The structural control of macro, micro and nano calcium phosphate and their combination with cells and polymeric material is likely to lead a significant development in bone tissue engineering. Newly, developed Silicon and wallastonite and wallastonite-hydroxyapatite provides effective results for bone tissue engineering. Recent developed smart bio-materials have tremendous potential and promise to significantly improves the efficiency of orthopedics device and tissue engineering. The smart bio-materials discussed in this paper is beneficial for the future development of biomedical devices and their clinical applications thus improving standard of patient life and advancement in biomedical sector.

References

1. Parida, P., Behera, A., Mishra, S.C.: Classification of bio materials used in medicine. *Int. J. Adv. Appl. Sci. (IAAS)* **1**(3), 31–35 (2012)
2. Ratner, B.D., Hoffman, A.S., Schoen, F.J., Lemons, J.E.: *Bio materials Science an Introduction to Materials in Medicine*, 3rd edn. Academic Press, Elsevier (2013)
3. Anderson, D.G., Burdick, J.A., Langer, R.: Smart bio materials. *Science* **305**, 1923–1924 (2004)
4. Nag, S., Banerjee, R.: Fundamentals of medical implant materials. *Mater. Med. Devices, ASM Handbook* **23**, 7–17 (2012)
5. Griffith1, L.G., Naughton, G.: Tissue Engineering—Current Challenges and Expanding Opportunities, *Science*, vol. 295, 1009–1014 (2002)
6. Poitout, D.G.: Biomaterials used in orthopaedics. In: *Biomechanics and Biomaterials in Orthopedics*, pp. 13–19. Springer, Berlin (2016)

7. Patil, N., Goodman, S.B.: The use of porous tantalum for reconstructing bone loss in orthopedic surgery. *Adv. Metal. Biomater.* **3**, 223–243 (2015)
8. Yamamuro, T.: Bioceramics. In: *Biomechanics and Biomaterials in Orthopedics*, pp. 21–32. Springer, Berlin (2016)
9. Colas, A., Curtis, J.: Silicone biomaterial: history and chemistry. In: *An Introduction to Materials in Medicine*, pp. 81–86 (2004)
10. Navarro, M., Michiardi, A., Castano, O., Planell, J.A.: Biomaterials in orthopedics. *J. R. Soc. Interface* **5**, 1137–1158 (2008)
11. Geetha, M., Singh, A.K., Asokamani, R., Gogia, A.K.: Ti based biomaterials, the ultimate choice for orthopaedics implants—a review. *Prog. Mater. Sci.* **54**, 397–425 (2009)
12. Kaur, M., Singh, K.: Review on titanium and titanium based alloys as bio materials for orthopaedics applications. *Mater. Sci. Eng. C* 1–19 (2019)
13. Findik, F.: Titanium based biomaterials. *Curr. Trend Biomed. Eng. Biosci.* **7**(3), 2–3 (2017)
14. Qazi, J.I., Rack, H.J.: Metastable beta titanium alloys for orthopedics applications. *Adv. Eng. Mater.* **7**(11), 993–998 (2005)
15. Taddei, E.B., Henriques, V.A.R., Silva, C.R.M., Cairo, C.A.A.: Production of new titanium alloy for orthopedics implants. *Mater. Sci. Eng., C* **24**(5), 683–687 (2004)
16. Niinomi, M., Nakai, M.: Titanium-based bio materials for preventing stress shielding between implant devices and bone. *Int. J. Bio mater.* 1–10 (2011)
17. Jakubowicz, J.: Special issue: Ti-based biomaterials: synthesis, properties and applications. *Materials* **13**, 1–5 (2020)
18. Correa, D.R.N., Kuroda, P.A.B., Grandini, C.R.: Structure, microstructure, and selected mechanical properties of Ti-Zr-Mo alloys for biomedical applications. *Adv. Mater. Res.* **922**, 75–80 (2014)
19. Zhou, F.Y., Wang, B.L., Qiu, K.J., Li, L., Lin, J.P., Li, H.F., Zheng, Y.F.: Micro structure, mechanical property, corrosion behavior, and in vitro bio compatibility of Zr–Mo alloys. *Willey Periodicals* 237–246 (2012)
20. Zhang, S., Liang, S.X., Yin, Y.X., Zheng, L.Y., Xie, H.L., Shen, Y.: Martensitic transition and shape memory effect of Ti-Zr-Mo series alloys. *Intermetallics* **88**, 55–60 (2017)
21. Laoble, C., Almedia, A., Vilar, R.: Laser-assisted development of new Ti-Mo-Zr alloy for biomedical application. *Inst. Mater. Surf. Sci. Eng.* 1–6 (2008)
22. Straskya, J., Harcubaa, P., Václavovaa, K., Horvatha, K., Landab, M., Srbac, O., Janeceka, M.: Increasing strength of a biomedical Ti-Nb-Ta-Zr alloy by alloying with Fe, Si and O. *J. Mech. Behav. Biomed. Mater.* **71**, 329–336 (2017)
23. Raducanu, D., Cojocaru, V.D., Nocivin, A., Cinca, I., Serban, N., Cojocaru, E.M.: Contributions to mechanical characteristics improvement of some biomedical TNTZ alloys by adding Fe, Si, and O: a comparative study. *Min. Met. Mater. Soc.* 1–8 (2018)
24. Achachea, S., Alhousseina, A., Guelorgeta, B., Salut, R., Françoisa, M., Sanchette, F.: Effect of oxygen addition on microstructure and mechanical properties of quaternary TNTZ superelastic thin films obtained by magnetron sputtering. *Mater. Chem. Phys.* **217**, 262–269 (2017)
25. Kalaiea, M.A., Zarei-Hanzakia, A., Ghambaria, M., Dastura, P., Málekb, J., Farghadany, E.: The effects of second phases on superelastic behavior of TNTZ bio alloy. *Mater. Sci. Eng. A* 513–520 (2017)
26. Liu, H., Niinomi, M., Nakai, M., Cong, X., Cho, K., Boehlert, C.J., Khademi, V.: Abnormal deformation behavior of oxygen-modified b-type Ti-29Nb-13Ta-4.6Zr alloys for biomedical applications. *Min. Met. Mater. Soc. ASM Int.* 139–149 (2016)
27. Guo, Z., Liu, R., Wang, C. T., He, Y., He, Y., Ma, Y., Hu, X.: Compressive mechanical properties and shock-induced reaction behavior of a Ti–29Nb–13Ta–4.6Zr alloy. *Met. Mater. Int.* 1–8 (2019)
28. Moduli, S., Guo, Y., Georarakis, K., Yokoyama, Y., Yavari, A.R.: On the mechanical properties of TiNb based alloys. *J. Alloys Compd.* **571**, 25–30 (2013)
29. Zhang, D.C., Mao, Y.F., Li, Y.L., Li, J.J., Yuan, M., Lin, J.G.: Effect of ternary alloying elements on micro structure and superelasticity of Ti–Nb alloys. *Mater. Sci. Eng., A* **559**, 706–710 (2013)

30. Yılmaz, E., Gökçe, A., Findika, F., Gülsoyc, H.Ö., İyibilgina, O.: Mechanical properties and electrochemical behavior of porous Ti-Nb biomaterials. *J. Mech. Behav. Biomed. Mater.* 1–19 (2018)
31. Ramarolahy, A., Philippe Castany, F., Prima, P.L., Péron, I., Gloriant, T.: Microstructure and mechanical behavior of superelastic Ti-24Nb-0.5O and Ti-24Nb-0.5N biomedical alloys. *J. Mech. Behav. Biomed. Mater.* **9**, 83–90 (2012)
32. Castany, P., Ramarolahy, A., Prima, F., Laheurte, P., Curfs, C., Gloriant, T.: In situ synchrotron X-ray diffraction study of the martensitic transformation in superelastic Ti-24Nb-0.5N and Ti-24Nb-0.5O alloys. *Acta Mater.* **88**, 102–111 (2015)
33. Firstov, G.S., Vitchev, R.G., Kumar, H., Blanpain, B., Van Humbeeck, J.: Surface oxidation of NiTi shape memory alloy. *Biomaterials* **23**, 4863–4871 (2002)
34. Michiardi, A., Aparicio, C., Planell, J.A., Gil, F.J.: New oxidation treatment of NiTi shape memory alloys to obtain Ni-free surface and to improve bio compatibility. *Wiley Interscience* 249–256 (2005)
35. Huang, T.-S., Hsieh, S.-F., Chen, S.-L., Lin, M.-H., Oua, S.-F., Changa, W.-T.: Surface modification of TiNi-based shape memory alloys by dry electrical discharge machining. *J. Mater. Process. Technol.* **221**, 279–284 (2015)
36. Kim, Y.: Mechanical Properties of Highly Porous Ti49.5Ni50.5. *Biomater. Intermetall.* **62**, 56–59 (2015)
37. Cai, X.L., Meng, L.C.Z.: Recent development of TiNi-based shape memory alloys. *Curr. Opin. Solid State Mater. Sci.* **9**, 296–302 (2005)
38. Lobo, S.E., Arinze, T.L.: Biphasic calcium phosphate ceramics for bone regeneration and tissue engineering application. *Materials* **3**, 815–826 (2010)
39. Chen, Y., Kawazoe, N., Chen, G.: Preparation of dexamethasone-loaded biphasic calcium phosphate nanoparticles/collagen porous composite scaffolds for bone tissue engineering. *Acta Biomater.* 1–15 (2017)
40. Daculsi, G., Miramond, T., Borget, P., Baroth, S.: Smart calcium phosphate bioceramic scaffold for bone tissue engineering. *Trans. Tech Publications*, pp. 19–23 (2013)
41. El-Ghannam, A.R.: Advanced bioceramics composites for bone tissue engineering. In: *Design Principles and Structure Bioactivity Relationship*, Wiley Interscience, pp. 490–501 (2004)
42. Kamboj, N., Marina Aghayan, C., Sara, R.-V., Rodriguez, M.A., Hussainova, I.: Novel Silicon-Wallastonite based scaffold for tissue engineering produced by selective laser melting. *Ceramic Int.* **45**, 24691–24701 (2019)
43. Ge, R., Xun, C., Yang, J., Jia, W., Li, Y.: In vivo therapeutic effect of wollastonite and hydroxyapatite on bone defect. *Biomed. Mater.* **14**, 1–13 (2019)

Chapter 41

Design and Development of Novel Multipoint Epicyclic Superfinishing Tool



Muhammad Osama, Faiz Iqbal, Dilshad Ahmad Khan, and Zafar Alam

Abstract As the field of superfinishing is progressing every day, the need for controlled and precisely finished complex industrial as well as medical components is emerging rapidly. However, the conventional finishing processes have limited capability when it comes to superfinishing. This work presents the design and development of a novel multipoint superfinishing tool. It utilizes magnetically energized hemispherical balls of polishing fluid formed at the tip of the tool to finish magnetic as well as non-magnetic materials using specially prepared magnetorheological polishing fluid. A modified epicyclic gear train mechanism is used for the design of the new tool with the shaft attached to the carrier and sun gear modified to be the non-movable integral component of the shaft with the cavity in the end for permanent magnet placement. The three planetary gears have extended shafts at both the ends with one end force-fitted to the carrier with a bearing and another end has the cavity for the placement of permanent magnets. The three planetary gears mesh with the ring gear which is directly mounted on the shaft. When the spindle/shaft rotates, the ring gear is kept stationary, and the planetary gears rotate around the common axis as well as spins on their respective axes simultaneously. This way the tool becomes multipoint and has a bigger diameter than the existing tools and can finish much larger area in the same period without affecting its ability to form the abrasive laden polishing fluid balls at the tip. Magnetic field analysis is done for the tool with the permanent magnets to simulate for the magnetic field interaction between tool and ferromagnetic workpiece. The finishing process is carried out on the 3-axis CNC

M. Osama

Department of Mechanical Engineering, Aligarh Muslim University, Aligarh, India

F. Iqbal

Institute of Integrated Micro and Nano Systems, School of Engineering, University of Edinburgh, Edinburgh, Scotland

D. A. Khan

Department of Mechanical Engineering, National Institute of Technology, Hamirpur, India

Z. Alam (✉)

Department of Mechanical Engineering, Indian Institute of Technology (Indian School of Mines), Dhanbad, Jharkhand, India

vertical milling machine for the precise control of the working gap (the gap between workpiece and tool) to control the applied finishing forces.

Keywords Magnetorheological · Epicyclic · Nanofinishing · Roughness · Magnetic · Non-magnetic

41.1 Introduction

Surface integrity can be defined as the properties of a component that are influenced by the physical and chemical effects of the machining processes. Apart from covering the interior effects of the machining processes, surface integrity also covers the outermost layers whose properties are different measurably from that of the base material [1].

The purpose of enhancing surface integrity or surface texture is to improve its functional ability during service. Better surface integrity can improve the component's load-bearing ability, endurance, fatigue strength, and frictional resistance. As each machining process generates a surface texture, the final finishing operation is the most critical in the manufacturing of precise parts. Generally, the finishing operations are employed to modify the texture if the manufacturing processes do not yield the intended surface texture suitable for the application. The finishing processes could be grinding, honing, lapping, etching, abrasive blasting, etc. However, when it comes to the precision, where surface roughness requirement is in nanometers, these conventional processes are rendered incapable. They tend to leave micro-cracks and generates unwanted residual stresses on the surface [2].

Moreover, there are two types of forces associated with the material removal process in nanofinishing [3]. The normal force which is responsible for the indentation of the abrasive particle in the workpiece, and the shear force which breaks away the surface roughness peaks. Control over the normal force is nearly impossible in conventional processes. Therefore, many advanced processes such as magnetic abrasive finishing (MAF) [4], magnetorheological finishing (MRF) [5], magnetorheological jet finishing (MRJF) [6], ball end magnetorheological finishing (BEMRF) [7], etc. have been developed in the last few decades.

Ball end magnetorheological finishing (BEMRF) is a process capable of finishing surfaces up to the order of nanometres using a smart fluid called magnetorheological polishing (MRP) fluid. Ferromagnetic and non-magnetic materials like polylactic acid (PLA) workpiece [8], copper mirrors [9, 10], aluminium, etc. can be finished using this process. MRP fluid containing abrasives and magnetizable iron particles is used as a finishing medium. The MRP fluid undergoes rheological changes under the influence of the magnetic field [11]. Due to the shape magnetic field produces at the BEMRF tool, the MRP fluid takes the shape of a hemispherical ball at the tip of the tool. The stiffness of this ball can be controlled by controlling the magnetizing current supplied in case of an electromagnet.

Many researchers have published insights into the BEMRF process. However, from the above literature archives, it is evident that the time taken to process a surface to the order of nanometers is very high. Also, the BEMRF tool tends to produce scuff or scratch marks called finishing marks around the periphery [12, 13].

Peng et al. [14] reported the main limitation of magnetorheological finishing. It is the wavy microstructure caused by plastic flow called ‘MRF’ marks which produce diffraction effects and stray light. They reported an effective post-polishing technique to remove these ‘MRF’ marks. However, post-polishing is extremely difficult on a spherical and free form surfaces, which leads to an inevitable contradiction between surface quality and the whole surface figure. Also, post finishing operations introduces multiple challenges apart from adding considerable finishing cost.

From the above literature, it can be observed that although magnetically aided abrasive finishing processes provide control over finishing forces, they still lag perfection in some aspects. In this research work, a novel magnetorheological superfinishing tool is designed and developed to cater to those drawbacks.

41.2 Design and Fabrication of Multipoint Epicyclic Superfinishing Tool

Researchers in the above literature devised and applied many kinds of finishing tool to achieve the intended surface roughness values. It includes a single point as well as multipoint tools, but they happen to have a small tip diameter. They can sweep minimal area at a time and takes an appreciable amount of time to complete a single workpiece. It would be highly expensive and time taking if it is to finish the workpieces of a bigger size such as telescopic mirrors. Also, the existing magnetorheological finishing tools tend to leave the scuff marks along their periphery. To overcome and eliminate the drawbacks mentioned in the above literature, this tool’s design is inspired by an epicyclic gear train mechanism. Designed using Solidworks software, this tool is multipoint and has a working diameter of 26 mm.

Epicyclic gear train has four necessary components, the sun gear attached with a driver/driven shaft, few planetary gears, an outer ring gear to make planetary gears revolve around the sun gear, and a carrier with a driven/driver shaft to which planetary gears are attached.

This tool is slightly modified to having only one shaft which is attached to the carrier and sun gear is modified to an integral component of the shaft having a cavity for the permanent magnet placement. There are three planetary gears in this tool. These planetary gears are designed to have extended shafts at both ends; one end is force-fitted to the bearing for the smooth operation, and the cavity is made on the other end to insert the permanent magnets as shown in Figs. 41.1 and 41.2.

The ring gear is held stationary for the rotary motion of planetary gears. Therefore, it is joined to the housing of bearing on the shaft and is anchored to the fixed part of the machine during the finishing operation. When the shaft/spindle is rotated,

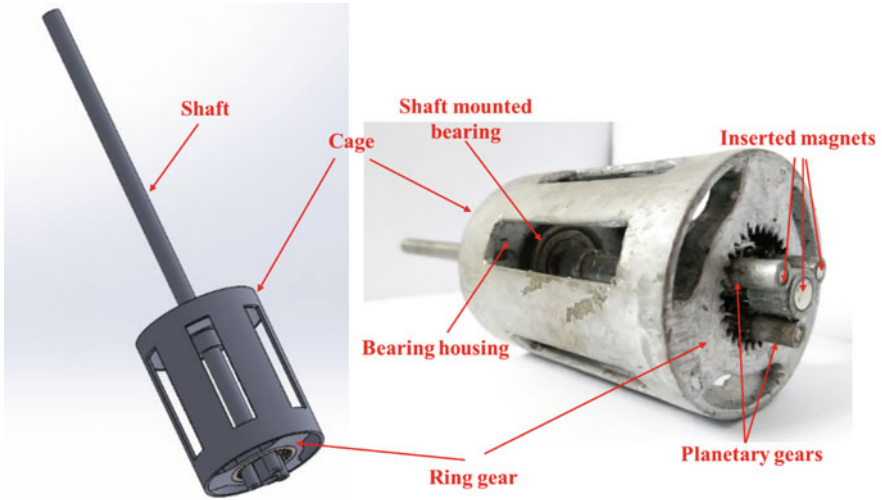


Fig. 41.1 CAD model and actual MR finishing tool



Fig. 41.2 Fabricated planetary gears

the planetary gear spins about their respective axes as well as revolves around the common axis. Due to the magnetic field produced by the permanent magnet attached to the end of each rotating gear, the MRP fluid takes the shape of hemispherical balls at each of the tips. Since these balls are flexible, they can adjust their shape according to the surface profile. Thus, forming the four small tools from spinning and giving a notion of one combined tool from the rotation. Also, the stiffness of these abrasive laden fluid balls can be controlled/changed either by increasing the

working gap (a gap between workpiece and tooltip) or by changing the permanent magnet. This helps in controlling the applied finishing forces.

The planetary gears, as shown in Fig. 41.2, are ten teethed having a unity module spur gear cut on the periphery of 12 mm. Their one end is force-fitted into the bearing of bore 3 mm and an outer diameter of 6 mm. On the other end, permanent magnets of 4 mm diameter are inserted in the 10 mm deep cavity. Material for gear has to be tough, hard, resilient and high in yield as well as fatigue strength. Therefore, these gears are turned and wire-EDM machined out of EN24 steel.

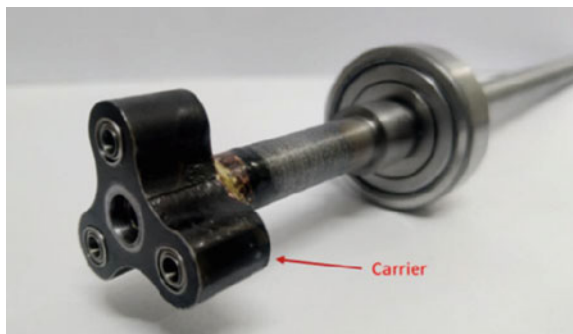
Ring gear also is a spur gear with a unity module having 30 teeth, as shown in Fig. 41.3. There are three projections on the ring gear's outer periphery, that is where it is joined to the bearing housing on the spindle, thus forming a cage. This cage is anchored to the stationary part of the machine to keep it from rotating with the spindle. The ring gear is also wire-EDM machined out of EN31 steel.

Shaft and carriers shown in Fig. 41.4 are machined from mild steel. The shaft is 150 mm long and 10 mm in diameter having a step along its length to support the

Fig. 41.3 Fabricated ring gear



Fig. 41.4 Photo showing shaft and carrier with the inserted bearings



bearing of bore 10 mm and an outer diameter of 26 mm on which the ring gear is supported through the cage.

Alternatively, the tool can be fabricated using the rapid prototyping technique also called 3D-printing. The readily available and most common type of technique which is Fused Filament Fabrication (FFF), has been used in this paper. The BEMRF tools, as available in the archived literature [15, 16], are fabricated out of certain grades of steel which is a ferromagnetic material. But this paper presents the findings of fabricating the tool out of non-magnetic materials as well.

The material chosen to print the tool is polyethylene terephthalate glycol (PETG) because of its availability and appreciable physical characteristics. The CAD model of the tool except the bearings and magnets is sliced and prepared for printing in the slicer called Cura. The 0.2 mm layer height has been considered with the infill density of 100% having a wall thickness of 1.2 mm. The nozzle temperature suitable for PETG is set to 240degC while bed temperature is fixed at 90 °C. Printing speed is 60 mm/s and supports were active for the minimum overhang angles of 45°. At these settings, the time to print the whole tool estimated by the slicer is 21 h and 17 min (Fig. 41.5).

41.3 Magnetostatic Simulation of Tool Model

To understand the interaction with the workpiece and shape of the magnetic field at the tip of the tool, a magnetostatic simulation has been carried out on Solidworks EMS (Electromagnetic Simulation) plugin version 2017. Two types of materials have been considered for the tool, one ferromagnetic material which is mild steel and another non-magnetic material namely polyethylene. The workpiece is a square of sides 60 mm with a thickness of 10 mm and a selection of materials from ferromagnetic and non-magnetic are considered. The simulation is done for four different types of materials including mild steel, copper, aluminium and a non-metallic polycarbonate. All four workpieces are tested with each of the types of tool material.

Permanent magnets are made of neodymium, and the direction of coercivity of all permanent magnets is always towards the workpiece. The whole tool model is enclosed in an air envelope to simulate for the conditions as realistic as possible.

The working gap is kept constant at 0.8 mm with MR fluid between the tooltip and the workpiece. The materials assigned and their properties given in Table 41.1 are taken from the Solidworks' EMS material directory except for the properties of MR fluid, which is taken from the literature [7, 15].

41.4 Results and Discussion

The results obtained from the magnetostatic simulation of the tool and workpiece are presented and discussed-upon in this section. The simulation has been carried out

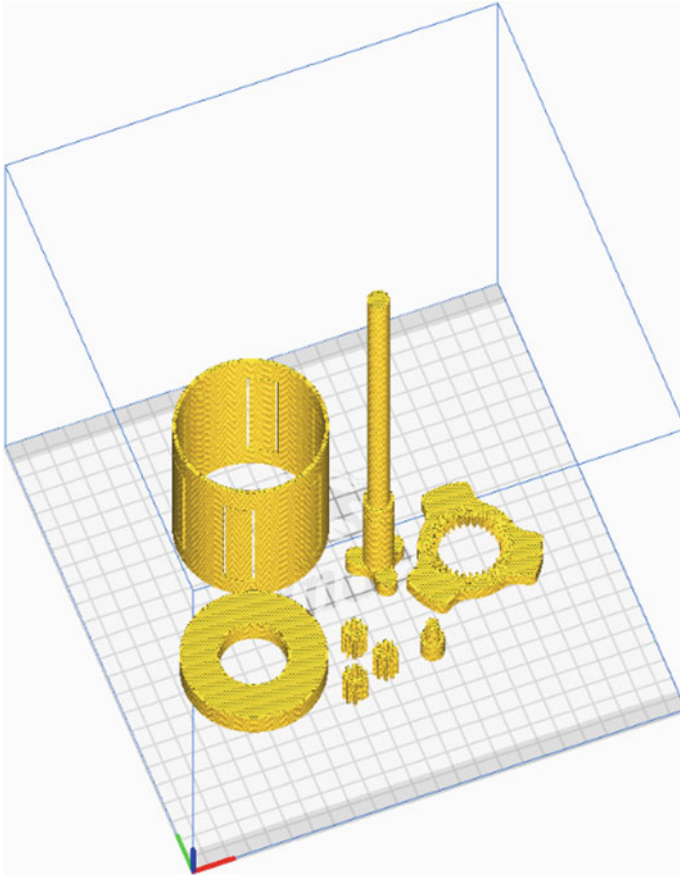


Fig. 41.5 Photo showing the preview of a sliced tool

for each of the combination of tool and workpiece material and the results obtained are presented in terms of magnetic flux density, Tesla (T).

41.4.1 Tool Material: Mild Steel

41.4.1.1 Workpiece: Ferromagnetic- Mild Steel

Using ferromagnetic workpiece of mild steel to simulate for the tool model with the MR fluid in the working gap, the side view of the tooltip components and workpiece shows the distribution of magnetic flux density (Tesla, T) in Fig. 41.6. It clearly shows the high concentration zones just beneath the tip of the magnet, and it decreases as the field pans out away from the tooltip. The highest flux density is in the centre because

Table. 41.1 Materials assigned and their magnetic properties

Material	Property	Type	Value
NdFeB Magnet (N5513)	Conductivity	Isotropic	Conductivity (Mho/m): 0
	Relative permeability	Isotropic	Relative permeability: 1.25
	Magnetization	Permanent magnetization	Coercivity (A/m): 954,929 Remanence (Tesla): 1.5
Air	Conductivity	Isotropic	Conductivity (Mho/m): 0
	Relative permeability	Isotropic	Relative permeability: 1
	Magnetization	Non-permanent magnetization	
Mild Steel	Conductivity	Isotropic	Conductivity (Mho/m): 1,100,000
	Relative permeability	Isotropic	Relative permeability: 2000
	Magnetization	Non-permanent magnetization	
Copper	Conductivity	Isotropic	Conductivity (Mho/m): 57,000,000
	Relative permeability	Isotropic	Relative permeability: 0.999991
	Magnetization	Non-permanent magnetization	
MR Fluid	Conductivity	Isotropic	
	Relative permeability	Isotropic	Relative permeability: 5
	Magnetization	Non-permanent magnetization	
Polycarbonate PC40	Conductivity	Isotropic	Conductivity (Mho/m): 1,724,137
	Relative permeability	Non-linear Isotropic	
	Magnetization	Non-permanent magnetization	
Polyethylene	Conductivity	Isotropic	Conductivity (Mho/m): 0
	Relative permeability	Isotropic	Relative Permeability: 1
	Magnetization	Non-permanent magnetization	
Aluminium	Conductivity	Isotropic	Conductivity (Mho/m): 38,200,000
	Relative permeability	Isotropic	Relative permeability: 1
	Magnetization	Non-permanent magnetization	

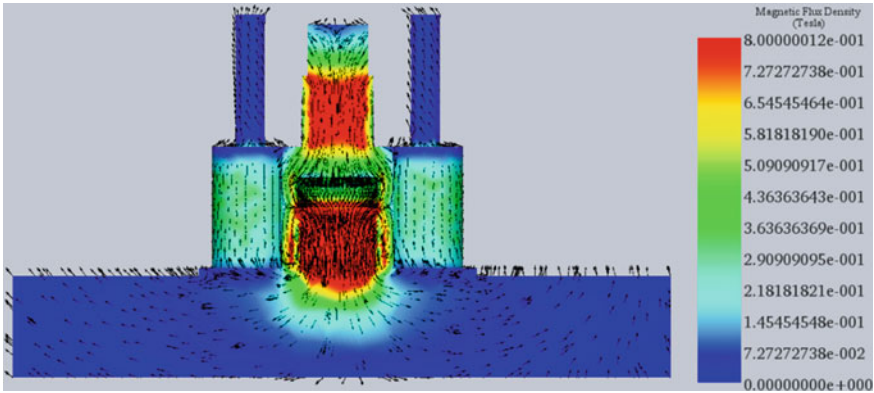


Fig. 41.6 The magnetic flux density distribution for the ferromagnetic workpiece

of the bigger size of the magnet. The result here is shown on the scale ranged from 0 to 0.8 T. Mild steel generally is finished at 0.6–0.8 T according to the data in the archived literature. Researchers have also finished the mild steel workpiece with the lesser magnitude of magnetic flux density [7, 15, 16]. However, at lower flux densities, the spindle rotation speed also needs to be lesser so that the MR fluid at the tip does not fly away because of the centrifugal force [16]. Therefore, the density of the magnetic flux considered here is well enough that the MRP fluid can form the hemispherical balls at the tip of the tool and can perform finishing operation even at higher spindle speeds.

Figure 41.7 shows the magnetic flux density on top of the mild steel workpiece. It

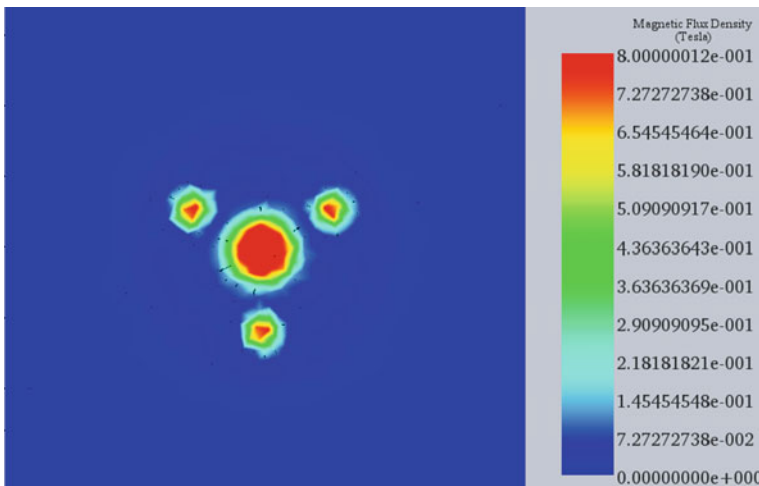


Fig. 41.7 Top view of the mild steel workpiece showing the magnetic flux density concentration zones

clearly shows the concentrations regions just beneath the tooltips. The hemispherical balls will form at the regions beneath the tooltip, as shown in Fig. 41.7, and the tool will rotate the stiffened MR fluid hemispherical balls to carry out the finishing operation of a ferromagnetic workpiece.

41.4.1.2 Workpiece: Non-magnetic-Copper

Figures 41.8 and 41.9 shows the magnetic flux distribution for the non-magnetic

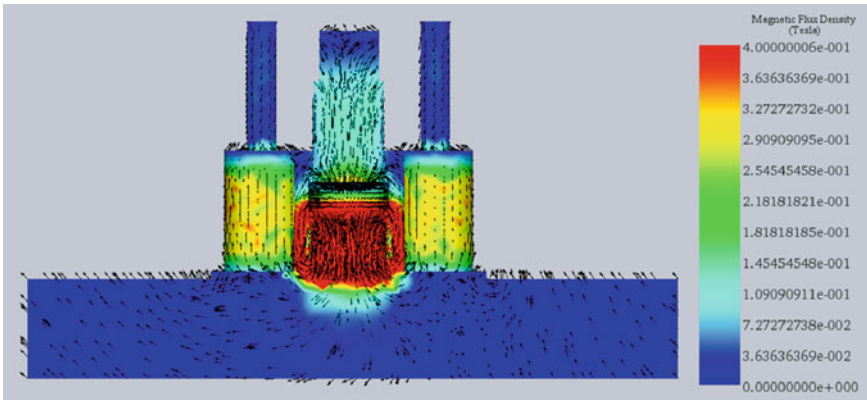


Fig. 41.8 The magnetic flux density distribution for the non-ferromagnetic copper workpiece

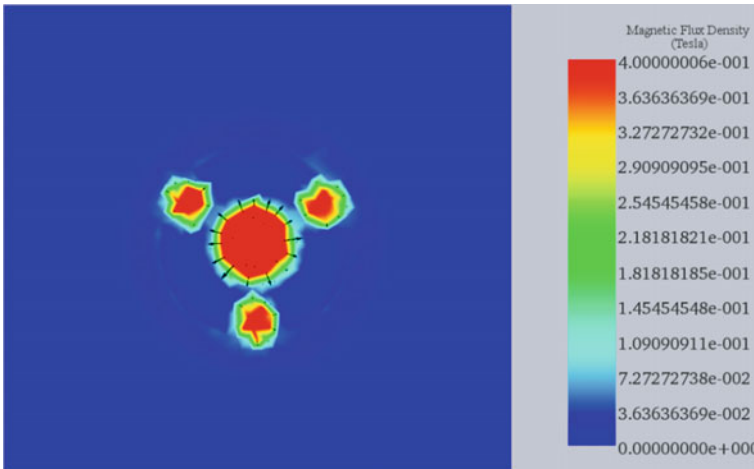


Fig. 41.9 Top view of the copper workpiece showing the magnetic flux density concentration zones

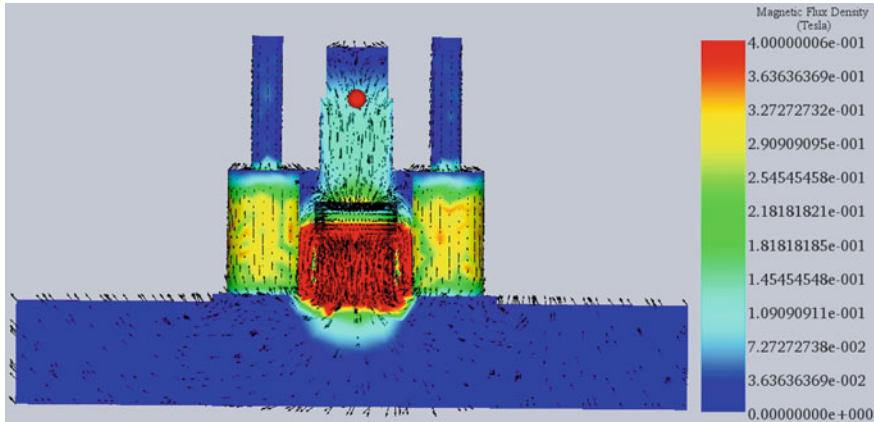


Fig. 41.10 The magnetic flux density distribution for the non-ferromagnetic aluminium workpiece

copper workpiece. The simulation results indicate the similar behaviour and interaction of the magnetic field as with the ferromagnetic workpiece. The magnetic field distribution is such that MRP fluid will form hemispherical balls and work effectively with the non-magnetic workpiece as well [2]. The scale considered for the copper workpiece ranges from 0 to 0.4 T. Because copper is a soft material as compared to the mild steel, hence it requires a lesser magnetic flux density to get finished [7, 15].

41.4.1.3 Workpiece: Non-magnetic-Aluminium

Similar to the case of a copper workpiece, the behaviour of magnetic flux density is the same for the aluminium workpiece as shown in Figs. 41.10 and 41.11. The red regions show the maximum concentration forming beneath each of the tips' centre. The range of the scale considered is similar to the copper which is 0–0.4 T because the aluminium and copper have a similar indentation hardness. In fact, aluminium exhibits a lesser indentation hardness than copper [17]. Therefore, the magnetic flux density obtained from the results of the simulation is sufficient to easily form hemispherical fluid balls and finish the workpiece.

41.4.1.4 Workpiece: Non-magnetic and Non-metallic-Polycarbonate

Figures 41.12 and 41.13 shows the distribution of magnetic flux density for the non-magnetic and non-metallic polycarbonate workpiece. The highest concentration although is achieved beneath the tips, however, the area of highest concentration zone seems smaller than the ones obtained for copper and aluminium.

Moreover, unlike non-magnetic metallic workpieces, the unusually high concentration is being achieved in the centre component of the tool as shown in Fig. 41.12.

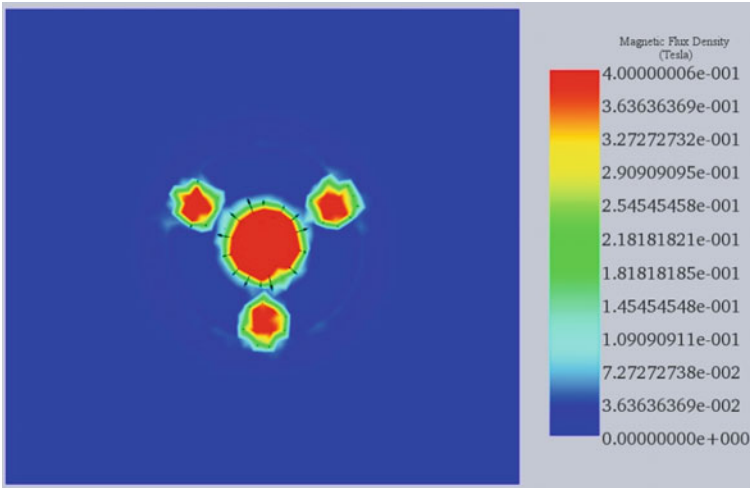


Fig. 41.11 Top view of the aluminium workpiece showing the magnetic flux density concentration zones

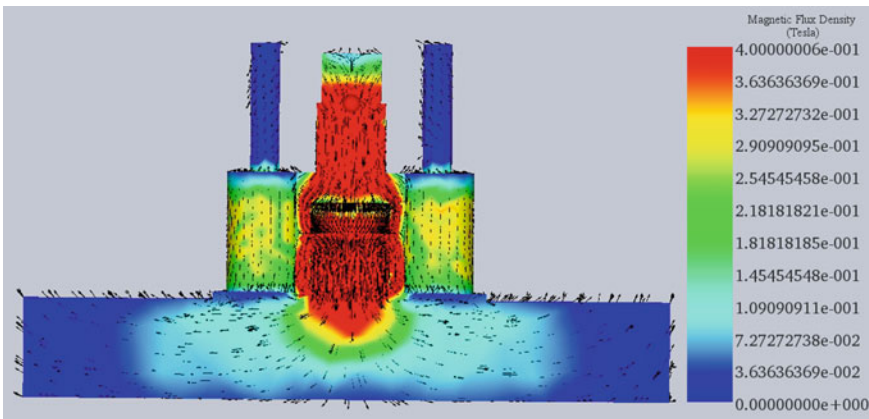


Fig. 41.12 The magnetic flux density distribution for the non-ferromagnetic polycarbonate workpiece

The magnetic fields seem to be more penetrant in the workpiece and distributed like a flare over a large area of the workpiece. The flux density scale for the polycarbonate workpiece also is set between the range of 0–0.4 T because polycarbonate is a softer material as compared to the metals and hence would require a lesser normal force to remove the material. Nevertheless, the simulation shows enough flux density distribution at the workpiece to carry-out the finishing process.

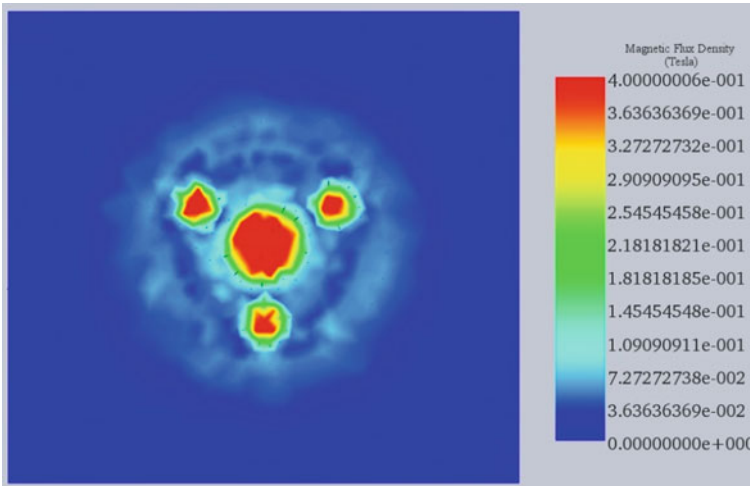


Fig. 41.13 Top view of the polycarbonate workpiece showing the magnetic flux density concentration zones

41.4.2 Tool Material: Polyethylene

The material for the tool is a polyethylene which is 3d-printable plastic available as PETG. Although, it is slightly different chemically, however, they are same for the permanent magnets. Apart from the neodymium magnets and readymade steel bearings, the rest of the component of the tool is plastic. The simulation results with each type of the workpiece material are presented in the following sub-sections.

41.4.2.1 Workpiece: Ferromagnetic-Mild Steel

The behaviour of the magnetic field for the non-metallic tool and ferromagnetic workpiece is shown in Figs. 41.14 and 41.15. In Fig. 41.14, the magnetic flux density is more directed towards the mild steel workpiece and seems to be more penetrant going from the top towards the bottom because the workpiece is ferromagnetic and is aiding the field line path.

Unlike the mild steel tool, the flux density in the plastic tool is close to zero. Due to the fact that the tool is non-magnetic, the flux density is higher and distinguished at the workpiece as shown in Fig. 41.15. The simulation result shows that the magnetic flux distribution is even more favourable for the required finishing conditions than ones with the mild steel tool.

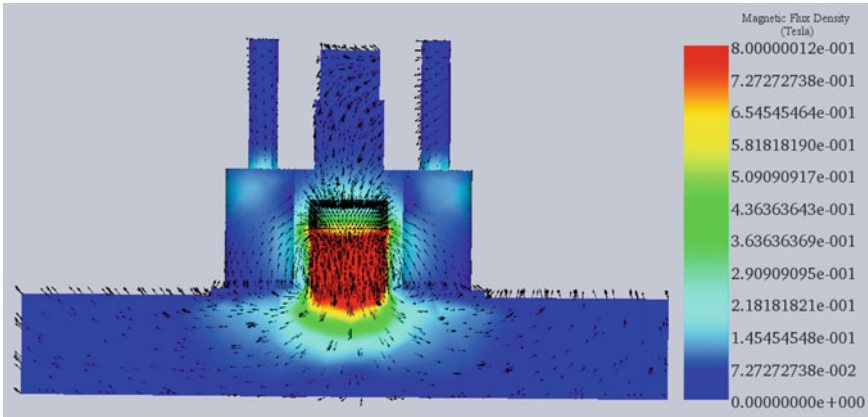


Fig. 41.14 The magnetic flux density distribution for the ferromagnetic workpiece

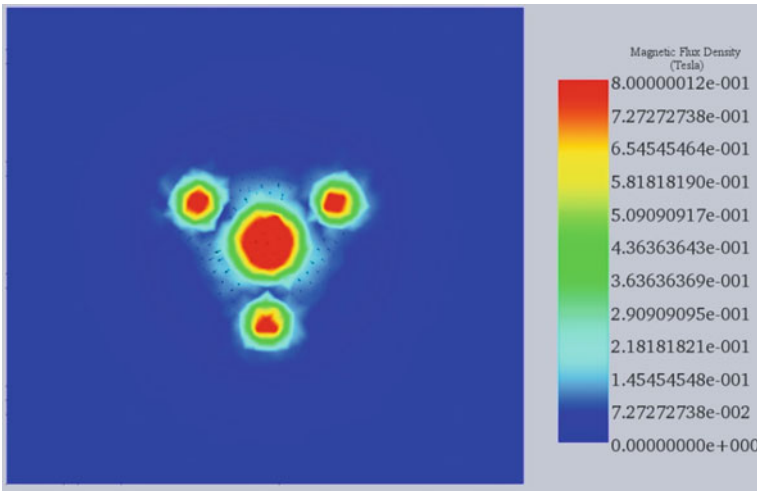


Fig. 41.15 Top view of the mild steel workpiece showing the magnetic flux density concentration zones

41.4.2.2 Workpiece: Non-magnetic-Copper

Now for the condition where the tool and the workpiece are non-magnetic, the simulation result in Figs. 41.16 and 41.17 shows that the flux density is higher in tool components as compared to the condition of plastic tool and mild steel workpiece. In the above condition, the workpiece is ferromagnetic and hence the magnetic flux density is more inside the workpiece than at the surface.

Here, in case of copper, the flux density is more distributed at the work surface. This fact is rather presenting a more favourable condition for the formation of strong

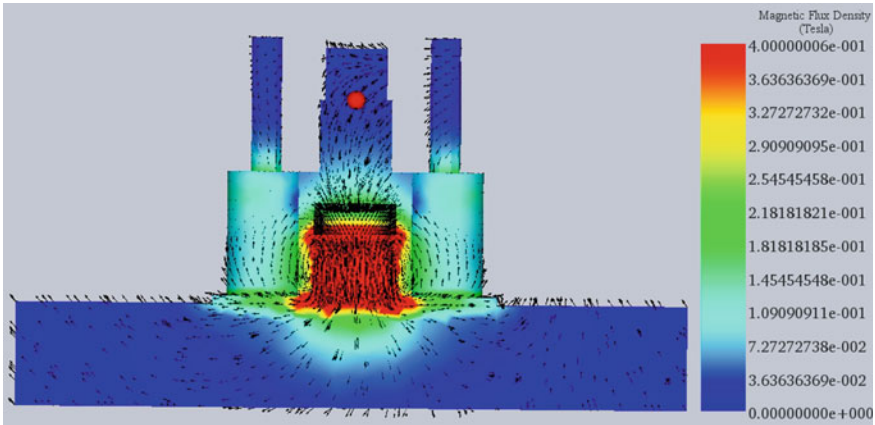


Fig. 41.16 The magnetic flux density distribution for the non-ferromagnetic copper workpiece

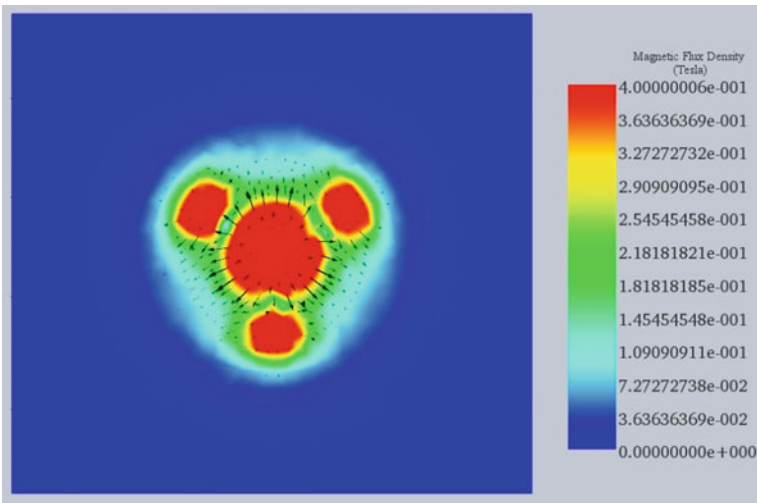


Fig. 41.17 Top view of the copper workpiece showing the magnetic flux density concentration zones

and stable hemispherical balls at the tool tip. Also shown in Fig. 41.17, most of the region beneath the tool is getting the maximum value of density distribution. And hence, the tool made out of non-magnetic material is equally capable to carry-out the magnetorheological finishing of magnetic as well as non-magnetic workpieces.

41.4.2.3 Workpiece: Non-magnetic-Aluminium

As shown in Figs. 41.18 and 41.19, the magnetic flux density distribution for aluminium workpiece is identical to the case of copper. The flux density, here as well, is superficial and distributed on the surface than being inside the workpiece. Moreover, the area beneath the tooltips is mostly shown in red colour indicating that the region is mostly getting the highest value of flux density. The results for this tool and work combination supposedly will give better results than the ones with the mild

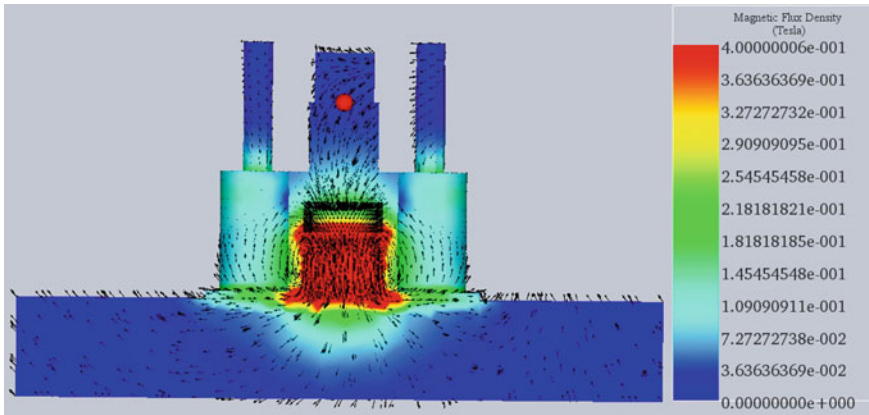


Fig. 41.18 The magnetic flux density distribution for the non-ferromagnetic aluminium workpiece

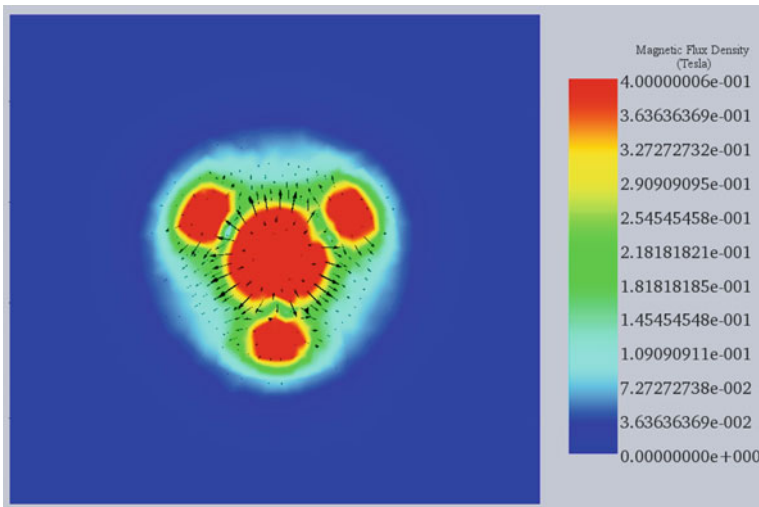


Fig. 41.19 Top view of the aluminium workpiece showing the magnetic flux density concentration zones

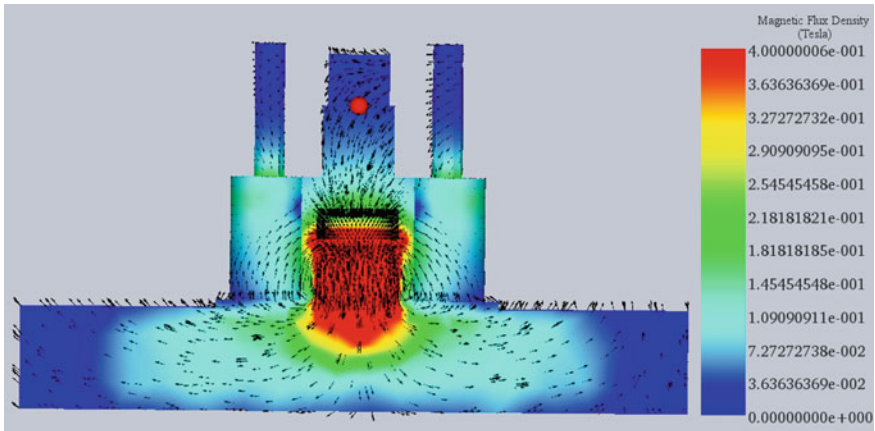


Fig. 41.20 The magnetic flux density distribution for the non-ferromagnetic polycarbonate workpiece

steel workpiece. Hence, the conditions in this scenario will also allow the formation of hemispherical balls of MRP fluid and will perform finishing.

41.4.2.4 Workpiece: Non-magnetic and Non-metallic-Polycarbonate

The non-magnetic plastic tool and non-metallic and non-magnetic polycarbonate workpiece seem to be getting the most favourable conditions for finishing. Unlike the mild steel tool where the flux density for polycarbonate workpiece has been seen going up the tool and flaring at the work surface, the flux density distribution in the tool components is very minimal. As a result of which, the flux density is very penetrant in the polycarbonate workpiece like a ferromagnetic workpiece as well as widely distributed at the surface, as shown in Figs. 41.20 and 41.21.

The magnetic flux density distribution at the top of the workpiece is visible in Fig. 41.21. It clearly shows the maximum regions in red colour and almost the whole area beneath the tooltips is getting the flux density of 0.4 T. This condition, in practical, will make the most ideal size of MRP fluid hemispherical balls at the tips, stiff enough to carry-out the finishing operation and able to sweep the maximum area intended according to the tool designed in this work.

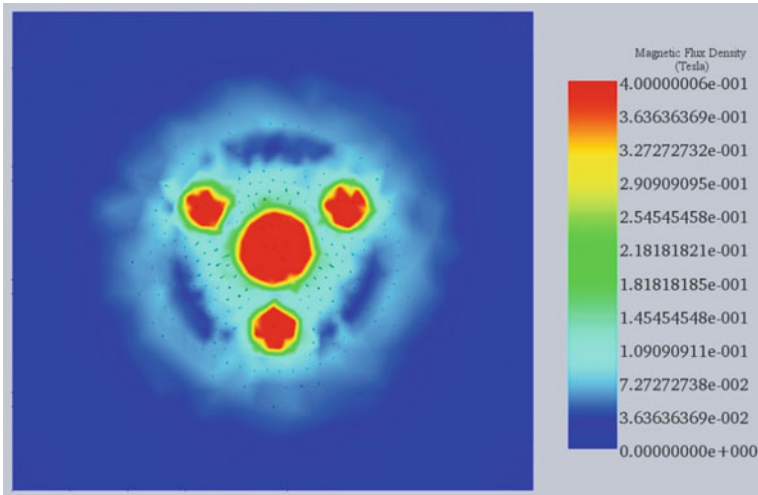


Fig. 41.21 Top view of the polycarbonate workpiece showing the magnetic flux density concentration zones

41.5 Conclusion

The following conclusions can be drawn from this study:

- A novel superfinishing tool is designed and developed here which can be used to finish magnetic as well as non-magnetic material using MRP fluid.
- A modified epicyclic gear train mechanism is used for the design of the new tool with the shaft attached to the carrier and sun gear modified to be the non-movable integral component of the shaft with the cavity in the end for permanent magnet placement.
- This tool design helps in reducing the finishing time and reduces the finishing marks associated with magnetorheological finishing processes.
- The tool has been fabricated from steel and required some advanced machining including wire-EDM and CNC milling. Steel tool though robust in construction, takes a lot of machine-hours as well as man-hours to fabricate, thereby increasing the cost as well. Also, customization is very costly and difficult for a conventionally fabricated tool.
- Rapid prototyping is relatively fast and doesn't require much man-hours but produces the parts with inferior physical characteristics. 3D printing from plastics requires a single machine with a very low setup time. The tool made here is printed from PETG and took only 21 h and 17 min. Also, customization is possible at the will and the complex shapes are possible to fabricate. Apart from that, FFF process has a far lower carbon footprint.

- Magnetostatic simulation of the tool along with the workpiece is carried out to validate the threshold intensity of magnetic flux density required for finishing of both ferromagnetic and non-magnetic materials.
- Tool materials namely mild steel and polyethylene were considered for the simulation, i.e. ferromagnetic as well as 3D printable non-magnetic.
- Workpieces considered from both ferromagnetic and non-magnetic categories. The ferromagnetic material is mild steel while non-magnetic taken were copper, aluminium and a non-metallic polycarbonate.
- The simulation results indicate magnetic flux density distribution beneath the tooltips confirming the formation of MRP fluid hemispherical ball formation to carry-out the finishing. The tool is equally capable of finishing ferromagnetic as well as non-magnetic materials.
- The plastic 3D printed tool seems to be performing better than the mild steel tool when it comes to the flux density distribution on the workpiece surface because of the fact that the tool material is non-magnetic.

Therefore, from the above points, it can be concluded that the BEMRF tool can be fabricated from plastics through the process of 3D printing and would perform the finishing operation well. This way, it would be faster, cheaper, highly customizable and would have a very minimal environmental impact. However, when required in masses, like in industry, it would be much better, robust and cheaper to fabricate the steel tool conventionally. Both types of the tool will perform the finishing operation well for ferromagnetic and non-magnetic as well as non-metallic workpieces.

References

1. Marinescu, I., Rowe, B., Ling, Y., Wobker, H.G.: Abrasive processes. In: Handbook of Ceramic Grinding & Polishing, pp. 94–189. William Andrew Publishing (1999)
2. Khan, D.A., Alam, Z., Jha, S.: Nanofinishing of copper using ball end magnetorheological finishing (BEMRF) process. In: ASME 2016 International Mechanical Engineering Congress and Exposition. American Society of Mechanical Engineers Digital Collection (2016)
3. Alam, Z., Jha, S.: Modeling of surface roughness in ball end magnetorheological finishing (BEMRF) process. *Wear* **374–375C**, 54–62 (2017)
4. Shinmura, T., Takazawa, K., Hatano, E., Matsunaga, M., Matsuo, T.: Study on magnetic abrasive finishing. *CIRP Ann.* **39**(1), 325–328 (1990)
5. Kordonski, W.I., Jacobs, S.D.: Magnetorheological finishing. *Int. J. Modern Phys. B* **10**(23n24), 2837–2848 (1996)
6. Kordonski, W.I., Shorey, A.B., Tricard, M.: Magnetorheological (MR) jet finishing technology. In: ASME 2004 International Mechanical Engineering Congress and Exposition, pp. 77–84. American Society of Mechanical Engineers Digital Collection (2004)
7. Singh, A.K., Jha, S., Pandey, P.M.: Magnetorheological ball end finishing process. *Mater. Manuf. Processes* **27**(4), 389–394 (2012)
8. Kumar, A., Alam, Z., Khan, D.A., Jha, S.: Nanofinishing of FDM-fabricated components using ball-end magnetorheological finishing process. *Mater. Manuf. Processes* **34**(2), 232–242 (2019)
9. Alam, Z., Iqbal, F., Ganesan, S., Jha, S.: Nanofinishing of 3D surfaces by automated five-axis CNC ball end magnetorheological finishing machine using customized controller. *Int. J. Adv. Manuf. Technol.* **100**(5–8), 1031–1042 (2019)

10. Alam, Z., Khan, D.A., Jha, S.: MR fluid-based novel finishing process for nonplanar copper mirrors. *Int. J. Adv. Manuf. Technol.* **101**, 995–1006 (2019)
11. Beverly, C.R., Tanner, R.I.: Numerical analysis of three-dimensional Bingham plastic flow. *J. Nonnewton. Fluid Mech.* **42**(1–2), 85–115 (1992)
12. Alam, Z., Khan, D.A., Jha, S.: A study on the effect of polishing fluid volume in ball end magnetorheological finishing process. *Mater. Manuf. Processes* **33**(11), 1197–1204 (2018)
13. Iqbal, F., Jha, S.: Experimental investigations into transient roughness reduction in ball-end magnetorheological finishing process. *Mater. Manuf. Processes* **34**(2), 224–231 (2019)
14. Peng, W., Li, S., Guan, C., Shen, X., Dai, Y., Wang, Z.: Improvement of magnetorheological finishing surface quality by nanoparticle jet polishing. *Opt. Eng.* **52**(4), 043401 (2013)
15. Singh, A.K., Jha, S., Pandey, P.M.: Nanofinishing of a typical 3D ferromagnetic workpiece using ball end magnetorheological finishing process. *Int. J. Mach. Tools Manuf.* **63**, 21–31 (2012)
16. Singh, A.K., Jha, S., Pandey, P.M.: Design and development of nanofinishing process for 3D surfaces using ball end MR finishing tool. *Int. J. Mach. Tools Manuf.* **51**(2), 142–151 (2011)
17. Lim, Y.Y., Chaudhri, M.M.: The influence of grain size on the indentation hardness of high-purity copper and aluminium. *Philos. Mag. A* **82**(10), 2071–2080 (2002)

Chapter 42

Investigation on Mechanical Properties of Himalyan Extract Reinforced Epoxy Composite



Ajay Chauhan, Vikram Singh, and Shiv Kumar

Abstract The prevailing scenario of whole material handling commercial enterprises is focused into utilization of highly durable material at lower rates. Thus, analysts focused for beneficial and greatest use of natural particulate reinforced (NPR) due to their cost effectiveness and sustainability. The NPR composite has capability to replace synthetic reinforced polymer composite. The epoxy was used as matrix material. Varieties of hard wood are available in himalyan region. The Oak particulates were used as Himalyan Fiber (HF) for reinforcing the epoxy. The weight fractions of OAK particles were 10%, 20% and 30%. The curing of epoxy was done in thermal oven at 120 °C for 124 min. It was discovered that the tensile strength, flexural strength as well as hardness were expanded with an increase in OAK particle content. There was decrement in impact strength in epoxy reinforced OAK composite with an increase in the concentration of OAK particle content due to their brittle nature. The water assimilation ability of epoxy/oak composite was investigated and it was found that an expansion in weight ratio of oak particles, the water absorption increases because of tendency of OAK particles to absorb moisture.

Keywords Epoxy · Oak · Curing · Mechanical behavior · Water assimilation

42.1 Introduction

The advancement in polymer substances with improved mechanical characteristics have susceptible scope for scientists and production engineers. These materials have capability to provide a better alternative over the other materials (e.g. metals, alloys). Due to insufficient mechanical properties of polymer, it alone cannot be used for application purposes. The reinforcement is necessary to achieve better mechanical properties. The various particulate reinforcement materials are alumina, boron carbide, silicon carbide etc. these reinforcements are very expensive. The natural particles may be used as an alternative over these expensive reinforced particles.

A. Chauhan (✉) · V. Singh · S. Kumar
SIRDA Institute of Engineering Technology, Mandi, Himachal Pradesh 175019, India

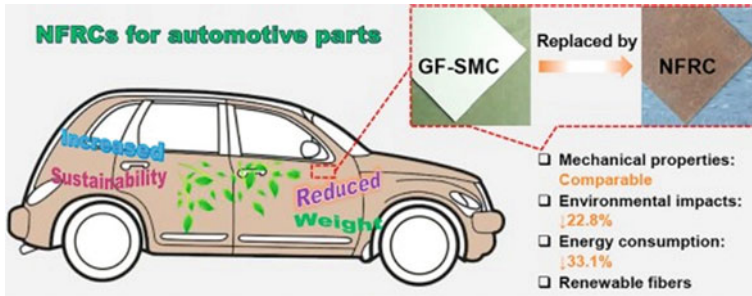


Fig. 42.1 Use of NFRC's in automobile industry [4]

The used of these reinforced particles may leads to sustainable development of engineering material. The available polymer matrix materials are thermosetting and thermoplastic material. It is well known that strength of thermosetting composite is better than thermoplastic. So, epoxy has been taken this research study. Thermal curing is required to decrease the curing time of epoxy. The curing time may be higher when it cured at room temperature. In the present days material fabrication in the polymers field, thermal curing take part a significant job because of their remarkable properties. The thermal waves can be reflected transmitted or retained based upon the matter to be fabricated via thermal curing [1–3]. Lately, the interest of researchers and designers has turned over on using all organic strands successfully, cost-effective as conceivable to deliver great quality strand-reinforced polymer composites for the framework, construction, and different necessities. This has prompted the advancement of alternate materials rather than conventional materials. Presently the goal of the aeronautic manufacturing units is concentrating on the development of lightweight and top-notch material. The lightweight and high strength materials are needed to diminish a load of planes for high performance [4, 5] (Fig. 42.1).

Organic strand composites are probably going to be naturally better than other synthetic strands because of the accompanying reasons, such as environment-friendly nature, less polluting content, and negligible carbon credits [6]. The organic strand reinforced polymer composite substances offered a broad area of characteristics that are appropriate for a considerable number of engineering utilization. The environmentally accessible plants have various lignocellulose strands. These strands may acknowledge as environmentally developed composites [7]. Practically all-organic strands, aside from cotton, are principally made out of cellulose, hemicellulose, lignin, waxes, and a few water-solvent mixes. The measure of cellulose in the strand decides the toughness and firmness of strands, which is given by bonds of hydrogen and different linkages in cellulose [8]. As the climate is a significant worldwide concern these days because of the growing rates of ozone harming substances. Conventional elements are typically answerable for transmitting carbon dioxide

(CO₂) gas during their transformation and utilization [9]. Among the different fabricated elements that have been examined as substitutes for iron and steel for the utilization in car, plastics holds a significant percentage. Plastics utilized for nearly everything from the components of the day by day use to confounded structures, various machine parts, and so on. It finds different applications due to the lightweight, less water assimilation high firmness, and durability. A number of plant strands discover usage as an asset for business materials. Polymers composite are not just famous in the aircraft sector, however, additionally famous in the implant business because of its incredible biodegradability. The conventional biomedical implant substance was metal and ceramics, which were disposed of because of their heavy weight and brittleness. Overwhelming inserts may likewise cause exhaustion to sick persons. In this manner, a few specialists have recommended bio compatible polymers as an option in contrast to conventional metals and ceramic inserts [10–12]. Now a day's polymeric foams have assortment of applications because of high adaptability, less weight, high water retention capacity and thermal protection. Due to non-biodegradability of traditional materials, scientists divert towards biodegradable polymeric foams. As a result, PCL might be a biodegradable option [13]. It was concluded from literature review that very less work has been on exploitation of natural resources as reinforcement in thermosetting resin (epoxy). As per knowledge of authors no work has been reported on study of mechanical behavior of epoxy/oak particulate composite.

42.2 Research Background

In a study, firmness and mechanical behavior of flax/bio-epoxy composites presented to various ecological circumstances were assessed. These circumstances were picked to clone those discovered outside that can influence the strength of these substances: water submersion, warm moist condition, and freeze-defrost circumstances. The results acquired in this examination recommend that flax/bio epoxy composites can utilize almost ecological circumstances, barring submerged applications that cause serious harm to the characteristics of the substance. Such material is inadvertently lowered in water for quite a while, dry the composites to three days will almost thoroughly restore the flexural quality and modulus, further Young's modulus, yet the elasticity will be diminished inevitably [9].

In the current work hygro-mechanical action of single hemp strand/epoxy interface was explored through its portrayal at micro scale through Microdroplet debonding tests. Debonding action examination related to strand/matrix interface crack perception highlights the modified stress position at the interface while expanding relative humidity. The extra hygroscopic stress produced during storage at different humidity are demonstrated the significant supporter of the ideal interface performance at 50% RH [14].

In this assessment study was done on mechanical performance of organic strand-based hybrid composite. accordingly, mechanical performance of hybrid composites was seen as upgraded linearly with volume. Additionally, the treatment of organic

strand with NaOH played significant job in improving the interfacial attachment among fiber and matrix. Deterioration in mechanical characteristics predominantly relied upon the period of vulnerability and temperature associated with different ecological conditions [15].

42.3 Material and Experimental Method

42.3.1 Material Used

High gloss and transparent epoxy resin (Grade: Bisphenol A) and hardener were supplied by chemzest techno products pvt ltd Chennai. The resin and hardener mixed with the ratio 60:40. For better curing, the epoxy was cured at 120 °C, which is glass transition temperature of epoxy as provided by supplier. The curing temperature was observed by non-contact pyrometer. The curing cycle was two hours. In order to prepare reinforced particles, Oak wood was crushed in Crusher (Make: Lyser, Model: 105, Germany). The particle passed from various sieves (higher to lower order). It was found that the particles pass from a sieve of 100 μm . The various weight fractions were used 10%, 20% and 30% along with neat epoxy (Fig. 42.2).

It was observed that glass transition temperature of epoxy expanded with increase in weight fraction of oak particles. This leads to increase in curing cycle time. The curing cycle time for pure epoxy, epoxy/10 Oak, epoxy/20 oak and epoxy/30 oak was 125, 157, 199 and 224 min, respectively. After curing, the mold permitted to cool at normal temperature upto 24 h.

Fig. 42.2 Extracted Oak fiber



42.3.2 Mechanical Testing

Tensile behavior of epoxy/oak composite was measured by using UTM according to ASTM D3039 specification. Specimens size were $50 \times 12.5 \times 4 \text{ mm}^3$ ($L \times W \times t$), respectively. Ten specimens of every sample were tested to acquire tensile strength value. Error bar was used to show standard deviation in results. Rectangular test piece $64 \times 16 \times 4 \text{ mm}^3$ was cut to according to ASTM D790 standard to perform flexural strength test. For impact strength test ASTM D256 standard was followed on impact strength testing machine. Samples were cut within the dimension $64 \times 12.7 \times 3.2$ for Izod test.

42.3.3 Physical Properties Analysis

Also, four specimens of about $10 \times 10 \text{ mm}^2$ was cut according to ASTM D5229 to check water assimilation. Specimen was immersed in the refined water at normal environment and the measure of water assimilated by the samples was estimated after 24 h. A Shore D Durometer was used to perform a hardness test procedure. Every durometer tests the intensity of an indentation in sample induced by a defined force of given geometric presser foot. The intensity of indentation indicates the hardness of samples. Specimens of size $10 \times 10 \times 10 \text{ mm}^3$ were cut according to ASTM 2240 to perform hardness test (Fig. 42.3).

42.4 Result and Discussion

42.4.1 Flexural Strength

Flexural strength is capability of substance to oppose the fracture beneath the load condition. The flexural quality of processed NFRC's was increased with an increment in oak strand inclusion. Flexural strength is calculated by equation (42.1) (Fig. 42.4).

$$\sigma = \frac{3FL}{2bd^2} \quad (42.1)$$

where,

- F = Force at fracture point,
- L = Length of support span,
- b = Width.
- d = Thickness of samples.

$$\sigma = 0.375 \times F \quad (42.2)$$

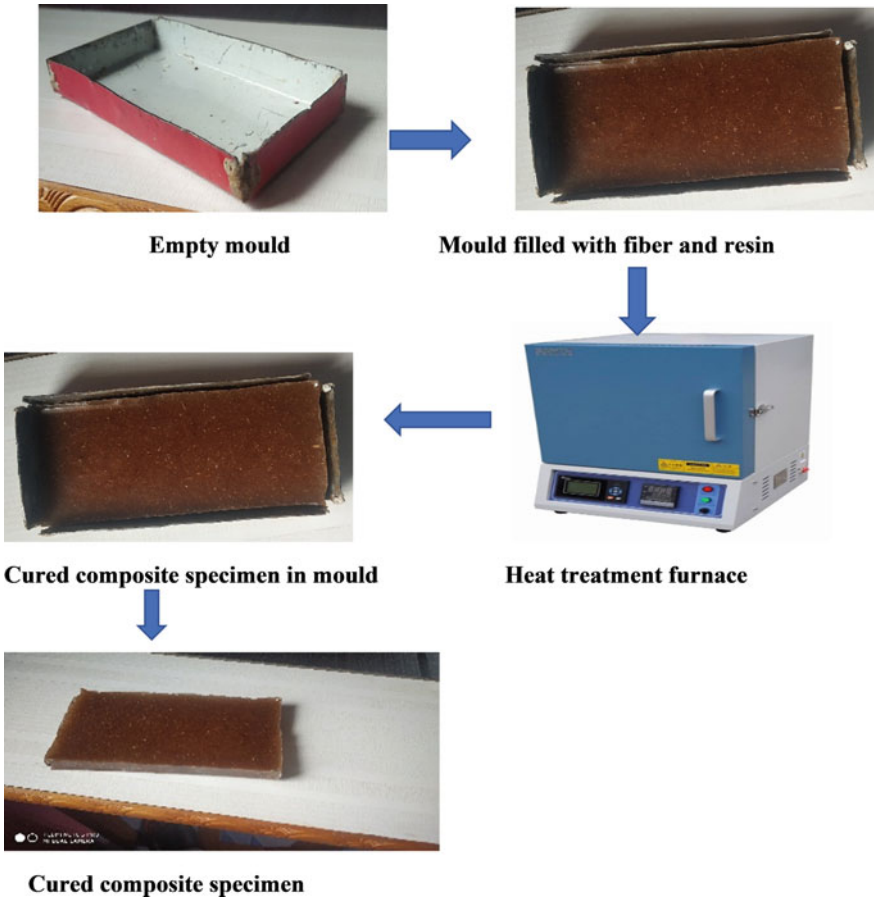
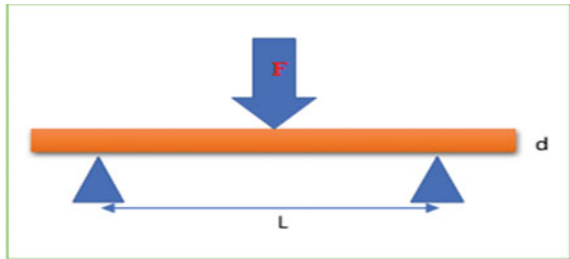


Fig. 42.3 Various steps followed to prepare the composite sample

Fig. 42.4 Beam under three-point bend test



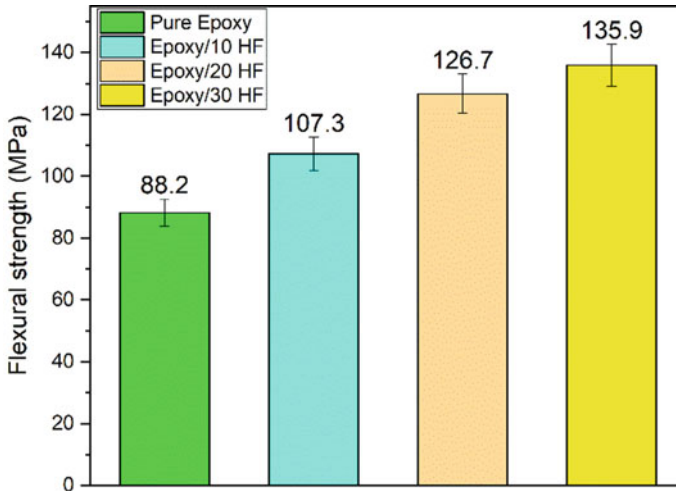


Fig. 42.5 Flexural strength comparison

The value of F has been obtained by the three-point bend analysis and flexural strength has been calculated from Eq. 2.

Figure 42.5 shows that as we compare the strength with pure epoxy sample having 0% reinforcement has less flexural strength i.e. 88.2 MPa. As we increase the reinforcement gradually by 10%, 20%, 30% flexural strength increases with increase in content of Himalayan fiber (HF). This is due to the reason that an increment in value of flexural strength in BFRC might be because of an increment in reinforcement (Ban fiber particulates) with the matrix. In case of neat epoxy the total bending load was focused on matrix only. While in case of ban fiber reinforced composite the load transfer from matrix to reinforcement particles successfully. The concentration of transmitted load in case of reinforced fibre composite having high wt% of fiber is more than that of reinforced composite having less wt% of fiber. The measured responses are similar with the other reported investigations of Verma and zafar [2].

42.4.2 Impact Strength

It shows the toughness of the material. It is capacity of material to absorb the shock vitality or to resist it. While the impact strength of the pure epoxy with 0% reinforcement have high impact value 32.2 kg/m² as compare to the reinforcement added to the pure epoxy. The impact strength decreases gradually with increase in reinforcement at 10%, 20%, 30% addition of fiber the impact strength value decreases with value 25.2, 22.8, 20.9 kJ/m² respectively as shown in Fig. 42.6. This decrease is due to the increase in brittleness in specimens. This could be due to reason that the particulates in general display low shock resistance, it happens because of inadequate interfacial

bond among matrix along with particulates, prompting the instance of cavities at intersection among matrix as well as particulates. There was more surface region for additional pits to made and served as intramural deformities diminishing the proficiency of vitality transferred inside the composites upon impact. The similar phenomenon was observed in Petchwattana and Covavisaruch [16].

42.4.3 Water Assimilation Test

As the water assimilation calculated which shows the water assimilation of pure epoxy is negligible as compare to the reinforcement added to the epoxy. The major reason of water assimilation in the reinforced composite specimen is organic strand. This organic strand absorbs moisture in presence of water. The neat epoxy has 0% increase in weight because the neat epoxy act as thermosetting plastic which absorb no moisture and 10%, 20%, & 30% reinforcement added to neat epoxy has respectively 0.4%, 1.0%, 2.4% increase in weight when sample dipped in distilled water for 24 h. The rate of water ingestion (WA%) was determined by utilizing the Eq. (42.3).

$$WA\% = [W - W_o] \div W_o \times 100 \quad (42.3)$$

where,

W_o = Dry weight in gm.

W = Wet weight in gm.

$W - W_o$ = Increase in weight.

Water assimilation test results shown in Table 42.1. This could be because of the reason that water retention in NFRC is because of aggregate impacts of many identical systems. Moisture can consumed through a single strand or particulate due to hygroscopic characteristic of cellulose strands. The other explanation that arrest the moisture is microgaps associate among strand as well as matrix. The gaps because of moist generate at the time of hot-melt process further advances toward water assimilation of materials due to increased porosity. Measured responses are similar with other documented studies of Tajvidi and Azad [17] (Table 42.1).

Table 42.1 Water assimilation test result

S. No	Specimen type	Dry weight (W_o) in gm	Wet weight (W) in gm	Increase in weight ($W - W_o$)	%age increase in weight ($WA\% = [(W - W_o)/W_o] \times 100$) (%)
1	Neat epoxy	4.510	4.510	0	0
2	Epoxy/10 HF	5.0	5.020	0.020	0.4
3	Epoxy/20 HF	5.0	5.050	0.050	1
4	Epoxy/30 HF	5.0	5.12	0.12	2.4

42.4.4 Tensile Strength

During tensile strength test result displays remarkable enhancement in tensile strength. When correlate to neat epoxy sample a gradual enhancemant found in durability of reinforced composite samples. 0% reinforced composite have tensile strength of 58.8 MPa while 10% reinforced composite sample have 78.7 MPa, 20% reinforced composite sample have 93.7 MPa, and 30% reinforced composite sample have 101.8 MPa tensile strength. The main reason of increase in strength of reinforced composite is inclusion of additional material. Increase in reinforcement cause increases the tensile strength shown in Fig. 42.7. Strength of BFRC advances with increment in wt% of Ban fiber reinforcement. As in case of neat eopxy the whole load is concentrate on matrix only. In the mean time when Ban fiber reinforcement added to matrix the weight move from neat epoxy to strands successfully and increase in tensile strength can be seen there. It might be happend because of the reason that tensile load focused on matrix substance successfully transfered toward reinforcement added to matrix because of improved bond quality enclosed by flexible matrix and stiff material added to matrix. The similar phenomenon was observed in Verma et al.[3]. This increase is due to the fact that the Oak particles are stiffer than epoxy, which causes increase in stiffness of pure epoxy and provide resistance during action of uniaxial loading.

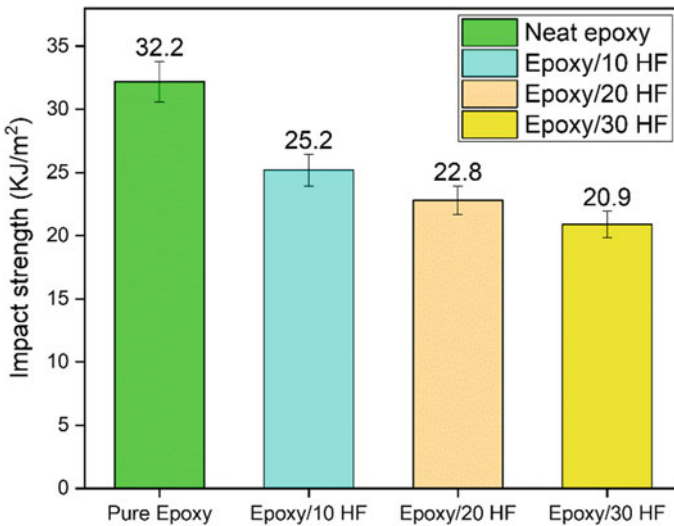


Fig. 42.6 Impact strength comparison

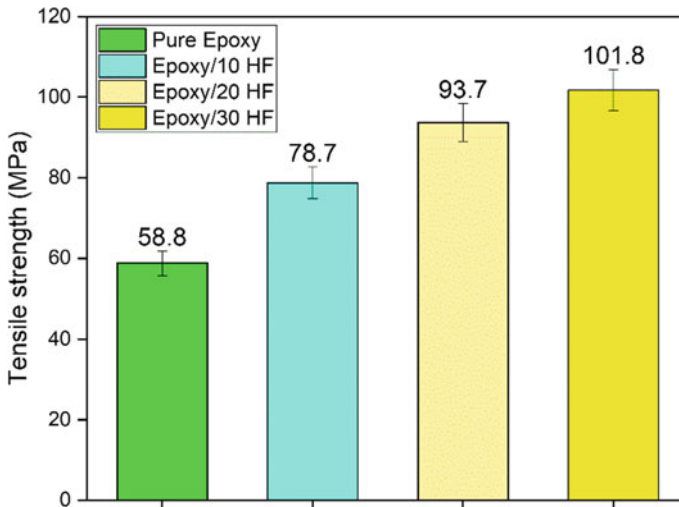


Fig. 42.7 Tensile strength comparison

42.4.5 Hardness Test

Hardness is the ability of material to resist the deformation against indentation scratch or abrasion. When the hardness test conducted the result shows that there is also increase in the hardness as compare to the neat epoxy sample. The neat epoxy material has 47.2 Shore D hardness, similarly for 10%, 20%, 30% reinforced composite samples have 60.3, 70.2, 78.8 Shore D hardness, respectively. As the reinforcement in the pure epoxy increases the hardness gradually increases. This is due to the presence of hard particle in epoxy. These hard particles offer a resistance to indenter and cause increase in hardness value. The increase in shore D hardness of composite material relies upon the kind of reinforcement and its properties (mechanical, chemical and physical) the degree of adhesion, and fiber stacking. Shore D hardness increases due to introduction of Ban fiber reinforcement in matrix. The Ban fiber particulates are harder then the matrix. Neat epoxy is softer and allow the indenter to penetrate easily. The similar phenomenon was observed in Verma et al. [3]. The increase in hardness represent in Fig. 42.8.

42.5 Conclusion

Mechanical characteristics as well as physical characteristics of organic strand reinforced composite are evaluated. Wide range of tests has been conducted on the different reinforced composition samples. The composite reinforced with organic strand have good flexural strength, rigidity as well as hardness in contrast with the

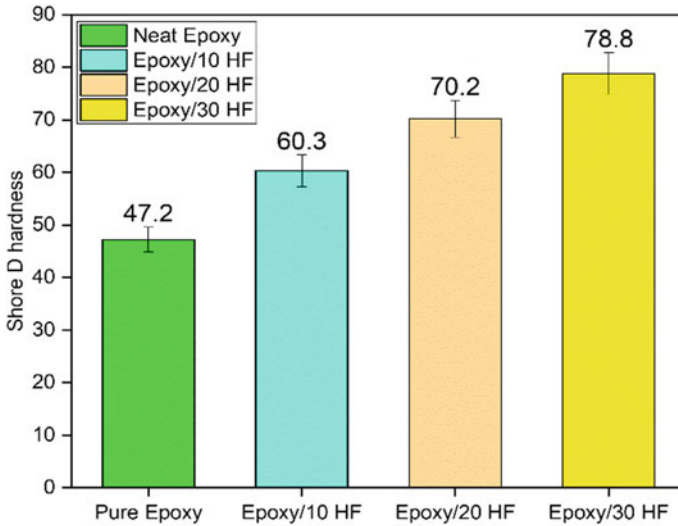


Fig. 42.8 Hardness test comparison

pure epoxy material. Whereas there is decrease in impact strength in reinforced composite as compare to the pure epoxy sample. There is also slightly increase in water assimilation in reinforced composite as in pure epoxy material have no water assimilation. Over all we can say that as there is an increase in reinforcement in pure epoxy strength like flexural, tensile, and hardness gradually increases and impact strength decreases when compared to the pure epoxy specimens.

References

1. Mathur, N.M., Bairwa, K.: A literature review on composite material and scope of sugar cane Bagasse. *Int. J. Eng. Develop. Res.* **5**(4), 125–133 (2017)
2. Verma, N., Zafar, S.: Investigations on mechanical performance of multi-layered microwave processed HDPE/ sisal composites for automobile applications. *App. Mech. and Mat.* **895**, 64–69 (2019)
3. Verma, N., Zafar, S., Talha, M.: Influence of nano-hydroxyapatite on mechanical behavior of microwave processed polycaprolactone composite foams. *J. Mater. Res. Express* **6**, 085336 (2019)
4. Thiruchitrabalam, M., Athijayamani, A., Sathiyamurthy, S., Thaheer, A., S., A.: A review on the natural fiber-reinforced polymer composites for the development of roselle fiber-reinforced polyester composite. *J. Nat. Fibers* **7**(4), 307–323 (2010)
5. Verma, N., Zafar, S., Pathak, H.: Vacuum-assisted microwave curing of epoxy/carbon fiber composite: an attempt for defect reduction in processing. *Manuf. Lett.* **24**, 127–131 (2020)
6. Joshi, S.V., Drzal, L.T., Mohanty, A.K., Arora, S.: Are natural fiber composites environmentally superior to glass fiber reinforced composites? *Compos. Part A Appl. Sci. Manuf.* **35**(3), 371–376 (2004)

7. Sathishkumar, T.P., Navaneethkrishnan, P., Shankar, S., Rajasekar, R., Rajini, N.: Characterization of natural fiber and composites—a review. *J. Reinf. Plast. Compos.* **32**(19), 1457–1476 (2013)
8. Thakur, V.K., Thakur, M.K., Gupta, R.K.: Review: Raw Natural Fiber-Based Polymer Composites. *Int. J. Polym. Anal. Charact.* **19**(3), 256–271 (2014)
9. Moudood, A., Rahman, A., Khanlou, H.M., Hall, W., Öchsner, A., Francucci, G.: Environmental effects on the durability and the mechanical performance of flax fiber/bio-epoxy composites *Compos. Part B Eng.* **171**, 284–293 (2019)
10. Venkateshwaran, N., Elayaperumal, A.: Banana Fiber Reinforced polymer composites—a review. *J. Reinf. Plast. Compos.* **29**, 2387–2396 (2010)
11. Guleria, T., Verma, N., Zafar, S., Jain, V.: Fabrication of Kevlar®-reinforced ultra-high molecular weight polyethylene composite through microwave-assisted compression molding for body armor applications. *J. Reinf. Plast. Compos.* (2020). <https://doi.org/10.1177/0731684420959449>
12. Verma, N., Zafar, S., Pathak, H.: Microwave-assisted composite fabrication of nano-hydroxyapatite reinforced ultra-high molecular weight polyethylene composite. *Mater. Res. Express* **6**, 115333 (2019)
13. Verma, N., Zafar, S., Thala, M.: Application of microwave energy for rapid fabrication of nanohydroxyapatite reinforced polycaprolactone composite foam. *Manuf. Lett.* **23**, 9–13 (2020)
14. Requile, S., Duigou, A.L., Bourmaud, A., Baley, C.: Interfacial properties of hemp fiber/epoxy system measured by microdroplet test: Effect of relative humidity. *J. Compos. Sci. Tech.* **181** (2019)
15. Nunna, S., Chandra, P.R., Shrivastava, S., Jalan, A.K.: A review on mechanical behavior of natural fiber-based hybrid composites. *J. Reinf. Plast. Compos.* **31**(11), 759–769 (2012)
16. Petchwattana, N., Covavisaruch, S.: Effects of rice hull particle size and content on the mechanical properties and visual appearance of wood plastic composites prepared from poly(vinyl chloride). *J. Bionic Eng.* **10**, 110–117 (2013)
17. Tajvidi, M., Azad, F.: Effect of particle size, fiber content and compatibilizer on the long-term water absorption and thickness swelling behavior of reed flour/polypropylene composites. *J. Reinf. Plast. Compos.* **28**, 2341–2351 (2009)

Chapter 43

Minimizing Solid Not Fat Loss in Whey During Paneer Manufacturing Using Taguchi Orthogonal Array



Sudip Banerjee, N. M. Suri, Sumankant, Subrata Kumar Bag, and Sandeep Kumar Khatkar

Abstract Paneer, a popular Indian dairy product, is obtained by acid coagulation of milk. Among several parameters that affect this process; the heating temperature of milk (A), coagulation temperature (B), the strength of coagulant (C) and immersion time in chilled water (D) are the most important. These factors affect the process of paneer production heavily and thus the correct combination of these four factors will minimize the loss incurred during processing. Here, L_{27} Taguchi Orthogonal array design was adopted with 4 factors and 03 levels to determine the conditions for the process to yield optimum result. Smaller the loss of Solid not fat (SNF) in whey, better was the combination of parameters. After each trial, paneer whey was tested for its final composition. It was perceived that the best result was realized using the combination of labelled as $A_3B_3C_2D_2$. The SNF content in whey, in this case, was minimum and was recorded as 5.5%. For validation, a confirmation test was conducted with the proposed combination of parameters and it was concluded that this combination is good enough to achieve the lowest SNF loss in whey or to maintain maximum milk solids in paneer.

Keywords Whey · Paneer · Fat · Solid not fat · Optimization · Taguchi · Waste reduction

S. Banerjee (✉) · N. M. Suri · Sumankant
Department of Production & Industrial Engineering, Punjab Engineering College, Chandigarh, India

S. K. Bag
Department of Dairy Engineering, West Bengal University of Animal & Fishery Sciences, West Bengal, Kolkata, India

S. K. Khatkar
Department of Mechanical Engineering, Chandigarh Engineering College, Landran, Punjab, India

43.1 Introduction

As per statistics from the year 2014–2019, it was recorded that the paneer marketplace in India nurtured with a CAGR of 12.5%. Paneer is a non-fermentative, non-renneted and non-melting type of cheese, attained by acid and heat coagulation of milk [1]. It is deliberated as one of the most widely consumed dairy product in India [2]. While producing paneer, cheese or chhana significant quantity of whey is produced. Whey constitutes about 45–50% of total milk solids, 70% of the milk sugar (lactose), 20% of the milk proteins and 70–90% of the milk minerals and almost all the water-soluble vitamins originally present in milk [3]. Whey when prepared during paneer manufacturing with the help of coagulant such as citric acid, a significant quantum of solid not fat removed from the paneer and incorporated in whey. Citrate content in paneer whey was higher due to the addition of citric acid as a coagulant during the preparation of paneer. The outcomes are in agreement with the observations reported by several scientists about the composition of paneer and cheese whey [4]. Khan and Pal [1] reported that the strength of coagulant has a significant consequence on the final body and texture of paneer. Rajashekhar et al. [5] observed that citric acid paneer produces softer body in comparison to other coagulants.

SNF % in whey is influenced by the entire paneer manufacturing process which requires many process parameters with a low, medium and high level of interactions resulting in the variance in final production. The Standard operating parameters traditionally designed are not based on optimization, taking into consideration of all majorly interacted process parameters. Hence the final output in terms of SNF in whey is required to be optimized (minimization of SNF in whey in this case). Several experimentations have to be conducted for a complete experiment [6–8]. To overcome this problem, the Taguchi method applies a special design of orthogonal arrays to examine the whole parameter space with only a small number of trials [9–11]. For the manufacturing of paneer four factors are measured as controlling factors. These are heating temperature, coagulation temperature, the strength of coagulant and immersion time of paneer blocks in chilled water.

For the Literature review, it has seen that consideration of multiple factors together such as heating temperature, coagulation temperature, the strength of coagulant, immersion time etc. have not experimented altogether [12,13]. It is fairly fascinating to understand the consequence of all these four factors and their interactions (combined effect) on the SNF content in whey. In addition to that, this investigation is meant to optimize the production factors put on Taguchi's orthogonal array. In convention, the standard operating process (SOP) for paneer manufacturing designed does not base upon any sort of optimization taking into consideration of all majorly interacted process parameters. Hence there is enough scope for the enhancement of the final output result in terms of lowermost SNF content in whey. Regarding the waste minimization, it has been observed that a significant volume of whey is drained during the production of paneer which contains an average 5.9% SNF. Therefore there is ample scope for more reduction of SNF in whey thereby saving the milk solids and ensuring the profitability. Therefore, in this investigation, the effect of

various control parameters such as heating temperature, coagulation temperature, the strength of coagulant and immersion time on SNF content in whey have been investigated using Taguchi optimization technique.

43.2 Material and Manufacturing of Paneer

The paneer was produced in Verka Ludhiana Dairy, Ludhiana. For manufacturing paneer, milk was taken at 4–6 °C and standardized to desired fat and SNF % [14]. Therefore, the same was transported through a plate heat exchanger to 85–95 °C for 10 min and impelled into a cheese vat where milk was cooled to 72–80 °C. One of the reasons for high heat treatment was to impart a desirable cooked flavour [15]. Moreover, the heating helped to cook the milk for speedy iso-electric precipitation, regulate the moisture content of paneer, mature distinctive body and consistency [13]. Therefore, hot milk was coagulated at 72–80 °C by adding citric acid at pH 5.3–5.4 with the help of citric acid. Here normally 1.8 kg of citric acid is immersed in 120 kgs of pasteurized hot water to get the desired concentration of 1.5% of citric acid (range 1–2%). The same may be sprinkled over the entire mass for better coagulation process. Higher concentration may impart an acidic flavour in paneer.

Three factors such as type of acid, its concentration and delivery mode and amalgamation into hot milk effect the yield of paneer and moisture withholding [16]. After coagulation, clear greenish-yellow whey splits out letting curd to shrink to the lowermost of the paneer vat. Therefore whey was drained through the filter and the curd mass was transferred to stainless steel grooved hoops kept inside the muslin cloth. The hoops have perforations on all edges to enable escaping out the whey. Four to five paneer hoops holding 7.5–10 kg paneer were placed one above another and pneumatic pressure of 6–10 kg/cm² is applied for 10–12 min. Finally cut paneer blocks are immersed in chilled water from 1 to 2 h for the preparation of the final composition of the product. After the immersion, paneer blocks are taken out of chilled water and kept on the SS table with the cover of wet muslin cloth. After that, the blocks are cut into pieces as per requirement, weight and packed below 15 °C. Paneer pieces then kept at the cold store at less than 4 °C for overnight to make it ready for dispatch. The SOP for paneer manufacturing depicted in Figs. 43.1 and 43.2.

43.3 Problem Identification and Design of Experiment

Problem identification stated with brainstorming followed by the voice of the customer (VOC). Then VOC turned to CTQ (Critical to Quality). Next probable reason for SNF loss in whey is grouped through the cause-effect diagram. After that pilot experimentation conducted to identify the manufacturing parameters and their

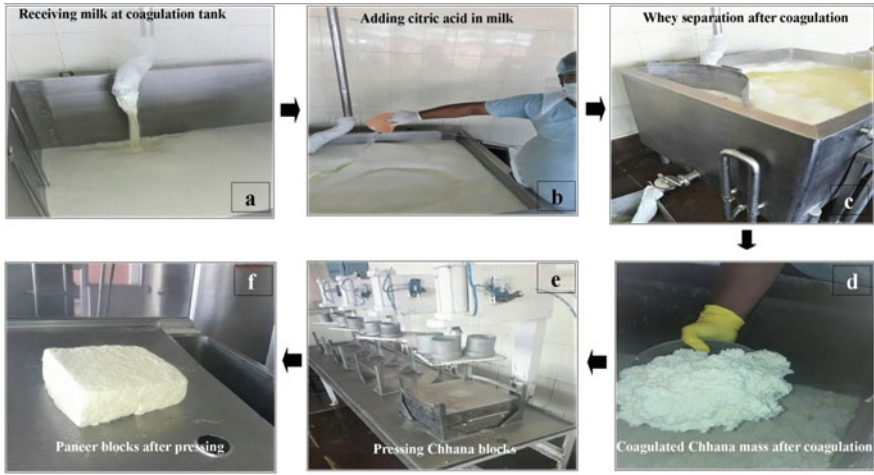


Fig. 43.1 a–f Process layout of manufacturing of paneer

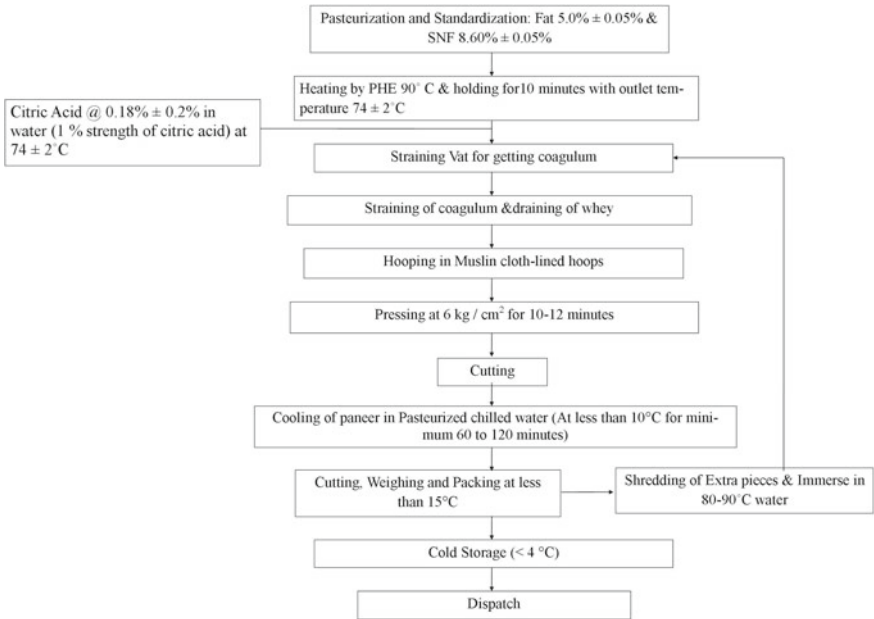


Fig. 43.2 Flow diagram for the manufacture of paneer

Table 43.1 Average SNF % in whey with different parameters at a different level of experiments

	Parameters	L1		L2		L3	
		%SNF in whey	S/N ratio	%SNF in whey	S/N ratio	%SNF in whey	S/N ratio
A	Heating temp. (°C)	5.9	-15.41	5.9	-15.41	5.8	-15.38
B	Coagulation temp. (°C)	6.0	-15.63	5.8	-15.41	5.7	-15.16
C	Strength of coagulant (%)	5.8	-15.38	5.8	-15.31	5.9	-15.51
D	Immersion time (h)	5.9	-15.49	5.8	-15.30	5.9	-15.41

*L1, L2 and L3 represent Levels 1,2 and 3 respectively

** S/N Ratio symbolizes Signal to Noise ratio

levels. The process factors for paneer were identified as heating temperature, coagulation temperature, the strength of coagulant and immersion time of paneer blocks in chilled water. Then research design was prepared by L27 Taguchi orthogonal array as shown in Table 43.1. From the paneer manufacturing trial, selected-response characteristic was recorded as SNF content in whey. Finally, the effect of all control parameters on response characteristics was studied individually applying Taguchi single response optimization [12]. The same was validated through a confirmation experiment for each factor. In the case of paneer whey “Smaller the better (SB)” concept is applied to minimize the SNF content in whey.

43.4 Result and Discussion

SNF content in whey during the manufacturing of paneer has been considered as a response, however, heating temperature, coagulation temperature, the strength of coagulant and immersion time have been taken as input parameters for the manufacturing of paneer. The raw data for average values of the responses for every factor considered in all three levels (L1, L2 and L3) and depicted in Table 43.1.

After conducting the three experiments for each of the 27 trials i.e. a total of 81 experiments, results were obtained in terms of average SNF% in paneer whey. Experimental results for % SNF in whey are summarized in Table 43.2. From the average values and main effect of the raw data of SNF in whey (Table 43.3), it is noticed that the control parameter coagulation temperature has the strongest influence on SNF % in whey followed by immersion time, the strength of coagulant and heating temperature. The coagulation is a process of curdling through precipitation. That is the settlement of solid not fat. Hence coagulation temperature has significant impact over the solid not fat of milk taken for the manufacturing of paneer.

Tabl 43.2 SNF Content in whey according to different experimentation combination

Trial No	Trial combination				% SNF in whey			Average % SNF in whey	S/N ratio
	A	B	C	D	S1	S2	S3		
1	85	72	1	1	6.70	6.60	6.40	6.57	-16.3485
2	85	72	1.5	1.30	6.00	6.20	6.30	6.17	-15.8028
3	85	72	2	2	6.50	6.40	6.30	6.40	-16.1243
4	85	76	1	1.30	6.00	5.80	5.90	5.90	-15.4179
5	85	76	1.5	2	5.80	5.60	5.40	5.60	-14.9675
6	85	76	2	1	6.00	6.00	6.00	6.00	-15.5630
7	85	80	1	2	5.40	5.30	5.80	5.50	-14.8139
8	85	80	1.5	1	5.40	5.30	5.80	5.50	-14.8139
9	85	80	2	1.30	5.40	5.30	5.80	5.50	-14.8139
10	90	72	1	1	6.20	6.30	6.00	6.17	-15.8028
11	90	72	1.5	1.30	5.80	5.90	6.00	5.90	-15.4179
12	90	72	2	2	6.00	6.30	6.10	6.13	-15.7557
13	90	76	1	1.30	6.00	5.80	6.00	5.93	-15.4671
14	90	76	1.5	2	6.00	6.00	5.90	5.97	-15.5149
15	90	76	2	1	6.00	5.80	5.90	5.90	-15.4179
16	90	80	1	2	5.80	5.60	5.40	5.60	-14.9675
17	90	80	1.5	1	6.00	6.00	6.00	6.00	-15.5630
18	90	80	2	1.30	5.40	5.30	5.80	5.50	-14.8139
19	95	72	1	1	5.40	5.30	5.80	5.50	-14.8139
20	95	72	1.5	1.30	5.40	5.30	5.80	5.50	-14.8139
21	95	72	2	2	6.20	6.30	6.00	6.17	-15.8028
22	95	76	1	1.30	5.80	5.90	6.00	5.90	-15.4179
23	95	76	1.5	2	5.80	5.90	5.90	5.87	-15.3681
24	95	76	2	1	6.00	6.00	6.00	6.00	-15.5630
25	95	80	1	2	5.90	5.90	5.80	5.87	-15.3681
26	95	80	1.5	1	6.00	6.00	6.00	6.00	-15.5630
27	95	80	2	1.30	6.00	6.20	6.10	6.10	-15.7074

*A, B, C and D denote Heating Temperature (OC), Coagulation Temperature(OC), the strength of coagulant(%) and Immersion Time respectively

For computing S/N ratio for smaller is better, the following formula is used:

Smaller is better: S/N_{LB} ratio = $-10 \log (1/r \sum yi^2)$,

Where yi = individual response.

Table 43.3 Percent contribution and optimum factors

Designation	Parameter	Optimum level	Optimum value	Mean of SW(% C)	S/N ratio of SW(%C*)
A	Heating temp (°C)	3	95 °C	0.16	0.12
B	Coagulation temp (°C)	3	80 °C	21.84	21.49
C	Strength of coagulant (%)	2	1.5%	3.75	3.69
D	Immersion time (h)	2	1.30 h	3.88	3.76

*% C denotes % contribution

The main effect and S/N ratios for SNF % in whey are stated in Figs. 43.2 and 43.3 respectively. The mean response denotes to the average measure of quality characteristics for every factor at altered levels. The average value of SNF % in whey for every factor at levels 1, 2, and 3 are computed. In Fig. 43.3a, it was observed that with an increase in temperature (i.e. 80, 85 and 90 °C) the SNF content was decreased. Also as shown in Fig. 43.3b with an increase in coagulation temp. the SNF content decreased significantly. In Fig. 43.3c SNF quantity decrease for raising coagulation strength from 1 to 1.5%. SNF further increases due to the increase in strength of coagulant from 1.5 to 2%. In case of increase of immersion time from 1 to 1.30 h, SNF in whey decreases and increase in immersion time from 1.30 to 2 h, SNF in whey increase.

Table 43.3 shows that the contribution of parameter i.e. coagulation temperature, to the responses is greatest (21.84%). The influence of other factors in downward

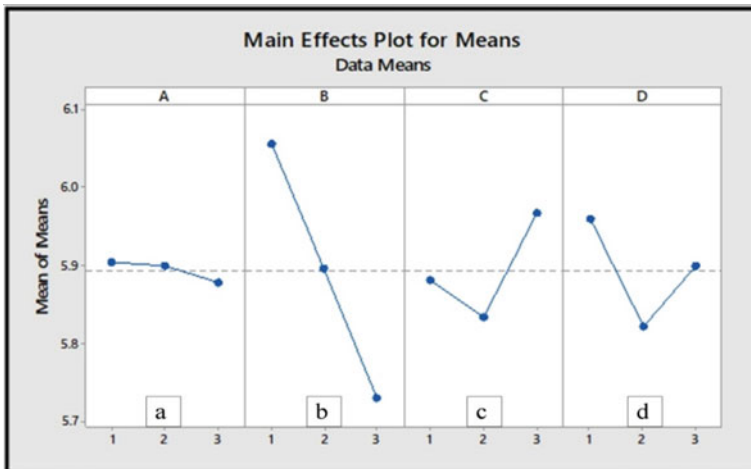


Fig. 43.3 Main effects graph with the mean for SNF% in whey

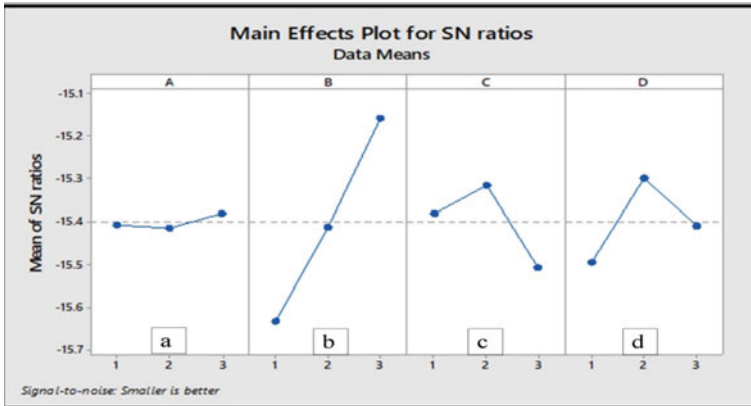


Fig. 43.4 Main effects graph with the S/N ratio for SNF% in whey

order is immersion time (3.88%), % coagulant used (3.75%), and heating temperature (0.16%). Thus, depending on the main effect, S/N ratio and ANOVA analysis, the optimal mixture of factors and their levels for attaining lowest SNF % in whey is A₃B₃C₂D₂ i.e. the Heating temperature at level 3 (95 °C), coagulation temperature at level 3 (80 °C), % Coagulant used at Level 2 (1.5%), and immersion time at level 2 (1.30 h).

As SNF % in whey is smaller is better type, the lower value of SNF % in whey is preferred. From Figs. 43.3 and 43.4, it is projected that the combination A₃B₃C₂D₂ provides the minimum value of SNF % in whey. Moreover, in almost all the factors A, B, C and D, the lowest value of mean response relate to the highest value of S/N ratio. It was observed that The optimal value of the predicted mean (μ) of different response characteristics can be available from the below-stated equation also adopted by [7, 8].

$$\mu = m + (m_{Aopt} - m) + (m_{Bopt} - m) + (m_{Copt} - m) + (m_{Dopt} - m)$$

$$m = \frac{T}{N}$$

where,

- m overall mean, average SNF % in whey = 5.89
- T a total of average SNF% in whey for each experiment = 477.4
- N total number of experiments = 81
- m_{Aopt} average SNF % in whey for factor A at its optimal level = 5.8
- m_{Bopt} average SNF % in whey for factor B at its optimal level = 5.7
- m_{Copt} average SNF % in whey for factor C at its optimal level = 5.8
- m_{Dopt} average SNF % in whey for factor D at its optimal level = 5.8

While Calculating we get the mean for selected trial conditions for parameters at (A₃B₃C₂D₂) is 0.72 (m)

$$\begin{aligned} \mu &= 5.89 + (5.8 - 5.89) + (5.7 - 5.89) + (5.8 - 5.89) + (05.8 - 5.89) \\ &= 5.89 - 0.09 - 0.19 - 0.09 - 0.0- \\ &= 5.43. \end{aligned}$$

43.4.1 The Confidence Interval Around the Estimated Mean

The optimum value of SNF % in whey is projected at the designated levels of factors. The production factors and their optimum levels have already been designated as A₃B₃C₂D₂ shown in Table 43.3.

There are three different types of confidence intervals (CIs) that Taguchi practices, depending on the purpose of the estimation [17]. The 95% confidence interval of confirmation experiments (CI_{CE}) and the population (CI_{POP}) is evaluated by applying the subsequent equations[10]:

$$\begin{aligned} CI_{CE} &= \left[F(\alpha, 1, v_e) V_e \left(\frac{1}{\eta_{eff}} + \frac{1}{r} \right) \right]^{1/2} \\ CI_{POP} &= \left[F(\alpha, 1, v_e) V_e \left(\frac{1}{\eta_{eff}} \right) \right]^{1/2} \end{aligned}$$

where,

α = the level of risk;

v_e = the degrees of freedom for the error;

$F(\alpha, 1, v_e)$ = The F ratio at the confidence level of (1- α) against DOF 1 and error DOF v_e ;

V_e = the error variance,

η_{eff} = the effective number of replications and r is the number of test trials.

r = Sample size for confirmation experiments;

η_{eff} = effective number of replications = (N/(1 + DOF));

Using the above values, the CI is calculated as given under

$$\eta_{eff} = N / (1 + Total\ degree\ of\ freedom\ associated\ in\ the\ estimate\ of\ mean)$$

$$= 81 / (1 + 8) = 9.$$

$$\alpha = 1 - confidence\ limits\ (95\%) = 0:05.$$

$$F_{ratio(1;0:05;6)} = 5.99.$$

Table 43.4 Result of the confirmation run

Experiment with $A_3B_3C_3D_3$	SNF % in whey
1	5.50
2	5.45
3	5.55
Average	5.50

43.4.2 Confirmation Experiments

Confirmations experiments are performed to endorse that the parameters and levels were designated from an experiment cause a product or technique to turn in a specific mode. If the average of the outcomes of the confirmation experiment is outside the range of the Confidence Interval, the factors voted and/or levels to regulate the fallouts for the anticipated value are indecorous or have extreme measurements, necessitatingextrainvestigation. Here $A_3B_3C_2D_2$ did not associate to any trial of the orthogonal array. A total of three (3) confirmation experiments was carried out in the same way as discussed (Table 43.4) and average SNF % in whey was computed.

The average of the respondent SNF % in whey in every trial is found to be 5.50%, which is within the CI $5.29 < 5.50 < 5.569$ of the predicted value of the SNF in whey. This suggests that nominated factors, as well as their suitable levels, are appropriate to attain the anticipated outcome.

43.5 Conclusion

In the current static investigation, the process parameters (such as heating temperature, coagulation temp., the strength of coagulant and immersion time) of fabrication of paneer with low SNF was optimized using the Taguchi approach. From the experimental investigation the following main conclusions can be drawn:

1. The optimal paneer manufacturing conditions for getting lower most SNF percentage in whey are Heating Temperature as 95 °C (level 3), coagulation temperature as 80 °C (level 3), the strength of coagulant as 1.5% (level 2) and Immersion Time as 1.30 h (level 2).
2. The percentage contribution of the parameter coagulation temperature on SNF content of paneer is highest (21.84%) followed by immersion time (3.88%), the strength of coagulant (3.75%) and heating temp. (0.6%).
3. Before the use of the Taguchi orthogonal array, the SNF content in whey was 5.90%, whereas, after the use of Taguchi's method, the SNF content in whey drastically reduced to 5.50% only, resulting in maximum SNF retention in paneer.

References

1. Khan, S.U., Pal, M.A., Wani, S.A., Mir, S.: Effect of different coagulants at varying strengths on the quality of paneer made from reconstituted milk. *J. Food Sci. Technol.* **51**, 565–570 (2014)
2. Girdharwal, D.N.: Microbiological study of Indian Paneer a case study of Delhi City. *Int. J. Pharmaceut. Sci. Res.* **9**(09), 4008–8014 (2018)
3. Pushpa, B.P., Kempanna, C., Murthy, N.: Formulation of hypotonic electrolyte re-hydration whey drinks from paneer and cheese whey. *Asian J. Dairy Food Res.* **37**(3), 197–201 (2018)
4. Goyal, N., Gandhi, D.N.: Comparative analysis of Indian paneer and cheese whey for electrolyte whey drink. *World J. Dairy Food Sci.* **4**(1), 70–72 (2009)
5. Rajashekar, G., Kempanna, C., Brunda, S.M., Roopa, O.M.: Influence of different coagulation temperature and coagulants on chemical and sensory qualities of paneer. *Int. J. Agric. Sci. and Res.* **6**(3), 7–12 (2016)
6. Bhadekar, S.V., Deshmukh, B.R., Baswade, S.V., Mule, R.S., Gatchearle, P.I.: Sensory evaluation and overall acceptability of paneer from buffalo milk added with sago powder. *J. Dairy. Foods Home Sci.* **27**(2), 99–103 (2008)
7. David, J.: Preparation of functional paneer from buffalo milk blended with coconut milk. *Res. J. Ani. Husband. Dairy Sci.* **3**(2), 88–90 (2012)
8. Masud, T., Athar, I.H., Shah, M.A.: Comparative study on paneer making from buffalo and cow milk. *Asian-Australasian J. Ani. Sci. (AJAS)* **5**(3), 563–565 (1992)
9. Elangovan, K., Narayanan, C.S.: Application of Taguchi approach on the investigation of formability for perforated Al 8011 sheets. *Int. J. Eng. Sci. Technol* **2**(5), 300–309 (2010)
10. Khatkar, S.K., Verma, R., Sumankant et al.: Optimization and effect of reinforcements on the sliding wear behavior of self-lubricating AZ91D-SiC-Gr hybrid composites. *Silicon* (2020)
11. Thakur, A.G., Nandedkar, V.M.: Application of Taguchi method to determine resistance spot welding condition of austenitic stainless steel AISI 304. *J. Sci. Indust. Res.* **69**(9), 680–683 (2010)
12. Peter, A., Sarathchandra, G., Manimehalai, N., Athmaselvi, K.A.: Assessment of microbiological quality and aflatoxin levels of paneer marketed in Chennai, India. *Int. J. Sci. Technol.* **3**(4), 118–125 (2015)
13. Ruby, K., Alok, J., Amrita, P.: Process optimization for the manufacture of filled milk dietetic paneer. *Asian J. Dairy Food Res.* **32**(2), 130–134 (2013)
14. Masud, T., Shehla, S., Khurram, M.: Paneer (White Cheese) from Buffalo Milk. *Biotechnol. Biotechnol. Equip.* **21**(4), 451–452 (2007)
15. Sahu, J.K., Das, H.: Effect of heating and cooling rates on the recovery of milk components during heat-acid coagulation of milk for preparation of chhana—an Indian soft cottage cheese. *Int. Food Res. J.* **17**, 163–172 (2010)
16. Shashikumar, C.S., Puranik, D.B.: Study on use of lactoferrin for the biopreservation of paneer. *Tropical Agricult. Res.* **23**(1), 70–76 (2011)
17. Pant, M., Sharma, T., Verma, O., Singla, R., Sikander, A. (eds): *Soft Computing: Theories and Applications. Advances in Intelligent Systems and Computing.* vol 1053. Springer, Singapore (2018)
18. Khatkar, S.K., Verma, R., Kant, S., Kharb, S., Thakur, A., Sharma, R.: Optimization and effect of reinforcements on the sliding wear behavior of self-lubricating AZ91D-SiC-Gr hybrid composites. *Silicon* (2020)
19. Singh, H., Kumar, P.: Optimizing cutting force for turned parts by Taguchi's parameter design approach. *Indian J. Eng. Mater. Sci.* **12**(2), 97–103 (2005)

Chapter 44

Features and Functions of Filament Operated 3D Printer Nozzles: A Review



Krishnanand, Vatsal Mittal, Varanjot Singh, Amar Kumar Branwal, and Mohammad Taufik

Abstract Filament assisted additive manufacturing (FAAM) techniques are widely used in different application sectors for the fabrication of the three-dimensional part in the current manufacturing scenario. A very limited research study reported in the literature on the features and functions of filament operated various 3D printer nozzles. However, for proper understanding, there must be some combined study for different nozzles available for these FAAM techniques. Therefore, a detailed study on the filament operated nozzle available in the literature has been presented in this review work. It has been seen that three common types of the nozzle are widely applied: direct and Bowden type nozzles, single and multi-extruder type nozzles and single and multi-type nozzles. These nozzles have their own features and function areas. To improve the applicability of these FAAM techniques, more efforts should be paid on the design and analysis of a new single nozzle system that will be incorporating strength and eliminates the weakness of previously developed nozzles.

Keywords Fused deposition modelling (FDM) · Fused filament fabrication (FFF) · Types of nozzles

44.1 Introduction

The process of manufacturing product by deposition of material layer over layer using 3D CAD model data is called Additive Manufacturing (AM) [1]. Initially this process was used for making prototypes during designing of product. This process was taking less time to prepare prototype, so it is also known as Rapid Prototyping [2]. Additive manufacturing is categorised in various category on the basis of technique of deposition of material in layers. Stereolithography (SLA) [3], Selective Laser Sintering (SLS) [4], and Fused Deposition Modelling (FDM) [5] are the some

Krishnanand · V. Mittal · V. Singh · A. K. Branwal · M. Taufik (✉)
Department of Mechanical Engineering, Maulana Azad National Institute of Technology (MANIT) Bhopal, Bhopal, Madhya Pradesh 462003, India
e-mail: mohammad.taufik@manit.ac.in

popular technologies in additive manufacturing. Among all the additive manufacturing technologies fused deposition modelling (FDM) is most popular and widely used technology because of its low cost and open-source availability [6, 7]. FDM process is based extrusion of melted or semi-solid material through nozzle to deposit in layers. The material to be extruded is in the form of filaments or may be in pellet form [8]. Generally, commercially available FDM based 3D printers uses filament form polymers like—ABS, PLA, etc. [9]. FDM process is also known as Fused Filament Fabrication (FFF) [10]. Extruder and nozzle are the prime mechanical components of any FFF based 3D printers [11].

In FFF 3D printers, there are mainly three types of nozzle systems—Direct extruder and Bowden type extruder [12] nozzle system, single and multi-extruder type nozzle system, and single and multi-nozzle system. Most widely used nozzle systems are Direct and Bowden type extruder nozzle systems as shown in Fig. 44.1. Extruder of FFF based 3D printer is mainly made up of two parts—hot end and cold end [13]. Cold end is consisting of stepper motor, gear, and bearing. All these components help to provide the controlled feed of filament in the hot end. Hot end is consisting of nozzle and filament liquefier which is used to melt the filament and extrude it out of nozzle to print on printing bed. For proper working of cold end of extruder, it must be ensured that there is no heat flow from hot end to cold end. Therefore, to prevent the heat flow, heat sink or heat insulators are used between cold end and hot end [14].

In this paper, various types of nozzles used in filament operated 3D printers along with their features and functions are discussed. In the first section, design and construction of direct and Bowden type extruder nozzle system is discussed. In the next section, a multi-extruder nozzle design for colour mixing is described, and then a multi-nozzle extrusion system for multi-material printing is explained.

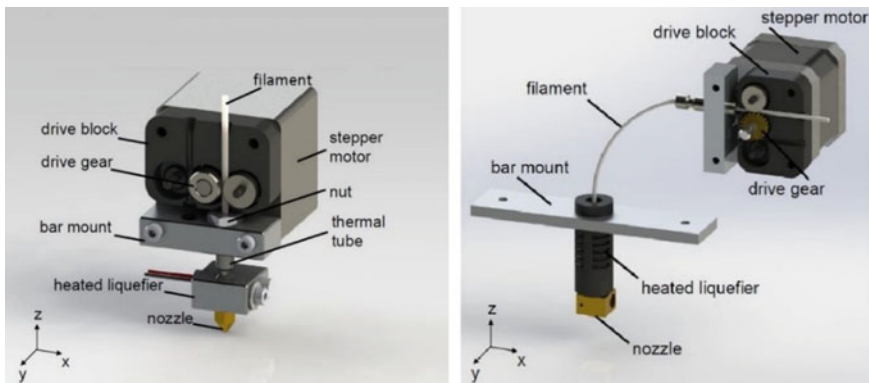


Fig. 44.1 a Direct extruder type Nozzle system and b Bowden Extruder type Nozzle system [12]

44.2 Direct and Bowden Extruder Nozzle System

Generally, commercially available FDM 3D printers use two categories of extruder one is direct type and another Bowden extruder. As shown in Fig. 44.2a, in direct extruder, hot end and cold ends are in close proximity, the filament is directly fed into the melting chamber, where it convert in semi solid form and extruded from the nozzle in a precise dimension [15]. Direct extruders are not as much fast as Bowden extruder. In a Bowden extruder, hot end and cold end are connected through a tube that is also named as Bowden tube. This tube works as guide-way for the filament to reach inside the hot end. Due to distance between hot end and cold end, flexible filaments are not suitable for Bowden extruder. Difference between direct and Bowden extruder is that, in Bowden extruder hot end is not in contact with moving parts as in case of direct extruder [14].

As shown in Fig. 44.3, Hoque et al. designed the Bowden extruder using. Bowden

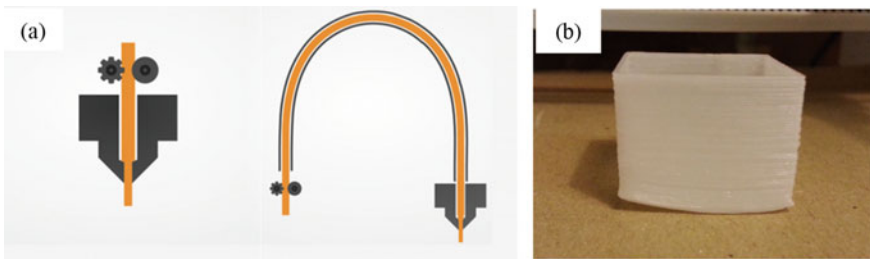


Fig. 44.2 a Schematic of Direct and Bowden Extruder [29], and b Warped 3D printed part [30]

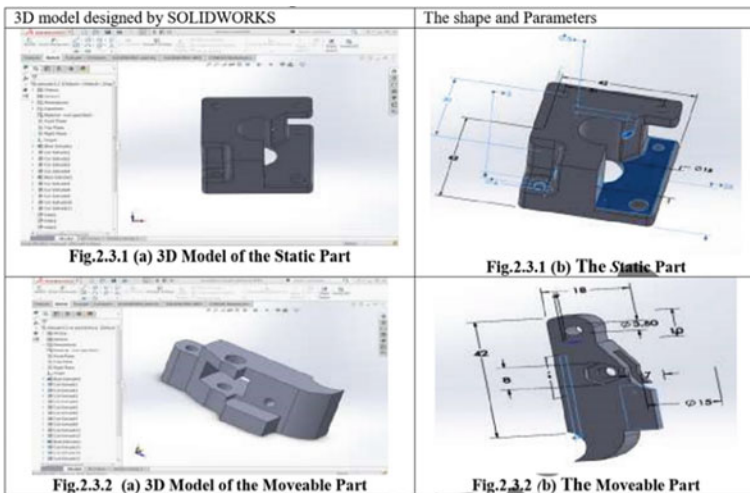


Fig. 44.3 Parts of Bowden Extruder [15]

extruder has two parts one is static part and other is solid part. Static part is in contact with stepper motor and the moveable in contact with the static part. Bowden extruder is having very good accuracy. Although, when the part to be printed is having sharp and very less thickness than there is some error can be seen. When part is printed using Bowden extruder then sometime warping can also be observed [16], as show in Fig. 44.2(b) [30].

44.3 Multi-Extruder Single Nozzle for Colour Mixing

In this system two extruder were used to feed two different colour filaments in a single nozzle, where both filaments get melted. Figure 44.4a shows the design of such type of nozzle. As shown in Fig. 44.4b, Han et al. used NX and ICEM CFD meshing software to design a CAD model and FEM model of this colour mixing multi-extruder nozzle [17]. They presented the velocity field and pressure field distribution at hole of nozzle. According to the combined effect of temperature field and feed speed, intersection area was built. After satisfactory results obtained from simulation, nozzle design was finalised and then experimental analysis was done which resulted in a nozzle which was capable of producing mixed colour artefacts stably.

Emphasis was given on reasonable simplification of model—like simplified heating block in which the angle between horizontal surface and the surface at which threaded hole for the filament pipe is located, is 30° . This inclination is helpful for the assembly of filament pipe and it also increased heat dissipation. To carry out the experiments ABS filament was used, as it is having good impact and tensile strength (Dudek 2013). The success design should provide complete melting and proper mixing of feed material at the point of intersection and optimal combination of filament feed speed and temperature field was found by comparing the results.

As shown in Fig. 44.4(c), molten filament accumulation was observed and also, at 230°C temperature it was seen that layers cannot stick to each other and liquidity is high due to which material is not able to extrude completely. All these outcomes show that there a design flaw exist at intersection in heating block.



Fig. 44.4 a Assembly of entire model, b 3D model of flow channel and c 3D printed objects [17]

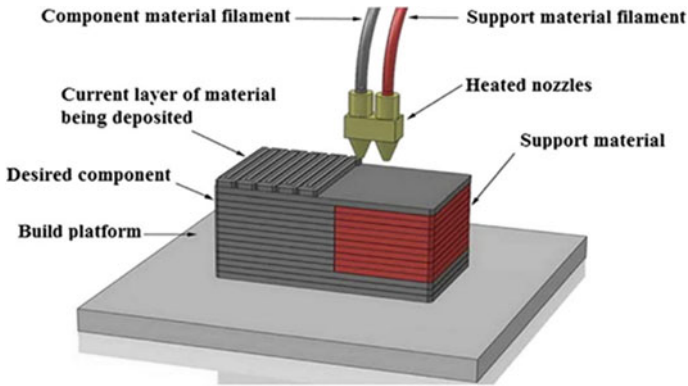


Fig. 44.5 Dual Nozzle 3D Printer [13]

44.4 Multi-Nozzle Extrusion System

Single nozzle FFF 3D printer has some limitation. It is having slow printing speed, it takes more time to print thin parts with increased accuracy, and multi-colour printing is not possible. For handling all these problems multi nozzle systems come in the picture. More than one nozzle is employed in such systems. Each nozzle can print different material. Working principle of multi nozzle extruder is not different from single nozzle extruder. One of the main aims to use multi nozzle system is to reduce the printing time by increasing the speed of printing. Generally, work of second nozzle is to print the support material for the hanging part [18] (Fig. 44.5).

Some 3D printers use more than two nozzles. RoVa3D is such 3D printer which is having five nozzles with five extruder [31]. The major constraint of the multi-extruder multi-nozzle system is the heavy weight and more power consumption because such systems having more than one melting chamber and extruder motor system. Bowden-type extruder are employed to separate hot-end and cold-end of an extruder. It increases the print volume and print speed significantly [13]. Ali et al. proposed extruder model in which five nozzles are present and each nozzle accept different filament. This design provides the flexibility of printing five different colours or materials without any hindrance [13]. This complete assembly of nozzle and extruder is embedded in the carriage and this carriage having movement as per the movement of stepper motor (Fig. 44.6).

44.5 Fused Deposition Modelling of Metals [20]

In this design, a FDM 3000 system is used because of its functions such altering build parameters viz, material flow rate, deposition head motion, liquefier and chamber temperature and tool path commands. Figure 44.7a and b show the initial design

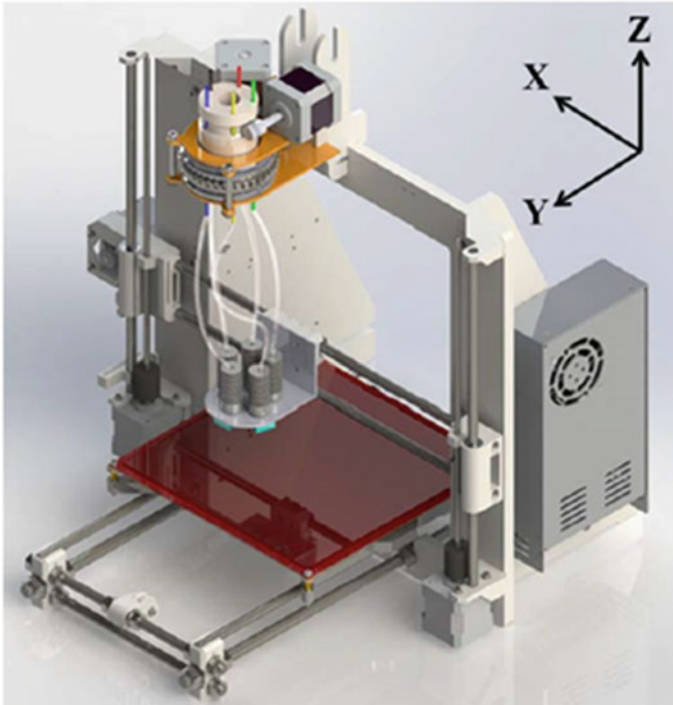


Fig. 44.6 Multi-Nozzle 3D Printer [19]

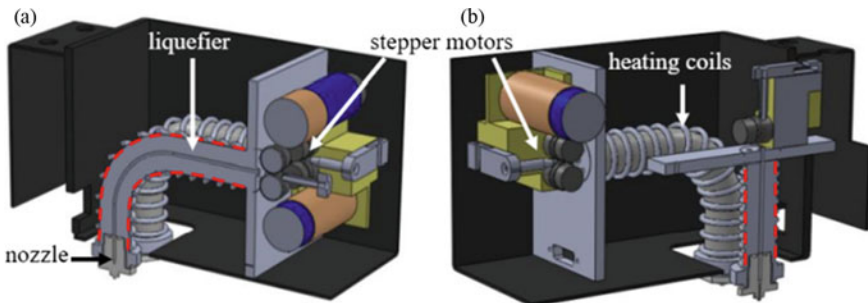


Fig. 44.7 a Initial design of liquefier and b redesigned liquefier [20]

for a FDM 3000 deposition head and the redesigned liquefier implemented here respectively.

The redesigned melting chamber/liquefier is straight in shape while previous one was curved. The objective of designing the melt chamber is to reduce the driving force required to deliver the material and also to reduce the puddling effect as well due to extra material which gets dispensed even after the stepper motors are stopped.

The length of liquefier was also reduced to achieve uniform thickness by improving transient response, to reduce the driving force, which is the cause of buckling and pudding by reducing pressure and to generate a small temperature difference between melt chamber inlet and outlet by improving heat transfer.

After modelling, assuming ideal conditions, significant differences were seen that justified the need for improved liquefier design over the original liquefier. Microstructural analysis showed stronger bonding between layers with variation in coarseness in microstructure along the layer interface which affects conductive and mechanical characteristics. This research opened the gateway towards the utilization of redesigned FDMs setups with various material deposition head to build metallic components using higher strength alloys.

44.6 Fused Filament Fabrication of Metallic Glasses [21]

Unlike the conventional 3d printing techniques which depends on thermoplastics this research focusses on the printing of the metallic glasses as a filament material like the bulk metallic glass (BMGs). As the metallic glasses has superior strength and better structural performance, but the main challenge is that unlike the thermoplastic they don't have go continuous softening with rise in temperature. But the BMG has a special property to acts like a super cooled liquid and undergoes continuous softening with rise in temperature. The BMGs has amorphous structure which enables it to possess high strength and elastic limits, along with other mechanical properties like corrosion resistance and fracture toughness. To optimise the metallic properties of BMG with its amorphous abilities researchers has originated a new processing route (FFF-based 3D printing) to a unique material class (BMGs).

The BMGs are acted by a series of operations in atmosphere of argon, heated upon crystallisation temperature, flipped several times and are cooled to room temperature to make ready as BMG rod to feed in FDM extruder as a filament. These rods were fed to extrusion head. The experimental data shows that the most optimised temperature for extrusion is about 460 degree having the appropriate viscosity and the time difference for crystallisation. The feeding system is installed with modified numerically controlled milling table, having custom written G codes for tool path but acted by automatic arrangements. A pulse joule heater is installed to heat the pre-extruded layer below nozzle. The experimental data shows that the feed rate achieved by the assembly is about 10 mm³/s and the and the feed force for the stepper motor is < 100 N which can vary during starting or stopping (Fig. 44.8).

The mechanical properties test on the 3D printed object applying the FFF-based 3D printing on BMGs it is obvious that they have better strength and toughness which provide an edge to it over the conventional 3d printing using thermoplastic. Also, unlike the conventional method having a close space for extrusion, extrusion can be carried out in air with the help of FFF technique. The surface of extruded object shows no significant effect with extrusion in open air (Figs. 44.9).

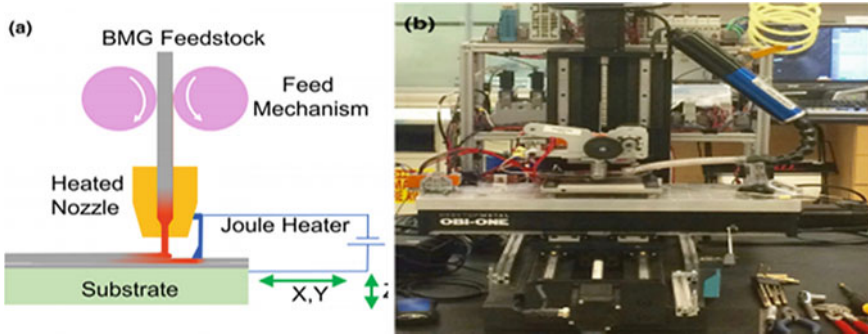


Fig. 44.8 a Schematics of BMG based FDM process; b BMG based 3D printer [21]

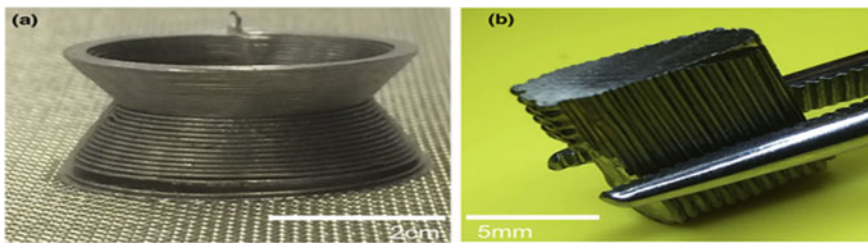


Fig. 44.9 FFF printed part using BMG a continuous 3D printing b start-stop 3D printing [21]

Much research is needed to be done in the field of FFF based 3D printing. Effects of Printing speed, nozzle diameter, and printing forces and other parameters, yet to be explored.

Also, mostly the feeding force needed in the stepper motor is between 10 and 100 N. But it can vary as the in starting and stopping and even when input conditions changes. In case of 3D printers, practically it is very difficult and expensive to realize forces more than 1000 N while forces below 10 N are difficult to control. The softening of the BMGs to form the feeding rod is a challenge. In the extrusion head as the range of optimality is minute for the temperature and pressure. at low temperatures, viscosity is high so it demands high extrusion torque, whereas at high temperature viscosity is low, which provides short processing timing.

44.7 Bonding Quality Affected by Processing Conditions [22]

The main objective of the researchers was to emphasis the phenomena of bonding between the adjacent layer of the filament wire after the extrusion. The bonding phenomena are largely affected by the thermal energy of the filament material.

This approach deals with the most common challenge of the conventional technique approach as its domain of validity is limited, they neglect the micro level phenomena of partial bonding between filament and they largely effected by the determination of fitting parameters. Researchers carried out the experiment on the pre-defined ABS specimen setting the temperature as 260° using nozzle of diameter 0.035 mm. the flow rate and the extrusion rate was fixed to a pre-defined value. during the extrusion, the temperature is monitored using 0.0118 mm K-type thermocouples. The filaments bond quality was validated on basis of the meso structure characteristics and three-point bending tests results. Figure 44.10a show the general FDM setup for experiment.

Figure 44.10b shows the bond formation process between two adjacent filaments. Temperature is the most promising character to determine the properties of the extruded part, and it depends of the rate of cooling after which it extruded from extrusion head. The experimental data indicates that the temperature gradients rapidly decreases along the width and height of the deposited filament. The result was obvious as the filament size is minute. To simplify the inference the cooling process of single filament is converted to one-dimensional transient heat transfer model and ellipse is assigned as moulded cross-sectional shape. It is observed that the temperature of liquefied is 260 degree but when it leaves the nozzle tip, the temperature degree. The liquefier control system, the delay in time in monitoring and the response time of thermocouple justify the temperature difference.

The neck growth phenomena are more frequent in the lower layer then the top layer due to the above observation that the bottom layer remains at higher temperature for long time then the top layer. The experimental data on the specimen agree with the theoretical prediction. When the extrusion process occurs due to the motion of filament, the temperature of region change. This changes the cooling rate effecting the bond strength. Healing theory explains the mechanical properties of healed surface with varying the temperature. Data results are affected by mesostructured, from sintering and creep behaviour. Change in cooling condition determines the surface finish of different locations. Experiments confirms that mesostructured, quality and finish of the bonding between filaments depends on the heating temperature and the changes in convective conditions within extrusion head. It can be concluded that the cooling rate is the most promising factor for determining the mechanical properties and accuracy of extruded part.

44.8 Real-Time Monitoring

For better quality control of printed part, real time monitoring is needed [23]. According to Turner and Gold controlling flow rate using process monitoring, FDM resolution can be improved [11]. According to Huang et al. unavailability of sophisticated sensors for real time monitoring is the one of the area to be explored in AM technologies [24]. During depositions of layers, temperature, flow rate, and shear rate of melt are important factor to decide the properties of printed part. These parameters

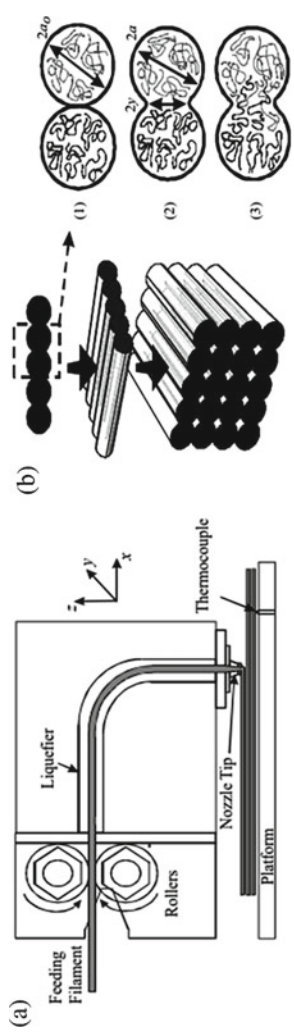


Fig. 44.10 a Schematic of the FDM 2000 filament extrude deposition; b Bonding between filaments; 1. surface contact; 2. neck growth; 3. molecular diffusion at interface and randomization [22]

should be monitored to get better properties of printed part. Coogan et al. designed an in-line sensor for the real-time monitoring of various process parameters of 3D printing process. They used a temperature sensor, encoder to measure feed rate of filament, and a pressure sensor to build rheometer [25]. Rheology helps to calculate force and torque requirements of extruder by determining material flow, shear rate and velocity profiles and all these parameters affect the final properties like strength and shape of printed part [11, 26].

Coogan et al. designed a nozzle system in which many elements, as shown in Fig. 44.11, were embedded. This nozzle is having a port hole which is to be used for pressure measurement (Fig. 44.11a). It is also having a load transfer bar as shown in Fig. 44.11b. This load transfer bar is attached with pressure port hole on the nozzle and directly contacting the melted filament. A temperature sensor is also embedded in this load transfer bar as shown in Fig. 44.11c. This load transfer bar is connected with a clamp at another end. A load cell is rigidly fixed with body of nozzle at one end and another end is connected with clamp. Pressure of melt is measure by this load cell. There is some voltage change in this load cell and this voltage change is mapped as per pressure change. A data acquisition system is used to collect the data from this rheometer. Pulses from stepper motor are counted by the data acquisition system and feed rate is calculated. Similarly, thermocouples also send the temperature data in form of voltage change through a signal conditioner to the data acquisition system. All these data collected by data acquisition system is sent to personal computer for analysis and interpretation. Figure 44.12 shows the complete set of data acquisition system.

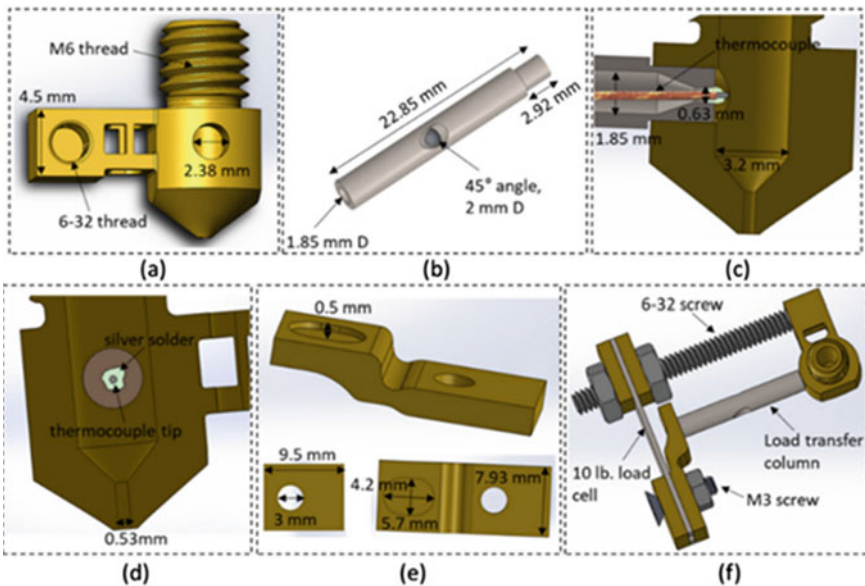


Fig. 44.11 Different components of customized in-line rheometer [25]

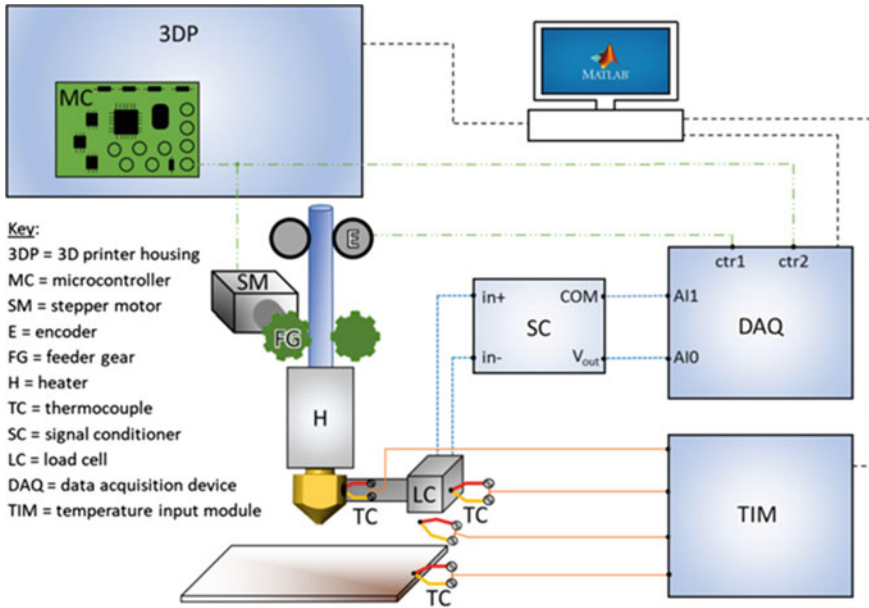


Fig. 44.12 Controllers, sensors, conditioners, and data acquisition system [25]

44.9 Numerical and Analytical Analysis of 3d Printer Extruder

The temperature distribution through the extruder, is helpful in design of extruder geometry of a filament-based 3D printer. S. Singh et al. developed a CFD model and different heat sink fins profile were analysed for working material poly-lactic-acid (PLA) [27]. In order to give continues supply of material to the heat block there should not be melting of material in the heat sink chamber. And hence the surface area of the heat sink is needed to increase and due to which fins are provided on heat sink. Tadmor et al. assumed a constant thermal conductivity of PLA, i.e. 0.195 W/m–K [26]. According to Pyda et al. specific heat capacity of PLA is dependent on temperature [28] (Fig. 44.13).

Boundary conditions applied in this model are—heat transfer coefficient of external surface, constant velocity at the point where filament is pushed in the melting chamber, pressure at the opening of nozzle, heating chamber as heat generation body. Effective heat transfer coefficient of exterior surfaces of hot end is calculated assuming the convection and radiation as the mode of heat transfer. Now temperature distribution inside the extruder is determined for different fins like circular, triangular, elliptical and rectangular having elliptical perforation fins. And it is found that temperature at the top of the heat sink is near about 370 K which is quite under the desirable conditions. And it is also less as compared to the other design of heat

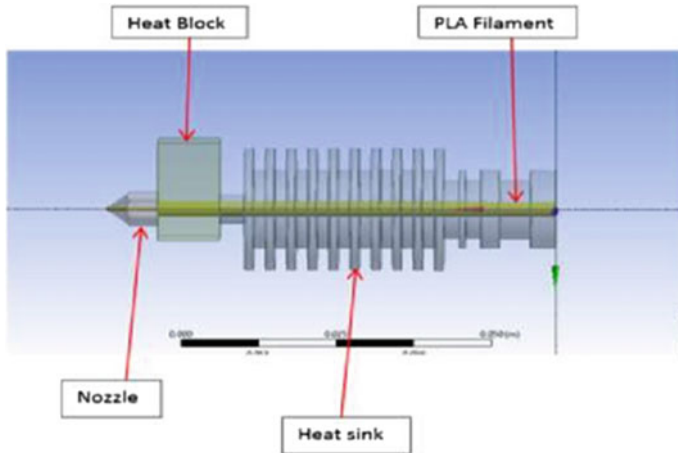


Fig. 44.13 Solid model of liquefier with PLA space filled [27]

sink and hence fulfilled the optimum condition and shows the desirable temperature variation throughout the liquefier.

44.10 Conclusion

In this paper various types of extruders and nozzles for filament operated 3D printers along with their features and functions has been discussed. It was found that direct type extruders are not faster and having slippage problem. On the other hand, Bowden type extruder cannot handle flexible filaments. Direct and Bowden extruder can be differentiated on the basis of distance between hot end and cold end of extruder. In multi extruder single nozzle type system, more than one filament can be feed in a liquefier, where the get melted and extrude out of nozzle to deposit as layer. Filaments could be of different colours to print a colourful part. In multi nozzle system more than one nozzle are used and each nozzle can print different materials. But more than one extruder, nozzle system would be bulky as it will carry a number of motors, rollers and bearing. It will slow down the printing speed as well as increase the power consumption. To handle this problem a suitable mechanism was discussed in the paper.

During depositions of layers temperature, flow, and shear rate are important factor to decide the properties of printed part. For real-time monitor all these parameters and process control, a rheometer, pressure sensor, and a thermocouple were incorporated in the nozzle. All the data for those parameters was collected by a data acquisition system and then sent to computer for analysis. This real time monitoring of 3D printing process is helpful in improving the parameters for better properties of 3D printed part.

From above study, it is clear that there is scope of development of a hybrid type FDM 3D printer. This hybrid FDM 3D printer will be capable to accept feed material in the form of filaments as well as pellets or granules. Real-time monitoring system can also be implemented in this hybrid FDM based 3D printer for better process control.

Acknowledgements This work was supported by the Science and Engineering Research Board (SERB)—DST under its Start-up Research Grant (SRG) scheme [Grant Number—SRG/2019/000943].

References

1. 52900: Standard Terminology for Additive Manufacturing—General Principles—Terminology. ASTM International (2015)
2. Sivadasan, M., Singh, N.K.: Rapid tooling road to rapid manufacturing. In: IEEE International Conference on Industrial Engineering and Engineering Management. vol. 2017-Decempp. 1556–1560 (2017)
3. Melchels, F.P.W., Feijen, J., Grijpma, D.W.: A review on stereolithography and its applications in biomedical engineering. *Biomaterials* (2010)
4. Yap, C.Y., Chua, C.K., Dong, Z.L., Liu, Z.H., Zhang, D.Q., Loh, L.E., Sing, S.L.: Review of selective laser melting: materials and applications. *Appl. Phys. Rev.* (2015)
5. Vyavahare, S., Teraiya, S., Panghal, D., Kumar, S.: Fused deposition modelling: a review. *Rapid Prototyp. J.* (2020)
6. Gokhare, V.G., Raut, D.N., Shinde, D.K.: A review paper on 3D-printing aspects and various processes used in the 3D-Printing. *Int. J. Eng. Res. Technol. (IJERT)* **6**, 953–958 (2017)
7. Jones, R., Haufe, P., Sells, E., Iravani, P., Olliver, V., Palmer, C., Bowyer, A.: Reprap—the replicating rapid prototyper. *Robotica*. **29**, 177–191 (2011)
8. Albu, S.C., NuȚiu, E.: Study on designing the extruder for 3D printers with pellets. *Acta Marisiensis. Seria Technologica* **16**, 19–22 (2019)
9. Medellin-Castillo, H.I., Zaragoza-Siqueiros, J.: Design and manufacturing strategies for fused deposition modelling in additive manufacturing: a review. *Chinese J. Mech. Eng. (English Edition)*. **32** (2019)
10. Osswald, T.A., Puentes, J., Kattinger, J.: Fused filament fabrication melting model. *Additive Manufacturing* (2018)
11. Turner, B.N., Strong, R., Gold, S.A.: A review of melt extrusion additive manufacturing processes: I. Process design and modeling. *Rapid Prototyp. J.* **20**, 192–204 (2014)
12. Tlegenov, Y., Hong, G.S., Lu, W.F.: Nozzle condition monitoring in 3D printing. *Robot. Comput.-Integrat. Manuf.* **54**, 45–55 (2018)
13. Ali, M.H., Mir-Nasiri, N., Ko, W.L.: Multi-nozzle extrusion system for 3D printer and its control mechanism. *Int. J. Adv. Manuf. Technol.* **86**, 999–1010 (2016)
14. Abilgazyev, A., Kulzhan, T., Raissov, N., Ali, M.H., Match, W.L.K.O., Mir-Nasiri, N.: Design and development of multi-nozzle extrusion system for 3D printer. 2015 4th International Conference on Informatics, Electronics and Vision, ICIEV 2015 (2015a)
15. Hoque, M., Kabir, H., Jony, M.H.: Design and construction of a bowden extruder for a Fdm 3D printer uses 1.75 Mm Filament. *Int. J. Tech. Res. Sci* **3** (2018)
16. Wang, T.M., Xi, J.T., Jin, Y.: A model research for prototype warp deformation in the FDM process. *Int. J. Adv. Manuf. Technol.* **33**, 1087–1096 (2007)
17. Han, S., Xiao, Y., Qi, T., Li, Z., Zeng, Q.: Design and analysis of fused deposition modeling 3D printer nozzle for color mixing. In: *Advances in Materials Science and Engineering* (2017)

18. 3DPrinterPrices.net: Dual Extruder 3D Printers—What You Need to Know (2007)
19. Abilgazyev, A., Kulzhan, T., Raissov, N., Ali, M.H., Match, W.L.K.O., Mir-Nasiri, N.: Design and development of multi-nozzle extrusion system for 3D printer. 2015 4th International Conference on Informatics, Electronics and Vision, ICIEV 2015. Institute of Electrical and Electronics Engineers Inc (2015b)
20. Mireles, J., Espalin, D., Roberson, D., Zinniel, B., Medina, F., Wicker, R.: Fused deposition modeling of metals. In: 23rd Annual International Solid Freeform Fabrication Symposium - An Additive Manufacturing Conference SFF 2012, 836–845 (2012)
21. Gibson, M.A., Mykulowycz, N.M., Shim, J., Fontana, R., Schmitt, P., Roberts, A., Ketkaew, J., Shao, L., Chen, W., Bordeenithikasem, P., Myerberg, J.S., Fulop, R., Verminski, M.D., Sachs, E.M., Chiang, Y.M., Schuh, C.A., John Hart, A., Schroers, J.: 3D printing metals like thermoplastics: fused filament fabrication of metallic glasses. *Mater. Today* **21**, 697–702 (2018)
22. Sun, Q., Rizvi, G.M., Bellehumeur, C.T., Gu, P.: Effect of processing conditions on the bonding quality of FDM polymer filaments. *Rapid Prototyp. J.* **14**, 72–80 (2008)
23. Mani, M., Lane, B., Donmez, M.A., Feng, S.C., Moylan, S.P., Fesperman, R.: Measurement Science Needs for Real-time Control of Additive Manufacturing Powder Bed Fusion Processes; NIST interagency/internal Report (NISTIR)—8036 NIST Interagency/Internal Report (NISTIR) 8036, 50 (2015)
24. Huang, Y., Leu, M.C., Mazumder, J., Donmez, A.: Additive manufacturing: current state, future potential, gaps and needs, and recommendations. *J. Manuf. Sci. Eng. Trans. ASME.* **137** (2015)
25. Coogan, T.J., Kazmer, D.O.: In-line rheological monitoring of fused deposition modeling. *J. Rheol.* **63**, 141–155 (2019)
26. Tadmor, Z., Gogos, C.G.: *Principles of Polymer Processing*. Wiley (2006)
27. Singh, S.K., Satankar, R.K.: Numerical and analytical analysis of 3D printer extruder in fused deposition modelling. *J. Emerg. Technol. Innov. Res.* **4**, 10–22 (2017)
28. Pyda, M., Bopp, R.C., Wunderlich, B.: Heat capacity of poly(lactic acid). *J. Chem. Thermodyn.* (2004)
29. Guide to Choosing My 3D Printer Extruder. Bitfab (n.d.)
30. Khau, V., Lourey, E., Napau, S.: 3D Printing Tips and Tricks (n.d.)
31. RoVa3D 5 Nozzle FDM 3D Printer (n.d.)

Chapter 45

Extruder Design in Pellets Operated 3D Printers: A Review



Krishnanand, Varanjot Singh, Vatsal Mittal, Amar Kumar Branwal, and Mohammad Taufik

Abstract The pellets/granulate/flakes operated 3D printer is a novel layer by layer part fabrication technique based on the extrusion of the pellets particles using the mechanism of screw extrusion and positioning system. When the mechanism of the screw extrusion has been complete in a single stage, the single screw design could be included to form a group of pellets operated 3D printers. Similarly, in the case of a double-stage screw extrusion system, two screws 3D printers could be used with a relatively large diameter for the first stage screw. The hopper, screw, heating system, temperature sensor, barrel, nozzle, and positioning system are the most common elements in the design of pellets operated 3D printers. Materials with high flexibility will have great potential as pellets operated 3D printer materials. In this paper, a single-stage screw extrusion, double-stage screw extrusion, flexible, and non-flexible material extruder designs for pellets operated 3D printers have been studied. Apart from this, the process parameter behaviour of the pellets operated 3D printers has also been studied. Literature showed that the based on the variation in the extruder design number of the process parameters varies. The number of the elements in the design of the extruder responsible for the overall build volume or size of the machine which greatly varied when compared with the conventional 3D printers. This effect may lead to an increase in resistance to large part fabrication, and thus increase the portability resistance of the pellets operated 3D printers.

Keywords FDM · Pellet operated 3D printer · Screw extrusion

45.1 Introduction

A modern manufacturing method in which product is manufactured in additive manner by layer by layer deposition of material using some digital data in the form of 3D CAD model, is known as Additive Manufacturing [1]. Additive manufacturing is also having various names such as rapid prototyping and 3D printing. There are

Krishnanand · V. Singh · V. Mittal · A. K. Branwal · M. Taufik (✉)
Department of Mechanical Engineering, Maulana Azad National Institute of Technology
(MANIT) Bhopal, Bhopal 462003, India
e-mail: mohammad.taufik@manit.ac.in

© The Author(s), under exclusive license to Springer Nature Switzerland AG 2022
R. Pratap Singh et al. (eds.), *Proceedings of the International Conference on Industrial and Manufacturing Systems (CIMS-2020)*, Lecture Notes on Multidisciplinary Industrial Engineering, https://doi.org/10.1007/978-3-030-73495-4_45

various additive manufacturing technologies but Stereolithography (SLA), Selective Laser Sintering (SLS), and Fused Deposition Modelling (FDM) or Fused filament Fabrication (FFF) are well known among them [3]. All these 3D printing technologies provides design freedom and complex geometry of product to be manufacturing is not a barrier [6]. FFF is widely used and most popular 3D printing technology [20, 21]. In FFF, some solid material is fed into a channel where it gets melted and convert into semi-solid form, and then this semi-solid material is extruded out of a very precise opening nozzle. Nozzle deposits the material in layer over layer by numerical control movement [12] (Fig. 45.1).

FFF technology is having numerous applications. FFF is widely used in medical industry for 3D printing prosthetic limb, other body parts, medical instruments, skin printing, and tissue engineering [19]. 3D printing having application in manufacturing industry for preparing automotive and aerospace parts [14]. It is also used in clothing, accessories and fashion industry [10]. FFF or FDM is also used in academics for better teaching methods [22] and it is also used in construction field [15].

In FFF or FDM, polymers [7], biomaterials, food materials, composites [17], and many other materials can be used as printing material, but polymers like—ABS and PLA are used at wider scale. Feed material for FFF is generally in the form of filament. To feed this filament in liquefier an extruder is used. Extruder is consisting of two parts—one is moving parts or cold end and the other is hot end. Cold is made up of a roller and a bearing, in between them filament is placed. Roller is attached with stepper motor to push the filament inside the liquefier. For proper working of this filament based FFF 3D printer, filament should not be flexible, it should not be buckle during printing process. Filament of flexible materials are not suitable for such 3D printers. Here, comes another type of extrusion-based 3D printer in which feed material is in form of pellets or granules rather than in form of filament. Such 3D printers are having different design and working principle of extruder and nozzle.

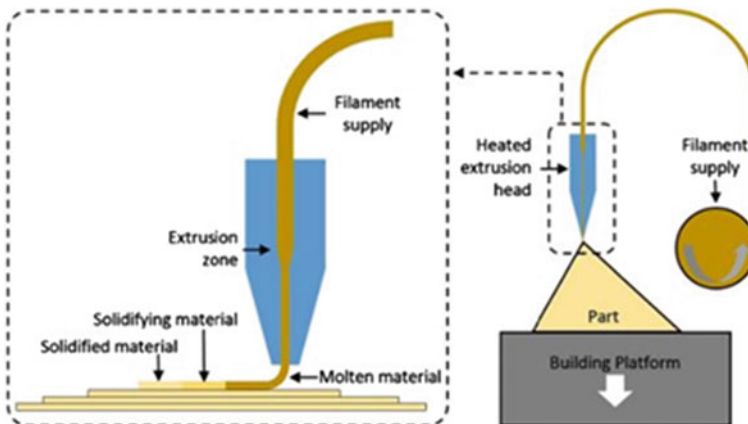


Fig. 45.1 Schematic of FFF 3D printer [6]

Hopper, rotating screw inside extruder, and numerically controlled nozzle are main components of such 3D printers.

45.2 Design of Pellet Operated Extruders

In this review paper, various designs of pellet (also called as granulate/flakes as per dimension and shape of the input material) operated 3D printers/extruders have been discussed. Pellet operated 3D printers use screw extrusion system. Single-stage screw extrusion, double-stage screw extrusion, flexible, and non-flexible material extruder designs for pellets operated 3D printers and similar have been discussed. Apart from this, the process parameter behaviour of the pellets operated 3D printers has also been studied.

As the name suggest, this type of 3D printers contains only one screw-extruder. Design mainly consisted of a hopper to contain the material that's going to be printed, motor driven screw to transport the material to the nozzle, heating system, temperature sensor and attachments to assemble the prototype to 3D printer. Stepper motor is used to drive 10 mm dia. 66 mm long auger. An aluminium extruder was made, to prevent extruder spinning in the hopper, it was locked using screws in the four holes in horizontal direction, at the top of it [23]. A cooling fan was installed for increasing heat dissipation and to increase print quality. Researcher used the final prototype for printing with shredded PET and PLA. An auger is used to pass the material from to nozzle via extruder and this auger is rotated by a DC motor. There is total two fans were used, one to prevent the hopper from being heated and another to make the temperature of printed part equal to surrounding temperature (Fig. 45.2).

Researcher printed various parts to show the working of this design but there are some limitations also. High working temperature may damage the hopper. Two solutions were provided in order to tackle with this problem. First is to make hopper

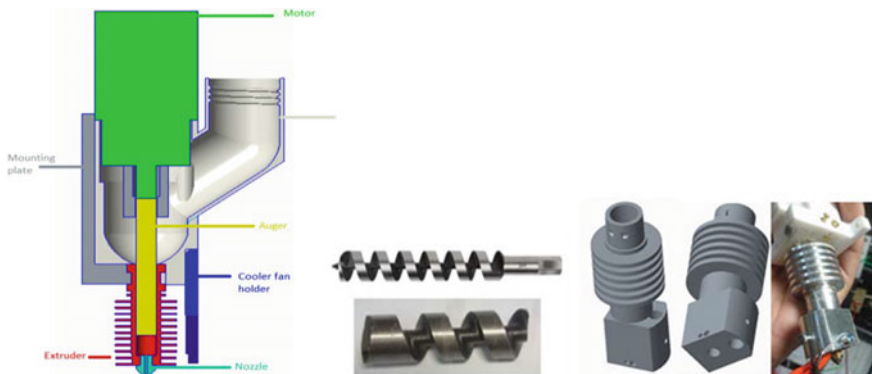


Fig. 45.2 Single stage screw extrusion design [23]

from high temperature resistant material that would increase its cost as well as weight. Secondly, we can apply insulation between hopper and extruder, so that there is no direct thermal contact. Another limitation which is general in pellet-based extruder is irregular flow of the melted plastic which degrades the print quality. Traditional filament-based printers have good melt flow control that is prime necessity. For poor flow control there may be various reasons like less time to heat, insufficient heat to melt properly. To sort out this problem, extruder of greater length can be used. Anna Bellini et al. presents the development of a set-up, which is having a small extruder at a highly precise positioning system [4]. This system accepts pellet or granules as feed material. Positioning system was made of high precision using servo drives, which allow to track the velocity and torque. The extruder assembly was installed on a table of high load wearing capacity and smooth motion with help of linear bearing.

Many experiments were done with different nozzle diameter but due to clogging of nozzle continuous flow is interrupted. Reason for this phenomenon is large amount of heat dissipation from the outer surface of the nozzle and adapter. From the repetitive experiments with the T16 (0.4064 mm diameter) nozzle, clogging problem was not seen, there is improvement in the flow [5]. So, it could be understood that using nozzle diameter greater than T16 will eliminate the clogging problem.

Liu et al. developed a double stage screw extrusion 3D printer. In this extrusion system two screw at different stages are used. Purposes of first stage screw are to melt and increase pressure and send the material to next stage [13]. First stage screw is also having larger diameter compared to second stage screw. The purpose of second stage screw is to plasticizing and controlling the melted material. To monitor the pressure, a pressure sensor is also inserted between these two stages. The pressure of melt could be controlled by controlling the speed screw at the first stage. Formation of bubbles is not desirable in the extrusion, to eliminate this problem, a vent hole is made at a place where two stages are in contact, to make the gas leak out of it. There are heating elements on the cylinder of heating zone, they generate heat to convert pellets into pressurised melt. Then rotating screw send this pressurised melt to next stage. In this process sufficient amount of pressure is generated due to the geometry of screw. Spiral groove on the screw makes its groove depth shallower at front-end compared to back-end. Melted pellets in second stage are extruded out of nozzle by rotation of metering screw, to print the parts (Fig. 45.3).

This extrusion system is having large print volume. It is having economically high printing speed for large parts. 3D Printing with filament has been extensively used for making products of different materials and sizes. During material selection to make filament, various properties of materials are checked. It should be rigid and melt should be viscous for easy squeezing out of nozzle. Commercially available filaments are not flexible [9]. These are made up of materials which is having high impact and tensile strength like—ABS [8]. Due to demand of these properties, filament making cost increases. Therefore, using polymer pellet in 3D printing is economical and easy to process.

Figure 45.4 shows the construction and design of pellet-based extrusion additive manufacturing process to produce a part made from flexible material like- EVA, PLA etc., which is difficult to produce from current famous 3D printing method i.e., from

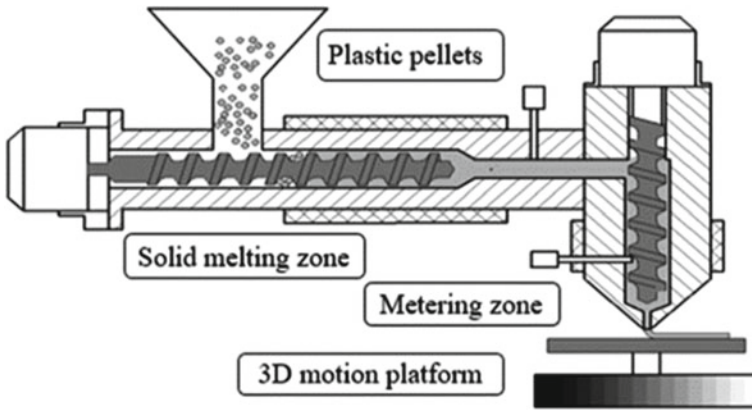


Fig. 45.3 Double stage screw extrusion design [13]

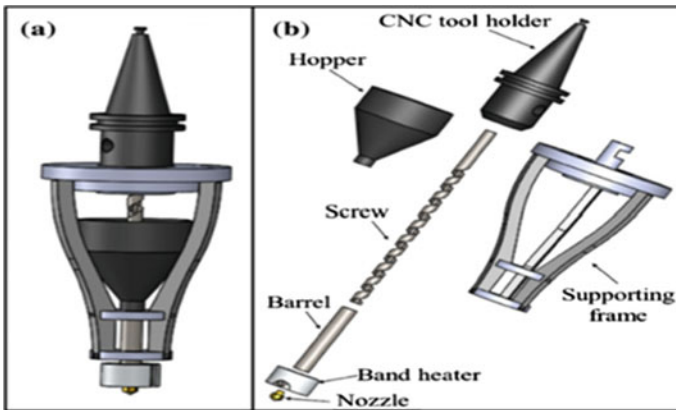


Fig. 45.4 Flexible material extruder design [11]

FDM process because it causes buckling of filament of flexible material. Kumar et al. developed a setup after doing many preliminary tests and through iterations [11]. This setup is categorised in two parts for better understanding of the whole system namely MDT (Material deposition tool) and Motion Subsystem.

As the name suggests, purpose of MDT is to deposit the material in layers and Motion to this tool in X, Y and Z directions, is provided by the motion subsystem. MDT is made up using a supporting frame on which all other components like—hopper, heater, melt channel, screw, etc., are installed. Material is extruded through the nozzle due to screw movement. Pressure difference helps this extruded material to take shape of a thin and long continuous filament (Fig. 45.5).

Singh et al. designed a model of extruder head which can be installed on CNC machine with three-axis [18]. This head could be used to perform FDM process using

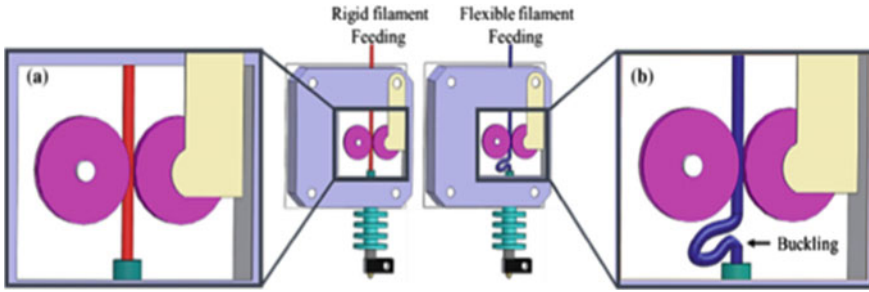


Fig. 45.5 Problem of buckling in flexible materials [11]

CNC. This extruder head is made for easy installation on different CNC-milling machines. Because of high cost of FDM machines compared to other computer-controlled manufacturing machines e.g., milling, turning, has a major obstacle to implementation of rapid product development machine in small and medium industries, therefore this design favourable for small scale industries to develop an economical FDM technique (Fig. 45.6).

Installation of this extruder design on different CNC milling machine because this design includes features like modular approach of selective extruder head, which having isolated, independent functional elements. This design is also having ease of change to achieve interfaces with different CNC machines. Different modules of the proposed extruder head are defined by elements like Nozzle head, Breaker plate, Barrel, Lead Screw, Ring, Cap and Heating Arrangement.

Kumar et al. done the process characterisation of MDT by conducting several experiments. Their process parameters for this characterisation were screw speed and temperature of barrel [11]. They find suitable screw speed below 75 RPM and barrel temperature in range of 100–150 °C (Fig. 45.7).

Furthermore, to know the quality of printed parts various tests per performed including tensile and hardness test. They found that printed part is having elongation

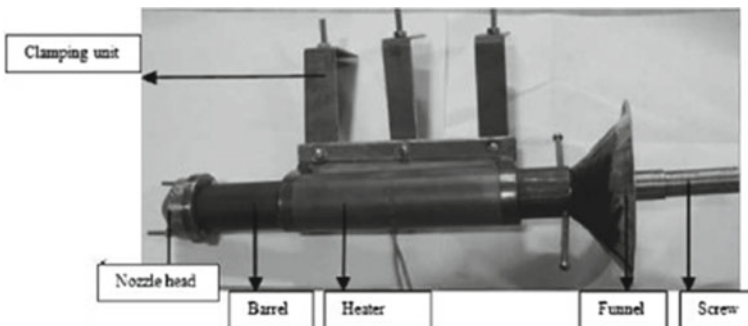


Fig. 45.6 Deign of Extruder head for CNC-assisted additive manufacturing [18]

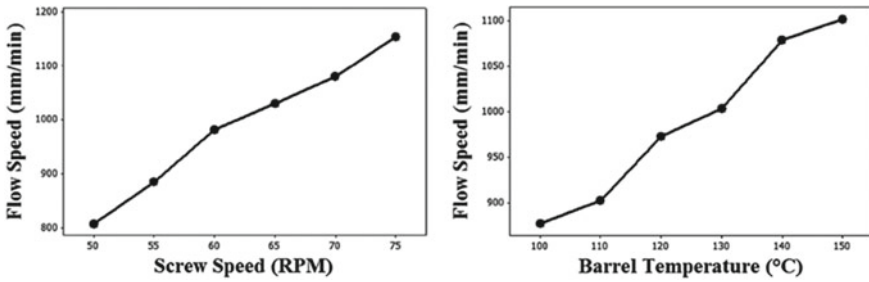


Fig. 45.7 Relation of flow speed with screw speed and barrel temperature [11]

up to 575.5% [11], which is much greater than ABS and PLA parts. After deformation, recovery of up to 60% of undeformed length was seen in hysteresis test.

Reddy et al. developed a process named as extruder deposition process, this process is based on polymer extrusion [16]. Elimination of drawbacks of extrusion-based system is possible using this process. It also produces parts with greater strength compared to other extrusion-based processes (like FDM) available in the market. In most cases failure of filament in FDM processes is because of flexibility or bending, to avoid this different polymer extrusion processes are designed. Bellini et al. designed a system for deposition of ceramics. An extrusion screw, which is having constant pitch and depth of channel, was used in their design. But they found that air is getting entrapped and aggregates a forming during feeding of material [4].

Reddy et al. designed a new system, as shown in Fig. 45.8a, for elimination of various issues in built part quality [16]. To eliminate the problem of air entrapment and to make the printed part stronger, the designed a screw extruder with variable pitch and depth of channel. To deal with aggregate formation in feeding channel, they installed a ceramic tube to feed the pellets of polymer. There is uneven pressure in radial direction around the screw, to reduce this a support is installed at exit point

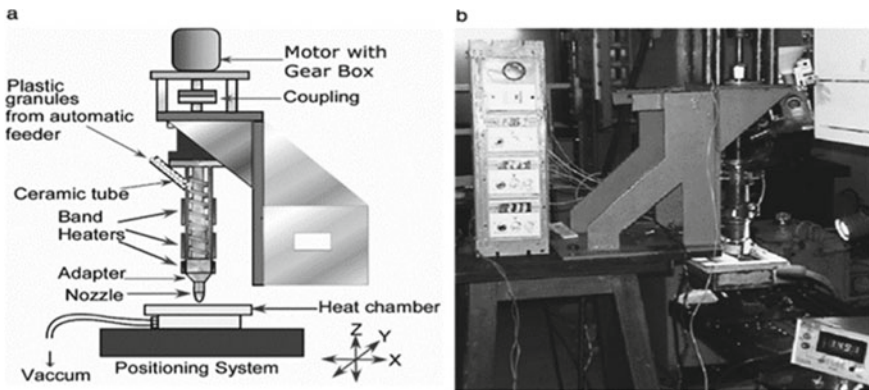


Fig. 45.8 Numerical control (NC) assisted Extruder deposition system: a Schematic; b actual [16]

of nozzle. This support is having an axial hole and also prevents deflections of screw. This whole system is installed on a numerical control (NC) bed (Fig. 45.8b).

For studying the effect of process parameters on surface finish and strength of bond formation, Box-Behnken design was used. Temperature of nozzle, inter road gap and temperature of melt chamber are the three parameters with three levels, which were selected by them for experimental design.

ABS material was used to print the parts so that bond strength can be compared with the FDM systems available in the market. On the basis of above three variables and their effect on inter-road bond strength and Surface finish is determined, and it is found road gap and temperature of nozzle plays much significant role than the chamber temperature. Inter-layer bond strength is also determined.

Whyman et al. design and developed biopolymer paellets extruder (Please refer Fig. 45.9). The design consists of a hopper, heating system, extruder, cooling system and a drip-feeding mechanism as shown in Fig. 45.9a. Material is filled in the hopper and then passed to melting zone in a controlled manner using drip feeder. To melt these pellets a band heater has been used. To reduce the conduction of heat from extruder to other parts, a cooling system has been used provided. In this design a modified auger bit (Fig. 45.9b) has been used to pushed down the pellets from hopper to heating zone and push the polymer melt out of nozzle. This auger bit needs less torque and reduce the stress acting on the drive motor. But in this type of auger lesser pressure is developed as compared to conventional auger with varying pressure regions. But this pressure loss can be easily compensated with help of drip feed (Fig. 45.9c).

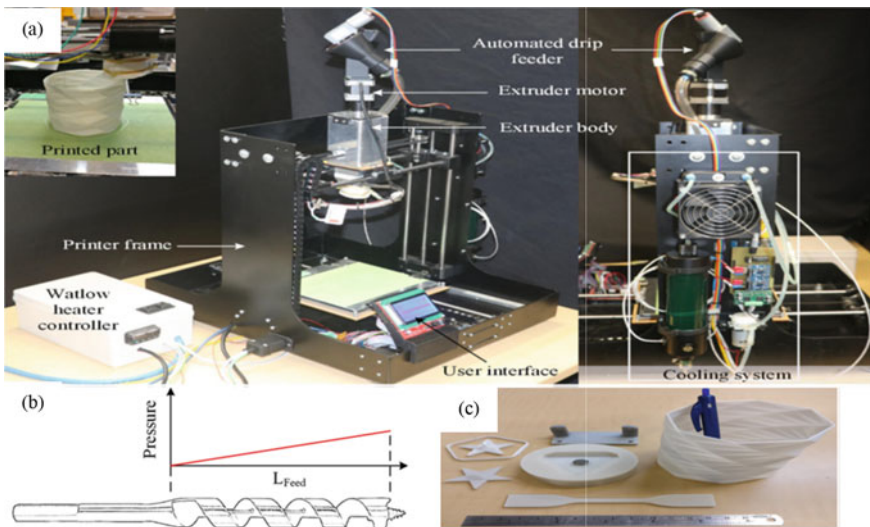


Fig. 45.9 a Complete setup of extrusion system for printing of biopolymer paellets; b Auger/drill bit; c Printed parts [25]

An electric heater along with PID controller has been used to maintain the required temperature. Heating is crucial step in pellet extrusion. If there is any conduction of heat from extruder to other parts like hopper and upper portion of screw, it could lead to partial melting of polymer particles. To deal with this problem a fluid channel around the neck of the extruder has been provided. A coolant with high concentration of glycol is pumped through this channel. Printing bed is a common XYZ cartesian design. Cylindrical guide rails have been provided to all the axis. X and Y axes are pulley driven while Z axis movement is based on lead screw. Researcher developed a compact pellet extrusion system which can print the part with strength, aesthetic quality and shine comparable to counterparts. This print quality is achieved due proper heating and melting of polymer. But there are problems of screw clogging, inconsistent bonding and colour change due to contamination. Solutions like the addition of more sensors to monitor the heating and cooling effects on the system and using a Transducer to determine if the correct pressure is obtained before turning on the drip feeder are still in research phase.

Researchers developed a vertical screw extruder with four feeding ports at different height along the barrel to feed the pellets/granules for wide range of residency time. This design is made up of barrel, screw, heater and nozzle. A stepper motor has been used to control the screw rotation and material deposition rate is controlled by the rotational speed of screw (Fig. 45.10).

Conventionally for filament extrusion of PVOH three steps are followed. In the first step, different compounds are mixed, then filament is extruded and in the last step material is extruded. Due to three step process, this elongated time of material processing leads to thermal decomposition of PVOH. But developed extruder reduced the residual time of polymer melt by a significant amount as all above mentioned steps

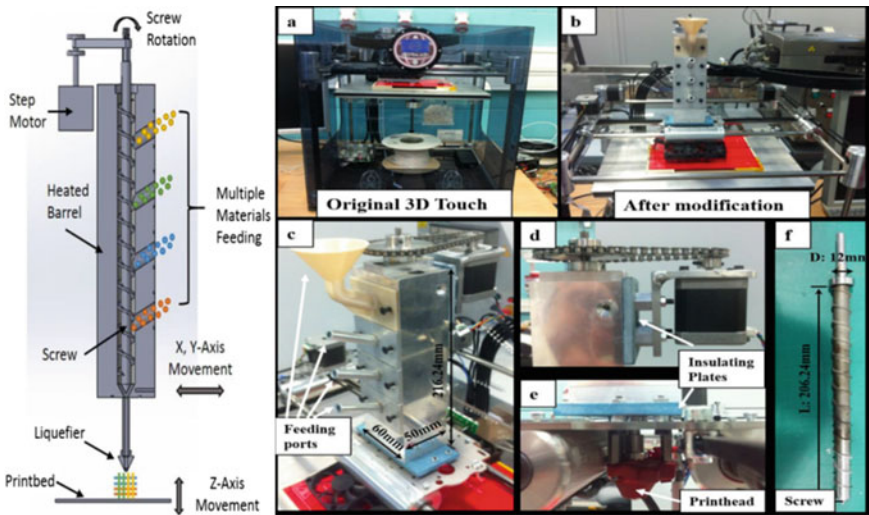


Fig. 45.10 Complete design of extruder with multiple feeding ports [26]

are combined into one. So, this design provides a best method to extrude filament from heat sensitive material or materials that are difficult to extrude into filament with constant diameter. This design can also be used to co-process multiple material at variable feed rates to make a compositionally heterogenous structure. Material being fed through different port has a different residency. Extruder with multiple feeding ports can used to print a wide range of materials by controlling residency time and temperature. Multiple materials with definite ratios can be mixed during the process.

FDM is one of the most popular additive manufacturing techniques used in 3D printing which uses plastic filament material as input. But the material used is little bit costly and generally imported. The main theme of Wankhade et al. work is to design a new extruder system at low cost in terms of material used and process of manufacturing. Here input material is taken in form of pellet and granules which can be of waste plastic materials. The design of this extrusion system used three ceramic band heaters in which two are used in heating the Barrel and one is used in heating the Die. The heater produces heat by positive temperature coefficient hence, producing high temperature by consuming less power input. Moreover, the temperature that can be produced is ranges from 100 to 1300 °C. The Ceramic heaters utilised in this work are shown in Fig. 45.11.

The pellet which is introduced through the hopper is reached to nozzle with the help of the screw, barrel, AC motor and the gear box which reduces the speed of motor to drive the screw with perfect RPM. The screw is divided into three zones feed zone, compression zone and metering zone. In feed zone, the rotation of the screw helps the granules to move down the barrel. In barrel granules are heated using heater and due to heating a contact develop between barrel walls and Plastic granules. This contact increases the friction and help them to move forward. If there is no friction, plastic would only rotate inside the screw. In compression zone plastic is melted due to different forces like compression and shear forces and finally in metering zone the plastic is pumped into the extruder die Fig. 45.12.

Barrel used here covers the screw and connected to the hopper and gear box, it is made up of hardened steel at the front end it is connected to the extruder die from where the extrusion of melted material takes place. The designed made is at low cost and the plastic made through it has better flexibility and remain hot when they

Fig. 45.11 Ceramic heaters
[24]





Fig. 45.12 Screw design and barrel [24]

are removed from the extruder and this allows for post-extrusion manipulations. The strength of the extruded plastics can be increased further by adding the fillers while reinforcing the input raw materials (Fig. 45.13).

In Additive Manufacturing FDM is the most common method of 3D printing and it uses the material in the filament form which are mainly thermoplastics polymer (e.g., ABS). In this paper a new design is made in which the input material is taken in pellet form which costs less as compare to filament one. Pellets are also available easily in market and it can be made from waste material too. The new extruder system is designed by Albu et al. (Fig. 45.14), by considering the aspect of eliminating the discontinuity in the flow of melted polymer and no material extrusion when printing head is changing the position.

To ensure the continuous flow, a conical conveyor worm with two beginnings is designed (Fig. 45.15). In the front of the screw a driver washer is fastened with help of bolts and holes provided on the screw. Whole design can be divided mainly in four sections. In one section an screw has been used to transposrt the pellets to heating zone. Then a section is provided to dessipate the extra heat so that it could not reach to other parts of extruder. This heat dessipation zone is followed by a bearing attachment zone. To drive the swinging mechanism a gear wheel is provided, this gear is connected to an electric motor using a coupler.

Fig. 45.13 Complete assembly [24]



Fig. 45.14 New extruder design for 3D printers [2]

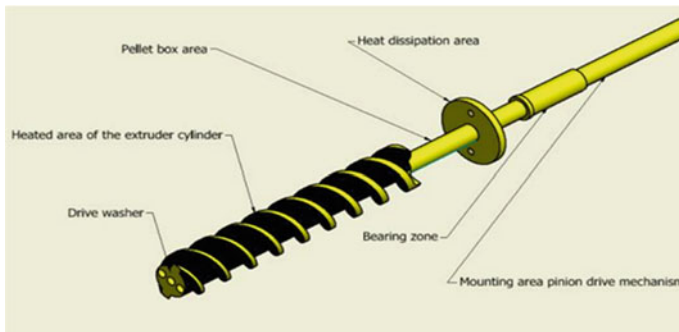
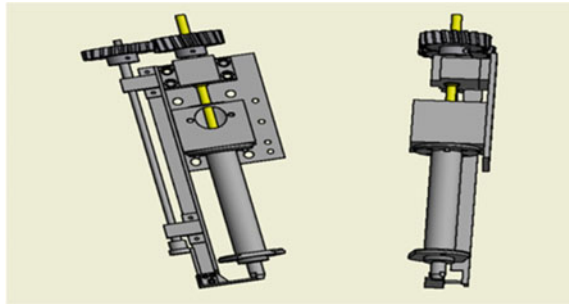


Fig. 45.15 Conveyor worm [2]

An assembly of drive washer and tapered piece was design, which is having two contact position according to the direction of rotation of the motor. This assembly has been used to ensure the retraction of material or to stop the flow of melted plastic.

There are recesses on circumference of drive washer to pass the molten material and enters the tapered piece through the four holes i.e., when the feed worm is rotated in the feed direction of the material, it continues in the recesses on the drive shaft. A cylinder is provided in the front of washer for providing centring between conical piece and two engagement zones. On rotating the feed worm in opposite to feed direction the contact surface would become the opposite of the holes on the conical piece and discontinuing in the recesses on the drive washer and hence through this, retraction of material was tried to be done (Fig. 45.16).

As per the designed discussed the printer was made and several attempts were made with different process parameter and a continuous flow of melted ABS pellets was obtained. On changing the direction of rotation of worm, the retraction was not under control i.e., melted material continues to flow in the projected version. Which was assumed due to high pressure generation inside the extruder and hence improvement was still needed (Fig. 45.17).

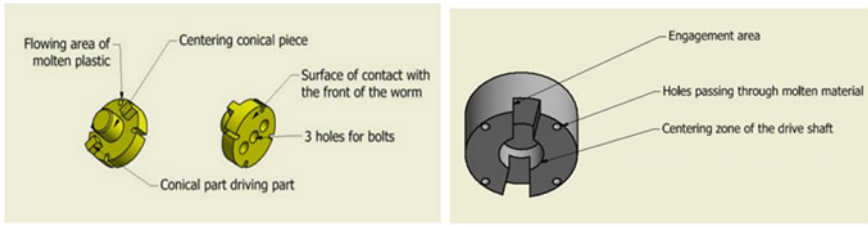
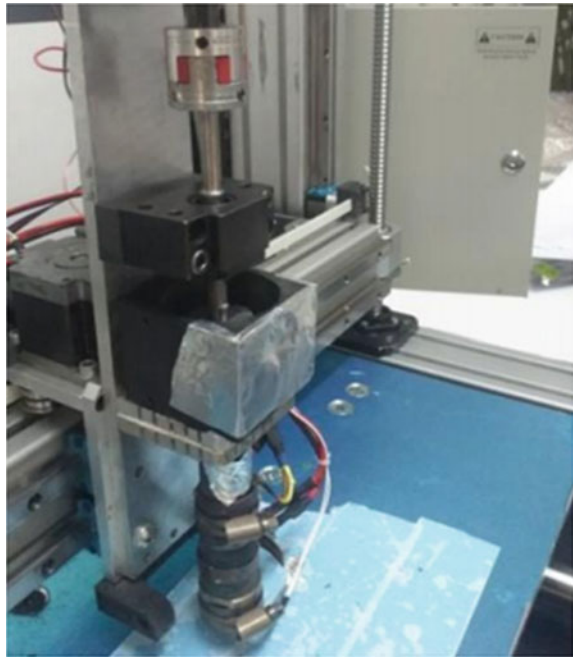


Fig. 45.16 Drive washer and tapered piece [2]

Fig. 45.17 Extruder assembly [2]



45.3 Conclusion

This paper presents a study of pellet or granules extrusion-based 3D printing methods. Filaments are used commercially for FDM 3D printing and flexible material are not suitable for filament, stiffness and strength limits the materials to be used as filament. Flexible materials can also be used in extrusion-based 3D printing in the form of pellets. These pellets can be extruded out of nozzle using screw-extrusion methods. Screw-extrusion are of mainly two types one is single stage screw extrusion and other is double stage screw extrusion. Like filament-based extruder, here also thermal insulation is needed between hopper and extruder. A pellet extrusion head can also be implemented in 3-Axis CNC machine to make it FDM 3D printer. Process

parameters like screw speed and barrel temperature play an important role in screw extrusion process. There should be suitable speed of extrusion screw and barrel temperature for the better quality of 3D printed part.

From this study, it is concluded that there is future scope of development of pellet extrusion-based 3D printing. A hybrid extrusion-based 3D printer can be developed in which both methods—filament extrusion as well as pellet or granule extrusion could be implemented.

Acknowledgements This work was supported by the Science and Engineering Research Board (SERB)—DST, New Delhi, India under its Start-up Research Grant (SRG) scheme [Grant Number—SRG/2019/000943].

References

1. ASTM International (2015) 52900: Standard Terminology for Additive Manufacturing—General Principles—Terminology
2. Albu, S.C., NuTiu, E.: Study on designing the extruder for 3D printers with pellets. *Acta Marisiensis. Seria Technologica*. **16**, 19–22 (2019)
3. ASTM F2792–12: Standard Terminology for Additive Manufacturing Technologies. ASTM International (2012)
4. Bellini, A., Shor, L., Guceri, S.I.: New developments in fused deposition modeling of ceramics. *Rapid Prototyp. J.* **11**, 214–220 (2005)
5. Bellini, A., Shor, L., Guceri, S.I.: New developments in fused deposition modeling of ceramics. *Rapid Prototyp. J.* (2005b)
6. Bikas, H., Stavropoulos, P., Chryssolouris, G.: Additive manufacturing methods and modeling approaches: a critical review. *Int. J. Adv. Manuf. Technol.* **83**, 389–405 (2016)
7. Caminero, M.A., Chacón, J.M., García-Moreno, I., Rodríguez, G.P.: Impact damage resistance of 3D printed continuous fibre reinforced thermoplastic composites using fused deposition modelling. In: *Composites Part B: Engineering* (2018)
8. Dudek, P.: FDM 3D printing technology in manufacturing composite elements. *Arch. Metall. Mater.* (2013)
9. Khondoker, M.A.H., Sameoto, D.: Design and characterization of a bi-material co-extruder for fused deposition modeling. *ASME Int. Mech. Eng. Congress Exposition Proc. (IMECE) ASME* **2**, 1–9 (2016)
10. Kim, S., Seong, H., Her, Y., Chun, J.: A study of the development and improvement of fashion products using a FDM type 3D printer. *Fashion Textiles* **6** (2019)
11. Kumar, N., Jain, P.K., Tandon, P., Pandey, P.M.: Extrusion-based additive manufacturing process for producing flexible parts. *J. Brazilian Soc. Mech. Sci. Eng.* **40**, 1–12 (2018)
12. Ligon, S.C., Liska, R., Stampfl, J., Gurr, M., Mülhaupt, R.: Polymers for 3D printing and customized additive manufacturing. *Chem. Rev.* (2017)
13. Liu, X., Chi, B., Jiao, Z., Tan, J., Liu, F., Yang, W.: A large-scale double-stage-screw 3D printer for fused deposition of plastic pellets. *J. Appl. Polym. Sci.* **134**, 1–9 (2017)
14. Ngo, T.D., Kashani, A., Imbalzano, G., Nguyen, K.T.Q., Hui, D.: Additive manufacturing (3D printing): a review of materials, methods, applications and challenges. *Composites Part B: Engineering* (2018)
15. Paolini, A., Kollmannsberger, S., Rank, E.: Additive manufacturing in construction: a review on processes, applications, and digital planning methods. *Add. Manuf.* **30**, 100894 (2019)
16. Reddy, B.V., Reddy, N.V., Ghosh, A.: Fused deposition modelling using direct extrusion. *Virt. Phys. Prototyp.* **2**, 51–60 (2007)

17. Sathishkumar, T.P., Satheeshkumar, S., Naveen, J.: Glass fiber-reinforced polymer composites—a review. *J. Reinf. Plast. Composit.* (2014)
18. Singh, S., Taufik, M., Jain, P.K.: Development of extruder head for fused deposition process. *J. Eng. Sci. Manage. Educat.* **7**, 1–5 (2014)
19. Soto, E., Baez, O., Sosa, S.: Modeling, design and construction of articulated hand for use in prosthetics, with adaptive control in neural networks based on mathematical model for finger. In: *Proceedings of Special Session—9th Mexican International Conference on Artificial Intelligence: Advances in Artificial Intelligence and Applications, MICAI 2010.*, pp. 107–112 (2010)
20. Taufik, M., Jain, P.K.: Laser assisted finishing process for improved surface finish of fused deposition modelled parts. *J. Manuf. Process.* **30**, 161–177 (2017)
21. Taufik, M., Jain, P.: On the Study of Effect of Coupled Parameters of Fused Deposition Modelling and CO₂ Laser Operation for Improved Surface Finish, pp. 86–89 (2017b)
22. Verner, I., Merksamer, A.: Digital design and 3D printing in technology teacher education. *Procedia CIRP.* **36**, 182–186 (2015)
23. von Krogh, P.: Direct Pellet Extruder Developed for LEDC 3D-print with Recycled Plastics (2017)
24. Wankhade, M.H., Bahaley, S.G.: Design and development of plastic filament extruder for 3D Printing. *IRA-Int. J. Technol. Eng.* **10**(23) (2018). (ISSN 2455–4480)
25. Whyman, S., Arif, K.M., Potgieter, J.: Design and development of an extrusion system for 3D printing biopolymer pellets. *Int. J. Adv. Manuf. Technol.* **96**, 3417–3428 (2018)
26. Zhou, Z., Salaoru, I., Morris, P., Gibbons, G.J.: Additive manufacturing of heat-sensitive polymer melt using a pellet-fed material extrusion. *Add. Manuf.* **24**, 552–559 (2018)

Chapter 46

Smart Magnetorheological (MR) Finishing Technology and Its Applications



Rahul Vaishya, Vivek Sharma, Vikas Kumar, and Rajeev Verma

Abstract Magnetorheological (MR) finishing technology utilise the novel behaviour of magnetorheological finishing fluid (MRFF) which changes its rheological properties under the influence of magnetic field. Generally surface roughness is a main predictor of engineering, medical, automobile parts performance, as irregularities tend to form nucleation sites which leads to wear, corrosion and thus, decreasing the efficiency of the components. In this chapter, we emphasis on the use of MR finishing technology and its application in finishing of various types of materials.

Keywords Magnetorheological finishing · Finishing operation · Surface roughness · Smart magneto-rheological finishing fluid

46.1 Introduction

The final phase in manufacturing of various components include finishing operations. Finishing operations usually increase the cost of the component by 15% to 20%. Surface roughness have a great influence on the aesthetic appearance, fatigue strength, durability, reliability and performance of the component. In many cases, rough surfaces of mating components generate a lot of friction and thus, wear out easily. High level finishing of the surface prevents corrosion and increase the wear-strength and life expectancy of the component. A number of conventional finishing processes (grinding, lapping and honing etc.) are in use from long times for the

R. Vaishya · V. Sharma
Punjab Engineering College, Chandigarh, India
e-mail: rahulvaishya@pec.ac.in

V. Sharma
e-mail: viveksharma.be18prod@pec.edu.in

R. Verma
NIT, Punjab, Punjab, Jalandhar, India
e-mail: vermar@nitj.ac.in

V. Kumar (✉)
Panjab University, Chandigarh, India

finishing of simple shapes components. Many times, traditional grinding damages the surface of the component by creating heat affected zone [1]. Invention of more and more hard material taking place with the advancement of technology and simultaneously the shape complexity of components also goes on increasing. Non-convention machining like EDM (electro discharge machining) [2, 3], ion milling [4] doesn't able to achieve ultra-fine quality surface. All such limitations led to the involvement of advanced finishing operations for precise finishing of varied complex shapes component made from different materials.

Researchers have developed various advanced finishing operations like Magnetic abrasive finishing (MAF) [5], Magnetorheological jet finishing (MRJF) [6], Magnetorheological abrasive flow finishing (MRAFF) [7], Rotational-magnetorheological abrasive flow finishing (R-MRAFF) [8] and Ball-end magnetorheological finishing (BEMRF) [9], Magnetorheological finishing (MRF) [10]. All the mentioned processes utilised the novel behaviour of Magnetorheological finishing fluids which works on the application of magnetic field.

46.2 Magnetorheological Finishing Fluid (MRFF)

MRFF comes under the classification of smart materials due to its novel rheological behavior. The composition of MRFF generally includes mixture of ferromagnetic particles (generally iron particles), abrasives particles and non-magnetic carrier liquid along with additives. The finishing performance of MRFF generally based on the ferromagnetic particles along with abrasives used in it.

MRFF changes its viscosity under the influence of magnetic field (M-Field) and the changed form becomes extremely viscous [11, 12]. The variation in the form of MRFF under different M-Field is shown in Fig. 46.1.

The carbonyl iron particles (CIPs) are generally used as ferromagnetic particle for the development of MRFF, because of its low coercive force and high magnetization. The sedimentation problem generally exists in MRFF due to high density of CIPs. Stability of MRFF increases with decrease in size of magnetic fillers. Nano sized particles show more stability than microns sized particles because of Van der Waals force and Brownian movement. Nano sized particles are used as dispersed phase in magnetic fluids [14–22].

46.3 Behavior of Magnetorheological Finishing Fluid

The condition of MRFF without any applied field is shown in Fig. 46.2a, while the condition under the effect of magnetic field is shown in Fig. 46.2b.

The magneto-dependent rheological behaviour of MRFF typically described by the Bingham model:

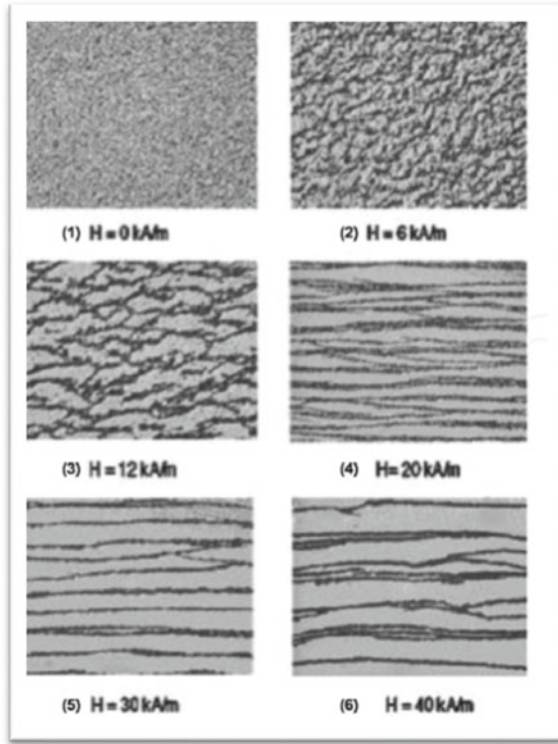


Fig. 46.1 variation in the form of MRFF under different M-Field [13]

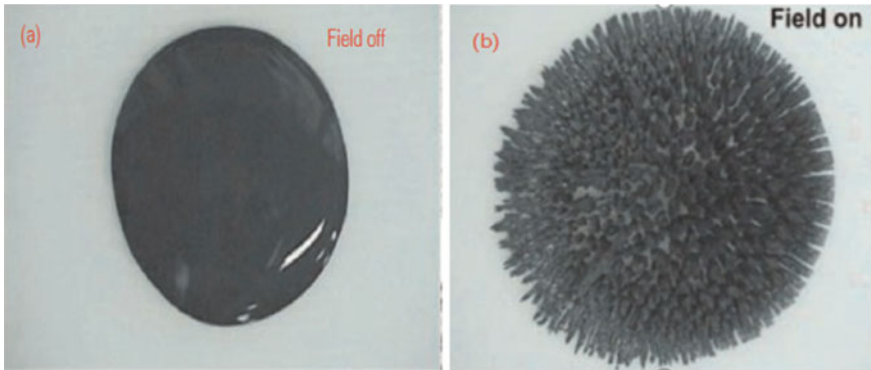


Fig. 46.2 a shows MRFF under no M-Field and b shows MRFF under M-Field [23]

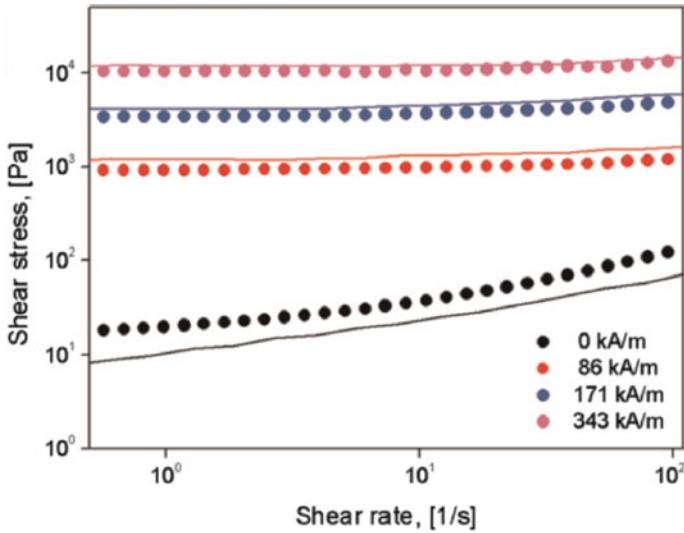


Fig. 46.3 Variation in shear stress (Pa) as a function of shear rate (1/s) at different M-Fields [24]

$$\begin{aligned}
 \tau &= \tau_y + \eta \dot{\gamma} \quad |\tau| \geq \tau_y \\
 \tau &= G_0 \gamma \quad |\tau| < \tau_y,
 \end{aligned}
 \tag{46.1}$$

where τ is shear stress, γ is shear strain rate, τ_y is magneto-dependent shear yield stress, G_0 is that the shear modulus before yield, and η is that the plastic viscosity. τ_y is defined as the minimum stress exhibited by MRFF before its deformation or flow, which may be calculated by using Bingham model (Eq. 46.1). Figure 46.3 shows relation between shear stress (Pa) and shear rate (1/s) because the shear stress increases rapidly as M-Field increases. Therefore, the magneto-dependence of τ_y are often used as a parameter to urge the magnetorheological effect of MRFF [25].

46.4 Applications of MR Finishing Technology

Researchers have used MR finishing technology in precise finishing of various components made of different materials. The present section gives detail on various types of materials which are precisely finished using it.

46.4.1 Cr12 Tool Steel

Cr12 tool steel is used for the cylindrical internal surface, plane position, the corner position and researchers get the surface roughness (Ra) of 132 and 278 nm at plane and corner surface, respectively [26].

46.4.2 Stainless Steel

Stainless Steel is used in the sanitary pipes. Researchers used permanent magnet as the source for generating magnetic field. Iron particles are used of size 80 microns diameter, aluminium oxide is used as abrasives particles along with the machining fluid (about 15%). The surface roughness (Rmax) was decreased from 4 to 0.1 micron [27].

46.4.3 BK-7 Glass

It is a top quality crown glass which is made up of two material. One is silicon dioxide and another one is boron dioxide. Lapping process gives a lot of cutting force as well as it creates heat affected zone. Such heat affected zone damages the surface of the glass. In place of this, MR-finishing technology founds to be more suitable which creates defect free good quality surface [28–36].

46.4.4 AlTiN-coated tool

Researchers have used MR finishing in the finishing of AlTiN-coated tool. They used iron particles of size 44-105 microns and steel grit of mean diameter 700 micron. The diamond abrasive particles were used in MR finishing of the tool. The life of the tool founds to be increases by 150% [37].

46.4.5 Mild Steel

Niranjan and Jha [38] worked on cylindrical external surface and plane position of mild steel. Authors achieved minimum surface roughness (Ra) of 0.0914 μm .

46.4.6 KDP Crystal

Chen et al. [39] worked on external surface of KDP Crystal and achieved final surface roughness (Ra) of 0.624 nm.

46.4.7 Stainless Steel

Das et al. [40] worked on cylindrical external surface of stainless steel and achieved final surface roughness (Ra) of 0.13 μm .

46.4.8 KDP Crystal

Ji et al. [41] worked on external surface of KDP Crystal and achieved final improved surface roughness.

46.4.9 Glass

Liu et al. [42] worked on backside of the cylindrical external surface of KDP Crystal and achieved final surface roughness (Ra) of 0.018 μm .

46.4.10 Glass BK7

Kim et al. [43] worked on external surface, deepest removal point of Glass BK7.

46.4.11 $\text{Al}_2\text{O}_3\text{-TiC}$

Bongsu et al. [44] worked on top surface of $\text{Al}_2\text{O}_3\text{-TiC}$ and achieved minimum Ra value of 131.9 nm.

46.5 Conclusion

MR finishing technology utilize the novel behavior of MRFF whose rheological properties are often altered with help of M-Field and with change in fluid composition. Use of MR finishing gives provision to control finishing forces effectively during operation. MR finishing used on sort of work piece materials (ranging glasses to alloys) without any damage of the work-surface. Also, the work-materials of complex shape geometries can be nano-finished with the utilization of MR finishing technology.

References

1. Liu, J.H., Pei, Z.J., Fisher, G.R.: Grinding wheels for manufacturing of silicon wafers: a literature review. *Int. J. Mach. Tools Manuf* **47**, 1–13 (2007)
2. Fleischer, J., Masuzawa, T., Schmidt, J., Knoll, M.: New applications for micro-EDM. *J. Mater. Process. Technol.* **149**, 246–249 (2004)
3. Abbas, N.M., Solomon, D.G., Bahari M.F. (eds.): A review on current research trends in electrical discharge machining (EDM). *Int. J. Mach. Tools Manuf.* **47**, 1214–1228 (2007)
4. Mitsuishi, K., Shimojo, M., Tanaka, M., Furuya, K.: Nano-fabrication using electron-beam-induced deposition combined with low energy ion milling. *Nuclear Instru. Methods Phys. Res. B* **242**, 244–246 (2006)
5. Shinmura, T., Takazawa, K., Hatano, E., et al.: Study on magnetic abrasive finishing. *CIRP Ann. Manuf. Technol.* **39**(1), 325–328 (1990)
6. Kordonski, W.I., Shorey, A.B., Tricard, M.: Magnetorheological jet (MR Jet™) finishing technology. *Trans. ASME J. Fluids Eng.* **128**, 20–26 (2006)
7. Das, M., Jain, V.K., Ghoshdastidar, P.S.: Analysis of magnetorheological abrasive flow finishing (MRAFF) process. *Int J Adv Manuf Techno* **38**(5), 613–621 (2008)
8. Das, M., Jain, V.K., Ghoshdastidar, P.S.: Nanofinishing of flat workpieces using rotational–magnetorheological abrasive flow finishing (R-MRAFF) process. *Int. J. Adv. Manuf. Technol.* **62**, 405–420 (2011)
9. Niranjana, M., Jha, S., Kotnala, R.K.: Mechanism of material removal in ball end magnetorheological finishing process. *Wear* **302**(1–2), 1180–1191 (2013)
10. Golini, D., Kordonski, W.I., Dumas, P., et al.: Magnetorheological finishing (MRF) in commercial precision optics manufacturing. *Proc. SPIE* **3782**, 80–91 (1999)
11. https://en.wikipedia.org/wiki/Bingham_plastic
12. https://en.wikipedia.org/wiki/Newtonian_fluid
13. Lloyd, J., Hayesmichel, M., Radcliffe, C.: Internal organizational measurement for control of magnetorheological fluid properties. *J. Fluids Eng.-Trans. ASME* **129**, 423–428 (2007)
14. Phule, P.: Synthesis of level magnetorheological fluids. *MRS Bull.* **23**, 23–25 (1998)
15. Sheikholeslami, M.: Influence of magnetic field on Al₂O₃-H₂O nanofluid forced convection heat transfer in a porous lid driven cavity with hot sphere obstacle by means of LBM. *J. Mol. Liq.* **263**, 472–488 (2018)
16. Sheikholeslami, M., Jafaryar, M., Li, Z.: Second law analysis for nanofluid turbulent flow inside a circular duct in presence of twisted tape turbulators. *J. Mol. Liq.* **263**, 472–488 (2018)
17. Sheikholeslami, M.: Application of Darcy law for nanofluid flow in a porous cavity under the impact of Lorentz forces. *J. Mol. Liq.* **266**, 495–503 (2018)
18. Sheikholeslami, M., Gerdroodbary, M., Moradi, R., Shafee, A., Li, Z.: Application of neural network for estimation of heat transfer treatment of Al₂O₃-H₂O nanofluid through a chan27nel. *Comput. Methods Appl. Mech. Eng.* **344**, 1–12 (2019)

19. Sheikholeslami, M., Haq, R., Shafee, A., Li, Z.: Heat transfer behavior of nanoparticle enhanced PCM solidification through an enclosure with V shaped fins. *Int. J. Heat Mass Transf.* **130**, 1322–1342 (2019)
20. Sheikholeslami, M.: Numerical approach for MHD Al₂O₃-water nanofluid transportation inside a permeable medium using innovative computer method. *Comput. Methods Appl. Mech. Eng.* **344**, 306–318 (2019)
21. Sheikholeslami, M.: New computational approach for exergy and entropy analysis of nanofluid under the impact of Lorentz force through a porous media. *Comput. Methods Appl. Mech. Eng.* **344**, 319–333 (2019)
22. Sheikholeslami, M., Mahian, O.: Enhancement of PCM solidification using inorganic nanoparticles and an external magnetic field with application in energy storage systems. *J. Cleaner Prod.* **215**, 963–977 (2019)
23. Tong, Y., Dong, X., Qi, M.: High performance magnetorheological fluids with flower-like cobalt particles. *Smart Mater. Struct.* **26**, 025023 (2017)
24. Fang, F., Choi, H., Seo, Y.: Sequential coating of magnetic carbonyl iron particles with polystyrene and multiwalled carbon nanotubes and its effect on their magnetorheology. *ACS Appl. Mater. Interfaces.* **2**, 54–60 (2010)
25. Kuzhir, P., Magnet, C., Bossis, G., Meunier, A., Bashtovoi, V.: Rotational diffusion may govern the rheology of magnetic suspensions. *J. Rheol.* **55**, 1297–1318 (2011)
26. Wang, J., Chen, W., Han, F.: Study on the magnetorheological finishing method for the WEDMed pierced die cavity. *Int J Adv Manuf Technol* **76**, 1969–1975 (2015)
27. Shinmura, T., Aizawa, T.: Study on internal finishing of a non-ferromagnetic tubing by magnetic abrasive machining process. *Bull. Japan Soc. Precision Eng.* **23**(1), 37–41 (1989)
28. Tsegaw, A.A., Shiou, F.J., Lin, S.P.: Ultra-precision polishing of N-Bk7 using an innovative self-propelled abrasive fluid multi-jet polishing tool. *J. Mech. Sci. Technol.* **19**, 262–285 (2015). <https://doi.org/10.1080/10910344.2015.1018532>
29. Lee, S.H., Lu, Z., Babu, S.V., Matijevic, E.: Chemical mechanical polishing of thermal oxide films using silica particles coated with ceria. *J. Mater. Res.* **17**, 2744–2749 (2011). <https://doi.org/10.1557/JMR.2002.0396>
30. Kordonski, W.I., Jacobs, S.D.: Magnetorheological finishing. *Int. J. Mod. Phys. B* **10**, 2837–2848 (1996). <https://doi.org/10.1142/S0217979296001288>
31. Singh, A.K., Jha, S., Pandey, P.M.: Nanofinishing of fused silicaglass using ball-end magnetorheological finishing tool. *Mater. Manuf. Processes* **27**, 1139–1144 (2012). <https://doi.org/10.1080/10426914.2011.654159>
32. Sidpara, A., Das, M., Jain, V.K.: Rheological characterization of magnetorheological finishing fluid. *Mater. Manuf. Processes* **24**, 1467–1478 (2009). <https://doi.org/10.1080/10426910903367410>
33. Cook, L.M.: Chemical processes in glass polishing. *J. Non-Cryst. Solids* **120**, 152–171 (1990). [https://doi.org/10.1016/0022-3093\(90\)90200-6](https://doi.org/10.1016/0022-3093(90)90200-6)
34. Das, C.R.: The reaction between borate glass and attacking agents-part iii: equilibrium pH of the Alkali borate glasses and their relationship with chemical durability and the glass composition. *Trans. Indian Ceram. Soc.* **26**, 155–158 (2014). <https://doi.org/10.1080/0371750x.1967.10855602>
35. Hoshino, T., Kurata, Y., Terasaki, Y., Susa, K.: Mechanism of polishing of SiO₂ Films by CeO₂ particles. *J. Non-Cryst. Solids* **283**, 129–136 (2001). [https://doi.org/10.1016/s0022-3093\(01\)00364-7](https://doi.org/10.1016/s0022-3093(01)00364-7)
36. DeGroot, J.E., Marino, A.E., Wilson, J.P., Bishop, A.L., Lambropoulos, J.C., Jacobs, S.D.: Removal rate model for magnetorheological finishing of glass. *Appl. Opt.* **46**, 7927–7941 (2007)
37. Yamaguchi, H., Srivastava, A.K., Tan, M., Hashimoto, F.: Magnetic Abrasive Finishing of cutting tools for high-speed machining of titanium alloys. *CIRP J. Manuf. Sci. Technol.* **7**, 299–304 (2014)
38. Niranjana, M.S., Jha, S.: Experimental investigation into tool aging effect in ball end magnetorheological finishing. *Int. J. Adv. Manuf. Technol.* **80**, 1895–1902 (2015)

39. Chen, S., Li, S., Hu, H., et al.: Analysis of surface quality and processing optimization of magnetorheological polishing of KDP crystal. *J. Opt.* **44**(4), 384–390 (2015)
40. Das, M., Jain, V.K., Ghoshdastidar, P.S.: A 2D CFD simulation of MR polishing medium in magnetic field-assisted finishing process using electromagnet. *Int. J. Adv. Manuf. Technol.* **76**, 173–187 (2015)
41. Ji, F., Xu, M., Wang, C. et al.: The magnetorheological finishing (MRF) of potassium dihydrogen phosphate (KDP) crystal with Fe_3O_4 nanoparticles. *Nanoscale Res. Lett.* **11**(79) (2016). <https://doi.org/10.1186/s11671-016-1301-4>
42. Liu, H., Chen, M., Yu, B., Fang, Z.: Configuration design and accuracy analysis of a novel magnetorheological finishing machine tool for concave surfaces with small radius of curvature. *J. Mech. Sci. Technol.* **30**(7), 3301–3311 (2016)
43. Kim, W.-B., Nam, E., Min, B.-K., et al.: Material removal of glass by magnetorheological fluid jet. *Int. J. Precis. Eng. Man.* **16**(4), 629–637 (2016)
44. Jung, B., Jang, K.I., Min, B.K., Lee, S.J., Seok, J.: Magnetorheological finishing process for hard materials using sintered iron-CNT compound abrasives. *Int. J. Mach. Tools Manuf* **49**(5), 407–418 (2009). <https://doi.org/10.1016/j.ijmachtools.2008.12.002>

Chapter 47

Development of Sheet Metal Die by Using CAD and Simulation Technology to Improvement of Quality



Amrapali L. Ramteke, Shubash N. Waghmare, Sagar D. Shelare, and Piyush M. Sirsat

Abstract Minimizing manufacturing time is a major advancement that decreases the entire cost of production and reduces the time for a commodity to be sold. One of the main titles of the sheet metal industry is the convergence of sheet metal product design, simplification, and fabrication applications. Sheet metal formation is one of the most common finished product procurement technologies in almost every industrial production field, especially in the aircraft, automobile, food and home appliance industries. Because of its intricate forms and the possibilities of applications it requires, the incorporation of sheet metal product design and development in a computer-aided setting is a challenge. To solve this problem, many methodologies are being developed, such as a Single Minute Exchange Die System (SMED) that considers only the methodology to minimize the installation of forming dies to almost 25–30%, but does not take into account the minimization of the phase or sequence of forming. Most of the time, the automotive industry reduces the time by standardizing some of the die components to mount the die issue. The paper is focused on the design of sheet metal die for the casting. It also focused to develop and optimize the performance of die. The performance of die is evaluated by using CAD simulation technology. Three different materials are checked to evaluate performance those are EN 8, SAE 4340, and SAE 4640. After the simulation results show that SAE 4640 material gives quality performance than are EN 8, SAE 4340 material.

Keywords Sheet metal · Die · CAD · Quality · Simulation technology

A. L. Ramteke
M.Tech in Mechanical Engineering Design, Priyadarshini College of Engineering Nagpur,
Nagpur, Maharashtra, India

S. N. Waghmare (✉) · S. D. Shelare · P. M. Sirsat
Department of Mechanical Engineering, Priyadarshini College of Engineering Nagpur, Nagpur,
Maharashtra, India

47.1 Introduction

The knowledge is about the different design parameters that affect the construction of sheet metal die. To make a sheet metal product, the sheet metal parts weighed and analysed. Because of this variety of potential production errors can be significantly reduced. The Die mould design principle, various research work can be carried out tribological simulation for mould invalidation analysis, creation of quality feature, Design for Manufacture and Assembly (DFMA), mould delamination and die fracture analysis. “Different approaches the virtual prototyping approach to mould design is taken into account. In virtual prototype is generated by combining automated and interactive approaches” [1]. There are some problems with the selection of alloy steel in the current die mould protection cap, sheet metal die mould product shape mistake, it is important to design the mould for protection cap and upgrade the existing design [2–4]. There is an attempt to look at different techniques of mould design for a protective cap. As mould design is a complex process involving in many decision factors, it is difficult to ensure both mould reusability and meeting manufacturing requirements without iteration of evaluating and modifying. Although other sheet metal Die mould product is less accurate & consistent [5–7]. Chances of the incidence of shape error are mostly from weak machining. There are new methods that are developed & technology is advancing to improve the quality of sheet metal die mould product. This product was specially designed and can be tailored to the needs and specifications of the customers. Several problems exist about alloy steel collection, sheet metal die mould form mistake. “Analysis of sheet metal die is required to overcome this difficulty” [8–10].

A simple die used for punching as shown in Fig. 47.1. It consist of Bed, bolster plate, die set, die, die block, lower shoe, punch, upper shoe, punch plate, back up plate, stripper, knockout, pitman, shut height, stroke [11].

As seen in Fig. 47.1, the upper shoe is directly fastened to the punch press ram. The lower shoe was attached to the blossom press pad. For improved compatibility of the punch holder with the die shoe [12–14], guide pots may be used. With two guide points, located at the rear of the die package, these main components are known as die set. Diagonally, one in front of the die set at the back, or with four guide posts, one in each die set corner. In the guide shoe, the lower ends of the guide posts are pressed. Guide posts have a slip fit with guide bushing at the upper end that is pushed into the punch holder. Have a free bushing motion with this guidance article. The punch is clamped to the punch holder and the die block is clamped to the die shoe [15–18]. The punch is associated with the Die Block opening. During the downward motion of the punch through the die block, the cutting operation takes place. Elastic regeneration in strip content happens after cutting action. The size of the blank increases and that of the cavity decreases as a result of this. So at the end of the process, the scrap strip clings to punch as punch begins to pass upward and blank gets clogged to die opening. A stripper is used to scrape scrap strips from the surface of the punch. The walls of the die opening are tapered to prevent sticking to the blank in the die opening.

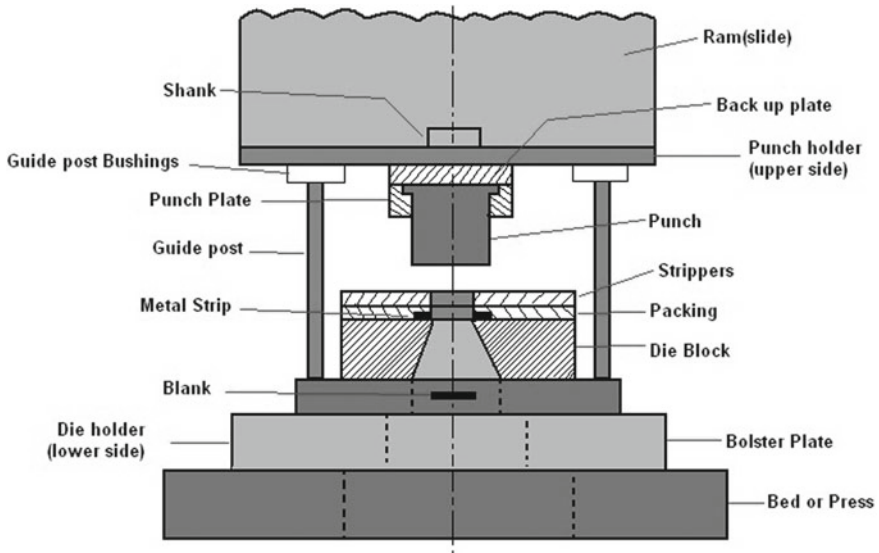


Fig. 47.1 Press tool terminology



Fig. 47.2 A Indicate the high stress induced in die

The high Stresses are induced in existing sheet metal die as shown in Fig. 47.2. Due to this high stresses induced in the Die resulting in crack propagation in sheet metal Die [19, 20]. The stresses Occur at the above four corners of Die. After punching pressure applies on the Die, Stresses induced are resulting in high stresses at the corners. The Stresses are induced in existing sheet metal die due to repetitive loading

conditions. Under repetitive load conditions, at one stage existing material EN8 crosses yield Strength resulting in crack propagation in sheet metal Die Along with high stresses, and more deformation occurs in sheet metal die. To overcome this difficulty, there is a Need to use CAD.

Software and simulation technology to redesign sheet metal die. That stresses occur in sheet metal die can be greatly reduced [21–24]. The Main Motivation in Designing Sheet Metal Die is to reduce the Stresses & Deformation produced by changing the material. Using software to analyse sheet metal die will find with greater accuracy & high precision along with achieving best material properties utilization with permissible stress level & less deformation in sheet metal die.

The outcome that comes from the literature survey is the analysis of sheet metal parts plays an important role to get improved accuracy, flexibility, and good efficiency advantages [25]. Analysis sheet metal of various parts gives assure quality and helps in reducing manufacturing cost. To achieve optimized die size, optimal die size rules with precision and lower complexity can be derived. Advanced processing technology such as high-pressure sheet metal formation (HPSMF) may be used to produce goods for sheet metal application with optimized thickness distribution [26, 27]. There is a constraint in the die wear analysis to maintain the efficiency of the shaping instrument and to estimate the risk of fixing or modifying the die. Theoretical prediction of the effective properties for materials is very important to the analysis of material performance.

The experimental set up is used to improve and study parameters related to the sheet metal die. To improve the life of sheet metal dies, different operations are performed on die mould. A literature survey helps to predict the shape of a sheet metal component and to achieve a quality of operation performed on sheet metal Die.

47.2 Research Background

The high Stresses are induced in existing sheet metal die. Due to this high stresses induced in the die resulting in crack propagation in sheet metal die [28, 29]. The stresses Occur at the above four corners of die. After punching pressure applies on the die, Stresses induced are resulting in high stresses at the corners as indicated in Figs. 47.2 and 47.3. The Stresses are induced in existing sheet metal die due to repetitive loading conditions, under repetitive load conditions, at one stage existing material EN8 crosses yield strength resulting in crack propagation in sheet metal die along with high stresses, deformation occurs in sheet metal die is more. To overcome this difficulty, there is need to use of CAD software and simulation technology to redesign sheet metal die. So that stresses occur in sheet metal die can be greatly reduced.

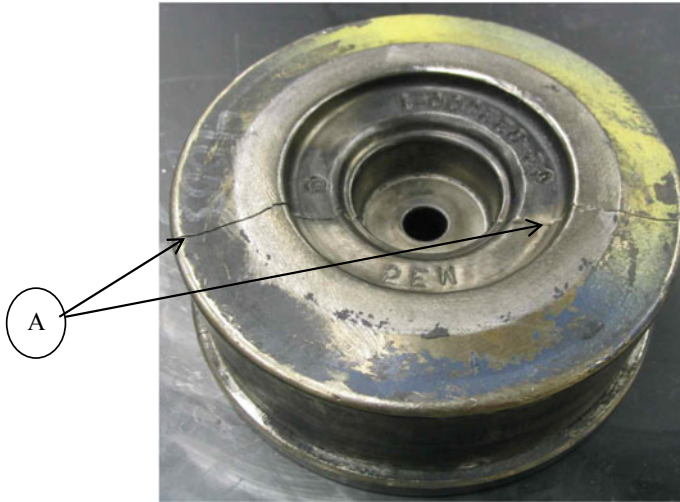


Fig. 47.3 Failure of die section where A-indicate the failure section

47.3 Methodologies

47.3.1 Methodologies to Be Used

- (1) Chemical composition of material.
- (2) Design of Sheet metal Die for protection cap.
- (3) CAD modelling using UNIGRAPHICS software (a) CAD modelling of Protection cap, (b) CAD modelling of sheet metal die.
- (4) Assembly of Die in UNIGRAPHICS software.
- (5) Analysis of sheet metal dies using Analysis software ANSYS 16.5.

To reduce the stresses and deformation of the material, research has to go through different analyses with different materials. Following Table 47.1, gives the available different materials for the testing purpose in CAD software with their physical properties.

To have the nature of stresses and deformation, one should the exact chemical composition. Following Tables 47.2, 47.3 and 47.4 shows the chemical composition

Table 47.1 Available data of material

Material	Poisson's ratio	Young's modulus (GPa)
EN 8 or SAE 1040	0.3	206
Copper Alloy SAE 4340	0.27	208
Stainless Steel or SAE 4640	0.28	211

Table 47.2 Chemical Composition EN8

Element	C	Si	Mn	Ni	Cr	Mo	S	P
Content	0.35–0.45	0.05	0.60/100	–	–	–	0.06 Max	0.06 Max

Table 47.3 Chemical Composition of SAE 4340

Element	C	Mn	Si	Cr	Ni	V	P	S
Content	0.37–0.44	0.10–0.35	0.55–0.90	0.65–0.95	1.55–2.00	0.20–0.35	0–0.04	0–0.04

Table 47.4 Chemical Composition of SAE 4640

Element	C	Mn	Si	Ni	Mo	P	S	Cu
Content	0.38–0.43	0.60–0.80	0.20–0.35	1.65–2.00	0.20–0.30	0.040	0.040	-

of the material EN8, SAE 4340 and SAE 4640.

47.4 Product Design

47.4.1 *Cad Modelling and Tool Path Generation*

Product design is the activity of designing a new product that will be marketed to its customers by a company. This is creating and implementing concepts quickly and effectively into a mechanism that leads to new goods [30, 31]. Consumer designers need all the details: how people use and misuse objects, defective goods, flaws in the design process, and the appropriate ways in which people want objects they can use. Many new designs will fail and many won't even make it to mark Different designs in the end become obsolete.

Generally taking 5 or 6 try to get the product design can be very frustrating for the design process itself. A product that go wrong in the marketplace for the first time can be renew to the market second times more. If it carry on to fail, then the company is deemed dead and the consumer thinks it is a failure most new products fail, even it is a brilliant idea [32–34]. The economic health of manufacturing industries is directly related to all forms of product design. Innovation brings much of the competitive momentum for new product development, with new technology also needing a different understanding of the design. Creating a new product model requires only one supplier to push the rest of the industry to catch up-sparking more innovation. Industrial design is the use of a mixture of applied art and applied science to improve a product's aesthetics, ergonomics, and usability, but it can also be used to increase the marketability and development of the product. An industrial designer has the task of designing and implementing design solutions for shape, usability,

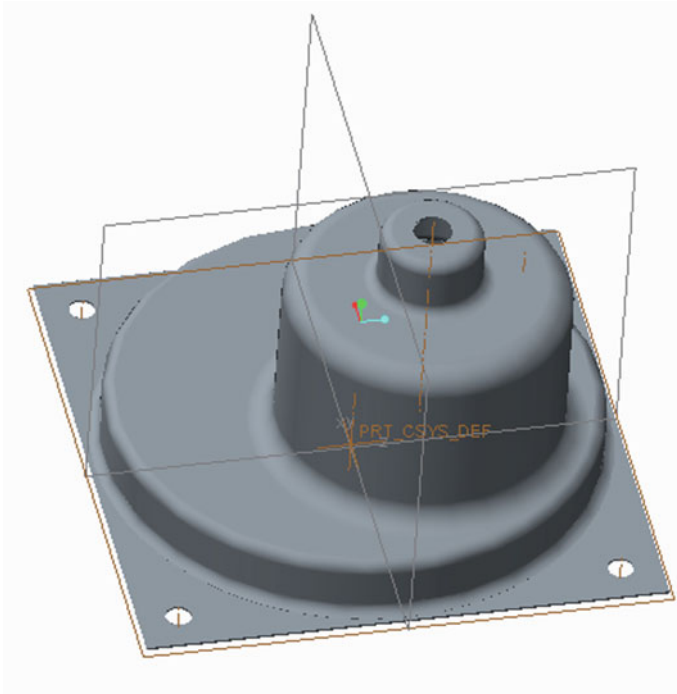


Fig. 47.4 Protection Cap of die

physical ergonomics, marketing, brand creation, and sales issues (Figs. 47.4 and 47.5).

47.4.2 Cavity Extraction

Cavity extraction is the process in making a die in which cavity can be extracted from die mould. Due to this extraction process, core and cavity in die mould becomes separated. The pull direction of material in cavity extraction process and core, cavity separated as shown in Figs. 47.6 and 47.7.

47.5 Analysis of Sheet Metal Dies

Product design is the process of designing a new product that will be marketed to its customers by a company. This is creating and implementing concepts quickly and effectively into a mechanism that leads to new goods. Consumer designers need all

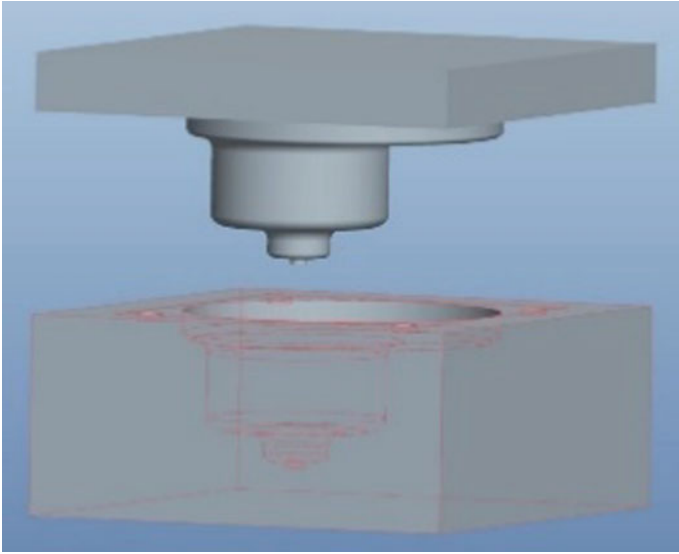


Fig. 47.5 Cavity of die

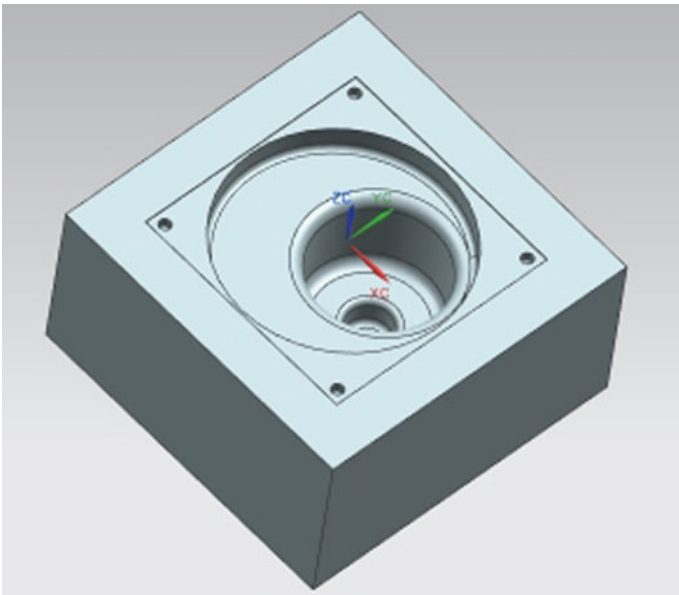


Fig. 47.6 CAD Design of Cavity of die

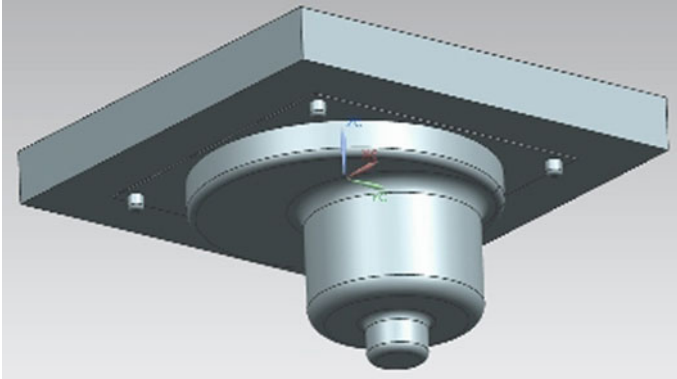


Fig. 47.7 CAD Design of core of die

the details: how people use and misuse objects, defective goods, flaws in the design process, and the appropriate ways in which people want objects they can use. Many new designs will fail and many won't even make it to market. Some designs eventually become obsolete.

It may typically be very difficult for the design process itself to take 5 or 6 attempts to achieve the product design. A commodity that fails for the first time in the industry can be reintroduced to the market 2 times again. If it manages to struggle, then the enterprise is considered dead and the buyer believes that any new products fail, even if it is a genius idea. The economic health of manufacturing industries is directly related to all forms of product design. Innovation brings much of the competitive momentum for new product development, with new technology also needing a different understanding of the design. Creating a new product model requires only one supplier to push the rest of the industry to catch up-sparking more innovation.

Industrial design is that the use of a mix of applied art and engineering to enhance a product's aesthetics, ergonomics, and usefulness, but it also can be used to increase the marketability and development of the product. An industrial designer has the task of designing and implementing design solutions for shape, advantages, physical comfort, marketing, brand formation, and sales issues (Figs. 47.8 and 47.9).

See Fig. 47.10.

47.5.1 Equivalent Stresses in Structural Steel EN8 Material

See Fig. 47.10.

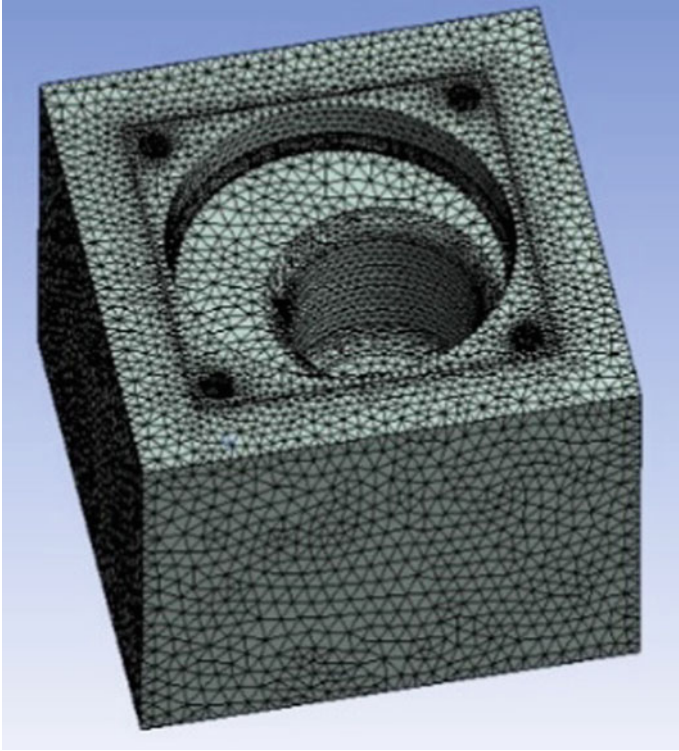


Fig. 47.8 Meshing of cavity of die

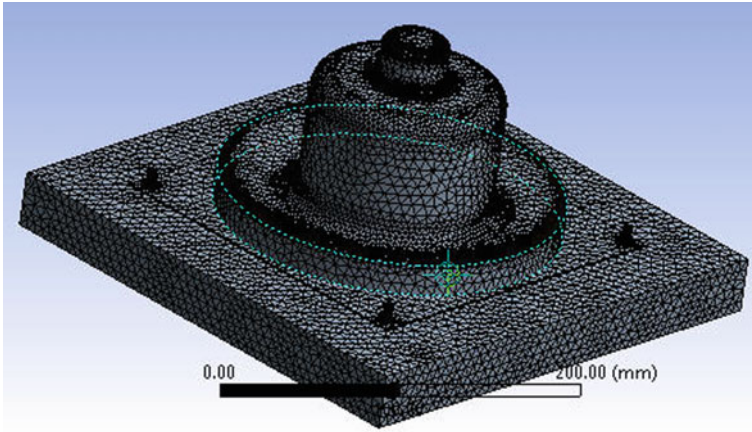


Fig. 47.9 Meshing of core of die

47.5.2 Equivalent Stresses in SAE 4340 Material

See Fig. 47.11.

47.5.3 Equivalent Stresses in SAE 4640 Material

See Fig. 47.12.

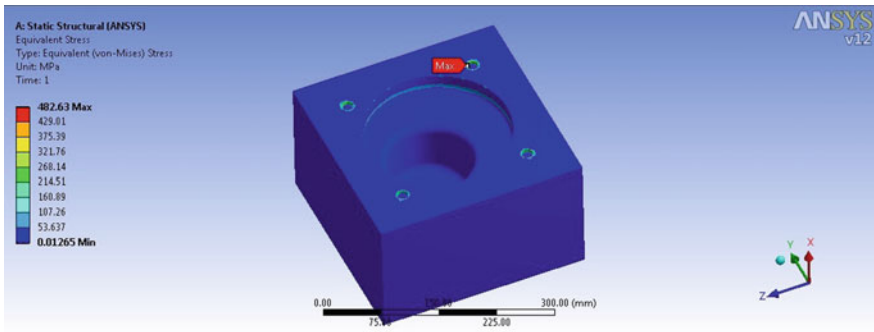


Fig. 47.10 Model showing stresses in EN8 material

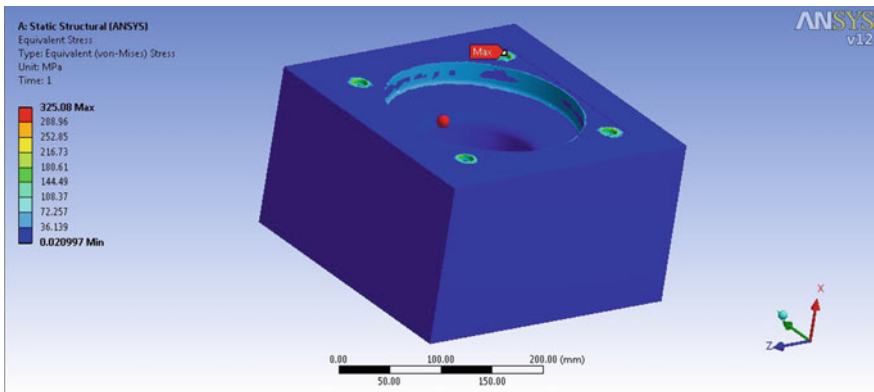


Fig. 47.11 Model showing stresses in copper alloy material

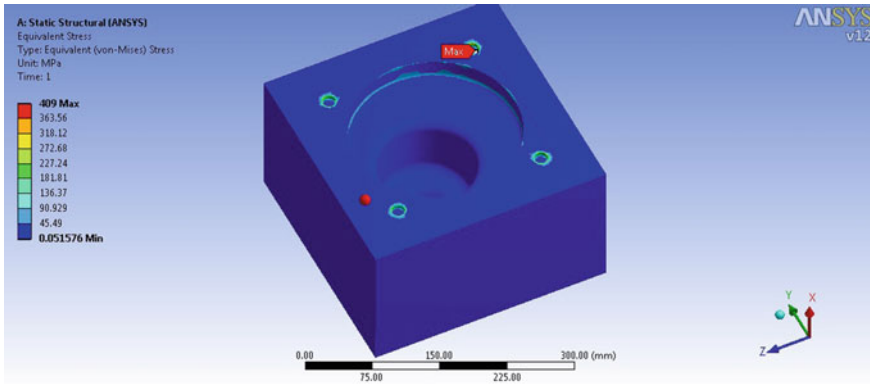


Fig. 47.12 Model showing stresses in SAE 4640 material

47.6 Result and Discussion

There is a need to understand why the model's answer varies from the real structures, as it does very massively. This can be due to a multitude of errors, errors in the parameters of the physical elements (material, thickness, etc.) or boundary conditions, or because the discretization of FEA is an insufficient solution to the real world. Modelling stiffness and mass can be unreliable due to an inadequate number of components, or because of the formulations of the underlying components.

The degree of accuracy of the manufacturing data is directly related to the product's quality and cost; thus, validation of data from manufacturing engineering is a crucial phase in the production cycle. Data packages for manufacturing engineering also contain errors that can lead to inefficient use of the production resources. The erroneous data corrected before the run of production. Individual data packets and related production processes reviewed before starting output. An NC software, for example, should be validated, a part of the manufacturing results. An NC software includes a series of instructions; these are the machining operations sequences on the piece of work. Traditionally, once an NC program has been created, it has been validated by checking the path plots of the NC tool or performing dry running on a real computer. Such conventional methods of validation can-not be effective and labour-intensive, risky and costly. There could be some undetectable errors left in the NC system. Those undetected errors can lead to poor quality of the part, premature wear out of the tool, or tool breakage. Table 47.5.

From the analysis as shown in Figs. 47.10, 47.11, and 47.12 of sheet metal die having EN8 material, stresses induced are 482.63 MPa. which exceeds yield strength 350 MPa of EN8 material. Due to repetitive loading, elongation occurs resulting in crack propagation in Die. This difficulty or problem can overcome by replacing EN8 material by copper alloy (SAE4340 Grade) stresses are reduced and are 325 MPa which below the yield strength 670 MPa of SAE 4340 Grade. Which even under repetitive loading condition, hardly crosses the yield strength. Along with that the

Table 47.5 Comparative stress values for die in ansys 12.0 for different die materials

Material	Loading condition (KM)	Yield strength (MPa)	Ultimate strength (MPa) (MPa)	Ansys result (MPa)
EN8 or SAE 1040Structural steel	395.127	350	632	482.63
SAE 4340 or copper alloy	395.127	670	755	325
SAE 4640 or Stainless steel	395.127	1160	1280	409

result ultimate strength of copper alloy grade is higher near about 755 MPa and hence chances of a crack occurring in die are greatly reduced. SAE 4640 grade is taken which is heavy-duty material which has the highest yield as well as ultimate strength. The Result shows improved performance parameters basis total equivalent stress by replacing EN8 material by SAE 4340 Grade.

47.7 Conclusion

It is seen that the use of suitable software has become essential to analyse stresses, deformation in sheet metal die and thereby improve the standard of the die by proper selection of material. This would result in cost reduction and material saving & reducing stresses. Several design rules, developed over the years through experience and observations, if rightly practiced, would lead to optimum design of various sheet metal components of die as a manufacturing process. However, it is vital to realize that each design is unique and studied exclusively to obtain the best results. With the use of CAD/CAE software's, standard design rules which is developed it is concluded that Different design parameters of a die are compared experimentally and selected the geometry having more accuracy and reliability From the analysis of sheet metal die having EN8 material has the stresses near about 482.63 MPa induced which exceeds yield strength results in crack propagation in Die under repetitive loading. This difficulty or problem can overcome by Replacing EN8 material by copper alloy (SAE 4340 Grade) that stresses are reduced & are 325 MPa which much below the yield strength.which even under repetitive loading conditions, hardly crosses the yield strength. The Result shows improved performance parameters of total equivalent stress.

The cost of SAE 4640 material is higher than EN8 material, the Die life of suggested SAE 4640 material becomes more than Die of EN8 material. There by improving the quality of the Die by proper selection of material. This would result in reducing stresses in Die.

References

1. Ashby, M.F., Johnson K.: The art and science of materials selection. *Mater. Today* **6**(12) (2003)
2. Chen-Fu, C., Chia-Chih, L., Chia-Yu, H., Hong-Shing, C., Chih-Wei.: Optimize Die Size Design to Enhance OWE for Design for Manufacturing. Institute of Electrical and Electronics Engineers (2007)
3. Dhande, H.K., Shelare, S.D., Khope, P.B.: Developing a mixed solar drier for improved postharvest handling of food grains. *Agricult. Eng. Int. CIGR J.* **22**(4), 17–24 (2020)
4. Dufflou, J.R., Callebaut, B., Verbert, J., De Baerdemaeker, D.: Laser assisted incremental forming: formability and accuracy improvement. *CIRP Ann.* **56**, 273–276 (2007)
5. Emad Al-Momani, Ibrahim R.: An application of finite element method and design of experiments in the optimization of sheet metal blanking process. *Jordan J. Mech. Indust. Eng.* **2**(1) (2008). ISSN 1995–6665
6. Göttmann, A., Dietrich, J., Bergweiler, G., Bambach, M., Hirt, G., Loosen, P., Poprawe, R.: Laser-assisted asymmetric incremental sheet forming of titanium sheet metal parts. *Prod. Eng.* **5**, 263–271 (2011)
7. Jawalekar, S.B., Shelare, S.D.: Development and performance analysis of low cost combined harvester for rabi crops. *Agricult. Eng. Int. CIGR J.* **22**(1), 197–201 (2020)
8. Lei, L.M., Hubert, W., Torsten, H.: Mold delamination and die fracture analysis of mechatronic packages. In: *Electronic Components and Technology Conference MerjaHuhtala, DFMA-Aspects of Sheet Metal* (2001)
9. Khan, Y.A., Ganesan, S.M., Valberg, H., Moe, P.T., Hansen, A.W.: Deformation conditions in conventional shearing dependent on geometry parameters of tooling. *Int. J. Mater. Forming* 535–538 (2008)
10. KalyaniAbhinav., K.A. Analysis of sheet metal bending by using finite element method. *Int. J. Eng. Res. Technol.* **2**(1), (2013)
11. Lawanwong, K., Natthasak, P., Ghit, L.: An investigation of adhesion wear behavior of tool steel on blanking die. In: *International Conference on Advanced Materials* (2011)
12. Kumbhare, H., Shelare, S.: (2020) Innovative advancement in drone technology for water sample collections -a review. *Int. J. Sci. Technol. Res.* **9**(03), 7266–7269 (2020)
13. Mali, P.K., Sakhale, C.N., Shelare, S.D.: A literature review on design and development of maize thresher. *Int. J. Pure Appl. Res. Eng. Technol.* **3**(9), 9–14 (2015)
14. Mathew, J.J., Sakhale, C.N., Shelare, S.D.: Latest Trends in Sheet Metal Components and Its Processes—A Literature Review. *Algorithms for Intelligent Systems*, 565–574 (2020). https://doi.org/10.1007/978-981-15-0222-4_54
15. Mats, R.: *Influence of Microstructure on Fatigue and Ductility Properties of Tool Steels*. Department of Materials Science and Engineering, Royal Institute of Technology. Stockholm, Sweden (2008). ISBN: 978-91-7178-859-7.
16. Mohammadi, A., Vanhove, H., Van Bael, A., Dufflou, J.R.: Towards accuracy improvement in single point incremental forming of shallow parts formed under laser assisted conditions. *Int. J. Mater. Form.* **9**, 339–351 (2016)
17. Mowade, S., Waghmare, S., Shelare, S., Tembhurkar, C.: Mathematical model for convective heat transfer coefficient during solar drying process of green herbs. In: *Computing in Engineering and Technology*, 867–877 (2019). https://doi.org/10.1007/978-981-32-9515-5_81
18. Sahu P., Shelare S., Sakhale C.: Smart cities waste management and disposal system by smart system: a review. *Int. J. Sci. Technol. Res.* **9**(03) 4467–4470 (2020)
19. Sartkulvanich, P., Kroenauer, B., Golle, R., Konieczny, A., Altan, T.: Finite element analysis of the effect of blanked edge quality upon stretch flanging of AHSS. *CIRP Ann. Manuf. Technol.* **59**, 279–282 (2010)
20. Sharma, P.C.: *A Textbook of Production Engineering*. S. Chand Publication Pvt. Ltd, India, chapter 2, section 2.5, 2.17, 76–127 (1982)
21. Shelare, S.D., Thakare, P.S., Handa, C.C.: (2012) Computer aided modelling and position analysis of crank and slotted lever mechanism. *Int. J. Mech. Eng. Prod. Eng. Res. Develop.* **2**(2), 47–52 (2012)

22. Shelare, S.D., Kumar, R., Khope, P.B.: Formulation of a Mathematical Model for Quantity of Deshelled Nut in Charoli Nut Deshelling Machine. *Advances in Metrology and Measurement of Engineering Surfaces*, pp. 89–97 (2020). Available at: https://doi.org/10.1007/978-981-15-5151-2_9
23. Tembhurkar, C., Kataria, R., Ambade, S., Verma, J.: Transient Analysis of GTA-Welded Austenitic and Ferritic Stainless Steel. *Advances in Materials Processing*, 59–65 (2020). https://doi.org/10.1007/978-981-15-4748-5_6
24. Shopping, Y., Han, D., Tso, S.K., Youlun, X.: A Virtual Prototyping Approach to Mould Design. *Institute of Electrical and Electronics Engineers* (1999). 0-7803-5731-0B9, 01
25. Tirupati, R., Chandrupatla., Ashok, D.B.: A Textbook of Introduction to Finite Elements in Engineering. Prentice-Hall of India Pvt. Ltd
26. Urban, M., Krahn, M.: Numerical research and optimisation of high pressure sheet metal forming of tailor rolled blanks. *J. Mater. Process. Technol.* **177**(1–3), 360–36 (2006)
27. Waghmare, S., Sirsat, P., Sakhale, C., Shelare, S., Awatade, S.: A case study on improvement of plant layout for effective production. *Int. J. Mech. Prod. Eng. Res. Develop.* **7**(5), 155–160. <https://dx.doi.org/10.24247/ijmperdoct201716>
28. Waghmare, S.N., Sakhale, C.N., Tembhurkar, C.K., Shelare, S.D.: Assessment of average resistive torque for human-powered stirrup making process. In: *Computing in Engineering and Technology*, 845–853 (2019). https://dx.doi.org/10.1007/978-981-32-9515-5_79
29. Waghmare, S., Mungle, N., Tembhurkar, C., Shelare, S., Sirsat, P., Pathare, N.: Design and analysis of power screw for manhole cover lifter. *Int. J. Recent Technol. Eng.* **8**(2), 2782–2786, <https://dx.doi.org/10.35940/ijrte.B2628.078219>
30. Waghmare, S.N., Shelare, S.D., Tembhurkar, C.K., Jawalekar, S.B.: Development of a model for the number of bends during stirrup making process. In: *Advances in Metrology and Measurement of Engineering Surfaces*, 69–78 (2020). https://dx.doi.org/10.1007/978-981-15-5151-2_7
31. Waghmare, S., Shelare, S., Sirsat, P., Pathare, N., Awatade, S.: (2020) Development of an innovative multi-operational furnace. *Int. J. Sci. Technol. Res.* **9**(04), 885–889 (2020)
32. Shao, W., Guo, J., Zhou, A.: A framework of measurement & analysis of sheet metal parts. *Inst. Electri. Electron. Eng.* (2009). <https://doi.org/10.1109/ICICTA.2009.323>
33. Yang, A.: Numerical simulation and optimization of process chain in high-pressure sheet metal forming. In: *Third International Conference on Measuring Technology and Mechatronics Automation* (2011)
34. Yan-fang, Y.: Tribological simulation for the invalidation analysis of mould. In: *Second International Conference on Mechanical and Electronics Engineering* (2010)